2 November 2012 | $10

Science

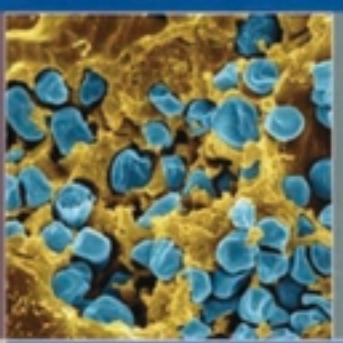

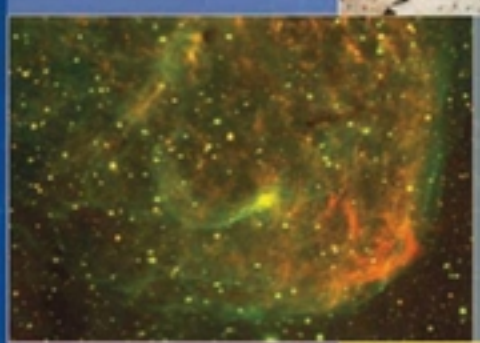

THE BEAUTY AND BENEFITS OF SCIENCE

AAAS ANNUAL MEETING

14–18 FEBRUARY 2013
HYNES CONVENTION CENTER
BOSTON

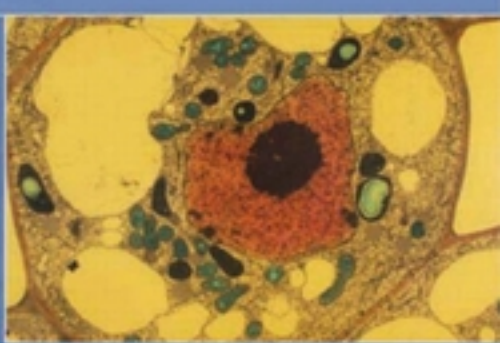

AAAS

EDITORIAL

NEWS OF THE WEEK

NEWS & ANALYSIS

NEWS FOCUS

LETTERS

BOOKS *ET AL.*

POLICY FORUM

PERSPECTIVES

CONTENTS continued >>

page 596

page 610

pages 617 & 682

COVER

The theme of the 2013 AAAS Annual Meeting, 14 to 18 February in Boston, Massachusetts, is *The Beauty and Benefits of Science*. This theme highlights the "unreasonable effectiveness" of the scientific enterprise in creating economic growth, solving societal problems, and satisfying the essential human drive to understand the world in which we live. The preliminary program begins on page 688.

Images (clockwise from top-left): wekwek/iStockphoto; Science Source; Biophoto Associates/Science Source; Eric Grave/Science Source; NASA; Ted Kinsman/Science Source

DEPARTMENTS

Published by AAAS

REVIEW

REPORTS

CONTENTS continued >>

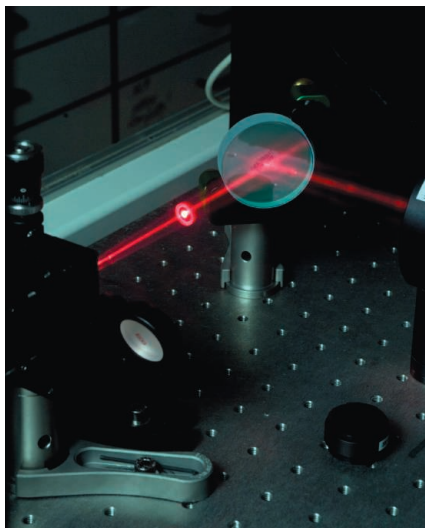

page 640

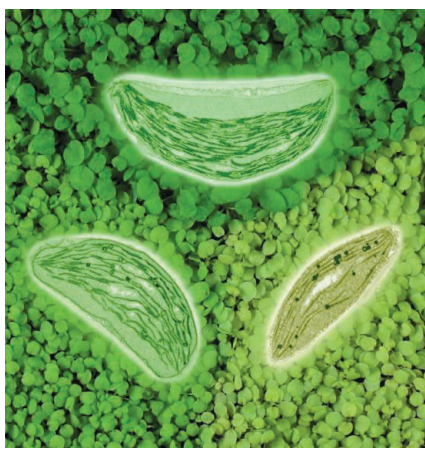

pages 622 & 655

ONLINE**HIGHLIGHTS**

*SCIENCE*EXPRESS

www.sciencexpress.org

Publication Ahead of Print

The Imprint of the Extragalactic Background Light in the Gamma-Ray Spectra of Blazars
M. Ackermann et al.
10.1126/science.1227160

Para-Aminosalicylic Acid Acts as an Alternative Substrate of Folate Metabolism in *Mycobacterium tuberculosis*
S. Chakraborty et al.
10.1126/science.1228980

Mice Lacking a *Myc* Enhancer That Includes Human SNP rs6983267 Are Resistant to Intestinal Tumors
I. K. Sur et al.
10.1126/science.1228606

Content-Specific Fronto-Parietal Synchronization During Visual Working Memory
R. F. Salazar et al.
10.1126/science.1224000

Influence of Threonine Metabolism on *S*-Adenosylmethionine and Histone Methylation
N. Shyh-Chang et al.
10.1126/science.1226603

TECHNICAL**COMMENTS**

Comment and Response on "Multiyear Prediction of Monthly Mean Atlantic Meridional Overturning Circulation at 26.5°N"
Comment: G. A. Vecchi et al.
http://dx.doi.org/10.1126/science.1222566
Response: D. Matei et al.
http://dx.doi.org/10.1126/science.1223200

*SCIENCE*NOW

www.sciencenow.org

Highlights From Our Daily News Coverage

Using Gut Bacteria to Fight Diarrhea
Mice show a treatment for chronic infection.
http://bit.ly/Gut_Bacteria

Dinosaurs Sprouted Wings Earlier Than Previously Thought
However, these wings were probably used for courtship or brooding rather than flight.
http://bit.ly/Dino_wings

Oceans Getting Too Hot to Handle?
Tropical marine organisms are shifting northward as temperatures rise.
http://bit.ly/Shifting_Plankton

*SCIENCE*SIGNALING

www.sciencesignaling.org

The Signal Transduction Knowledge Environment

30 October issue: http://scim.ag/ss103012

RESEARCH ARTICLE: Mice Lacking the ITIM-Containing Receptor G6b-B Exhibit Macrothrombocytopenia and Aberrant Platelet Function
A. Mazharian et al.

PODCAST
Y. A. Senis and A. M. VanHook
An inhibitory receptor ensures that megakaryocytes produce proper numbers of functional platelets.

MEETING REPORT: Stress Response and Child Health
E. Charmandari et al.
Endocrine and inflammatory responses to stress affect many aspects of development, physiology, and cognition.

PRESENTATION: Prenatal Stress, Telomere Biology, and Fetal Programming of Health and Disease Risk
S. Entringer et al.
Telomere biology may link intrauterine stress to newborn, child, and adult health and disease risk.

PRESENTATION: Protein Complexes and Target Genes Identification by in Vivo Biotinylation—The STAT5 Paradigm
E. Katsantoni
A transcription factor's interacting partners and target genes can reveal context-specific signaling and transcriptional outputs.

*SCIENCE*TRANSLATIONAL MEDICINE

www.sciencetranslationalmedicine.org

Integrating Medicine and Science

31 October issue: http://scim.ag/stm103112

RESEARCH ARTICLE: Food-Grade Bacteria Expressing Elafin Protect Against Inflammation and Restore Colon Homeostasis
J. P. Motta et al.
Gut bacteria engineered to make a protease inhibitor inhibit inflammation and heal colitis in mice.

RESEARCH ARTICLE: Immune Parameters Correlate with Protection Against Ebola Virus Infection in Rodents and Nonhuman Primates
G. Wong et al.
Antibody induction may serve as a surrogate for survival in protecting against Ebola infection.

RESEARCH ARTICLE: Window Reveals a Pre-Micrometastasis Stage During Liver Metastasis
L. Ritsma et al.

FOCUS: A Window into Metastasis
D. Brucker et al.
An abdominal window allows imaging of cancer metastasis in real time.

EDITORIAL: Emerging Economies, Enduring Partnerships
B. Onaral

PODCAST
B. Onaral and K. LaMarco
Mutually beneficial innovation alliances are built on belief in a joint mission and a shared vision.

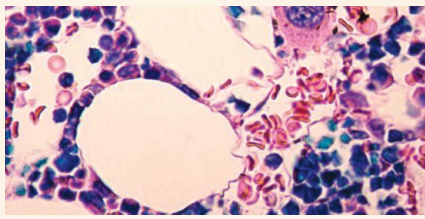

SCIENCE**SIGNALING**
Platelet-producing megakaryocytes.

REVIEW: Computational Medicine—Translating Models to Clinical Care
R. L. Winslow et al.
Modeling molecular networks, physiology, and anatomy could improve personalized medicine.

*SCIENCE*CAREERS

www.sciencecareers.org/career_magazine

Free Career Resources for Scientists

http://scim.ag/SciCareers2November2012

A Modest Workforce Proposal
M. Price
An NAS report forgoes skills-gap rhetoric and focuses on DOD's needs.

Taken for Granted: Ethics Across Borders
B. L. Benderly
Different approaches to responsible research conduct challenge scientists working internationally.

myIDP: Interests
B. Lindstaedt et al.
It sounds obvious, but when choosing a career path, you need to think hard about what you like to do.

*SCIENCE*PODCAST

www.sciencemag.org/multimedia/podcast

Free Weekly Show for 2 November 2012

Listen to stories on delaying quantum decisions, perpetuating poverty, growing global universities, and more.

SCIENCE (ISSN 0036-8075) is published weekly on Friday, except the last week in December, by the American Association for the Advancement of Science, 1200 New York Avenue, NW, Washington, DC 20005. Periodicals Mail postage (publication No. 484460) paid at Washington, DC, and additional mailing offices. The title SCIENCE is a registered trademark of the AAAS. Domestic individual membership and subscription (51 issues): $149 ($74 allocated to subscription). Domestic institutional subscription (51 issues): $990; Foreign postage extra: Mexico, Caribbean (surface mail) $55; other countries (air assist delivery) $85. First class, airmail, student, and emeritus rates on request. Canadian rates with GST available upon request, GST #1254 88122. Publications Mail Agreement Number 1069624. **Printed in the U.S.A.**

Change of address: Allow 4 weeks, giving old and new addresses and 8-digit account number. **Postmaster:** Send change of address to AAAS, P.O. Box 96178, Washington, DC 20090–6178. **Single-copy sales:** $10.00 current issue, $15.00 back issue prepaid includes surface postage; bulk rates on request.

AAAS
ADVANCING SCIENCE, SERVING SOCIETY

CREDIT: WBENSMITH/WIKIMEDIA COMMONS

EDITED BY CAROLINE ASH

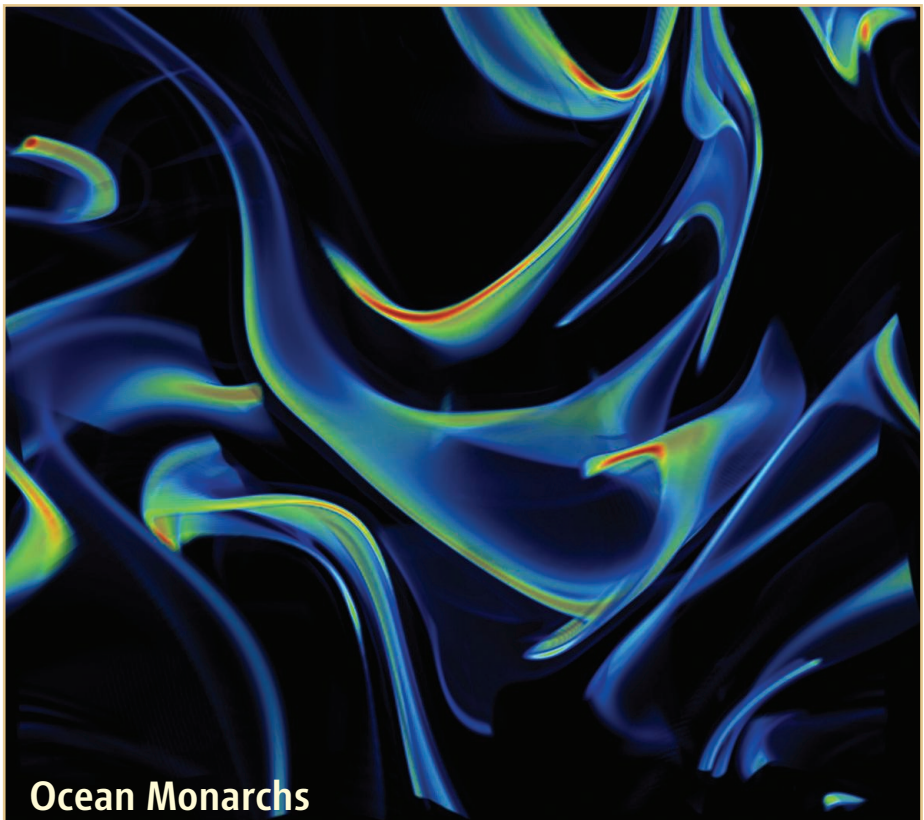

Ocean Monarchs

It is hard to grasp that the unseen microorganisms of the oceans are the most productive on the planet, at orders of magnitude greater than sharks and whales or even terrestrial forests. The plankton is thus a major contributor to the geochemical cycles that are currently under pressure from climate change. **Stocker** (p. 628) reviews the state of knowledge of the web of myriad ephemeral microenvironments within the ocean's bulk and how microorganisms respond to the ever-shifting chemical spectrum. To this end, **Taylor and Stocker** (p. 675) report experiments on the effects of turbulence on nutrient uptake by chemotactic marine bacteria. They propose that turbulence favors motile bacteria that adopt an optimal foraging strategy, which trades off the relative high cost of motility to gain the benefits of plumes of nutrients by zipping between them at optimized speeds. Scaled up, such apparently "micro" behavior will influence the rate of remineralization of dissolved organic matter and in turn will feed into global patterns of geochemical cycling.

Twist and Entangle

Entanglement is a key feature in quantum information science and plays an important role in various applications of quantum mechanics. **Fickler *et al.*** (p. 640) present a method for converting the polarization state of photons into information encoded into spatial modes of a single photon. From this, superposition states and entangled photons with very high orbital angular momentum quantum numbers were generated.

Push Me, Release, Pull You

In eukaryotic cells, nearly all long-distance transport of cargos is carried out by the microtubule-based motors kinesin and dynein. These opposite-polarity motors move cargos bidirectionally so that they reach their cellular destinations with spatial and temporal specificity. To understand transport by motor ensembles, **Derr *et al.*** (p. 662, published online 11 October; see the Persective by **Diehl**) used a DNA scaffold for building an artificial cargo that could be programmed to bind different numbers and types of molecular motors with defined geometry. A cargo with multiple copies of the same motor was transported with minimal interference, suggesting that similar-polarity motors can coordinate without the need for additional cellular factors. However, ensembles of opposite-polarity motors frequently engaged in a sort of "tug of war," which could only be resolved by releasing one motor from the microtubule track. Thus, within the cell, it is likely that regulation is required for bidirectional transport.

Dating the First Solids

The solar system's first solids: calcium-aluminum–rich inclusions and chondrules are found in meteorites and provide a direct record of the dynamics of the solar protoplanetary disk that led to the formation of the solar system. Previous results indicate that chondrules formed 1 to 2 million years after the inclusions—an age difference that has been used in constructing models of chondrule formation. Based on uranium- and lead-isotope measurements of a collection of these primitive materials, **Connelly *et al.*** (p. 651) show that chondrules in fact started to form at the same time as the inclusions, 4.567 billion years ago, and that their formation took about 3 million years.

PolII Goes Loopy

To execute their function, genes must be transcribed into RNA, often by RNA polymerase II (PolII), which binds at the 5′ end of genes and therefore transcribes through the coding region to make messenger RNA. But, presented with nucleosome-depleted chromatin, PolII will, wastefully, initiate transcription nonspecifically and bidirectionally away from the gene. Noting that actively transcribed genes often form loops, such that their 5′ and 3′ ends are juxtaposed. **Tan-Wong *et al.*** (p. 671, published online 27 September; see the Perspective by **Hampsey**) showed that PolII's propensity for promiscuous bidirectional transcription is reined in by gene loop formation.

Delaying Quantum Choice

Photons can display wavelike or particle-like behavior, depending on the experimental technique used to measure them. Understanding this duality lies at the heart of quantum mechanics. In two reports, **Peruzzo *et al.*** (p. 634) and **Kaiser *et al.*** (p. 637; see the Perspective on both papers by **Lloyd**) perform an entangled version of John Wheeler's delayed-choice gedanken experiment, in which the choice of detection can be changed after a photon passes through a double-slit to avoid the

CREDITS (TOP TO BOTTOM): JOHN R. TAYLOR AND ROMAN STOCKER; UNIVERSITY OF BRISTOL

Published by AAAS

measurement process affecting the state of the photon. The original proposal allowed the wave and particle nature of light to be interchanged after the light had entered the interferometer. By contrast in this study, entanglement allowed the wave and particle nature to be interchanged after the light was detected and revealed the quantum nature of the photon, for example, it displays wave- and particle-like behavior simultaneously.

Perovskite Photovoltaics

For many types of low-cost solar cells, including those using dye-sensitized titania, performance is limited by low open-circuit voltages. **Lee *et al.*** (p. 643, published online 4 October; see the Perspective by **Norris and Aydil**) have developed a solid-state cell in which structured films of titania or alumina nanoparticles are solution coated with a lead-halide perovskite layer that acts as the absorber and n-type photoactive layer. These particles are coated with a spirobifluorene organic-hole conductor in a solar cell with transparent oxide and metal contacts. For the alumina particles, power conversion efficiencies of up to 10.9% were obtained.

Chloroplast Rescued by Ubiquitin

The ubiquitin proteasome system is important in the regulation of many nucleocytosolic processes. However, its regulatory reach was not thought to extend to the chloroplast. Using a forward-genetic screen in *Arabidopsis,* **Ling *et al.*** (p. 655; see the Perspective by **Kessler**) identified a ubiquitin E3 ligase, termed SP1, embedded in the chloroplast outer envelope membrane. SP1 was found to target components of the chloroplast protein import machinery for degradation by the ubiquitin proteasome and was important for changes in chloroplast biogenesis.

Necrophilic Bandit Fungi

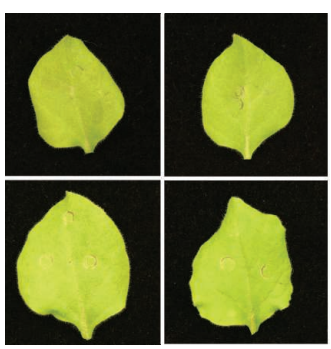

The immune systems that plants use to defend against pathogens normally deflect attack. However, **Lorang *et al.*** (p. 659, published online 18 October) have identified a rearguard susceptibility that a necrotrophic fungus exploits. The fungal toxin victorin interacts with the defense protein LOV1 in *Arabidopsis* and activates it, but the result, counterintuitively, is that the plant succumbs to the disease rather than fighting it off. What seems to be happening is that victorin targets a thioredoxin that regulates the systemic acquired resistance pathway. That interaction triggers activity of LOV1, which in turn incites cell death. The invading fungus then benefits from the ready access to dead cells.

Epigenetic Inheritance

A long-standing question is whether and how stem cells maintain their epigenetic information. Knowing that many types of stem cells undergo asymmetric cell divisions, **Tran *et al.*** (p. 679) probed the asymmetric division of *Drosophila* male germline stem cells and found that preexisting histones were selectively segregated to the stem cell, whereas new histones were enriched in the daughter cell that underwent differentiation. By contrast, asymmetric histone distribution was not seen in progenitor cells. This study suggests that stem cells retain preexisting canonical histones during asymmetric cell divisions in vivo.

Poor Choices

Two categories of reasons for why poor people make economically unsound choices, such as obtaining a payday loan at an extraordinarily high rate of interest, reflect, first, the environment: Poor people are more likely to be living in poor neighborhoods with higher rates of crime and lower rates of social services. Second, they reflect the individual: People are poor in part because of their own psychological dispositions toward impatience and impulsiveness. For both cases, obtaining causal evidence in controlled experiments has been challenging. **Shah *et al.*** (p. 682; see the Perpective by **Zwane**) propose a third category of reasons whereby being poor exerts a bias on cognitive processes and provide evidence for it in laboratory experiments performed in scenarios of scarcity.

CREDIT: LORANG *ET AL.*

Mary-Claire King is president of the American Society of Human Genetics and a professor in the Department of Genome Sciences and the Department of Medicine at the University of Washington, Seattle, WA. E-mail: mcking@uw.edu.

The Scientist as World Citizen

IN EARLY 2011, LISTENING ON U.S. PUBLIC RADIO TO REPORTS FROM TAHRIR SQUARE, I LOOKED forward particularly to those from Mona Seif, a young citizen journalist from Cairo. Her reports were rich in detail, and even when difficult to hear over gunfire, they were clear and informative to a listener on the other side of the world.

In a profile a few months later, Seif was asked about her work when not in Tahrir Square. She was a graduate student, she responded, working in cancer biology. "My work in particular is on the *BRCA1* gene," she said, "which is one of the genes connected with breast cancer incidence, and I'm investigating the mutation pattern in Egyptian patients. . . . Both [science and activism] are very consuming, time and energy—and emotions. And I'm only starting to get the handle of doing both at the same time and juggling between my activism and my work."* Hearing this interview on a quiet evening in my lab, I had three thoughts: "Fantastic!" and, "You must be getting way behind on DNA sequencing," and, "At least we can help you with that."

Mona Seif's story illustrates for me the essence of the scientist as a citizen of the world. Scientists insist on believable data both in work and in public life. Bright young scientists do not accept nonsense from those in power, and they will not be eternally patient with those responsible for it. The response of the scientist to nonsense is both conceptual and practical: to recognize it, expose it, and try to fix it. And because scientists are connected through worldwide networks, we can stimulate each other to do the same. This power was demonstrated by young computer-savvy scientists in Beijing when they informed the world about the Tiananmen Square protests in June 1989, and more recently by youthful bloggers of the Arab Spring such as Mona Seif.

This week, the American Society of Human Genetics holds its annual meeting in San Francisco. As human geneticists, we are particularly privileged world citizens. Our field is inherently global in both content and talent. All people share the same biology. A gene responsible for a human trait in any family, anywhere, is part of the biology underlying that trait in everyone, everywhere. The discovery and characterization of genes responsible for serious human conditions are therefore best undertaken by studying the families most informative about those conditions, wherever they live. The scientists best qualified to work with such families, understanding cultural context, historical demography, and environment/gene interactions, are those from the same places as the families they are studying. The extraordinary success of contemporary human genetics is due both to the revolution in genomic technology and to advanced training of scientists from across the globe. Collaborations formed using the very best talent for each project lead to both productive science and an understanding of people and places outside of one's home turf. The job of the citizen scientist is to put this understanding to use.

One rarely knows in advance when opportunities will arise. Solving complex problems, whether scientific, social, or political, requires honest and critical appraisal of data. Truth ultimately matters more than consolidating power, securing funding, or furthering agendas. In my experience, the most important questions come from people on the front lines, and no question is too big to ask.

– Mary-Claire King

10.1126/science.1231607

*www.onthemedia.org/2011/apr/15/state-run-newspapers-and-mona-seif/transcript/.

Published by AAAS

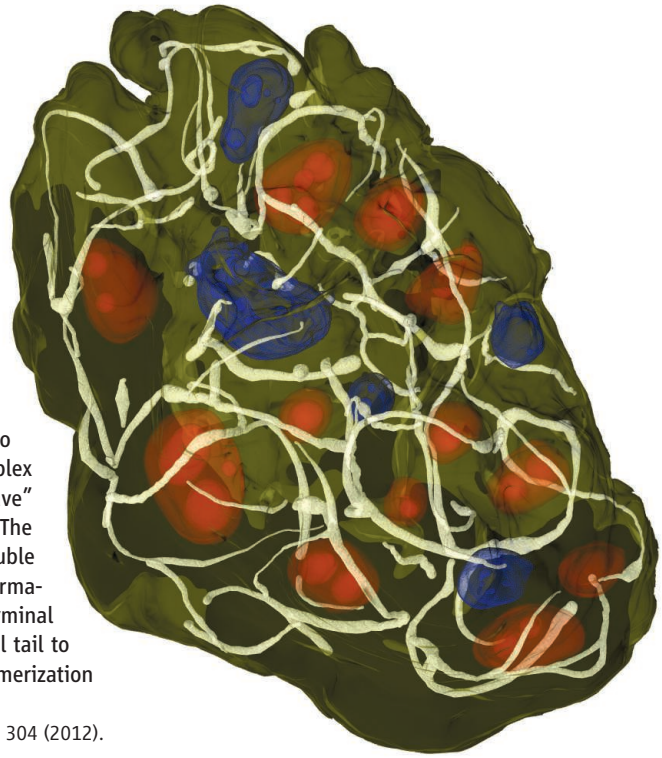

CELL BIOLOGY

Spinning a E4dly Weave

Adenovirus is a small DNA tumor virus. It expresses a number of "early" proteins during infection that take over the host cell for virus production by subverting cellular pathways. These early proteins are often quite small: E4-ORF3 is a mere 13 kD and yet can disrupt large protein complexes, interfere with tumor suppressors in a number of critical cellular pathways, and forms long cablelike structures in the host cell. Using super-resolution and electron microscopy, Ou *et al.* show that these cablelike assemblies appear to form a single continuous polymer with variable curvature and loops. This complex architecture requires nothing more than the E4 protein itself. The intricate "weave" of the polymer partitions the host cell nucleus into viral replication domains. The structure of a mutant form of the protein that forms dimers, rather than insoluble polymers, together with mutagenesis studies, suggest a model for polymer formation in which dimers can reciprocally or nonreciprocally domain-swap their C-terminal tails with other dimers. Glycine residues form a hinge allowing the C-terminal tail to adopt many different conformations that produce polymer branch points. Polymerization is required for E4 to target cellular tumor suppressors. — GR

Cell **151**, 304 (2012).

PLANT SCIENCE

Biofuel Self-Engineering

Biofuels could be a useful substitute for fossil fuels, but various aspects of the production process need improvement to increase yield and reduce costs. One approach would be to express processing enzymes in the growing plant itself. However, to avoid damage to the growing plant, the enzymes need to be held at bay until the time comes to convert cell walls into soluble sugars. Shen *et al.* have tackled this challenge in maize, for which xylanase can be used to break down cell walls into fermentable carbohydrates. Expression of xylanase in the plant alleviates problems of enzyme production and access to substrates, but at the same time produces problems in damaging plant growth, for example, yielding shriveled seeds. The xylanase was brought under control by adding an intein, a self-splicing peptide from the bacterium *Thermus thermophilus*. Use of a thermostable xylanase meant that treatment of the plant material containing the hybrid protein with temperatures in the range of 60° to 70°C resulted in removal of the inhibitory peptide and the generation of functional xylanase. With an optimized version of the hybrid xylanase-intein, transgenic plants showed normal development and normal seed set, and improved biomass conversion to glucose and xylose. — PJH

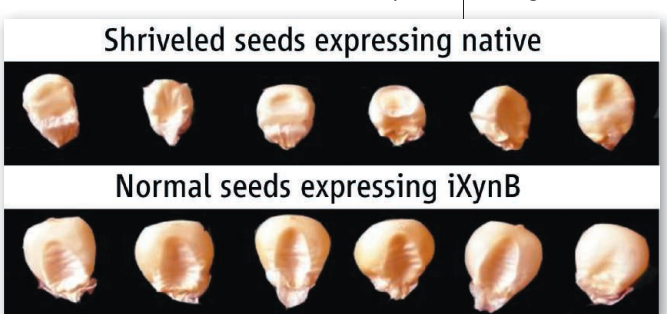

Nat. Biotechnol. **30**, 10.1038/nbt.2402 (2012).

EVOLUTION

Origins of Variation

It is not clear whether the majority of selection on human genetic variation originates from de novo mutations (SDN) or from selection on previously neutral, or nearly neutral, standing genetic variation (SSV). Peter *et al.* examined theoretical models to determine parameters that distinguish between SDN and SSV. Identifying the origin of the genetic variant was dependent on the strength of selection and the frequency of the variant under selection. Examining genes previously identified to be under selection, but not yet fixed within humans, revealed that both models were applicable; save for the gene that encodes glucose-6-phosphate dehydrogenase, which appears to be under balancing selection and, because of the lack of a selective sweep, did not fit either model. Furthermore, when regions currently not under selection were examined, it was not possible to discriminate between selected and neutral variants. These results support the notion that the origin of human genetic variation that is subject to selection is complex and that an understanding of both standing variation and the de novo mutation rate is important to trace our evolution. — LMZ

PLoS Genet. **8**, 10.1371/journal.pgen.1003011 (2012).

VIROLOGY

Viruses Gone Haywire

One of the hallmarks of human immunodeficiency virus (HIV) infection in people or pathogenic simian immunodeficiency virus (SIV) infection in nonhuman primates is intestinal pathology. Such enteropathy causes breakdown of the intestinal barrier and is thought to result in the leakage of microbial constituents into wider circulation that then drive immune activation and worsening of disease. Whether enteropathy is a direct effect of HIV or SIV infection, however, has not been established. Handley *et al.* used next-generation sequencing, viral culture, and polymerase chain reaction testing to show that pathogenic SIV infection in two independent cohorts of rhesus macaques was associated with an expansion of the intestinal virome (gut-associated viral genomes). Such an expansion was not seen in nonpathogenically SIV-infected African green monkeys. The expanded virome included several previously undescribed viruses as well as adenoviruses. Adenovirus-associated enteritis was observed in some pathogenic SIV-infected animals. Furthermore, parvovirus viremia was associated with advanced AIDS. These findings suggest that an expanded range of viruses within the infected individual rather than SIV/HIV infection itself may cause SIV/HIV-associated enteropathy. — KLM

Cell **151**, 253 (2012).

PHYSICS

Splitting Pairs

Entanglement is a property of quantum systems whereby correlations exist between the entangled particles, so that measuring the state of one particle instantaneously reveals that of the other. Such quantum-mechanical correlations are a powerful resource for applications in quantum information processing and secure communication. Although much work has focused on the generation and manipulation of entangled photons, the condensed-matter version in the form of superconducting Cooper pairs of electrons offers the potential of fabricating entangled electronic circuits. However, extracting and then splitting the Cooper pairs has been experimentally challenging, with competing processes giving rise to impractically low efficiencies. Schindele *et al.* developed a carbon nanotube–based device that can be used to extract the Cooper pairs from a superconductor and then split and store them on two separate quantum dots defined within the nanotube. The experiments revealed splitting efficiencies up to 90%, sufficient for practical applications in quantum electronic circuits. — ISO

Phys. Rev. Lett. **109**, 157002 (2012).

CHEMISTRY

Cavity Complexities

High-energy irradiation of water can transiently liberate reactive electrons, which are implicated in pathways that chemically damage biomolecules. Such hydrated electrons have been spectroscopically detected, and decades of associated modeling suggested that the charge resides in a cavity, with surrounding water molecules displaced. Recently, however, a theoretical study challenged this model and instead supported a region of increased water density in the vicinity of the charge. Yet, more studies, performed in response, claimed reaffirmation of the traditional structure. In each of these cases, the simulations involved parameterized pseudopotentials. Seeking to resolve the impasse, Uhlig *et al.* carried out a series of ab initio calculations that treated the electron as well as a subset of surrounding water molecules quantum-mechanically; a molecular mechanics approach was applied to model long-range effects. The result did suggest that ~40% of the spin density resides in a cavity, but also partitioned the remaining fraction among neighboring water molecules and a diffuse tail between them. Thus, the cavity description alone appears to oversimplify a complex geometry. — JSY

J. Phys. Chem. Lett. **3**, 3071 (2012).

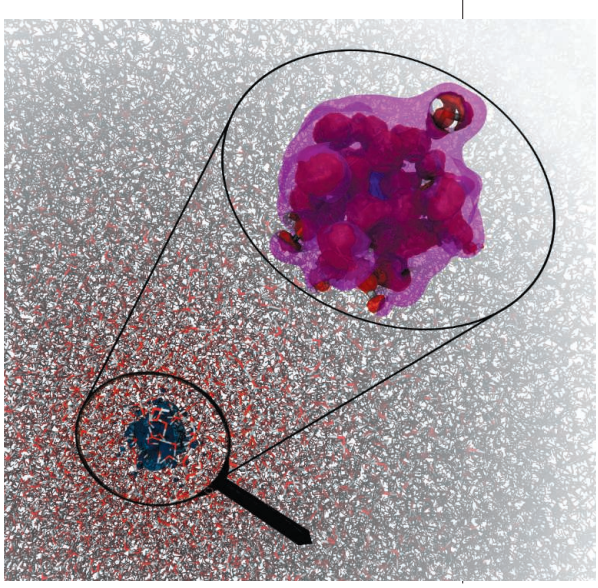

CREDIT: F. UHLIG *ET AL., J. PHYS. CHEM. LETT.* **3**, 3071 (5 OCTOBER 2012) © 2012 AMERICAN CHEMICAL SOCIETY

EDUCATION

Gauging Competitiveness

Supported by data showing that U.S. students perform substantially below their international peers, politicians justify their education policies by linking them to the need to be competitive in a global economy. How does this type of policy motivation influence voters' attitudes toward supporting public schooling? Using a survey designed to randomize exposure to international competitiveness across respondents, Morgan and Poppe tested 1000 U.S. adults for differential responses to the perceived quality of local public schools and the preferred expenditures for the nation's education system. A randomly selected treatment group was asked two questions on international competitiveness before taking the survey. This group reported lower assessments of their local schooling, coupled with decreased support for increasing the national budget for education, suggesting that although the public may be concerned about the quality of their schools, these concerns do not translate into support for additional education spending. Framing education policy as essential to the United States being competitive in the global economy may thus be counterproductive if politicians are also looking to increase education spending. — MM

Educ. Researcher **41**, 262 (2012).

AROUND THE WORLD

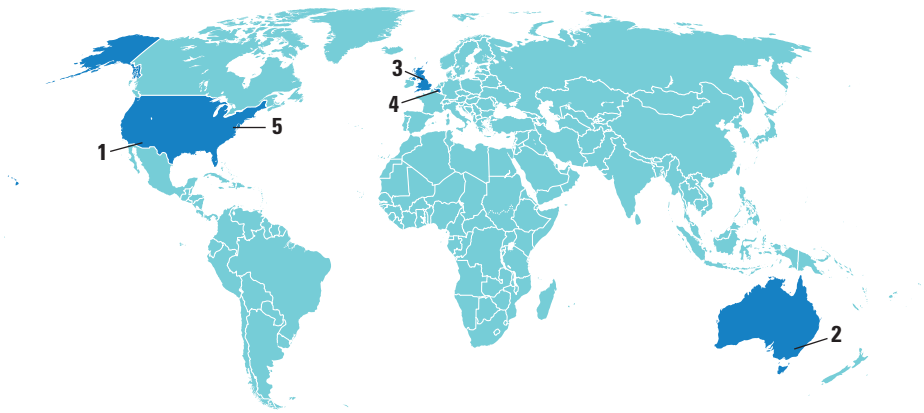

Tucson, Arizona **1**

Smooth Mirror for Giant Telescope

Twenty tons of glass—that's what went into casting the first of seven mirrors that comprise the light-collecting area of the 25-meter Giant Magellan Telescope (GMT). The 8.4-meter-diameter, single-piece mirror was finished last week. The GMT will peer at the heavens from a remote Chilean mountaintop when it is ready for operations by the end of this decade.

The mirror was cast using a technique pioneered by University of Arizona astronomer Roger Angel. It has been polished to such a high degree of precision that any surface aberrations lie within a margin one-twentieth the wavelength of light. Six other such mirrors will be fashioned over the next few years. Assembled into a floral design, they will collect enough light to produce images of unprecedented sharpness, helping researchers answer fundamental questions in astrophysics, planetary science, and cosmology.

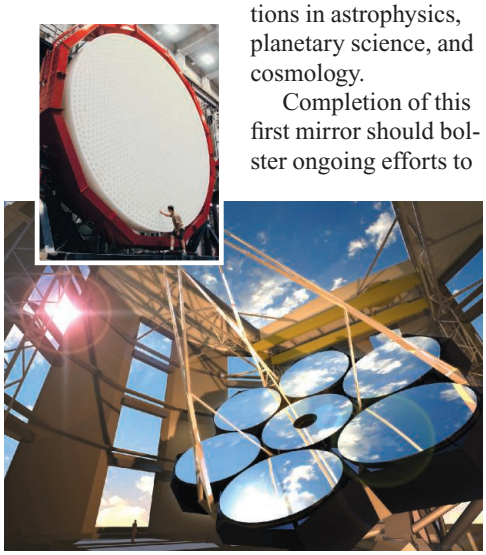

Completion of this first mirror should bolster ongoing efforts to raise funds for the $1 billion project, which has so far received commitments of about $300 million from its various partners.

Canberra **2**

Relief, Pain in Australia's Science Budget

The limbo is over for Australian researchers as grants are flowing once again. Over the past several tense weeks, the federal government froze all science grants while seeking to balance the nation's budget. But the midyear budget released on 22 October had welcome relief: AUS $1.686 billion for the Australian Research Council, the National Health and Medical Research Council, and the Cooperative Research Centres.

But the government is also reneging on a pledge to increase allotments for indirect costs, trimming AUS $499 million from the original Sustainable Research Excellence grants budget of the Department of Innovation, Industry, Science and Research. The move will effectively cap overhead funding rates at 30% over the next 4 years, instead of raising those rates from 20% to 50% by 2014 as originally promised.

University officials say they were counting on that money. "We can expect to struggle to provide our researchers with the level of support they require, and we will start losing them," says James McCluskey, deputy vice-chancellor of research at the University of Melbourne. **http://scim.ag/AusBudget**

United Kingdom **3**

Britain Fights Ash Dieback

The U.K. government banned the import of ash trees Monday in the face of a spreading fungal disease threatening Britain's iconic ash woodlands. The fungus *Chalara*

fraxinea causes ash dieback disease, which has devastated ash trees in Denmark and is spreading through central Europe. The fungus was detected in a Buckinghamshire nursery shipment from the Netherlands in February. In the following months, cases were identified in several other locations that had received recent tree imports. In late October, the U.K. Food and Environment Research Agency confirmed the disease in 10 woodland sites in East Anglia that had no known connection to nursery stock. The U.K. Forestry Commission calls the fungus "potentially a very serious threat" to Britain's ash trees, which make up about 5% of the country's woodlands. *C. fraxinea* was first identified in Poland in 1992, but researchers aren't sure where it originated.

Brussels **4**

European Researchers Protest Looming Cuts

A petition asking European heads of state to spare research funding when they wield their budget axes was closing in on 100,000 signatures as *Science* went to press this week. The petition was sparked by an open letter, published in leading European newspapers, from 42 Nobel laureates and five Field medalists arguing that in the face of tightening budgets across Europe, research funding should not be cut.

European heads of state will meet on 22 and 23 November to decide on the E.U.

NOTED

>ScienceDebate, a coalition of science groups (including AAAS, the publisher of *Science*), received answers from nine lawmakers on science and science policy questions that it sent to 33 Republican and Democratic leaders of congressional committees that shape U.S. science policy. Answers touched on energy, climate change policy, the role of scientific research in fueling technological innovation and economic growth, and the importance of funding research even in tough fiscal times. http://scim.ag/SciDebAnsw

Published by AAAS

budget from 2014 until 2020, and the continent's economic crisis has triggered calls to freeze the overall budget at current levels. That would seriously jeopardize plans to spend €80 billion on Horizon 2020, an E.U. research program that will be part of the new budget. Cuts to Horizon 2020 would "risk losing a generation of talented scientists just when Europe needs them most," the letter states.

The petition, coordinated by the Initiative for Science in Europe and the Young Academy of Europe, collected 40,000 signatures on its first day on 23 October; by 29 October, it had close to 90,000 signatures from more than 50 countries around the world.

Washington, D.C. **5**

Foreign Talent Hires for DOD?

In order to keep a high-quality technical workforce, the U.S. Department of Defense (DOD) should consider revising security rules that now exclude hiring foreign-born scientists and engineers—and think about starting "unconventional" research projects that might attract the best and the brightest, according to a new study on the Pentagon's future workforce needs. The good news is that DOD is not facing an immediate crisis in finding technical employees to replace an aging workforce, says C. Daniel Mote Jr., the former University of Maryland, College Park, president who co-chaired the study for the U.S. National Academies' National Research Council and the National Academy of Engineering. "But it's clear that DOD needs to be more assertive and prepared to compete" with industry, academia, and other nations for the best workers, he says. Jump-starting exciting, innovative projects may be one way to attract recruits. Another is for DOD to "reexamine" the need for the strictest security clearances for some positions. But implementing such changes could be difficult, because it would require rewriting a host of laws and policies.

http://scim.ag/DODrep

NEWSMAKERS

X-ray Scientist Leads SLAC

Chi-Chang Kao, an x-ray physicist at SLAC National Accelerator Laboratory in Menlo Park, California, is the new director of the lab, which is managed by Stanford University and owned by the Department of Energy (DOE).

SLAC was once a dedicated particle physics lab. But in 2008, SLAC researchers turned off their last particle smasher. In 2009, they turned on the world's first x-ray laser, the Linac Coherent Light Source, which serves experiments in materials science, chemistry, structural biology, and other fields. Kao, 54, hopes to expand the lab's portfolio into basic research in energy storage, solar technology, and catalysis. "We have a very aggressive growth agenda that needs the budget [from DOE] to support it," he says.


Kao

Kao is a top-flight researcher, says Peter Siddons of Brookhaven National Laboratory in Upton, New York, where Kao worked from 1988 until 2010: "It was clear from the get-go that he was leadership material." **http://scim.ag/_Kao**

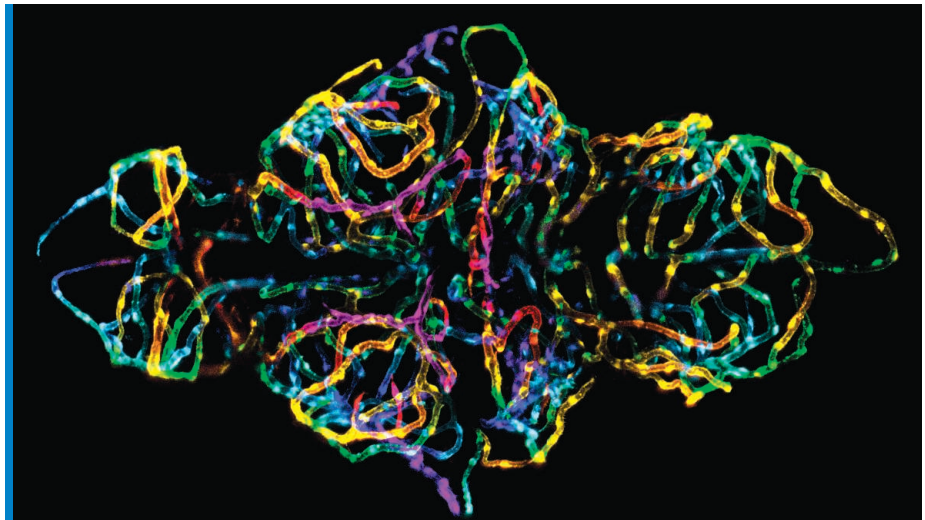

Beauty in the Blood-Brain Barrier

More than just a pretty picture, this image may be the first of the blood-brain barrier in a live animal. It took top honors last week in the 2012 Nikon Small World Photomicrography Competition. Microscopy specialist Jennifer Peters and chemical biologist Michael Taylor from St. Jude Children's Research Hospital in Memphis, Tennessee, compiled the picture from 41 images taken with a confocal microscope of a zebrafish embryo 6 days after fertilization. They wanted to study the barrier's development and, eventually, generate ways to screen for drugs that modify the structure. To observe the barrier in real time, the researchers gave the zebrafish a gene for a protein that glows red in the barrier's endothelial cells. Later, they color-coded the blood vessels in the image, with blue representing the ones deepest in the brain, then green, yellow, red, and finally pink for vessels closest to the brain's surface. Unfortunately, beauty only goes so far. "The manuscript hasn't gotten past the editors of top journals," Taylor laments, even one that put this picture on its cover.

Ireland Scraps Office Of Science Adviser

Mark Ferguson, who heads the Science Foundation Ireland (SFI), a research funding agency, is now also Ireland's chief scientific adviser. He takes over for animal geneticist Patrick Cunningham, who finished his 5-year term at the end of August. On 26 October, the government announced that Cunningham's office, created in 2004, will be abolished as part of a "wider drive for reform and greater efficiency within the Department of Jobs, Enterprise and Innovation." The move has drawn criticism from researchers.

"We now have one civil servant doing this as a part-time job, on top of his already significant workload," says Stephen Sullivan, chief scientific Officer of the Irish Stem Cell Foundation. Sullivan also sees a "huge conflict of interest," because the director of SFI, funded by taxpayers, "is also the man now advising the government on how taxpayers' money should be spent."

CREDITS (TOP TO BOTTOM): (PHOTOMICROGRAPHERS) JENNIFER L. PETERS AND MICHAEL R. TAYLOR/ST. JUDE CHILDREN'S RESEARCH HOSPITAL, COURTESY OF NIKON SMALL WORLD; SLAC

Published by AAAS

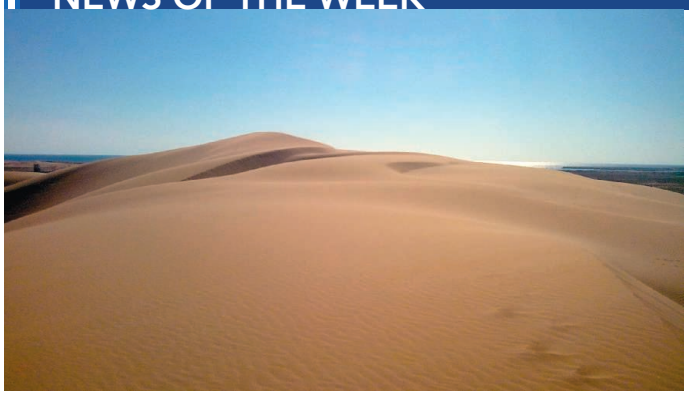

FINDINGS

Sand Grains Make Dunes Sing

When whipped by desert winds, sand dunes signal their displeasure with haunting moans that reverberate across the arid landscape. Some emit single notes while others mimic a jumbled chorus, but what causes different dunes to sing different songs has been a mystery—until now. Scientists at Université Paris Diderot collected sand from a singing dune in Morocco that moans at around 105 hertz (Hz)—or, to a musician, G-sharp two octaves below middle C. They compared those grains to sand collected from a dune in Oman, which produces notes ranging from 90 Hz to 150 Hz (F-sharp to D). As they reported in a paper published online last week in *Geophysical Research Letters,* the scientists reproduced these desert songs by sliding sand down inclines in the lab, indicating that the synchronized movement of sand grains produces the famed moaning. When they sieved the Omani sand so the grains were similarly sized, the resulting "avalanche" produced a single-note song. Grain size, they conclude, determines the notes contained in a dune's song. **http://scim.ag/singsand**

Random Sample

Repellent Marketing

When it comes to the truth, Bart Knols is prepared to suffer for it. In July, Knols, a malaria specialist with the Dutch Malaria Foundation, heard that the São Paulo, Brazil-based advertising agency Talent had won a Grand Prix at the prestigious Cannes Lions International Festival of Creativity for an unlikely stunt. To promote the adventure magazine *Go Outside*, the agency had persuaded a radio station to add a 15 kHz signal to its normal music broadcast to Campos, Brazil, and São Paulo between 6 p.m. and 8 p.m. for 3 weeks. The agency claimed the signal deterred mosquitoes, allowing listeners to "go outside" without fear of being bitten.

The scientific consensus, however, is clear that such "repellents" do not work. The advertisements endanger people by "giving them a false sense of security," Knols says. To prove the point, he made a video of himself holding an iPhone emitting the 15 kHz signal in a cage full of hungry female mosquitoes. Within minutes, his hand was covered with feasting insects. But festival organizers were unswayed when Knols asked them to withdraw Talent's prize. Neither the agency nor the festival responded to e-mails from *Science* seeking a comment.

Dozens of apps in the Apple and Google online stores claim to repel mosquitoes with similar high-frequency sounds, Knols says. The prize "is fueling the industry of these bogus products," he charges. "It's fraud, it's criminal, and it's unethical." He hopes that the app stores will be more responsive to his arguments than the advertisers have been.

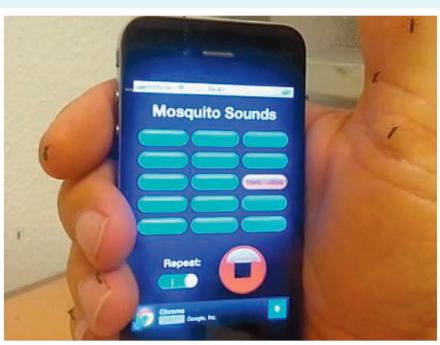

Cool as a Ball of Dung

If you've ever run barefoot across a sizzling beach in summertime, imagine what the dung beetle endures as it works the African savanna, where midday surface temperatures can exceed 60°C. The beetles, however, have an ingenious trick for keeping cool, according to a study published on 23 October in *Current Biology*. They take periodic breaks from rolling their balls of dung and climb atop their cargo, which stays up to 30° cooler than the ground because of evaporating moisture.

The researchers, from Sweden and South Africa, noticed that the beetles clambered onto their dung balls more frequently as the surface temperature rose.

Using infrared thermography, they found that the temperature of the beetles' front legs decreased up to 10°C during these interludes. When they dipped the beetles' front legs in silicone to form tiny insulating boots, the beetles could better tolerate the hot sand and climbed on the dung balls less often. A dung ball provides a "mobile thermal refuge," the researchers conclude, by providing elevation above the ground and absorbing heat directly from a beetle's legs when it climbs atop, and by cooling the the sand in front of the beetle as it pushes the ball along.

CREDITS (TOP TO BOTTOM): SIMON DAGOIS-BOHY; UNIVERSITÉ PARIS DIDEROT; J. SMOLKA *ET AL.*, *CURRENT BIOLOGY* **22**, 20 (23 OCTOBER 2012); BART KNOLS (2)

Published by AAAS

Aftermath. CGR President Luciano Maiani (*left*) offered his resignation last week, while a phone conversation between Guido Bertolaso (*center*) and Enzo Boschi (*right*) shed new light on the commission's relation to Bertolaso.

SCIENCE AND THE LAW

Convictions Leave Italy's Civil Protection in Chaos

ROME—Italy's government was left without experts to advise it on natural hazards following the conviction last week of six scientists and a government official for advice they gave ahead of the deadly earthquake in L'Aquila in 2009. The president and several members of the National Commission for the Forecast and Prevention of Major Risks (CGR) have resigned in response to the convictions, while others have threatened to resign. As *Science* went to press this week, the commission remained out of action, its future unclear.

The seven convicted men took part in a CGR meeting on 31 March 2009, 6 days before the magnitude-6.3 earthquake, which killed more than 300 people. Last week, each of the seven were sentenced to 6 years in prison by a judge after having been accused of falsely reassuring L'Aquila's citizens as a result of discussions they held during the meeting (*Science*, 26 October, p. 451). CGR is a consultative body to Italy's Civil Protection Department (DPC); in a note to the press last week, DPC warned that the conviction could lead to "paralysis" of risk forecasting and prevention in Italy.

In an e-mail written on 23 October, the day after the conviction, CGR president, particle physicist Luciano Maiani, told his fellow commission members that he was sending his resignation letter to Prime Minister Mario Monti because he believed CGR could not work "serenely and effectively." The jail terms had highlighted the "fragility" of the commission, Maiani wrote. He also expressed his "most complete solidarity" with the convicted seven.

The commission's president emeritus and vice president also resigned, and about two-thirds of the 60-strong membership have at least announced their intention to do so. In a 26 October Cabinet meeting, however, the Italian government rejected the resignations, leaving the commission's future uncertain for the moment.

CGR members argue that their role as scientific advisers isn't clearly distinguished from that of the decision-makers. The way the CGR works was overhauled last year to avoid the confusion that took place in its now-infamous meeting ahead of the L'Aquila quake, which civil protection officials, local administrators, and others also attended, and which did not result in a summary at the meeting's close. Today, deliberations take place behind closed doors and result in official documents that are sent to DPC. But, says resigning commission member Aldo Zollo of the University of Naples Federico II, the regulations do not explicitly free the scientists of all responsibility for decisions made on the basis of their advice, which may stifle their ability to speak their minds.

A pair of earthquakes earlier this year in the north of Italy provides a case in point, Zollo says. CGR's advice regarding the possibility of a third quake led DPC to take emergency measures; when the quake didn't materialize, the mayor of a town called Finale Emilia threatened to sue the commission because the measures hampered local business.

Not all commission members agree with the resignations, however. Francesco Mulargia, a geophysicist at the University of Bologna, says the judge's decision must be respected: "[I]n a civilized country, justice is administered in courts and not in talk shows, in newspapers, in streets or by 'resigning in protest,' " Mulargia wrote in an e-mail. He maintains that the resigning scientists mistakenly believe science itself to be on trial, whereas, he says, the defendants were actually charged with not correctly conveying that science.

But Mulargia agrees that in the wake of the verdict, new regulations are needed, arguing that "CGR cannot have any responsibility if not the scientific one." Stefano Gresta, president of the National Institute of Geophysics and Volcanology (INGV), says that new rules might be forthcoming as early as this week, either in the form of DPC regulations or new laws. He points out that Maiani and the other heads of CGR were due to meet on 30 October to clarify the commission's role in civil protection.

That a solution is needed was driven home by a magnitude-5 earthquake that struck near the border between the Calabria and Basilicata regions in southern Italy just 3 days after Maiani resigned. The quake was the latest tremor in a more than 2-year-long seismic "swarm," and it represented a significant jump in magnitude—a situation fairly similar to that in L'Aquila a week before the fatal quake. But DPC head Franco Gabrielli could not draw on the expertise of CGR to assess the risks of more significant tremors last week. Fortunately, the commission had analyzed the swarm earlier in the month. "This earthquake is well characterized by that analysis," Gresta says.

In a separate development, the newspaper *La Repubblica* published another recorded phone conversation last week suggesting that scientists serving on CGR were under pressure to bring their public statements in line with the wishes of Guido Bertolaso, then-head of the DPC. (Bertolaso's phone was tapped at the time by prosecutors investigating his possible involvement in corrupt government contracting.) In the call, recorded 3 days after the L'Aquila quake, Bertolaso discusses a CGR meeting scheduled for that day with commission member and then-INGV Director Enzo Boschi. "Today's meeting is aimed at this, so the truth is not to be said," Bertolaso said. At the end of the brief conversation, during which the meeting's aim and "the truth" were not revealed, Boschi reas-

Published by AAAS

sures Bertolaso that "ours is a very cooperative attitude. We will do a press release which we will first submit to your attention." In January of this year, *La Repubblica* published the recording of another call in which Bertolaso, talking with a regional official ahead of the 31 March 2009 meeting, says that that meeting was to be "more of a media operation" in which "we want to reassure the public."

Meanwhile, the flood of protests from outside Italy has continued. Michael Halpern of the Union of Concerned Scientists wrote in a blog post last week that the conviction "for failing to accurately predict an earthquake" is "an absurd and dangerous decision," while a *Nature* editorial said: "The verdict is perverse and the sentence ludicrous." But a statement by the American Geophysical Union (AGU) was more reserved, calling the prison sentences "troubling" and pointing out that they "could ultimately be harmful" to combating the threat of natural disasters. Although AGU had called the charges against the seven "unfounded" in 2010, it now merely said that "the facts of the L'Aquila case are complex."

–EDWIN CARTLIDGE

Edwin Cartlidge is a science writer in Rome.

STEM CELLS

Immune Reactions Help Reprogram Cells

When under threat, it pays to be flexible. That principle may help explain why scientists have been able to use viruses to reprogram differentiated cells into stem cells, an advance that was recognized as part of this year's Nobel Prize in physiology or medicine. In the 26 October issue of *Cell*, a U.S. research team reports that a cell's defensive reaction to viruses seems to make it more open to expressing genes that are usually shut down—whether they be those that trigger inflammation or those that are active in stem cells. The find could help scientists better understand how cellular reprogramming works, and may also help them develop more efficient and safer ways to reprogram cells.

Exactly what happens inside cells during reprogramming remains a mystery. The technique as first described in 2006 by Shinya Yamanaka of Kyoto University in Japan, who shared this year's Nobel Prize, involves giving a cell extra copies of four key genes by infecting it with a retrovirus that inserts the genes into the host cell's genome. In a poorly understood process, the proteins encoded by those genes set off a cascade of signals that turns mature cells into pluripotent cells, which can become any of the body's tissue types. These so-called induced pluripotent stem (iPS) cells have allowed scientists to derive cell lines that are a genetic match with patients, enabling them to study diseases in new ways. They may also someday provide genetically matched tissue for regenerative medicine.

The first techniques used to reprogram cells had a major drawback, however. The virus-inserted genes remained in the iPS cells, raising the possibility that they might cause tumors. Although scientists have found several ways to ferry reprogramming genes into cells without permanently altering the genome, they are still looking for new methods. One especially attractive alternative is protein-only reprogramming, which would avoid the use of foreign genes altogether. By directly inserting the proteins that the reprogramming genes code for, scientists can set off the same signaling cascade, but the process is very inefficient.

John Cooke, a cardiologist at Stanford University School of Medicine in Palo Alto, California, and his colleagues wanted to understand why the proteins worked so poorly. They carefully examined what happened when they treated cells with a single reprogramming factor, either via a gene in a retrovirus or with specially designed versions of the reprogramming proteins that can traverse cell membranes. The cells that received the retrovirus began to express the inserted gene and its downstream counterparts within hours. The proteins took days to have any effect.

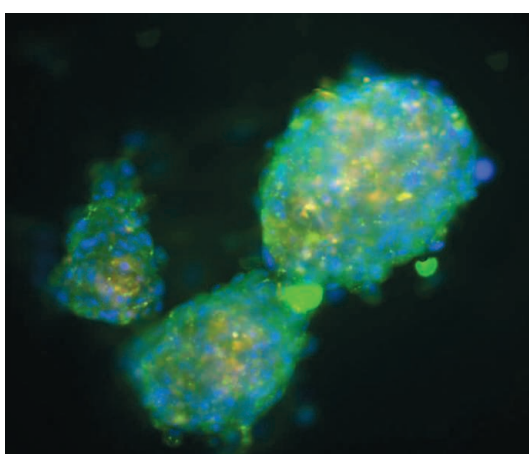

Protein makeover. These cells were reprogrammed into stem cells with proteins alone.

Cooke wondered if the virus might be doing more than just ferrying genes. When the researchers added a virus that carried only a marker gene to cells that received copies of a single reprogramming protein, the effect was immediate: Within a few hours, the cells began to react to the protein, expressing the signaling pathway it triggered. Further experiments showed that the virus triggers the cell's innate immune response, primarily through a protein called toll-like receptor 3 (TLR3), and this ends up unwinding chromatin, the complex of DNA and proteins that usually keeps genes that aren't in use tightly bound in compact coils.

"When a cell meets a pathogen, it assumes a more plastic phenotype, which allows it to adapt to survive the pathogenic challenge," says Cooke, who calls this ready-for-anything state "transflammation." For those trying to make stem cells, the looser chromatin apparently allows the reprogramming factors better access to the genes involved in pluripotency.

Cooke's group found that blocking the TLR3 pathway also blocked reprogramming by viral vectors and by another method, the introduction of messenger RNAs that code directly for reprogramming factors. When the researchers added a TRL3-triggering molecule to their protein-only reprogramming recipe, they significantly improved the speed and efficiency of the technique.

"It is intriguing and unexpected that inflammatory pathways play a role in reprogramming," says Konrad Hochedlinger, a stem cell researcher at Harvard University. He notes that TLR3 may affect not only chromatin but also other processes such as a cell's replication rate. The find "adds to the deeper understanding of reprogramming mechanisms," agrees George Daley, a stem cell scientist at Harvard Medical School in Boston.

Cooke says he hopes that the transflammation might also help researchers looking for ways to turn one kind of mature cell directly into another, skipping the pluripotent state altogether. Cooke and his colleagues would ideally like to use it to change skin or other cells into cardiac cells that might help patients suffering from heart disease—turning a cell's perceived threat into a powerful opportunity.

–GRETCHEN VOGEL

CREDIT: JULIUS T. CSOTONYI

Agile flyer? New studies suggest the feathered dromaeosaurid *Microraptor* used its hind legs as rudders to steer among the trees.

PALEONTOLOGY

Flying Dinos and Baby Birds Offer New Clues About How Avians Took Wing

RALEIGH—Most scientists agree that birds are living dinosaurs, survivors of the mass extinction that did in all other dinos at the end of the Cretaceous period 65 million years ago. Birds are also the result of a remarkable series of evolutionary events that transformed dinosaurs from mighty masters of the land into light and feathery lords of the skies. At a meeting of vertebrate paleontologists here last month,* researchers pondered fresh clues about the origins of flight from studies of feathered dinosaurs and baby birds.

"This was one of the most important morphological and behavioral transitions in the history of vertebrate life," says Stephen Brusatte, a paleontologist at the American Museum of Natural History in New York City. And some of the most tantalizing clues to how it may have happened have been uncovered during the past dozen or so years: Nearly 30 species of feathered dinosaurs have been reported during that time, mostly from China, although just last week a team from Canada announced that a closer look at previously discovered dinosaurs from Alberta revealed that they were also covered with feathers (*Science*, 26 October, p. 510).

Perhaps the most spectacular of these finds have been beautifully preserved fossils of a crow-sized dinosaur called *Microraptor*, reported by Chinese paleontologists in 2000 (*Science*, 8 December 2000, p. 1871). *Microraptor* belongs to a group of carnivorous dinosaurs called the dromaeosaurids, which includes *Velociraptor* of *Jurassic Park* fame. The dromaeosaurids, many of which had feathers, were closely related to the earliest birds, although whether they were the closest of all dinosaur groups—and whether any of them could actually fly—is still a matter of debate.

Yet, if any dromaeosaurid could fly, researchers generally agree, it would be *Microraptor*. This slender dino had feathers on both its forelimbs and hind limbs, as well as a feathery tail. The Chinese scientists who originally reported it, including famed dino hunter Xu Xing, have argued that *Microraptor* was a glider that spread its four feathered limbs out wide as it launched itself from trees. They and other researchers have also suggested that the transition from nonflying dinosaurs to flying birds involved just such a four-winged stage, but that birds eventually lost the feathers on their hind limbs as they evolved more elaborate wings and feathers on their forelimbs. However, some paleontologists, including Brusatte, have challenged this hypothesis, countering that the dromaeosaurid body plan would not have allowed *Microraptor* to spread its hind limbs out far enough to serve as wings (*Science*, 24 January 2003, p. 491).

In a pair of companion papers presented at the Raleigh meeting, a team led by biologists Michael Habib of the University of Southern California in Los Angeles and Justin Hall of USC and the Natural History Museum of Los Angeles County described new studies using three-dimensional models and computer simulations to figure out how *Microraptor* might have flown. After modeling how much lift and maneuverability *Microraptor* would have achieved with its limbs in various positions, the researchers found that it would have been a much better flyer if it kept its forelimbs spread but its hind limbs tucked under its body, where they could be used as rudders to keep the animal under control as it banked and turned. By using the hind limbs in this way, the team concluded, *Microraptor* would have been able to turn twice as fast as a two-winged animal.

The team also found that *Microraptor*'s long tail—which is relatively longer than that of *Velociraptor* and many other dromaeosaurids—would have been a key part of this control and stabilization apparatus, helping to adjust the animal's pitch as it maneuvered among closely spaced trees. These adaptations, Hall tells *Science*, "let you get this dinosaur body into the air with very little [anatomical] overhaul" of its basic body plan.

Kevin Padian, a paleontologist at the University of California, Berkeley, who has also challenged the notion that *Microraptor* splayed its hind limbs out laterally, says the team has "advanced over some earlier work and gotten rid of stuff that was obviously anatomically wrong." But Padian objects that the model is still based on the old assumption that birds evolved from dinosaurs that glided down from trees. Many researchers now favor "ground up" scenarios in which feathered dinosaurs and early birds flapped their wings to get into the air. Habib and Hall counter that their model would work for either type of scenario.

Thomas Holtz, a geologist at the University of Maryland, College Park, says the debate over the two hypotheses "ended with the end of the 20th century," when paleontologist Kenneth Dial of the University of Montana in Missoula proposed that flight evolved after bird ancestors began using their feathery forelimbs to provide a bit of lift as they ran up trees and other inclined surfaces (*Science*, 17 January 2003, p. 329). Dial's "wing-assisted incline running" hypothesis makes evolutionary sense, Holtz says, because many animals—including today's chickens and peacocks—hide in trees to escape predators. "There would have been selective pressure to ascend

*Society of Vertebrate Paleontology 72nd annual meeting, Raleigh, North Carolina, 17–20 October.

Published by AAAS

into the trees and then get out of them once you got up there," he says.

In Raleigh, Dial's graduate student Ashley Heers argued in a widely applauded talk that paleontologists should search for clues to the origins of flight by studying the stages that young birds go through as they begin to fly. Although the 19th century idea that "ontogeny recapitulates phylogeny" has been widely discredited, Heers said, many young animals do retrace key evolutionary steps between birth and adulthood. For example, she argued, young birds such as chukars, a member of the partridge family, have many features that are typical of extinct carnivorous dinosaurs but are not present in adult birds. They include unfused thoracic vertebrae and a small pelvis and very small keel, an extension of the sternum that protrudes outward from the ribs. Young chukars and other juvenile birds also have symmetrical feathers that give way to asymmetrical ones in adult birds, a pattern that reflects differences between early and later feathered dinosaurs. And Heers and Dial have documented wing-assisted incline running in baby chukars; although they cannot yet fly, if their wings are clipped or blocked, their ability to run up inclines is greatly reduced.

The study of living juvenile birds is important to understanding the evolution of flight, Heers tells *Science*, because "if you saw them as a fossil, you would probably not guess what they were actually using their wings for." Holtz agrees, although he stresses the importance of new fossil discoveries as well: "We are getting a nice, coherent picture of the phases of avian evolution that was totally unguessable without these wonderful new fossils from China."

–MICHAEL BALTER

EDUCATION

Indonesia to Drop Science for Youngest Students

Indonesian children lag far behind their peers on global measures of science aptitude. But rather than use that poor performance as a call to arms, the Indonesian government wants to eliminate science as a subject in the nation's elementary schools as part of a "streamlining" of the curriculum.

The proposed changes were unveiled at the end of September but have only recently attracted widespread attention. And not surprisingly, some scientists are fuming. "While other countries are introducing science early, the proper way, Indonesia is going backwards," says Sangkot Marzuki, director of the Eijkman Institute for Molecular Biology in Jakarta and president of the Indonesian Academy of Sciences.

Challenging assignment. Teachers will need to work harder to get science into Indonesian classrooms.

The new curriculum will have six subjects: arts and culture, civics, Indonesian language, math, religion, and sports. The natural sciences, social sciences, and English will be dropped from grades 1 to 3, starting next year with the first grade.

"[P]rimary school students will be involved in moral and character building instead of focusing on the content of subjects," Deputy Education and Culture Minister Musliar Kaslim told *The Jakarta Post* last month. Students will learn science as part of their Indonesian language studies, he explained, as part of an effort to lighten a curriculum that now is "too heavy."

Some see the hidden hand of Islamic fundamentalists in the move to jettison science. "A science education is a secular education," says a Jakarta-based scientist who requested anonymity. The curriculum revisions, he asserts, are "symptomatic of the ongoing struggle by this nation to retain its secular identity and soul."

"Rubbish," says C. W. Watson, a social anthropologist who has rallied to the education ministry's defense. "The government is very secular and there are no Islamicist moles working there," says Watson, who teaches at the Bandung Institute of Technology.

Indonesian students have fared poorly on recent global science tests. For example, in the 2007 Trends in International Mathematics and Science Study exam, Indonesian eighth graders placed 35th out of 48 countries. Indonesia's 15-year-olds ranked sixth from last in science proficiency in the 2009 Program for International Student Assessment.

Some backers of the revisions laud the emphasis on morality. "We don't just need experts in physics and mathematics, but people who understand human values," Dedi Gumelar, a legislator in Indonesia's House of Representatives was reported as saying in the *Jakarta Globe*.

Watson believes the new curriculum is on the right track. "It's excellent in terms of its aim to instill a sense of curiosity about the natural world and the immediate material environment of pupils." Watson, a professor emeritus at the University of Kent in the United Kingdom, says the revised curriculum resembles that of primary schools in the United Kingdom.

Observers of all stripes agree that Indonesian schools need more innovative teaching. The new curriculum takes a step toward inquiry-based learning by asking students "to observe their surroundings," according to Musliar.

Still, schoolteachers will need more training and support to get students to "learn science by doing it," Marzuki says. "It's not the science that's wrong, but the way science is taught," he says. He says the education system now emphasizes rote memorization.

Marzuki and other scientists hope to persuade the government to restore natural sciences to the curriculum before the changes are finalized later this year. The education ministry's revisions may be "wrong," Marzuki says, but "they are not an attack on science."

–RICHARD STONE

CREDIT: AGUNG KUNCAHYA B./XINHUA/LANDOV

Published by AAAS

GENETICS

Cancer Gene Data Casts Doubt on Popular Research Method

The online catalog PubMed contains more than 25,000 biology papers about *Myc*, a gene linked to aggressive cancers, says David Levens, a pathologist at the National Cancer Institute in Bethesda, Maryland. But most of this work now needs to be reevaluated, according to Levens and a colleague, molecular biologist Richard Young of the Whitehead Institute for Biomedical Research in Cambridge, Massachusetts. They argue that *Myc*'s cancerous effects are much broader than most people have assumed, and that a flawed experimental method may have thrown off a decade's worth of *Myc* research.

Perhaps as important, the pair says that the problem may extend beyond studies of cells with *Myc*. Gene-expression studies that used proliferating cells of any kind may need to be reinvestigated, says Young, who claims to have done this for experiments involving "key concepts we have published in the past 5 years." In a paper in *Cell* last week, he and Levens call for "revisiting" all gene-expression results. That could be a well-nigh-impossible task, as the technique is widely used throughout biology research; there are more than 750,000 gene-expression data sets in just one public database.

Both Levens and Young say they started rocking the boat when James Watson, winner of the 1962 Nobel Prize in physiology or medicine and co-discoverer of DNA's structure, began pushing a year ago for a better explanation of how a mutated *Myc* promotes cancer. According to them, Watson, now chancellor emeritus at Cold Spring Harbor Laboratory in New York, helped set up a conference on *Myc* at the lab in November 2011.

It was at that meeting, Levens says, that he proposed "with a great deal of trepidation" that a cancer-promoting *Myc* doesn't activate specific genes, as had been assumed for years. Instead, he argued, it works like a "universal" switch to boost RNA output by all genes expressed in a cell—an idea that Young was also investigating. The two published independent papers on *Myc*'s function back-to-back in the 28 September issue of *Cell*. But they went further last week in a *Cell* commentary, suggesting that this type of universal gene activation was more common than thought. The pair called for a broad reconsideration of almost all gene-expression data.

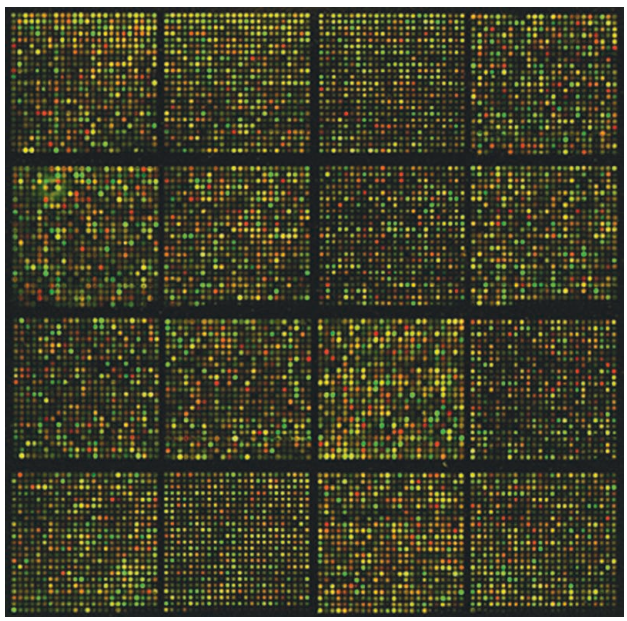

CREDIT: LOUIS M. STAUDT/NATIONAL CANCER INSTITUTE

Missed effects? New biology may require a reevaluation of gene-expression data like this view of mouse DNA, researchers say.

Not everyone agrees about the significance of the new *Myc* insight. Chi Van Dang, one of the most published experts on *Myc* and director of the Abramson Cancer Center at the University of Pennsylvania, suggests that some of the new claims about *Myc* are exaggerated. He objects especially to Levens's use of the word "universal" to describe how *Myc* operates to increase the RNA output of genes. By Dang's reckoning, at least 10% of the genes affected by the oncogene are suppressed. As for the broader issue, Todd Golub, a cancer researcher at the Broad Institute in Cambridge, says that it would be a mistake to think that "all previously reported gene-expression studies are suspect."

A persistent critic of such research, Simon Melov, a molecular biologist at the Buck Institute for Research on Aging in Novato, California, says he often tells people that "80% of expression studies in the literature are bad" because the experiments are designed poorly. The specific issue flagged by Young and Levens—that gene expression varies a lot from one cell to another and that RNA assays need to be normalized better to account for this—is pretty "obvious," according to Melov.

The problem highlighted by the *Myc* studies may sound modest, but after thinking about it for a year, Levens and Young don't see a simple fix. The only way to update the older work on *Myc* and gene expression, they say, is to go back to the lab and redo the experiments. That view, Young says, causes "the most angst" among biologists. He says he understands the "desperation" of bioinformaticists seeking a way to tweak existing data into better shape, but he can't offer one that doesn't require lab work.

Levens suggests that this problem arose partly because scientists viewed *Myc* as a "master regulator of master regulators," one that sends a signal along defined pathways to an array of specific targets that send out additional signals, creating a dizzying pattern of interactions. In reality, Levens says, "*Myc* is not a high executive making lots of decisions but a dumb bureaucrat enforcing a rule." And the rule itself seems pretty simple: If a gene is expressed, increasing *Myc* in nearly all cases increases that gene's level of expression. Genes that are already highly expressed are boosted more, so the impact of *Myc* is "exponential," Levens says.

The broad effects of *Myc* were overlooked, according to Levens and Young, because the standard procedure in gene-expression experiments has been to use similar quantities of RNA from the samples being compared and to normalize results to mean RNA. Young calculates that this practice erroneously deflates *Myc*'s effects two- to threefold. He says it also creates the impression that some genes are turned down when they are not.

Levens and Young acknowledge that more studies are needed to show that this problem extends beyond *Myc*-driven cancer cells. But there is one clear way to prevent being misled in the future. To get accurate gene-expression results, Young says, researchers should "spike in" known amounts of labeled RNA so that assays will contain a yardstick for RNA quantity tied to the source.

Young says that his "biggest concern" for a time was that "misinterpretations" of gene-expression data might affect patient care. But based on conversations with clinicians whose judgment he trusts, he's decided that isn't a problem. Levens agrees. He says that diagnostic and therapeutic methods exploiting gene-expression data are held to much more demanding standards than research papers; they have to work in the clinic.

–ELIOT MARSHALL

Published by AAAS

SCIENTIFIC MEETINGS

U.S. Agencies Feel the Pinch of Travel Cutbacks

Two years ago, the General Services Administration, which is responsible for improving efficiency across the U.S. government, held a conference in Las Vegas, Nevada, that became notorious. Attendees enjoyed delights such as artisanal cheese, expensive sushi, and a mind-reading session—at a cost to taxpayers of $800,000. An investigation and a congressional hearing earlier this year prompted the Office of Management and Budget (OMB) to impose government-wide restrictions on conference travel—and now some scientific meetings are paying the price.

The restrictions, spelled out in an 11 May OMB memo, have shrunk attendance at several meetings over the past few months. Recently, they caused the American Astronautical Society (AAS) to cancel its annual conference on space science, which was to be held at the Jet Propulsion Laboratory in Pasadena, California, on 28 and 29 November. Ironically, the conference, which promised to feature several speakers from NASA headquarters, was devoted to the theme of "Space Science and Planetary Exploration in an Age of Austerity."

"We were going to discuss how to do meaningful space science in a tight fiscal climate," says AAS President Frank Slazer. When key NASA speakers dropped out because of travel restrictions, the meeting fell apart. "Bottom line, to avoid spending a small amount of money on our conference, we had to cancel a meeting that was going to be focused on doing challenging—and expensive—space research at lower cost."

The OMB memo specifically requires that agencies conduct a senior-level review before participating in conferences that might cost the agency more than $100,000. It also prohibits agencies from spending more than $500,000 on any single conference without obtaining an exemption from the agency head. In addition, the memo directs agencies to cut annual travel expenditures 30% below fiscal year 2010 levels starting in FY 2013, which began on 1 October.

The impact began to be felt within weeks of OMB's ruling. To fit under the $100,000 expenditure cap, NASA whittled down its participation in the International Space Station Research and Development Conference in mid-June, a Denver meeting also organized by AAS. Some 84 NASA employees were supposed to attend, but only 50 went—enough, AAS reasoned, to proceed. For the Pasadena meeting, however, more than eight speakers who had been invited from NASA headquarters said they could not make it. The depleted roster made the meeting unviable, and the association decided to cut its losses.

Other disciplines are bearing the brunt as well. A symposium on environmental technology sponsored each year by the Department of Defense—to be held in Washington, D.C., in November—was called off, the organizers say, because they did not have enough time to obtain the budgetary approvals for travel required under the new rules. Nearly 80 employees of the National Weather Service had to drop out of the National Weather Association meeting held in Madison in October because the Department of Commerce, which oversees NWS, did not approve the travel in time.

Exception. NIH's role in the Society for Neuroscience's annual meeting is one of a rare few exemptions from new federal travel restrictions.

CREDIT: JEFF NYVEEN/© 2011 SOCIETY FOR NEUROSCIENCE

The Department of Energy (DOE) has cut the number of laboratory staff members who will attend the premier supercomputing conference, SC12, being held in Salt Lake City from 10 to 16 November. Last year, 550 DOE lab people attended; only 400 are going this year. DOE labs, which typically sponsor booths at the conference to tout their latest research and foster recruiting, won't have any this year. DOE's reduced involvement is of serious concern, says SC12 Chair Jeffrey Hollingsworth, a computer scientist at the University of Maryland, College Park. "This affects their ability to be engaged in the cutting edge of science and could affect U.S. competitiveness in the high-performance computing field," he says.

The OMB memo appears to have had far less impact at the National Institutes of Health (NIH). Initially, NIH officials worried that the restrictions would apply to peer-review panels. After NIH Director Francis Collins made a personal appeal, OMB responded that meetings of peer-review panels and federal advisory committees are not considered conferences and are exempt from the spending limits.

Nor has the OMB memo affected grants for conferences that cost more than $100,000, NIH says. The secretary of Health and Human Services has given waivers for several big meetings with more than $500,000 in NIH expenditures, including the International AIDS Conference and the Society for Neuroscience's annual meeting.

Travel restrictions may be causing some problems now, but things could get a lot worse if Congress enacts the Government Spending Accountability Act of 2012, which passed the House of Representatives in September. That legislation would make the OMB travel restrictions permanent and make it harder to obtain waivers. Several scientific societies, including the Federation of American Societies for Experimental Biology (FASEB) and the American Physical Society, have objected to the bill.

Howard Garrison, FASEB's deputy executive director for policy, acknowledges the need to rein in spending on conferences in hard times. But he says researchers across the life sciences and other disciplines are already making efforts to cut down on meeting costs—for instance, by taking public transportation instead of jumping into a cab to get from their hotel to the conference venue. However, he says, meetings are especially important for young scientists, and scientists inside and outside the government need to continue interacting face-to-face: "Administrative officials who run grant programs need to be able to get out there and speak to the research community."

–YUDHIJIT BHATTACHARJEE

With reporting by Robert F. Service and Jocelyn Kaiser.

Published by AAAS

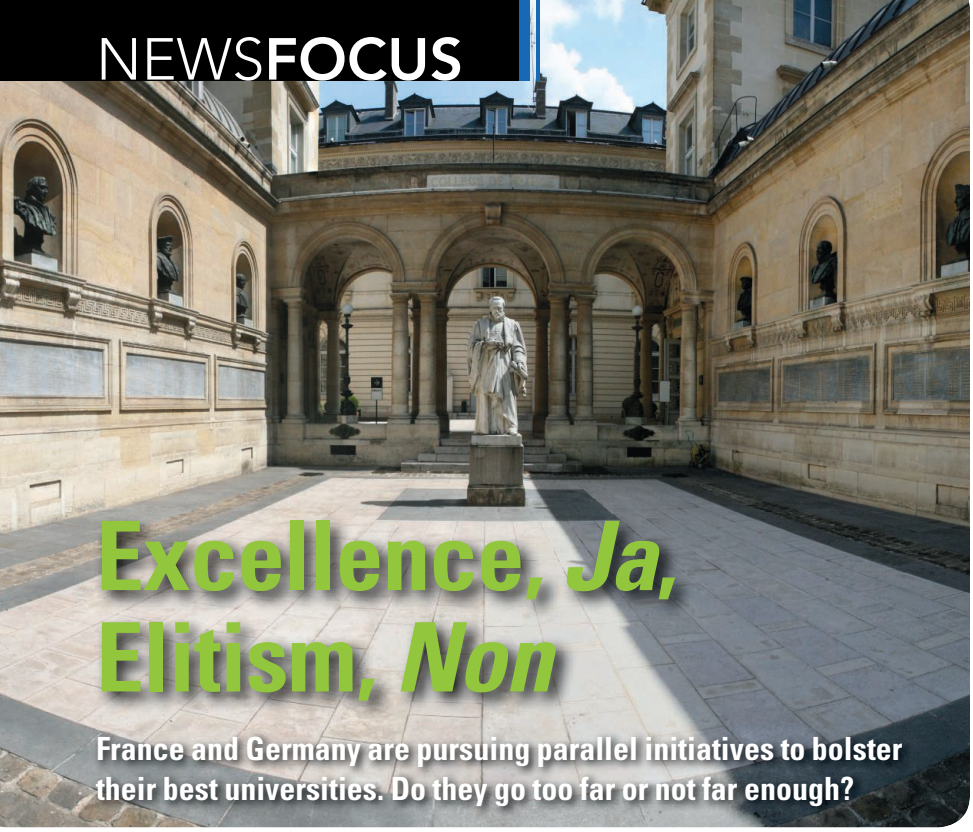

Excellence, *Ja*, Elitism, *Non*

France and Germany are pursuing parallel initiatives to bolster their best universities. Do they go too far or not far enough?

"We're developing an institution with all of the characteristics of a research university."

—MONIQUE CANTO-SPERBER, PARIS SCIENCES ET LETTRES

"Everyone says that a large university is hard to turn round, like a supertanker," proclaims Axel Freimuth, rector of the University of Cologne in Germany. "But that's simply wrong. We have 40 new appointments every year. Our size gives us the potential to act dynamically."

A solid-state physicist, Freimuth personifies what a German university leader needs to be: three-parts persuader and one-part autocrat. That combination has worked well for Freimuth, a bear of a man who became rector at Cologne in 2005. In June, his 40,000-student university competed successfully for a €50 million, 5-year "future concepts" grant, one of 11 winners in a federally funded "Excellence Initiative" designed to build stronger German research universities.

The grant supports a strategic plan to develop the entire university. It builds on earlier support for a research "cluster" in Cellular Stress Responses in Aging-Associated Diseases. The cluster grant alone, Freimuth says, has helped attract €300 million of investment—including brand-new Max Planck and Helmholtz centers—at the university. "Cologne is now *the* focus of aging research in Germany," Freimuth says.

Yet Freimuth acknowledges that some of his colleagues at Cologne are skeptical that the initiative will be able to turn a handful of German universities into global powerhouses. In addition, some faculty members outside the sciences still question whether they should be judged on their ability to obtain competitive funding.

The Excellence Initiative, launched in 2005 by then-Chancellor Gerhard Schröder, was born of politicians' and scientists' fears that Germany's research universities were falling behind in the global race to attract the best faculty members and students. Two years later, French President Nicolas Sarkozy began pushing through a set of measures with the same goal. After passing laws that gave university presidents more autonomy and greater control over their institutions, France established a program to select and support eight major research universities, eventually granting them public funds as the basis for building private endowments.

Both initiatives assume that world-class research universities are essential drivers of economic growth. And the initiatives follow the same game plan: Inject money into a small number of leading universities and allow newly empowered administrators to spend it on developing the institutions' strengths.

But this drive runs counter to egalitarian traditions in both countries. Although the quality of universities in each country varies, the gap isn't as large as, say, between Harvard University and some U.S. state universities. Many European scientists are queasy at what they see as attempts to mimic the U.S. system.

There are also institutional roadblocks to rewarding excellence. In Germany, the drive for reform comes primarily from the federal government, but control of higher education rests with the states, or Länder. In France, students and nonacademic staff members have a strong say in university governance. That democratic tradition runs counter to the notion of strong, strategic leadership.

Germany's universities have long featured a weak, ponderous central administration, combined with near-total autonomy for professors. That autonomy has led to much inbreeding, with faculty members giving junior staff positions to their own best students rather than outsiders, never mind foreigners. Much of the best German research is undertaken in adjacent but separately managed Max Planck institutes and Helmholtz centers.

France's university system is centrally funded from Paris. But the country's best students customarily attend selective, research-free *grandes écoles* and bypass university altogether.

The value of international rankings in assessing a nation's scientific prowess is debatable. But there's no denying their influence. This year, France had only three institutions in one such yardstick, known as the Shanghai Top 100, and Germany's total was only one greater (see chart, p. 599).

Superficial as this metric may be, it has led to much public soul-searching. "You can say what you like about the rankings," muses Louis Vogel, head of the Paris-based Conference of University Presidents. "But there's no question that a high ranking attracts people to a university."

Online

sciencemag.org

Podcast interview with author Colin Macilwain (http://scim.ag/pod_6107).

Published by AAAS

"Our size gives us the potential to act dynamically."

—AXEL FREIMUTH, UNIVERSITY OF COLOGNE

Despite their differences, the same questions are being asked of both efforts: Were they fair? Do they go far enough? Will they strengthen the university system as a whole? And, above all, will they endure?

The German initiative is set to expire in 2017. But the current German government, led by Angela Merkel, remains firmly behind it until then. In France, the new Socialist government of François Hollande is reviewing the entire program. And although the general thrust of the reforms seems safe, the government is under considerable pressure to modify them.

German teamwork

Graduate education in Germany is well-respected around the world. But its traditional structure, based on a tight one-to-one relationship between the student and a professor, excludes the taught components and multiple academic inputs now commonplace internationally.

In designing the Excellence Initiative, German officials were struck by the autonomy enjoyed by U.S. researchers once they won their own grants, recalls Reinhard Grunwald, then–secretary-general of the DFG, Germany's main research agency. "We paid special attention to American universities, because many of our scientists spent their formative years there," he says.

However, the aim of the initiative was not to "get even" with other countries in the rankings, Grunwald recalls. Rather, it was intended to help universities foster greater innovation in Germany and across Europe. Reaching that goal required the intervention of the federal government, Grunwald adds. "We knew the universities were having a hard time because the Länder couldn't come up with enough of a financial contribution," he says.

The Excellence Initiative comprises three components: graduate schools, clusters of excellence, and future concepts. The first two were continuations of older DFG programs. The funding has been implemented in two rounds: The first injected €1.9 billion into the universities between 2006 and 2012, and an additional €2.7 billion will be spent between 2012 and 2017.

The graduate school component of the Excellence Initiative has given grants of about €1 million a year to dozens of departments. Germany has about 100 Ph.D.-granting universities that this funding has been spread across (39 in the first round and 45 in the second) to support programs that will incorporate more teaching and have students mentored by several faculty members. The second component of the initiative awarded about €6.5 million annually to 80 "clusters" of research excellence—37 in the first round, 43 in the second.

The most radical element of the Excellence Initiative, however, is the third component, called future concepts. The scramble for this money sparked an unprecedented rush among senior faculty members, university rectors, consultants, and outside organizations to develop strategic plans that would bolster their research strengths. Some plans identified particular disciplines for investment and development; Cologne's, unusually, pledged to build a broad base of excellence across all fields of research.

"People started to talk with one another across faculty," says Stefan Hornbostel, director of the Institute for Research Infor-

GLOBAL RESEARCH UNIVERSITIES

www.sciencemag.org/extra/global

This is the third in a series of articles on global research universities. The first article (7 September, p. 1162) examined the importance of mobility by exploring the reasons for the increased flow of talent to Hong Kong and Singapore. The second article (28 September, p. 1600) looked at cross-national collaborations created through satellite laboratories, a relatively new phenomenon. This article focuses on Europe, where two of the continent's scientific powerhouses have launched separate initiatives with the same goal: to strengthen research at a handful of elite universities without eroding the quality of the country's other academic institutions.

CREDITS (TOP TO BOTTOM): ALEKSANDER PERCOVIC (2); ISTOCKPHOTO

Published by AAAS

mation and Quality Assurance in Berlin. "Even those universities who weren't successful had a 'plan B' of how to act without government money."

Particular emphasis was placed on forging stronger links with industry and with the Max Planck institutes and Helmholtz centers. "We wanted the universities to be more alert to their roles, not just in research and teaching, but as agenda-setters for innovation," Grunwald says.

The process of selecting universities for future concepts funding was bound to be contentious, and the final approach struck a less elitist tone than did the original version. Nine institutions were funded in the first round, as opposed to the three initially suggested by the Schröder administration. In addition, after international peer review narrowed the field, the winners were selected not by the DFG but by Germany's science council, the Wissenschaftsrat, whose membership includes representatives of the federal government and the Länder, as well as leading scientists.

Christiane Gaehtgens, a former secretary-general of the German Rectors' Conference, believes that the process has greatly strengthened university leadership. But she worries about the middle-ranked institutions that failed to win awards: "We're seeing stratification. We're losing out in the middle, which is where many of our strengths used to lie."

Others think the reforms don't go far enough, either in concentrating resources or in updating the patchwork of governance laws decreed by the Länder. "The Excellence Initiative did put money into the system—but it didn't achieve true excellence," says Ernst Winnacker, who stepped down as president of the DFG in 2006 and now runs the Human Frontier Science Program in Strasbourg, France. "The extra money really did a lot of good, but a world-class standard has not been reached."

Winnacker had pushed for the government to select a single national winner in the future concepts competition. He would now like the Max Planck institutes to create a single, distributed graduate university. Such an institution, he says, would "illustrate the high quality of the German research system."

Tim Stuchtey, an economist and director of the Brandenburg Institute for Society and Security in Potsdam, Germany, thinks that permanent change would require governance reform. North Rhine-Westphalia, of which Cologne is part, introduced reforms including greater autonomy and performance-related pay, but other Länder have not followed suit.

When the initiative draws to a close in 2017, universities can expect no extra help from the Länder, which will shortly face severe new borrowing limits. But many predict that a constitutional amendment will pass after next year's elections, allowing the federal government to continue some form of block-grant support for the elite.

Paris match

The obstacles facing French university leaders are yet more daunting. After the governance laws were passed, Sarkozy introduced a set of measures as part of an economic stimulus package known as the Big Loan. A program called LABEX supports centers of excellence in specific disciplines, while a second piece, EQUIPEX, pays for equipment.

The largest component, Initiatives d'Excellence (IDEX), aims to build an elite club of research universities. So far, eight groups of institutions have won IDEX awards. Most of the winners plan to merge fully, but others will form confederations and seek to be classed as single entities in the institutional rankings.

Financing is generous but not guaranteed: Selected proposals have been initially funded for 4 years, to the tune of about €30 million each annually. Projects deemed successful could then receive permanent endowments of about €1 billion from the government.

The headquarters of Paris Sciences et Lettres (PSL)—one of the first three IDEX projects selected in July 2011—is inauspiciously located in a side street in the Latin Quarter. But its leader, Monique Canto-Sperber, compensates for her modest, half-complete surroundings with a steely determination to build something new and distinctive.

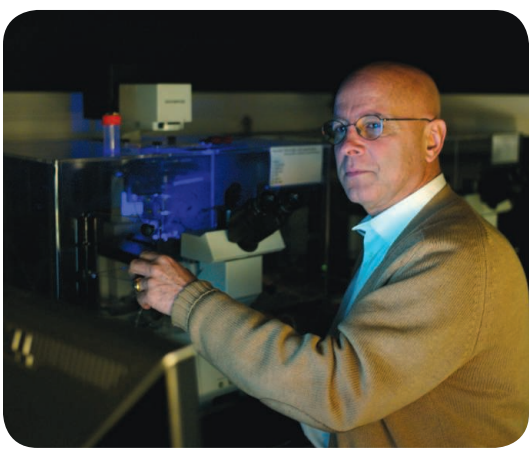

Common purpose. Biologist Antoine Triller (*left*) is trying to "develop a community" of scientists in Paris; Ernst Winnacker (*right*) cautions that "a world-class standard" has yet to be attained at German universities.

"We're developing an institution with all of the characteristics of a research university," Canto-Sperber says. The 16 institutions participating in PSL will not be merged, but they plan to submit a single set of data to the rankings systems. "We believe in the benefits of having scientific inputs from autonomous components," she says.

The PSL project isn't the first attempt to build stronger ties among several outstanding academic institutions in the Latin Quarter. But it is, by far, the most comprehensive effort. The goal is a confederacy of 2500 researchers, with a private endowment worth €1.24 billion.

Antoine Triller, the director of the prestigious biology institute at École Normale Supérieure (ENS) in Paris, says he's long immunized himself against the frustrations of working inside a system in which researchers from agencies such as CNRS and INSERM operate cheek-by-jowl with colleagues at universities and other institutes. "It's not so easy, but we get used to it," he says. "It's like if you speak Chinese, you don't go on complaining about how hard it is to speak Chinese."

As dean of research at PSL, Triller is hoping to streamline the existing potpourri of institutes. "We all have our own histories," Triller wryly observes. "The idea is to respect each other and develop a community. I am Dean of Research here. I didn't want to be 'research director'—I'm not going to direct anybody!"

Scientists acknowledge that it will be a major feat to get 16 institutions, many of them with their own illustrious histories, to sing from

CREDITS (LEFT TO RIGHT): INSTITUT DE BIOLOGIE DE L'ENS; ADRIEN COQUARD

Published by AAAS

the same song sheet. "It will take time for us to think of ourselves as part of PSL," says Patrick Tabeling, a prominent physicist at the École Supérieure de Physique et de Chimie Industrielles. He notes that the school has a long history and a superb recent record in establishing start-up companies: "We don't want to homogenize, that's for sure!"

The new institution may not even make the type of leap in the Shanghai ranking that many had hoped for. Some have calculated it would "only gain a few places" above the 73rd position now held by its highest-ranked component, ENS, Tabeling says: "That came as a surprise to me."

In its application last year, PSL said it "would appear within the first 20 academic institutions on a worldwide level." Canto-Sperber says that predicting PSL's place in the Shanghai ranking has proven harder than expected. While speaking with *Science*, Canto-Sperber heard that Serge Haroche, a physicist at ENS and the College de France—both part of PSL—had won this year's Nobel Prize in physics for his work in quantum mechanics. That honor will certainly help boost PSL's Shanghai ranking, which gives weight to recent Nobels.

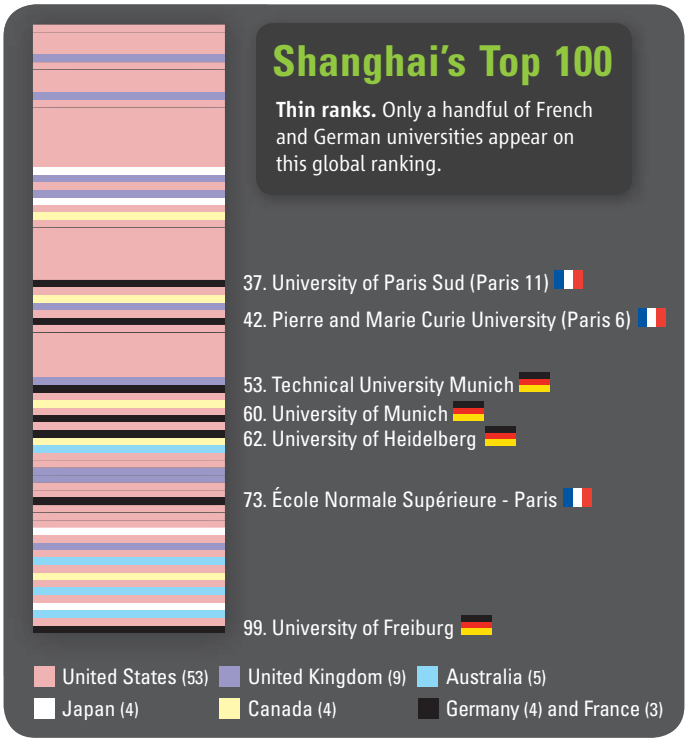

Some full-blown mergers between established institutions with IDEX awards have already run into trouble. The Toulouse IDEX, for example, was approved in May. But it stalled after one of its partners, Université Paul Sabatier, elected as president mathematician Bertrand Monthubert. As former leader of the grassroots researchers' group Sauvons La Recherche, he was an outspoken critic of the reforms.

In common with most critics, Monthubert professes full support for IDEX's goals but disputes its means. He takes issue, for example, with the enhanced powers for university presidents, narrower franchises for their election (which removes the influence of students and junior staff members), and the focus on a small number of winning institutions. Monthubert also opposes the idea of the state transferring an endowment to the IDEX institutions: "Public universities should be funded by the state," he says.

Even researchers who are generally sympathetic to Hollande fear what now lies ahead. "I'm not optimistic," says Philippe Froguel, a geneticist at Imperial College London and the Pasteur Institute in Lille. "At least with Sarkozy, he tried to do something." Froguel gives Sarkozy credit for promoting the idea "that universities should lead the system and that it should be based on excellence. That was something people like me can endorse. Nothing has been achieved yet—but if the effort gets further support, it can still be a big success."

But some now fear that whatever gains have been made could be reversed. Jacques Crémer is research director of the Toulouse School of Economics (TSE), a cluster affiliated with the University of Toulouse, which obtained its first backing under RTRA, a research network program launched under Sarkozy's predecessor, Jacques Chirac. The money was used to start a private, €30 million endowment to help support a growing, international school of 160 researchers and 100 graduate students.

"I think it would be a pity if the Toulouse IDEX didn't go through—although more for the university than for TSE," he says. "And, speaking personally, I think it would be catastrophic if we went backwards, in terms of autonomy for the universities. There are some elements in the French university system who would like to take us back to the 1950s. I think that's the wrong road to follow."

Along with the rest of Sarkozy's reforms, however, IDEX is now being subjected to a consultation exercise led by France's new Socialist research minister, Geneviève Fioraso. The ministry declined to comment for this article pending the outcome of the consultation, but interviews with a dozen senior university officials and observers suggest that the government is likely to retain some of the autonomy measures granted in the 2007 law and honor its short-term financial commitments to the universities. However, it's anyone's guess what will happen to the transfer of substantial endowments to the universities, a central tenet of IDEX.

"We are proceeding exactly as we had planned," Canto-Sperber says emphatically. "There's been no signal at all that we should change track." Within weeks, PSL will issue its first call for internal research projects to be supported from IDEX funds. Canto-Sperber says PSL will also be holding discussions with rankings organizations on a joint entry next year for the combined institution.

Making it work

As the former convener of the policy working group at the League of European Research Universities, which represents 21 elite institutions, Geoffrey Boulton is quite familiar with the German reform effort. And he's impressed with its impact thus far.

"The Excellence Initiative has made German universities think more deeply about their strategic futures, and that's a good thing," says Boulton, a geologist at the University of Edinburgh in the United Kingdom who now heads the Science Policy Advisory Group at the Royal Society of London. Boulton also chairs the Academic Advisory Council at Heidelberg University, which won backing under all three components of the initiative. The selection process administered a "salutary shock" to prestigious German universities that lost out early on, he notes.

The French initiative is more problematic, Boulton says: "For the last 10 or 15 years, French governments have been thrashing around, looking for the 'magic bullet' that will bring their universities up to what they regard as international standards."

He's especially concerned about the sustainability of the new federations backed by IDEX. "They look good on paper," he says. "But the operational challenges of making them work will be really severe."

–COLIN MACILWAIN

Colin Macilwain is a writer in Edinburgh, Scotland.

CREDIT: (SOURCE) ARWU.ORG

Published by AAAS

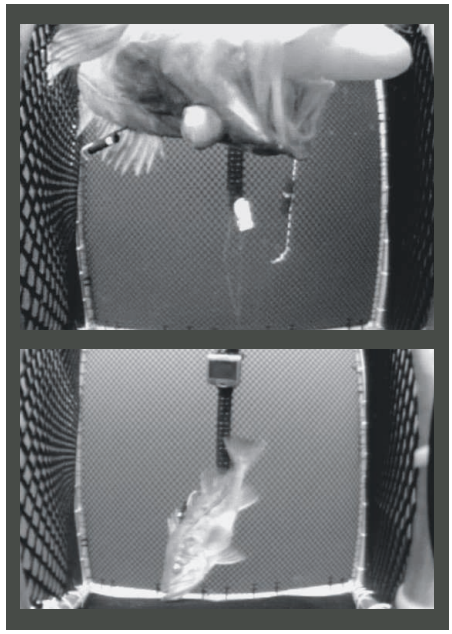

MARINE BIOLOGY

Putting Rockfish Back Where They Belong

New gadgets for releasing by-catch of critically overfished rockfish could help ease a regulatory bottleneck on the West Coast recreational groundfish fishery

On an overcast September day, fishing in a small boat off the coast of San Diego, California, marine biologist John Hyde has just reeled in a 10-inch, bright-orange starry rockfish that looks like a creature in a horror show: Its eyes are freakishly inflated, popping out of their sockets, and glazed milky white from tiny air bubbles inside. Its pale stomach sticks out of its mouth. The fish is stiff, "just like an inflated balloon," says Hyde, a program leader at the National Oceanic and Atmospheric Administration's (NOAA's) Southwest Fisheries Science Center in San Diego. Hyde and Nicholas Wegner, a NOAA biologist and postdoc, have been studying a new technique that hook-and-line fishers can use to resuscitate unwanted by-catch of severely overfished rockfish stocks.

Hyde's fish is suffering from barotrauma. When rockfish (*Sebastes*) are hauled up from deep waters, the gas in their swim bladder swells with the pressure change, often triggering the dramatic symptoms and leaving the fish too buoyant to swim back down, explains Hyde, a lifelong angler. Fishers and biologists traditionally thought that these "floaters" were goners; they either succumbed or got picked off by seagulls. But Wegner grabs a small, black, cylindrical gadget with articulated, noninvasive jaws and locks them onto the rockfish's lower lip. The device, called a SeaQualizer, is hooked onto a PVC pipe that the researchers lower into the water with a rope. The pressure-sensitive device is preset to pop open at about 45 meters down, releasing the fish. It's like giving a rockfish an ambulance ride home after an angler catches it.

Over the last decade, a growing body of studies and dramatic underwater research videos has shown that barotrauma can largely be reversed. Bulging eyes and stomachs go back into place, and many rockfish can swim away and survive, at least short term, if they are released back down to depth with so-called descender or recompression devices. On the boat, Wegner and Hyde demonstrate several gadgets, from the $55 SeaQualizer to an inexpensive weighted, inverted barbless hook—and even an upside-down milk crate on a rope. As with CPR in people, timing is critical. "If you don't get 'em down quickly, they'll die," Hyde says.

View video of fish with barotrauma.
www.scim.ag/vid_6107

Although the science on recompression is in many ways still preliminary, interest in the work has reached the point where, at a 5 November meeting, the federal Pacific Fishery Management Council (PFMC) will begin considering proposals to give recreational fishers regulatory "credit" for releasing depleted rockfish species with descender devices. If such a move were eventually approved, the premise is that anglers not only would get to spend more time angling, but their voluntary use of recompression tackle could also potentially help restore some depleted fish stocks over time.

Off the West Coast, seven species of rockfish, including cowcod, yelloweye, canary, and bocaccio, were federally listed as overfished about 10 years ago. These fish are long-lived and slow to reproduce (yelloweye, for example, can live up to 120 years), and some of the species will likely take decades to recover under rebuilding plans managed by PFMC. To protect these and other groundfish stocks off the coasts of California, Oregon, and Washington, in the early 2000s the federal council and state agencies closed large ocean areas to bottom-fishing, restricted fishing depths, and reduced daily catch limits for anglers. New rules also mandated that if hook-and-line fishers caught certain depleted species, they had to throw them back. Upset about the floaters going to waste, some fishers began experimenting with resubmerging them.

So did biologists, who started studying the issue. Barotrauma is caused by "gas breaking out of the swim bladder and going wherever it's going to go" as tissues fail, says marine biologist Robert Hannah of the Oregon Department of Fish and Wildlife (ODFW) in Newport. The expanding gas can force air bubbles beneath the corneas and may tear blood vessels, lacerate the liver and other organs, and leak out through the skin or from under the gill flap. The extent of injuries is species-specific,

CREDITS: (LEFT) ALENA PRIBYL/NOAA; (RIGHT, TOP AND BOTTOM) NICHOLAS WEGNER AND JOHN HYDE/NOAA

Published by AAAS

Bloated from barotrauma. With its eyes bulging and stomach protruding from its mouth, this bocaccio rockfish shows injuries from barotrauma after being reeled in from 146-meter-deep waters. When NOAA researchers lowered the fish back to 42.5 m in a camera-equipped cage, the fish recovered enough to swim away when the cage door opened.

but the deeper the capture depth, the worse the damage can be.

Studies have demonstrated that recompression can achieve high short-term survival in several types of rockfish when taken from depths of up to 65 m, says marine biologist Alena Pribyl, although how effectively the technique works in much deeper waters or in the long term is less certain. In a study published this spring in the *Journal of Fish Diseases*, Pribyl (then a Ph.D. student) and colleagues at Oregon State University, Corvallis, tracked 1-month survival in 30 black rockfish that underwent simulated catch-and-release in pressurized aquaria. "Most of them did just fine," she says, with tissue and blood samples and a gene expression analysis revealing a surprising capacity for physiological recovery. Some fish, however, had nonfatal swim bladder ruptures that hadn't healed after 30 days.

Although few rockfish recompression studies have been done in the field, the latest results include a recently published study by Hannah's team. After catching 287 rockfish from depths of up to 64 m and lowering them to the sea floor in modified plastic barrels, the biologists observed 2-day survival rates ranging from 100% in canary and yelloweye to 78% in blue rockfish. Hannah is now running a similar field trial at depths up to about 80 m and tracking 4-day survival.

Other deepwater data have come in from Wegner and Hyde. Working with Pribyl, they recently finished a 4-month acoustic tagging study of 50 rockfish (including cowcod and bocaccio) that they reeled in from 80 m to 180 m of depth off southern California and released with cages or SeaQualizers. Preliminary analysis of the tagging data indicates that about 93% of the animals survived after 2 days, and 77% after 10 days. However, those numbers are based only on "the fish we heard from," Wegner says. By day 10, 40% of the study subjects moved out of detection range; whether they swam off happily, died from barotrauma, or got eaten by a shark is unknown, which increases the uncertainty of the survival estimates, the scientists say.

But a number of tagged fish were still alive at 4 months. And the data the researchers did gather indicated no signs of barotrauma-related deaths occurring beyond 6 days, Wegner says. "What we have is a good sense that this technique works for a lot of the species that we care about," Hyde says, but much more research is needed to better characterize the survival rates for the different species and capture depths.

Among other unanswered questions, can rockfish recover from multiple captures, and would barotrauma injuries keep them from functioning or reproducing normally over a potentially long life span? "There's a lot of work left to do," says ODFW's Hannah, who adds that the actual benefits of recompression in helping to rebuild the overfished stocks are hard to predict.

Nonetheless, after learning that floaters may survive if released properly, recreational fishing groups such as the Sportfishing Association of California and the Oregon Coalition for Educating Anglers have distributed thousands of descender devices. Avoiding depleted rockfish species is best whenever possible, but as a next-best practice, using recompression tackle "is the right thing to do," says Dan Wolford, the science director of the Coastside Fishing Club, which represents anglers in the San Francisco Bay Area. "We can make a difference saving one fish at a time." Wolford, a retired aerospace engineer, is also chair of PFMC.

In June, PFMC directed its scientific staff to develop possible methods for estimating and incorporating the reduced mortality of rockfish released with descender devices into its catch accounting models—starting with cowcod and yelloweye. For most rockfish species, current metrics count any fish caught from deeper than 55 m and released at the surface as dead, a 100% mortality rate. At the council's November meeting, its groundfish management team will propose different options for applying lower mortality rates when fish are recompressed, based on the existing research data; where data are insufficient, conservative buffers for uncertainty could be built into estimates. Although the committee wishes to encourage anglers' good stewardship in using recompression tackle, it also wants "to make sure we aren't jumping in too fast," says team member Lynn Mattes, a fisheries manager at ODFW. PFMC's scientific and statistical committee will give feedback on the proposals, and the council will decide next year whether or how to proceed with adopting survival-rate credits.

For anglers, Wolford says, such credits could mean having a longer fishing season targeting other, abundant groundfish species before getting shut down if they reach the federally allotted annual by-catch quotas on cowcod, yelloweye, canary, or other key depleted species. Down the road, he says, the use of descender devices could help in particular to rebuild yelloweye and canary—of which recreational fishers take a third or more of the overall catch allocations compared with commercial fishers—and might open the door for the council to consider reopening some areas now closed to fishing.

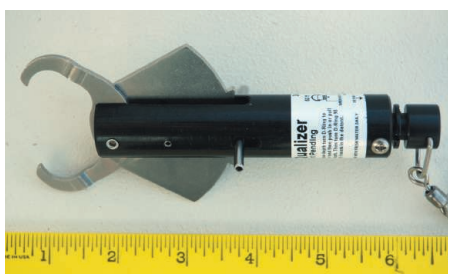

Recompressing rockfish. Anglers can clip a variety of descender devices to a fishing line to grip onto and release bloated rockfish by-catch underwater. Gadgets range from low-tech (*left*) to high-tech (the SeaQualizer, *above*).

It's unknown, however, exactly how many recreational fishers currently use descender devices—Oregon and California have begun collecting usage data—or how effectively. Some gadgets take practice to handle well, and each has pros and cons.

Still, even as they cite the need for further data, some scientists are cautiously supportive of bringing descender devices into rockfish management policy. As NOAA's Hyde says of the techniques for recompressing rockfish, "there's no question that it's better than letting them die."

–INGFEI CHEN

Ingfei Chen is a writer in Santa Cruz, California.

CREDITS: (RIGHT) DAN WOLFORD; (LEFT) MARK HUPP/ECOLEESER

Published by AAAS

How poverty affects behavior
617

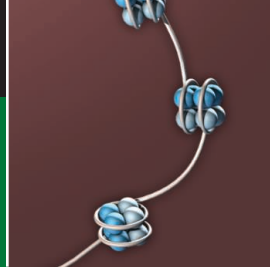

Gene loops
624

LETTERS | BOOKS | POLICY FORUM | EDUCATION FORUM | PERSPECTIVES

LETTERS

edited by Jennifer Sills

Antarctic Treaty System Ready for a Challenge

IN THEIR POLICY FORUM "CHALLENGES TO THE FUTURE CONSERvation of the Antarctic" (13 July, p. 158), S. L. Chown *et al*. discuss concerns about the Antarctic Treaty System's (ATS's) ability to navigate future challenges. We believe ATS has demonstrated that it is both robust and adaptable.

Chown *et al*. raise the issue of marine resource harvesting, biological prospecting, and potential mineral and hydrocarbon exploitation. The Commission for the Conservation of Antarctic Marine Living Resources (CCAMLR) regulates the harvesting of marine resources in the Southern Ocean, and it has arguably the most highly developed system for ecosystem-based management of any international agreement (*1*). Underpinning CCAMLR's decision-making processes is the precautionary approach which, as it has evolved, has set very conservative catch limits on fish stocks and provided other mechanisms for reducing harvesting impacts. The Southern Ocean krill fishery is arguably the largest underexploited fishery in the world. For many years, CCAMLR has been developing mechanisms in advance of projected escalation of interest in the fishery, including setting precautionary catch limits, establishing small-scale management areas, and invoking trigger points where, when a predesignated catch is exceeded, additional conservation measures will apply.

United. Treaty nation flags fly over the South Pole.

In their discussion of the submissions of several Antarctic claimant states to the Commission on the Limits of the Continental Shelf (CLCS), Chown *et al*. have misconstrued both the actions of those Antarctic Treaty Parties and the effects of those actions. All Antarctic Treaty Parties are bound by the Antarctic mining ban (*2*). Submission of data to the CLCS in relation to Antarctic or other continental shelves has no bearing on that ban or a party's obligation to uphold it. Mitigating unacceptable human impacts in Antarctica is a substantial focus for the Antarctic Treaty Consultative Parties, as Chown *et al*. note. There is no evidence that human interest in Antarctica will outpace the capacity of the ATS to respond.

The historically steady climb in Antarctic tourism numbers from the 1990s has been reversed since the 2008 financial crisis (*3*) and also since the International Maritime Organization introduced a ban on the use and carriage of heavy and intermediate fuel into the Antarctic Treaty Area in 2011 (*4*). Tourism is subject to ongoing monitoring, oversight, and management, mainly through the International Association of Antarctica Tour Operators (IAATO)—an organization mindful of the extraordinary responsibilities it carries for maintaining the integrity of the pristine Antarctic environment. Local impact is minimized by a system of site guidelines and rules about behavior ashore—the latter originally adopted by IAATO in its by-laws and later formalized by the ATS.

The Antarctic Treaty Consultative Parties have addressed past challenges firmly and overtly within the Antarctic Treaty's twin pillars of peace and science (*5*). Reforms to the operation of the Antarctic Treaty Consultative Meeting, increased opportunities for engagement with relevant international organizations, and the presence of nongovernmental organizations as observers to ATS meetings and as members of national delegations since the mid-1980s all work to strengthen the institutional resilience of the ATS. The number of parties acceding to instruments of the Antarctic Treaty System has steadily increased (including, notably, Malaysia and Pakistan in 2011). At the same time, the Antarctic Treaty Consultative Parties have increased engagement with relevant international organizations: among them, the UN Food and Agriculture Organization regarding IUU fishing; the International Hydrographic Office in relation to charting Antarctic waters; and the International Maritime Organization in the development of the Polar Shipping Code. We concur that the challenges facing the region defy complacency. The quickening pace of global change requires scientists and policymakers to work together. With this as a fundamental underpinning for future action, we believe the ATS is well placed to meet these challenges.

MARCUS HAWARD,[1]* JULIA JABOUR,[1] A. J. PRESS[2]

[1]Marine and Antarctic Futures, Institute for Marine and Antarctic Studies, University of Tasmania, Hobart, Tasmania 7001, Australia. [2]Antarctic Climate and Ecosystems Cooperative Research Centre, Hobart, Tasmania 7001, Australia.

*To whom correspondence should be addressed. E-mail: m.g.haward@utas.edu.au

References

1. A. Constable, *Fish Fisheries* **12**, 138 (2011).
2. Article 7, Protocol on Environmental Protection to the Antarctic Treaty, Antarctic Treaty Secretariat (www.ats.aq/e/ep.htm).
3. International Association of Antarctica Tour Operators, Tourism Statistics (http://iaato.org/tourism-statistics).
4. Annex I, Chapter 9, "Special requirements for the use or carriage of oils in the Antarctic area," International Convention for the Prevention of Pollution from Ships (MARPOL) (International Maritime Organization Resolution MEPC.189(60), 26 March 2010).
5. Articles I and III of the Antarctic Treaty, Antarctic Treaty Secretariat (www.ats.aq/documents/ats/treaty_original.pdf).

Letters to the Editor

Letters (~300 words) discuss material published in *Science* in the past 3 months or matters of general interest. Letters are not acknowledged upon receipt. Whether published in full or in part, Letters are subject to editing for clarity and space. Letters submitted, published, or posted elsewhere, in print or online, will be disqualified. To submit a Letter, go to www.submit2science.org.

CREDIT: PETTY OFFICER 2ND CLASS JOHN K. SOKOLOWSKI/U.S. NAVY

Published by AAAS

China's Wastewater Treatment Goals

CHINA SUFFERS FROM SEVERE WATER POLlution, primarily resulting from substantial discharge of wastewater. In 2011, China generated 65.21 billion tons of wastewater (*1*), and the total amount is expected to continue growing as a result of rapid urbanization and industrialization, reaching 78.4 billion tons by 2015 based on an annual increase rate of 4.7% (*2*).

On 6 August, China issued the Twelfth Five-Year Plan of Energy Conservation and Emission Reduction (2011 to 2015), in which the importance of wastewater treatment is addressed (*3*). The plan sets a goal: By 2015, the municipal wastewater treatment rate (wastewater treated divided by wastewater generated) and wastewater recycle rate (wastewater recycled divided by wastewater treated) should reach 85 and 15%, respectively.

The 85% target will be difficult to meet if rural areas are taken into account. Currently, national statistics for wastewater treatment rate in China only include urban areas and industrial sectors. If the wastewater treatment conditions in rural areas, which make up more than 50% of total population in China, are factored in, the wastewater treatment rate [currently 82.3% (*2*)] would drop dramatically. Most villages (96%) do not have drainage or wastewater treatment systems, and the remaining 4% treat wastewater with simple technologies such as septic tanks (*4*).

Municipal wastewater reclamation is also in its infancy. The recycle rate in developed countries is 70 to 80% (*5*). In China, it was 2.7% in 2007 (*5*) and less than 8.5% in 2010 (*6*). This explains why the target set for 2015 is only 15%.

Even if the target could be successfully achieved in a 5-year time frame, wastewater treatment in China would remain a challenge. More stringent discharge standards are needed, particularly in developed areas in China. For municipal wastewater discharges, the national Discharge Standard of Pollutants for wastewater treatment plants (WWTPs) (GB 18918-2002) applies. According to this standard, the effluent total nitrogen and total phosphorus concentrations must not exceed 15 and 0.5 mg/liter, respectively. WWTPs can meet these requirements, but doing so does not prevent the discharge of substantial nitrogen and phosphorus into nearby lakes and rivers, causing rampant eutrophication (*7*–*9*).

ZHIWEI WANG

State Key Laboratory of Pollution Control and Resource Reuse, School of Environmental Science and Engineering, Tongji University, Shanghai, 200092, China. E-mail: zwwang@tongji.edu.cn

References

1. Ministry of Environmental Protection of the People's Republic of China, National Report on Environmental Quality of 2011 (http://jcs.mep.gov.cn/hjzl/zkgb/2011zkgb/) [in Chinese].
2. Ministry of Environmental Protection of the People's Republic of China, National Report on Environmental Statistics of 2010 (http://zls.mep.gov.cn/hjtj/nb/) [in Chinese].
3. The State Council, The Twelfth Five-Year Plan of Energy Conservation and Emission Reduction (www.gov.cn/zwgk/2012-08/21/content_2207867.htm) [in Chinese].
4. J. Li, *Application of Decentralized Wastewater Treatment in Small Towns and Villages of China* (Chalmers Univ. of Technology, Gothenburg, Sweden, 2010).
5. Innovation Center Denmark, Shanghai, "Wastewater Treatment in China" (2009).
6. Y. L. Liu, Recycle rate of wastewater reaches 8.5% in China (2010); http://info.water.hc360.com/2010/04/160933182857.shtml [in Chinese].
7. L. Guo, *Science* **317**, 1166 (2007).
8. R. Stone, *Science* **333**, 1210 (2011).
9. M. Yang *et al.*, *Science* **319**, 158 (2008).

CORRECTIONS AND CLARIFICATIONS

Letters: "Friends in fungi" by G. D. A. Werner and E. T. Kiers (21 September, p. 1452). The image of the rare ericoid mycorrhizal fungus was misleading. The Letter's discussion applies more closely to arbuscular mycorrhizal fungi. The image has been replaced in the HTML and PDF versions online. The caption has been changed to "Arbuscular mycorrhizal fungi" and the credit has been changed to Jan Jansa.

This Week in Science: "Modulating the clock" (31 August, p. 1017). The image with this description should have been placed with the description below: "Keeping DNA flexible." The placement has been corrected in the HTML and PDF versions online.

Perspectives: "Walking on solid ground" by B. F. Dickey (24 August, p. 924). In panel A of the figure, the path of the mucus (going up the trachea, making a turn, and going down the esophagus) should have been indicated in dark blue. The HTML and PDF versions online have been corrected.

News Focus: "Stopping Alzheimer's before it starts" by G. Miller (17 August, p. 790). Matthew Reiswig should have been referred to as Matt throughout the story. Also, in the family portrait caption, Matt and his brother were misidentified. Matt is the second adult from the left, and his brother Marty is in the red shirt just right of center. The HTML and PDF versions online have been corrected.

Review: "Valorization of biomass: deriving more value from Waste" by C. O. Tuck *et al*. (special section on Working with Waste, 10 August, p. 695). In Fig. 3, the bracketed portion of the cyanophycin structure should have shown an amide, rather than an amine. The complete figure has been corrected in the HTML version online. The corrected structure is shown here.

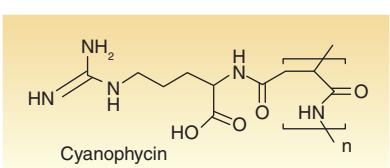

Cyanophycin

Perspectives: "Recycling of the #5 polymer" by M. Xanthos (special section on Working with Waste, 10 August, p. 700). The figure credit was omitted. It should be the following: Photo collage by L. Blizard; Thinkstock; iStockphoto; Shutterstock; Wikimedia Commons. The credit is correct in the HTML version online.

News Focus: "An evolutionary theory of dentistry" by A. Gibbons (25 May, p. 973). The article implied that both European countries and the United States added fluoride to their drinking water in the 1970s. In fact, water in most European nations was not fluoridated. However, European improvements in public dental health from the 1970s to the present have matched or even exceeded those of the United States. Reasons include fluoridated toothpastes, which became widely available in the 1970s, and changing criteria for diagnosing caries. See T. M. Marthaler, *Caries Res*. **38**, 173 (2004).

TECHNICAL COMMENT ABSTRACTS

Comment on "Multiyear Prediction of Monthly Mean Atlantic Meridional Overturning Circulation at 26.5°N"

Gabriel A. Vecchi, Rym Msadek, Thomas L. Delworth, Keith W. Dixon, Eric Guilyardi, Ed Hawkins, Alicia R. Karspeck, Juliette Mignot, Jon Robson, Anthony Rosati, Rong Zhang

Matei *et al*. (Reports, 6 January 2012, p. 76) claim to show skillful multiyear predictions of the Atlantic Meridional Overturning Circulation (AMOC). However, these claims are not justified primarily because the predictions of AMOC transport do not outperform simple reference forecasts based on climatological annual cycles. Accordingly, there is no justification for the "confident" prediction of a stable AMOC through 2014.

Full text at http://dx.doi.org/10.1126/science.1222566

Response to Comment on "Multiyear Prediction of Monthly Mean Atlantic Meridional Overturning Circulation at 26.5°N"

Daniela Matei, Johanna Baehr, Johann H. Jungclaus, Helmuth Haak, Wolfgang A. Müller, Jochem Marotzke

Vecchi *et al*. question the skill of our initialized multiyear predictions of Atlantic Meridional Overturning Circulation (AMOC), arguing that our predictions do not outperform their suggested climatological reference forecast—using a single measure of skill. We show that our initialized AMOC predictions do outperform the climatological reference forecast, using both measures of hindcast performance that were presented in our original paper.

Full text at http://dx.doi.org/10.1126/science.1223200

Published by AAAS

Denuclearization's Indirect Consequences

THE FUKUSHIMA NUCLEAR DISASTER HAS led to a global review of nuclear power. Germany has declared a complete phasing out of its 17 nuclear reactors by 2022 (*1*); the Swiss government has voted not to replace their nuclear plants, which means they all have to be decommissioned by 2034 (*2*); and the French government has committed to reducing the share of nuclear power in its energy mix.

Although we do not discount the appeal of a cleaner and nonnuclear world, we caution that widespread, rapid denuclearization may well have unintended consequences, given that nuclear power accounts for 13.5% of global electricity production (*3*). The acute shortfall from a sudden, rapid denuclearization of electricity production can only feasibly be compensated by increasing the burning of fossil fuels, resulting in much greater emissions of greenhouse gases and worsening the climate change problem. Given the current poor economic outlook in nuclear-powered economies such as Japan, the loss of nuclear expertise as an export industry and the added burden of further fossil fuel imports are likely to force these nations to abandon their emission targets. Developing emitter nations such as India and China will be even less likely to commit to extensive emission cuts.

Further down the line, the heavier involvement of major manufacturing economies, such as Japan and Germany, in the global oil and gas market could create increased market competition for these finite resources, which could in turn increase oil prices. Given that all nations pay about the same price for primary energy sources, the inflated electricity prices would hit the poorest nations the hardest. Reduction of affordable electricity access would exacerbate numerous public health, education, and gender equality problems, making it harder to meet UN Millennium Development goals.

Although there are calls to ramp up renewable energy production, it would be difficult to scale up existing technologies quickly enough to offset the deficit, given the substantial investment in required infrastructure, which cannot be recovered if the electrical generation method is changed, and the inertia that pervades the energy sector (*4*).

Most of the problems associated with nuclear power can be resolved with newer, modified technologies, which could make it safer to use. Given the value of nuclear energy in combating climatic change in the short to medium term, let's not be too hasty in phasing it out completely.

SHUN DENG FAM,[1]* DING LI YONG,[2] DANIEL NG,[3] GORDON XIONG[2]

[1]School of Archaeology and Anthropology, The Australian National University, Canberra, ACT 0200, Australia. [2]South-East Asian Biodiversity Society, Singapore, 680504, Singapore. [3]Department of Biological Sciences, National University of Singapore, 117543, Singapore.

*To whom correspondence should be addressed. E-mail: shun.deng.fam@anu.edu.au

References

1. D. Jarn, S. Korolczuk, *Environ. Polit.* **21**, 159 (2012).
2. World Nuclear Association, Nuclear Power in Switzerland (www.world-nuclear.org/info/inf86.html).
3. P. L. Joskow, J. E. Parsons. *Econ. Energ. Environ. Sci.* **1**, 99 (2012).
4. S. O. Negro, F. Alkemade, M. P. Hekkert. *Renew. Sust. Energ. Rev.* **16**, 3836 (2012).

Published by AAAS

Comment on "Multiyear Prediction of Monthly Mean Atlantic Meridional Overturning Circulation at 26.5°N"

Gabriel A. Vecchi,[1]* Rym Msadek,[1] Thomas L. Delworth,[1] Keith W. Dixon,[1] Eric Guilyardi,[2,3] Ed Hawkins,[3] Alicia R. Karspeck,[4] Juliette Mignot,[2] Jon Robson,[3] Anthony Rosati,[1] Rong Zhang[1]

Matei *et al*. (Reports, 6 January 2012, p. 76) claim to show skillful multiyear predictions of the Atlantic Meridional Overturning Circulation (AMOC). However, these claims are not justified, primarily because the predictions of AMOC transport do not outperform simple reference forecasts based on climatological annual cycles. Accordingly, there is no justification for the "confident" prediction of a stable AMOC through 2014.

Matei *et al*. (*1*) claimed that an initialized global climate model (GCM) could produce skillful multiyear forecasts of the Atlantic Meridional Overturning Circulation (AMOC) strength at 26.5°N over the time period 2004 to 2008. We show that their statistical evaluation of forecast skill is not robust, resulting largely from the limited forecast evaluation period and the use of inappropriate reference forecasts. Due to these shortcomings, we argue that the claim in (*1*) of meaningful forecast skill as a basis for making future predictions of AMOC variability is unjustified.

Since 2004, a unique and exciting observing system has been providing records of the strength of the AMOC at 26.5°N Rapid Climate Change-Meridional Overturning Circulation and Heatflux Array (RAPID-MOCHA) (*2*, *3*). Matei *et al*. use data from RAPID-MOCHA to assess the ability of a GCM (*4*) to predict the evolution of the AMOC strength after the GCM's oceanic state is "spun up" with estimates of the observed momentum and heat fluxes between the atmosphere and ocean, in an attempt to capture the initial state of the climate system at a given time (these forecasts are referred to as "initialized").

As a skill metric, Matei *et al*. use the correlation between the observed and predicted monthly AMOC strength over a year and show this metric at different leads (1 to 4 years) from four starting dates (2004 through 2007). A critical element of their analysis is the inclusion of the annual cycle in both the observations and the predictions. This is crucial because over the time period 2004 to 2008, the observed and predicted

[1]National Oceanic and Atmospheric Administration, Geophysical Fluid Dynamics Laboratory, Princeton, NJ 08540–6649, USA. [2]Universite Pierre et Marie Currie/CNRS/IRD/MNHN LOCEAN-IPSL, Paris, France. [3]National Centre for Atmospheric Sciences-Climate, Department of Meteorology, University of Reading, Reading, UK. [4]National Center for Atmospheric Research, Boulder, CO, USA.

*To whom correspondence should be addressed. E-mail: Gabriel.A.Vecchi@noaa.gov

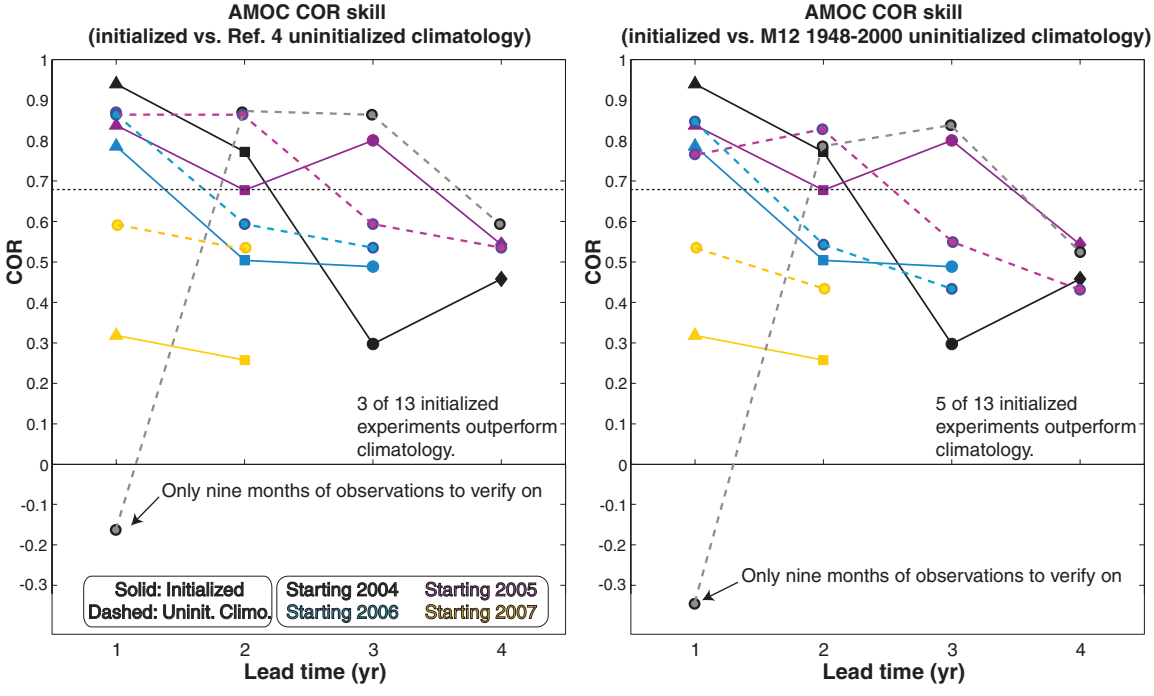

Fig. 1. Skill of initialized forecasts of AMOC strength from (*1*) against two repeating climatologies [figure adapted from figure 2 in (*1*)]. Black, violet, blue, and yellow solid lines and symbols indicate the 12-month correlation of forecasts initialized in 2004, 2005, 2006, and 2007, respectively, over the first, second, third, and fourth year of the forecast. Circles connected by a dashed line indicate the 12-month correlation of the monthly climatology of AMOC strength at 26.5°N based on the repeating climatology of uninitialized experiments with the Fifth Generation of the Max Planck Institute Atmospheric GCM (MPI-ECHAM5) model (*4*), with color coding consistent with the solid lines. The left panel shows results using the 1861 to 2000 climatology from the historical radiative forcing (20c3m) MPI-ECHAM5 model run submitted to the Third Coupled Model Intercomparison Project (CMIP3) (*13*); the right panel is based on the 1948 to 2000 uninitialized MPI-ECHAM5 (*4*) used in (*1*). The initialized forecast outperforms a repeating climatology if, for a given lead time, a symbol connected to a solid line has a higher correlation than the symbol connected to the dashed line of the same color. The 1860 to 2000 climatology (left panel) outperforms the initialized forecasts except for 2004 at Lead 1 (first black symbol, which was a year with only 9 months of observations), 2007 at Lead 3, and 2008 at Lead 4 (third and fourth violet symbols). Meanwhile, the 1948 to 2000 climatology (right panel) outperforms the initialized forecasts except for 2004 at Lead 1 (first black symbol), 2005 at Lead 1, 2007 at Lead 3, and 2008 at Lead 4 (first, third, and fourth violet symbols) and 2008 at Lead 3 (third blue symbol). Horizontal black dashed line indicates the $P = 0.1$ confidence level on correlation (*14*). [The correlations of the uninitialized climatologies to observations shown in both panels were computed by the authors of (*1*) using data of (*1*, *4*) and provided to us in the process of preparing this Comment; the correlations from the initialized experiments were taken from figure 2 of (*1*).]

AMOC is dominated by a strong annual cycle, which can inflate the apparent performance of the prediction system without any practical benefit. For example, a useful forecast of monthly mean temperatures in Europe does not consist of determining whether it will be warmer in August than February but whether it will be warmer or cooler than what we expect for a typical August.

Therefore, our baseline knowledge of the climatological mean annual cycle must be taken into account in assessing the skill of the forecasts. A typical method for removing the artificial inflation of skill from the annual cycle is to subtract a repeating climatology from observations and predictions or to work with quantities that have been averaged over a year or multiple years. Alternatively, should the mean annual cycle be retained, as was done in the Matei *et al*. analysis, we argue that a proper metric of forecast performance involves comparing the skill of the initialized forecasts against that from a simple repeating climatological annual cycle.

Figure 1 [adapted from figure 2 of (*1*)] compares the skill of the Matei *et al*. initialized forecasts of AMOC transport with the skill obtained from simply assuming a repeating climatological annual cycle. Two slightly different AMOC climatologies, both based on "uninitialized" GCM integrations (i.e., with initial conditions not constrained by observations), were used for this baseline (or "null") forecasting strategy: (i) an average over 1860 to 2000 from the GCM simulations of (*4*) and (ii) an average over 1948 to 2000 using the GCM of (*1*). For only 3 of 13 cases do the initialized forecasts have nominally larger correlation scores than the climatological null forecasts made using (*4*) (GCM climatology). Similarly, initialized forecasts outperform the Matei *et al*. climatology in only 5 of the 13 cases. Thus, there is no evidence in (*1*) of skill from these initialized AMOC forecasts.

We note that Matei *et al*. did show a comparison with uninitialized predictions from their model, but the comparison was against the average correlation over the entire record (2004 to 2008) rather than for each year individually as was done by Matei *et al*. for the "initialized" forecasts and in our Fig. 1 for both the initialized and climatological forecasts. In other words, Matei *et al*. presented an "apples-to-oranges" comparison of initialized and uninitialized predictions, whereas Fig. 1 puts them on an even footing.

The skill of the AMOC forecasts in (*1*) is no better than that from a repeating annual cycle (Fig. 1), and the skill assessment in (*1*) treats each year independently. That is, Matei *et al*. did not present any evidence of year-to-year or multiyear predictive skill in AMOC transport or its stability. Therefore, their claim that "we confidently predict a stable AMOC at least until the end of 2014" is not justified and is further contradicted by the assertion that "we cannot at present distinguish between predictability of climatological and anomalous seasonality."

We are keen to stress that the absence of meaningful skill in AMOC predictions in Matei *et al*. should not be taken as evidence of an inherent lack of AMOC predictability or that predictive skill cannot be achieved in the future. Rather, our analysis highlights the difficulty in assessing skill from a short data set. Because of its scientific merit, its likely societal importance (*5*–*7*), and the growing model-based evidence that there may be predictability of AMOC variations (*8*–*10*), we believe that it is important to build our capability to understand and predict AMOC variations and associated climatic impacts. Essential to building this capability are sustained climate observations, particularly of the AMOC. Observations from the RAPID-MOCHA array (*2*, *3*) have already identified key dynamical processes for the annual cycle of the AMOC (including some mechanisms suggested by Matei *et al*., which appear to successfully capture aspects of the annual cycle of the AMOC), and observations from the recent anomalous years will provide crucial information on processes controlling AMOC variability.

Development of our understanding of AMOC, its potential climate impact, and our future ability to predict it depends on sustained observations, the assessment and enhancement of GCMs, and improved methodologies for initializing GCMs for AMOC predictions. Finally and crucially, to ensure confidence in GCM predictions, a rigorous assessment of skill against reliable and meaningful null hypotheses is essential.

References and Notes

1. D. Matei *et al*., *Science* **335**, 76 (2012).
2. S. A. Cunningham *et al*., *Science* **317**, 935 (2007).
3. T. Kanzow *et al*., *Science* **317**, 938 (2007).
4. J. H. Jungclaus *et al*., *J. Clim.* **19**, 3952 (2006).
5. J. R. Knight, R. J. Allan, C. K. Folland, M. Vellinga, M. E. Mann, *Geophys. Res. Lett.* **32**, L20708 (2005).
6. R. T. Sutton, D. L. R. Hodson, *Science* **309**, 115 (2005).
7. R. Zhang, T. L. Delworth, *Geophys. Res. Lett.* **33**, L17712 (2006).
8. M. Collins *et al*., *J. Clim.* **19**, 1195 (2006).
9. H. Pohlmann *et al*., *J. Clim.* **17**, 4463 (2004).
10. R. Msadek, K. W. Dixon, T. L. Delworth, W. J. Hurlin, *Geophys. Res. Lett.* **37**, L19608 (2010).
11. P. J. Bickel, K. A. Doksum, *Mathematical Statistics: Basic Ideas and Selected Topics* (Holden-Day, San Francisco, 1977).
12. N. L. Johnson, S. Kotz, N. Balakrishnan, *Continuous Univariate Distributions: Volume 2* (Wiley, New York, 1995).
13. G. A. Meehl *et al*., *Bull. Am. Meteorol. Soc.* **88**, 1383 (2007).
14. We note that the $P = 0.1$ significance level indicated in figures 2 and 3 in (*1*) included an error that we correct in our version [the single-sided Student's t test applied in (*1*) erroneously used the sample size, rather than the sample size minus two (*11*), as the degrees of freedom in the test]. The significance threshold changes from 0.55 to 0.69. A similar number (0.68) is found using the full distribution of the correlation coefficient (*12*) instead of its Student's t approximation. Similarly, the significance level in figure 3 in (*1*) should be 0.8.

Acknowledgments: We are grateful to Matei *et al*. for cordial discussions and exchanges in the process of preparing this Comment. We thank G. Danabasoglu, S. Griffies, W. Hazeleger, T. Knutson, J. Lanzante, G.-J. van Oldenborgh, and G. Villarini for useful comments. J.M. and E.G. were supported by the Gestion des Impacts du Changement Climatique Programme (GICC) under the Evaluation de la Prévisibilité Interannuelle à Décennale à partir des Observations et des Modèles (EIPDOM) project funded by MEDDTL (French Minister of Ecology and Sustained Development). A.K. was supported by the National Oceanographic and Atmospheric Administration under the Climate Variability and Predictability Program (NA09OAR4310163) and through a cooperative agreement with GFDL (NA06OAR4310119). J.R. received financial support from the NERC VALOR project.

28 March 2012; accepted 31 August 2012
10.1126/science.1222566

Response to Comment on "Multiyear Prediction of Monthly Mean Atlantic Meridional Overturning Circulation at 26.5°N"

Daniela Matei,[1]* Johanna Baehr,[2] Johann H. Jungclaus,[1] Helmuth Haak,[1] Wolfgang A. Müller,[1] Jochem Marotzke[1]

Vecchi *et al*. question the skill of our initialized multiyear predictions of Atlantic Meridional Overturning Circulation (AMOC), arguing that our predictions do not outperform their suggested climatological reference forecast—using a single measure of skill. We show that our initialized AMOC predictions do outperform the climatological reference forecast, using both measures of hindcast performance that were presented in our original paper.

In Matei *et al*. (*1*), we demonstrated multiyear predictability of monthly mean strength of Atlantic Meridional Overturning Circulation (AMOC). We established the skill of our initialized AMOC predictions not only from high anomaly correlation (COR) but also from a more realistic amplitude of AMOC variations quantified by root-mean-square (RMS) variability. We diagnosed the skill improvement from the initialization by testing hindcast simulations against a persistence forecast based on observations (*2*, *3*) and against a forecast with the uninitialized coupled model for the same forecast period (*4*).

Vecchi *et al*. (*5*) now propose a reference forecast based on a repeated seasonal cycle of the uninitialized coupled model (CLIMREF hereafter) (*6*). Vecchi *et al*. find that our initialized AMOC predictions outperform CLIMREF in only 5 of 13 cases, using COR as the sole skill measure (their figure 1) (*7*). However, a high COR skill just indicates a substantial phase coherence between the observed and hindcasted AMOC variations.

Here, we reply to Vecchi *et al*. by showing for CLIMREF both measures of hindcast performance presented in (*1*). In (*1*), we analyzed, in addition to COR, RMS variability. We used RMS variability, even though it is not strictly a skill score, because the original submission combined the correlation and RMS analysis by showing Taylor diagrams (*8*). In an attempt to simplify the presentation, we switched in the review process to a representation of COR and RMS analysis in separate plots [(*1*), figure 2 and fig. S2, respectively]. As already discussed in (*1*) concerning individual hindcasts and ensemble mean, there appears to be a tension between obtaining high correlation skill and high enough RMS variability.

Because correlation and RMS variability combine geometrically to RMS error (RMSE) with an overall bias removed (*8*), we now summarize the two measures of hindcast performance used in (*1*) to RMSE. Specifically, we compute the RMSE skill score (*9*) using CLIMREF as a reference forecast. With the RMSE skill score, our initialized AMOC predictions outperform CLIMREF in 8 of 13 cases (Fig. 1). With this demonstration that the model initialization leads to a substantial reduction in forecast error, we maintain that the conclusions about AMOC predictive skill as stated in (*1*) are justified.

We also test CLIMREF against the updated observational record (Table 1), verifying the AMOC predictions that we made in (*1*). Using COR, our initialized AMOC predictions outperform CLIMREF in 14 of 22 cases. Using the RMSE skill score, our initialized AMOC predictions outperform CLIMREF in 16 of 22 cases. Hence, with a larger sample size, our initialized AMOC predictions clearly outperform CLIMREF more often than not, using the RMSE skill score and even using COR as a sole measure of skill.

In conclusion, we have shown that with a combination of correlation and root-mean-square skill measure, as in (*1*), our ocean initialization results in AMOC prediction skill enhancement over the alternative reference forecast proposed by Vecchi *et al*. Also, as we showed in (*1*), we do understand where the skill enhancement arises from: It is the initialization of the upper-ocean zonal density difference. Therefore, we maintain that the conclusions about AMOC predictive skill as stated in (*1*) are robust.

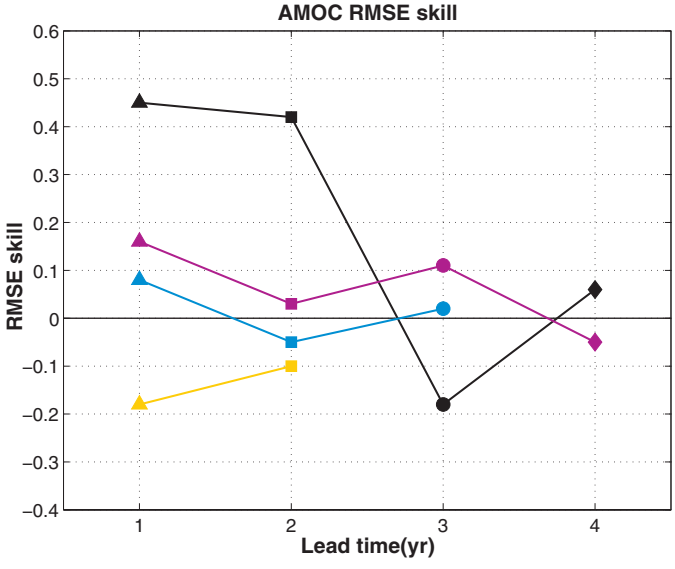

Fig. 1. RMSE skill scores of AMOC with respect to the CLIMREF forecast. RMSE skill scores for the ensemble mean hindcasts started in January 2004, January 2005, January 2006, and January 2007 are shown by black, violet, blue, and yellow filled symbols, respectively, connected by solid lines.

Table 1. Comparison of COR and RMSE skill scores of AMOC against CLIMREF for different lengths of the RAPID time series [4/2004 to 12/2008 as used in (*1*), and an extension until 12/2010].

AMOC skill measure	Number of AMOC predictions from (*1*) outperforming CLIMREF, using RAPID (4/2004 to 12/2008)	Number of AMOC predictions from (*1*) outperforming CLIMREF, using RAPID (4/2004 to 12/2010)
COR skill	5 of 13	14 of 22
RMSE skill score	8 of 13	16 of 22

[1]Max Planck Institute for Meteorology, Bundesstrasse 53, 20146 Hamburg, Germany. [2]Institute of Oceanography, KlimaCampus, University of Hamburg, Bundesstrasse 53, 20146 Hamburg, Germany.

*To whom correspondence should be addressed. E-mail: daniela.matei@zmaw.de

References and Notes

1. D. Matei *et al*., *Science* **335**, 76 (2012).
2. S. A. Cunningham *et al*., *Science* **317**, 935 (2007).
3. T. Kanzow *et al*., *Science* **317**, 938 (2007).
4. Because our model underwent some technical changes since the Coupled Model Intercomparison Project phase 3 (CMIP3), we constructed and used in (*1*) a different 20th-century realization from that in the CMIP3 archive (*10*).
5. G. A. Vecchi *et al*., *Science* **338**, 604 (2012); www.sciencemag.org/cgi/content/full/338/6107/604-c.
6. Vecchi *et al*. motivate their alternative reference forecast by arguing that the reference forecasts used in (*1*) ignored the issue of a repeating annual cycle. Although both reference forecasts used in (*1*) do include baseline knowledge of seasonality, we stand by our discussion in (*1*) that the limitation of observational record to half a decade does not allow a robust estimation of the seasonal cycle from the observations (*11*, *12*); we therefore decided to keep the seasonal cycle in both modeled and observed AMOC time series and investigated the predictability of the full AMOC signal using monthly means. As already discussed in (*1*), the observed AMOC seasonal cycle with a maximum in October and a minimum in April has highly nontrivial causes (*11*, *12*). The representation of the AMOC seasonal cycle in the model, and the improvement of monthly mean predictions of the AMOC strength through initialization, should therefore not be considered straightforward.
7. Figure 1 in (*5*), and the associated note 14, prompted us to revisit the computation of the significance level. In (*1*), we have computed the significance level using a single-sided *t* test taking into account the serial autocorrelation of both time series. However, because the determination of the effective number of degrees of freedom (df) in short time series is associated with uncertainty (*13*), we have repeated our significance test by constructing an empirical probability density function of correlations. We have calculated the correlations of each year of monthly means of the observed AMOC with the 350 years of uninitialized runs of our model. The 10% significance level now lies at a correlation value of 0.61, compared with 0.55 in the paper. In a similar way, we have reestimated the 10% significance level for the correlation skill of upper-mid-ocean transport and upper-ocean zonal density difference to be 0.65 and 0.67, instead of 0.6 used in the original paper. Hence, we should have been slightly more conservative, but this modification does not change the conclusions drawn from both figures 2 and 3 of (*1*).
8. K. E. Taylor, *J. Geophys. Res.* **106**, (D7), 7183 (2001).
9. The RMSE skill score (*14*) is defined as $RMSE_{\mathrm{skill}} = 1 - \frac{RMSE_{\mathrm{hindcast}}}{RMSE_{\mathrm{CLIMREF}}}$.
10. J. H. Jungclaus *et al*., *J. Clim.* **19**, 3952 (2006).
11. T. Kanzow *et al*., *J. Clim.* **23**, 5678 (2010).
12. M. P. Chidichimo, T. Kanzow, S. A. Cunningham, W. E. Johns, J. Marotzke, *Ocean Sci.* **6**, 475 (2010).
13. H. von Storch, F. W. Zwiers, *Statistical Analysis in Climate Research* (Cambridge University Press, Cambridge, 1999), p. 484.
14. I. T. Jolliffe, D. B. Stephenson, *Forecast Verification. A Practitioner's Guide in Atmospheric Science* (Wiley and Sons, Chichester, UK, 2003), p. 240.

Acknowledgments: This work was supported by the Bundesministerium für Bildung und Forschung North Atlantic project (D.M.) and the Deutsche Forschungsgemeinschaft–funded Cluster of Excellence CliSAP (J.B. and W.A.M.). All model simulations were performed at the German Climate Computing Centre (DKRZ). Data from the RAPID-WATCH MOC monitoring project are funded by the Natural Environment Research Council and are freely available from www.noc.soton.ac.uk/rapidmoc.

7 May 2012; accepted 31 August 2012
10.1126/science.1223200

MEDICAL GENETICS

Healing Through Heredity

Angela N. H. Creager

Medical genetics is often represented as a baby boomer field, emerging only after the postwar decline of its pseudoscientific, unsavory predecessor, the eugenics movement. Nathaniel Comfort dismantles this comfortable but misleading myth in *The Science of Human Perfection*, his beautifully written account of how genes became central to American medicine. The pedigree of medical genetics, he conclusively shows, leads right back to eugenics, defined by its proponent Charles Davenport as "the science of human improvement through better breeding." In part, this was because eugenics has always been tightly linked to preventive medicine and public health. In illuminating the neglected connections between eugenics and medicine during the first half of the 20th century, Comfort (a historian of science at Johns Hopkins University) expands on existing scholarship—such as Daniel Kevles's widely read *In The Name of Eugenics* (*1*)—in important ways.

The Science of Human Perfection
How Genes Became the Heart of American Medicine
by Nathaniel Comfort
Yale University Press, New Haven, CT, 2012. 334 pp. $35, £25. ISBN 9780300169911.

Standard works on American eugenics revolve around the Eugenics Record Office (ERO) at Cold Spring Harbor, which Davenport founded and Harry H. Laughlin managed. The ERO was both a research site—collating hundreds of family pedigrees collected by its field workers to create the "Trait Book"—and a clearinghouse for popular publications and organizations advocating the control of human breeding. Comfort covers these canonical developments but also casts a wider net, examining the contributions of economist Irving Fisher, who created the Race Betterment Foundation, and Raymond Pearl, a statistician who founded the Division of Medical Genetics at Johns Hopkins. From the outset, he argues, eugenics drew its energy from middle-class health reform and evangelical self-improvement, not only from racism or elitism. Those who were committed to eugenics were initially equally enthused about public health and euthenics (improvement of the environment), although by the 1920s improving human genetic stock began to predominate in considerations of what was then called race hygiene.

The reckless overreach of Laughlin at the ERO, in conjunction with the chilling Nazi racial policies, discredited eugenics. However, the search for hereditary determinants of human conditions continued unabated in the United States. Even negative eugenics did not disappear, but its target became "health rather than sociality," as Comfort puts it. The torch was initially passed to physicians who oversaw the founding of a handful of heredity clinics in the 1940s. Most trained geneticists had already turned to better experimental subjects: flies, maize, mice, and, increasingly, microbes. After 1947, the newly founded Atomic Energy Commission became the main patron of genetics, because its atomic weapons program and push for civilian nuclear power made the human costs of exposure to ionizing radiation an urgent issue. The postwar focus on mutation clearly reflects the legacy of the involvement of this government agency in human genetics, as could still be seen in the sponsorship of the Human Genome Project by the Department of Energy.

Comfort stresses the longdurée continuities that animated medical genetics. Into the 1960s, researchers in human genetics continued to draw on two approaches that dated to the turn of the 20th century. One, the biometrical orientation, traced back to Francis Galton's initial work on eugenics. This quantifying approach tended to posit, in analogy with the germ theory, hereditary causes of disease, or genes as "seeds of disease." The other, derived from Archibald Garrod, stressed inborn errors of metabolism; its emphasis on constitutionalism and predisposition can be understood in terms of genes as the soil on which the seeds fell. After becoming the Galton Professor at University College London in 1965, biochemist Harry Harris brought the Garrodian and Galtonian strands together through his pioneering work on enzyme polymorphisms in human populations. In addition, in his 1963 reissue of Garrod's *Inborn Errors of Metabolism* (*2*), he pointed to DNA as the principal material of heredity (*3*).

Comfort is an astute commentator on what James Watson and Francis Crick's 1953 paper meant—and what it didn't—for medical research. To stake a claim on the centrality of the double helix did not answer the question of why and how genes cause disease, knowledge that often relied on laborious biochemistry and cell biology. Comfort discusses several well-known developments that reinforced the relevance of molecular genetics to medicine, though he only gestures to the explosion of research in the 1970s and 1980s that made use of techniques for somatic cell genetics, mapping, and sequencing. In effect, only in the era of the Human Genome Project did *Homo sapiens* begin to catch up with other model organisms whose molecular genetics had been studied for decades. The genetic code was cracked with *E. coli*, not John Doe.

Above all, Comfort is interested in the people who shaped medical genetics, their motivations and methods. He offers vivid

CREDIT: OSULEO/ISTOCKPHOTO.COM

The reviewer is at the Department of History, Princeton University, 136 Dickinson Hall, Princeton, NJ 08544–1017, USA. E-mail: creager@princeton.edu

Published by AAAS

biographical sketches of towering figures such as internist Victor McKusick (author of the catalog *Mendelian Inheritance in Man*) as well as lesser-known contributors such as blood-group geneticist Laurence Snyder. Comfort does not provide a comprehensive history of human genetics; the role of key techniques and tools, particularly in the molecular era, likewise remains to be written. But the book covers much ground and accomplishes a great deal in a spare 246 pages of text. Given how radically its author recasts the history of American eugenics, *The Science of Human Perfection* is a remarkably unpolemical work. Comfort does not seek to rehabilitate eugenics, but he does compel the reader to recognize that the American impulse to improve health through science was a key ingredient of eugenics and remains a driver of medical genetics today.

References

1. D. J. Kevles, *In the Name of Eugenics: Genetics and the Uses of Human Heredity* (Knopf, New York, 1985).
2. A. E. Garrod, *Inborn Errors of Metabolism* (H. Froude and Hodder and Stoughton, London, 1909).
3. H. Harris, in *Garrod's Inborn Errors of Metabolism*, H. Harris, Ed. (Oxford Univ. Press, London, 1963), pp. 120–183.

10.1126/science.1230490

THEORETICAL BIOLOGY

Benefits and Perils of Synthesis

Manfred D. Laubichler

In the preface to his seminal *What Is Life?* Erwin Schrödinger recognized a predicament facing those who attempt a grand synthesis rather than remain on the safe ground of their narrow fields of specialization: "I see no other escape from this dilemma (lest our true aim be lost forever) than that some of us should venture to embark on a synthesis of facts and theories, albeit with second hand and incomplete knowledge of some of them—and at the risk of making fools of ourselves" (*1*). As it turned out, Schrödinger was no fool (at least not with regard to his insights into the fundamental principles of science).

In *Cells to Civilizations*, Enrico Coen, a plant developmental biologist at the John Innes Center and author of the acclaimed *The Art of Genes* (*2*), takes his inspiration (albeit not explicitly) from Schrödinger. This attempt at a grand theoretical synthesis within biology explores the transformative powers and creative forces that have brought about the living world from the first cells to the latest developments in cultural and technological evolution.

Coen focuses on similarities (without ignoring the differences) among four major processes of life: evolution, development, learning, and culture. He argues that all four domains are governed by a set of seven fundamental principles. These generative mechanisms bring about novel solutions to life's challenges and therefore account for the diversity and persistence we observe today and throughout the history of life. By formulating those principles on the basis of their functional roles rather than their historically contingent origins, he aims to develop a unifying theory of transformation or of phenotypic evolution in its most inclusive meaning.

Cells to Civilizations
The Principles of Change That Shape Life
by Enrico Coen
Princeton University Press, Princeton, NJ, 2012. 340 pp. $29.95, £19.95. ISBN 9780691149677.

The first four principles reformulate the basic argument for evolution by means of natural selection. All systems that show population variation, persistence (a more general formulation for heredity), reinforcement (capturing the cumulative effects of selection), and competition will change through time and develop creative solutions to environmental challenges. The next three principles can best be illustrated (more as a matter of convenience than intuition) in the context of development. Here we have cooperation (among parts at all levels and among levels), combinatorial richness (as a result of interactions among modular elements), and recurrence. The third accounts for the cumulative effects of history, both within a system and in its complex interactions with multiple environments (for example, think niche construction, canalization, and constraints). The bulk of the book offers an exposition of these principles as they apply to evolution, development, learning, and culture.

Coen responds to a real and damaging lack of theory within the biological sciences, which are still largely dominated by empiricism in overdrive. With few accepted general principles, the life sciences have developed a large number of domain-specific generalizations and concepts. Complexity theory represents one recent unifying attempt, but its core abstractions are difficult to communicate (*3*). What has been missing is a clearly formulated conceptual framework that lucidly communicates the deep unity of life's fundamental properties and processes.

Throughout the book, to convey complex conceptual abstractions Coen illustrates his arguments with references to and discussions of art. This is more than just pedagogy—cultural transformations are, after all, squarely within the purview of his synthesis. Transformations in artistic expression—for example, those visible in the versions of the *Portrait of Ambroise Vollard* by Paul Cézanne (1899) and Pablo Picasso (1909)—can be understood as a case of cultural evolution governed by a domain-specific application of the seven processes. Coen thus proposes a fundamental isomorphism between art and nature, which places him in a lineage of thinkers that includes such biologist-artists as Johann Wolfgang von Goethe and Ernst Haeckel.

Does Coen succeed in providing a unified view of "life's remarkable transformative powers"? Yes and no. It would be foolish to expect that one short book could contain all the answers, and incomplete knowledge of all the intricate details necessarily leads to some misguided assumptions and claims. Coen is clearly on solid ground in his discussions of development, but experts in any of the other three domains will inevitably find some of his interpretations or metaphors problematic. Still, this does not invalidate his daring attempt at synthesis.

Focusing on the problem of inheritance and evolution from a physicist's point of view, Schrödinger was able to see more clearly some fundamental theoretical aspects and formulate those more precisely than most biologists of his time (who were burdened by a plethora of often confusing details). Similarly, Coen attempts to highlight the underlying unity and generality of processes that not only generate variation and novelty at all stages of life's drama but also select among those creative solutions. His eloquently written book offers a programmatic synthesis and an empirically grounded proposal for a theory of biology. Will this be the last word? Most certainly not, but *Cells to Civilizations* will stimulate many productive discussions about the origins and development of life in all its complexities.

References

1. E. Schrödinger, *What Is Life? The Physical Aspect of the Living Cell* (Cambridge Univ. Press, Cambridge, 1944).
2. E. Coen, *The Art of Genes: How Organisms Make Themselves* (Oxford Univ. Press, Oxford, 2000).
3. D. C. Krakauer *et al.*, *J. Theor. Biol.* **276**, 269 (2011).

10.1126/science.1222822

The reviewer is in the School of Life Sciences and the Center for Biology and Society, Arizona State University, Tempe, AZ 85287–4501, USA. E-mail: manfred.laubichler@asu.edu

SCIENCE AND GOVERNMENT

Obama and the Promotion of International Science

Has the U.S. president's record on promoting international science fulfilled the promise of his early rhetoric?

Thomas J. Bollyky[1]* and Paul L. Bollyky[2]

Six months after his 2009 inauguration, U.S. President Obama spoke at Cairo University in Egypt and called for a new beginning in relations between the United States and Muslim-majority countries, defined by collaboration in science and technology (*1*). Innovation, according to the president, is the "currency of the 21st century" and the means by which the United States and its partners would create new jobs and tackle the global challenges of climate change, hunger, and disease. The Cairo speech remains a seminal moment in President Obama's broader initiative to ramp up U.S. cooperation in international science as a core component of his foreign policy agenda (*2*).

On the eve of the next U.S. presidential election, now is an opportune moment to evaluate whether the Obama Administration's record on promoting international science has fulfilled the promise of its early rhetoric. This question will be considered through the lenses of diplomacy, international development, and the operational requirements for scientific exchange. For this analysis, we, like the president, refer to international scientific cooperation in its broadest sense, including not only research but also capacity-building and the application of technological innovations to achieve global goals.

President Obama speaks at Cairo University. In his speech, he promoted international science cooperation to create new jobs, tackle global challenges, and provide a basis for a new beginning between the United States and Muslim-majority countries.

Diplomacy and International Development

Although U.S. science diplomacy dates back to the Cold War and détente, its use to promote international scientific collaboration has expanded under the Obama Administration (*3*). The U.S. Department of State enlisted eminent U.S. scientists, including Nobelist Ahmed Zewail and Bruce Alberts, editor-in-chief of *Science*, to serve as envoys to engage and collaborate with their counterparts in Africa, Asia, and the Middle East. The White House established high-level joint commissions on science and technology with Brazil, China, India, Japan, Russia, and South Korea. The U.S. Department of Energy launched a cofunded, $150 million United States–China Clean Energy Research Center to promote collaboration, protection of intellectual property, and advanced technology development. The Obama Administration founded networks of foreign-born U.S. researchers, engineers, and entrepreneurs to encourage collaboration and to promote the spread of scientific values, such as meritocracy and transparency, in their countries of origin (*4*). An expanded corps of Environment, Science and Technology, and Health officers at U.S. embassies supports these diplomatic initiatives.

The integration of science and foreign policy objectives under the Obama Administration, however, has not been seamless. The Central Intelligence Agency's use of a fake hepatitis B immunization campaign to identify Osama bin Laden's whereabouts sparked violence against World Health Organization workers and a ban on polio immunization in parts of Pakistan (*5*), threatening the same 24-year, nearly $10 billion polio eradication campaign on which President Obama proposed in Cairo that the United States and Muslim-majority countries should collaborate.

Obama Administration efforts to integrate science into its international development policies build on a long and distinguished history that includes expanding access to HIV/AIDS drugs, increasing global agriculture production through the Green Revolution, and reducing child mortality from cholera and diarrhea with oral rehydration therapy. Nonetheless, the current administration has distinguished itself in the degree to which it has promoted science and technology as the best means to achieve its development objectives (*6*). The U.S. Agency for International Development (USAID) hired its first Science and Technology Adviser since the 1980s, created the post of Chief Innovation Officer, and recruited dozens of scientists. In

[1]Council on Foreign Relations, Washington, DC 20006, USA. [2]Division of Allergy and Infectious Diseases, University of Washington, Seattle, WA 98195, USA.

*Author for correspondence. E-mail: tbollyky@cfr.org

Published by AAAS

2007, USAID had five Science and Technology Policy Fellows sponsored by the American Association for the Advancement of Science; today, it has 54 fellows, including 11 deployed overseas (*7*). USAID also instituted the Grand Challenges program, which leverages outside funding to support domestic and international research on U.S. development priorities, and the Development Innovation Ventures fund, which provides seed capital to high-risk, high-return development-friendly technologies (*8*, *9*). The U.S. Department of Agriculture (USDA) participates in the USAID-led Feed the Future initiative and sought to orient its funding priorities toward research that would yield compound benefits for U.S. agriculture and global food security (*10*). Although these programs involve modest funds, they are an important foundation for future work.

Requirements for Scientific Exchange

In comparison with its progress on scientific diplomacy and international development, the Obama Administration yet had only modest success in facilitating the collaborations that account for the majority of cooperation between U.S. scientists and their foreign counterparts.

Most international science is self-organizing (*11*). Government-directed international research initiatives, such as ITER (formerly the International Thermonuclear Energy Reactor) and the Human Genome Project, are rare. Most U.S. government agencies, such as the National Science Foundation (NSF) and USDA, predominantly or exclusively fund U.S. researchers. Scientists pursue collaborations, international or otherwise, to share costs and access the best minds, equipment, and data. Improved information communication technologies and cheaper travel have made these collaborations easier. More than a third of the research papers produced globally now have coauthors from multiple countries, twice the share in 1990 (*12*). As emerging countries, such as China, dramatically increase their research and development (R&D) expenditures, international collaborations have become increasingly diverse geographically (*13*).

It is too soon to know whether these self-organizing international scientific collaborations have increased during the Obama Administration. The U.S. National Institutes of Health (NIH), NSF, and other U.S. government agencies that fund scientific research do not systematically track the international collaborators of their domestic grantees. Coauthored publications are a lagging indicator of international scientific cooperation, coming months or, more often, years after the collaboration formed.

It is not too early, however, to assess U.S. government policies on ensuring the operational requirements of international science: funding, quality data, and talent.

Since 2009, U.S. government R&D budgets under the Obama Administration, have remained stagnant or have declined, in the case of National Aeronautics and Space Administration (NASA), amid high unemployment and a poisonous political environment in the U.S. Congress. Reduced or stagnant R&D funding, of course, limits the opportunities for U.S. researchers to engage in international collaboration. The budgets of the few U.S. government agencies that fund international researchers directly have likewise flat-lined. For example, international research expenditures of the global-minded National Institute of Allergy and Infectious Diseases (NIAID) have remained roughly constant since 2008, after a fourfold increase over the prior decade (supplementary materials). USDA's International Science and Education program, which provided grants to U.S. researchers to engage in international collaboration, has been defunded (*14*). One exception is the USAID and NSF-supported Partnership for Enhanced Engagement in Research (PEER), which provides modest funding for non-U.S. researchers to work with U.S. counterparts on research on international development issues (*15*). Although small in scale, PEER represents an important departure from the Bush Administration, which did not, as a matter of policy, fund foreign researchers as part of its international scientific cooperation initiatives (*16*).

In comparison with the billions of dollars devoted through the U.S. President's Emergency Plan for AIDS Relief (PEPFAR) and the Feed the Future program to delivering treatment and sustenance to the world's poor, the Obama Administration has underinvested in the research capacity, regulatory oversight, and training that would enable developing country researchers to produce quality data, collaborate, and address their own health and development needs. Such investments would facilitate existing U.S. global health and development initiatives and encourage future research in these countries (*17*, *18*). Modest seed funding would likewise help engage female scientists, underrepresented in international collaborations generally, in U.S. development initiatives on women and girls (*19*). The Medical Education Partnership Initiative, a new U.S. interagency program to support operational medical research and education in Africa, is a step in the right direction (*20*). The NSF Global Research Council, an initiative to promote the quality and compatibility of international research, likewise deserves support (*21*).

Cumbersome immigration processes and visa shortages continue to hinder the face-to-face interactions that scientists need to connect and collaborate. The Obama Administration streamlined the Mantis clearance process for U.S. visa applicants with experience working with nuclear, chemical, and biological materials, but it remains a challenge to U.S. conference attendees and organizers (*22*). Although F-1 student visas have increased nearly 25% since 2009, the number of H-1B work visas available for scientists, programmers, and engineers has remained stuck at 65,000 since 2004 (*23*). Restricting the ability of foreign-born scientists and engineers to travel to and work in the United States undermines continued U.S. scientific leadership. It also deprives the United States of its greatest ambassadors: the living testimonials to the research and economic opportunities that America provides.

A Work in Progress

Four years after being elected, the Obama Administration's initiative on international scientific collaboration remains a work in progress. According to the Pew Global Attitudes Project, approval of the United States has declined in Muslim-majority countries since 2009, from 25 to 15%, with U.S. drone attacks and the unresolved Israeli-Palestinian conflict among the cited reasons (*24*). Meanwhile, admiration of U.S. scientific and technological prowess in these countries has remained high (*24*). Building on the international respect for American science to create good will toward U.S. policies is smart. Investing in the immigration reforms, international research, and capacity-building that would help ensure that the best scientific minds come together to address the biggest global challenges is even smarter. Both are laudable goals for a future administration.

References and Notes

1. B. H. Obama, Remarks by the President on a New Beginning, Cairo University, Cairo, Egypt, 4 June 2009.
2. B. H. Obama, Remarks by the President at the National Academy of Sciences Annual Meeting, 27 April 2009.
3. R. D. Hormats, *Sci. Diplomacy* no. 2 (March 2012).
4. Office of the Spokesman, U.S. Department of State, Department of State Announces Two New Science Outreach Platforms, 26 July 2012; www.state.gov/r/pa/prs/ps/2012/07/195525.htm.
5. O. Levine, L. Garrett, The fallout from the CIA's vaccination ploy in Pakistan, *Washington Post*, 15 July 2011.
6. R. Shah, remarks for Conference on science, technology, and innovation in development, USAID, Washington, DC, 13 to 14 July 2010.
7. R. Shah, Remarks by USAID Administrator Rajiv Shah at the University of Michigan, 28 September 2012.

8. USAID, Grand Challenges for Development (2012); www.usaid.gov/grandchallenges/.
9. USAID, Development Innovation Ventures (2012); www.usaid.gov/what-we-do/science-technolog-and-innovation/development-innovation-ventures.
10. National Institute of Food and Agriculture, U.S. Department of Agriculture (USDA), Global Engagement: NIFA and Feed the Future (2012); www.csrees.usda.gov/nea/international/in_focus/intl_if_feed_future.html.
11. C. Wagner, *The New Invisible College: Science for Development* (Brookings Institution Press, Washington, DC, 2008).
12. The Royal Society, *Knowledge, Networks, and Nations: Global Scientific Collaboration in the 21st Century* (The Royal Society, London, 2011).
13. National Science Board, *National Science and Engineering Indicators 2012* (National Science Foundation, Arlington, 2012).
14. USDA, Grants: International Science and Education (ISE) Competitive Grants Program (2011); http://nifa.usda.gov/fo/internationalscienceandeducation.cfm.
15. USAID, USAID and the National Science Foundation expand PEER Global Researcher Program to new countries and development challenges, 11 September 2012; www.usaid.gov/news-information/press-releases/usaid-and-national-science-foundation-nsf-expand-peer-global.
16. D. D. Stine, *Science, Technology, and American Diplomacy: Background and Issues for Congress* (Congressional Research Service, Washington, DC, 2009).
17. T. J. Bollyky, *Safer, Faster, Cheaper: Improving Clinical Trials and Regulatory Pathways to Fight Neglected Diseases: Report of Center for Global Development Working Group on Clinical Trials and Regulatory Pathways* (Center for Global Development, Washington, DC, 2011).
18. T. J. Bollyky, *Intellectual Property Rights and Climate Change: Principles for Innovation and Access to Low-Carbon Technology* (Center for Global Development, Washington, DC, 2009).
19. L. M. Frehill, S. Vlaicu, K. Zippel, paper presented at International Workshop on International Scientific Collaborations, Arlington, VA, 23 October 2010, http://nuweb.neu.edu/zippel/nsf-workshop/docs/NSF_PI_Study_Oct23_2010.pdf.
20. F. Collins *et al.*, *Science* **330**, 1324 (2010).
21. S. Suresh, *Science* **336**, 959 (2012).
22. V. C. Johnson, *A Visa and Immigration Policy for the Brain-Circulation Era* (National Association of Foreign Student Advisers, Washington, DC, 2009).
23. U.S. Citizenship and Immigration Services, H-1B Specialty Occupations, DOD Cooperative Research and Development Project Workers, and Fashion Models (2012); www.uscis.gov.
24. Global Attitudes Project, Pew Research Center, Global Opinion of Obama Slips, International Policies Faulted (Pew Research Center, Washington, DC, 2012).

Supplementary Materials
www.sciencemag.org/cgi/content/full/338/6107/610/DC1

10.1126/science.1230970

PUBLIC HEALTH

Optimizing Investments in Malaria Treatment and Diagnosis

Better targeting of antimalarials to people who need them will maximize the impact of interventions in the private sector.

Justin M. Cohen,[1]* Aaron M. Woolsey,[1] Oliver J. Sabot,[1] Peter W. Gething,[2] Andrew J. Tatem,[3] Bruno Moonen[1]

The Roll Back Malaria (RBM) Partnership has set an ambitious target of achieving near zero deaths from malaria by 2015 (*1*). Scale-up of insecticide-treated nets, indoor residual spraying of insecticide, and increased access to treatment with artemisinin-based combination therapies (ACTs) over the past decade have led to reductions in malaria incidence of more than 50% in 43 countries, including 8 in Africa (*2*). However, as an estimated 655,000 malaria deaths still occurred in 2010 (*2*), with the great majority in sub-Saharan Africa, substantial challenges remain.

Prominent among these challenges is the fact that the private sector is an important source of treatment for suspected malaria in many countries, but drugs available there are primarily composed of affordable, yet often ineffective, monotherapies (*3*, *4*). ACTs, the recommended first-line treatment for malaria (*5*), are often prohibitively expensive outside of the public sector (*6*), and drug quality is often poor (*7*). Beginning in 2009, the Affordable Medicines Facility for Malaria (AMFm), a "factory-gate" subsidy for ACTs, represented one prominent effort to increase access to effective drugs even in the private sector. The first phase of that program ends this year, and initial evaluation suggests that it was largely successful in increasing availability and affordability of ACTs in most, although not all, participating countries, particularly in the private sector (*8*). Regardless of whether the AMFm initiative continues, the RBM Partnership will confront critical questions about the future of overall diagnosis and treatment strategies, especially regarding how to engage with the private sector.

These decisions will be made in the context of a rapidly evolving epidemiological and financial landscape. Malaria burden varies greatly from country to country, which leads to goals of elimination in Zanzibar (*9*) and Swaziland (*10*), even as incidence rates have remained consistently high in parts of West and Central Africa (*11*). Resistance to artemisinin-based drugs has been detected in Southeast Asia (*12*, *13*). Availability of the artemisinin monotherapies that may promote resistance in Africa has been found to range widely, from virtually absent in Madagascar to nearly half of drug shops sampled in Nigeria (*3*). Targeting resources properly and maximizing their effectiveness has been rendered even more crucial by the fact that international donations for malaria control declined in 2012 for the first time in a decade (*14*).

Improved diagnosis has led to steep declines in reported malaria incidence and presumptive treatment in regions of Senegal (*15*) and Tanzania (*16*), where malaria makes up only a small fraction of febrile disease (*15*). However, there are still many places where febrile illness is assumed to be synonymous with malaria (*17*). Because many private-sector outlets are drug shops that sell medications without confirmatory diagnosis, it is likely that a substantial fraction of antimalarials obtained through the private sector are taken for nonmalarial illnesses, which limits their impact.

Analysis of Private-Sector Antimalarial Demand

Increased focus on private-sector antimalarial markets through the work of groups like ACTwatch (*18*) and evaluation activities surrounding the AMFm (*8*) have begun to provide data that we have used to better understand the volume of antimalarials distributed through the private sector, the importance of the private sector in treating febrile disease, and the number of malaria infections reached

[1]Clinton Health Access Initiative, Boston, MA 02127, USA. [2]Spatial Ecology and Epidemiology Group, Department of Zoology, University of Oxford, Oxford OX1 3PS, UK. [3]Emerging Pathogens Institute and Department of Geography, University of Florida, Gainesville, FL 32610, USA.

*Author for correspondence. E-mail: jcohen@clintonhealthaccess.org

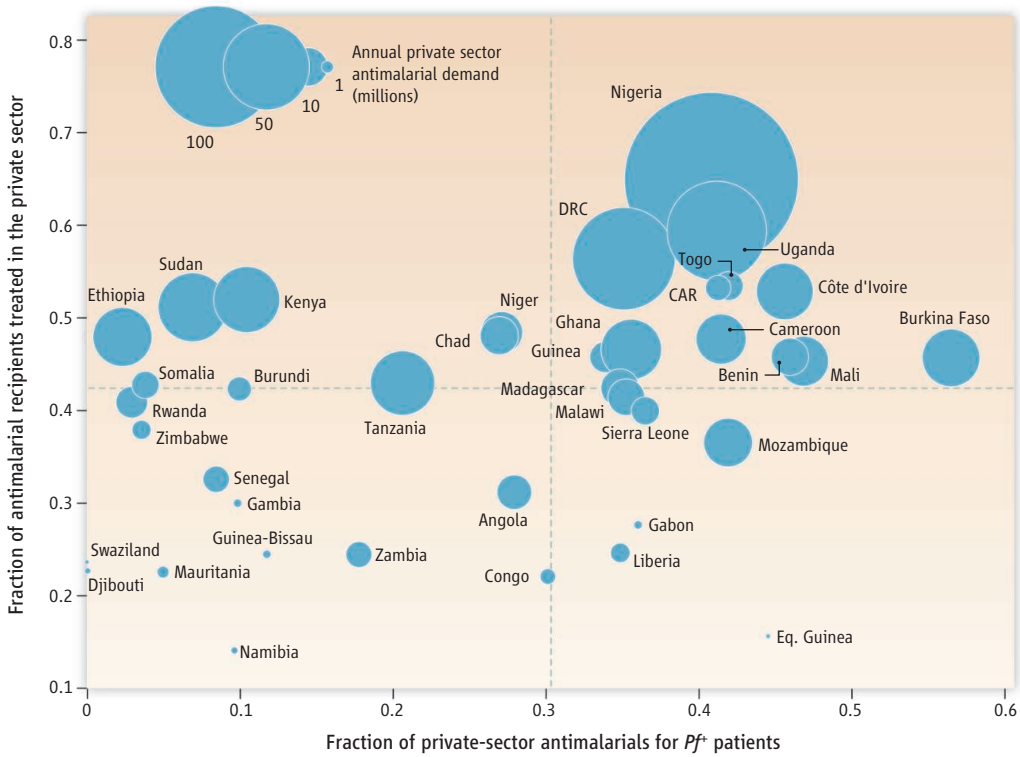

Private-sector patients receive antimalarials for malaria or fever. Distribution of sub-Saharan African countries by the fraction of antimalarial recipients estimated to be positive for *P. falciparum* (*x* axis), the relative importance of the private sector for febrile treatment (*y* axis), and the overall size of the private-sector antimalarial market (bubble size). Dotted lines represent median values. Values for each country are given in the SM, table S3.

by these drugs. Full details of data collection and analysis can be found in the supplementary materials (SM). In summary, data on reported febrile illness in children younger than 5 years and the fraction of those receiving antimalarial drugs from the private sector were assembled from all population-representative household surveys conducted since 2000 in malaria-endemic countries in sub-Saharan Africa for which individual survey responses were available (n = 96). The combined data set included records on 680,964 children from 43 countries for whom reports of fever status were recorded; all but two of these surveys did not include fever or treatment-seeking behaviors for ages older than 5. All surveys used multistage cluster randomized sampling from subnational administrative divisions, allowing fever prevalence to be recorded separately at a regional level. Repeated-measures regression models (*19*) were fitted to adjust survey responses for timing of the survey during the year and to account for variation over surveyed years by extrapolating trends to 2013. Literature reviews were conducted to facilitate extrapolations of fever incidence (fig. S2) and treatment-seeking behavior (fig. S3) to those ≥5 years old, based on surveys recording these measures for both age groups.

Rates for both age groups were applied to a high-resolution map of populations across Africa (*20*) in order to estimate the number of individuals receiving an antimalarial drug for fever annually from the private sector in each administrative unit as the product of the population, the annual fever rate, the fraction receiving antimalarials for fever, and the fraction of antimalarials reportedly received in the private sector.

The expected number of antimalarials received by individuals infected and not infected with malaria was then estimated by multiplying the antimalarial demand in each age group by the prevalence of *Plasmodium falciparum* malaria (*Pf*PR) in febrile individuals in that age group for each administrative unit. Malaria prevalence in fevers was estimated from a *Pf*PR map in the general population in 2010 (*21*) adjusted according to an empirical relation between population and febrile prevalence derived from household survey data (*22*). This multiplication assumed that the decision to seek treatment in the private sector is independent of true malaria infection status, an assumption corroborated by nearly identical positivity rates in those seeking treatment for fever in the public and private sectors in Tanzania (*23*). The inverse of the malaria prevalence in febrile private-sector treatment seekers represented the fraction of antimalarials taken by individuals with nonmalarial fevers. To capture the uncertainty surrounding these estimates and derive an interquartile range (IQR), values were drawn from distributions for each input variable through 10,000 Monte Carlo repetitions and combined into a distribution of outcomes. Details on assumptions and conversions are provided in SM (tables S1 to S3 and figs. S1 to S3).

The median estimated demand for private-sector antimalarial drugs for fever in 2013 was 153 million (M) for children <5 years old (IQR = 140M to 167M) and 502M for ≥5s (IQR= 426M to 585M) for a total of 655M (IQR= 571M to 746M). More than 90% of the variation in this total was caused by uncertainty in the relative probability of a ≥5-year-old receiving an antimalarial compared with a <5-year-old. Overall, a median of 33.81% of antimalarial drugs (IQR = 29.69 to 37.94%) were estimated to be intended for *P. falciparum*–positive individuals. Positivity was higher among <5-year-old antimalarial recipients (49.83%, IQR = 43.80 to 55.84%) than ≥5-year-old recipients (28.83%, IQR = 25.34 to 32.36%). An estimated 437M private-sector antimalarials (IQR = 384M to 491M) went to individuals not infected with malaria.

Although considerable uncertainty surrounds these estimates, the magnitude of this market is striking and has important implications for how the malaria community must tackle private-sector case management. It accompanies a substantial public-sector market that saw sales of ACTs alone numbering 181 million in 2011 (*2*). Given that ACTs are estimated to be about 20% of antimalarials received by febrile children in the public sector in such large markets as Nigeria and the Democratic Republic of the Congo (*3*), it is plausible that the total annual demand for antimalarials in Africa may be well over one billion treatments. The size of the antimalarial market in the private sector alone dwarfs the number of actual incident malaria cases that occur, estimated to be 174M (range 113M to 239M) in Africa in 2010 (*2*), which indicated substantial overtreatment of febrile disease as malaria. The analysis conducted here confirms that

Published by AAAS

the majority of private-sector antimalarial drugs are currently received by *P. falciparum*–negative patients, although this estimate is based on malaria prevalence in 2010 and is likely to change over time as malaria prevalence declines and treatment-seeking behaviors evolve (details of this calculation are provided in SM). This overtreatment means both that most febrile patients are not being treated for the true cause of their illness and that limited global funding and drug supplies could be better targeted to individuals who truly need them.

These averages mask substantial heterogeneities (Fig. 1). Of the consumers estimated to have bought an antimalarial medicine in the private sector, the fraction who were likely infected with malaria varied widely, from <1% in Djibouti and Swaziland to 56% in Burkina Faso. In eight countries, more than half of all antimalarials were estimated to be received in the private sector. Considerable heterogeneity existed within countries as well as across countries (SM and fig. S4).

Conclusions

Ultimately, all individuals with fever should receive appropriate treatment following accurate diagnosis according to World Health Organization (WHO) guidelines. Achieving this aim in the African private sector, however, will require a diagnostic test for the estimated 655M febrile individuals who purchase treatment there; only about 50 million rapid diagnostic tests were delivered globally in 2010 (*2*). Resources available for rolling out diagnostic tests and distributing ACTs in the private sector are likely to remain insufficient to reach the significant demand estimated here in the short term (*24*). Until resources are sufficient to properly diagnose and effectively treat all patients, it will be necessary to prioritize attempts to improve the availability of diagnostic tests and effective malaria drugs so that they will have the greatest impact on morbidity and mortality.

Interventions like private-sector ACT subsidies that can improve access to effective drugs will have the greatest probability of each treatment curing a malaria infection even in the absence of strong diagnosis if implemented in those countries on the right of the figure (Fig. 1), where estimated malaria prevalence in fevers is highest. Given the relatively lesser importance of the private sector for febrile treatment in countries in the bottom quadrants, private-sector interventions may be considered a lower priority in these areas. ACT subsidies are likely to be most cost-effective if implemented in countries in the upper-right quadrant. Although this quadrant includes only 13 out of 39 countries, they tend to have some of the highest demand for antimalarials in the private sector, together accounting for 70% of all estimated volumes (461 million annually). Improved accessibility of diagnostic tests in these countries has the greatest potential to prevent the unnecessary antimalarial treatments, but prioritizing deployment to the private sector of countries in the upper-left quadrant, where the highest proportions of antimalarials are currently taken unnecessarily, has the potential to be the most cost-effective use of resources available for diagnosis. Intranational heterogeneity indicates that some countries may benefit from prioritization at a subnational level.

These metrics are dynamic. Investment and policy decisions will need to be updated accordingly. The private-sector axis may be adjusted over time as new population-representative surveys reveal changes in treatment-seeking behavior and fever incidence, and the increasing frequency of population prevalence surveys (*21*) should permit regular updating of malaria maps. In addition, our consideration of the private sector in general could not detect variations in how interventions might affect more informal outlets versus private health-care facilities. Patterns of ACT overtreatment may differ from those estimated here for antimalarials in general if taken more frequently by certain age groups or in certain sectors.

Our analysis shows that, across sub-Saharan Africa, about one-quarter of private-sector antimalarials are obtained for children under the age of 5 years, but these children are much more likely to be infected with malaria than the general population. Malaria deaths in children under 5 also account for ~90% of all deaths from the disease (*2*). These numbers suggest that substantial opportunities exist to improve the value for money of malaria case-management interventions by prioritizing resources not only by geography but also age.

As long as resources remain insufficient to fully implement universal diagnosis and treatment, the short-term goal should be to target investments in private-sector diagnosis to places where overtreatment is high, while ensuring that affordable ACTs are used instead of the current, suboptimal treatments, even in the absence of diagnosis, in places where overtreatment is low. In the longer term, three transformations are needed across most countries. First, diagnosis rather than presumptive treatment should be the first response for fever management. Second, only effective combination treatments should be widely available in both the public and private sectors. Third, everyone should have access to quality and affordable care and treatment. Until those transformations occur, country-tailored interventions supported by optimally distributed global funding could have a tremendous impact in further accelerating progress against malaria.

References and Notes

1. Roll Back Malaria Partnership, *The Global Malaria Action Plan for a Malaria-Free World* (Roll Back Malaria, Geneva, 2008).
2. WHO, *World Malaria Report 2011* (WHO, Geneva, 2011).
3. K. A. O'Connell *et al.*, *Malar. J.* **10**, 326 (2011).
4. WHO, *World Malaria Report 2010* (WHO, Geneva, 2010).
5. WHO, *Guidelines for the Treatment of Malaria* (WHO, Geneva, ed. 2, 2010).
6. B. A. Larson, A. A. Amin, A. M. Noor, D. Zurovac, R. W. Snow, *BMC Public Health* **6**, 314 (2006).
7. G. M. L. Nayyar, J. G. Breman, P. N. Newton, J. Herrington, *Lancet Infect. Dis.* **12**, 488 (2012).
8. F. Arnold *et al.*, *Preliminary Report of the Independent Evaluation of AMFm Phase 1* (ICF Macro and London School of Hygiene and Tropical Medicine, Calverton, MD, 2012).
9. Zanzibar Malaria Control Program, *Malaria Elimination in Zanzibar: A Feasibility Assessment* (Zanzibar Malaria Control Program, Stone Town, Zanzibar, 2009).
10. S. Kunene, A. A. Phillips, R. D. Gosling, D. Kandula, J. M. Novotny, *Malar. J.* **10**, 313 (2011).
11. W. P. O'Meara, J. N. Mangeni, R. Steketee, B. Greenwood, *Lancet Infect. Dis.* **10**, 545 (2010).
12. A. M. Dondorp *et al.*, *N. Engl. J. Med.* **361**, 455 (2009).
13. R. M. Fairhurst *et al.*, *Am. J. Trop. Med. Hyg.* **87**, 231 (2012).
14. Clinton Health Access Initiative, Evidence to Policy Initiative of the Global Health Group at the University of California San Francisco, and the African Leaders Malaria Alliance, *Maintaining the Gains in Global Malaria Control* (CHAI, E2Pi, ALMA, 2011).
15. S. Thiam *et al.*, *PLoS ONE* **6**, e18419 (2011).
16. G. J. Bastiaens *et al.*, *Malar. J.* **10**, 76 (2011).
17. V. D'Acremont, C. Lengeler, B. Genton, *Malar. J.* **9**, 240 (2010).
18. T. Shewchuk *et al.*, *Malar. J.* **10**, 325 (2011).
19. G. Johnston, Repeated measures analysis with discrete data using the SAS system (SAS Institute Inc., Cary, NC, 1996); www2.sas.com/proceedings/sugi22/STATS/PAPER278.PDF.
20. C. Linard, M. Gilbert, R. W. Snow, A. M. Noor, A. J. Tatem, *PLoS ONE* **7**, e31743 (2012).
21. P. W. Gething *et al.*, *Malar. J.* **10**, 378 (2011).
22. E. A. Okiro, R. W. Snow, *Malar. J.* **9**, 99 (2010).
23. D. L. Smith, C. A. Guerra, R. W. Snow, S. I. Hay, *Malar. J.* **6**, 131 (2007).
24. D. M. Pigott, R. Atun, C. L. Moyes, S. I. Hay, P. W. Gething, *Malar. J.* **11**, 246 (2012).

Acknowledgments: J.M.C. and B.M. received support from the Bill & Melinda Gates Foundation (BMGF) and the UK Department for International Development; J.M.C. and A.M.W. were also supported by UNITAID. A.J.T. received support from BMGF and National Institute for Allergy and Infectious Diseases, NIH. P.W.G. was funded by the Wellcome Trust.

Supplementary Materials

www.sciencemag.org/cgi/content/full/338/6107/612/DC1

10.1126/science.1229045

PUBLIC HEALTH

From Financing to Fevers: Lessons of an Antimalarial Subsidy Program

Better approaches to affordable drugs, diagnostic tests, and patient-centered treatment are needed in Africa.

Ramanan Laxminarayan,[1] Kenneth Arrow,[2] Dean Jamison,[3] Barry R. Bloom[4]*

In 2001, the World Health Organization (WHO) recommended that countries use artemisinin-based combination therapies (ACTs) to treat malaria patients (*1*), as continued use of artemisinin monotherapies and substandard drugs had the potential to lead to widespread resistance to artemisinin, the most effective drug for malaria. But ACTs were unaffordable for most people in malaria-endemic countries, particularly in the private for-profit sector where most people seek treatment. Artemisinin monotherapies and the threat of resistance remain a problem. Resistance has now emerged in Cambodia and is spreading to Myanmar and Vietnam (*2*). Despite WHO's efforts, monotherapies are produced by 37 pharmaceutical companies and marketed in 29 countries (*3*). Although resistance to artemisinin had not been detected at the time of the Institute of Medicine (IOM) report in 2004 (*4*), an IOM committee proposed a global subsidy high in the distribution chain, both to make ACTs inexpensive and to displace artemisinin monotherapy and other ineffective drugs.

After 5 years of planning by many organizations under the Roll Back Malaria Partnership to design the financing mechanism, the Affordable Medicines Facility for malaria (AMFm) phase 1 was launched in 2010 under the auspices of the Global Fund to Fight AIDS, Tuberculosis, and Malaria. AMFm's four goals were to make quality-assured ACTs (i) available in both the public and private sectors, (ii) affordable through price negotiations with the producers and a subsidy, (iii) used in malaria-endemic countries, and (iv) able to crowd out monotherapy. The pilot study has been going on in urban and rural populations in seven countries in Africa (Ghana; Kenya; Madagascar; Niger; Nigeria; and Tanzania, including Zanzibar and Uganda) (*5*). AMFm has become a powerful market force in the antimalarials sector (*6, 7*). Over the past 2 years, price reductions for ACTs ranged from U.S.$1.28 to $4.82 per dose, at a subsidy cost to donors of roughly $1 per dose in the five countries where the program was substantially implemented. Although having improved health outcomes is the eventual goal, it was not feasible as a benchmark that could be evaluated in the 2-year duration of the pilots (*8*). In remote areas of Ghana and Kenya, measurements showed a reduced gap between rural and urban areas in availability of quality-assured ACTs. However, the program's future is uncertain, and in November 2012, the Board of the Global Fund will vote either to continue AMFm in a modified form or to terminate the program. In either case, future actions should be informed by the following lessons from phase 1.

A drug shop in Kenya selling ACT for malaria. The green leaf logo on the package indicates that the drugs are AMFm quality-assured.

Online
sciencemag.org
Podcast interview with Barry Bloom (http://scim.ag/ed_6107).

The more countries involved, the lower the drug prices and risk of leakage to other countries. Although AMFm subsidies ensure that ACTs are affordable, retail prices are lowered largely through negotiations with manufacturers: Wholesale prices have dropped by up to 80%, from between $2 and $5 to roughly $1 (*6, 7*). Even without a subsidy, providing first-line buyers with access to the negotiated price reductions could lower the retail price of ACTs substantially and make ACTs affordable in many countries. Negotiating with all wholesalers in malaria-endemic countries would retain the advantages of using existing channels (public, private, and nongovernmental organizations) to deliver quality-assured ACTs and to discourage monotherapies. With assured artemisinin supply, an expanded AMFm could lower price differentials across borders and thus discourage arbitrage (taking advantage of a price difference between markets) and leakage. The expansion would cost donors nothing beyond the small cost of supporting interventions and improving awareness about quality ACTs.

There should be a transition to reduce subsidies over time. The subsidy, although secondary to negotiated wholesale prices, is necessary in the AMFm pilot countries and in other countries with high malaria burden and low purchasing capacity for a few more years. However, sustainability is a key concern for donors who do not want to be locked into a long-term commitment

[1]Research Scholar, Princeton University, and Director of the Center for Disease Dynamics, Economics and Policy, Washington, DC 20036, USA. [2]Professor of Economics at Stanford University, Stanford, CA 94305, USA, and joint recipient of the Nobel Prize in Economics in 1972. [3]Professor of Global Health at the University of Washington Seattle WA 98195, USA. [4]Harvard University Distinguished Service Professor at Harvard School of Public Health. Boston, MA 02115, USA. He chairs the AMFm Expert Advisory Group of the Global Fund.

*Author for correspondence. E-mail: bbloom@hsph.harvard.edu

CREDIT: GLOBAL FUND

Published by AAAS

on financing ACTs. Even subsidizing drugs only for children may be infeasible, given that adults will likely purchase these drugs and receive an incorrect dose. However, the level of needed subsidy should fall with time as ACT prices decline as a result of technological improvement, greater demand for products from AMFm, and economies-of-scale increase. More resources would then be available for introducing antigen-based malaria rapid diagnostic tests (mRDTs), the subject of our next recommendation.

Rapid diagnostic tests for malaria are needed in the private sector. Because many fevers in malaria-endemic countries are not caused by malaria (*9*), WHO, in 2010, recommended a move from presumptive treatment of fever with antimalarials for children under 5 years of age to universal parasitological diagnosis (where feasible) before treatment. Surveys done in 2010, during the course of the AMFm pilot program, indicated that availability of mRDTs was generally low, under 10% of all outlets in all countries except Zanzibar, where availability was 36%. In most countries, low availability reflected the situation in private for-profit outlets (under 5% in all countries). In public health facilities, availability ranged from a low in Uganda (4%) to the highest in Madagascar (88%).

Presumptive treatment with antimalarials wastes precious treatment resources, potentially increases selection pressure for emergence of resistance, and delays access to the appropriate treatment for the actual cause of febrile illness (*10*). Significant improvements in quality and reductions in cost of mRDTs have been achieved over the past few years—they are expected to cost about half as much as malaria treatment. However, there is little private sector demand for mRDTs; they were routinely available in private shops and clinics only in Kenya, Uganda, and Zanzibar (*6, 7*). Public-sector clinics in pilot countries were more likely to perform malaria diagnostics; nonetheless, public-sector availability of diagnostic tests ranged from a low of 29% in Nigeria to a high of 98% in Zanzibar.

The challenge raised by the diagnostic tests is what to do for a child with a high fever and an anxious mother when an mRDT reveals no evidence of malaria. The need of health providers to do something in this circumstance explains the common provision of antimalarials for febrile illness, regardless of its cause. In the public sector, a significant proportion of patients who test negative for malaria receive an antimalarial (*11*), ranging from 12% in Zanzibar to more than 80% in Burkina Faso. Clearly, patients who test negative for malaria need appropriate treatments that may include antipyretics or antibiotics (*12*). Development of rapid tests and other diagnostic tools for non-malaria fevers (including pneumonias) is a major research opportunity. Even without them, however, community health workers, with some training, can distinguish severe pneumonia in children and effectively treat it with antibiotics (*13*).

It is possible to design pricing strategies that assure the private providers that they will not lose money by having an mRDT that can prevent a customer from buying an antimalarial, as well as benefit patients who do not inappropriately purchase ACTs that will be ineffective. Strategies will need to incorporate the likelihood that mRDTs will not be uniformly cost-effective in all settings, for example, in locations with either high or very low malaria prevalence (*10*). It will be necessary to provide some training of shopkeepers and community health workers (although there are regulatory issues in some countries as to who can take a blood drop).

A broader febrile illness agenda is crucial. We believe it is time to expand our approach to fever case management from disease-focused treatment to patient-centered treatment. Respiratory disease (principally severe pneumonia) is the largest cause of death of children in developing countries. Health systems could more effectively manage both malaria and pneumonia by addressing the more general problem of febrile illness, rather than proceeding from a specific etiology or funding source. This is not entirely new, of course: Fever management via an action-oriented classification system and case-management process is a core component of the Integrated Management of Childhood Illness (IMCI) strategy, which, since 1992, has been implemented in more than 75 countries (*14*). This broader "febrile illness" framing is not reflected in the way malaria treatment has been financed, particularly in sub-Saharan Africa. Moreover, there is little financing for treatment of pneumonias or other non-malaria causes of fevers in the private sector, where treatment is most frequently sought.

The United Nation's Every Woman Every Child program (*15*) provides a broader framework for thinking about the children who are at risk. The new UN Commission on Life-Saving Commodities for Women and Children recently recommended bulk buying, local manufacturing, and innovative marketing to help transform the supply, demand, and use of quality life-saving products including amoxicillin (*16*). The preliminary successes of ACTs and RDTs suggest that they could be considered for inclusion in this framework as well.

Conclusion

Termination of AMFm will create instability in artemisinin production, will reduce access to affordable ACTs, and will be seen as abandonment—both by the many people who depend on AMFm and by ACT producers. It will cause the kind of reaction that will detract from efforts to reduce deaths from malaria, to engage the private sector in providing community-based health care in poor countries, and to build credible health diplomacy. In the short term, we would recommend expanding ACT access to negotiated manufacturer prices to private-sector wholesalers in more malaria-endemic countries and allocating financial resources to support both ACTs and rapid diagnostic tests. The longer-term direction is supporting a broader, patient-centered approach to treatment of febrile illness.

References and Notes

1. WHO, *Antimalarial Drug Combination Therapy*: *Report of a WHO Technical Consultation* (WHO, Geneva, 2001).
2. WHO, WHO urges regulatory measures to stop marketing of oral artemisinin-based monotherapies and to promote access to artemisinin-based combination therapies (ACTs); www.who.int/malaria/publications/ who_ measures_to_stop_monotherapies.pdf.
3. H. Noedl *et al*., *N. Engl. J. Med.* **359**, 2619 (2008).
4. K. J. Arrow, C. B. Panosian, H. Gelband, Eds., *Saving Lives, Buying Time: Economics of Malaria Drugs in an Age of Resistance* (Institute of Medicine, Washington, DC, 2004).
5. O. Adeyi, R. Atun, *Lancet* **376**, 1869 (2010).
6. Independent Evaluation of Phase 1 of the Affordable Medicines Facility—malaria (AMFm): Multi-Country Independent Evaluation Report (ICF International, Calverton, MD, and the London School of Hygiene and Tropical Medicine, London, 2012).
7. AMFm Expert Advisory Group, AMFm, and the Global Fund for AIDS, TB, and Malaria, meeting report of the review of the preliminary independent evaluation of the AMFm Program; www.theglobalfund.org/en/amfm/independentevaluation/.
8. G. Yamey, M. Schäferhoff, D. Montagu, Piloting the Affordable Medicines Facility-malaria: what will success look like? *Bull. World Health Organ.* **90**, 452 (2012).
9. V. D'Acremont *et al*., *PLoS Med.* **6**, e252 (2009).
10. J. M. Cohen *et al*., *Science* **338**, 612 (2012).
11. D. H. Hamer *et al*., *J. Am. Med. Assoc.* **297**, 2227 (2007).
12. L. J. Frost, M. R. Reich, in *Access: How Do Good Health Technologies Get to Poor People in Poor Countries?* (Harvard Univ. Press, Cambridge MA, 2008).
13. K. Yeboah-Antwi *et al*., *PLoS Med.* **7**, e1000340 (2010).
14. I. M. C. I. Handbook, Integrated Management of Childhood Illnesses; http://whqlibdoc.who.int/publications/2005/9241546441.pdf.
15. Every Woman Every Child, www.everywomaneverychild.org/.
16. UN Commission sets out plan to make life-saving health supplies more accessible [press release], www.unicef.org/media/media_65942.html.

10.1126/science.1231010

ECONOMICS

Implications of Scarcity

The concept of scarcity helps to understand and aid decision-making, particularly in the case of very poor people.

Alix Peterson Zwane

Are the very poor really different? Modern development economics has struggled to answer this question, which turns F. Scott Fitzgerald's indictment of the rich on its head. Yet, the effects that poverty has on people's behavior have far-reaching implications. What price to charge for health and education? What specifications to include in research and development goals for new products? What information to include in public education campaigns? Answers to all these questions depend on whether we believe that the poor are "efficient" optimizers and arrive at first-best outcomes given their circumstances (*1*); optimizers who often achieve second-best outcomes as a result of missing markets; or not fully rational in the spirit of (*2*–*4*). On page 682 of this issue, Shah *et al*. (*5*) bring evidence of a distinct claim about what it is that makes the poor different.

The authors present data from laboratory experiments showing that people with smaller endowments of both time and "tries" perform worse in simple games: They borrow too much and spend inefficient amounts of time making decisions. This experimental evidence is consistent with the claim that scarcity, a broader concept than economic poverty, engages the mind, and that this engagement causes neglect along other dimensions, leading to substandard outcomes. The examples given by the authors are easily accessible to readers of this journal: Worrying about paying for groceries can make it hard to plan accurately to have money to make rent; stressing out over a looming work deadline can have the knock-on effect of poor planning for routine tasks.

Shah *et al*.'s results about the implications of scarcity for decision-making are not confined to people who face absolute poverty: the 1.3 billion people who live on less than $1.25 per day, or the 2.5 billion who live on less than $2 per day (see the figure) (*6*). For this population, however, there is a growing body of empirical evidence about decision-making that can be reconsidered through the lens of scarcity as a determinant of decision quality.

Take, for example, the observation that among the absolute poor, valuation—or what economists call willingness to pay—is low for basic preventive health products such as deworming medication (*7*), vaccination (*8*), insecticide-treated bed nets (*9*), and clean water (*10*). In the case of clean water, a series of experiments in Kenya and in other settings suggests not only that valuation is low and very sensitive to small changes in price but also that price is a more important determinant of adoption than nonprice determinants such as information about contamination or marketing and persuasion efforts (*11*).

This result may indeed reflect the preferences of poor but rational people. In light of Shah *et al*.'s work, however, another possible explanation emerges. If the absolute poor perceive their economic poverty as more salient than their information poverty, decision-making when positive prices are involved may invoke the engagement and cognitive load that Shah *et al*. describe, to the detriment of decision-making that fully uses information provided through other signals; people may not know that they do not know the relationship between water and diarrhea, or diarrhea and child morbidity.

Kremer and Miguel (*12*) report that many people living in Western Kenya, a region where the average income is close to $1 per day and where intestinal worms are common, do not correctly understand the relationships between infection and nutritional status. The low willingness to pay for deworming may at least in part result from the salience of economic scarcity and lack of salience of information scarcity.

Such a phenomenon would suggest that, just as Shah *et al*. propose to urge people to save for specific life events, we should inform people about common misconceptions so that they can balance or manage scarcity across domains. Dupas (*13*) provides some recent evidence on the value of this specific sort of evidence to improving decision-making: Informing teenage Kenyan girls about the relationship between HIV status and age in their country, which is not generally common knowledge, helps them make choices that reduce pregnancy rates and their own chances of infection.

Shah *et al*.'s results can also help deepen our understanding of the growing body of evidence that small changes in prices around zero can have large effects on behavior (*14*). We can interpret this set of results in a traditional framework, but, as with the low valuation of a range of preventive health products, this would imply that people have a low willingness to pay for child health and well-being. Shah *et al*.'s insights suggest that removing the information that draws cognitive engagement because of scarcity (that is, the price) enables better-quality decision-making: indeed, decision-making that more closely reflects

Decision-making under scarcity. Many people in developing countries, for example, in rural parts of Mali, live in absolute poverty. Shah *et al*. show that conditions of scarcity affect the ability to make decisions, helping to explain why poor people appear to make irrational decisions.

CREDIT: TREVOR KITTELTY/SHUTTERSTOCK

Bill & Melinda Gates Foundation, Seattle, WA 98109, USA. E-mail: alix.zwane@gatesfoundation.org

Published by AAAS

true preferences, including those for child health. This is an important area for further exploration because it implies that seemingly paternalistic policies, or expenditures that change outcomes relative to what would be chosen independently, may help people to arrive at outcomes that they would themselves choose in the absence of scarcity.

Banerjee and Duflo (*15*) have recently made the case for improving well-being by reducing the number of decisions that people have to make. They argue that in the United States, people do not have to decide whether to chlorinate their drinking water—it comes that way; similarly, many employers enroll people into retirement plans by default, lessening the need to actively make a choice to save. In developing countries, on these topics as well as others, people must make choices, decisions, and trade-offs. The evidence from Shah *et al*. provides another argument for why having so many choices can result in bad outcomes; scarcity makes quality decision-making difficult. Under such circumstances, defaults and guide rails, such as default option retirement plans, make quality decision-making easier and can have big payoffs for well-being.

References

1. T. W. Schultz, *Transforming Traditional Agriculture* (Yale Univ. Press, New Haven, London, 1964).
2. D. Kahneman, A. Tversky, *Econometrica* **47**, 263 (1979).
3. A. Tversky, D. Kahneman, *Science* **211**, 453 (1981).
4. E. Duflo, in *Understanding Poverty*, A. Banerjee, R. Benabou, D. Mookherjee, Eds. (Oxford Univ. Press, Oxford/New York, 2006), chap. 24.
5. A. K. Shah *et al*., *Science* **338**, 682 (2012).
6. *World Bank World Development Report 2011*, (World Bank and Oxford University Press, Washington, DC, 2011).
7. E. Miguel, M. Kremer, *Econometrica* **72**, 159 (2004).
8. A. V. Banerjee, E. Duflo, R. Glennerster, D. Kothari, *BMJ* **340**, c2220 (2010).
9. J. Cohen, P. Dupas, *Q. J. Econ.* **125**, 1 (2010).
10. M. Kremer, J. Leino, E. Miguel, A. P. Zwane, *Q. J. Econ.* **126**, 145 (2011).
11. A. Ahuja, M. Kremer, A. P. Zwane, *Annual Review of Resource Economics* **2**, 237 (2010).
12. M. Kremer, E. Miguel, *Q. J. Econ.* **122**, 1007 (2007).
13. P. Dupas, *Appl. Econ.* **3**, 1 (2011).
14. H. Holla, M. Kremer, in *What Works in Development? Thinking Big and Thinking Small*, J. Cohen, W. Easterly, Eds. (Brookings Institution Press, Washington, DC, 2009), ch. 4.
15. A. Banerjee, E. Duflo, *Poor Economics: A Radical Rethinking of the Way to Fight Global Poverty* (Public Affairs, New York, 2011).

10.1126/science.1230292

EVOLUTION

Getting to the Root of Aging

Why do patterns of aging differ widely across the tree of life?

Annette Baudisch[1,2] and James W. Vaupel[2,3,4]

As people live longer, the question arises of how malleable aging is and whether it can be slowed or postponed. The classic evolutionary theories of aging (*1*–*4*) provide the theoretical framework that has guided aging research for 60 years. Are the theories consistent with recent evidence?

At the heart of the theories lies the observation that the old count less than the young: Unfavorable traits are weeded out by evolution more slowly at higher ages (*2*); traits that are beneficial early in life are selected for despite late life costs (*3*); and resources are used to enhance reproduction at younger ages instead of maintaining the body at ages that do not matter much for evolution (*1*). The decline in the force of selection with age is viewed as the fundamental cause of aging (*4*). It is why, starting at reproductive maturity, senescence—increases in susceptibility to death and decreases in fertility—should be inevitable in all multicellular species capable of repeated breeding (*4*). Yet, this is not the case. Increasing, constant, and decreasing mortality (and fertility) patterns (see the figure) are three generic variants that compose the rich diversity of life trajectories observed in nature. For vertebrates, reproductive trajectories are commonly hump-shaped, and death rates may start rising much later than reproductive maturity (*5*). Thus, a new view on the fundamental causes of aging is needed to explain the clash of theory and data.

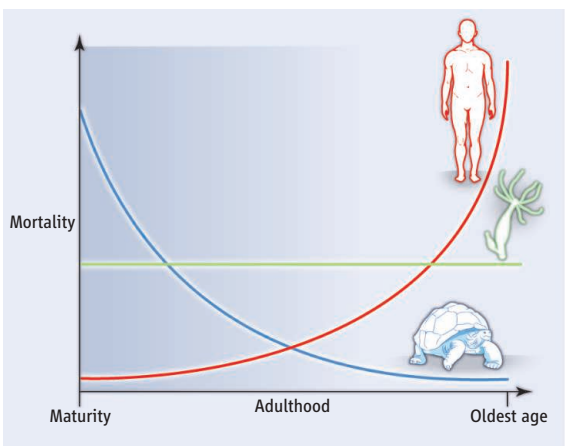

Aging patterns. The illustration is a schematic view of how species age in radically different ways. The life courses of humans and of many mammals and birds, at least at the oldest ages, are generally marked by rising mortality. For the tortoise *Gopherus agassizii* (*17*) and many other reptiles, amphibians, fish, and plants, mortality decreases throughout adult life. For the freshwater polyp *Hydra vulgaris* (*18*) and various other species across the tree of life, daily survival is more or less constant with age.

Allocation theory, which seeks to explain how resource limitations determine life-history patterns, provides a possible, promising perspective (*6*). Nature strikes compromises in allocating limited resources to growth versus maintenance versus reproduction versus escaping predators and pathogens. The scarcity of resources available for competing needs requires that an organism "makes difficult choices" at every moment of life. For instance, more energy dedicated to growth at one moment may reduce reproductive output but improve chances of survival to the next breeding opportunity, when conditions might be better and reproductive potential (because of growth) higher (*6*). Current theory of aging acknowledges the necessity of such compromises (*7*) but neglects their fundamental importance. Because the declining force of selection with age dominates evolutionary thinking about aging, classic theory focuses on life-history choices that specifically confer early-life advantages at the cost of late-life losses.

By widening horizons to consider not only early- versus late-life compromises but all the difficult choices an organism must make in allocating limited resources to competing needs over its life span, it is possible to gain insights into the diverse demographic patterns observed in nature (*6*, *8*, *9*). Even the effects of purely deleterious mutations that act only

[1]Max Planck Research Group for Modeling the Evolution of Aging, Rostock, Germany. [2]Max Planck Institute for Demographic Research, Rostock, Germany. [3]University of Southern Denmark, Odense, Denmark. [4]Duke University, Durham, NC 27705, USA. E-mail: baudisch@demogr.mpg.de

at older ages can be accounted for by appropriate allocation models (*10*). In such models, the force of selection declines with age, but though important, this decline is not decisive in molding fertility and mortality patterns.

What is decisive is the "option set" of a species, which can be summarized by the feasible combinations of survival and reproduction at all ages over the life span. Option sets differ widely: For some species, extra investment in repair and maintenance substantially reduces fertility; for other species there is little impact; for yet other species enhanced repair and maintenance decrease current but increase future fecundity. The details of such option sets shape age patterns of growth, fertility, and mortality (*8*, *11*).

Little is known about what types of constraints favor a pattern of aging with increasing mortality and decreasing fertility (senescent) versus alternative patterns with constant or declining mortality and constant or increasing fertility (nonsenescent). Life-history models suggest that the marginal costs and benefits of energy allocation play a central role (*8*, *11*). To test this and to explore other hypotheses, it would be informative to compare plants, for which growth and reproduction flexibly adapt to environmental conditions (*12*), to animals, for which growth and reproduction are more rigid and distinct (*8*). In contrast to vertebrates, plants capable of vegetative reproduction can create offspring by splitting off body parts. Thereby an investment in growth effectively becomes an investment in reproduction. Species that are small but long-lived (such as hydra in the laboratory), that can reproduce either sexually or asexually (such as daphnia), or that face highly uncertain environments [such as desert plants (*12*)] may also be good candidates for studies of how allocation options shape patterns of aging.

Research on the evolution of aging should focus on unraveling those differences in species' option sets that lead to senescent versus nonsenescent aging patterns. A major barrier in accomplishing this has been the lack of laboratory, zoo, and field evidence about age patterns of growth, maintenance, fertility, and mortality for species across the tree of life. New statistical methods and software now permit the extraction of mortality patterns from field data that are sporadic or are missing observations (*13*). Further development of life-history models hinges on more extensive and reliable data as well as on experiments to reveal how much allocation of additional resources to, say, faster growth or a more effective immune system affects lifetime fertility and survival. Fundamental understanding of why humans deteriorate so sharply (*14*) compared with other species, why human mortality has fallen so dramatically (*15*), and whether aging can be further delayed or even slowed (*16*) depends on knowledge of why some species senesce and others do not.

References and Notes

1. T. B. L. Kirkwood, *Nature* **270**, 301 (1977).
2. P. B. Medawar, in *Uniqueness of the Individual* (Lewis, London, 1952), pp. 44–70.
3. G. C. Williams, *Evolution* **11**, 398 (1957).
4. W. D. Hamilton, *J. Theor. Biol.* **12**, 12 (1966).
5. O. R. Jones *et al.*, *Ecol. Lett.* **11**, 664 (2008).
6. S. C. Stearns, *The Evolution of Life Histories* (Oxford Univ. Press, Oxford, New York, 1992).
7. L. Partridge, R. Sibly, R. J. H. Beverton, W. G. Hill, *Philos. Trans. Biol. Sci.* **332**, 3 (1991).
8. A. Baudisch, *Inevitable Senescence? Contributions to Evolutionary Demographic Theory*, Demographic Research Monographs (Springer, Berlin, 2008).
9. J. W. Vaupel *et al.*, *Theor. Popul. Biol.* **65**, 339 (2004).
10. M. J. Dańko *et al.*, *PLoS ONE* **7**, e34146 (2012).
11. A. Baudisch, *Gerontology* 10.1159/000341861 (2012).
12. R. Salguero-Gómez, B. C. Casper, *J. Ecol.* **98**, 312 (2010).
13. F. Colchero *et al.*, *Methods Ecol. Evol.* **3**, 466 (2012).
14. A. Baudisch, *Methods Ecol. Evol* **2**, 375 (2011).
15. O. Burger, A. Baudisch, J. W. Vaupel, *Proc. Natl. Acad. Sci. U.S.A.* 10.1073/pnas.1215627109 (2012).
16. J. W. Vaupel, *Nature* **464**, 536 (2010).
17. F. B. Turner, K. H. Berry, D. C. Randall, G. C. White, "Population ecology of the desert tortoise at Goffs, California, 1983–1986. Report No. 87-RD-81" (Southern California Edison Company, 1987).
18. D. E. Martínez, *Exp. Gerontol.* **33**, 217 (1998).

Acknowledgments: We thank L. Partridge, F. Colchero, D. Conde, D. Levitis, O. Jones, R. Salguero-Gomez, A. Scheuerlein, and the Evodemo group at the Max Planck Institute for Demographic Research. Supported by NIH grant AG-031719.

10.1126/science.1226467

EVOLUTION

How Cichlids Diversify

The extreme diversity of cichlid fishes in East Africa helps to elucidate how and why organisms diversify.

M. Emília Santos and Walter Salzburger

How is genetic variation connected to morphological evolution? How did Earth's spectacular organismal diversity evolve and how is it maintained? To answer these fundamental questions, scientists must understand how organisms function and diversify and how they interact with other organisms and the environment. Recent studies of cichlids, including (*1*–*7*), are beginning to provide insights into the basis of diversification in this exceptionally diverse fish family.

Many widely used biological model systems only provide limited insights into organismal diversification. Traditional laboratory-based model organisms tell us little about how organisms survive, adapt, behave, and reproduce in the wild. Model organisms used in evolutionary and ecological research, on the other hand, are often difficult to breed, their genomes are poorly characterized, and few genetic and developmental tools are available to study them. Furthermore, most established model systems are not very diverse taxonomically and phenotypically. Notable exceptions are instances of adaptive radiation, that is, the rapid origination of a multitude of phenotypically diverse species from a common ancestor through adaptation to distinct ecological niches (*8*, *9*). Famous examples of adaptive radiations include Darwin's finches on the Galápagos archipelago, silversword plants on Hawaii, anole lizards on islands of the Caribbean, and cichlid fishes in East Africa.

In the case of cichlids, hundreds of endemic species evolved independently in each of the three East African Great Lakes: Victoria, Malawi, and Tanganyika. Cichlids thus form by far the most species-rich extant adaptive radiations. They split up into distinct species in such little time that their DNA is still almost identical, a situation comparable to an experimental mutagenesis screen, yet in a natural environment (*10*).

Analyses of draft genome and transcriptome sequences have demonstrated the potential provided by such data (*1*, 2, *5*, *7*, *11*). Loh *et al.* (*1*), for example, investigated microRNA genes, which are important agents for the regulation of gene expression, and detected signatures of divergent natural selection in microRNA target sites among Lake Malawi cichlids. A comparative transcriptome analysis revealed little divergence at protein-coding sequences but high diversity in untranslated regions that are impor-

Zoological Institute, University of Basel, Vesalgasse 1, CH-4051 Basel, Switzerland. E-mail: emilia.santos@unibas.ch; walter.salzburger@unibas.ch

tant for gene regulation (*2*). These studies suggest that regulatory evolution plays a key role in cichlid diversification.

Draft genome sequences have also facilitated developmental studies and the quest for genes underlying adaptive morphological traits (*11*). Because of their close relatedness and amenability to aquarium life, it is possible to cross cichlid species with distinct phenotypes in the laboratory to then genetically map key evolutionary traits (*12*, *13*). It has now become possible to directly and causally link molecules to phenotypes through phenotypic engineering. Fujimura and Kocher (*14*) created transgenic tilapia that express green fluorescent protein under the control of a *Xenopus* promoter. This method allows the function of genes in cichlids to be studied directly.

A wealth of information, spanning decades of research (*15*, *16*), is available on the evolution, ecology, morphology, and behavior for many cichlid species and communities. These diverse data open up various possibilities to examine the relative importance of natural and sexual selection, contingency, and determinism to cichlid evolution and to observe the evolution of fitness-relevant traits as well as their underlying genes in action.

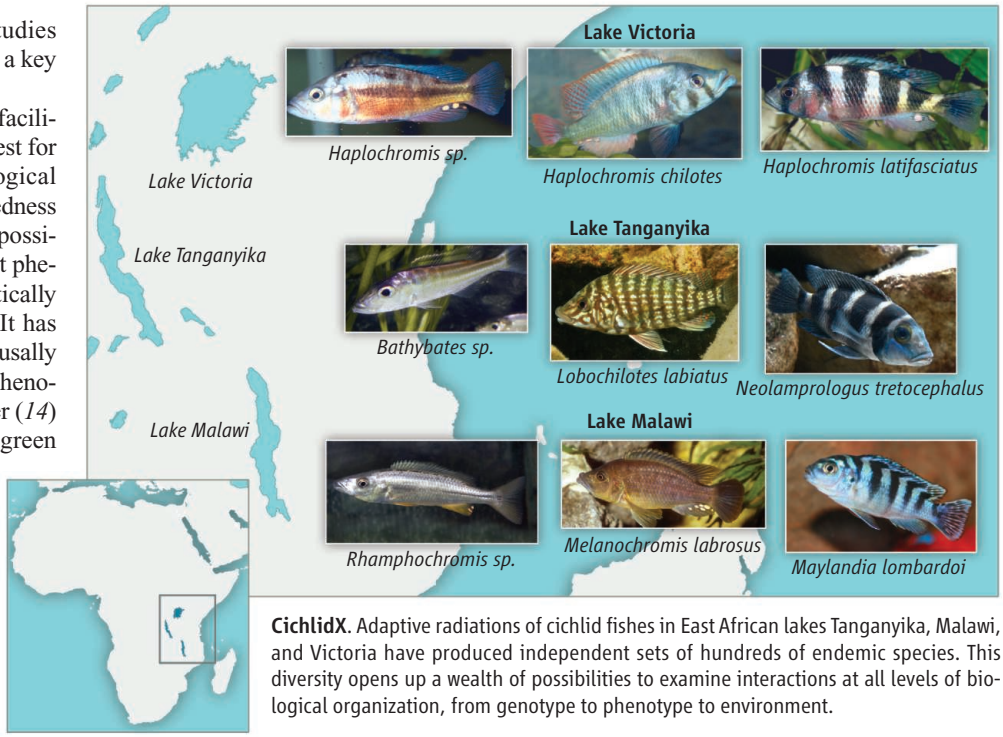

CichlidX. Adaptive radiations of cichlid fishes in East African lakes Tanganyika, Malawi, and Victoria have produced independent sets of hundreds of endemic species. This diversity opens up a wealth of possibilities to examine interactions at all levels of biological organization, from genotype to phenotype to environment.

For example, Seehausen *et al*. (*17*) and Miyagi *et al*. (*3*) have examined the role of visual pigments in the recent divergence of Lake Victoria cichlids. The heterogeneous light conditions in this lake led to diversifying selection on *opsin* genes as a function of water depth. The divergence in opsins, in turn, affects sexual selection, because differences in color perception influence the female preference for male coloration (*17*). Here, the interplay between natural and sexual selection resulted in speciation in the absence of geographic barriers through selection on a sensory system ("sensory drive").

In other cases, natural and sexual selection act in opposite directions. An orange-blotch coloration is common among females of Lake Malawi cichlids and provides camouflage over boulders. Blotched males, on the other hand, seem to have a selective disadvantage because they do not possess the nuptial coloration that attracts females. Roberts *et al*. have recently shown (*12*) how this conflict between natural selection (the orange blotch pattern provides camouflage) and sexual selection (orange blotch males are less likely to reproduce) is resolved. A new female sex-determining gene has evolved in linkage with the *pax7* gene that makes the orange blotch coloration. This linkage leads to low recombination; therefore, mostly females have this coloration.

Perhaps the most important feature of cichlid adaptive radiations, at least in the context of speciation, is that they come in replicates, because lakes Malawi, Victoria, and Tanganyika each have their own cichlid assemblage (see the figure). "Nature's grand experiment in evolution" (*16*) therefore provides an opportunity for comparing patterns and processes of diversification—especially because both very species-rich (radiating) and species-poor (nonradiating) groups of cichlids exist.

In a recent analysis focusing on 46 African lakes (*4*), Wagner *et al*. concluded that cichlids are more prone to radiate if they are sexually dichromatic (with males and females showing different pigmentation patterns), live in deeper and older lakes, and occupy regions with more solar energy input. The combination of environmental conditions and sexual dichromatism does not explain all cichlid radiations; for example, there are no differences in coloration between males and females in the ~100 species of lamprologines in Lake Tanganyika. Nevertheless, Wagner *et al*. demonstrate that patterns of diversification can at least partially be predicted.

The main outcome of "evolution in replicates" is a high abundance of convergent phenotypes, which are perfectly suited to elucidate the molecular mechanisms and/or developmental constraints involved in parallel evolution. Colombo *et al*. (*5*), for example, identified striking similarities in the genetics underlying the thick-lipped phenotype found in East African and Central American cichlid radiations, which are separated by almost 100 million years of independent evolution. That phenotypic parallelism is not restricted to morphology in cichlids is, for example, highlighted by the repeated transition of parental care strategies in the Ectodini, a group of mouthbrooding cichlids from Lake Tanganyika (*6*), illustrating once more the broad scope of traits and topics that can be tackled with the cichlid model system.

The release of five cichlid genomes provides further opportunity for the molecular characterization of diversification. The five sequenced species encompass the phylogenetic and geographic diversity of East African cichlids (*18*). These genomes will serve as important resources, anchoring points, and templates for comparative genomic studies.

Sequencing of many more genomes, from many more species, will help to determine the contribution of mutation, selection, drift, and migration to diversification. This endeavor would also allow the detection of regulatory and coding polymorphisms that segregate in natural populations, which in turn would facilitate the linking of genotypes to phenotypes. East African cichlid fishes thus offer the possibility to dissect the interplay of thousands of genes from many genomes, found in many cells, forming tissues in many individuals, in many popula-

PHOTO CREDITS: *M. LOMBARDOI* AND *N. TRETOCEPHALUS*, WIKIMEDIA.ORG; *L. LABIATUS*, M. MUSCHICK/UNIV. OF SHEFFIELD; ALL OTHERS, E. SCHRAML

Published by AAAS

tions, encompassing hundreds of species that occupy various ecological niches across replicate adaptive radiations.

To keep up with these advances on the molecular and genomic aspects of cichlid diversification, it will be important to increase the efforts at the organismal and life-history level by surveying ecology, morphology, and behavior. This integration would make cichlids a role model not only for adaptive radiation and explosive speciation but also for the survey of interactions at all levels of biological organization.

References

1. Y. H. Loh, S. V. Yi, J. T. Streelman, *Genome Biol. Evol.* **3**, 55 (2011).
2. L. Baldo, M. E. Santos, W. Salzburger, *Genome Biol. Evol.* **3**, 443 (2011).
3. R. Miyagi *et al.*, *Mol. Biol. Evol.* **29**, 3281 (2012).
4. C. E. Wagner, L. J. Harmon, O. Seehausen, *Nature* **487**, 366 (2012).
5. M. Colombo *et al.*, *Mol. Ecol.* 10.1111/mec.12029 (2012).
6. M. R. Kidd, N. Duftner, S. Koblmüller, C. Sturmbauer, H. A. Hofmann, *PLoS ONE* **7**, e31236 (2012).
7. T. Manousaki *et al.*, *Mol. Ecol.* 10.1111/mec.12034 (2012).
8. D. Schluter, *The Ecology of Adaptive Radiation* (Oxford Univ. Press, New York, 2000).
9. S. Gavrilets, J. B. Losos, *Science* **323**, 732 (2009).
10. T. D. Kocher, *Nat. Rev. Genet.* **5**, 288 (2004).
11. G. J. Fraser *et al.*, *PLoS Biol.* **7**, e31 (2009).
12. R. B. Roberts *et al.*, *Science* **326**, 998 (2009).
13. R. C. Albertson, J. T. Streelman, T. D. Kocher, P. C. Yelick, *Proc. Natl. Acad. Sci. U.S.A.* **102**, 16287 (2005).
14. K. Fujimura, T. D. Kocher, *Aquaculture* **319**, 342 (2011).
15. G. Fryer, T. D. Iles, *The Cichlid Fishes of the Great Lakes of Africa: Their Biology and Evolution* (Oliver & Boyd, Edinburgh, 1972).
16. G. W. Barlow, *The Cichlid Fishes. Nature's Grand Experiment in Evolution* (Perseus, Cambridge, MA, 2000).
17. O. Seehausen *et al.*, *Nature* **455**, 620 (2008).
18. Four members of radiating clades were sequenced, plus a sister taxon, the Nile tilapia. See www.broadinstitute. org/models/tilapia.

10.1126/science.1224818

PHYSICS

Quantum Procrastination

Entangling two photons allows the wave and particle nature of light to be interchanged even after the light has already been detected.

Seth Lloyd

Do you have a decision you have to make but you just can't bring yourself to do it? As the irrevocable moment approaches, you squirm more and more, but something inside you says, "Not now, not yet." Then when it's already almost too late, in a burst of energy and shame, you come through—or not. Afterward, you are irrationally resentful, as if someone other than yourself is responsible for disturbing your peace of mind. You vow that the next time a decision arises, you will make it expeditiously. If you are a severe procrastinator like me (at least when it came to starting this article), have hope—quantum mechanics is coming to your rescue. On pages 637 and 634 of this issue, experiments by Kaiser *et al*. (*1*) and Peruzzo *et al*. (*2*) show that in the presence of quantum entanglement (in which outcomes of measurements are tied together), it is possible to hold off making a decision, even if events seem to have already made one. Quantum procrastination ("proquastination") allows you to put off for tomorrow what you should have done today.

The experiments are based on Wheeler's famous delayed-choice experiment (*3*). Although photons are particles of light, they also possess a wavelike nature and can exhibit interference effects. Suppose that the path lengths of a Mach-Zehnder interferometer (*4*, *5*) have been tuned to make the photon come out of one port of the final beam splitter with probability 1 (see the figure). After the photon has passed the first beam splitter, so that it is fully inside the interferometer, and before it has reached the second beam splitter, you decide to whisk away that second beam splitter, preventing any interference between the photon's two paths from taking place. Without interference, the photon behaves like a particle and emerges with equal probability out of either of the two ports of the apparatus where the second beam splitter used to be.

If instead you choose to leave the beam splitter in, the wavelike nature of the photon asserts itself to exhibit interference between the two paths that the single particle takes in quantum superposition, and the photon would emerge from only one port with probability 1. That is, even though you have delayed the choice of removing the beam splitter until after the photon—if it really were a classical particle—should be traveling along one path or the other, by restoring the beam splitter, you can reinstate the photon's wavelike nature and have it report that it was traveling along both paths simultaneously.

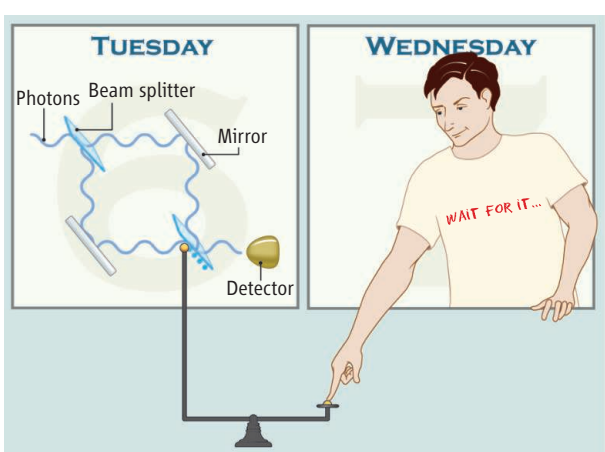

Welcomed delays. Two studies use quantum entanglement in delayed choice experiments; the outcome for the first photon detected (whether it is a particle or a wave or has intermediate character) is determined by later measurements. Kaiser *et al*. entangle the first photon's polarization with that of the second photon, so that its outcome depends on the second photon's polarization. Peruzzo *et al*. entangle the photon with the presence or absence of a beam splitter in the setup and again delay the outcome of the first photon's state. If the photon states could be stored in quantum memories, it might be possible to delay the outcome of the first photon detection (on a Tuesday) until the observer makes a choice on Wednesday.

Since Wheeler proposed his delayed-choice gedanken experiment in 1984, a horde of theories and experiments exhibiting weird quantum effects has spread across the scientific landscape, including experimental demonstrations of Wheeler's proposal (*6*). Quantum information theory has supplied a general language for discussing such quantum weirdness, and small but effective quantum information processors have provided the wherewithal to demonstrate virtually any effect of quantum superposition and entanglement on a small number of quantum bits (*7*). As effects such as Wheeler's delayed-choice experiment and its relatives, such as the quantum eraser (*8*), have become commonplace, they have lost some of their power to amaze.

Department of Mechanical Engineering, Massachusetts Institute of Technology, Cambridge, MA 02139, USA. E-mail: slloyd@mit.edu

For quantum weirdness with more kick to it, we need look no further than the two delayed-choice experiments of Kaiser *et al*. and Peruzzo *et al*. Both experiments use quantum entanglement to delay the choice of what quantum effects are demonstrated not merely until after the photon has entered the interferometer, but until after the photon has emerged from the interferometer and the measurement that detects it has already taken place. In the first proquastination experiment, polarizing beam splitters ensure that vertically polarized photons entering the Mach-Zehnder interferometer undergo quantum interference, while horizontally polarized photons do not. Photons whose polarization is in between vertical and horizontal—diagonally polarized photons—exhibit partial interference.

There is nothing here that the two Ludwigs, Mach and Zehnder, couldn't already have observed in the early 1890s, but now the tricky part comes in. Kaiser *et al*. do not send a photon with a definite polarization into the interferometer. Rather, they send a photon whose polarization is entangled with the polarization of a second photon. After the first photon has already emerged from the interferometer and the port by which it has emerged has been detected, Kaiser *et al*. measured the polarization of the second photon. If they measure the polarization of the second photon along the vertical/horizontal axis and obtain the result "horizontal," then the first photon has behaved like a particle: No interference has taken place. If they obtain the result "vertical," then the first particle has behaved like a wave, and interference has taken place.

So far, the results of the experiment could be explained simply by saying the two photons are either both horizontally polarized or both vertically polarized. If one chooses to measure the second photon along the diagonal/antidiagonal axis however, so that first photon exhibits partial interference, then Bell's inequalities (*9*) can be used to show that this convenient classical explanation won't wash. It is the measurement on the second photon—apparently retroactively—that made interference take place or not.

The second demonstration of quantum procrastination, by Peruzzo *et al*., is if anything even more audacious. In this experiment, a photon is sent through a Mach-Zehnder interferometer as before, but the presence or absence of the second beam splitter in the Mach-Zehnder interferometer is entangled with the state of a second photon. As a result, even after the first photon has been detected, the question of whether it has exhibited wave nature, particle nature, or something in between, is determined by measurements made on the second photon. Strong violations of Bell's inequalities again rule out easy classical explanation.

Although the two quantum procrastination experiments reported here delay the choice of whether to exhibit wave- or particle-like nature of entangled particles for just a few nanoseconds, if one has access to quantum memory in which to store the entanglement, the decision could be put off until tomorrow (or for as long as the memory works reliably). So why decide now? Just let those quanta slide! Sadly, the applications of quantum procrastination are for the moment limited to making only a few highly quantum types of decision ex post facto. I wish I had decided to start writing this article a week before it was due, but no amount of entanglement can hide that I decided to the day before.

References

1. F. Kaiser *et al*., *Science* **338**, 637 (2012).
2. A. Peruzzo, P. Shadbolt, N. Brunner, S. Popescu, J. L. O'Brien, *Science* **338**, 634 (2012).
3. J. A. Wheeler, in *Quantum Theory and Measurement*, J. A. Wheeler, W. H. Zurek, Eds. (Princeton Univ. Press, Princeton, NJ, 1984), pp. 182–213.
4. L. Zehnder, *Z. Instrumentenkunde* **11**, 275 (1891).
5. L. Mach, *Z. Instrumentenkunde* **12**, 89 (1891).
6. V. Jacques *et al*., *Science* **315**, 966 (2007).
7. M. A. Nielsen, I. L. Chuang, *Quantum Computation and Quantum Information* (Cambridge Univ. Press, Cambridge, UK, 10th anniversary ed., 2011).
8. Y.-H. Kim, R. Yu, S. P. Kulik, Y. Shih, M. O. Scully, *Phys. Rev. Lett.* **84**, 1 (2000).
9. J. S. Bell, *Physics* **1**, 3 (1964

10.1126/science.1229825

PLANT SCIENCE

Chloroplast Delivery by UPS

Identification of a membrane-anchored E3 ligase in plants reveals a role for the ubiquitin proteasome system in chloroplast development.

Felix Kessler

Chloroplasts are the organelles of photosynthesis in plants and are responsible for much of the food and biomass production on our planet. But chloroplasts are only the best-known members of an extended family of organelles termed plastids. Their name suggests plasticity and, indeed, plastids exist in various incarnations depending on developmental cues (e.g., nonphotosynthetic etioplasts in dark-grown leaves, colored chromoplasts in petals and fruit, and starch-storing amyloplasts in roots). Yet, the mechanisms underlying the transformation from one plastid type to another are largely unknown. On page 655 in this issue, Ling *et al*. (*1*) show that the ubiquitin-26*S* proteasome system (UPS) directly targets plastids and promotes chloroplast biogenesis, controlling yet another important facet of cell biology.

Plastids originate from an endosymbiotic process that started ~1.5 billion years ago when a eukaryotic host cell engulfed a photosynthetic prokaryote. Over time, the two organisms became almost completely integrated. A permanent and ongoing flow of genetic material from the prokaryotic endosymbiont resulted in the transfer of most plastid protein-encoding genes to the host nucleus (*2*). The *Arabidopsis* chloroplast today has ~2000 proteins (*3*, *4*), only 87 of which are encoded in the organelle. Concurrently with their transfer to the nucleus, the former endosymbiont genes acquired genetic information encoding amino-terminal targeting sequences resulting in synthesis of preproteins in the cytosol. The amino-terminal sequences enable the recognition and the translocation of preproteins across the dual-membrane chloroplast envelope and are later removed.

Preprotein recognition and envelope translocation are facilitated by the chloroplast protein import machinery (*5*), which consists of translocon complexes at the outer (TOC) and inner envelope membranes of the chloroplast. The main components (identified by their molecular mass in kilodaltons) of the Toc complex (Toc159, Toc34, and Toc75) were first identified in isolated pea chloroplasts (*6*–*8*) and play essential roles in chloroplast biogenesis in *Arabidopsis thaliana* (*9*, *10*). Toc159 and Toc34 are outer membrane preprotein receptors shar-

Institute of Biology, University of Neuchâtel, CH-2000 Neuchâtel, Switzerland. E-mail: felix.kessler@unine.ch

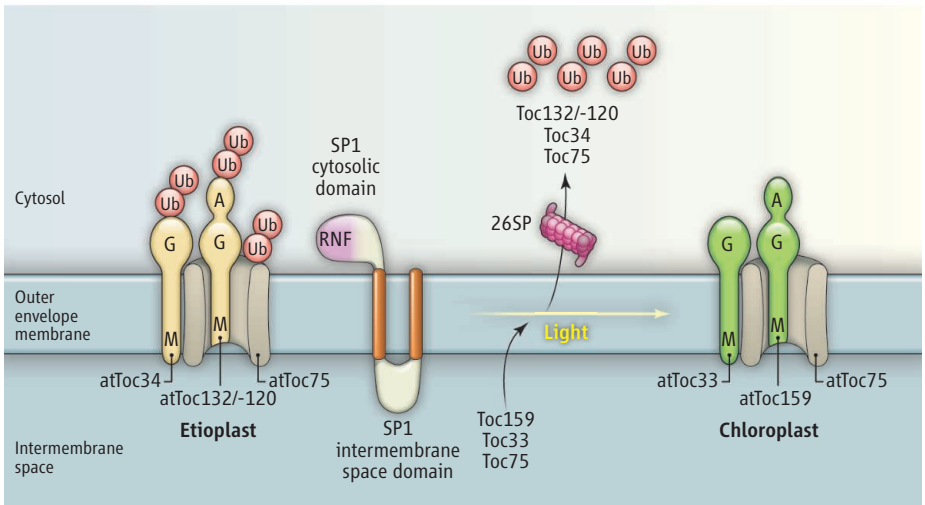

Model of chloroplast biogenesis. Nonphotosynthetic, undifferentiated plastids in the dark (etioplasts) import housekeeping proteins via a translocon at the outer membrane of the chloroplast (Toc) complex consisting of the preprotein receptors Toc132/-120 and Toc34 together with the protein-translocating channel Toc75. Light triggers the transformation of etioplasts into chloroplasts. Developing chloroplasts import large quantities of photosynthesis-associated proteins using a Toc complex consisting of the preprotein receptors Toc159 and Toc33 together with Toc75. The remodeling of the Toc complex during chloroplast biogenesis implicates an outer membrane E3 ligase, SP1, that targets components of the protein import machinery for degradation by the 26*S* proteasome (26SP). A, acidic; at, *Arabidopis thaliana*; G, GTP-binding; M, membrane insertion; RNF, RING-finger domain; Ub, ubiquitin.

ing homology in their guanosine 5′-triphosphate (GTP)–binding domains, and they extend into the cytosol. Toc75 forms the protein-conducting channel, deeply buried in the outer membrane. The *Arabidopsis* genome revealed that a small gene family of Toc GTPases (Toc159, -132, -120, -90, -34, and -33) engage in separate, preprotein-specific pathways (*11*, *12*). Toc159 and -33 are present predominantly in the chloroplast and mediate the import of the highly abundant proteins associated with photosynthesis. By contrast, Toc132/-120 and Toc34 are present mostly in other plastid types and are required for the import of housekeeping proteins.

Chloroplast biogenesis occurs when a dark-grown (etiolated) plant senses the light and consists of a series of developmental processes called photomorphogenesis (*13*). This results in extensive changes in gene expression that dramatically increase the components of the photosynthetic machinery and enables the greening of young plants. Greening directly reflects chloroplast biogenesis and leads to remodeling of the import machinery and then of the entire chloroplast proteome that becomes dominated by highly abundant photosynthesis-associated proteins.

For the import machinery, the balance is shifted from Toc120/-132 and Toc34 to Toc159 and Toc33. Both *toc33* (*ppi1*) (*9*) and *toc159* (*ppi2*) (*10*) mutants give rise to chloroplast phenotypes (pale green and albino, respectively), emphasizing the relevance of these components and their specific role in preprotein import. But what brings about this switch of components in the import machinery during chloroplast biogenesis?

In a screen for second site suppressors of *ppi1*, Ling *et al*. discovered SP1 (suppressor of *ppi1* locus 1), a "really interesting new gene" (RING)–type ubiquitin E3 ligase. Together with E2, E1, and the proteasome, E3 ligases regulate protein degradation and thereby a range of processes in animals and plants, and occupy 6% of the *Arabidopsis* genome (*14*). SP1 has a "really interesting" topology: It is anchored in the plastid outer envelope membrane by two transmembrane helices and exposes a carboxyl-terminal C3HC4-type RING-finger domain to the cytosol. The domain between the two transmembrane helices faces the envelope intermembrane space and interacts with its TOC targets. Thus, SP1 is ideally positioned to ubiquitinate targets at the chloroplast surface.

The *sp1 ppi1* double-mutant plants generated by Ling *et al*. are larger and greener and contain more extensively developed chloroplasts than *ppi1* but still less so than wild-type plants. By contrast, the *sp1* single mutant showed a slower transformation of etioplasts to chloroplasts, and from chloroplasts to gerontoplasts (aging chloroplasts in older plants). This indicates a role in the transformation of one plastid type to another (see the figure). In vitro and in vivo experiments by the authors show that Toc complex components are directly ubiquitinated by the action of SP1. But how could loss of ubiquitination activity by the *sp1* mutations rescue the pale phenotype and the defective chloroplasts in the *ppi1* mutant? The answer may lie in the reduced degradation and consequent increase in amounts of other Toc components that may compensate for the absence of Toc33 in the *ppi1 sp1* double mutant.

Why would the loss of SP1 function disrupt transition between different plastid types? Chloroplast biogenesis, as well as the differentiation of other plastid types, is linked to the import of functionally specific proteins that in turn require specific combinations of the import receptor homologs (i.e., Toc159 and Toc33 for photosynthesis-associated proteins and Toc132/-120 and Toc34 for housekeeping proteins). SP1-dependent ubiquitination followed by proteasome-mediated degradation may therefore allow modulation of the composition of the Toc complex with regard to the preprotein demands of the developing plastid type.

Are the Toc components the only targets of SP1, or are there other substrates? SP1 has a close homolog, SPL1, that also localizes to the chloroplast outer membrane. Genetic evidence indicates that SPL1 is not redundant with SP1, but its function remains unknown. The findings of Ling *et al*. have opened an exciting new door to regulatory mechanisms at the chloroplast import machinery. No doubt, many interesting secrets remain to be discovered.

References and Notes

1. Q. Ling, W. Huang, A. Baldwin, P. Jarvis, *Science* **338**, 655 (2012).
2. J. N. Timmis, M. A. Ayliffe, C. Y. Huang, W. Martin, *Nat. Rev. Genet.* **5**, 123 (2004).
3. B. Zybailov *et al.*, *PLoS One* **3**, e1994 (2008).
4. K. Baerenfaller *et al.*, *Science* **320**, 938 (2008).
5. F. Kessler, D. Schnell, *Curr. Opin. Cell Biol.* **21**, 494 (2009).
6. S. E. Perry, K. Keegstra, *Plant Cell* **6**, 93 (1994).
7. D. J. Schnell, F. Kessler, G. Blobel, *Science* **266**, 1007 (1994).
8. S. Hirsch, E. Muckel, F. Heemeyer, G. von Heijne, J. Soll, *Science* **266**, 1989 (1994).
9. P. Jarvis *et al.*, *Science* **282**, 100 (1998).
10. J. Bauer *et al.*, *Nature* **403**, 203 (2000).
11. S. Kubis *et al.*, *Plant Cell* **16**, 2059 (2004).
12. Y. Ivanova, M. D. Smith, K. Chen, D. J. Schnell, *Mol. Biol. Cell* **15**, 3379 (2004).
13. C. Kami, S. Lorrain, P. Hornitschek, C. Fankhauser, *Curr. Top. Dev. Biol.* **91**, 29 (2010).
14. R. D. Vierstra, *Nat. Rev. Mol. Cell Biol.* **10**, 385 (2009).

Acknowledgments: F.K. is funded by the Swiss National Science Foundation, the National Center of Competence in Research Plant Survival, SystemsX, and the University of Neuchâtel. I regret not citing some work because of space limitations.

10.1126/science.1230658

MOLECULAR BIOLOGY

A New Direction for Gene Loops

Genes adopt a loop conformation to focus the direction of transcription and block the production of noncoding RNAs.

Michael Hampsey

The textbook illustration of a gene depicts a linear structure, with flanking regulatory sequences—a promoter on the left and a terminator on the right, to start and stop transcription, respectively. However, recent analyses of chromatin architecture have revealed that the promoter and terminator elements are not necessarily separate in three-dimensional space, but can be juxtaposed to form "gene loops" (*1*, *2*). Gene loops are not static structures; they form transiently in a transcription-dependent manner. But what function do they serve? On page 671 of this issue, Tan-Wong *et al*. report that gene loops restrict divergent transcription from inherently bidirectional promoters, repressing the synthesis of noncoding RNA (*3*).

The yeast *SSU72* gene was key to the discovery of gene loops. An *ssu72* mutant was initially identified on the basis of genetic interaction with the general transcription initiation factor TFIIB (*4*). The Ssu72 protein associates directly with TFIIB, and defects in either protein can affect transcription start site selection at target genes. It was subsequently found that Ssu72 is a protein phosphatase with specificity for phosphorylated serine residues in the C-terminal domain of the largest subunit of RNA polymerase II (Pol II) (*5*, *6*). This dephosphorylation event occurs early in the transcription cycle. Yet Ssu72 is an integral component of the cleavage and polyadenylation factor (CPF) complex that couples 3′-end processing of precursor mRNA (pre-mRNA) with transcription termination (*7*). How does a component of the 3′-end processing machinery interact with TFIIB to affect initiation?

It turns out that the terminating element of a gene is not necessarily distal to its promoter, but can physically interact with it in three-dimensional space. This was demonstrated by chromosome conformation capture (3C), a powerful technique that detects and quantifies physical interaction between any two regions of a genome (*8*). 3C revealed not only that yeast genes form loops, but that looping might be a general feature of Pol II transcription (*1*, *2*). Furthermore, defects in TFIIB and Ssu72, as well as in other initiation and 3′-end processing proteins, impair loop formation (*9*). A current model proposes that looping requires a pioneer round of transcription to recruit the 3′-end pre-mRNA processing proteins, followed by physical interaction with transcription initiation factors to generate the loop. Gene loops might enhance transcription by facilitating handoff of Pol II from the terminator to the promoter of the same gene. Whether loops are formed and dissociate with each transcription cycle remains to be determined. However, persistence of loops at some genes has been associated with "transcriptional memory," a phenomenon defined as rapid reactivation of genes after a cycle of activation and repression (*10*, *11*).

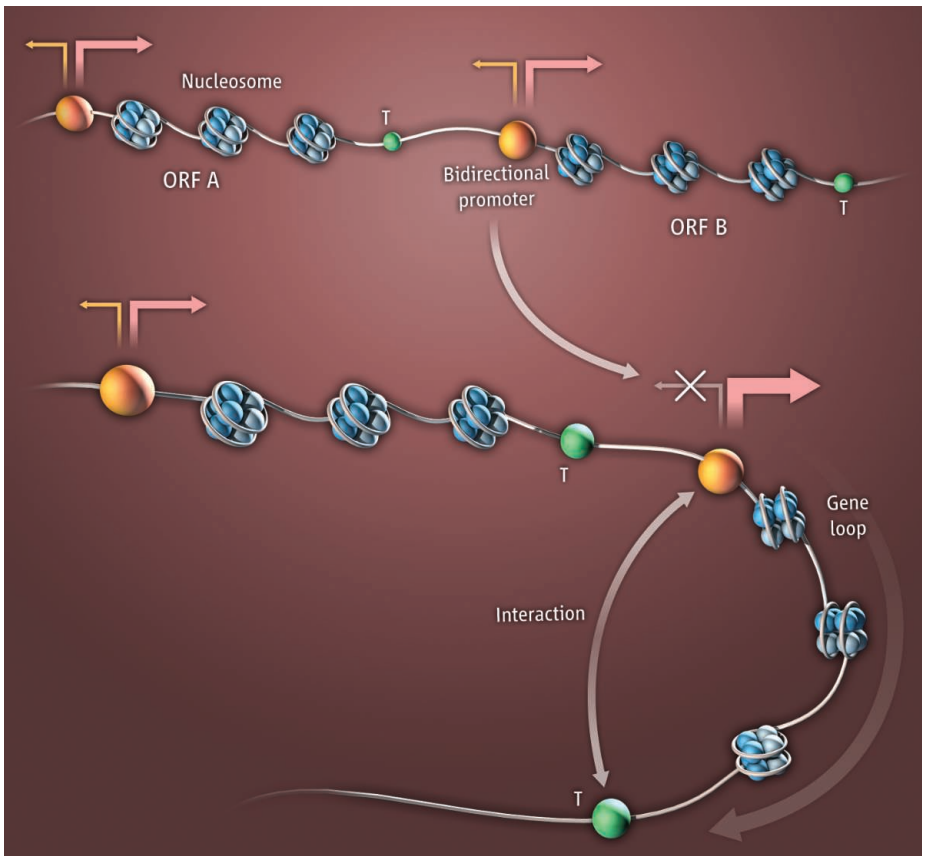

Gene loops. Transcription-dependent juxtaposition of a terminator (T) with its promoter forms a gene loop that facilitates transcription in the sense direction (mRNA) while repressing antisense transcription (ncRNA). Loop formation requires components of the transcription initiation and 3′-end pre-mRNA processing machineries, although the mechanism by which loops are formed and maintained remains to be established. ORF, open reading frame.

In this study, Tan-Wong *et al*. observed that the *ssu72-2* mutation blocks looping and confers a pronounced growth defect in combination with a Δ*rrp6* deletion. The protein Rrp6 is a component of the nuclear surveillance machinery that degrades aberrant noncoding RNAs (ncRNAs) synthesized by Pol II (*12*). Indeed, Δ*rrp6* was instrumental in discovering the pervasive nature of cryptic unstable transcripts (CUTs), most of which originate from nucleosome-free regions flanking protein-encoding genes (*13*). Thus, terminator regions can be transcribed in the antisense direction, and many promoters are inherently bidirectional, yielding either mRNA or ncRNA.

Does Ssu72, and more generally gene looping, repress transcription of CUTs? Tan-Wong *et al*. show that inactivation of Ssu72 (*ssu72-2* mutant) enhances production of

CREDIT: BICKEL/*SCIENCE*

Department of Biochemistry and Molecular Biology, Robert Wood Johnson Medical School, Piscataway, NJ 08854, USA. E-mail: michael.hampsey@umdnj.edu

Published by AAAS

ncRNAs across the yeast genome. Furthermore, by focusing on pairs of tandem genes where the promoter of the downstream gene is far from the termination region of the upstream gene, the authors established that enhanced synthesis of ncRNAs originates from the downstream bidirectional promoter, rather than from the upstream polyadenylation site (see the figure). Enhanced expression of CUTs, previously detected in the Δ*rrp6* deletion mutant, as well as an extensive set of new CUTs called SRTs (Ssu72-restricted transcripts), were observed in the *ssu72-2* mutant. However, enhanced synthesis of these ncRNAs was not specific to the *ssu72-2* mutation; other mutations that block looping—including *sua7-1* (which encodes a mutated form of TFIIB) and defects in the Pta1, Rna14, and Rna15 components of the 3′-end pre-mRNA processing machinery—exhibited similar enhancement of CUTs and SRTs. Accordingly, Tan-Wong *et al*. define a new function for gene loops: repression of ncRNA synthesis from bidirectional promoters.

It remains to be determined how gene loops repress upstream transcription. One scenario is that bidirectional transcription is mutually exclusive: Formation of one initiation complex precludes formation of an adjacent complex of opposite polarity. In this case, a promoter-terminator loop would simply repress ncRNA transcription by default. This possibility is consistent with the small decrease in mRNA production associated with the *ssu72-2* mutant observed by Tan-Wong *et al*. Alternatively, gene loops might actively block ncRNA synthesis, perhaps by localized recruitment of a repressive histone deacetylase complex.

Gene loops are not unique to yeast. For example, the HIV provirus forms a transcription-dependent gene loop between the 5′ long terminal repeat (LTR) promoter and the 3′ LTR polyadenylation site (*14*). Interestingly, proper 3′-end formation of mammalian β-globin mRNA stimulates transcription initiation of the β-globin gene —an effect that is most easily explained by looping-mediated recycling of Pol II (*15*). The extent to which gene loops might be a general feature of Pol II transcription awaits further investigation.

References and Notes

1. J. M. O'Sullivan *et al*., *Nat. Genet.* **36**, 1014 (2004).
2. A. Ansari, M. Hampsey, *Genes Dev.* **19**, 2969 (2005).
3. S. M. Tan-Wong *et al*., *Science* **338**, 671 (2012); 10.1126/science.1224350.
4. M. Hampsey, B. N. Singh, A. Ansari, J. P. Lainé, S. Krishnamurthy, *Adv. Enzyme Regul.* **51**, 118 (2011).
5. A. R. Bataille *et al*., *Mol. Cell* **45**, 158 (2012).
6. D. W. Zhang *et al*., *J. Biol. Chem.* **287**, 8541 (2012).
7. J. N. Kuehner, E. L. Pearson, C. Moore, *Nat. Rev. Mol. Cell Biol.* **12**, 283 (2011).
8. J. Dekker, K. Rippe, M. Dekker, N. Kleckner, *Science* **295**, 1306 (2002).
9. S. Medler *et al*., *J. Biol. Chem.* **286**, 33709 (2011).
10. S. M. Tan-Wong, H. D. Wijayatilake, N. J. Proudfoot, *Genes Dev.* **23**, 2610 (2009).
11. J. P. Lainé, B. N. Singh, S. Krishnamurthy, M. Hampsey, *Genes Dev.* **23**, 2604 (2009).
12. P. Preker *et al*., *Science* **322**, 1851 (2008).
13. Z. Xu *et al*., *Nature* **457**, 1033 (2009).
14. K. J. Perkins, M. Lusic, I. Mitar, M. Giacca, N. J. Proudfoot, *Mol. Cell* **29**, 56 (2008).
15. C. K. Mapendano, S. Lykke-Andersen, J. Kjems, E. Bertrand, T. H. Jensen, *Mol. Cell* **40**, 410 (2010).

Acknowledgments: M.H. is supported by NIH grant R01 GM039484.

10.1126/science.1230576

MATERIALS SCIENCE

Getting Moore from Solar Cells

Exploring alternative device designs and component materials will be crucial in improving solar cell performance.

David J. Norris[1] and Eray S. Aydil[2]

Biological organisms, when faced with a difficult environment, take advantage of the process of mutation. Beneficial mutations can help to optimize a known survival strategy or even reveal a new one. In solar cell research, a similar process is occurring. Solar cells must continue to improve in efficiency and cost if they are to thrive as a viable energy technology. Through the implementation of variations on known device architectures, "mutant" solar cells are leading not only to important incremental improvements but also to surprising new approaches. On page 643 of this issue, Lee *et al*. (*1*) demonstrate an example of the latter, introducing a new species of solar cell for study.

Photovoltaic solar cells convert sunlight into usable electrical power. After decades of research, several device archetypes have been established. These include long-standing approaches, such as the common silicon solar cell (*2*, *3*), and newer alternatives at various stages in their development (*4*). One example is the dye-sensitized solar cell (*5*), first reported in 1991. Unlike the silicon cell, it is a hybrid device made of both inorganic and organic components. A porous film of inorganic titania particles is deposited on an electrode. When a single layer of an organic dye molecule decorates the surface of these particles, sunlight is absorbed by the dye, generating electrons. If extremely small (nanometer-scale) titania particles are used, even a thin film contains sufficient surface area that most of the sunlight is absorbed by the dye. A voltage can then be established between the titania-coated electrode and a counterelectrode when a liquid electrolyte is placed in between. In this configuration, the device produces power when the film of titania particles performs several functions simultaneously: It provides a scaffold for the dye, collects the generated electrons, and transports these charges to the electrode.

Initially, dye-sensitized solar cells converted full sunlight into electricity with an efficiency of 7.1% (5). By comparison, crystalline silicon solar cells convert full sunlight into electricity with an efficiency of 25%. However, because titania particles are inexpensive to produce and spread on a surface, dye-sensitized solar cells were pursued as a low-cost alternative to silicon. Moreover, through optimization of the dye and the electrolyte, their efficiency now stands at an impressive 12.3% (6).

The basic concept of the dye-sensitized solar cell has also provided a good launching point for "mutations" to further improve this performance. The titania nanoparticles have been replaced with other structures, such as semiconductor nanowires (*7*, *8*); the dye replaced with other light absorbers, such as semiconductor quantum dots (*9*); and the liquid electrolyte replaced with solid conductors, such as organic semiconductors (*10*). Changing two of these simultaneously has also been explored (*11*). However, so far, none of these mutations have yielded cost or efficiency benefits over the conventional dye-sensitized solar cell.

By changing three elements of the dye-sensitized solar cell simultaneously, the results reported by Lee *et al*. suggest a shift in that stalemate. They replaced the titania

[1]Optical Materials Engineering Laboratory, ETH Zürich, 8092 Zürich, Switzerland. [2]Department of Chemical Engineering and Materials Science, University of Minnesota, Minneapolis, MN 55455, USA. E-mail: dnorris@ethz.ch; aydil@umn.edu

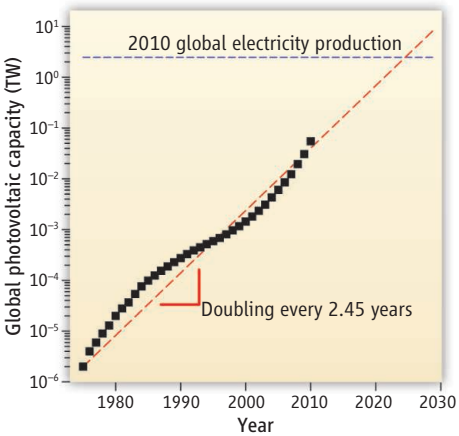

Moore's law for solar cells. The accumulated amount of photovoltaic solar cells manufactured from 1975 to 2010, in terawatts (*13*). The red dashed line is a linear fit to the data and represents a doubling of the global capacity every 2.45 years since 1975. The blue dashed line is the gross electricity produced globally from all sources in 2010 (*14*) for comparison.

nanoparticles with alumina nanoparticles, the dye with a thin layer of an organic-inorganic perovskite (*12*), and the liquid electrolyte with a solid organic conductor. The outcome was a device that converted full sunlight with an efficiency of 10.9%, a truly impressive number, especially for a combination one might not expect to perform at all.

In particular, alumina is nonconductive and cannot transport the light-generated electrons to the electrode. Consequently, the alumina performs only one of the three required functions—a high-surface-area scaffold upon which the light-absorbing perovskite is placed. But then how does the device work? The other functions are apparently assumed by the perovskite, which is a hybrid solid consisting of an inorganic framework (a metal halide) with small organic molecules in its voids. Although this sounds exotic, these materials are known to behave like semiconductors, allowing them to absorb the sunlight and create electrons. Without the titania, the perovskite also has to transport this charge to the electrode. Because the overall device performance is high, the perovskite apparently accomplishes all of these tasks surprisingly well.

Replacing the simple organic dye with the perovskite also sounds complicated (and expensive). However, Lee *et al*. show that highly crystalline layers of these materials can be grown simply by coating the surfaces of the alumina particles with a solution of low-cost molecular precursors followed by mild heating. The high structural quality of the resulting films is presumably one reason the perovskite can collect and transport the electrons so efficiently. Because the absorbing layer is produced by simple and inexpensive solution processing, the Lee *et al*. device also maintains a primary advantage of the conventional dye-sensitized solar cell: low cost.

On the basis of this first report, researchers can now evolve the new device and search for further improvements. An obvious target is the organic-inorganic perovskite. The specific lead halide used is only one example of a large class of possible perovskites (*12*). Exploring related materials can also provide an opportunity to eliminate the lead, a worthwhile goal for environmental protection.

These and other "mutants" are intended to help photovoltaic solar cells make an impact on the world's electricity production (see the figure). Global photovoltaic solar cell capacity has doubled every 2.5 years between 1975 and 2010. Such exponential growth is reminiscent of the famous Moore's law in integrated circuits, which states that the number of transistors on a computer chip doubles every 2 years. Although not a physical law, it has provided a self-fulfilling prophecy for the computer industry for several decades. Will solar cell manufacturers be able to maintain their Moore-like growth? In particular, recent increases have occurred during a period of government subsidies. If the political or economic environment changes, then technological improvements in performance and cost will be needed more than ever to stay on track. Research on mutant solar cells, which can lead to improvements in both efficiency and cost, has an important role to play in achieving this goal.

References

1. M. M. Lee, J. Teuscher, T. Miyasaka, T. N. Murakami, H. J. Snaith, *Science* **338**, 643 (2012); 10.1126/science.1228604.
2. D. M. Chapin, C. S. Fuller, G. L. Pearson, *J. Appl. Phys.* **25**, 676 (1954).
3. C. A. Wolden *et al*., *J. Vac. Sci. Technol. A* **29**, 030801 (2011).
4. M. Graetzel, R. A. J. Janssen, D. B. Mitzi, E. H. Sargent, *Nature* **488**, 304 (2012).
5. B. O'Regan, M. Gratzel, *Nature* **353**, 737 (1991).
6. A. Yella *et al*., *Science* **334**, 629 (2011).
7. J. B. Baxter, E. S. Aydil, *Appl. Phys. Lett.* **86**, 053114 (2005).
8. M. Law, L. E. Greene, J. C. Johnson, R. Saykally, P. D. Yang, *Nat. Mater.* **4**, 455 (2005).
9. A. J. Nozik, *Physica E* **14**, 115 (2002).
10. U. Bach *et al*., *Nature* **395**, 583 (1998).
11. K. S. Leschkies *et al*., *Nano Lett.* **7**, 1793 (2007).
12. D. B. Mitzi, *Prog. Inorg. Chem.* **48**, 1 (1999).
13. Earth Policy Institute, *World Solar Photovoltaics Production, 1975–2010* (2011); www.earth-policy.org/datacenter/xls/indicator12_2011_1.xls.
14. International Energy Agency, *Electricity Information 2012* (2012); www.oecd-ilibrary.org/energy/electricity-information-2012_electricity-2012-en.

10.1126/science.1230283

BIOCHEMISTRY

Templating a Molecular Tug-of-War

Michael R. Diehl

Tying cytoskeletal motors together on a DNA rope reveals how opposing motors compete to determine the direction of cargo transport.

The activated transport of organelles, vesicles, and many other subcellular commodities along cytoskeletal filaments is central to mechanisms that regulate the internal organization of eukaryotic cells (*1*). The motions of these cargos are driven by several classes of ATP–dependent enzymes called motor proteins that are capable of converting chemical energy into mechanical work. A variety of bulk biochemical and single-molecule techniques have been developed over the past decade to characterize the principles that allow these enzymes to function effectively as molecular machines (*2*, *3*). Yet most cargos are transported by multicomponent motor systems containing multiple copies of the same motor, or even by mixtures of different classes of motors that move with different velocities, in opposite directions, and along different types of cytoskeletal filaments (*4*, *5*). Understanding how motors cooperate productively and compete antagonistically has therefore become increasingly important for dissecting mechanisms that regulate intracellular transport as well as the impact of motor mutations in diseases. On page 662 of this issue, Derr *et al*. (*6*) demonstrate a new materials approach to these problems that allows the characterization of key relationships among the structural organization of multiple motor systems, the

Departments of Chemistry and Bioengineering, Rice University, Houston, TX 77030, USA. E-mail: diehl@rice.edu

properties of motors within these complexes, and their collective dynamic behaviors.

Current studies of collective motor functions have been confounded by the fact that the number and spatial arrangement of motors on a cargo are unknown in most assays and must be inferred from analyses of cargo motions. The combination of these experimental deficiencies and the inherent complexities of collective motor behaviors have left many aspects of multiple motor dynamics poorly defined and controversial. To address these challenges, several groups have developed methods to generate organized motor complexes using molecular scaffolds composed of protein-based polymers, linear DNA duplexes, and other biomacromolecules (*7*–*9*). These approaches provide important abilities to quantify differences between single and multiple motor run lengths, velocities, and force production. However, they have allowed small motor complexes to be prepared that typically only contain two identical motors. Derr *et al*. have overcome this limitation by engineering DNA scaffolds, called DNA origami, in order to create motor complexes that better reflect the size and complexity of the motor systems responsible for the transport of natural cargos. The DNA origami is formed by folding a long viral single-stranded DNA strand into an organized structure by annealing this strand with collections of small oligonucleotides called "staple strands," which hybridize to different regions of the viral DNA (*10*). This method allows long molecular scaffolds to be synthesized whose persistence length can far exceed that of a single DNA duplex because multiple duplexes can be tied together. The staple strands can also be extended from the structure and used to specify sites where DNA-tagged motors and fluorescent labeling strands are linked to the scaffold. The resulting ability to program the number, sequence, and spatial presentation of these handles allows near-arbitrarily complex, three-dimensional scaffolds to be prepared that can template the self-assembly of multiple protein systems containing collections of different proteins.

The development of recombinant yeast dynein expression constructs that can be outfitted with oligonucleotides also provided Derr *et al*. with new opportunities to engineer motor complexes containing oppositely directed kinesin and dynein motors and then examine how these microtubule motors compete to control the direction of cargo motion. Single kinesin motors move processively toward the plus end of microtubules and can produce forces up to 7 pN. Yeast dynein is a minus end–directed motor and has been found to stall at somewhat smaller forces (5 pN) (*11*). One may therefore expect that teams of kinesins would prevail over similar-sized teams of dyneins during a molecular tug-of-war. However, Derr *et al*. found that collections of dyneins tended to win this competition, except in extreme cases where the number of kinesins far outweighed the number of dyneins in a complex. These results show that factors other than a motor's stalling force can play key roles determining how motors cooperate in groups. They are also consistent with recent optical trapping studies that have suggested that teams of kinesins use only a small fraction of their motors at a time when transporting cargos against opposing loads on average (*9*, *12*). This weak cooperative response has been attributed to kinesin's relatively high stepping rate under load and large stalling force relative to its critical detachment force (*8*, *13*). Although these properties allow kinesin to function efficiently as single motor molecules, they can produce kinetic constraints that limit the ability of multiple kinesins to cooperate productively by sharing their applied loads (see the figure). The present dynein motors possess much higher filament affinities than kinesin and advance at much lower rates, which appears to relieve these constraints, yielding net minus end–directed motions even at low dynein-to-kinesin ratios.

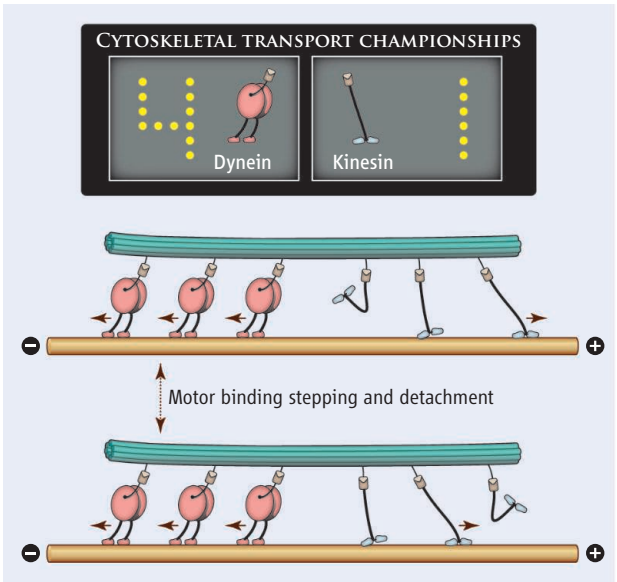

Oppositely directed motors compete in a tug-of-war. Many cargos are outfitted with different types of antagonistic cytoskeletal motors in cells and move bidirectionally along cytoskeletal filaments. Using molecular scaffolds call DNA origami to generate organized multiple motor complexes, Derr *et al*. show that teams of yeast dyneins tend to win tug-of-war competitions with multiple kinesins. Despite its lower stalling force, dynein's high microtubule affinity tips the scale in the dynein team's favor because this property allows more dyneins to remain engaged during a tug-of-war against a team of kinesins, which tend to use only a small fraction of their motors during the competition.

The ability to controllably tune the motor ratios will likely shed light on intracellular transport regulatory mechanisms. The dominant role of high-affinity motors in the present ensembles suggests that controlling their number and activities will be particularly influential to tug-of-war competitions. Nevertheless, the mechanochemical properties of motors can vary appreciably depending on their structure and association with specific accessory factors, indicating that characteristically different collective responses can potentially be produced by other motor systems. Analogously rich collective behaviors are known to occur when nonmotile proteins interact in groups and operate as integrated biosynthetic factories and signaling complexes (*14*, *15*). Consequently, the ability to make use of DNA self-assembly techniques to engineer organized multiple protein assemblies and deterministically modulate their composition will likely constitute an important new approach to dissecting the functions of various integrated macromolecular systems of proteins.

References

1. R. D. Vale, *Cell* **112**, 467 (2003).
2. M. T. Valentine, S. P. Gilbert, *Curr. Opin. Cell Biol.* **19**, 75 (2007).
3. K. Visscher, M. J. Schnitzer, S. M. Block, *Nature* **400**, 184 (1999).
4. A. L. Jolly, V. I. Gelfand, *Biochem. Soc. Trans.* **39**, 1126 (2011).
5. A. G. Hendricks *et al*., *Curr. Biol.* **20**, 697 (2010).
6. N. D. Derr *et al*., *Science* **338**, 662 (2012).
7. M. R. Diehl, K. Zhang, H. J. Lee, D. A. Tirrell, *Science* **311**, 1468 (2006).
8. D. K. Jamison, J. W. Driver, M. R. Diehl, *J. Biol. Chem.* **287**, 3357 (2012).
9. J. Xu, Z. Shu, S. J. King, S. P. Gross, *Traffic* **13**, 1198 (2012).
10. P. W. K. Rothemund, *Nature* **440**, 297 (2006).
11. A. Gennerich, A. P. Carter, S. L. Reck-Peterson, R. D. Vale, *Cell* **131**, 952 (2007).
12. D. K. Jamison, J. W. Driver, A. R. Rogers, P. E. Constantinou, M. R. Diehl, *Biophys. J.* **99**, 2967 (2010).
13. J. W. Driver *et al*., *Biophys. J.* **101**, 386 (2011).
14. C. T. Walsh, *Science* **303**, 1805 (2004).
15. J. G. Zalatan, S. M. Coyle, S. Rajan, S. S. Sidhu, W. A. Lim, *Science* **337**, 1218 (2012).

10.1126/science.1230818

Marine Microbes See a Sea of Gradients

Roman Stocker

Marine bacteria influence Earth's environmental dynamics in fundamental ways by controlling the biogeochemistry and productivity of the oceans. These large-scale consequences result from the combined effect of countless interactions occurring at the level of the individual cells. At these small scales, the ocean is surprisingly heterogeneous, and microbes experience an environment of pervasive and dynamic chemical and physical gradients. Many species actively exploit this heterogeneity, while others rely on gradient-independent adaptations. This is an exciting time to explore this frontier of oceanography, but understanding microbial behavior and competition in the context of the water column's microarchitecture calls for new ecological frameworks, such as a microbial optimal foraging theory, to determine the relevant trade-offs and global consequences of microbial life in a sea of gradients.

Twenty years ago much of microbial oceanography was based on the assumption that molecules and organisms are randomly distributed, with little regard for gradients and behavioral responses (*1*). There is now abundant evidence that nutrients are not homogeneously distributed at the scales relevant to the microorganisms and instead frequently arise as microscale hot spots. Many bacteria exploit heterogeneity by swimming toward the epicenter of hot spots, whereas others survive in low-concentration, uniform background conditions.

Although tools to interrogate the behavior of marine microbes at the level of single cells and their microenvironment have begun to be developed, the conceptual frameworks needed to evaluate the trade-offs and ecosystem implications of life in microscale gradients lag behind. Integrating microscale observations with ecological frameworks will shed light on important unexplored questions in microbial oceanography. What are the effects of gradients on microbial diversity in the ocean? How do they affect productivity? Do the consequences of heterogeneity simply average out, justifying mean-field descriptions based on bulk concentrations and a neglect of behavior, or do microscale gradients affect the rates and fluxes of biogeochemical transformation? This Review describes the nature and prevalence of microscale gradients in the ocean, the response of microbes to these gradients, and the putative mechanisms by which these processes can affect the marine ecosystem at a global scale.

At What Scales Do Marine Microbes Interact with Their Environment?

To understand the behavior of an organism, it must be studied in relation to its immediate environment. Marine microorganisms affect large-scale processes in the sea, including the cycling of most elements, the rates and fate of primary production, and the generation of climatically active gases (*2*), yet they live and interact with the ocean at the microscale. In terms of relative scale, environmental conditions at tens of meters resolution are to a microbe what the mean world temperature is to an African lion: a useful metric for global trends, but hardly a mechanistic ecological predictor.

How large, then, is a microbial microenvironment in the ocean? Rather than being a fixed volume (*3*), it depends on behavior and time, as simple calculations exemplify. For a nonmotile bacterium (or archaeon), cell size (~0.4- to 2-μm diameter) defines the microenvironment. For example, nutrient uptake occurs from a small region surrounding the organism, the diffusion boundary layer, which spans a few cell diameters. There is little motion of the cell relative to the surrounding water, with Brownian diffusion allowing a 0.4-μm–diameter cell to explore 45 pl of seawater (a ~35-μm cube) in 10 min and 80 nl (a ~430-μm cube) in a day.

In contrast, the microenvironment of a swimming bacterium is largely defined by its motility range. One can calculate that randomly swimming at 50 μm/s enables a bacterium to experience 0.5 μl (a ~0.8-mm cube) of new water every 10 min and 0.8 ml (a ~1 cm cube) every day. Chemotaxis (the ability to sense chemical gradients and direct motility accordingly) further increases the distance a microbe can traverse: a chemotactic velocity (the directional component of swimming) of 10 μm/s results in a net displacement of 6 mm in 10 min.

Microbial microenvironments can thus be large compared with cell size but are still tiny relative to most oceanographic sampling methods. With rare exceptions, these volumes remain difficult to interrogate in situ, owing to the small size and intermittency of microenvironments and the minuscule amount of matter they contain. We must gain better access to the marine microscale, in terms of tools and conceptual frameworks, if we are to understand the consequences of resource heterogeneity and microbial behavior on diversity, productivity, and biogeochemistry.

How Heterogeneous Is the Ocean at the Microscale?

It has long been recognized that the water column is dotted with copious sources of microscale heterogeneity (Fig. 1). A ubiquitous case is the "phycosphere," the region surrounding a phytoplankton cell, which harbors gradients of dissolved organic matter [DOM; operationally defined as the organic material <0.7 μm in size (*2*)] and oxygen that attract heterotrophic bacteria (*4*, *5*). This attraction can result in diverse ecological interactions between bacteria and algae, from symbiosis to parasitism, and can increase the fraction of primary production used by bacteria (*6*). Equally widespread are marine snow particles, aggregates that also contain gradients of DOM and oxygen (*7*) and emanate intense DOM plumes as they sink (*8*, *9*). The particles and their plumes can attract and become growth hot spots for bacteria (*9*, *10*). Strong gradients are further created by excretions from larger organisms, cell lysis, and sloppy feeding. These sources of heterogeneity, along with a multitude of particle types ranging from colloids to fecal pellets to exopolymers, can vary in size from micrometers to centimeters, and harbor resource concentrations orders of magnitude above background levels.

These processes have led to the view that even a milliliter of seawater is far from homogeneous (*3*). I suggest that microscale gradients are in fact considerably more pervasive than even these sources of heterogeneity indicate, for three reasons. First, the majority of inputs of microbial resources are heterogeneous at microbial scales: 10- to 1000-μm oil droplets originating from spills or natural seeps, 50- to 5000-μm gas bubbles released from natural vents or injected by breaking waves, sediment grains resuspended by currents, and dust particles of aeolian origin are all constituents of large-scale events that for marine microorganisms resolve into a patchy landscape peppered with discrete resources and microscale gradients.

Second, turbulence converts macroheterogeneity into microheterogeneity. In the process of mixing a solute such as DOM, turbulent whirls stir the solute into ever-finer sheets and filaments (see Box 1 and associated figure). This stretching and folding continues down to a scale below which molecular diffusion dissipates gradients to truly mix the solute. For typical marine turbulence levels, this scale, known as the Batchelor scale, ranges from 30 to 300 μm. Thus, irrespective of the size of the DOM source, turbulence produces a rich fabric of gradients at the scale of microbial microenvironments.

Third, chemical gradients are compounded by physical gradients. Microscale viscosity gradients can develop inside and around particles, but also

Ralph M. Parsons Laboratory, Department of Civil and Environmental Engineering, 49-213, Massachusetts Institute of Technology, 77 Massachusetts Avenue, Cambridge, MA 02139, USA. E-mail: romans@mit.edu

in the bulk medium, where colloids and mucus sheets can form tangled polymer webs (*3*). Gradients in fluid velocity due to turbulent shear can occur at millimeter scales and result in subtle hydrodynamic interactions with cell shape (*11*). Salinity can equally vary on submillimeter scales, owing, for example, to pockets of interstitial fluid carried by porous particles sinking through the water column (*12*).

Likely as a consequence of this heterogeneity, bacteria are also heterogeneously distributed, with recorded variations in cell concentration of up to 20-fold over 10 to 30 mm (*13*). Thus, despite its superficial homogeneous appearance, the water column can have a rich physical, chemical, and biological microarchitecture, not unlike that of environments dominated by surfaces, such as sediments or animal hosts. In the following, I focus on a specific adaptation to this heterogeneity: chemotactic motility.

How Pervasive Are Behavioral Responses to Microscale Gradients?

Chemotactic motility is not only the most conspicuous adaptation to microscale chemical gradients, but also a de facto demonstration of their existence. A subtle distinction is in order: motility alone does not increase microbial nutrient uptake, whereas chemotaxis can. The description of marine bacteria as the "ultimate swimming stomachs" [J. Stern in (*14*)] should not be interpreted in the same manner as whales swimming open-mouthed to catch plankton: The uptake rate of a bacterium while it swims is the same as when it rests, except for very high molecular weight solutes (*15*). In contrast, cells can increase uptake by residing in high-concentration microenvironments, which they find by chemotaxing along gradients. Thus, chemotactic motility is intimately linked to microscale gradients. But how prevalent is motility among marine bacteria?

It contrast to phytoplankton, whose motility is a well-studied, distinguishing trait (e.g., in the competition between diatoms and dinoflagellates), or enteric bacteria, whose chemotaxis is among the best understood cellular processes, bacterial motility and its prevalence have been given less attention in the ocean. On one hand, we know that some numerically abundant organisms, such as *Pelagibacter ubique* of the SAR11 clade, are nonmotile (*16*). On the other hand, direct observation has shown that many marine bacteria are motile (*17*), and the fraction of motile cells can be as high as 20 to 60% (*18*, *19*). Further, metagenomic studies have revealed that genes for motility and chemotaxis can be common in the photic zone (*20*). Nutrient enrichment can elevate the motile fraction from <10 to >50% in 12 hours (*21*), which suggests either a lag time for the activation of motility or the occurrence of a rapid community shift upon episodic resource inputs.

Motility is typically associated with the ability to respond to gradients. Laboratory observations have shown that marine strains are capable of chemotaxing into the DOM plumes emanating from settling particles (*10*), to high phosphate concentrations in phosphate-limited environments (*22*), toward dimethylsulfoniopropionate to associate with algae (*23*, *24*), and toward lysing organisms (*5*) and cyanobacterial exudates (*25*). In a dynamic version of the phycosphere, they can even briefly pursue swimming algae (*26*).

Motility demarcates two evolutionary strategies among marine bacteria. These are broadly aligned with the dichotomy between oligotrophs and copiotrophs. Oligotrophs, such as *P. ubique*, are adapted to life in nutrient-poor conditions. Their minute size (~0.4 μm in diameter) allows them to maximize uptake per unit biomass and to extract nutrients at the minuscule bulk concentrations characteristic of the ocean (*27*). Their streamlined genome lacks many functional and regulatory genes, including those for motility and chemotaxis (*16*); The latter would be vain at any rate, because directed swimming is trounced by Brownian effects for cells <0.6 μm in diameter (*28*). Streamlining also implies poor metabolic plasticity and an inability to exploit high-resource conditions (*29*).

In contrast, copiotrophs are adapted to take advantage of rare, resource-rich conditions: Their abundance of motility and chemotaxis genes, together with fast uptake kinetics, indicate that their success is linked to an ability to exploit microscale gradients (*27*), and their abundance will be a reflection of the texture of the resource landscape. The metabolic flexibility of copiotrophs allows them to adapt rapidly to newly encountered microenvironments (*30*), for example, by disproportionately increasing protease activity upon attachment to particles (*31*), though their size and uptake kinetics would make them less competitive at low resource concentrations.

The numerical abundance of marine bacteria is often dominated by nonmotile oligotrophs, such as members of the SAR11 clade (*29*). However, to assess the importance of copiotrophs relative to oligotrophs—and therefore the importance of microscale gradients—in shaping large-scale ecosystem properties, one must go beyond abundance and consider activity. The relation between abundance and activity in the ocean remains unclear (*32*), but there is evidence that rare taxa have proportionately higher potential growth rates

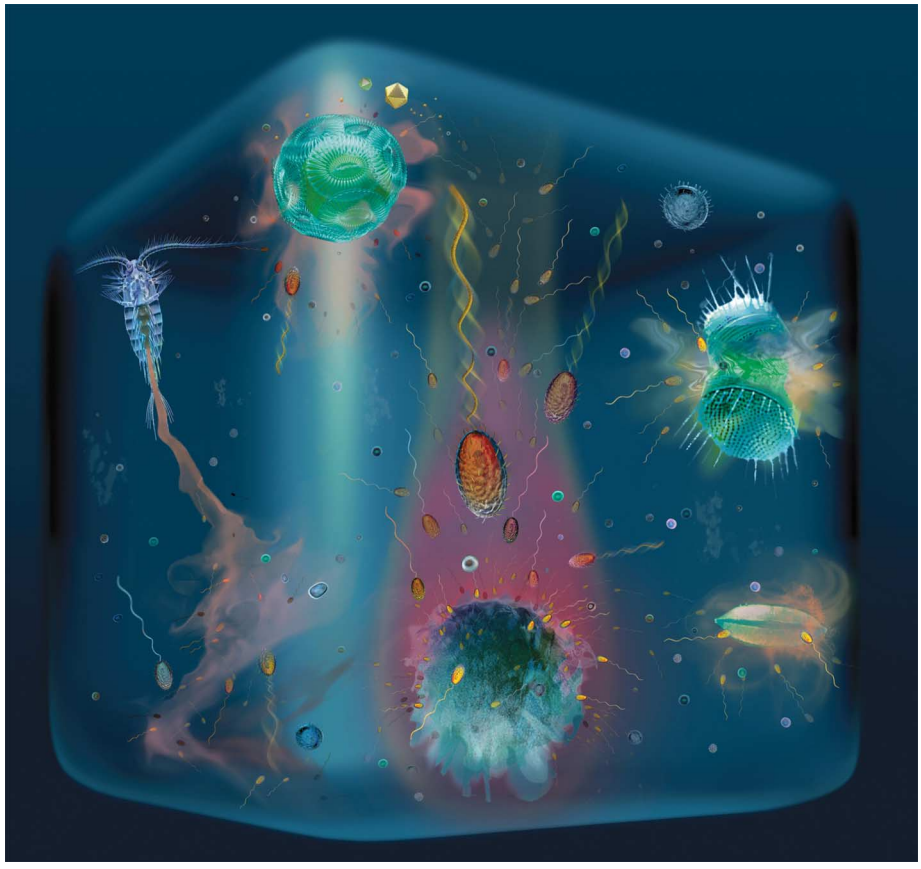

Fig. 1. Marine microbial microenvironments. Disparate processes contribute to make the ocean a sea of gradients, from the vantage point of microorganisms, including DOM exudation by phytoplankton (top), cell lysis events (top right), stationary or sinking detritus and marine snow particles (bottom center), and copepod excretions (left). Marine bacteria adopt one of two broad strategies: They can be motile, propelling themselves with corkscrewlike flagella to exploit microscale gradients, or nonmotile, optimizing uptake of solutes diffusing to them and saving the cost of swimming. [Modified from the cover of *Science*, 5 February 2010, with permission; original image credits: R. Stocker, J. R. Seymour, G. Gorick]

Box 1. The Batchelor scale in the ocean

The shape of a solute patch is affected by two transport processes: diffusion and turbulence. Turbulence stirs the patch into ever-finer filaments. As a filament thins, the associated gradient (the concentration contrast with the background, divided by the filament width) grows. This increases the effect of diffusion, which is proportional to the magnitude of the gradient, in erasing the gradient. There is, hence, a scale where the effects of turbulence and diffusion balance. This scale is the Batchelor scale (*54*), $(\nu D^2/\varepsilon)^{1/4}$, which in the sea ranges from 30 to 300 μm depending on the turbulent dissipation rate ε, the diffusivity of the solute D, and the kinematic viscosity of seawater, ν.

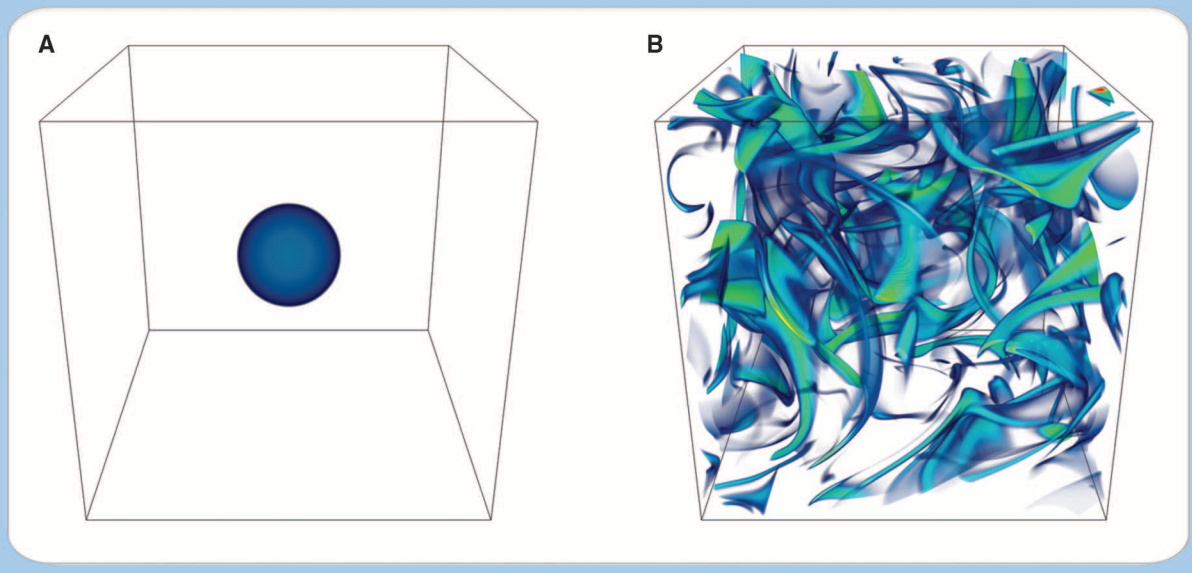

Turbulence stirs chemical resources of any size into a complex web of microscale gradients. Any source of a dissolved substance in the ocean (**A**), even if macroscopic, will produce a tangle of sheets and filaments (**B**). The characteristic scale of the resulting gradients is set by the Batchelor scale. The image on the right is the result of a direct numerical simulation modeling the fate of a centimeter-scale patch exposed to turbulence for 30 s (with a turbulent dissipation rate ε of 10^{-6} W/kg). [Image courtesy of J. R. Taylor]

than abundant taxa (*32*). Bacteria on particles are less numerous than free-living bacteria, but they are frequently larger and more active (*30*). In an example from a different aquatic environment, an oligotrophic lake, the large (270 μm^3) motile bacterium *Chromatium okenii* was found to be responsible for >40% of total ammonium uptake and >70% of total carbon uptake, despite accounting for only 0.3% of the total cell number (*33*). In contrast, the small (1.2 μm^3) nonmotile *Chlorobium clathratiforme* only contributed 15% to total ammonium uptake and 15% to total carbon uptake, despite having a 100-fold larger numerical abundance and a 10% larger total biovolume compared with *C. okenii*. Geographic distribution also matters: Copiotrophs are most abundant in the coastal ocean, where DOM inputs are greater (*34*) and impacts on biogeochemistry proportionally larger. Furthermore, the metabolic plasticity of copiotrophs suggests that they are the early responders to biogeochemical perturbations, as evidenced by increases in motility and chemotaxis after drastic events such as algal blooms (*19*) and nutrient enrichments (*21*). Whether these higher levels of activity and readiness to respond to change often exhibited by copiotrophs outweigh the numerical dominance of oligotrophs in shaping marine biogeochemistry remains a fundamental open question in microbial oceanography.

Do Gradients Drive Specific Adaptations Among Marine Microbes?

The abundance of oligotrophs testifies to the stringent trade-offs in the utilization of microscale gradients in the ocean. Because most hot spots are ephemeral, chemotaxis is a race against time, which suggests selection for advanced chemotactic strategies. Evidence for specific adaptations for exploiting microscale gradients includes the discovery of the high swimming speeds of many marine bacteria, whose mean velocities, often exceeding 60 to 80 μm/s (*10*, *21*, *22*, *24*), dwarf the 15 to 30 μm/s of *Escherichia coli* and allow fast chemotactic responses and large increases in potential nutrient uptakes (*10*, *24*).

Rapid swimming has major energetic implications. The persistent viewpoint that motility is inexpensive for bacteria was developed for slow swimmers (*E. coli*) in nutrient-rich (e.g., enteric) environments (*35*) and is unlikely to apply in the ocean, where nutrients are orders of magnitude scarcer and the required propulsive power, proportional to speed squared, is more than 10 times as great. A model of competition for a nutrient patch between motile and nonmotile bacteria revealed a trade-off between the additional uptake afforded by swimming toward nutrient-rich filaments (see the Box) and the energetic cost of motility to find and reach filaments (*36*). Optimal predicted swimming velocities (~60 μm/s) fall within the observed range, which suggests that bioenergetic trade-offs are important in determining adaptations to microscale gradients.

Given the high energetic cost of motility, cells might have evolved adaptive strategies to exploit gradients, for example by activating motility only when the resource landscape justifies it. The question is "Can marine bacteria actively modulate motility, and over what time scales?" Recorded lags of several hours (*21*) suggest that motility is not tunable over the lifetime of an individual patch (~10 min), but can be resumed after episodic nutrient inputs. Yet, other evidence suggests that motility is highly intermittent at time scales of tens of seconds (*19*).

Another potentially ocean-specific adaptation is the hybrid swimming pattern of some monotrichous (i.e., having a single flagellum) marine bacteria, such as *Vibrio alginolyticus* and *Pseudoalteromonas haloplanktis*. These bacteria deviate from *E. coli*'s prototypical swimming behavior, alternating reversals in direction with strong reorientations caused by a rapid "flick" of the

flagellum (*37*). This is likely a strategy that guarantees effective turning, while requiring the synthesis of only a single flagellum, again highlighting that microbial motility in the ocean might be best understood in a cost-benefit framework.

Do Microscale Gradients Affect Species Composition and Diversity?

Gradients can provide a fitness advantage to motile cells. Mathematical models predict that growth rates increase 50% for cells that cluster around nutrient patches (*38*) and up to 10-fold for those chemotaxing into DOM plumes (*9*). These estimates are consistent with microfluidic experiments, which revealed a fourfold increase in potential uptake rates for bacteria responding to plumes over those that cannot (*10*).

Likely as a result of the fitness implications of gradients, microenvironments can affect species composition. For example, bacteria on particles are taxonomically different from free-living bacteria (*39*), and laboratory manipulations have shown that the dominant phylotypes change during a diatom bloom (*40*). Can gradients, i.e., the intricacy of the microscale nutrient landscape, also affect species diversity? Because spatial and temporal gradients in the nutrient landscape represent two formidable dimensions in niche space, it seems plausible that the diversity of motile bacteria is, on average, larger than the diversity of nonmotile bacteria. On the one hand, the high diversity among copiotrophs such as *Vibrios* and the association of clusters of closely related *Vibrionaceae* with distinct microenvironments (*41*) is in line with this prediction: Could chemotactic motility, widespread among *Vibrios*, have contributed to determine these diversity patterns? On the other hand, it remains difficult to compare the degree of diversity among clades and thus to determine whether microscale gradients represent a fundamental determinant of diversity and whether the diversity of copiotrophs is in general larger than the diversity of oligotrophs. These questions represent exciting targets for future molecular investigations.

Can Microscale Gradients Affect Ocean Biogeochemistry?

The consequences of microscale gradients on biogeochemical dynamics and productivity are less intuitive. The most naïve interpretation is that microscale interactions simply average out. Several pieces of evidence indicate that this is not the case, but a consistent framework is lacking.

Macroscopic dynamics in patchy environments can differ significantly from mean-field descriptions based on bulk seawater concentrations. For

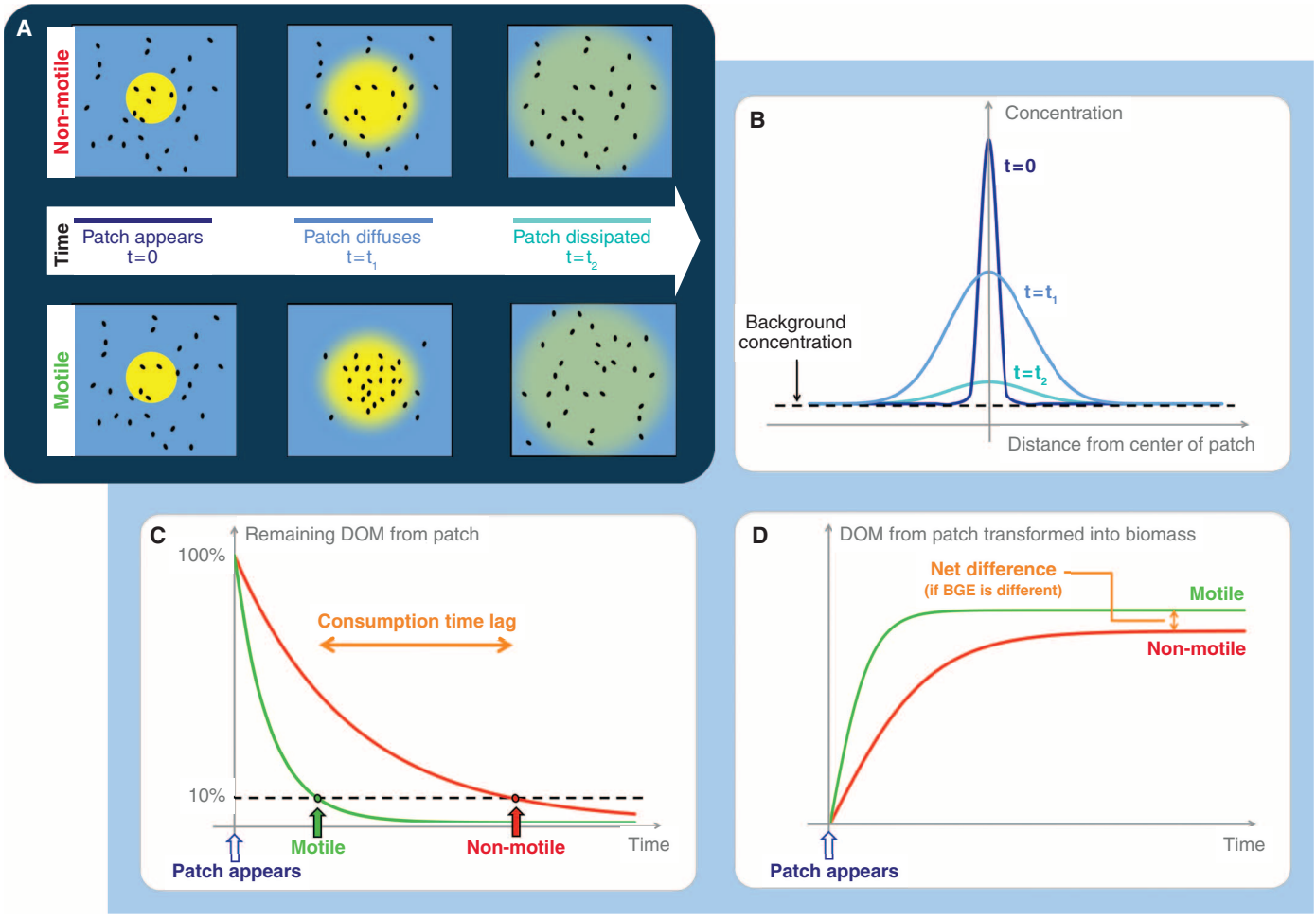

Fig. 2. The fate of the DOM from a patch. In order to understand the consequences of motility and the utilization of microscale gradients, it is useful to consider two scenarios: an ocean of nonmotile bacteria and one of motile (and chemotactic) bacteria. (**A**) A patch of DOM appearing within a suspension of bacteria can attract motile cells, whereas nonmotile cells remain randomly distributed. (A and **B**) DOM eventually diffuses into background concentrations, typically over time scales of minutes. (A and **C**) Chemotaxis into the patch can result in faster DOM consumption by motile bacteria, compared with nonmotile bacteria. Ultimately, however, the entire DOM from the patch is consumed in both cases, unless other processes intervene to reduce the bioavailability of DOM during the short (~minutes) time lag in DOM consumption between nonmotile and motile bacteria (see text). (**D**) Consumption by motile bacteria could increase the fraction of DOM that is transformed into biomass, if motile bacteria have higher BGE than nonmotile bacteria. Differences in BGE would have direct effects on the flow of carbon through the microbial loop and on biogeochemical fluxes and, thus, represent an important target for experimental quantification.

example, bacterial chemotaxis to microscale DOM gradients has been predicted to increase remineralization rates twofold (*42*). For phytoplankton, modeling predicts that productivity is several times larger in heterogeneous than in homogeneous conditions (*43*). Similarly, observations of phytoplankton growth in the face of nondetectable levels of limiting nutrients have been attributed to intermittent nutrient pulses (*44*).

To identify potential effects of microscale gradients on biogeochemical fluxes, it is instructive to consider how a small DOM patch affects bacteria, for nonmotile bacteria and for chemotactic bacteria (Fig. 2A). Only a minuscule fraction of the bacteria will initially find themselves by chance inside the patch, yet typically, most are within 100 to 1000 μm of the next patch (*45*). As the patch diffuses (Fig. 2, A and B), nonmotile cells remain randomly distributed, whereas many motile cells cluster inside the patch within tens of seconds (*5*, *10*, *24*). Does this behavior affect the total amount of DOM transformed into bacterial biomass? We need to consider that the entire DOM from the patch, which diffuses to uniformity within minutes, might ultimately be consumed in both the motile and the nonmotile scenarios, in which case DOM consumption may simply be accelerated if perpetrated by motile bacteria (Fig. 2C). In other words, do responses to microscale gradients purely change the time scale over which DOM is remineralized or also the total amount of DOM that is remineralized?

There are several mechanisms by which differential gradient utilization may affect total amounts, not only time scales. A first mechanism relates to the bacterial growth efficiency (BGE), the fraction of carbon taken up that cells incorporate as biomass (the remainder, they respire). BGE increases with growth rate and with resource concentration when measured across different marine provinces (*6*). Given the higher concentrations within patches and the higher maximum growth rates of copiotrophs, might copiotrophs have larger BGEs than oligotrophs? If metabolic studies were to verify this hypothesis, then DOM uptake by copiotrophs would channel more carbon into the microbial loop than uptake by oligotrophs (Fig. 2D).

A second mechanism concerns the feedback between primary production and remineralization. By clustering near phytoplankton (*4*), motile bacteria may not only accelerate remineralization of algal DOM but also enhance the productivity of phytoplankton by supplying them with inorganic nutrients. Evidence for the pervasiveness of these associations has come from atomic force microscopy measurements, which recently revealed that heterotrophic bacteria and cyanobacteria are "conjoint" on average 30% of the time (*46*). Calculations predict that motile bacteria have orders-of-magnitude higher chances of ending up conjoint than nonmotile bacteria and that this propinquity markedly increases solute fluxes between heterotrophs and autotrophs. A further example is the remineralization of organic matter on sinking marine snow particles, which favors the retention of limiting elements in the upper water column and thereby stimulates primary production and the formation of more marine snow. Motility can enhance this process by increasing particle colonization rates up to fivefold (*9*).

Finally, the time lag in DOM consumption by nonmotile bacteria compared with motile bacteria (Fig. 2C), which are faster at locating DOM patches, may reduce the metabolic accessibility of DOM, because the latter becomes increasingly refractory over time (*3*, *47*). It remains to be determined whether this degradation affects DOM bioavailability on the time scale (~minutes) of the consumption lag.

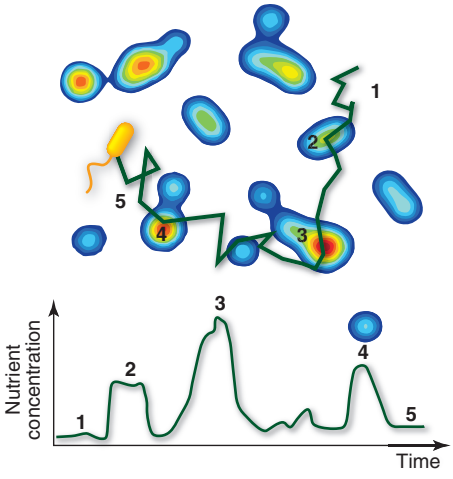

Fig. 3. Optimal foraging. The nutrient concentration encountered by marine bacteria varies considerably over time scales as short as seconds to minutes, owing to pervasive chemical and physical gradients in their immediate environment. For motile bacteria, which actively exploit nutrient gradients, this variability is greater than for nonmotile bacteria. Optimal foraging frameworks—where utilization of nutrient patches is weighted against the cost of motility but also, e.g., against the increased risks of predation and viral infection—promise to help determine the dominant foraging strategies of marine bacteria as a function of the environmental conditions. These frameworks will require new information on bacterial metabolism, including, for example, the dependence of uptake kinetics and BGE on nutrient concentration, to determine to what extent the behavioral responses of bacteria to microscale gradients affect ocean ecosystem-level properties.

Behavioral responses to microenvironments can also have indirect effects on biogeochemistry. The attachment of heterotrophic bacteria to diatoms can favor diatom aggregation by stimulating the production of sticky extracellular polymers (*48*). Aggregation accelerates sinking and, thus, the efficiency of the biological pump in transporting carbon from the surface ocean to depth. Bacterial attachment to diatoms, in turn, could be strongly favored by algal exudate gradients and bacterial motility, particularly during the algae's stickier senescent phase (*4*).

Outlook: Shrinking Our Fields of View While Expanding Our Ecological Frameworks

Advances in microbial oceanography have been repeatedly triggered by new tools, from the fluorescent staining of cells to flow cytometry to metagenomics. As we begin to appreciate how heterogeneous and diverse the world of marine microbes is, there is now scope for techniques that probe this world at the scale of single cells and microenvironments. Bulk sampling techniques, where liters of water are collected and homogenized, provide valuable information on the mean microbial environment but cannot capture the local conditions experienced by microbes. To do so, we must shrink our operational field of view. Exciting opportunities are in sight on a number of fronts: Genomics is reaching single-cell resolution (*49*), secondary ion mass spectrometry (nanoSIMS) is revealing the chemical signature of individual cells (*50*), atomic force microscopy is shedding light on the spatial organization of marine microbes (*46*), and microfluidic technology is unveiling microbial behavior within realistic microenvironments (*10*, *24*, *25*, *51*). Yet, it remains difficult to interrogate microenvironments in situ, owing to their small volumes and intermittent nature: There is "plenty of room at the bottom" for measurements of microbial behavior and the microscale chemical concentration gradients that shape it.

Tools, however, are not the sole limiting factor in our understanding of microbial ecology in the context of a heterogeneous microlandscape. We also lack quantitative ecological frameworks to rationalize and scale up microenvironmental processes. Unraveling the relation between gradients and motility; between patchiness and diversity; and between behavior, uptake kinetics, and biogeochemical fluxes calls for theoretical ecologists to dive into microbial oceanography. Microbes' fast generation times, vast numbers, disparate interactions, and rich spatial organization make microbial oceanography an intriguing, yet underappreciated, model system for testing ecological theory. Glimpses of this trend can be seen in microbial biogeography, where predictions for taxa-area relations and longitudinal gradients in species abundance have been recently tested on marine microorganisms (*52*).

In contrast, little ecological theory has been applied at the scale of microbial microenvironments. Fitness-based models can provide unifying frameworks to evaluate the role of specific adaptations, such as high swimming speeds, hybrid locomotion, and metabolic plasticity. For example, the bacterial nutrient quest in a sea of microscale patches is a quintessential optimal foraging problem (Fig. 3). Optimal foraging theory predicts the movement behavior that maximizes the fitness of an organism whose resources are heterogeneous (*53*). Motile marine bacteria live in a dynamic equilibrium between disparate micro-

environments: What strategies do they adopt to optimize foraging and fitness? Might only a minority of cells stumble upon the right combination of nutrient patches and survive, i.e., is the mean motile bacterium a dead bacterium? How are gene expression and uptake kinetics tuned to the intermittency of nutrient encounters? How do episodic events, such as blooms and spills, and top-down controls, such as predation and viral lysis, play into the competition and succession between oligotrophs and copiotrophs? If new approaches to quantify the metabolism and behavior of marine bacteria at the level of single cells can be brought to bear onto these questions and if the resulting insights can be integrated into comprehensive ecological frameworks, we will achieve a deeper understanding of the functions of bacteria in the oceans and, ultimately, improve our ability to predict the dynamics of Earth's biosphere.

References and Notes

1. F. Azam, D. C. Smith, in *Particle Analysis in Oceanography*, S. Demers, Ed. (NATO ASI Series G27, Springer, Berlin, 1991), pp. 213–236.
2. D. L. Kirchman, *Microbial Ecology of the Oceans* (Wiley & Sons, New York, 2008).
3. F. Azam, F. Malfatti, *Nat. Rev. Microbiol.* **5**, 782 (2007).
4. W. Bell, R. Mitchell, *Biol. Bull.* **143**, 265 (1972).
5. N. Blackburn, T. Fenchel, J. Mitchell, *Science* **282**, 2254 (1998).
6. P. A. del Giorgio, J. J. Cole, *Annu. Rev. Ecol. Syst.* **29**, 503 (1998).
7. A. L. Alldredge, Y. Cohen, *Science* **235**, 689 (1987).
8. D. C. Smith, M. Simon, A. L. Alldredge, F. Azam, *Nature* **359**, 139 (1992).
9. T. Kiørboe, G. A. Jackson, *Limnol. Oceanogr.* **46**, 1309 (2001).
10. R. Stocker, J. R. Seymour, A. Samadani, D. E. Hunt, M. F. Polz, *Proc. Natl. Acad. Sci. U.S.A.* **105**, 4209 (2008).
11. H. Marcos, H. C. Fu, T. R. Powers, R. Stocker, *Proc. Natl. Acad. Sci. U.S.A.* **109**, 4780 (2012).
12. K. Kindler, A. Khalili, R. Stocker, *Proc. Natl. Acad. Sci. U.S.A.* **107**, 22163 (2010).
13. J. R. Seymour, J. G. Mitchell, L. Pearson, R. L. Waters, *Aquat. Microb. Ecol.* **22**, 143 (2000).
14. F. Azam, *Science* **280**, 694 (1998).
15. J. S. Guasto, R. Rusconi, R. Stocker, *Annu. Rev. Fluid Mech.* **44**, 373 (2012).
16. S. J. Giovannoni *et al.*, *Science* **309**, 1242 (2005).
17. J. E. Johansen, J. Pinhassi, N. Blackburn, U. L. Zweifel, A. Hågström, *Aquat. Microb. Ecol.* **28**, 229 (2002).
18. T. Fenchel, *Aquat. Microb. Ecol.* **24**, 197 (2001).
19. H.-P. Grossart, L. Riemann, F. Azam, *Aquat. Microb. Ecol.* **25**, 247 (2001).
20. E. F. DeLong *et al.*, *Science* **311**, 496 (2006).
21. J. G. Mitchell *et al.*, *Appl. Environ. Microbiol.* **61**, 877 (1995).
22. A. Hütz, K. Schubert, J. Overmann, *Appl. Environ. Microbiol.* **77**, 4412 (2011).
23. T. R. Miller, R. Belas, *Environ. Microbiol.* **8**, 1648 (2006).
24. J. R. Seymour, R. Simó, T. Ahmed, R. Stocker, *Science* **329**, 342 (2010).
25. J. R. Seymour, T. Ahmed, W. M. Durham, R. Stocker, *Aquat. Microb. Ecol.* **59**, 161 (2010).
26. G. M. Barbara, J. G. Mitchell, *FEMS Microbiol. Ecol.* **44**, 79 (2003).
27. F. M. Lauro *et al.*, *Proc. Natl. Acad. Sci. U.S.A.* **106**, 15527 (2009).
28. D. B. Dusenbery, *Living at Micro Scale* (Harvard Univ. Press, Cambridge, MA, 2009).
29. S. Yooseph *et al.*, *Nature* **468**, 60 (2010).
30. B. Ayo *et al.*, *Mar. Biol.* **138**, 1071 (2001).
31. H.-P. Grossart, K. W. Tang, T. Kiørboe, H. Ploug, *FEMS Microbiol. Lett.* **266**, 194 (2007).
32. B. J. Campbell, L. Yu, J. F. Heidelberg, D. L. Kirchman, *Proc. Natl. Acad. Sci. U.S.A.* **108**, 12776 (2011).
33. N. Musat *et al.*, *Proc. Natl. Acad. Sci. U.S.A.* **105**, 17861 (2008).
34. H. Ducklow, in *Microbial Ecology of the Oceans*, D. L. Kirchman, Ed. (Wiley, New York, 2000), pp. 85–120.
35. E. M. Purcell, *Am. J. Phys.* **45**, 3 (1977).
36. J. R. Taylor, R. Stocker, *Science* **338**, 675 10.1126/science.1219417 (2012).
37. L. Xie, T. Altindal, S. Chattopadhyay, X.-L. Wu, *Proc. Natl. Acad. Sci. U.S.A.* **108**, 2246 (2011).
38. N. Blackburn, F. Azam, A. Hågström, *Limnol. Oceanogr.* **42**, 613 (1997).
39. E. F. DeLong, D. G. Franks, A. L. Alldredge, *Limnol. Oceanogr.* **38**, 924 (1993).
40. L. Riemann, G. F. Steward, F. Azam, *Appl. Environ. Microbiol.* **66**, 578 (2000).
41. D. E. Hunt *et al.*, *Science* **320**, 1081 (2008).
42. T. Fenchel, *Science* **296**, 1068 (2002).
43. S. J. Brentnall, K. J. Richards, J. Brindley, E. Murphy, *J. Plankton Res.* **25**, 121 (2003).
44. J. J. McCarthy, J. C. Goldman, *Science* **203**, 670 (1979).
45. F. Azam, J. W. Ammerman, in *Marine Phytoplankton and Productivity*, O. Holm-Hansen, L. Bolis, R. Gilles, Eds. (Springer, Berlin, 1984).
46. F. Malfatti, F. Azam, *Aquat. Microb. Ecol.* **58**, 1 (2009).
47. R. G. Keil, D. L. Kirchman, *Mar. Chem.* **45**, 187 (1994).
48. A. Gärdes, M. H. Iversen, H.-P. Grossart, U. Passow, M. S. Ullrich, *ISME J.* **5**, 436 (2011).
49. T. Kalisky, S. R. Quake, *Nat. Methods* **8**, 311 (2011).
50. M. Wagner, *Annu. Rev. Microbiol.* **63**, 411 (2009).
51. J. R. Seymour, T. Ahmed, R. Marcos, R. Stocker, *Limnol. Oceanogr. Methods* **6**, 477 (2008).
52. J. A. Fuhrman, *Nature* **459**, 193 (2009).
53. G. H. Pyke, *Annu. Rev. Ecol. Syst.* **15**, 523 (1984).
54. G. K. Batchelor, *J. Fluid Mech.* **5**, 113 (1959).

Acknowledgments: I thank E. F. DeLong, W. M. Durham, V. Fernandez, M. S. Garren, M. Gatto, D. L. Kirchman, F. M. Lauro, F. Malfatti, J. G. Mitchell, M. F. Polz, J. R. Seymour, S. Smriga, and B. Ward for insightful discussions and comments on the manuscript, and J. R. Taylor for the figure on turbulence. I am grateful for support by NSF through grants OCE-0744641-CAREER and CBET-0966000, and by NIH through grant 1R01GM100473.

10.1126/science.1208929

A Quantum Delayed-Choice Experiment

Alberto Peruzzo,[1]* Peter Shadbolt,[1]* Nicolas Brunner,[2]† Sandu Popescu,[2] Jeremy L. O'Brien[1]‡

Quantum systems exhibit particle- or wavelike behavior depending on the experimental apparatus they are confronted by. This wave-particle duality is at the heart of quantum mechanics. Its paradoxical nature is best captured in the delayed-choice thought experiment, in which a photon is forced to choose a behavior before the observer decides what to measure. Here, we report on a quantum delayed-choice experiment in which both particle and wave behaviors are investigated simultaneously. The genuinely quantum nature of the photon's behavior is certified via nonlocality, which here replaces the delayed choice of the observer in the original experiment. We observed strong nonlocal correlations, which show that the photon must simultaneously behave both as a particle and as a wave.

Quantum mechanics predicts with remarkable accuracy the result of experiments involving small objects, such as atoms and photons. However, when looking more closely at these predictions we are forced to admit that they defy our intuition. Indeed, quantum mechanics tells us that a single particle can be in several places at the same time, and that distant entangled particles behave as a single physical object no matter how far apart they are (*1*).

In trying to grasp the basic principles of the theory—in particular, to understand more intuitively the behavior of quantum particles—the notion of wave-particle duality was introduced (*2*). A quantum system—for instance, a photon—may behave either as a particle or a wave. However, the way in which it behaves depends on the kind of experimental apparatus with which it is measured. Hence, both aspects, particle and wave, which appear to be incompatible, are never observed simultaneously (*3*). This is the notion of complementarity in quantum mechanics (*4*–*7*), which is central in the standard Copenhagen interpretation and has been intensely debated in the past.

In an effort to reconcile quantum predictions and common sense, it was suggested that quantum particles may in fact know in advance to which experiment they will be confronted, via a hidden variable, and could thus decide which behavior to exhibit. This simplistic argument was, however, challenged by Wheeler in his elegant "delayed choice" arrangement (*8*–*10*). In this gedanken experiment, as shown in Fig. 1A, a quantum particle is sent toward a Mach-Zender interferometer. The relative phase φ between the two arms of the interferometer can be adjusted so that the particle will emerge in output D' with certainty. That is, the interference is fully constructive in output D' and fully destructive in output D''. This measurement thus clearly highlights the wave aspect of the quantum particle. However, the observer performing the experiment has the choice of modifying the above experiment, in particular by removing the second beamsplitter of the interferometer. In this case, he will perform a which-path measurement. The photon will be detected in each mode with probability one half, thus exhibiting particle-like behavior. The main point is that the experimentalist is free to choose which experiment to perform (interference or which-path, thus testing the wave or the particle aspect) once the particle is already inside the interferometer. Thus, the particle could not have known in advance (for instance via a hidden variable) the kind of experiment with which it will be confronted because this choice was simply not made when the particle entered the interferometer. Wheeler's experiment has been implemented experimentally by using various systems, all confirming quantum predictions (*11*–*15*). In a recent experiment with single photons, a spacelike separation between the choice of measurement and the moment the photon enters the interferometer was achieved (*16*).

We explored a conceptually different take on Wheeler's experiment. Our starting point is a recent theoretical proposal (*17*) of a delayed-choice experiment based on a quantum-controlled beamsplitter, which can be in a superposition of present and absent. Hence, the interferometer can be simultaneously closed and open, thus testing both the wave and the particle behavior of the photon at the same time. Using a reconfigurable integrated quantum photonic circuit (*18*), we implemented an interferometer featuring such a quantum beamsplitter, observing continuous morphing between wave and particle behavior (*17*). However, this morphing behavior can be reproduced by a simple classical model, and this loophole also plagues both the theoretical proposal of (*17*) as well as two of its recent nuclear magnetic resonance (NMR) implementations (*19*, *20*). In order to overcome this issue, we then experimentally demonstrated a quantum delayed-choice scheme based on Bell's inequality (*21*), which allowed us to test the most general classical model. The main conceptual novelty of this scheme is that the temporal arrangement of Wheeler's original proposal—the delayed choice of closing the interferometer or not—is not necessary anymore. Instead, we certify the quantum nature of the photon's behavior by observing the violation of a Bell inequality. This demonstrates in a device-independent way—that is, without making assumptions about the functioning of the devices—that no local hidden variable model can reproduce the quantum predictions. In other words, no model in which the photon decided in advance which behavior to exhibit—knowing in advance the measurement setup—can account for the observed statistics. In our experiment, we achieve strong Bell inequality violations, hence giving an experimental refutation to such hidden variable models, up to a few additional assumptions about the implementation that are regularly used in experimental Bell tests.

Our scheme is presented in Fig. 1B. A single photon (our system) is sent through an interferometer. At the first beamsplitter, the photon evolves into a superposition of the two spatial modes, represented by two orthogonal quantum states $|0\rangle_s$ and $|1\rangle_s$. Formally, this first beam-

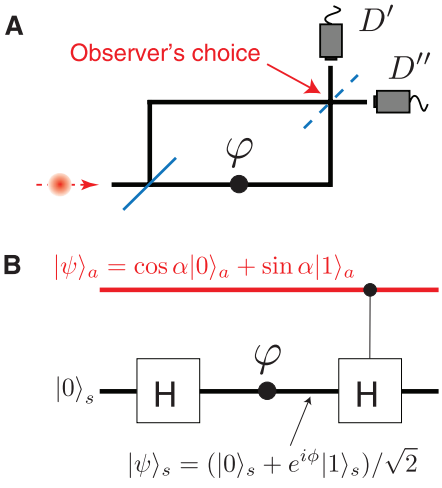

Fig. 1. Quantum delayed-choice experiment. (**A**) Schematic of Wheeler's original delayed-choice experiment. A photon is sent into a Mach-Zehnder interferometer and split into a superposition across both paths at the first beamsplitter (solid blue line). By inserting (or not) the second beamsplitter (dashed blue line), wave (or particle) behavior can be observed at detectors D' or D''. (**B**) Schematic of the quantum delayed-choice experiment. The second beamsplitter is now a quantum beamsplitter (represented by a controlled-Hadamard operation), which can be set in a superposition of present and absent by controlling the state of an ancilla photon $|\psi\rangle_a$.

[1]Centre for Quantum Photonics, H. H. Wills Physics Laboratory and Department of Electrical and Electronic Engineering University of Bristol, Bristol BS8 1UB, UK. [2]H. H. Wills Physics Laboratory, University of Bristol, Tyndall Avenue, Bristol BS8 1TL, UK.

*These authors contributed equally to this work.
†Present address: Département de Physique Théorique, Université de Genève, 1211 Genève, Switzerland.
‡To whom correspondence should be addressed. E-mail: jeremy.obrien@bristol.ac.uk

splitter is represented by a Hadamard operation (*22*), which transforms the initial photon state $|0\rangle_s$ into the superposition $(|0\rangle_s + |1\rangle_s)/\sqrt{2}$. A phase shifter then modifies the relative phase between the two modes, resulting in the state $|\psi\rangle_s = (|0\rangle_s + e^{i\varphi}|1\rangle_s)/\sqrt{2}$. Both modes are then recombined on a second beamsplitter before a final measurement in the logical $(\{|0\rangle_s, |1\rangle_s\})$ basis. In the standard delayed-choice experiment, the presence of this second beamsplitter is controlled by the observer (see Fig. 1A). For a closed interferometer, the statistics of the measurements at detectors D' and D'' will depend on the phase φ, revealing the wave nature of the photon. For an open interferometer, both detectors will click with equal probability, revealing the particle nature of the photon.

Here, on the contrary, the presence of the second beamsplitter depends on the state of an ancillary photon. If the ancilla photon is prepared in the state $|0\rangle_a$, no beamsplitter is present; hence, the interferometer is left open. Formally, this corresponds to the identity operator acting on $|\psi\rangle_s$, resulting in the state

$$|\psi\rangle_{s,\text{particle}} = \frac{1}{\sqrt{2}}(|0\rangle_s + e^{i\varphi}|1\rangle_s) \qquad (1)$$

The final measurement (in the $\{|0\rangle_s, |1\rangle_s\}$ basis) indicates which path the photon took, revealing the particle nature of the photon. The measured intensities in both output modes are equal and phase-independent, $I_{D'} = I_{D''} = 1/2$.

If, however, the ancilla photon is prepared in the state $|1\rangle_a$, the beamsplitter is present, and the interferometer is therefore closed. Formally, this corresponds to applying the Hadamard operation to $|\psi\rangle_s$, resulting in the state

$$|\psi\rangle_{s,\text{wave}} = \cos\frac{\varphi}{2}|0\rangle_s - i\sin\frac{\varphi}{2}|1\rangle_s \qquad (2)$$

The final measurement gives information about the phase φ that was applied in the interferometer, but indeed not about which path the photon took. The measured intensities are $I_{D'} = \cos^2(\varphi/2)$ and $I_{D''} = \sin^2(\varphi/2)$.

The main feature of this quantum controlled beamsplitter is that it can be put in a superposition of being present and absent. Indeed, if the ancilla photon is initially in a superposition—for instance, in the state $|\psi\rangle_a = \cos\alpha|0\rangle_a + \sin\alpha|1\rangle_a$—then the global state of the system evolves into

$$|\Psi_f(\alpha,\varphi)\rangle = \cos\alpha|\psi\rangle_{s,\text{particle}}|0\rangle_a + \sin\alpha|\psi\rangle_{s,\text{wave}}|1\rangle_a \qquad (3)$$

The system and ancilla photons now become entangled, when $0 < \alpha < \pi/2$.

The measured intensity at detector D' is then given by

$$I_{D'}(\varphi,\alpha) = I_{\text{particle}}(\varphi)\cos^2\alpha + I_{\text{wave}}(\varphi)\sin^2\alpha = \frac{1}{2}\cos^2\alpha + \cos^2\left(\frac{\varphi}{2}\right)\sin^2\alpha \qquad (4)$$

whereas intensity at D'' is $I_{D''}(\varphi, \alpha) = 1 - I_{D'}(\varphi, \alpha)$.

We fabricated the quantum circuit shown in Fig. 2 in a silica-on-silicon photonic chip (*18*). The Hadamard operation is implemented by a directional coupler of reflectivity 1/2, which is equivalent to a 50/50 beamsplitter. The controlled-Hadamard (CH) is based on a nondeterministic control-phase gate (*23*, *24*). The system and ancilla photon pairs are generated at 808 nm via parametric down conversion and detected with silicon avalanche photodiodes at the circuit's output.

We first characterized the behavior of our setup for various quantum states of the ancilla photon. We measured the output intensities $I_{D'}(\varphi, \alpha)$ and $I_{D''}(\varphi, \alpha)$ for $\alpha \in [0, \pi/2]$, and $\varphi \in [-\pi/2, 3\pi/2]$. In particular, by increasing the value of α we observe the morphing between a particle measurement ($\alpha = 0$) and a wave measurement ($\alpha = \pi/2$). For $\alpha = 0$ (no beamsplitter), the measured intensities are independent of φ. For $\alpha = \pi/2$, the beamsplitter is present, and the data shows interference fringes. Our results are in excellent agreement with theoretical predictions (Fig. 3).

To achieve our main goal—to refute models in which the photon knows in advance with which setup it will be confronted—we must go one step further. Indeed, the result of Fig. 3 does not refute such models. Although we have inserted the ancilla photon in a superposition, hence testing both wave and particle aspects at the same time, we have in fact not checked the quantum nature of this superposition. This is because the final measurement of the ancilla photon was made in the logical $(\{|0\rangle_a, |1\rangle_a\})$ basis. Therefore, we cannot exclude the fact that the ancilla may have been in a statistical mixture of the form $\cos^2\alpha|0\rangle\langle 0|_a + \sin^2\alpha|1\rangle\langle 1|_a$, which would lead to the same measured statistics. Hence, the data can be explained by a classical model, in which the state of the ancilla represents a classical variable (a classical bit) indicating which measurement, particle or wave, will be performed. Because the state of the ancilla may have been known to the system photon in advance—indeed, here no delayed choice is performed by the observer—no conclusion can be drawn from this experiment. This loophole also plagues the recent theoretical proposal of (*17*), as well as two of its NMR implementations (*19*, *20*).

In order to show that the measurement choice could not have been known in advance, we must ensure that our quantum controlled beamsplitter behaves in a genuine quantum way. In particular, we must ensure that it creates entanglement between the system and ancilla photons, which is the clear signature of a quantum process. The global state of the system and ancilla photons, given in Eq. 3, is entangled for all values $0 < \alpha < \pi/2$. Because $\langle\psi_{\text{particle}}|\psi_{\text{wave}}\rangle \sim \cos\varphi$, the degree of entanglement depends on φ and α; in particular, for $\alpha = \pi/4$ and $\varphi = \pi/2$ the state in Eq. 3 is maximally entangled.

In order to certify the presence of this entanglement, we tested the Clauser-Horne-Shimony-Holt (CHSH) Bell inequality (*25*), the violation

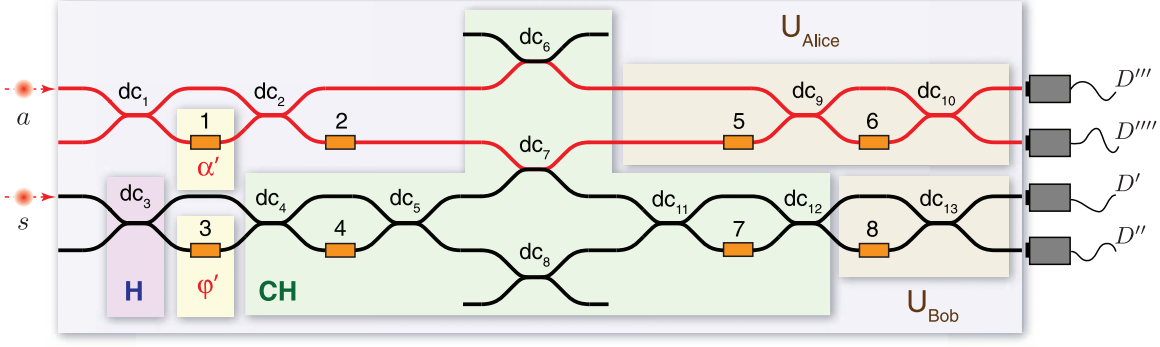

Fig. 2. Implementation of the quantum delayed-choice experiment on a reconfigurable integrated photonic device. Nonentangled photon pairs are generated by using type I parametric down-conversion and injected into the chip by using polarization maintaining fibers (not shown). The system photon (*s*), in the lower part of the circuit, enters the interferometer at the Hadamard gate (*H*). A relative phase φ is applied between the two modes of the interferometer. Then, the controlled-Hadamard (CH) is implemented by a nondeterministic CZ gate with two additional MZ interferometers. The ancilla photon (*a*), in the top part of the circuit, is controlled by the phase shifter α, which determines the quantum state of the second beamsplitter—a superposition of present and absent. Last, the local measurements for the Bell test are performed through single-qubit rotations (U_A and U_B) followed by APDs. The circuit is composed of directional couplers of reflectivity 1/2 (dc_{1-5} and dc_{9-13}) and 1/3 (dc_{6-8}) and resistive heaters (orange rectangles) that implement the phase shifters (*25*).

of which would imply in a device-independent way that the measured data could not have been produced by a classical model. In the CHSH Bell scenario, each party (here, Alice holds the system photon while Bob holds the ancilla photon) chooses among two possible measurement settings, denoted $x = 0,1$ for Alice and $y = 0,1$ for Bob. Each measurement is dichotomic, giving a binary result $A_x = \pm 1$ and $B_y = \pm 1$. The CHSH inequality then reads

$$S = \langle A_0 B_0 \rangle + \langle A_0 B_1 \rangle + \langle A_1 B_0 \rangle - \langle A_1 B_1 \rangle \leq 2 \quad (5)$$

This represents a Bell inequality in the sense that any local model must satisfy it.

Indeed, this inequality can be violated by making judiciously chosen local measurements on certain entangled states. We measured S for the output state $|\Psi_f(\alpha, \varphi)\rangle$ for $\alpha \in [0, \pi/2]$ and $\varphi \in [-\pi/2, 3\pi/2]$. We tailored the local measurement operators of Alice and Bob [adjusting phase shifters 5, 6, and 8 (*26*)] for the maximally entangled state $|\Psi_f(\alpha = \pi/4, \varphi = \pi/2)\rangle$. Hence, for this state we expect the maximal possible violation of the CHSH inequality in quantum mechanics—namely, $S = 2\sqrt{2}$ (*27*). The choice of apparatus in Wheeler's original setup is here, in some sense, replaced by the choice of measurement settings for the Bell test. The latter choice is nevertheless conceptually different from the former, in that it can be performed after the photon left the interferometer.

Experimentally, we observed a maximal violation of $S = 2.45 \pm 0.03$ for $\alpha = \pi/4$ and $\varphi = \pi/2$, which is in good agreement with theoretical predictions (Fig. 4). Therefore, our data could not have been accounted for by any model in which the system photon would have known in advance whether to behave as a particle or as a wave. However, for this claim to hold without making further assumptions, a loophole-free Bell inequality violation is required. This is not the case in our experiment, as in all optical Bell tests performed so far, which forces us to make a few additional assumptions. We make the standard fair-sampling assumption (allowing us to discard inconclusive results and postselect only coincidence events), which must here be slightly strengthened because of the nondeterministic implementation of the controlled Hadamard operation. We must also assume independence between the photon source and the choice of measurement setting used in the Bell inequality test. As usual, if the photons could know in advance the choice of measurement setting in the Bell test, then a local model can mimic Bell inequality violations. It would be interesting to perform a more refined experiment in which these assumptions could be relaxed (*28*, *29*).

We have reported on a quantum delayed-choice experiment, giving a novel demonstration of wave-particle duality, Feynman's "one real mystery" in quantum mechanics. In our experiment, the delayed choice of Wheeler's proposal is replaced by a quantum controlled beamsplitter followed by a Bell inequality test. In this way, we demonstrate genuine quantum behavior of single photons. The demonstration of a quantum controlled beamsplitter shows that a single measurement device can continuously tune between particle and wave measurements, hence pointing toward a more refined notion of complementarity in quantum mechanics (*17*, *30*–*32*).

Note added in proof. We note a related work of Kaiser *et al*. (*33*), who performed a similar quantum delayed-choice experiment.

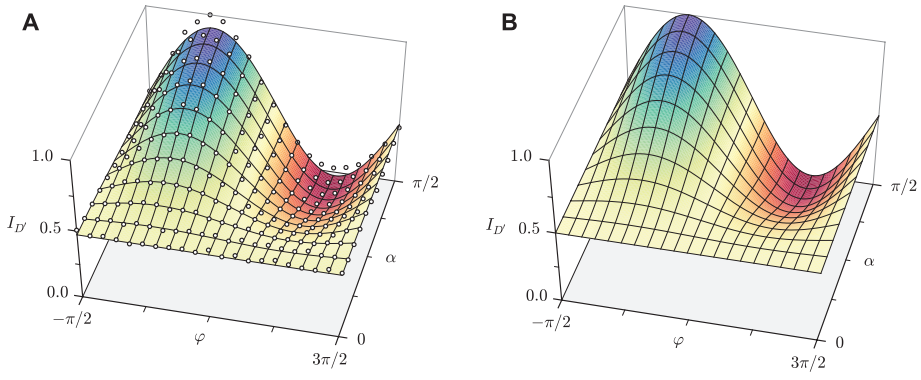

Fig. 3. Characterization of the continuous transition between wave and particle behavior. (**A**) Measured and (**B**) simulated intensity at detector D' when continuously tuning the state of the ancilla photon $|\psi\rangle_a$. The experimental data (white dots) were fitted by using Eq. 4. The data shows excellent agreement with theoretical predictions. Error bars due to Poissonian noise are smaller than the data points; hence, they are not drawn. The discrepancy between the experimental and theoretical results is not due to statistical fluctuations but to imperfection in the device calibration.

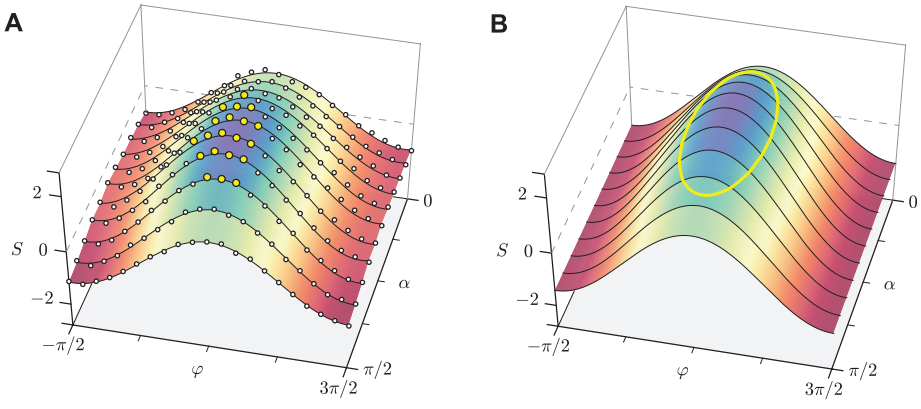

Fig. 4. Experimental Bell-CHSH inequality test. (**A**) Measured and (**B**) simulated Bell-CHSH parameter S (Eq. 1). When the CHSH inequality is violated—when $S > 2$ [yellow dots in (A) and yellow circle in (B)]—no local hidden variable model can explain the observed data, hence demonstrating genuine quantum behavior. The maximal experimental violation ($S = 2.45 \pm 0.03$) is achieved for $\alpha = \pi/4$ and $\varphi = \pi/2$, as expected. The data are in excellent agreement with theoretical predictions. Error bars due to Poissonian noise are smaller than the data points; hence, they are not drawn. The discrepancy between the experimental and theoretical results is not due to statistical fluctuations but to imperfection in the device calibration.

References and Notes

1. J. S. Bell, *Speakable and Unspeakable in Quantum Mechanics* (Cambridge Univ. Press, Cambridge, 2004).
2. R. P. Feynman, R. B. Leighton, M. L. Sands, *Lecture Notes on Physics* (Addison-Wesley, Reading, MA, 1965).
3. N. Bohr, in *Quantum Theory and Measurement*, J. A. Wheeler, W. H. Zurek, Eds. (Princeton Univ. Press, Princeton, NJ, 1984), pp. 9–49.
4. M. O. Scully, B.-G. Englert, H. Walther, *Nature* **351**, 111 (1991).
5. B.-G. Englert, *Phys. Rev. Lett.* **77**, 2154 (1996).
6. W. K. Wootters, W. H. Zurek, *Phys. Rev. D Part. Fields* **19**, 473 (1979).
7. V. Jacques *et al*., *Phys. Rev. Lett.* **100**, 220402 (2008).
8. J. A. Wheeler, in *Mathematical Foundations of Quantum Mechanics*, A. R. Marlow, Ed. (Academic, New York, 1978), pp. 9–48.
9. J. A. Wheeler, in *Quantum Theory and Measurement*, J. A. Wheeler, W. H. Zurek, Eds. (Princeton Univ. Press, Princeton, NJ, 1984), pp. 182–213.
10. A. J. Leggett, in *Compendium of Quantum Physics*, D. Greenberger, K. Hentschel, F. Weinert, Eds. (Springer, Berlin, 2009), pp. 161–166.
11. T. Hellmut, H. Walther, A. G. Zajonc, W. Schleich, *Phys. Rev. A* **35**, 2532 (1987).
12. B. J. Lawson-Daku *et al*., *Phys. Rev. A* **54**, 5042 (1996).
13. Y.-H. Kim, R. Yu, S. P. Kulik, Y. Shih, M. O. Scully, *Phys. Rev. Lett.* **84**, 1 (2000).
14. A. Zeilinger, G. Weihs, T. Jennewein, M. Aspelmeyer, *Nature* **433**, 230 (2005).

15. A. Zeilinger, G. Weihs, T. Jennewein, M. Aspelmeyer, *Nature* **446**, 342 (2007).
16. V. Jacques *et al.*, *Science* **315**, 966 (2007).
17. R. Ionicioiu, D. R. Terno, *Phys. Rev. Lett.* **107**, 230406 (2011).
18. P. J. Shadbolt *et al.*, *Nat. Photonics* **6**, 45 (2012).
19. S. S. Roy, A. Shukla, T. S. Mahesh, *Phys. Rev. A* **85**, 022109 (2012).
20. R. Auccaise *et al.*, *Phys. Rev. A* **85**, 032121 (2012).
21. J. S. Bell, *Physics* **1**, 195 (1964).
22. M. A. Nielsen, I. L. Chuang, *Quantum Computation and Quantum Information* (Cambridge Univ. Press, Cambridge, MA, 2000).
23. T. C. Ralph, N. K. Langford, T. B. Bell, A. G. White, *Phys. Rev. A* **65**, 062324 (2002).
24. H. F. Hofmann, S. Takeuchi, *Phys. Rev. A* **66**, 024308 (2002).
25. J. F. Clauser, M. Horne, A. Shimony, R. A. Holt, *Phys. Rev. Lett.* **23**, 880 (1969).
26. Materials and methods are available as supplementary materials on *Science* Online.
27. B. S. Cirel'son, *Lett. Math. Phys.* **4**, 93 (1980).
28. A. Aspect, J. Dalibard, G. Roger, *Phys. Rev. Lett.* **49**, 1804 (1982).
29. G. Weihs, T. Jennewein, C. Simon, H. Weinfurter, A. Zeilinger, *Phys. Rev. Lett.* **81**, 5039 (1998).
30. J.-S. Tang, Y.-L. Li, C.-F. Li, G.-C. Guo, *Nat. Photonics* **6**, 602 (2012).
31. T. Qureshi, *Quantum Phys.*, arXiv:1205.2207.
32. X.-s. Ma, *Quantum Phys.*, arXiv:1206.6578.
33. F. Kaiser, T. Coudreau, P. Milman, D. B. Ostrowsky, S. Tanzilli, *Science* **338**, 637 (2012).

Acknowledgments: We thank R. Ionicioiu, S. Pironio, T. Rudolph, N. Sangouard, and D. R. Terno for useful discussions, and acknowledge financial support from the UK Engineering and Physical Sciences Research Council (EPSRC), European Research Council (ERC), the Quantum Integrated Photonics (QUANTIP) project, A Toolbox for Photon Orbital Angular Momentum Technology (PHORBITECH) project, the Quantum InterfacES, SENsors, the Communication based on Entanglement (Q-ESSENCE) integrating project, Nokia, the Centre for Nanoscience and Quantum Information (NSQI), the Templeton Foundation, and the European Union Union Device-Independent Quantum Information Processing (DIQIP) project. J.L.O. and S.P. acknowledge a Royal Society Wolfson Merit Award. A.P. holds a Royal Academy of Engineering Research Fellowship.

Supplementary Materials

www.sciencemag.org/cgi/content/full/338/6107/634/DC1
Materials and Methods
Fig. S1

28 June 2012; accepted 18 September 2012
10.1126/science.1226719

Entanglement-Enabled Delayed-Choice Experiment

Florian Kaiser,[1] Thomas Coudreau,[2] Pérola Milman,[2,3] Daniel B. Ostrowsky,[1] Sébastien Tanzilli[1]*

Wave-particle complementarity is one of the most intriguing features of quantum physics. To emphasize this measurement apparatus–dependent nature, experiments have been performed in which the output beam splitter of a Mach-Zehnder interferometer is inserted or removed after a photon has already entered the device. A recent extension suggested using a quantum beam splitter at the interferometer's output; we achieve this using pairs of polarization-entangled photons. One photon is tested in the interferometer and is detected, whereas the other allows us to determine whether wave, particle, or intermediate behaviors have been observed. Furthermore, this experiment allows us to continuously morph the tested photon's behavior from wavelike to particle-like, which illustrates the inadequacy of a naive wave or particle description of light.

Although the predictions of quantum mechanics have been verified with marked precision, subtle questions arise when attempting to describe quantum phenomena in classical terms (*1*, *2*). For example, a single quantum object can behave as a wave or as a particle. This concept is illustrated by Bohr's complementarity principle (*3*) which states that, depending on the measurement apparatus, either wave or particle behavior is observed (*4*, *5*). This is demonstrated by sending single photons into a Mach-Zehnder interferometer (MZI) followed by two detectors (Fig. 1A) (*6*). If the MZI is closed [that is, if the paths of the interferometer are recombined at the output beam splitter (BS_2)], the probabilities for a photon to exit at detectors D_a and D_b depend on the phase difference θ between the two arms. The which-path information remains unknown, and wavelike intensity interference patterns are observed (Fig. 1B). On the other hand, if the MZI is open (i.e., if BS_2 is removed), each photon's path can be known, and consequently, no interference occurs. Particle behavior is said to be observed, and the detection probabilities at D_a and D_b are equal to ½, independent of the value of θ (Fig. 1C). In other words, these two different configurations—BS_2 present or absent—give different experimental results. Recently, Jacques *et al.* have shown that, even when performing Wheeler's original gedanken experiment (*7*) in which the configuration for BS_2 is chosen only after the photon has passed the entrance beam splitter BS_1, Bohr's complementarity principle is still obeyed (*8*). Intermediate cases, in which BS_2 is only partially present, have been considered in theory and led to a more general description of Bohr's complementarity principle expressed by an inequality limiting the simultaneously available amount of interference (signature of wavelike behavior) and which-path information (particle-like behavior) (*9*, *10*). This inequality has also been confirmed experimentally in delayed-choice configurations (*11*, *12*).

We take Wheeler's experiment one step further by replacing the output beam splitter by a quantum beam splitter (QBS), as theoretically proposed of late (*13*, *14*). In our experiment (Fig. 2), we exploit polarization entanglement as a resource for two reasons. First, doing so permits implementing the QBS. Second, it allows us to use one of the entangled photons as a test photon sent to the interferometer and the other one as a corroborative photon. Here, as opposed to previous experiments (*8*, *11*), the state of the interferometer remains unknown, as does the wave or particle behavior of the test photon, until we detect the corroborative photon. By continuously modifying the type of measurement performed on the corroborative photon, we can morph the test photon from wave to particle behavior, even after the test photon was detected. To exclude interpretations based on either mixed states, associated with preexisting state information (*15*), or potential communication between the two photons, the presence of entanglement is verified via the violation of the Bell inequalities with a space-like separation (*16*–*18*).

The QBS is based on the idea that when a photon in an arbitrary polarization state enters an interferometer that is open for $|H\rangle$ (horizontally polarized) and closed for $|V\rangle$ (vertically polarized) photons, the states of the interferometer and the photon become correlated. Our apparatus, shown in the right-hand side of Fig. 2 and detailed in fig. S1, therefore reveals a particle behavior for the $|H\rangle$ component of the photon state and a wave behavior for the $|V\rangle$ component. Note that such an experiment has been realized with the use of single photons prepared in a coherent superposition of $|H\rangle$ and $|V\rangle$ (*12*). However, we take this idea a step further by achieving genuine quantum behavior for the output beam splitter by exploiting an intrinsically quantum resource, entanglement. This allows us to entangle the quantum beam splitter and test photon system with the corroborative photon. Thus, measurement of the corroborative photon enables us to project the test photon–QBS system into an arbitrary coherent wave-particle superposition, which is a purely quantum object. In other words, our QBS is measured by another quantum object, which projects it into a particular superposition of present and absent states. More precisely, we use as a test photon one of the photons from the maximally polarization-entangled Bell state $|\Phi^+\rangle = \frac{1}{\sqrt{2}}(c_H^\dagger t_H^\dagger + c_V^\dagger t_V^\dagger)|vac\rangle$, produced at the wavelength of 1560 nm using the source described in (*19*). Here, using the notation of Fig. 2,

[1]Laboratoire de Physique de la Matière Condensée, CNRS UMR 7336, Université de Nice–Sophia Antipolis, Parc Valrose, 06108 Nice Cedex 2, France. [2]Laboratoire Matériaux et Phénomènes Quantiques, Université Paris Diderot, Sorbonne Paris Cité, CNRS, UMR 7162, 75013 Paris, France. [3]Institut de Sciences Moléculaires d'Orsay (CNRS) Bâtiment 210, Université Paris Sud 11, Campus d'Orsay, 91405, Orsay Cedex, France.

*To whom correspondence should be addressed. E-mail: sebastien.tanzilli@unice.fr

$c_H^\dagger(t_H^\dagger)$ and $c_V^\dagger(t_V^\dagger)$ represent creation operators for horizontally and vertically polarized photonic modes, respectively, propagating toward the corroborative (test) photon apparatus. Moreover, $|vac\rangle$ represents the vacuum state. Using an entangled state of this form ensures maximum randomness of the input polarization state of the test photon (t), which enters an MZI with a QBS for the output beam splitter.

The actual QBS device is made up of two components. The first is a polarization-dependent beam splitter (PDBS) that shows close to 100% reflection for horizontally polarized photons and provides an ordinary 50/50 splitting ratio for the vertically polarized photons. The PDBS is realized using a combination of standard bulk optical components, as described in supplementary text S1. The whole state after the PDBS reads

$$|\Psi\rangle = \frac{1}{2}\left(c_H^\dagger(-e^{i\theta}a_H^\dagger + ib_H^\dagger) + \frac{1}{\sqrt{2}}c_V^\dagger(b_V^\dagger(i + ie^{i\theta}) + a_V^\dagger(1 - e^{i\theta}))\right)|vac\rangle \quad (1)$$

Here, θ is an adjustable phase shift in the interferometer, i is the complex imaginary unit, and $a_H^\dagger$, $a_V^\dagger$, $b_H^\dagger$, and $b_V^\dagger$ symbolize creation operators for test photons propagating toward PBS_1 and PBS_2, respectively. At this point, each polarization state of the test photon is associated with one of the two complementary types of behaviors, wave and particle.

The second stage consists of polarizing beam splitters (PBS_1 and PBS_2) oriented at 45° to the $\{H, V\}$ basis, which permits the erasure of all polarization information that potentially existed at the PDBS output (*4*, *5*, *20*). Equation 1 becomes

$$|\Psi\rangle = \frac{1}{\sqrt{2}}(c_H^\dagger[particle]^\dagger + c_V^\dagger[wave]^\dagger)|vac\rangle \quad (2)$$

with

$$[particle]^\dagger = \frac{1}{2}(-e^{i\theta}(a'^\dagger + a''^\dagger) + i(b'^\dagger + b''^\dagger)) \quad (3)$$

and

$$[wave]^\dagger = \frac{1}{2\sqrt{2}}((1 - e^{i\theta})(-a'^\dagger + a''^\dagger) + i(1 + e^{i\theta})(-b'^\dagger + b''^\dagger)) \quad (4)$$

Here, the creation operators $a'^\dagger$, $a''^\dagger$, $b'^\dagger$, and $b''^\dagger$ denote photons propagating toward detectors $D_{a'}$, $D_{a''}$, $D_{b'}$, and $D_{b''}$, respectively. Consequently, the only way of knowing if wave or particle behavior was observed is by examining the corroborative photon.

The corroborative photon measurement apparatus, as shown on the left-hand side of Fig. 2, consists of two stages. The first is an electro-optic phase modulator that allows us to rotate the

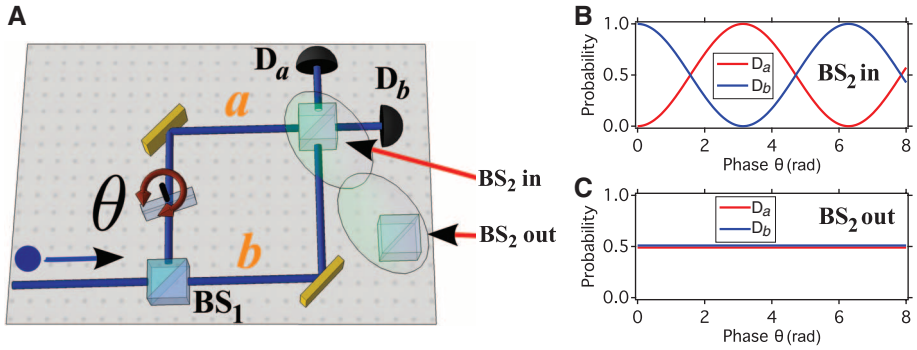

Fig. 1. (**A**) Wheeler's gedanken experiment using an MZI. The device consists of two beam splitters, BS_1 and BS_2; a glass plate introducing a phase shift θ; and two detectors, D_a and D_b, at its output. (**B**) Simulated photon-detection probabilities at detectors D_a and D_b as a function of the phase θ. The sinusoidal oscillations are related to unknown path information and, therefore, to single-photon interference, which is a wavelike phenomenon. rad, radians. (**C**) Detection probabilities without BS_2. No interference is observed, which is the signature of particle behavior.

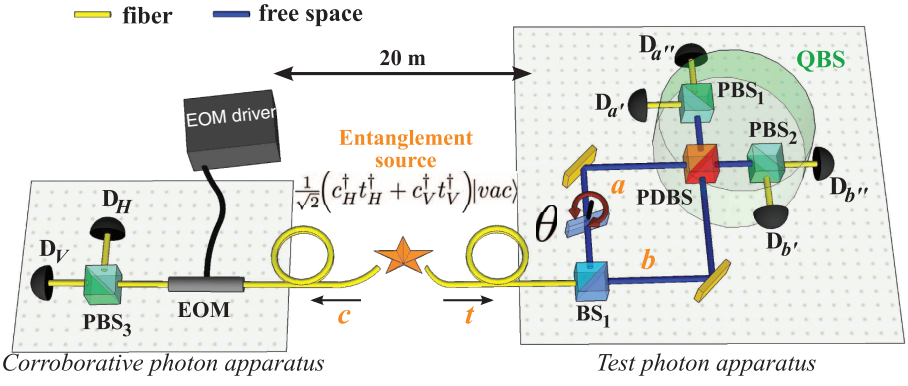

Fig. 2. Experimental setup. Via a single-mode optical fiber, a source of polarization-entangled photons [λ = 1560 nm, see (*13*) for more details] sends one photon (t) to a QBS apparatus, which is an open (or closed) MZI for horizontally (or vertically) polarized photons. This is enabled by the use of a PDBS. The second photon (c) of the entangled state is sent to another laboratory 20 m away (spacelike separation) and used as a "corroborative" photon, which allows us to determine whether we observed wavelike, particle-like, or both behaviors of photon t. EOM, electro-optic phase modulator.

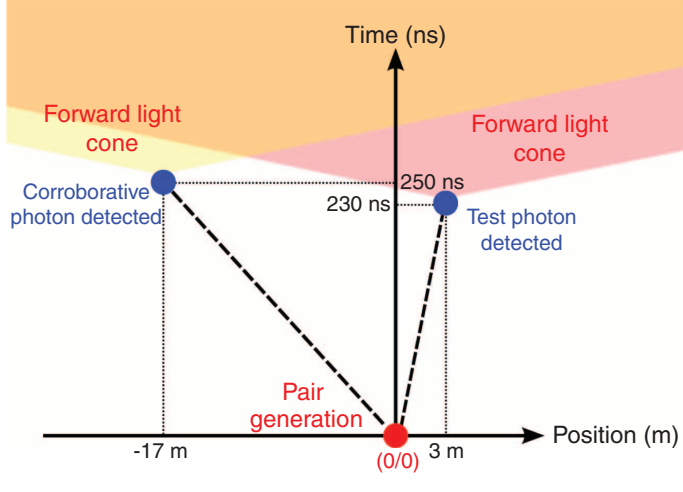

Fig. 3. Space-time diagram of the experimental apparatus. The paired photons are said to be generated and separated at the origin (0/0). The test photon travels ~50 m in an optical fiber before entering the QBS apparatus, which is located in the same laboratory as the entangled photon pair source. The corroborative photon is sent through a 55-m fiber to another laboratory. The corroborative and test photon apparatuses are physically separated by 20 m. The corroborative photon was measured 20 ns after the test photon was detected, thus revealing the MZI configuration in a delayed fashion. The forward light cones from both photon-detection events do not overlap, demonstrating that spacelike separation is achieved. In other words, no causal connection between these events can be established.

polarization state of the corroborative photon by an angle α. From Eqs. 2 to 4, we now have

$$|\Psi\rangle = \frac{1}{\sqrt{2}}\left(c_H^\dagger(\cos\alpha[particle]^\dagger - \sin\alpha[wave]^\dagger\right) + c_V^\dagger\left(\cos\alpha[wave]^\dagger + \sin\alpha[particle]^\dagger\right)\Big)|vac\rangle \quad (5)$$

After passing PBS_3, which is oriented on the {*H*, *V*} axis, the corroborative photon is transmitted (|H⟩) or reflected (|V⟩). This projects the test photon into a state defined by the terms in the parentheses of Eq. 5. Therefore, the firing of detector D_H indicates that the test photon is in the state $\cos\alpha[particle]^\dagger - \sin\alpha[wave]^\dagger$, whereas the firing of D_V shows that it is in the state $\cos\alpha[wave]^\dagger + \sin\alpha[particle]^\dagger$. By choosing $0 < \alpha < 90°$, we obtain a continuous morphing between wave and particle behavior. The expected intensity correlations, given by the coincidence count probability between detectors D_H (corroborative) and $[D_{b'} \oplus D_{b''}]$ (test), where ⊕ denotes an exclusive OR (XOR) gate, are

$$I_{H,b}(\theta,\alpha) = \cos^2\frac{\theta}{2}\sin^2\alpha + \frac{1}{2}\cos^2\alpha \quad (6)$$

Note that the correlations between detectors D_V and $[D_{a'} \oplus D_{a''}]$ follow the same function. On the contrary, the complementary intensity correlations (that is, correlations between detectors D_H and $[D_{a'} \oplus D_{a''}]$ or between D_V and $[D_{b'} \oplus D_{b''}]$) are given by $1 - I_{H,b}(\theta,\alpha)$. The use of XOR gates permits counting the photons from both outputs of each quantum eraser (PBS_1 or PBS_2), and reaching an average coincidence rate of 70 s^{-1} for each of them. Note that Eq. 6 does not depend on the relative detection times of the two photons. In the experiment reported here, the detection of the corroborative photon is delayed until after the detection of the test photon. This is ensured by inserting an extra 5-m length of optical fiber in the path of the corroborative photon (*c*). In this case, for each of the four correlation functions mentioned above, the configuration of the interferometer remains undetermined, even after the test photon has been detected. In other words, there is no information available yet from the corroborative photon that could influence the behavior of the test photon. Furthermore, a space-time analysis shows that no classical communication can be established between the photon-detection events, as they have spacelike separation (Fig. 3).

We now measure the correlations between detectors D_H and $[D_{b'} \oplus D_{b''}]$ via counting coincidence events on the corresponding single-photon detectors (InGaAs avalanche photodiodes). As shown in Fig. 4A, the experimentally measured results are in near-perfect agreement with the theoretical predictions of Eq. 6. For the angle $\alpha = 0°$, $I_{H,b}(\theta,0)$ is independent of the phase θ, as predicted for particle-like behavior. Setting $\alpha = 90°$ results in sinusoidal intensity oscillations as a function of θ, which corresponds to wavelike behavior. For $0° < \alpha < 90°$, a continuous transition from wave to particle behavior is observed, expressed by the continually reducing fringe visibility. As outlined in (*9*, *10*), a generalization of Bohr's complementarity principle implies the interference fringe visibility *V* and the path distinguishability *D*, also called the which-way information, to be limited by the following inequality

$$V^2 + D^2 \le 1 \quad (7)$$

The experimental measurement of these two quantities is described in supplementary text S2 (*11*, *12*). Figure 4B shows the obtained results for V^2, D^2, and $V^2 + D^2$ as a function of the angle α. With our experimental data, Eq. 7 is confirmed for all angles of α.

To prove the existence of a coherent quantum superposition of wave and particle behavior of the

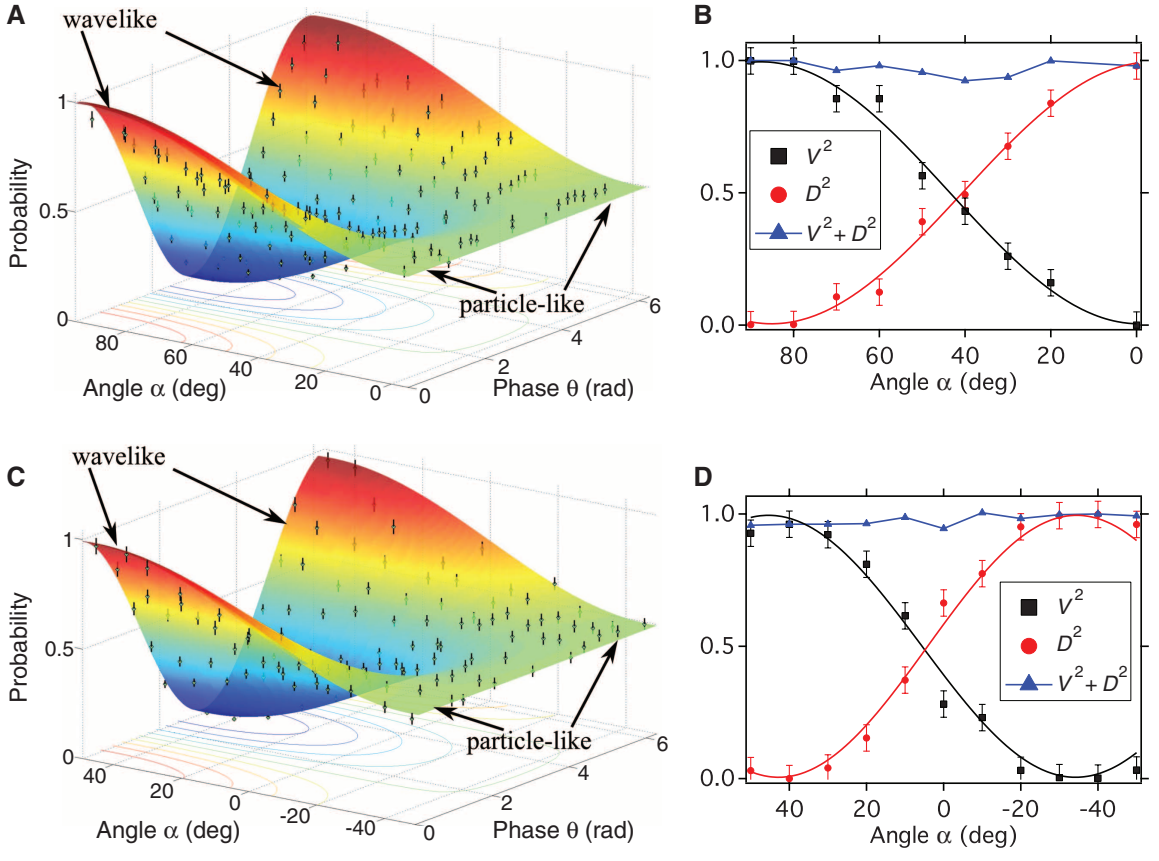

Fig. 4. Experimental results for the quantum delayed-choice experiment. (**A** and **C**) Plots of the intensity correlations, $I_{H,b}(\theta,\alpha)$, as defined by Eq. 6, expressed as the probability of a coincidence event between detectors D_H and $[D_{b'} \oplus D_{b''}]$ as a function of α and θ. Dots and associated vertical lines represent experimental data points and their corresponding standard deviations. Wave-particle morphing is observed for the natural {*H*, *V*} basis (**A**), as well as for the complementary {*D*, *A*} basis (**C**). The colored surfaces in these graphs represent the best fits to the experimental data using Eq. 6. Note that the result obtained for the {*D*, *A*} basis is essential because it represents the signature of the entangled state, proving the correct implementation of the desired quantum beam-splitting effect. We obtain average coincidence rates of 350 events per 5 s. The noise contribution, on the order of three events per 5 s, has not been subtracted. (**B** and **D**) Plots and related sinusoidal fits (solid lines) of the fringe visibility *V* (black) and path distinguishability *D* (red) as a function of the angle α. For all angles, we verify $V^2 + D^2 \le 1$, as predicted by Eq. 7; the blue solid line serves as a guide for the eyes. Note that the same experimental results would be obtained if the timing order of the measurements of the test and corroborative photons were inverted (*26*). Error bars indicate the relative uncertainty obtained in the photon-counting measurements.

test photon created by the detection of the corroborative photon, the presence of entanglement must be verified (*16*, *21*). Note that several recent works did not do this; therefore, the presence of a QBS has not been proven unambiguously (*22*, *23*). In our realization, entanglement is proven by performing the same experiment as before, but using the complementary analysis basis, namely the diagonal basis $\{D, A\}$. Now, the initial quantum state is rotated by 45°—i.e., $\frac{1}{\sqrt{2}}(c_V^\dagger t_V^\dagger + c_H^\dagger t_H^\dagger)|vac\rangle \rightarrow \frac{1}{\sqrt{2}}(c_D^\dagger t_D^\dagger + c_A^\dagger t_A^\dagger)|vac\rangle$—where D and A symbolize diagonally and antidiagonally polarized photon contributions, respectively. In this configuration, every single photon is unpredictably subjected to a closed or open Mach-Zehnder configuration by the PDBS. In this case, as opposed to the experiment in the $\{H, V\}$ basis, if a statistical mixture was analyzed instead of an entangled state, no correlations should be observed when measuring $I_{H,b}(\theta,\alpha)$. However, the strong correlations shown in Fig. 4C exclude a statistical mixture and are in good agreement with the theoretical predictions of Eq. 6. This emphasizes that wave and particle behavior coexist simultaneously for the entire range $0° < \alpha < 90°$ in the $\{H, V\}$ basis and for $-45° < \alpha < 45°$ in the $\{D, A\}$ basis. Figure 4D shows the measurements for V^2, D^2, and $V^2 + D^2$ as a function of α and confirms the upper limits imposed by Eq. 7. The quality of the entangled state is measured via the Bell parameter S, which is deduced from the phase oscillation visibilities at $\alpha = 90°$ in the $\{H, V\}$ basis and $\alpha = 45°$ in the $\{D, A\}$ basis. We obtain $S = 2.77 \pm 0.07$, which is very close to the optimal value of $2\sqrt{2}$ attained with maximally entangled states and is 11 standard deviations above the classical/quantum boundary $S = 2$ (*16*, *21*).

The detection loophole remains open in our experiment, because some of the initial entangled photons are lost during their propagation in the fiber or bulk channels or are not detected by the single-photon detectors that show nonunit quantum detection efficiencies (*24*). Therefore, we make the reasonable assumption that the detected photons represent a faithful sample (*17*).

In conclusion, we have carried out a quantum delayed-choice experiment, enabled by polarization-entangled photons and the associated property of nonlocality. We used an MZI in which the output beam splitter has been replaced by its quantum analog (i.e., a beam splitter in a coherent superposition of being present and absent). In this configuration, we observed that single photons can behave as waves and as particles in the same experiment, meaning that the simple view of photons being either waves or particles is refuted. We experimentally excluded interpretations based on local hidden variables and/or information exchange between the photon and the quantum beam splitter. The state of the quantum beam splitter is determined by the detection of the corroborative photon. We have, therefore, demonstrated delayed interference between wave and particle behavior, which underlines the subtleness of Bohr's complementarity principle.

We note that, parallel to this work, Peruzzo *et al.* realized another version of a quantum delayed-choice experiment based on entangled photons (*25*).

References and Notes

1. E. Schrödinger, *Naturwissenschaften* **23**, 807 (1935).
2. G. Greenstein, A. Zajonc, *The Quantum Challenge: Modern Research on the Foundations of Quantum Mechanics* (Jones and Bertlett Publishers, Sudbury, MA, 2006).
3. N. Bohr, in *Quantum Theory and Measurement*, J. A. Wheeler, W. H. Zurek, Eds. (Princeton Univ. Press, Princeton, NJ, 1984), p. 949.
4. Y.-H. Kim, R. Yu, S. P. Kulik, Y. Shih, M. O. Scully, *Phys. Rev. Lett.* **84**, 1 (2000).
5. S. P. Walborn, M. O. Terra Cunha, S. Pádua, C. H. Monken, *Phys. Rev. A* **65**, 033818 (2002).
6. P. Grangier, G. Roger, A. Aspect, *Europhys. Lett.* **1**, 173 (1986).
7. J. A. Wheeler, in *Quantum Theory and Measurement*, J. A. Wheeler, W. H. Zurek, Eds. (Princeton Univ. Press, Princeton, NJ, 1984), pp. 182–213.
8. V. Jacques *et al.*, *Science* **315**, 966 (2007).
9. W. K. Wootters, W. H. Zurek, *Phys. Rev. D* **19**, 473 (1979).
10. B.-G. Englert, *Phys. Rev. Lett.* **77**, 2154 (1996).
11. V. Jacques *et al.*, *Phys. Rev. Lett.* **100**, 220402 (2008).
12. J.-S. Tang *et al.*, *Nat. Photonics* **6**, 602 (2012).
13. R. Ionicioiu, D. R. Terno, *Phys. Rev. Lett.* **107**, 230406 (2011).
14. M. Schirber, *Physics* **4**, 102 (2011).
15. A. Einstein, B. Podolsky, N. Rosen, *Phys. Rev.* **47**, 777 (1935).
16. J. S. Bell, *Physics* **1**, 195 (1964).
17. A. Aspect, J. Dalibard, G. Roger, *Phys. Rev. Lett.* **49**, 1804 (1982).
18. G. Weihs, T. Jennewein, C. Simon, H. Weinfurter, A. Zeilinger, *Phys. Rev. Lett.* **81**, 5039 (1998).
19. F. Kaiser, A. Issautier, O. Alibart, A. Martin, S. Tanzilli, *Phys. Rev. Lett.* **75**, 3034 (1995).
21. J. F. Clauser, M. A. Horne, A. Shimony, R. A. Holt, *Phys. Rev. Lett.* **23**, 880 (1969).
22. S. S. Roy, A. Shukla, T. S. Mahesh, *Phys. Rev. A* **85**, 022109 (2012).
23. R. Auccaise *et al.*, *Phys. Rev. A* **85**, 032121 (2012).
24. J. F. Clauser, M. A. Horne, *Phys. Rev. D Part. Fields* **10**, 526 (1974).
25. A. Peruzzo, P. Shadbolt, N. Brunner, S. Popescu, J. L. O'Brien, *Science* **338**, 634 (2012).
26. X.-S. Ma *et al.*, *Nat. Phys.* **8**, 480 (2012).

Acknowledgments: We thank L. A. Ngah for his help on data acquisition and O. Alibart for fruitful discussions. This work was supported by the CNRS, l'Université de Nice–Sophia Antipolis, l'Agence Nationale de la Recherche for the "e-QUANET" project (grant ANR-09-BLAN-0333-01), the European ICT-2009.8.0 FET open program for the "QUANTIP" project (grant 244026), le Ministère de l'Enseignement Supérieur et de la Recherche, la Fondation iXCore pour la Recherche, and le Conseil Régional PACA for the "QUANET" project in the exploratory call.

Supplementary Materials

www.sciencemag.org/cgi/content/full/338/6107/637/DC1
Supplementary Text
Fig. S1

29 June 2012; accepted 18 September 2012
10.1126/science.1226755

Quantum Entanglement of High Angular Momenta

Robert Fickler,[1,2]* Radek Lapkiewicz,[1,2] William N. Plick,[1,2] Mario Krenn,[1,2] Christoph Schaeff,[1,2] Sven Ramelow,[1,2] Anton Zeilinger[1,2,3]*

Single photons with helical phase structures may carry a quantized amount of orbital angular momentum (OAM), and their entanglement is important for quantum information science and fundamental tests of quantum theory. Because there is no theoretical upper limit on how many quanta of OAM a single photon can carry, it is possible to create entanglement between two particles with an arbitrarily high difference in quantum number. By transferring polarization entanglement to OAM with an interferometric scheme, we generate and verify entanglement between two photons differing by 600 in quantum number. The only restrictive factors toward higher numbers are current technical limitations. We also experimentally demonstrate that the entanglement of very high OAM can improve the sensitivity of angular resolution in remote sensing.

Quantum entanglement—the nonclassical phenomenon of joint measurements of at least two separate systems showing stronger correlations than classically explainable (*1*, *2*)—is widely considered one of the quintessential features of quantum theory. Since its discovery and first experimental demonstration (*3*), photon entanglement has been shown in various degrees of freedom (*4*–*7*). In the field of photonic quantum optics, studies of the orbital angular momentum (OAM) of light have been productive. The natural solutions of the paraxial wave equation in cylindrical coordinates, Laguerre-Gauss modes, have a helical phase dependence that leads to a vortex or phase singularity and thus zero intensity along the beam axis. These Laguerre-Gauss modes carry an OAM that can take any integer value (*8*). Entanglement of OAM of photons (*5*) has led to many novel insights and applications in quantum foundations and quantum information—for example, qutrit quantum com-

[1]Quantum Optics, Quantum Nanophysics, Quantum Information, University of Vienna, Vienna A-1090, Austria. [2]Institute for Quantum Optics and Quantum Information, Austrian Academy of Science, Vienna A-1090, Austria. [3]Vienna Center for Quantum Science and Technology, Faculty of Physics, University of Vienna, Vienna A-1090, Austria.

*To whom correspondence should be addressed. E-mail: robert.fickler@univie.ac.at (R.F.); anton.zeilinger@univie.ac.at (A.Z.)

munication protocols (*9*), uncertainty relations with angular position and OAM (*10*), or higher-dimensional entanglement (*11*–*13*).

An important motivation for our work is the open question of the existence of macroscopic entanglement, which is intricately connected to the very definition of "macroscopicity" (*14*). The OAM degree of freedom offers the possibility to create entanglement of quantum numbers in principle up to arbitrarily high values. In optomechanical experiments, which already make use of linear momentum (*15*), such photons can be used to create entanglement of a mechanical system with high angular momentum. Also, relative to classical methods, quantum remote sensing offers an improved angular resolution that is amplified by large OAM values (*16*).

Because of the rapidly decreasing efficiency of the downconversion process for the direct generation of entanglement of higher OAM (*17*, *18*), we use a different approach similar to the ideas in (*7*, *19*–*21*). We start with high-fidelity two-dimensional entanglement in the polarization degrees of freedom and transfer it to various OAM subspaces with chosen amounts of angular momentum (Fig. 1). The polarization-entangled photon pairs propagating in single-mode fibers enter the transfer setups in the two-photon state described by the tensor product of two degrees of freedom (polarization and OAM):

$$|\psi_{in}\rangle = [\alpha|H\rangle|V\rangle + \beta \exp(i\varphi)|V\rangle|H\rangle]\otimes|0\rangle|0\rangle \quad (1)$$

where α, β, and φ are real and normalized ($\alpha^2 + \beta^2 = 1$), *H* and *V* denote horizontal and vertical polarization, 0 indicates the amount of OAM per photon (Gauss mode), and the positions of the ket vectors, which describe the quantum mechanical states of the photon, label the different photons. The transfer is realized with a folded interferometric structure that is intrinsically phase-stable and has by design equal arm lengths. Depending on their polarization, the photons are transferred to a well-defined Laguerre-Gauss mode by a spatial light modulator (SLM), which modulates the phase of the light (*22*). The SLM is programmed such that photons that take the path for horizontally polarized light are changed to $+l$ after leaving the interferometer, and those that take the path for vertically polarized light are changed to $-l$ after leaving the interferometer. Finally, a polarizer projects the photons onto the diagonal polarization (*D*), erasing any information about path and creating the state

$$|\psi_{out}\rangle = |D\rangle|D\rangle\otimes[\alpha|+l\rangle|-l\rangle + \beta \exp(i\varphi)|-l\rangle|+l\rangle] \quad (2)$$

Our method does not rely on phase matching, as in the generation of OAM entanglement via spontaneous parametric downconversion (SPDC), but instead benefits from the efficient and high-quality polarization entanglement. The resulting states can be entangled in any two-dimensional subspace of the infinite-dimensional OAM space or even in the general space of all spatial modes that can be generated with SLMs (*23*–*25*).

To realize projective measurements onto high-OAM superposition states in order to demonstrate entanglement, we use a technique that takes advantage of the specific spatial structure of the created photonic states (Fig. 2). Any equal Laguerre-Gauss superposition, $|\chi\rangle = 2^{-1/2}[|l\rangle + \exp(i\varphi)|-l\rangle]$, has an intensity distribution showing a radially symmetric structure with $2l$ maxima arranged in a ring (Fig. 2, B to D). Because the angular position $\gamma = (\varphi/2l)\cdot(360°/2\pi)$ of this petal structure is determined by the phase φ, a mask with $2l$ slits maximally transmits only a specific superposition. By rotating the mask, all possible superpositions with equal amplitude are accessible. For analysis of the created state and demonstration of entanglement, one mask is installed after each transfer setup

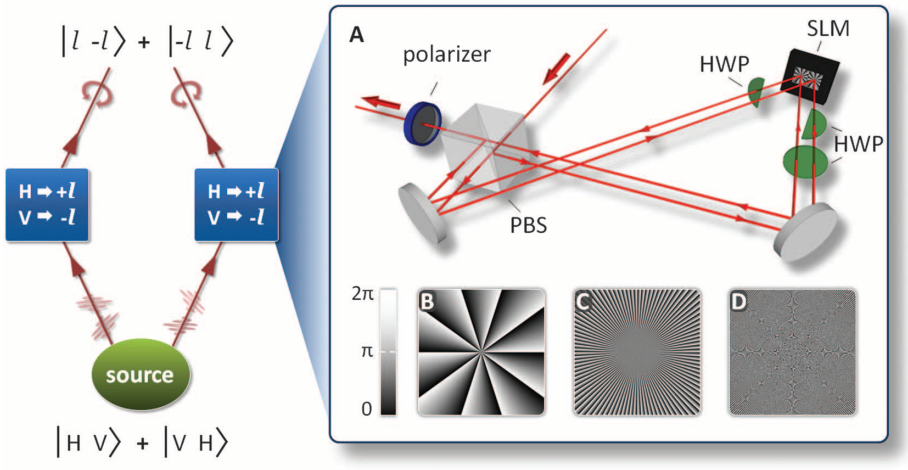

Fig. 1. Left panel: Schematic sketch of the setup. Polarization entanglement is created in a parametric downconversion process (source) and afterward transferred to modes with high quanta of OAM (transfer setups, shown as blue boxes). (**A**) Experimental layout for one of the two identical transfer setups where the photon is split by a polarization beam splitter (PBS) and its spatial mode is transformed to a higher-order Laguerre-Gauss mode by a spatial light modulator (SLM). Half-wave plates (HWP) in the paths ensure that the SLM works optimally and that the output is separated from the input. A polarizer (blue) projects the photon to diagonal polarization and completes the transfer. (**B** to **D**) Three-phase pattern of increasing complexity of the structure: l = 10 (B), l = 100 (C), and l = 300 (D). Because the SLM has finite resolution, a Moiré pattern emerges.

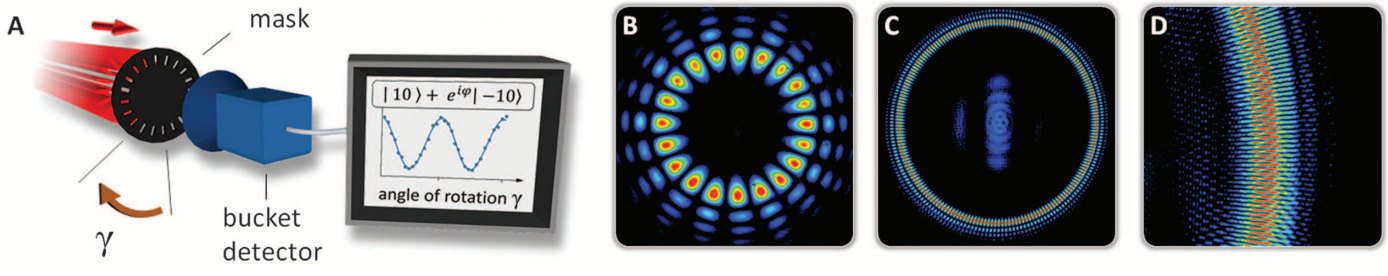

Fig. 2. Sketch of the measurement principle. (**A**) The angular position of the radial superposition structure (red) is dependent on the phase φ of the state, here $|\chi\rangle = |10\rangle + \exp(i\varphi)|-10\rangle$. A mask with the same rotational symmetry (20 slits) is able to detect any superposition depending on the mask's angular position γ. (**B** to **D**) Three superpositions (false colors denote intensity gradations) for $l = \pm 10$ (B), $l = \pm 100$ (C), and a section of the mode for $l = \pm 300$ (D), experimentally created with a laser imaged by a charge-coupled device camera. Additional structures around and inside of the main intensity pattern (higher-order Laguerre-Gauss modes with the same OAM and unmodulated photons, respectively) arise from the imperfect creation of the modes at the SLM but will be blocked by the slit mask. For $l = \pm 300$, only the section of the mode shown here was used in the measurements, because of the noise from diffraction at the SLM housing and distorted modulation due to the limitations of the finite resolution.

and the coincidence of two transmitted photons for different combinations of γ is measured.

In our experiment, polarization-entangled photon pairs (uncorrected average visibility 97.99 ± 0.03%) at 810 nm were created using a type II nonlinear crystal in a Sagnac-type configuration (*26*, *27*). The SLM in the transfer setup is programmed such that the reflected photons acquire l multiples of 2π azimuthal phase (l quanta of OAM), which leads to complex patterns when OAM is large (Fig. 1, B to D). Therefore, we used a high-resolution SLM (1920 × 1080, full HD; Holoeye Photonics AG, Berlin) with small pixel size (8 μm). Nonetheless, for values of $l \geq 300$ we observed a clear reduction of mode transformation efficiency, which is the main limiting factor (*22*). This is only a technical limitation that can be overcome by higher-resolution SLMs or novel techniques for creating photons with higher l values (*28*). After the transfer setups, the modes are enlarged to fit the masks (laser-cut black cardboard) and transmitted photons are focused to bucket detectors.

As a demonstration of the flexibility of our setup, we created two-dimensional spatial mode entanglement with highly asymmetric OAM states, in which one photon is transferred to $l = \pm 10$ and the second photon to $l = \pm 100$ (Fig. 3A). Because of its intrinsic conservation of angular momentum, the SPDC process could not create this asymmetric state directly. We then transferred both photons to $l = \pm 100$, showing the ability to create OAM modes with very high difference in quantum number (Fig. 3B). The highest value of OAM per single photon where strong correlations were still measurable was $l = \pm 300$ for both photons (Fig. 3C). The decrease in mode transformation efficiency of the SLM, however, strongly affects the coincidence rate (about 1 coincidence count per minute in the maximum) and therefore the statistical significance of our results.

To demonstrate successful transfer, we constructed an entanglement witness [similar to (*29*)], which verifies entanglement if the sum of two visibilities in two mutually unbiased bases is above the classical bound of $(2^{1/2} + 1)/2 \approx 1.21$ (*22*, *29*). The data for the visibilities were taken in addition to the fringe measurements (apart from $l = \pm 300$) with longer integration. For the asymmetric OAM state $l = \pm 10/\pm 100$, we achieved a witness value of 1.48 ± 0.01. When both photons were transferred to $l = \pm 100$, the witness value was 1.55 ± 0.01. Both values were calculated without any correction of the data and violate the classical limit by ~30 standard deviations, demonstrating the successful entanglement transfer. Because of the significantly smaller creation and detection efficiencies (hence a lower pair detection rate) for $l = \pm 300$, we corrected for accidental coincidence counts (*22*), yielding a value of 1.6 ± 0.3 for our entanglement witness. With a statistical significance of more than 80%, we thus violate the bound for separable states with photons that each carry $l = \pm 300$ quanta of OAM.

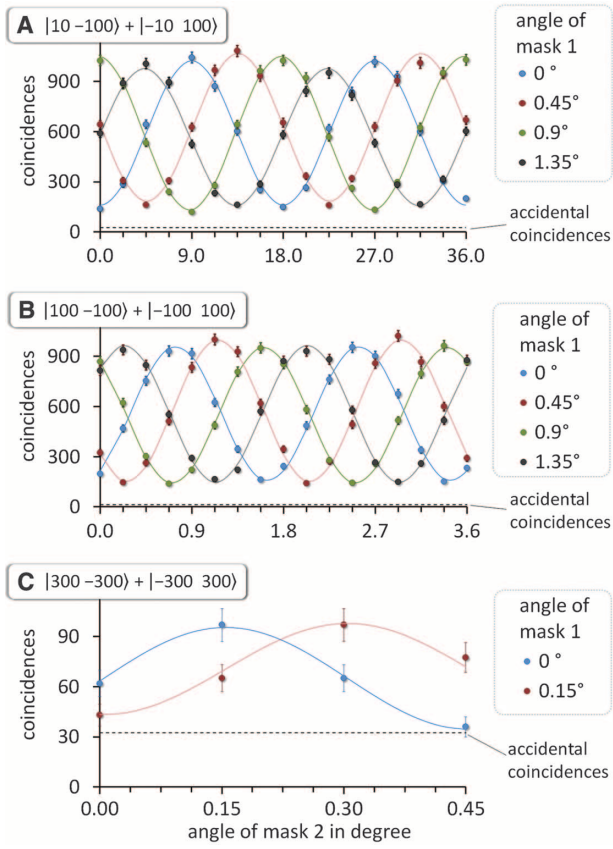

Fig. 3. Measured coincidence counts as a function of the angle of one mask and different angles of the other mask. The measured coincidence counts (points) show a sinusoidal dependence (fitted lines) and depend only on the difference between the angles of the masks, which is a clear signature of nonclassical correlations. **(A)** The first photon is transferred to $l = \pm 10\hbar$ and the second to $l = \pm 100\hbar$, showing the ability to create asymmetric OAM entangled states. **(B)** Both photons are transferred to $l = \pm 100\hbar$. **(C)** Both photons carry $l = \pm 300\hbar$ and nonclassical correlations can still be measured. Here, the count rate decreased significantly (about 1 coincidence count per minute) primarily because of limited conversion efficiency. The integration times in (A), (B), and (C) were 2 min, 9 min, and 64 min, respectively, for each data point. Error bars in all plots (if large enough to be seen) are estimated from Poissonian count statistics.

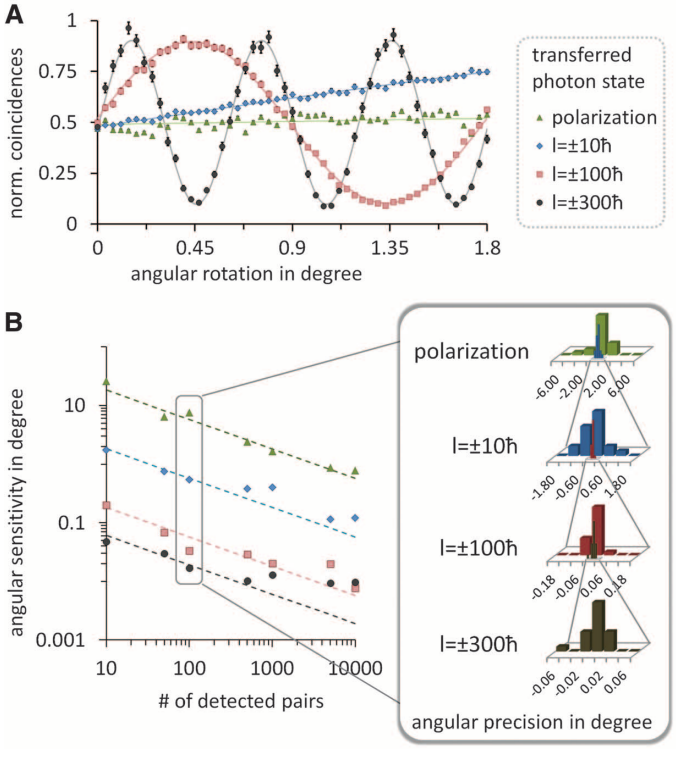

Fig. 4. Measurements of remote angular sensitivity enhancement. **(A)** Normalized coincidence count rates where one photon is projected on diagonal polarization, and the second photon is either kept polarization-encoded while the polarizer is rotated (green triangles) or transferred to $l = \pm 10\hbar$ (blue diamonds), to $l = \pm 100\hbar$ (red squares), or to $l = \pm 300\hbar$ (black circles) while the appropriate mask is rotated. The errors are estimated assuming Poissonian count statistics. **(B)** From the steepest part of the fringes (0°), it is possible to calculate the corresponding angular sensitivity limited by statistical fluctuations for different numbers of detected pairs. The dashed lines are the theoretically expected sensitivities (assuming 100% visibility and Poissonian fluctuation) and the points are the measured values. To illustrate the enhancement for 100 detected pairs, we measured the angular position of the randomly rotated mask by correcting the change in the coincidence counts with a rotation of the remote polarizer. The right panel shows histograms of 20 different random angles that were measured for each arrangement. For $l = \pm 300\hbar$, the limit of our high-precision rotation stage (±0.016°) was determined with the polarizer in a low-precision mount (±1°). To reach the same precision without OAM-induced angular resolution enhancement, about 3.3 million detected pairs would have been necessary.

To further corroborate this successful entanglement creation, we transferred only one photon to $l = \pm 300$ and measured the other photon in the polarization bases. The measured witness value was 1.628 ± 0.004. Therefore, our results demonstrate that single photons can carry $300\hbar$ of OAM (where $\hbar$ is Planck's constant divided by 2π) and that entanglement between two photons differing by 600 in quantum number can be achieved. Even in classical optics, the highest value of OAM that had been created with an SLM was $l = 200$ (*30*).

Apart from the fundamental interest of entangling high quantum numbers, we also demonstrate the use of high-OAM entanglement for remote sensing. For this we use the same method as before for creating high-OAM entangled states (folded interferometric scheme including SLM) and analyzing them (slit wheel method). When we transfer one photon to high OAM values and keep the other in its polarization state, the pair can be used to remotely measure an angular rotation with a precision that is increased by a factor l relative to the situation when only polarization-entangled photon pairs are used (Fig. 4) (*22*). This can lead to notable improvements for applications in the field of remote sensing, especially where low light intensities are required, such as in biological imaging experiments with light-sensitive material. An analogous improvement can be achieved classically if diagonally or circularly polarized light enters our transfer setup. However, the important difference is that entanglement enables the measurements to be done remotely, with the photons being spatially separated or even in unknown locations at some later time.

Our approach could be generalized to higher-dimensional entanglement for spatial modes—for example, by starting with higher-dimensional (hybrid) entanglement and a more complex interferometric scheme. Such a development would have potential benefits in applications such as quantum cryptography, quantum computation, and quantum metrology.

References and Notes

1. A. Einstein, B. Podolsky, N. Rosen, *Phys. Rev.* **47**, 777 (1935).
2. J. S. Bell, *Physics* **1**, 195 (1965).
3. S. J. Freedman, J. F. Clauser, *Phys. Rev. Lett.* **28**, 938 (1972).
4. P. G. Kwiat, A. M. Steinberg, R. Y. Chiao, *Phys. Rev. A* **47**, R2472 (1993).
5. A. Mair, A. Vaziri, G. Weihs, A. Zeilinger, *Nature* **412**, 313 (2001).
6. J. C. Howell, R. S. Bennink, S. J. Bentley, R. W. Boyd, *Phys. Rev. Lett.* **92**, 210403 (2004).
7. S. Ramelow, L. Ratschbacher, A. Fedrizzi, N. K. Langford, A. Zeilinger, *Phys. Rev. Lett.* **103**, 253601 (2009).
8. L. Allen, M. W. Beijersbergen, R. J. C. Spreeuw, J. P. Woerdman, *Phys. Rev. A* **45**, 8185 (1992).
9. N. K. Langford *et al.*, *Phys. Rev. Lett.* **93**, 053601 (2004).
10. J. Leach *et al.*, *Science* **329**, 662 (2010).
11. A. Vaziri, G. Weihs, A. Zeilinger, *Phys. Rev. Lett.* **89**, 240401 (2002).
12. A. C. Dada, L. Leach, G. S. Buller, M. J. Padgett, E. Andersson, *Nat. Phys.* **7**, 677 (2011).
13. B.-J. Pors, F. Miatto, G. W. 't Hooft, E. R. Eliel, J. P. Woerdman, *J. Opt.* **13**, 064008 (2011).
14. A. J. Leggett, *J. Phys. Condens. Matter* **14**, R415 (2002).
15. M. Aspelmeyer, P. Meystre, K. Schwab, *Phys. Today* **65**, 29 (2012).
16. A. K. Jha, G. S. Agarwal, R. W. Boyd, *Phys. Rev. A* **83**, 053829 (2011).
17. J. Romero, D. Giovannini, S. Franke-Arnold, S. M. Barnett, M. J. Padgett, http://arxiv.org/abs/1205.1968 (2012).
18. H. Di Lorenzo Pires, H. C. B. Florijn, M. P. van Exter, *Phys. Rev. Lett.* **104**, 020505 (2010).
19. M. Żukowski, J. Pykacz, *Phys. Lett. A* **127**, 1 (1988).
20. E. Nagali *et al.*, *Phys. Rev. Lett.* **103**, 013601 (2009).
21. E. J. Galvez, S. M. Nomoto, W. H. Schubert, M. D. Novenstern, paper presented at the International Conference on Quantum Information, Ottawa, 6 June 2011; www.opticsinfobase.org/abstract.cfm?URI=ICQI-2011-QMI18.
22. See supplementary materials on *Science* Online.
23. S. Chávez-Cerda *et al.*, *J. Opt. B* **4**, S52 (2002).
24. J. B. Bentley, J. A. Davis, M. A. Bandres, J. C. Gutiérrez-Vega, *Opt. Lett.* **31**, 649 (2006).
25. G. A. Siviloglou, J. Broky, A. Dogariu, D. N. Christodoulides, *Phys. Rev. Lett.* **99**, 213901 (2007).
26. T. Kim, M. Fiorentino, F. N. C. Wong, *Phys. Rev. A* **73**, 012316 (2006).
27. A. Fedrizzi, T. Herbst, A. Poppe, T. Jennewein, A. Zeilinger, *Opt. Express* **15**, 15377 (2007).
28. G. Campbell, B. Hage, B. Buchler, P. K. Lam, *Appl. Opt.* **51**, 873 (2012).
29. O. Gühne, G. Tóth, *Phys. Rep.* **474**, 1 (2009).
30. A. Jesacher, S. Fürhapter, C. Maurer, S. Bernet, M. Ritsch-Marte, *Opt. Express* **14**, 6342 (2006).

Acknowledgments: Supported by the European Research Council (advanced grant QIT4QAD, 227844) and the Austrian Science Fund (FWF) within the Special Research Programs (SFB) F40 (Foundations and Applications of Quantum Science; FoQuS) and W1210-2 (Vienna Doctoral Program on Complex Quantum Systems; CoQuS). R.F. participated in the design and building of the experimental apparatus, collected and analyzed the data, and wrote the manuscript. R.L., C.S., and S.R. participated in the design and building of the experiment and assisted on the experimental side. W.N.P., S.R., and M.K. assisted on the theoretical side. A.Z. initiated the work and supervised the experiment. All authors contributed to conceiving the experiment, discussing the results, and contributing to the final text of the manuscript.

Supplementary Materials

www.sciencemag.org/cgi/content/full/338/6107/640/DC1
Materials and Methods
Supplementary Text
Table S1
Fig. S1

9 July 2012; accepted 20 September 2012
10.1126/science.1227193

Efficient Hybrid Solar Cells Based on Meso-Superstructured Organometal Halide Perovskites

Michael M. Lee,[1] Joël Teuscher,[1] Tsutomu Miyasaka,[2] Takurou N. Murakami,[2,3] Henry J. Snaith[1]*

The energy costs associated with separating tightly bound excitons (photoinduced electron-hole pairs) and extracting free charges from highly disordered low-mobility networks represent fundamental losses for many low-cost photovoltaic technologies. We report a low-cost, solution-processable solar cell, based on a highly crystalline perovskite absorber with intense visible to near-infrared absorptivity, that has a power conversion efficiency of 10.9% in a single-junction device under simulated full sunlight. This "meso-superstructured solar cell" exhibits exceptionally few fundamental energy losses; it can generate open-circuit photovoltages of more than 1.1 volts, despite the relatively narrow absorber band gap of 1.55 electron volts. The functionality arises from the use of mesoporous alumina as an inert scaffold that structures the absorber and forces electrons to reside in and be transported through the perovskite.

An efficient solar cell must absorb over a broad spectral range, from visible to near-infrared (near-IR) wavelengths (350 to ~950 nm), and convert the incident light effectively into charges. The charges must be collected at a high voltage with suitable current in order to do useful work (*1*–*8*). A simple measure of solar cell effectiveness at generating voltage is the difference in energy between the optical band gap of the absorber and the open-circuit voltage (V_{oc}) generated by the solar cell under simulated air mass (AM) 1.5 solar illumination of 100 mW cm^{-2} (*9*). For instance, gallium arsenide (GaAs) solar cells exhibit V_{oc} of 1.11 V and an optical band gap of 1.4 eV, giving a difference of ~0.29 eV (*2*). For dye-sensitized and organic solar cells, this difference is usually on the order of 0.7 to 0.8 eV (*2*, *9*). For organic solar cells, such losses are predominantly caused by their low dielectric constants. Tightly bound excitons form, which require a heterojunction with an electron acceptor with a large energy offset to enable ionization and charge separation (*10*, *11*). Likewise, dye-sensitized solar cells (DSSCs) have losses, both from electron transfer from the dye (or absorber) into the TiO_2, which requires a certain "driving force," and from dye regeneration from

[1]Clarendon Laboratory, Department of Physics, University of Oxford, Oxford OX1 3PU, UK. [2]Graduate School of Engineering, Toin University of Yokohama, 1614 Kurogane, Aoba, Yokohama 225-8503, Japan. [3]Research Center for Photovoltaic Technologies, National Institute of Advanced Industrial Science and Technology, Central 5, 1-1-1 Higashi, Tsukuba, Ibaraki 305-8565, Japan.

*To whom correspondence should be addressed. E-mail: h.snaith1@physics.ox.ac.uk

the electrolyte, which requires an overpotential. Efforts have been made to reduce such losses in DSSCs by moving from a multielectron iodide–tri-iodide redox couple to one-electron outer-sphere redox couples, such as cobalt complexes or a solid-state hole conductor (*1*, *4*, *12*, *13*).

Inorganic semiconductor–sensitized solar cells have recently become a focus of interest (*14*, *15*). An extremely thin absorber (ETA) layer, 2 to 10 nm in thickness, is coated upon the internal surface of a mesoporous TiO_2 electrode and then contacted with an electrolyte or solid-state hole conductor. These devices have achieved power conversion efficiencies of up to 6.3% (*15*). However, the ETA concept suffers from rather low V_{oc}; the problem may lie in the electronically disordered, low-mobility n-type TiO_2 (*16*). Perovskites are relatively underexplored alternatives (Fig. 1A) that provide a framework for binding organic and inorganic components into a molecular composite. With careful consideration of the interaction between organic and inorganic elements and suitable control of the size-tunable crystal cell (*17*), rudimentary wet chemistry can be used to create new and interesting materials. Era, Mitzi, and coworkers have shown that layered perovskites based on organometal halides demonstrate excellent performance as light-emitting diodes (*18*, *19*) and transistors with mobilities comparable to amorphous silicon (*20*). Organometal halide perovskites have been used as sensitizers in liquid electrolyte–based photoelectrochemical cells with conversion efficiencies from 3.5 to 6.5% (*21*, *22*). Recently, a $CsSnI_3$ perovskite was shown to function efficiently as a hole conductor in solid-state DSSCs, delivering up to 8.5% power conversion efficiency (*23*, *24*).

We report on a solution-processable solar cell that overcomes the fundamental losses of organic absorbers and disordered metal oxides. We followed the ETA approach and used a perovskite absorber, mesoporous TiO_2 as the transparent n-type component, and 2,2′,7,7′-tetrakis-(*N*,*N*-di-*p*-methoxyphenylamine)9,9′-spirobifluorene (spiro-OMeTAD) as the transparent p-type hole conductor. These devices exhibited power conversion efficiencies near 8%. Remarkably, we also found that replacement of the mesoporous n-type TiO_2 with insulating Al_2O_3 improved the power conversion efficiency. The Al_2O_3 is an insulator with a wide band gap (7 to 9 eV) and purely acts as a "scaffold" upon which the perovskite is coated. We observed that electron transport through the perovskite layer was much faster than through the n-type TiO_2. In addition, we observed an increase in V_{oc} (moving from the TiO_2 to the insulating Al_2O_3 scaffold) of a few hundred millivolts and a power conversion efficiency of 10.9% under simulated AM1.5 full solar illumination.

The specific perovskite we used is of mixed-halide form: methylammonium lead iodide chloride ($CH_3NH_3PbI_2Cl$), which was processed from a precursor solution in *N*,*N*-dimethylformamide via spin-coating in ambient conditions. X-ray diffraction analysis for $CH_3NH_3PbI_2Cl$ prepared on glass (fig. S1) (*25*) showed diffraction peaks at 14.20°, 28.58°, and 43.27°, which we assigned as the (110), (220), and (330) planes, respectively, of a tetragonal perovskite structure with lattice parameters $a = 8.825$ Å, $b = 8.835$ Å, $c = 11.24$ Å, similar to the $CH_3NH_3PbI_3$ previously reported (*21*). The extremely narrow diffraction peaks suggest that the films have long-range crystalline domains (>200 nm, peak width limited by instrument broadening) and are highly oriented with the *a* axis (*21*, *26*). In contrast to the methylammonium trihalogen plumbates previously reported in solar cells (i.e., $CH_3NH_3PbI_3$) (*21*, *22*), this iodide-chloride mixed-halide perovskite was remarkably stable to processing in air. The absorption spectra (Fig. 1B) demonstrated good light-harvesting capabilities over the visible to near-IR spectrum and was also stable to prolonged light exposure, as demonstrated by 1000 hours of constant illumination under simulated full sunlight. The absorbance of the film at 500 nm remained around 1.8 throughout the entire measurement period (absorbance of 1.8 corresponds to 98.4% absorption) (Fig. 1B, inset). Note that the scale is optical density, where absorbance of ~0.5 at 700 nm corresponds to ~70% attenuation in a single pass; in the solar cell, there are two passes of light leading to ~91% absorption at this wavelength.

The solar cells were fabricated on semitransparent fluorine-doped tin oxide (FTO)–coated glass coated with a compact layer of TiO_2 that acted as an anode. The porous oxide films were fabricated from sol-gel–processed sintered nanoparticles. The perovskite precursor solution was infiltrated into the porous oxide mesostructure via spin-coating and was dried at 100°C, which enabled the perovskite to form via self-assembly of the constituent ions. Dark coloration was observed only after this drying step.

With respect to the perovskite coating process, there has been extensive work done on investigating how solution-cast materials infiltrate into mesoporous oxides (*27*–*32*). If the concentration of the solution is low enough and the solubility of the cast material high enough, the material will completely penetrate the pores as the solvent evaporates. Typically, the material forms a "wetting" layer upon the internal surface of the mesoporous film that uniformly coats the pore walls throughout the thickness of the electrode (*28*–*31*). The degree of "pore filling" can be controlled by varying the solution concentration (*29*–*32*). If the concentration of the casting solution is high, then maximum pore filling occurs, and any "excess" material forms a "capping layer" on top of the filled mesoporous oxide.

For the optimum perovskite precursor concentrations we used, there was no appearance of a capping layer, which implies that the perovskite was predominantly formed within the mesoporous film. We verified that the perovskite was within and uniformly distributed throughout the meso-

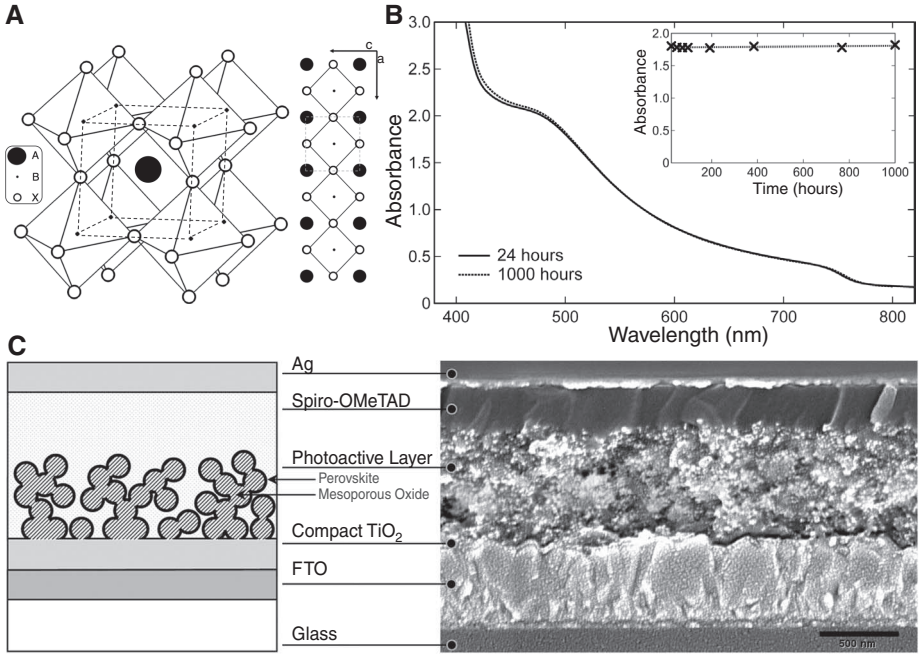

Fig. 1. (**A**) Left: Three-dimensional schematic representation of perovskite structure ABX_3 (A = CH_3NH_3, B = Pb, and X = Cl, I). Right: Two-dimensional schematic illustrating the perovskite unit cell. (**B**) Ultraviolet to visible (UV-Vis) absorbance spectra of the photoactive layer in the solar cell (mesoporous oxide; perovskite absorber; spiro-OMeTAD) sealed between two sheets of glass in nitrogen and exposed to simulated AM1.5 sunlight at 100 mW cm^{-2} irradiance for up to 1000 hours. No additional UV filtration was used for the solar irradiance. Inset: Extracted optical density at 500 nm as a function of time. (**C**) Left: Schematic representation of full device structure, where the mesoporous oxide is either Al_2O_3 or anatase TiO_2. Right: Cross-sectional SEM image of a full device incorporating mesoporous Al_2O_3. Scale bar, 500 nm.

porous oxide films by performing cross-sectional scanning electron microscopy (SEM) with elemental mapping via energy-dispersive x-ray (EDX) analysis (fig. S2) (*25*). To complete the photoactive layer, the perovskite-coated porous electrode was further filled with the hole transporter, spiro-OMeTAD, via spin-coating; as shown in Fig. 1C, the spiro-OMeTAD forms a capping layer that ensures selective collection of holes at the silver electrode.

In Fig. 2A, the incident photon-to-electron conversion efficiency (IPCE) action spectrum is shown for the devices that use mesoporous TiO_2 and Al_2O_3, exhibiting spectral sensitivity spanning from the visible to the near-IR (400 to 800 nm) with a peak IPCE of >80% for both oxides. The slight difference in shape arises from the slightly different perovskite concentrations in the optimized devices. In Fig. 2B, we show current density–voltage (*J-V*) curves measured under simulated AM1.5 illumination of 100 mW cm^{-2}. The sensitized TiO_2 solar cell exhibited a short-circuit photocurrent (J_{sc}) = 17.8 mA cm^{-2}, V_{oc} = 0.80 V, and a fill factor of 0.53, yielding an overall power conversion efficiency (η) of 7.6%. We present two different *J-V* curves for the Al_2O_3-based device. The most efficient device exhibited J_{sc} = 17.8 mA cm^{-2}, V_{oc} = 0.98 V, and a fill factor of 0.63, yielding η = 10.9%. The third curve (dashed trace) shows a device with J_{sc} = 15.4 mA cm^{-2} and V_{oc} = 1.13 V but a low fill factor of 0.45, yielding η = 7.8%. [See (*25*) for histograms of device performance parameters for the TiO_2- and Al_2O_3-based devices (fig. S3)].

The general trend is that the Al_2O_3 cells generated open-circuit voltages that were >200 mV higher than those generated by the sensitized TiO_2 solar cells, with comparable short-circuit currents and slightly lower fill factors. From the solar cell measurements on alumina-based devices, it was apparent that the perovskite layer could function as both absorber and n-type component, transporting electronic charge out of the device. We further illustrate the "semiconducting" nature of the perovskite by the construction of a planar-junction diode with the structure FTO / compact TiO_2 / $CH_3NH_3PbI_2Cl$ / spiro-OMeTAD / Ag. The perovskite film was ~150 nm thick in this configuration, and the solar cell exhibited J_{sc} = 7.13 mA cm^{-2}, V_{oc} = 0.64 V, a fill factor of 0.4, and η = 1.8%.

If we take the optical band gap of $CH_3NH_3PbI_2Cl$ to be 1.55 eV from the IPCE onset at 800 nm (*33*) and the open-circuit voltage to be 1.1 V, this represents a difference in energy of only 0.45 eV, competitive with the best thin-film technologies (*2*). To understand why we observed such an increase in voltage over the TiO_2 cells, we need to consider the operational mode of the two concepts (Fig. 3A). For sensitized TiO_2 devices, we would expect that after light absorption in the perovskite, electrons would be transferred to the TiO_2 (with subsequent electron transport to the FTO electrode through the TiO_2) and holes would be transferred to the spiro-OMeTAD (with subsequent transport to the silver electrode). For Al_2O_3-based cells, the electrons must remain in the perovskite phase (*34*) until they are collected at the planar TiO_2-coated FTO electrode, and must hence be transported throughout the film thickness in the perovskite. Hole transfer from the photoexcited perovskite to the spiro-OMeTAD should occur in much the same way as in the sensitized device. Al_2O_3 did not act as an n-type oxide in DSSCs (fig. S4) (*25*).

To examine the charge generation in these devices, we performed photoinduced absorption (PIA) spectroscopy on the oxide films coated with the perovskite, both with and without the addition of spiro-OMeTAD. For the mesoporous TiO_2 film coated with perovskite, the PIA spectrum revealed features in the near-IR assigned to the free electrons in the titania (*35*), confirming effective sensitization of the titania by the perovskite. In contrast, films made of Al_2O_3 coated with perovskite exhibited no PIA signal, confirming the insulating role of alumina. After addition of spiro-OMeTAD, we could efficiently monitor the oxidized species of spiro-OMeTAD created after photoexcitation of the perovskite. They had absorption features at 525 and 750 nm, as well as a broad band around 1200 nm, assigned to the hole located on the triarylamine moieties (*28*, *36*), which dominated the spectra in both the TiO_2- and Al_2O_3-based samples. These results indicate that hole transfer is highly effective from the photoexcited perovskite to spiro-OMeTAD, and specifically that a hole conductor is required to enable long-lived charge species within the perovskite coated on the Al_2O_3. We note that the PIA signal depended both on the concentration and lifetime of the species monitored; hence, from this measurement alone, quantification of the relative charge-generated yield is not possible.

To probe the effectiveness of the perovskite layer at transporting electronic charge out of the device, we performed small-perturbation transient photocurrent decay measurements (*37*). The solar cells were exposed to simulated sunlight and "flashed" with a small red light pulse; in such experiments, the decay rate of the transient photocurrent signal is approximately proportional to the rate of charge transport out of the photoactive layer (*37*). As shown in Fig. 3C, we observed that charge collection in the Al_2O_3-based devices was faster than in the TiO_2-based sensitized devices by a factor of >10, indicating faster electron diffusion through the perovskite phase than through the n-type TiO_2.

Because there is no n-type oxide in the Al_2O_3-based cells, the devices are not "sensitized" solar cells, but rather two-component hybrid solar cells. As designed, the Al_2O_3 is simply acting as a mesoscale "scaffold" upon which the device is structured; we term this concept a "meso-superstructured solar cell" (MSSC). The above measurements demonstrate that long-lived charge carriers can be generated via hole transfer from the perovskite to spiro-OMeTAD and that the perovskite layer is faster at transporting electronic charge than the mesoporous TiO_2. However, they do not explain the increase in V_{oc} values. The V_{oc} is generated by the build-up of electrons in

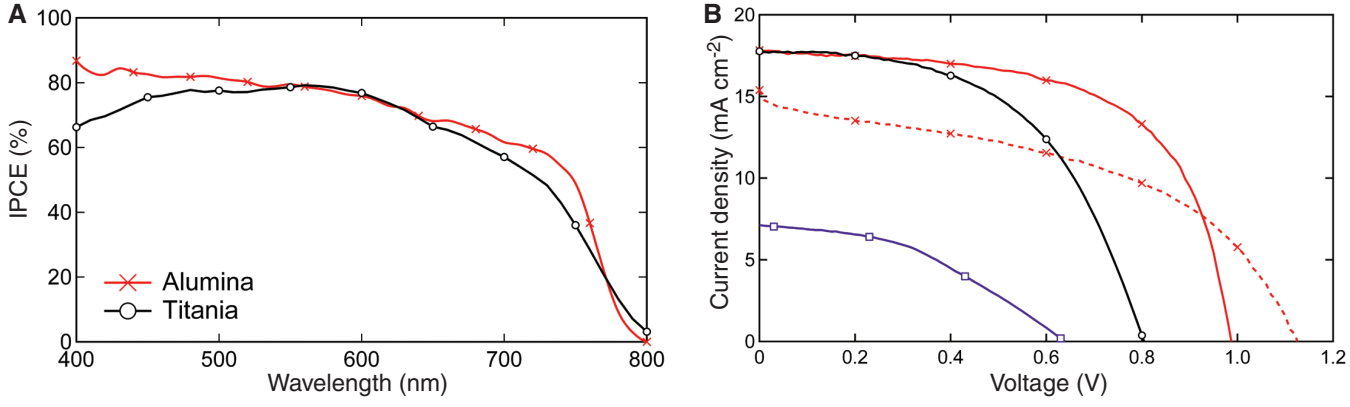

Fig. 2. (**A**) IPCE action spectrum of an Al_2O_3-based and perovskite-sensitized TiO_2 solar cell, with device structure as follows: FTO / compact TiO_2 / mesoporous Al_2O_3 (red trace with crosses) or mesoporous TiO_2 (black trace with circles) / $CH_3NH_3PbI_2Cl$ / spiro-OMeTAD / Ag. (**B**) Current density–voltage characteristics under simulated AM1.5 100 mW cm^{-2} illumination for Al_2O_3-based cells, one cell exhibiting high efficiency (red solid trace with crosses) and one exhibiting V_{OC} > 1.1 V (red dashed line with crosses); for a perovskite-sensitized TiO_2 solar cell (black trace with circles); and for a planar-junction diode with structure FTO / compact TiO_2 / $CH_3NH_3PbI_2Cl$ / spiro-OMeTAD / Ag (purple trace with squares).

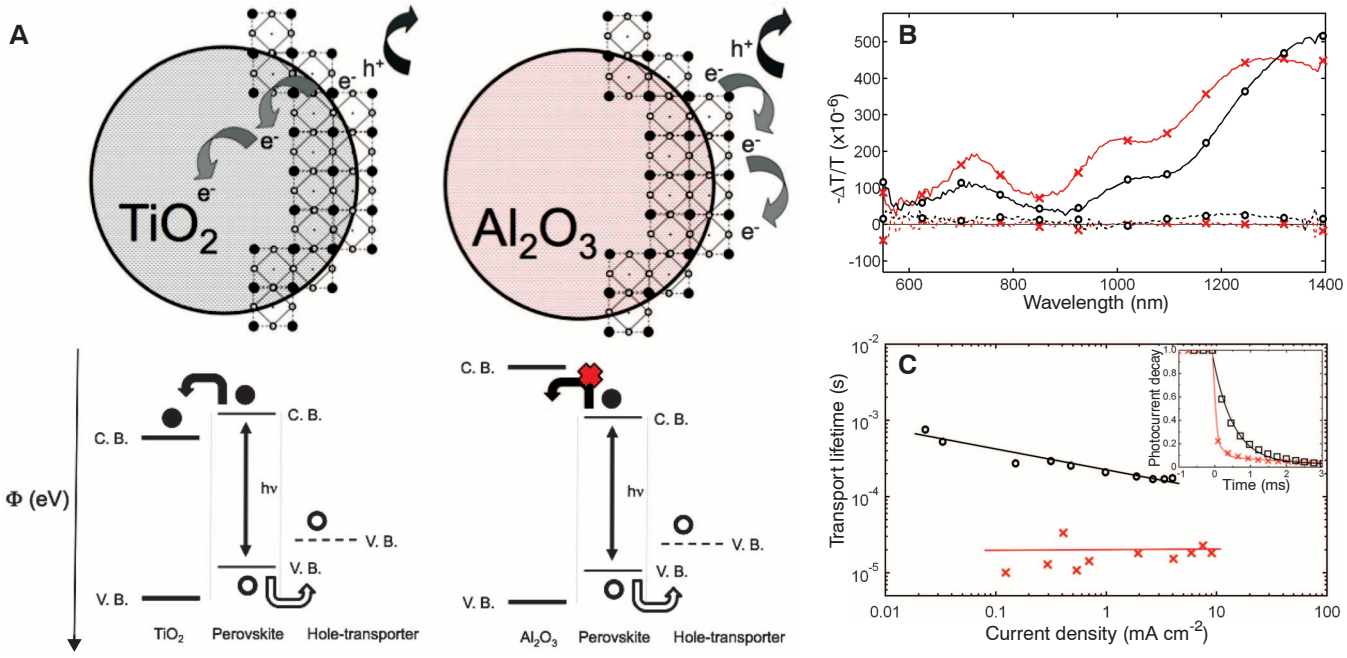

Fig. 3. (**A**) Schematic illustrating the charge transfer and charge transport in a perovskite-sensitized TiO_2 solar cell (left) and a noninjecting Al_2O_3-based solar cell (right); a representation of the energy landscape is shown below, with electrons shown as solid circles and holes as open circles. (**B**) Photoinduced absorbance (PIA) spectra of the mesoporous TiO_2 films (black circles) and Al_2O_3 films (red crosses) coated with perovskite with (solid lines) and without (dashed lines) spiro-OMeTAD hole transporter, under 496.5 nm excitation at 23 Hz repetition rate. (**C**) Charge transport lifetime determined by small-perturbation transient photocurrent decay measurement of perovskite-sensitized TiO_2 cells (black circles) and Al_2O_3 cells (red crosses), both with lines to aid the eye. Inset shows normalized photocurrent transients for Al_2O_3 cells (red trace with crosses every 7th point) and TiO_2 cells (black trace with circles every 7th point), set to generate 5 mA cm^{-2} photocurrent from the background light bias.

the n-type material and holes in the p-type material, resulting in splitting of the quasi Fermi levels for both electrons and holes. For mesoporous TiO_2, there exist sites in the tail of the density of states that extend into the band gap (*38*). These fill with electrons under illumination; the result is that the quasi–Fermi level for electrons (E^*_{Fn}) is farther from the conduction band, for any given charge density, than would be the case if these states did not exist (i.e., in a highly crystalline semiconductor). The increased charge-storing capacity of materials with a high density of sub–band gap states is termed "chemical capacitance" (*38*). There is, in essence, no chemical capacitance of the Al_2O_3, and for the MSSCs all the electronic charge resides in the perovskite, moving the E^*_{Fn} in this material nearer to the conduction band for the same charge density. The higher voltage indicates that there are fewer surface and sub–band gap states in the perovskite films than in the mesoporous TiO_2. Hence, the increased voltage is caused by a substantial reduction of the chemical capacitance of the solar cell. We used a compact layer of TiO_2 as the electron-selective anode, but the chemical capacitance of this extremely thin (50 to 100 nm) TiO_2 layer was very low because of the low volume and surface area (i.e., flat). In addition, the compact layer deposited via spray pyrolysis has a donor density of ~10^{18} cm^{-3} (*39*), and the sub–band gap sites responsible for the chemical capacitance may be full.

A central question is whether the MSSC is excitonic or a distributed p-n junction. The perovskites tend to form layered structures, with continuous two-dimensional metal halide planes perpendicular to the *z* axis and the lower dielectric organic components (methyl amine) between these planes. The possible quasi–two-dimensional confinement of the excitons can result in an increased exciton binding energy, which can be up to a few hundred millielectron volts (*40*). The reasonably high photocurrents from the planar-junction solar cells (Fig. 2B) could be explained by either moderately delocalized and highly mobile excitons being quenched at the perovskite–spiro-OMeTAD interface, or the generation of free charges in the bulk of the perovskite films with reasonably good electron and hole migration out of the devices.

The key limitation in performance of the MSSC at present is a balance between series and shunt resistance. The perovskite absorber is reasonably conductive, measured to be on the order of 10^{-3} S cm^{-3}; thus, short-circuiting of the device occurs if contact exists between the silver electrode and the perovskite absorber. A thick capping layer of p-type spiro-OMeTAD readily resolves this issue, however; spiro-OMeTAD is less conductive (~10^{-5} S cm^{-1}), so a thicker capping layer results in high series resistance. Thus, we are presented with a compromise.

Our work represents an evolution of the solid-state sensitized solar cell with low fundamental losses. The application of a mesostructured insulating scaffold upon which extremely thin films of n-type and p-type semiconductors are assembled, termed the meso-superstructured solar cell (MSSC), has proven to be extraordinarily effective with an n-type perovskite, delivering more than 10.9% power conversion efficiency under full solar illumination. Further advances in overall power conversion efficiency are expected by extending the absorption onset toward 940 nm, through the implementation of new perovskites or broadening this concept to other solution-processable semiconductors. Enhancing the light absorption near the band edge through carefully engineered mesostructures or better photon management would lead to increased photocurrent. Reduced series resistance through the use of higher-mobility hole transporters, or better control over the capping layer thickness, would improve the fill factor. Finally, extending this system to multijunction devices (without the requirement for lattice matching, as in conventional multijunction solar cells) would further enhance performance.

References and Notes

1. B. O'Regan, M. Grätzel, *Nature* **353**, 737 (1991).
2. M. A. Green, K. Emery, Y. Hishikawa, W. Warta, E. D. Dunlop, *Prog. Photovolt. Res. Appl.* **20**, 12 (2012).
3. L. Han *et al.*, *Energy Environ. Sci.* **5**, 6057 (2012).
4. A. Yella *et al.*, *Science* **334**, 629 (2011).
5. G. Yu, J. Gao, J. C. Hummelen, F. Wudl, A. J. Heeger, *Science* **270**, 1789 (1995).
6. J. J. M. Halls *et al.*, *Nature* **376**, 498 (1995).
7. A. H. Ip *et al.*, *Nature Nano.* **7**, 577 (2012).
8. T. K. Todorov, K. B. Reuter, D. B. Mitzi, *Adv. Mater.* **22**, E156 (2010).
9. H. J. Snaith, *Adv. Funct. Mater.* **20**, 13 (2010).
10. G. Dennler, M. C. Scharber, C. J. Brabec, *Adv. Mater.* **21**, 1323 (2009).

11. B. E. Hardin, H. J. Snaith, M. D. McGehee, *Nat. Photonics* **6**, 162 (2012).
12. U. Bach *et al.*, *Nature* **395**, 583 (1998).
13. J. Burschka *et al.*, *J. Am. Chem. Soc.* **133**, 18042 (2011).
14. Y. Itzhaik, O. Niitsoo, M. Page, G. Hodes, *J. Phys. Chem. C* **113**, 4254 (2009).
15. J. A. Chang *et al.*, *Nano Lett.* **12**, 1863 (2012).
16. J. Nelson, *Phys. Rev. B* **59**, 15374 (1999).
17. D. B. Mitzi, C. A. Field, W. T. A. Harrison, A. M. Guloy, *Nature* **369**, 467 (1994).
18. K. Chondroudis, D. B. Mitzi, *Chem. Mater.* **11**, 3028 (1999).
19. M. Era, T. Tsutsui, S. Saito, *Appl. Phys. Lett.* **67**, 2436 (1995).
20. C. R. Kagan, D. B. Mitzi, C. D. Dimitrakopoulos, *Science* **286**, 945 (1999).
21. A. Kojima, K. Teshima, Y. Shirai, T. Miyasaka, *J. Am. Chem. Soc.* **131**, 6050 (2009).
22. J. H. Im, C. R. Lee, J. W. Lee, S. W. Park, N. G. Park, *Nanoscale* **3**, 4088 (2011).
23. I. Chung, B. Lee, J. He, R. P. H. Chang, M. G. Kanatzidis, *Nature* **485**, 486 (2012).
24. H. J. Snaith, *Energy Environ. Sci.* **5**, 6513 (2012).
25. See supplementary materials on *Science* Online.
26. A. Poglitsch, D. Weber, *J. Chem. Phys.* **87**, 6373 (1987).
27. T. Leijtens *et al.*, *ACS Nano* **6**, 1455 (2012).
28. H. J. Snaith *et al.*, *Nanotechnology* **19**, 424003 (2008).
29. J. Melas-Kyriazi *et al.*, *Adv. Energy Mater.* **1**, 407 (2011).
30. A. Abrusci *et al.*, *Energy Environ. Sci.* **4**, 3051 (2011).
31. I.-K. Ding *et al.*, *Adv. Funct. Mater.* **19**, 2431 (2009).
32. P. Docampo *et al.*, *Adv. Funct. Mater.* 10.1002/adfm.201201223 (2012).
33. D. A. R. Barkhouse, O. Gunawan, T. Gokmen, T. K. Todorov, D. B. Mitzi, *Prog. Photovolt. Res. Appl.* **20**, 6 (2012).
34. A. Kojima, M. Ikegami, K. Teshima, T. Miyasaka, *Chem. Lett.* **41**, 397 (2012).
35. G. Rothenberger, D. Fitzmaurice, M. Graetzel, *J. Phys. Chem.* **96**, 5983 (1992).
36. G. Boschloo, A. Hagfeldt, *Inorg. Chim. Acta* **361**, 729 (2008).
37. P. Docampo *et al.*, *Adv. Funct. Mater.* **20**, 1787 (2010).
38. J. Bisquert, *Phys. Chem. Chem. Phys.* **5**, 5360 (2003).
39. L. Kavan, M. Grätzel, *Electrochim. Acta* **40**, 643 (1995).
40. T. Ishihara, J. Takahashi, T. Goto, *Phys. Rev. B* **42**, 11099 (1990).

Acknowledgments: Supported by the European Research Council (HYPER project no. 279881), the Strategic International Research Cooperative Program of the UK Engineering and Physical Sciences Research Council, and the Japan Science and Technology Agency. T.M. thanks the funding program for World-Leading Innovative R&D on Science and Technology (FIRST Program), Japan, for hybrid solar cell research. We thank the New Energy and Industrial Technology Development Organization for support. M.M.L. is grateful for support from the Simms Bursary granted by Merton College, Oxford. We thank S. K. Pathak for assistance with x-ray diffraction measurements and analysis, and A. Abrusci, J. Ball, P. Docampo, A. Hey, T. Leijtens, N. Noel, and A. Kojima for valuable discussions. The University of Oxford has filed three patents related to this work.

Supplementary Materials

www.sciencemag.org/cgi/content/full/science.1228604/DC1
Materials and Methods
Supplementary Text
Figs. S1 to S4

31 May 2012; accepted 7 September 2012
Published online 4 October 2012;
10.1126/science.1228604

Photoinduced Ullmann C–N Coupling: Demonstrating the Viability of a Radical Pathway

Sidney E. Creutz,[1]* Kenneth J. Lotito,[1]* Gregory C. Fu,[1,2]† Jonas C. Peters[1]†

Carbon–nitrogen (C–N) bond-forming reactions of amines with aryl halides to generate arylamines (anilines), mediated by a stoichiometric copper reagent at elevated temperature (>180°C), were first described by Ullmann in 1903. In the intervening century, this and related C–N bond-forming processes have emerged as powerful tools for organic synthesis. Here, we report that Ullmann C–N coupling can be photoinduced by using a stoichiometric or a catalytic amount of copper, which enables the reaction to proceed under unusually mild conditions (room temperature or even −40°C). An array of data are consistent with a single-electron transfer mechanism, representing the most substantial experimental support to date for the viability of this pathway for Ullmann C–N couplings.

Arylamines (anilines) are a commonly encountered subunit in organic compounds and are important in fields ranging from pharmaceuticals to materials science (*1*–*3*). Because many aryl halides and amines are readily available, coupling these two reactants provides a particularly attractive, convergent approach to the synthesis of arylamines. Thus, the discovery by Ullmann in 1903 that this C–N bond construction can be accomplished by heating these partners in the presence of a stoichiometric amount of copper was a landmark achievement (Fig. 1A) (*4*, *5*). During the past 20 years, there have been numerous advances in C–N coupling reactions, ranging from the discovery of milder, copper-catalyzed Ullmann processes to the development of methods based on palladium and other transition metals (*6*–*11*).

Despite the importance of copper-based Ullmann C–N coupling reactions, understanding of the mechanism of these processes has evolved only slowly (*6*–*9*, *12*). It is believed that Ullmann couplings generally begin with Cu–N bond formation; however, a variety of pathways for the subsequent cleavage of the Ar–X bond have been proposed, including a concerted oxidative addition (*13*, *14*) and a single-electron transfer (SET, which encompasses halogen-atom transfer) mechanism with radical intermediates (Fig. 1B) (*15*). It is likely that different pathways operate under different conditions.

Currently, there is virtually no direct experimental evidence for the viability of an SET mechanism for Ullmann C–N couplings (*12*), although Buchwald and Houk have recently published a computational study in support of this pathway for certain processes (*15*, *16*). With respect to Ullmann C–C bond formation, Kim has observed that oligothiophenes can be generated upon ultraviolet irradiation (~140 nm) of 2,5-diiodothiophene on a copper metal surface, presumably via direct photodissociation of the C–I bond (*17*, *18*). In this report, we provide an array of experimental data for the reaction of aryl halides with well-defined copper(I) amido complex **1**, all of which are consistent with an SET/radical mechanism for Ullmann C–N coupling. In addition to furnishing the strongest evidence to date for the viability of an SET pathway, this study introduces a photoinduced variant of this powerful transformation.

During the past several years, we have explored the chemistry of copper(I) amido complexes (*19*, *20*), and we have determined that adducts such as carbazolide complex $(Ph_3P)_2Cu(carbazolide)$ (**2**) are photoluminescent when irradiated between 300 and 400 nm (*21*). We envisioned that we could capitalize on the photophysical properties of this family of complexes as a mechanistic tool in order to examine the viability of an SET/radical pathway for Ullmann C–N bond formation (Fig. 1C). Thus, irradiation of a copper–carbazolide complex could lead to electron transfer to the aryl halide to afford a radical anion, which would rapidly fragment to form an aryl radical and a halide anion (Fig. 1C, top) (*22*). This aryl radical could then react with the copper complex to furnish the C–N coupling product. Alternatively, the aryl radical could be generated directly through halogen atom transfer from the aryl halide to the copper–carbazolide complex (inner-sphere electron-transfer) (Fig. 1C, bottom). Regardless of which mechanism is followed, this would provide a photoinduced (*23*, *24*) pathway for Ullmann C–N coupling.

In a preliminary investigation, we determined that the luminescence of $(Ph_3P)_2Cu(carbazolide)$ (**2**) is quenched upon the addition of iodobenzene; furthermore, irradiation of the mixture leads to C–N bond formation. However, our desire for improved solubility properties led us to synthesize a related copper complex in which the PPh_3

[1]Division of Chemistry and Chemical Engineering, California Institute of Technology, Pasadena, CA 91125, USA. [2]Department of Chemistry, Massachusetts Institute of Technology, Cambridge, MA 02139, USA.

*These authors contributed equally to this work.
†To whom correspondence should be addressed. E-mail: gcfu@caltech.edu (G.C.F.); jpeters@caltech.edu (J.C.P.)

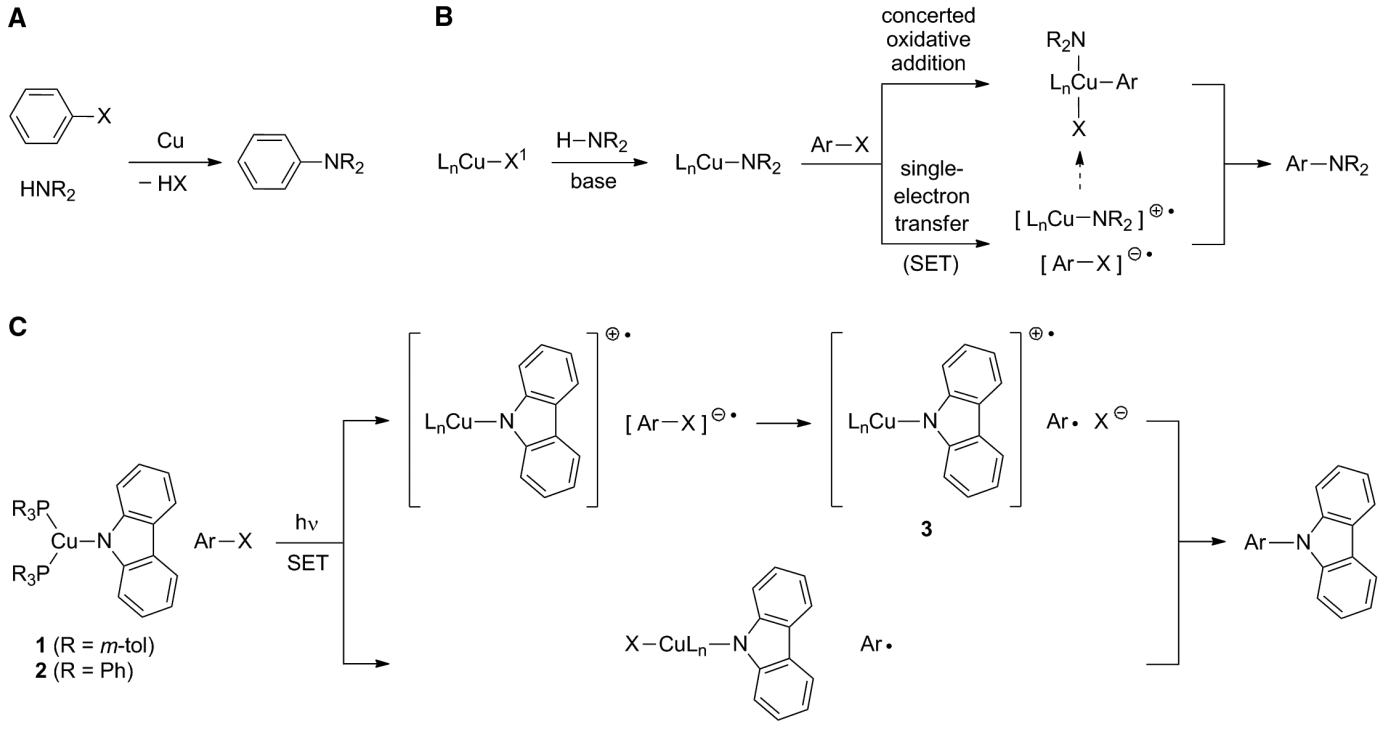

Fig. 1. (**A**) Generalized equation for an Ullmann coupling to form an arylamine. (**B**) Outline of two of the possible mechanisms for Ullmann C–N bond formation. (**C**) Outline of a possible pathway for photoinduced Ullmann C–N bond formation via a copper–carbazolide complex.

ligands are replaced with P(*m*-tol)$_3$ (*25*). A single-crystal x-ray diffraction study confirmed that copper–carbazolide complex **1** maintains a three-coordinate trigonal-planar geometry in the solid state (Fig. 2A). Complex **1** is colorless and is not visibly luminescent in acetonitrile; however, emission and excitation spectra confirm that it has accessible excitations in the near ultraviolet (Fig. 2B).

When an acetonitrile solution of copper–carbazolide complex **1** and iodobenzene is irradiated with a standard 13-W compact fluorescent light bulb (CFL) at room temperature for 10 hours, C–N bond formation proceeds in good yield (77%) (Table 1A, entry 1); an even higher yield is obtained in CD_3CN (84%) (Table 1A, entry 2). Irradiation with a 100-W mercury lamp results in C–N bond formation even at –40°C (Table 1A, entry 3). Previously described couplings of carbazole with iodobenzene in the presence of copper have used temperatures of at least 90°C (*26*).

Under otherwise identical conditions in the absence of light, no *N*-phenylcarbazole is observed (<1%) (Table 1A, entry 4), and negligible coupling occurs in the dark even upon heating at 65°C for 12 hours. Irradiation of a mixture of carbazole and iodobenzene (without **1**) leads to no detectable *N*-phenylcarbazole (<1%).

For these photoinduced Ullmann C–N coupling reactions, we postulate that upon photoexcitation, copper complex **1** transfers an electron to iodobenzene to produce a radical ion pair (Fig. 1C). The higher yield obtained in CD_3CN (Table 1A, entry 2) as compared with that in CH_3CN (Table 1A, entry 1) can be attributed to a kinetic isotope effect for undesired abstraction of a hydrogen/deuterium from the solvent by the phenyl radical or by radical cation **3** (Fig. 1C). Consistent with this hypothesis, we observed benzene and unsubstituted N*H*/N*D* carbazole as side products in these photoinduced couplings (*25*), and we have established that when we independently generate radical cation **3** via chemical oxidation of **1** in CH_3CN, the unsubstituted N*H* carbazole is formed (Fig. 2C) (*27*).

Bromobenzene also undergoes Ullmann coupling when irradiated with a 13-W CFL in the presence of copper–carbazolide complex **1**. As would be expected on the basis of relative reduction potentials [PhI, –1.91 V; PhBr, –2.43 V; PhCl, –2.76 V versus saturated calomel electrode (SCE) in dimethylformamide (DMF) on a platinum electrode] (*28*), photoinduced C–N bond formation is considerably slower for bromobenzene (Table 1A, entry 5) than for iodobenzene (Table 1A, entry 1). Nevertheless, a good yield of the desired product can be obtained at room temperature if a 100-W mercury lamp is used (Table 1A, entry 6), and a moderate yield is observed even at –40°C (Table 1A, entry 7). In the absence of light, no Ullmann coupling occurs (Table 1A, entry 8).

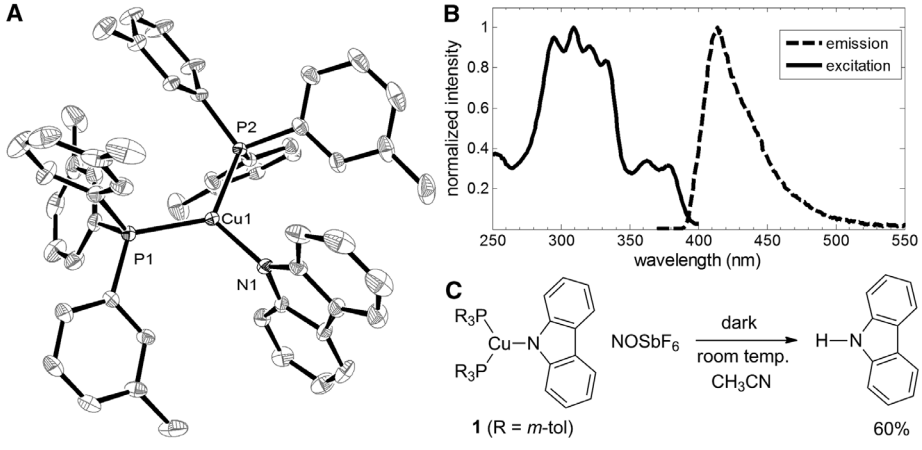

Fig. 2. (**A**) X-ray structure of copper complex **1** (thermal ellipsoids drawn at 50% probability and H atoms omitted for clarity). (**B**) Excitation and emission spectra of copper complex **1** in CH_3CN. (**C**) Chemical oxidation of copper complex **1**.

Table 1. (**A**) Photoinduced Ullmann C–N coupling reactions of copper–carbazolide complex **1** with PhX (X = I, Br, Cl). (**B**) Photoinduced Ullmann C-N coupling reactions catalyzed by copper–carbazolide complex **1**. Yields were determined by means of gas chromatographic analysis versus a calibrated internal standard (4,4′-di-*t*-butylbiphenyl) and are reported as averages of at least two experiments; yields of purified product are in parentheses. The conditions described in each equation are designated as the "standard" conditions for the set of entries immediately below the equation. CFL, compact fluorescent light bulb.

A

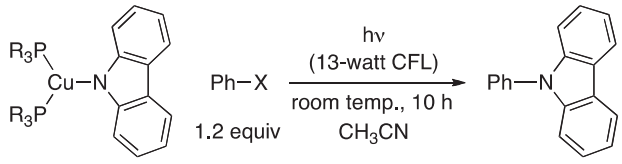

1 (R = *m*-tol)

Coupling with iodobenzene (X = I)

Entry	Conditions	Yield (%)
1	Standard conditions	77 (74)
2	CD_3CN instead of CH_3CN	84 (82)
3	–40 °C, 100-watt Hg lamp	69 (68)
4	dark	<1

Coupling with bromobenzene (X = Br)

Entry	Conditions	Yield (%)
5	Standard conditions	40
6	100-watt Hg lamp	76 (72)
7	–40 °C, 100-watt Hg lamp, 5 equiv PhBr	59
8	dark	<1

Coupling with chlorobenzene (X = Cl)

Entry	Conditions	Yield (%)
9	Standard conditions	5
10	100-watt Hg lamp, 24 h, 5 equiv PhCl	68 (66)
11	–40 °C, 100-watt Hg lamp, 5 equiv PhCl	11
12	dark	<1

B

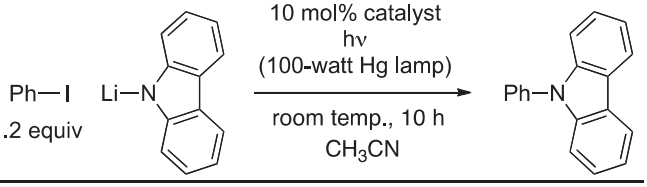

Entry	Catalyst	Conditions	Yield (%)
1	**1**	Standard conditions	64 (52)
2	**1**	dark	<1
3	None	Standard conditions	3
4	**1**	–40 °C	45
5	1.5 mol% **1**	Standard conditions	30
6	CuI	Standard conditions	65 (58)
7	CuI	dark	<1

We roughly estimate the excited-state reduction potential of copper–carbazolide complex **1** to be ~ –2.6 V versus SCE in CH_3CN, on the basis of its electrochemistry (fig. S4) and the approximate value of E^{00} = 3.1 eV, the energy value obtained from the intersection of its emission and excitation profiles. This reduction potential is sufficiently close to the outer-sphere reduction potential of chlorobenzene (–2.76 V in DMF) to expect electron transfer to occur. Under the standard conditions for the reaction of copper–carbazolide complex **1** with iodobenzene, chlorobenzene undergoes cross-coupling in low yield (5%) (Table 1A, entry 9). However, irradiation by a 100-W mercury lamp in the presence of excess chlorobenzene leads to efficient photoinduced Ullmann coupling at room temperature (Table 1A, entry 10).

A variety of data are consistent with radical intermediates in these photochemical Ullmann reactions. For example, we detected benzene as a side product (vide supra); furthermore, monodeuterated arene is generated when the reaction is conducted in CD_3CN, along with a small amount of succinonitrile (>5%) due to dimerization of the resulting cyanomethyl radical (*29*). Last, we observed the formation of iodobiphenyls when a large excess of iodobenzene is used (*30*).

Low-temperature (77 K) electron paramagnetic resonance (EPR) data are consistent with photoinduced generation of a copper-containing radical when copper–carbazolide complex **1** and iodobenzene are irradiated with a 100-W mercury lamp at –40°C for 15 min in a 4:5 mixture of propionitrile/butyronitrile (Fig. 3A); this signal and the deep-blue color of the reaction mixture rapidly disappear upon warming to room temperature. The EPR spectrum has nearly axial symmetry. Coupling to $^{63/65}$Cu is too small relative to the broadness of the signal to be observed (*31*); nevertheless, the strongly anisotropic *g*-values suggest that this species has at least partial metalloradical [Cu(II)] character. The same EPR spectrum is produced when complex **1** is treated at –100°C with 0.3 equivalents of the oxidant Magic Blue [tris(4-bromophenyl)aminium hexachloridoantimonate], indicating that the same radical species can be generated by chemical and by photoinduced oxidation. We speculate that rather than being radical cation **3** itself (Fig. 1C), the detected radical is likely a more stable derivative, such as $Cu_2[P(m\text{-tol})_3]_4(carbazolide)_2^{+\bullet}$, which could be formed via trapping of radical cation **3** by complex **1**. The lack of resolved $^{63/65}$Cu hyperfine coupling in the EPR signal is consistent with such a species (*32*), as is our observation that this signal is absent when one equivalent of Magic Blue is used.

To provide further support for radical intermediates in these photoinduced Ullmann reactions, we examined the coupling of copper–carbazolide complex **1** with 2-(allyloxy)iodobenzene (**4**), a radical probe (Fig. 3B). Because radical **5** is known to cyclize very rapidly [rate constant (k) = 9.6×10^9 s^{-1} in dimethyl sulfoxide] (*33*), the consistent failure to observe cyclized products in other studies of Ullmann C–N bond-forming reactions with this substrate has been cited as evidence against a radical pathway (*12*–*15*). In contrast, in the case of our photoinduced Ullmann coupling we observed exclusive formation of cyclized compounds (**6** and 3-methyl-2,3-dihydrobenzofuran) (Fig. 3B). This dichotomy of reaction products under thermal versus photochemical conditions does not require a divergence in pathways (radical versus nonradical) for C–X cleavage; for example, the thermal process could, in principle, proceed through an aryl radical intermediate that is captured by copper faster than it adds to the pendant olefin.

Control reactions establish that copper complex **1** does not couple with **4** in the dark, even upon heating to 65°C. Furthermore, no cyclized products are detected when compound **4** is irradiated in the absence of complex **1**.

Formation of dihydrobenzofuran **6** does not conclusively support a radical pathway because this product could in principle be generated via concerted oxidative addition of **4** to form an aryl–copper reagent, followed by β-migratory insertion and reductive elimination. However, our observation

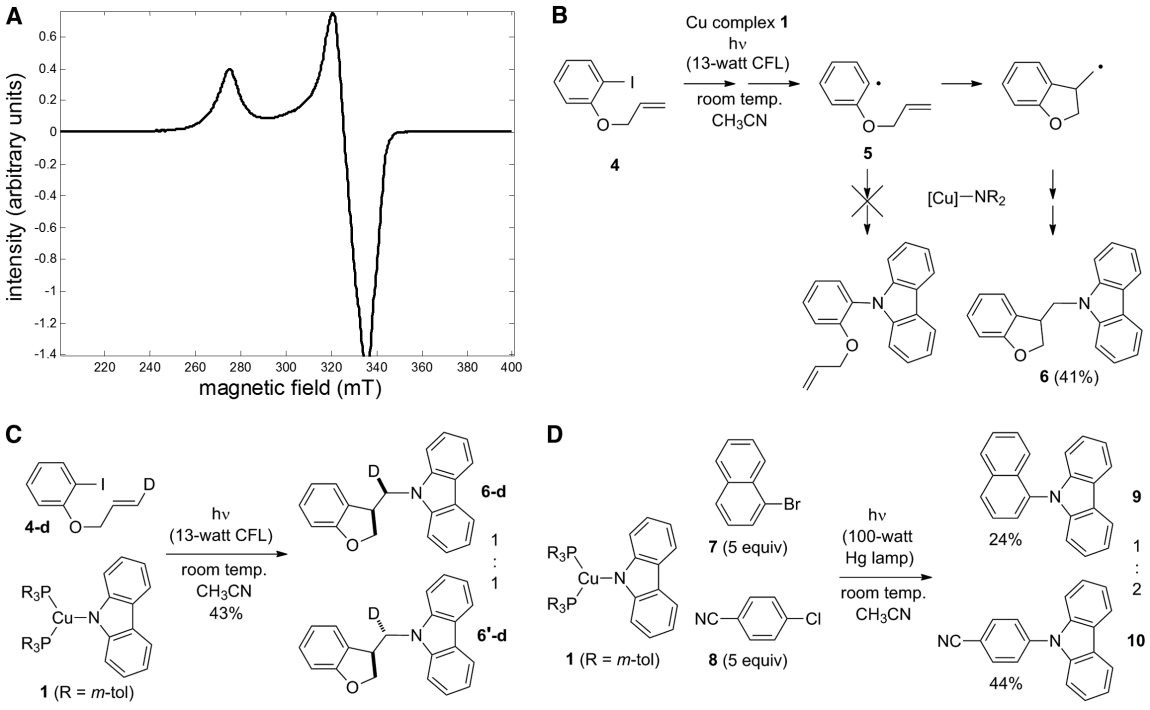

Fig. 3. Experimental observations that are consistent with a radical pathway. (**A**) X-band EPR spectrum of a frozen (77 K) reaction mixture. Parameters are g = [2.440, 2.055, 1.990]. (**B**) Cyclization, followed by C–N bond formation, in a photoinduced Ullmann reaction of an aryl iodide bearing a pendant olefin. (**C**) Stereochemical study of a photoinduced Ullmann reaction. (**D**) Substrate-competition study in a photoinduced Ullmann reaction.

that deuterium-labeled aryl iodide **4-d** furnishes a 1:1 mixture of diastereomers (Fig. 3C) is fully consistent with a radical pathway, whereas the oxidative-addition/syn-insertion/reductive-elimination sequence should only produce diastereomer **6-d**.

A control experiment established that olefin **4-d** does not undergo cis/trans isomerization under the reaction conditions. We have also performed this stereochemical study with the bromo analog of **4-d**; again, a 1:1 mixture of diastereomers is generated, and no uncyclized products are observed.

An additional mechanistic probe that has been used to distinguish between concerted oxidative addition of Ar–X and a pathway involving SET to the haloarene is the relative reactivity of 1-bromonaphthalene (**7**) and 4-chlorobenzonitrile (**8**) (Fig. 3D) (*13*). According to this analysis, if C–X cleavage proceeds via concerted oxidative addition, then preferential coupling of 1-bromonaphthalene is expected, whereas if the reaction occurs via an SET mechanism, then 4-chlorobenzonitrile should react more rapidly because of its more favorable reduction potential (–2.03 V for **8**; –2.17 V for **7** versus SCE in DMF) (*28*).

When copper–carbazolide complex **1** is irradiated in the presence of a 1:1 mixture of 1-bromonaphthalene and 4-chlorobenzonitrile, Ullmann coupling product **10**, derived from 4-chlorobenzonitrile, is predominant (Fig. 3D). This observation is consistent with a radical-based SET pathway for C–N bond formation and stands in sharp contrast with a previous investigation in which only the bromoarene was reactive, which was interpreted as supporting a concerted mechanism for oxidative addition under those conditions (*13*).

Because copper-catalyzed Ullmann C–N couplings are of substantial interest (*6*–*9*), we have pursued preliminary studies to ascertain whether turnover can be achieved in these photoinduced processes. We have determined that irradiation of iodobenzene and lithium carbazolide in an acetonitrile solution of 10 mole percent (mol %) of copper–carbazolide complex **1** does indeed furnish the C–N coupling product in 64% yield, establishing the viability of copper catalysis in this photochemical reaction manifold (Table 1B, entry 1). In the absence of light, no detectable coupling is observed (Table 1B, entry 2), and irradiation of the coupling partners in the absence of complex **1** leads to very little *N*-phenylcarbazole (3%) (Table 1B, entry 3). These copper-catalyzed, photoinduced Ullmann couplings can even be effected at –40°C (Table 1B, entry 4). In the presence of 1.5 mol % of copper–carbazolide complex **1**, a turnover number of ~20 can be achieved (Table 1B, entry 5). CuI also serves as a catalyst for photoinduced Ullmann C–N couplings, likely via electron transfer from a luminescent copper–carbazolide complex generated in situ (Table 1B, entries 6 and 7).

When aryl iodide **4-d** (Fig. 3C) and lithium carbazolide are used as coupling partners in the presence of copper–carbazolide complex **1** under the catalytic conditions outlined in Table 1B, a 1:1 mixture of diastereomers **6-d** and **6′-d** is formed (with no accompanying uncyclized products). This observation is consistent with a common radical-based SET pathway for catalyzed and uncatalyzed Ullmann couplings effected by complex **1**.

Until now, the available experimental data regarding the mechanism (or mechanisms) of the classic Ullmann C–N coupling reaction could be accommodated by C–X cleavage via concerted oxidative addition to copper. The present report demonstrates that Ullmann C–N coupling can be achieved via a photoinitiated step in which C–X cleavage proceeds instead via a radical intermediate. Although we do not suggest that our findings establish a general SET mechanism for Ullmann coupling reactions, they do show that if a carbon-centered radical is generated, copper-mediated C–N bond formation can ensue. In addition, our demonstration—that photochemical initiation can lead, under unusually mild conditions, to C–N bond formation with carbazole—opens the door to the development of practical photoinduced, copper-catalyzed C–N bond-forming processes, including both N-arylation and N-alkylation reactions (Fig. 3C). Indeed, this approach may also be applicable to the formation of other carbon–heteroatom bonds.

References and Notes

1. A. S. Travis, in *Chemistry of Anilines*, Z. Rapaport, Ed. (John Wiley & Sons, New York, 2007), vol. 1, pp. 1–73.
2. A. S. Travis, in *Chemistry of Anilines*, Z. Rapaport, Ed. (John Wiley & Sons, New York, 2007), vol. 2, pp. 715–782.
3. *Atorvastatin in the Management of Cardiovascular Risk: From Pharmacology to Clinical Evidence*, S. Grundy, Ed. (Kluwer, Auckland, New Zealand, 2007).
4. F. Ullmann, *Ber. Deutsch. Chem. Ges.* **36**, 2382 (1903).
5. I. Goldberg, *Ber. Deutsch. Chem. Ges.* **39**, 1691 (1906).
6. F. Monnier, M. Taillefer, *Angew. Chem. Int. Ed.* **48**, 6954 (2009).
7. G. Evano, N. Blanchard, M. Toumi, *Chem. Rev.* **108**, 3054 (2008).
8. I. P. Beletskaya, A. V. Cheprakov, *Coord. Chem. Rev.* **248**, 2337 (2004).
9. S. V. Ley, A. W. Thomas, *Angew. Chem. Int. Ed.* **42**, 5400 (2003).
10. L. Jiang, S. L. Buchwald, in *Metal-Catalyzed Cross-Coupling Reactions*, A. De Meijere, F. Diederich, Eds. (Wiley–VCH, New York, 2004), vol. 2, pp. 699–760.
11. J. F. Hartwig, S. Shekhar, Q. Shen, F. Barrios-Landeros, in *Chemistry of Anilines*, Z. Rapaport, Ed. (John Wiley & Sons, New York, 2007), vol. 1, pp. 455–536.

12. E. Sperotto, G. P. M. van Klink, G. van Koten, J. G. de Vries, *Dalton Trans.* **39**, 10338 (2010).
13. J. W. Tye, Z. Weng, A. M. Johns, C. D. Incarvito, J. F. Hartwig, *J. Am. Chem. Soc.* **130**, 9971 (2008).
14. R. Giri, J. F. Hartwig, *J. Am. Chem. Soc.* **132**, 15860 (2010).
15. G. O. Jones, P. Liu, K. N. Houk, S. L. Buchwald, *J. Am. Chem. Soc.* **132**, 6205 (2010).
16. H.-Z. Yu, Y.-Y. Jiang, Y. Fu, L. Liu, *J. Am. Chem. Soc.* **132**, 18078 (2010).
17. S. Natarajan, S. H. Kim, *Chem. Commun. (Camb.)* **7**, 729 (2006).
18. S. Natarajan, G. Liu, S. H. Kim, *J. Phys. Chem. B* **110**, 8047 (2006).
19. S. B. Harkins, J. C. Peters, *J. Am. Chem. Soc.* **127**, 2030 (2005).
20. J. C. Deaton *et al.*, *J. Am. Chem. Soc.* **132**, 9499 (2010).
21. K. J. Lotito, J. C. Peters, *Chem. Commun. (Camb.)* **46**, 3690 (2010).
22. R. A. Rossi, *Acc. Chem. Res.* **15**, 164 (1982).
23. J. M. R. Narayanam, C. R. J. Stephenson, *Chem. Soc. Rev.* **40**, 102 (2011).
24. D. A. Nicewicz, D. W. C. MacMillan, *Science* **322**, 77 (2008).
25. Materials and methods are available as supplementary materials on *Science* Online.
26. Z. Xi, F. Liu, Y. Zhou, W. Chen, *Tetrahedron* **64**, 4254 (2008).
27. N. P. Mankad, W. E. Antholine, R. K. Szilagyi, J. C. Peters, *J. Am. Chem. Soc.* **131**, 3878 (2009).
28. R. J. Enemærke, T. B. Christensen, H. Jensen, K. Daasbjerg, *J. Chem. Soc. Perkin Trans. 2* **9**, 1620 (2001).
29. C. L. Keller, J. D. Dalessandro, R. P. Hotz, A. R. Pinhas, *J. Org. Chem.* **73**, 3616 (2008).
30. R. L. Dannley, E. C. Gregg Jr., R. E. Phelps, C. B. Coleman, *J. Am. Chem. Soc.* **76**, 445 (1954).
31. E. I. Solomon, *Inorg. Chem.* **45**, 8012 (2006).
32. M. Hay, J. H. Richards, Y. Lu, *Proc. Natl. Acad. Sci. U.S.A.* **93**, 461 (1996).
33. A. Annunziata, C. Galli, M. Marinelli, T. Pau, *Eur. J. Org. Chem.* **2001**, 1323 (2001).

Acknowledgments: This work was supported by the National Science Foundation (graduate research fellowships for S.E.C. and K.J.L.) and by the Gordon and Betty Moore Foundation. Metrical parameters for the structure of copper complex **1** are available free of charge from the Cambridge Crystallographic Data Centre under reference CCDC-896019.

Supplementary Materials

www.sciencemag.org/cgi/content/full/338/6107/647/DC1
Materials and Methods
Figs. S1 to S41
Tables S1 to S3
References (*34*–*46*)

22 June 2012; accepted 10 September 2012
10.1126/science.1226458

The Absolute Chronology and Thermal Processing of Solids in the Solar Protoplanetary Disk

James N. Connelly,[1]* Martin Bizzarro,[1]* Alexander N. Krot,[1,2] Åke Nordlund,[3] Daniel Wielandt,[1] Marina A. Ivanova[4]

Transient heating events that formed calcium-aluminum–rich inclusions (CAIs) and chondrules are fundamental processes in the evolution of the solar protoplanetary disk, but their chronology is not understood. Using U-corrected Pb-Pb dating, we determined absolute ages of individual CAIs and chondrules from primitive meteorites. CAIs define a brief formation interval corresponding to an age of 4567.30 ± 0.16 million years (My), whereas chondrule ages range from 4567.32 ± 0.42 to 4564.71 ± 0.30 My. These data refute the long-held view of an age gap between CAIs and chondrules and, instead, indicate that chondrule formation started contemporaneously with CAIs and lasted ~3 My. This time scale is similar to disk lifetimes inferred from astronomical observations, suggesting that the formation of CAIs and chondrules reflects a process intrinsically linked to the secular evolution of accretionary disks.

The only record of our solar system's formative stages comes from the earliest solids preserved from the protoplanetary disk that now reside as millimeter- to centimeter-sized objects—calcium-aluminum–rich inclusions (CAIs) and chondrules—in chondrite meteorites. These complex objects have been the subject of intense study in an attempt to decipher their origins and, in turn, use them as records of the dynamics of the protoplanetary disk that led to the formation of the solar system (*1*–*8*). Most CAIs formed as fine-grained condensates from a gas of approximately solar composition in a high-temperature environment (>1300 K) at total pressure $\leq 10^{-4}$ bar, with a subset experiencing re-melting to form distinct coarser igneous textures (*9*). In contrast, most chondrules represent coalesced dust aggregates that were subsequently rapidly melted and cooled in lower-temperature regions (<1000 K) and higher ambient vapor pressures ($\geq 10^{-3}$ bar) than CAIs, resulting in igneous porphyritic textures (*10*). Despite their formation by different mechanisms (condensation versus dust accretion) in distinct environments (*11*), these objects share common histories of exposure to brief, high-temperature events at least once in their respective evolutions.

The current perception of the relative timing of CAI and chondrule formation is based on the short-lived ^{26}Al-^{26}Mg chronometer [^{26}Al decays to ^{26}Mg with a half-life of 0.73 million years (My)], which has led to a growing consensus that chondrules formed 1 to 2 My after CAIs (*12*). This age difference has long been used as a central observation in defining models of chondrule formation and, in addition, implies that the melting of CAIs and chondrules was produced by different mechanisms and/or heat sources. However, the ^{26}Al-^{26}Mg dating method critically depends on the disputed assumption of homogeneous distribution of ^{26}Al in space and time within the protoplanetary disk (*13*). In contrast, chronologies based on long-lived radioisotope systems rely on the knowledge of the present-day abundances of the parent and daughter isotopes in a sample and therefore are free from assumptions of parent nuclide homogeneity. Of the various long-lived radioisotope systems, the Pb-Pb dating method is the most powerful tool to establish a high-resolution chronology of the first 10 My of the solar system. This chronometer is based on two isotopes of U, ^{238}U and ^{235}U, that decay in a chain to stable Pb isotopes, ^{206}Pb and ^{207}Pb, respectively, resulting in $^{207}Pb_R/^{206}Pb_R$ (where R = radiogenic) ratios that correspond to the amount of time passed since the system closed, by Eq. 1

$$\frac{^{207}Pb_R}{^{206}Pb_R} = \left(\frac{^{235}U}{^{238}U}\right)\left(\frac{(e^{\lambda_1 t} - 1)}{(e^{\lambda_2 t} - 1)}\right) \quad (1)$$

where λ_1 and λ_2 reflect the decay constants for ^{235}U and ^{238}U, respectively; t, time. The $^{207}Pb_R/^{206}Pb_R$ ratio of an inclusion is calculated by extrapolating from an array of measured Pb isotopic values that represent varying mixtures of radiogenic Pb and its initial Pb isotopic composition, which should approximate that of the solar system defined by the Nantan iron meteorite (*14*). However, attempts to date individual CAIs and chondrules by this approach have historically been frustrated by the difficulties in analyzing the small amounts of Pb in these inclusions. In addition, the $^{238}U/^{235}U$ ratio required for Eq. 1, which has traditionally been assumed to be 137.88 in all solar system materials, was demonstrated to vary in CAIs by 35 ε units (deviations in parts per 10^4), corresponding to offsets in calculated Pb-Pb ages of up to 5 My (*15*). The observation of U isotope variability, attributed to the decay of the short-lived ^{247}Cm nuclide (^{247}Cm decays to ^{235}U with a half-life of 15.6 My) voided all published Pb-Pb ages for solar system materials that were based on an assumed $^{238}U/^{235}U$ ratio and made clear the need to have measurements of the U isotopic compositions for all materials dated by the Pb-Pb method.

To establish an assumption-free absolute chronology of CAI and chondrule formation, we have developed improved methods for the precise analysis of small amounts of Pb and U by thermal

[1]Centre for Star and Planet Formation and Natural History Museum of Denmark, University of Copenhagen, DK-1350 Copenhagen, Denmark. [2]Hawai'i Institute of Geophysics and Planetology, University of Hawai'i at Manoa, HI 96822, USA. [3]Centre for Star and Planet Formation and Niels Bohr Institute, University of Copenhagen, DK-2100 Copenhagen, Denmark. [4]Vernadsky Institute of Geochemistry and Analytical Chemistry, Moscow 119991, Russia.

*To whom correspondence should be addressed. E-mail: connelly@snm.ku.dk (J.N.C.); bizzarro@snm.ku.dk (M.B.)

ionization mass spectrometry and high-resolution inductively coupled plasma source mass spectrometry, respectively (*16*). We measured the $^{238}U/^{235}U$ ratios of three CAIs from the reduced CV chondrite Efremovka, three chondrules from the oxidized CV chondrite Allende, and whole-rock chondrites and differentiated meteorites in an attempt to understand the extent and origin of $^{238}U/^{235}U$ variations in the early solar system (Fig. 1 and Table 1). The Efremovka CAIs show a range of $^{238}U/^{235}U$ ratios (Table 1), confirming the presence of U isotope variability in refractory inclusions. In contrast, our analyses of meteorites derived from chondritic and differentiated asteroids as well as three individual chondrules from Allende show identical $^{238}U/^{235}U$ ratios within analytical uncertainty (Fig. 1), defining a weighted mean of 137.786 ± 0.013. These observations indicate a uniform $^{238}U/^{235}U$ ratio in the inner solar system outside the CAI-forming region. This is consistent with an earlier study (*17*) but at odds with the solar system initial $^{247}Cm/^{235}U$ value of ~1.1×10^{-4} inferred from $^{238}U/^{235}U$ variability in Allende CAIs (*15*). Moreover, our analyses of Efremovka CAIs show significant departure from the apparent correlation between the $^{144}Nd/^{238}U$ [an assumed proxy for Cm/U (*18*)] and $^{235}U/^{238}U$ ratios of Allende CAIs (*15*), similarly to another recent study (*19*). Thus, we infer that the $^{238}U/^{235}U$ variability in CAIs largely reflects mass-dependent fractionation associated with the CAI-forming process and not ^{247}Cm decay (supplementary materials text 1).

The subset of chondrite meteorites we analyzed includes the Ivuna carbonaceous chondrite, a member of the rare clan of primitive meteorites referred to as CI chondrites. Composed of matrix material with the highest abundances of presolar grains, CI chondrites are generally considered to represent the least chemically fractionated and least thermally processed meteorites: They have solar abundances of most elements (*20*) and, by extension, have the solar $^{247}Cm/^{235}U$ ratio. Therefore, we interpret the $^{238}U/^{235}U$ value of 137.786 ± 0.013 obtained for bulk inner solar system materials as representing the best estimate of the bulk $^{238}U/^{235}U$ ratio of the solar system and hence that of the Sun.

To constrain the timing and duration of CAI and chondrule formation, we have obtained Pb isotope data for a suite of three CAIs from Efremovka (22E, 31E, and 32E), two ferromagnesian porphytitic olivine-pyroxene chondrules from Allende (C20 and C30), and three ferromagnesian porphyritic olivine (C1) and barred olivine-pyroxene chondrules (C2 and C3) from the unequilibrated ordinary chondrite NWA 5697. 22E is a fine-grained inclusion with a porous, nearly monomineralic hibonite core surrounded by a mantle composed of concentrically zoned objects having a spinel-hibonite-perovskite core rimmed by the layers of melilite ± anorthite and pyroxene. The texture and mineralogy of 22E indicate that it is an unmelted nebular condensate. 31E is a coarse-grained type B1 CAI with a pyroxene-melilite-spinel core surrounded by a melilite mantle and a multilayered Wark-Lovering rim sequence of spinel, melilite, pyroxene, and forsterite. 32E is a coarse-grained type B1 CAI with a melilite-pyroxene-anorthite-spinel core surrounded a melilite mantle, thin Wark-Lovering rim layers of pyroxene and spinel, and a forsterite-rich accretionary rim. Both coarse-grained CAIs experienced melting after their initial formation by condensation and evaporation processes. To calculate the Pb-Pb ages of the Efremovka CAIs, we used their measured $^{238}U/^{235}U$ ratios, which are characterized by a range of ~15 ε units (Table 1) with compositions that are both isotopically heavy and light relative to the bulk solar $^{238}U/^{235}U$ value of 137.786. The three CAIs yield ages of 4567.35 ± 0.28 My (22E), 4567.23 ± 0.29 My (31E), and 4567.38 ± 0.31 My (32E) (Table 1), with uncertainties including errors associated with both the Pb and U isotope measurements. The age concordancy of these inclusions, despite the wide range of their $^{238}U/^{235}U$ ratios, supports our interpretation that the $^{238}U/^{235}U$ variability was imparted during CAI formation and does not represent a secondary event such as, for example, mass-dependent fractionation resulting from variable redox conditions during alteration processes on the CV chondrite parent body. The ages we report for Efremovka CAIs overlap with the age of 4567.18 ± 0.50 My recently obtained for the coarse-grained type B CAI SJ101 from Allende (*19*), which is the only CAI age currently available in the literature calculated with a measured $^{238}U/^{235}U$ ratio. Pooling the ages we obtained for Efremovka CAIs with that of the SJ101 CAI from Allende yields a weighted mean age of 4567.30 ± 0.16 My, suggesting that the time scale of the CAI-forming event inferred from our absolute chronology may be as short as 160,000 years. Therefore, these data collectively support a single and brief time interval for the formation of CV CAIs, in agreement with the rapid time scales of less than 50,000 years required for their condensation and evaporative melting based on bulk ^{26}Al-^{26}Mg systematics (*6*, *13*). However, our preferred age for the CAI-forming event and, by extension, the formation of the solar system, is based on the best-constrained age of 4567.35 ± 0.28 My obtained for the 22E CAI (Fig. 2A). This interpretation is founded on the petrographic features of this inclusion, suggesting an origin as a gas-solid condensate,

Table 1. Summary of Pb-Pb ages, $^{238}U/^{235}U$ ratios used in age calculations, and ^{54}Cr compositions of individual CAIs and chondrules. The Pb concentrations are based on the total amount of Pb analyzed. $\mu = {}^{238}U/^{204}Pb$. The $\varepsilon^{54}Cr$ values represent 10^4 deviation of the $^{54}Cr/^{52}Cr$ value of a sample relative to the terrestrial chromium reference standard and were acquired following Trinquier *et al.* (*41*). Uncertainties reflect the external reproducibility of 9 ppm. The $\varepsilon^{54}Cr$ value for the 31E CAI is from Larsen *et al.* (*13*).

Sample	Type	Weight (mg)	μ	Pb (ppb)	Age (My)	$^{238}U/^{235}U$	$\varepsilon^{54}Cr$
22E	CAI	25.9	46	178.8	4567.35 ± 0.28	137.627 ± 0.022	
31E	CAI	57.6	247	119.4	4567.23 ± 0.29	137.770 ± 0.022	6.8 ± 1.2
32E	CAI	18.0	116	322.3	4567.38 ± 0.31	137.832 ± 0.022	
C30	Chondrule	29.7	246	24.1	4567.32 ± 0.42	137.786 ± 0.013	−0.58 ± 0.09
C1	Chondrule	30.0	23	78.3	4566.67 ± 0.43	137.786 ± 0.013	−0.60 ± 0.09
C20	Chondrule	28.5	26	40.8	4566.24 ± 0.63	137.786 ± 0.013	−0.36 ± 0.09
C3	Chondrule	107.6	183	27.6	4566.02 ± 0.26	137.786 ± 0.013	−0.87 ± 0.09
C2	Chondrule	58.9	63	77.7	4564.71 ± 0.30	137.786 ± 0.013	−0.24 ± 0.09

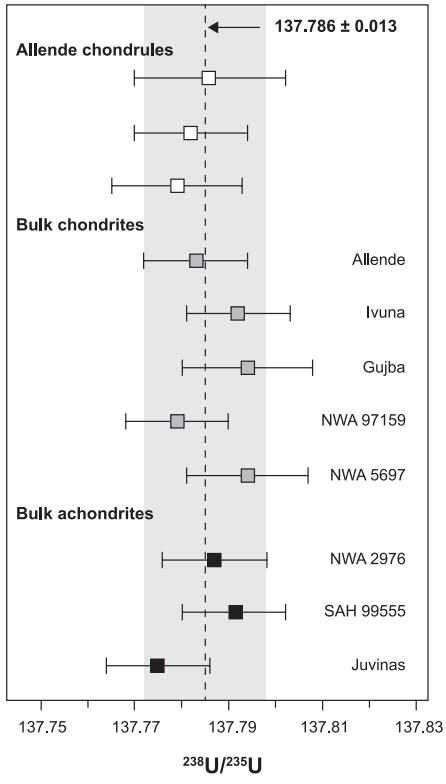

Fig. 1. $^{238}U/^{235}U$ ratios of individual chondrules, bulk chondrites, and achondrites. These samples define a mean of 137.786 ± 0.013 [mean square of weighted deviations (MSWD) = 1.2], which we interpret as the present-day solar $^{238}U/^{235}U$ ratio. The vertical gray band reflects the 2 SD uncertainty of the $^{238}U/^{235}U$ solar value. Uncertainties of sample measurements reflect external reproducibility or the internal precision of individual analyses, whichever is larger.

together with the combined effect of the slightly smaller errors on the age due to the greater spread in Pb-Pb data to define the $^{207}Pb_R/^{206}Pb_R$ ratio, greater number of points defining the isochron, acceptable sample/blank ratios for all measurements used to define the array (table S4), and the low amount of terrestrial Pb contamination (*21*).

Because of the lack of $^{238}U/^{235}U$ variability among bulk inner solar system reservoirs, including three individual chondrules from the Allende meteorite (Fig. 1), we used the well-constrained solar $^{238}U/^{235}U$ value of 137.786 ± 0.013 to calculate the absolute Pb-Pb ages of our subset of chondrules. In contrast to the narrow age span defined by CAIs, the chondrule ages

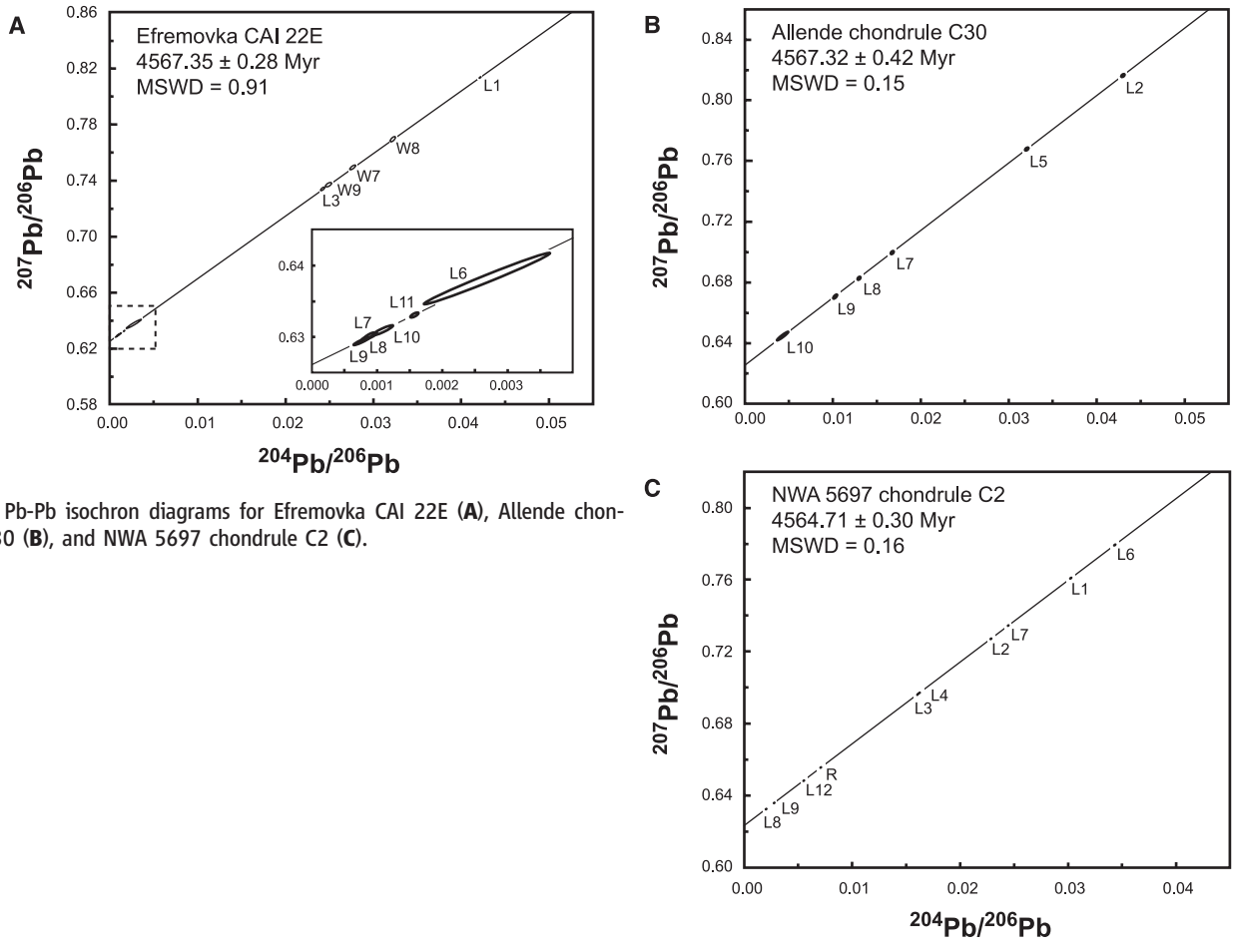

Fig. 2. Pb-Pb isochron diagrams for Efremovka CAI 22E (**A**), Allende chondrule C30 (**B**), and NWA 5697 chondrule C2 (**C**).

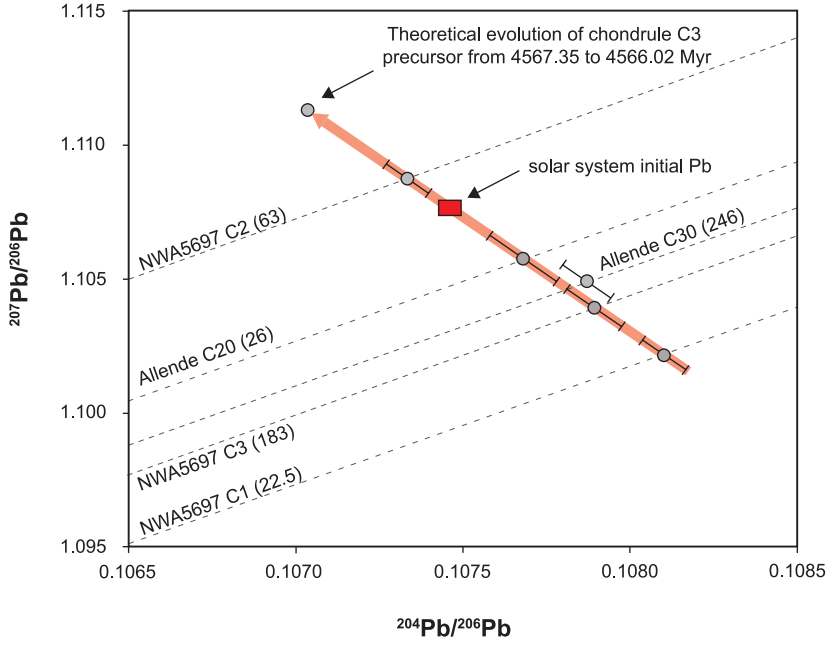

Fig. 3. Initial Pb isotopic compositions of individual chondrules. The initial Pb isotope compositions are defined by the intersection of the individual isochrons and a Pb evolution array anchored on the solar system initial Pb isotope composition defined by the Nantan iron meteorite (*14*). The μ values ($^{238}U/^{204}Pb$) of chondrules are indicated in parentheses. Chondrule C30 was displaced to the right-hand side of the solar system initial Pb array for clarity. The uncertainty of the solar system initial Pb value is smaller than the symbol.

range from 4567.32 ± 0.42 My to 4564.71 ± 0.30 My (Fig. 2, B and C, and Table 1). The oldest chondrule age overlaps with our estimate of CAI formation and thus requires that aggregation of the chondrule precursor material and its thermal processing occurred within the uncertainty of its Pb-Pb age. Moreover, the age of the oldest chondrule indicates that it was not heated to temperatures above the Pb closure temperature after 4567.32 ± 0.42 My and therefore has a formation and thermal history indistinguishable from that of CAIs. These data demonstrate that chondrule formation started contemporaneously with CAIs (within the uncertainty of our measurements) and continued for at least ~3 My.

The majority of chondrules are believed to have formed as dust aggregates of near-solar composition subsequently thermally processed by a flash heating mechanism creating the igneous textures we observe today (*10*). However, the presence of relict grains, igneous rims, and compound chondrules suggests that some chondrules may have grown by collisions and remelting (*22*, *23*). Given the low solar $^{238}U/^{204}Pb$ ratio (μ) of ~0.15 (*24*), the Pb isotopic composition of a chondrule precursor is not expected to evolve measurably during the lifetime of the protoplanetary disk (~3 My) until its μ value is increased by Pb devolatilization during thermal processing. As such, internal isochron relationships of chondrules are expected to project back to nonevolved initial Pb isotopic compositions, unless an object experienced a complex thermal history involving multiple heating and melting events. The isochron for the oldest Allende chondrule (C30) projects back to an initial Pb isotopic composition that is less radiogenic than the most primitive estimate of the initial Pb isotopic composition of the solar system (Fig. 3), based on the Nantan iron meteorite (*14*). The low μ value of the precursor material for chondrules in general and the antiquity of this chondrule in particular indicate that the Pb isotopic composition of the Nantan iron meteorite does not represent the initial Pb isotopic composition of the solar system, but instead an evolved composition inherited after accretion and differentiation of its parent body before core formation. Similar to chondrule C30, three of the four younger chondrules we analyzed define isochron relationships that project back to Pb isotopic compositions that are more primitive than the current estimate of the solar system initial Pb composition. This implies that the precursor material of these chondrules, especially C3 with its high μ value of ~183, were not thermally processed until at or near the derived Pb-Pb age. Thus, the range of ages we observe for individual chondrules reflects primary ages associated with a chondrule-forming event and not secondary disturbance of the Pb-Pb chronometer. Only the youngest chondrule, C2, yields an isochron that projects to a more evolved Pb isotopic composition, requiring that this inclusion was thermally processed for the first time early enough to have accumulated substantial radiogenic Pb by the time the last melting event occurred at 4564.71 ± 0.30 My.

Chondrules from the Allende and NWA 5697 chondrites define age ranges (Fig. 4) that indicate the presence of multiple generations of chondrules in individual chondrite groups. To explore the spatial significance of this age range, we have measured the $^{54}Cr/^{52}Cr$ ratios of these chondrules, because $^{54}Cr/^{52}Cr$ variations within the inner solar system track genetic relationships between early-formed solids and their respective reservoirs (*25*). The five chondrules analyzed here show significant ^{54}Cr variability (Table 1) that is not correlated with their ages. Moreover, most chondrules have $^{54}Cr/^{52}Cr$ ratios that are distinct from those of their host chondrites (*26*). Collectively, these observations indicate that chondrules from individual chondrite groups formed from isotopically diverse precursor material in different regions of the protoplanetary disk and were subsequently transported to the accretion regions of their respective parent bodies. This is consistent with the proposal that radial transport of material in the protoplanetary disk, such as by radial diffusion (*27*) and/or stellar outflows (*3*), was important during the epoch of CAI and chondrule formation (*28*).

Some models of chondrule formation such as current sheets (*29*), colliding molten planetesimals (*30*), and recycling of fragmented differentiated planetesimals (*31*) are based on the presumed offset of 1 to 2 My between the formation of CAIs and chondrules and therefore are inconsistent with the contemporaneous formation of CAIs and the oldest chondrules inferred from our study. Moreover, differentiated planetesimals typically have enhanced U/Pb values (*32*), which would result in chondrules with radiogenically evolved initial Pb isotopic compositions. However, the initial Pb isotopic composition of individual chondrules suggests that, in most cases, chondrule precursors retained the solar U/Pb value up to the chondrule-forming event(s).

Nebular shock waves are currently the favored mechanism for chondrule formation. The proposed sources of shock waves include infalling clumps of dust and gas (*33*), bow shocks generated by planetary embryos (*34*), spiral arms and clumps in a gravitationally unstable protoplanetary disk (*35*), and x-ray flares (*3*). Similar to the colliding planetesimals model, the formation of chondrules by bow shocks requires at least 1 My to allow for the growth of planetary embryos of adequate size and therefore cannot explain the existence of old chondrules. Accretion-driven shock models, including models based on a gravitationally unstable disk, require copious mass accretion rates to the central star on the order of ~10^{-5} solar mass ($M_\odot$) $year^{-1}$ to be plausible (*36*). Astronomical observations indicate that such high accretion rates are achieved only in the deeply embedded class 0 phase of star formation (*37*), and such accretion rates can only last for ~0.1 My. Thus, chondrule formation via accretion-driven

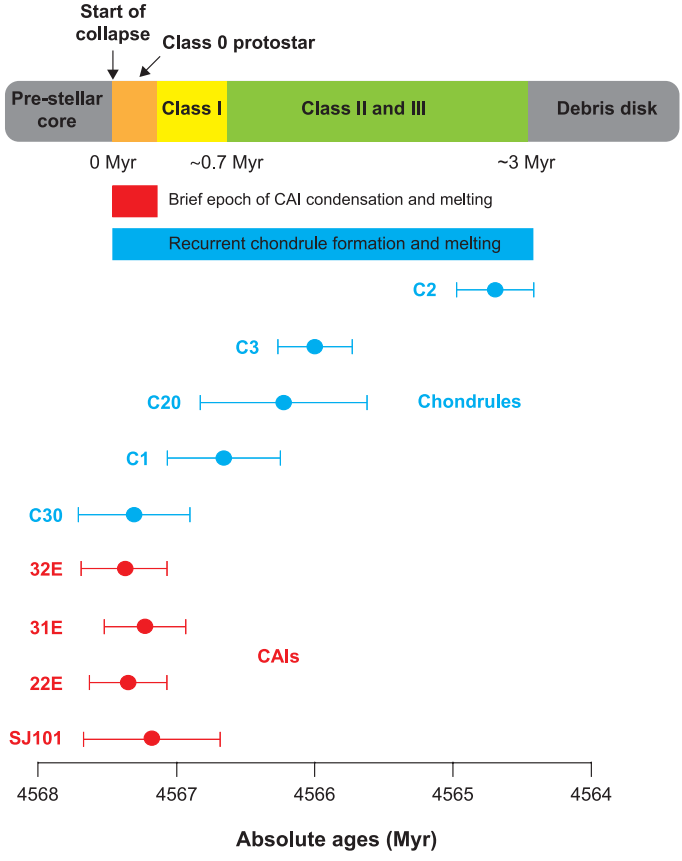

Fig. 4. Time scales of solid formation and disk evolution. The brief formation interval of 160,000 years for the CAI-forming event is similar to the median lifetimes of class 0 protostars of ~0.1 to 0.2 My inferred from astronomical observation of star-forming regions (*37*). Therefore, the thermal regime required for CAI condensation may only have existed during the earliest stages of disk evolution typified by high mass accretion rates (~10^{-5} $M_\odot$ $year^{-1}$) to the central star.

shocks is limited to the earliest stage of disk evolution. As such, different sources of shock waves would be required to account for the observed ~3 My age range of chondrule formation inferred from our study.

Our revised chronology of the formation of solids and their thermal processing refutes the long-held view of a time gap between the formation of CAIs and chondrules, thereby allowing for the possibility that the energy required for melting CAIs and chondrules may have been associated with the same physical process. Statistical studies based on astronomical observations of young stellar objects within star-forming regions indicate that the median lifetime of disks around low-mass stars is ~3 My (*37*). These time scales are comparable to the timing of melting of disk solids inferred from our Pb-Pb dates (Fig. 4), suggesting that the formation of CAIs and chondrules may reflect a process intrinsically linked to the secular evolution of protoplanetary disks (*38*) and is not unique to our solar system. Transfer of mass from the disk to the central protostar is the most energetic process during the lifetime of the protoplanetary disk. Although the energy generated during this process is only gradually released, part of which is converted into kinetic energy expressed as magnetically driven bipolar outflows from the protostar (*39*), a substantial amount of it is available for the thermal processing of solids during transient mass-accretion events. Indeed, models of the innermost structure of protoplanetary disks predict temperatures in excess of 1400 K within 1 astronomical unit for mass accretion rates as low as ~10^{-6} $M_{\odot}$ year^{-1} (*40*). Because the conservation of energy requires dissipation per unit of area of the disk that scales as the inverse cube of the distance from the central star, accretion-based processes may produce similar thermal regimes over a large range of accretion rates, albeit at different orbital radii. Whether accretion-based processes can provide thermal histories for CAIs and chondrules that are consistent with their heating and cooling rates, as well as the chronology provided here, requires robust numerical simulations of the evolving thermal structure of accreting disks.

References and Notes

1. T. Lee, D. A. Papanastassiou, G. J. Wasserburg, *Astrophys. J.* **211**, L107 (1977).
2. C. Göpel, G. Manhès, C. J. Allègre, *Meteoritics* **26**, 338 (1991).
3. F. H. Shu, H. Shang, T. Lee, *Science* **271**, 1545 (1996).
4. A. Galy, E. D. Young, R. D. Ash, R. K. O'Nions, *Science* **290**, 1751 (2000).
5. Y. Amelin, A. N. Krot, I. D. Hutcheon, A. A. Ulyanov, *Science* **297**, 1678 (2002).
6. M. Bizzarro, J. A. Baker, H. Haack, *Nature* **431**, 275 (2004).
7. C. M. Alexander, J. N. Grossman, D. S. Ebel, F. J. Ciesla, *Science* **320**, 1617 (2008).
8. J. N. Connelly, Y. Amelin, A. N. Krot, M. Bizzarro, *Astrophys. J.* **675**, L121 (2008).
9. G. J. MacPherson, *Treatise on Geochemistry, Volume 1*, A. M. Davis, Ed. (Elsevier, Amsterdam, 2003), pp. 201–246.
10. E. R. D. Scott, *Annu. Rev. Earth Planet. Sci.* **35**, 577 (2007).
11. A. N. Krot *et al.*, *Geochim. Cosmochim. Acta* **73**, 4963 (2009).
12. N. T. Kita *et al.*, in *Chondrites and the Protoplanetary Disk*, A. N. Krot, E. R. D. Scott, B. Reipurth, Eds. (Astronomical Society of the Pacific, San Francisco, 2005), vol. 341, pp. 558–587.
13. K. K. Larsen *et al.*, *Astrophys. J.* **735**, L37 (2011).
14. J. Blichert-Toft, B. Zanda, D. S. Ebel, F. A. Albarède, *Earth Planet. Sci. Lett.* **300**, 152 (2010).
15. G. A. Brennecka *et al.*, *Science* **327**, 449 (2010).
16. Materials and methods are available as supplementary materials on *Science* Online.
17. C. H. Stirling, A. N. Halliday, D. Porcelli, *Geochim. Cosmochim. Acta* **69**, 1059 (2005).
18. J. B. Blake, D. N. Schramm, *Nature* **289**, 138 (1973).
19. Y. Amelin *et al.*, *Earth Planet. Sci. Lett.* **300**, 343 (2010).
20. M. Asplund, N. Grevesse, J. A. Sauval, P. Scott, *Annu. Rev. Astron. Astrophys.* **47**, 481 (2009).
21. Confidence in this age is also enhanced by the fact that the well-constrained isochron projects to an initial Pb isotopic composition that is more consistent with an initial Pb component from the CAI source reservoir than a modern terrestrial contamination (supplementary materials text 2).
22. A. N. Krot, J. T. Wasson, *Geochim. Cosmochim. Acta* **59**, 4951 (1995).
23. R. H. Jones, J. N. Grossman, A. E. Rubin, in *Chondrites and the Protoplanetary Disk*, A. N. Krot, E. R. D. Scott, B. Reipurth, Eds. (Astronomical Society of the Pacific, San Francisco, 2005), vol. 341, pp. 251–285.
24. H. Palme, A. Jones, in *Treatise on Geochemistry*, H. D. Holland, K. K. Turekian, Eds., Vol. 1, *Meteorites, Comets and Planets*, A. M. Davis, Ed. (Elsevier-Pergamon, Oxford, 2003), pp. 41–61.
25. A. Trinquier *et al.*, *Science* **324**, 374 (2009).
26. A. Trinquier, J.-L. Birck, C. G. Allègre, *Astrophys. J.* **655**, 1179 (2007).
27. F. J. Ciesla, *Science* **318**, 613 (2007).
28. D. Brownlee *et al.*, *Science* **314**, 1711 (2006).
29. M. K. Ryan Joung, M.-M. Mac Low, D. S. Ebel, *Astrophys. J.* **606**, 532 (2004).
30. E. Asphaug, M. Jutzi, N. Movshovitz, *Earth Planet. Sci. Lett.* **308**, 369 (2011).
31. G. Libourel, A. N. Krot, *Earth Planet. Sci. Lett.* **254**, 1 (2007).
32. J. N. Connelly, M. Bizzarro, K. Thrane, J. A. Baker, *Geochim. Cosmochim. Acta* **72**, 4813 (2008).
33. A. P. Boss, J. A. Graham, *Icarus* **106**, 168 (1993).
34. S. J. Weidenschilling, F. Marzari, L. L. Hood, *Science* **279**, 681 (1998).
35. A. P. Boss, R. H. Durisen, *Astrophys. J.* **621**, L137 (2005).
36. E. I. Vorobyov, S. Basu, *Astrophys. J.* **719**, 1896 (2010).
37. N. J. Evans II *et al.*, *Astrophys. J.* **181** (suppl.), 321 (2009).
38. R. Salmeron, T. R. Ireland, *Earth Planet. Sci. Lett.* **327–328**, 61 (2012).
39. C. Zanni, A. Ferrari, R. Rosner, G. Bodo, S. Massaglia, *Astron. Astrophys.* **469**, 811 (2007).
40. P. D'Alessio, N. Calvet, D. H. Woolum, in *Chondrites and the Protoplanetary Disk*, A. N. Krot, E. R. D. Scott, B. Reipurth, Eds. (Astrophysical Society of the Pacific, San Francisco, (2005), pp. 353–372.
41. A. Trinquier, J.-L. Birck, C. G. Allègre, *J. Anal. At. Spectrom.* **23**, 1565 (2008).

Acknowledgments: All the data reported in this paper are presented in the supplementary materials. The Centre for Star and Planet Formation is financed by the Danish National Research Foundation. We thank C. Paton for help in the mass spectrometer laboratory and J. K. Jørgensen for discussion.

Supplementary Materials

www.sciencemag.org/cgi/content/full/338/6107/651/DC1
Materials and Methods
Supplementary Text
Figs. S1 to S22
Tables S1 to S4
References (*42*–*55*)

3 July 2012; accepted 14 September 2012
10.1126/science.1226919

Chloroplast Biogenesis Is Regulated by Direct Action of the Ubiquitin-Proteasome System

Qihua Ling,* Weihua Huang,*† Amy Baldwin,‡ Paul Jarvis§

Development of chloroplasts and other plastids depends on the import of thousands of nucleus-encoded proteins from the cytosol. Import is initiated by TOC (translocon at the outer envelope of chloroplasts) complexes in the plastid outer membrane that incorporate multiple, client-specific receptors. Modulation of import is thought to control the plastid's proteome, developmental fate, and functions. Using forward genetics, we identified *Arabidopsis SP1*, which encodes a RING-type ubiquitin E3 ligase of the chloroplast outer membrane. The SP1 protein associated with TOC complexes and mediated ubiquitination of TOC components, promoting their degradation. Mutant *sp1* plants performed developmental transitions that involve plastid proteome changes inefficiently, indicating a requirement for reorganization of the TOC machinery. Thus, the ubiquitin-proteasome system acts on plastids to control their development.

Chloroplasts belong to a family of plant organelles called plastids, which includes several nonphotosynthetic variants (such as etioplasts in dark-grown seedlings and carotenoid-rich chromoplasts in fruits) (*1*). A specific feature of the plastid family is the ability to interconvert in response to developmental and environmental cues—for example, during de-etiolation or fruit ripening (*1*). Such plastid interconversions are linked to reorganization of the organellar proteome (*2*, *3*).

Over 90% of the thousands of proteins in plastids are nucleus-encoded and imported from the cytosol posttranslationally (*1*). The translocon at the outer envelope of chloroplasts (TOC) recognizes chloroplast pre-proteins and initiates

Department of Biology, University of Leicester, Leicester LE1 7RH, UK.

*These authors contributed equally to this work.
†Present address: Shanghai Institute of Plant Physiology and Ecology, Shanghai Institutes for Biological Sciences, Chinese Academy of Sciences, Shanghai 200032, China.
‡Present address: School of Medicine, Cardiff University, Cardiff CF14 4YS, UK.
§To whom correspondence should be addressed. E-mail: rpj3@le.ac.uk

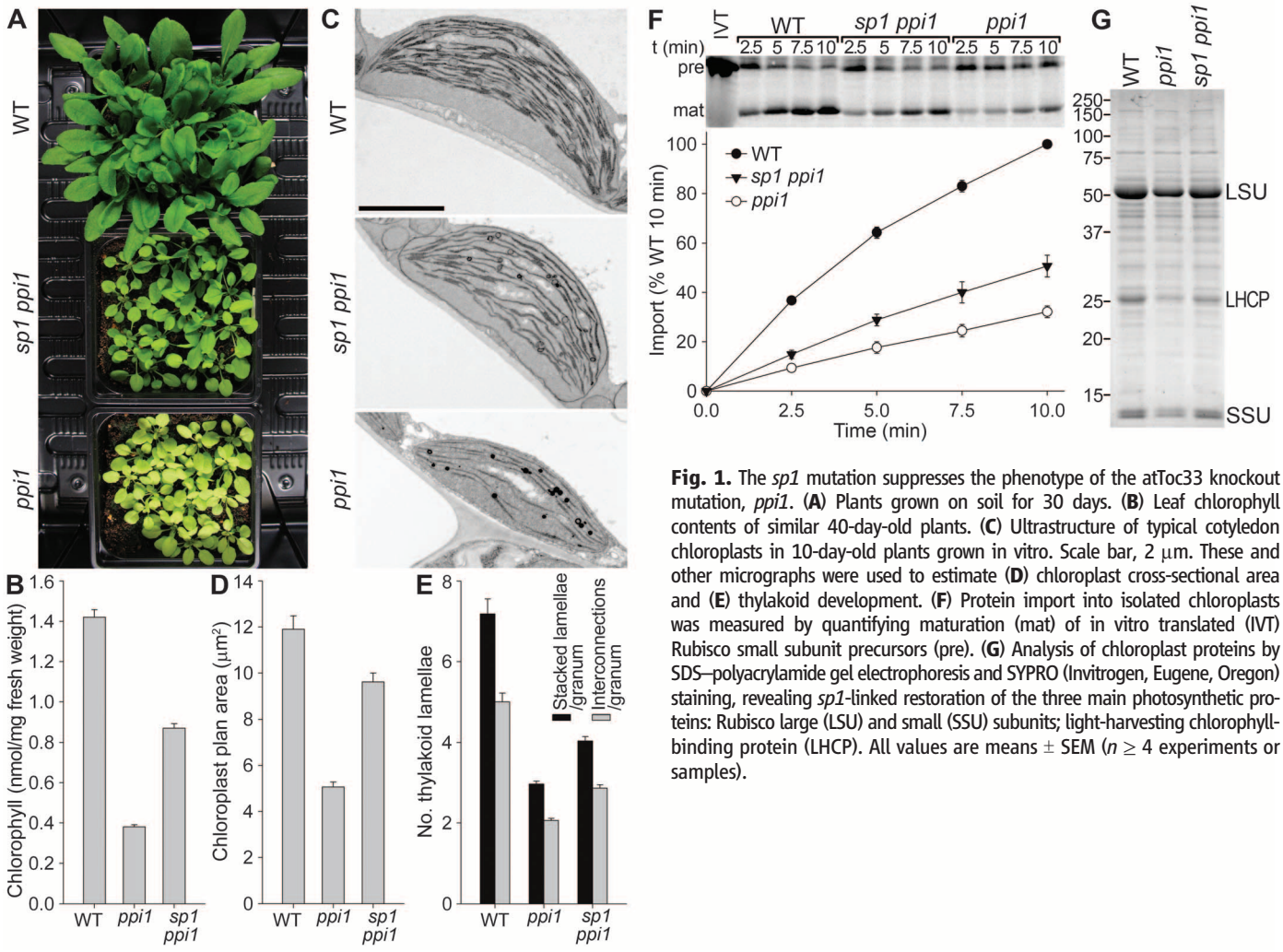

Fig. 1. The *sp1* mutation suppresses the phenotype of the atToc33 knockout mutation, *ppi1*. (**A**) Plants grown on soil for 30 days. (**B**) Leaf chlorophyll contents of similar 40-day-old plants. (**C**) Ultrastructure of typical cotyledon chloroplasts in 10-day-old plants grown in vitro. Scale bar, 2 μm. These and other micrographs were used to estimate (**D**) chloroplast cross-sectional area and (**E**) thylakoid development. (**F**) Protein import into isolated chloroplasts was measured by quantifying maturation (mat) of in vitro translated (IVT) Rubisco small subunit precursors (pre). (**G**) Analysis of chloroplast proteins by SDS–polyacrylamide gel electrophoresis and SYPRO (Invitrogen, Eugene, Oregon) staining, revealing *sp1*-linked restoration of the three main photosynthetic proteins: Rubisco large (LSU) and small (SSU) subunits; light-harvesting chlorophyll-binding protein (LHCP). All values are means ± SEM ($n \geq 4$ experiments or samples).

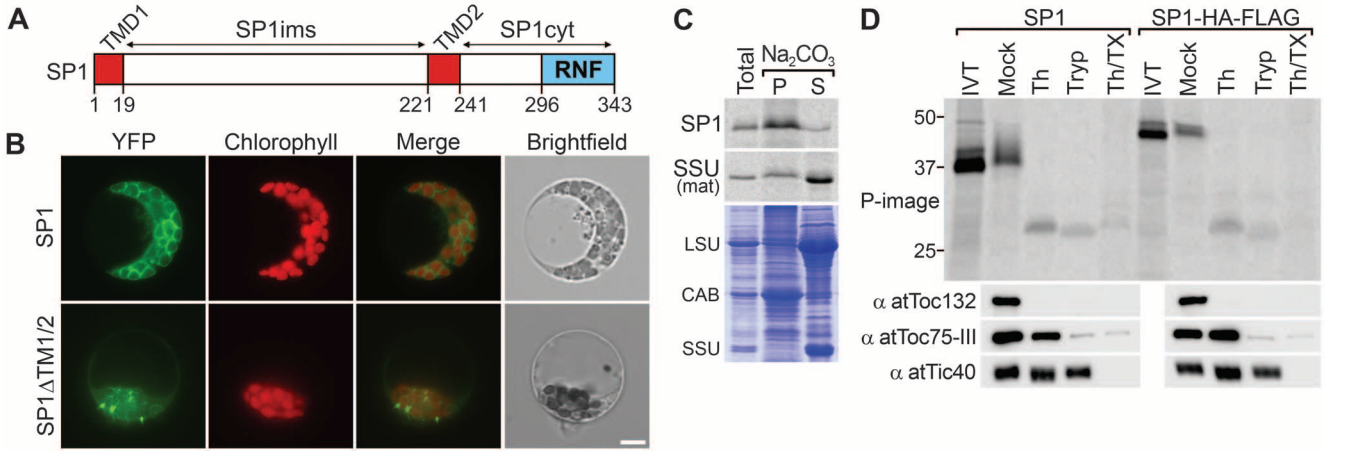

Fig. 2. SP1 is located in the chloroplast outer-envelope membrane with its RING domain facing the cytosol. (**A**) SP1 protein map showing transmembrane (TMD), intermembrane space (SP1ims), cytosolic (SP1cyt), and RING finger (RNF) domains. (**B**) Localization of SP1-YFP to chloroplast envelopes (top) depended on the transmembrane domains, as revealed by a double-deletion mutant (bottom). Scale bar, 10 μm. (**C**) Radiolabeled SP1 in isolated chloroplasts was located in the membrane pellet (P) fraction after high-pH washing, in contrast with imported mature SSU which was in the soluble (S) fraction. Endogenous markers partitioned as expected (Coomassie stain; bottom). (**D**) Radiolabeled SP1 and C-terminally tagged SP1–hemagglutinin (HA)–FLAG were imported into chloroplasts before their treatment with thermolysin (Th), trypsin (Tryp), thermolysin plus Triton X-100 (Th/TX) (Fisher Scientific, Fair Lawn, New Jersey), or buffer lacking protease (Mock). Phosphor-imaging revealed protease sensitivity and protected fragments (of sizes not influenced by the C-terminal tag) consistent with outer membrane localization and the topology shown in (A). Immunoblot analysis of three endogenous markers confirmed efficacy of the treatments.

their translocation (*4*–*6*). The TOC machinery comprises the Omp85 (outer membrane protein, 85 kD)–related channel Toc75 and the receptor guanosine triphosphatases Toc34 and Toc159. The receptors protrude into the cytosol, where different isoforms contact pre-proteins with differing specificity: In *Arabidopsis*, the major isoforms (atToc33 and atToc159) recognize abundant precursors of the photosynthetic apparatus, whereas the minor isoforms (atToc34 and atToc132/atToc120) recognize housekeeping pre-proteins (*7*–*10*). Receptor isoform levels vary developmentally depending on biochemical requirements of the plastids.

Although the main TOC components were identified more than a decade ago, regulatory mechanisms that govern their action are poorly understood. To shed light in this area, we screened an ethyl methanesulfonate–mutagenized population of *Arabidopsis* for second-site suppressors of the atToc33 knockout mutation, *plastid protein import1* (*ppi1*; which causes chlorosis due to defective protein import) (*7*), and identified *suppressor of ppi1 locus1* (*sp1*). Double-mutant *sp1 ppi1* plants were larger and greener than were *ppi1* and exhibited improved chloroplast ultrastructural organization and protein import capacity (Fig. 1). Recovery mediated by *sp1* was specific; two other mutations that cause chlorosis were not suppressed (fig. S1). The only other mutation found to be suppressed by *sp1* was a hypomorphic allele of the gene encoding Toc75 (*toc75-III-3*) (*11*, *12*), implying a close functional relationship between SP1 and the TOC apparatus.

The *SP1* locus (At1g63900) was identified by means of map-based cloning; the original *sp1-1* allele carries a splice-junction mutation, causing frame-shifts, whereas two insertional mutants (*sp1-2* and *sp1-3*) also lack the native *SP1* transcript and are phenotypically similar (fig. S2). SP1 is a putative C3HC4-type really interesting new gene (RING) ubiquitin E3 ligase (*13*, *14*). Such E3s perform a crucial role in the ubiquitin-proteasome system (UPS), along with E1 and E2 enzymes and the 26*S* proteasome. The UPS is a central proteolytic system in eukaryotes with numerous components, accounting in *Arabidopsis* for ~6% of the proteome (*15*). The E1, E2, and E3 enzymes cooperate to attach ubiquitin to target proteins, which are then typically degraded by the proteasome. Targets are identified primarily by the E3s, of which there are many (~90% of 1600 UPS components in *Arabidopsis* are E3s), enabling specific recognition (and regulation) of numerous, functionally diverse substrates (*15*). Unimported plastid pre-proteins in the cytosol are UPS substrates (*16*, *17*), but whether the plastid itself is a target is not clear. Overexpression of *SP1* accentuated the phenotypes of TOC mutants, supporting the notion that it regulates the import machinery (fig. S3).

The SP1 protein has two predicted transmembrane spans (Fig. 2A). Translational fusions to yellow fluorescent protein (YFP) indicated localization to the chloroplast envelope that was dependent on these transmembrane domains (Fig. 2B). In isolated chloroplasts, SP1 was resistant to alkaline extraction and partially sensitive to applied proteases (Fig. 2, C and D, and fig. S4), indicating that it is an integral outer-membrane protein with an intermembrane-space domain, and that the RING domain is cytosolically oriented and accessible to UPS components. Localization of SP1 to chloroplasts (a major source of reactive oxygen species) may

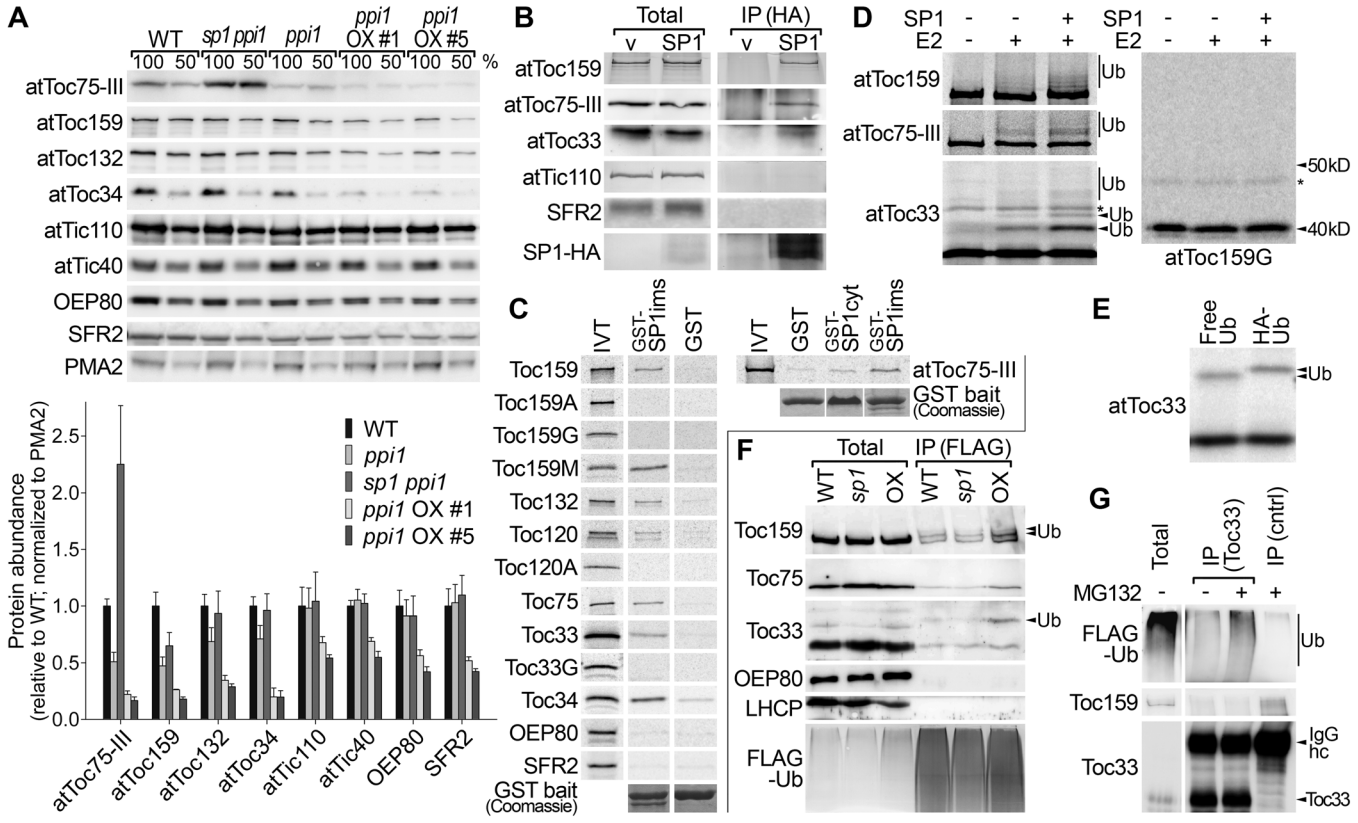

Fig. 3. SP1 associates with TOC complexes and targets TOC components for UPS-mediated degradation via ubiquitination. (**A**) Immunoblot analysis of total leaf protein from different genotypes, including SP1 overexpressors (OX). Plasma membrane H^+-ATPase, PMA2, acted as a loading control. Bars show means ± SEM (n = 4 to 6 experiments). (**B**) Coimmunoprecipitation (IP) of TOC components with HA-tagged SP1 from protoplast extracts. Cells were transfected with an SP1-HA construct or empty vector (v). (**C**) In vitro pull-down of radiolabeled TOC components [or domains (*25*)] with GST-SP1 baits. (**D**) In vitro ubiquitination of radiolabeled TOC components (but not atToc159G) by recombinant GST-SP1flex. Asterisks indicate a nonspecific 48-kD band seen in all translations. Mono-ubiquitinated atToc159G would be expected to migrate near the 50 kD marker. (**E**) Ubiquitination of atToc33 as in (D) using free and HA-tagged ubiquitin (8.5 and 9.4 kD, respectively). (**F**) Immunoprecipitation of TOC components with FLAG-tagged ubiquitin from transfected protoplasts. (**G**) Immunoprecipitation under denaturing conditions of FLAG-ubiquitin with atToc33; a control IP used excess anti-atTic110. Immunoglobulin G heavy chain (hc) is shown. Ubiquitinated species (Ub) are indicated [(D) to (G)].

explain why SP1 is linked to programmed cell death (*18*).

Two SP1 homologs exist in *Arabidopsis*: SP1-Like1 (SPL1) and SPL2. They share topological similarity and considerable sequence identity with SP1, and both were located in the chloroplast envelope (fig. S5). However, overexpression of *SP1*'s closest relative, *SPL1*, did not complement *sp1* (fig. S6), suggesting that SP1 and its homologs have distinct clients. Also related to SP1 is the human mitochondrial outer-membrane protein MULAN/MAPL, which controls mitochondrial dynamics (*19*–*22*).

In planta, activity of SP1 depended on the presence of a functional RING domain (fig. S7, A to D), which in E3s is required for E2 recruitment (*14*, *15*). Purified SP1 had self-ubiquitination activity (*13*), typical for E3s, which was similarly dependent on RING functionality (fig. S7, E and F). Polyubiquitinated SP1 was also detected in plants, in amounts proportional to RING integrity (fig. S8A). Such auto-ubiquitination implies that SP1 itself is subject to UPS control, as E3s frequently are (*14*). Accordingly, cellular SP1 protein levels were elevated upon treatment with the proteasome inhibitor MG132 (fig. S8B) (*17*, *23*).

Phenocopy of *sp1*-mediated suppression was observed when 26*S* proteasome mutants (*24*) were crossed to *ppi1* or *toc75-III-3* (fig. S9), suggesting that the UPS indeed controls chloroplast development. We thus set about identifying the target (or targets) of SP1 E3 activity. All tested TOC proteins were deficient in *ppi1* relative to wild type but substantially recovered in *sp1 ppi1* (Fig. 3A); other envelope proteins [Tic110, Tic40, OEP80, and SFR2 (*25*)] were largely unaffected by *sp1*. These changes were not attributable to pretranslational events because TOC transcript levels were comparable in the different genotypes (fig. S10A). Similar TOC protein abundance recovery was apparent in *sp1 toc75-III-3* (fig. S10B). TOC protein levels were also elevated in the visibly normal *sp1* single mutant, arguing against the possibility that the protein changes in *sp1 ppi1* and *sp1 toc75-III-3* were a consequence (rather than a cause) of the phenotypic recovery. Moreover, SP1 overexpression preferentially depleted TOC proteins (Fig. 3A and fig. S10C); effects on other envelope proteins in the *ppi1* background were likely indirect consequences of general phenotype severity (Fig. 3A and fig. S3).

Consistent with the notion that TOC proteins are targeted for UPS-mediated degradation by SP1, all three principal TOC components coimmunoprecipitated with epitope-tagged SP1 from plant extracts (Fig. 3B). In vitro pull-down experiments revealed SP1 interactions with Toc75 and all tested TOC receptors (Fig. 3C), which is not unusual because E3s often have diverse substrates (*14*, *15*). These interactions were mediated primarily by the SP1 intermembrane-space domain and the membrane/intermembrane-space domains of the receptors.

In vitro ubiquitination assays using radiolabeled TOC proteins, purified SP1, and UPS components revealed high-molecular-weight species indicative of TOC ubiquitination (Fig. 3D). Some ubiquitination occurred in the absence of E3 [presumably mediated by E2 alone (*26*)], but for each TOC substrate, the extent of ubiquitination was enhanced in the presence of SP1. The identity of mono-ubiquitinated atToc33 was confirmed by a size shift upon utilization of different forms of ubiquitin (Fig. 3E).

In an in vivo assay for ubiquitination, the three main TOC components all co-immunoprecipitated with epitope-tagged ubiquitin in amounts proportional to the expression of SP1 (in *sp1*, amounts were less than in wild type; in an *SP1* overexpressor, amounts were more) (Fig. 3F). Moreover, modified forms of atToc159 and atToc33 were apparent in the precipitates, which likely correspond to ubiquitinated species. Absence of clearly ubiquitinated forms of Toc75 may indicate that it is less readily ubiquitinated than the receptors in vivo, or more readily deubiquitinated (*27*). Regardless, its association with other ubiquitinated TOC proteins may be sufficient to promote its turnover via the UPS (*28*). In a reciprocal experiment (performed under denaturing conditions to disrupt noncovalent

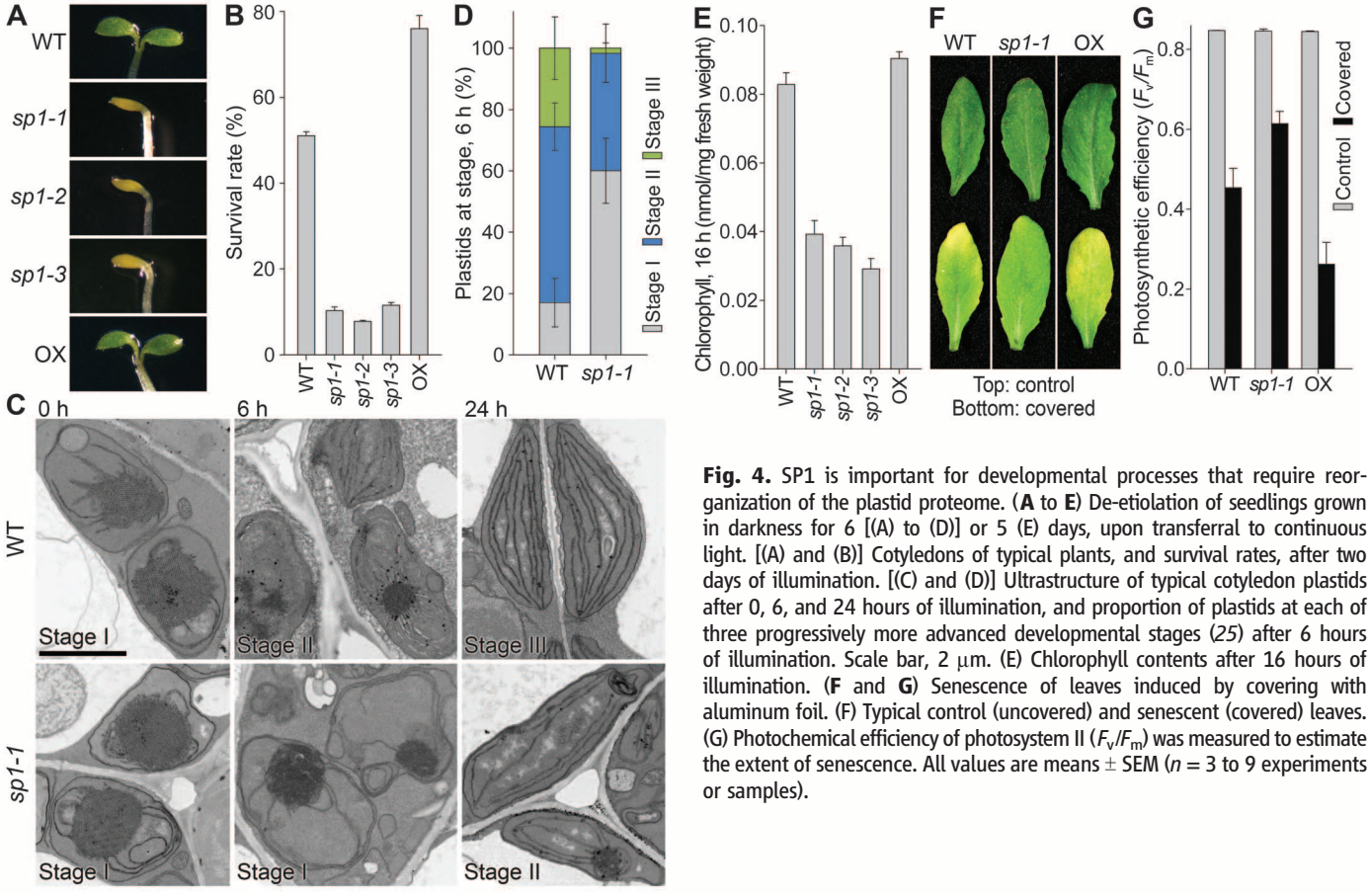

Fig. 4. SP1 is important for developmental processes that require reorganization of the plastid proteome. (**A** to **E**) De-etiolation of seedlings grown in darkness for 6 [(A) to (D)] or 5 (E) days, upon transferral to continuous light. [(A) and (B)] Cotyledons of typical plants, and survival rates, after two days of illumination. [(C) and (D)] Ultrastructure of typical cotyledon plastids after 0, 6, and 24 hours of illumination, and proportion of plastids at each of three progressively more advanced developmental stages (*25*) after 6 hours of illumination. Scale bar, 2 μm. (E) Chlorophyll contents after 16 hours of illumination. (**F** and **G**) Senescence of leaves induced by covering with aluminum foil. (F) Typical control (uncovered) and senescent (covered) leaves. (G) Photochemical efficiency of photosystem II (F_v/F_m) was measured to estimate the extent of senescence. All values are means ± SEM (n = 3 to 9 experiments or samples).

protein-protein associations; see atToc159 control), high-molecular-weight ubiquitin smears were apparent in atToc33 immunoprecipitates (Fig. 3G). Abundance of polyubiquitinated atToc33 was controlled by proteasomal activity, as revealed by MG132 treatment. Thus, TOC components are indeed ubiquitinated in vivo, which controls their turnover. Genetic suppression by *sp1* is likely due to the stabilization of TOC components (such as atToc75-III and atToc34).

Our data imply a role for SP1 in the reorganization of the TOC machinery (fig. S11) and a mechanism for the regulation of plastid biogenesis. This might be important during developmental phases in which plastids convert from one form to another through organellar proteome changes (*1*–*3*). For example, during fruit ripening in crops such as tomato and citrus, chloroplasts differentiate into chromoplasts, which accumulate carotenoid pigments of dietary importance (*3*). In *Arabidopsis*, when etiolated seedlings are exposed to light, heterotrophic etioplasts rapidly differentiate into chloroplasts (*29*). This is essential for initiation of photoautotrophic growth after seed germination beneath the soil. In accordance with the hypothesis, *sp1* single mutants de-etiolated inefficiently, displaying reduced survival rates linked to delayed organellar differentiation (Fig. 4, A to E), reduced accumulation of photosynthetic proteins, and imbalances in TOC receptor levels (fig. S12). At the other end of the life cycle, chloroplasts transform into gerontoplasts as catabolic enzymes accumulate to recover resources from the organelles of senescent leaves for use elsewhere in the plant. This response is characterized by declining photosynthetic performance and can be induced prematurely by dark treatment (*30*). The *sp1* mutation also attenuated this transition (Fig. 4, F and G), whereas *SP1* overexpression enhanced both senescence and de-etiolation (Fig. 4), presumably because of the hastening of organellar proteome changes.

Identification of plastids as targets of UPS activity extends the known field of influence of this remarkably pervasive eukaryotic regulatory network. Although its direct action may be limited to cytosolically exposed proteins of the plastid's outer membrane, this may orchestrate wholesale internal changes through reorganization of the protein import machinery.

References and Notes

1. E. López-Juez, K. A. Pyke, *Int. J. Dev. Biol.* **49**, 557 (2005).
2. T. Kleffmann *et al.*, *Plant Physiol.* **143**, 912 (2007).
3. C. Barsan *et al.*, *J. Exp. Bot.* **61**, 2413 (2010).
4. H. M. Li, C. C. Chiu, *Annu. Rev. Plant Biol.* **61**, 157 (2010).
5. P. Jarvis, *New Phytol.* **179**, 257 (2008).
6. F. Kessler, D. J. Schnell, *Traffic* **7**, 248 (2006).
7. P. Jarvis *et al.*, *Science* **282**, 100 (1998).
8. J. Bauer *et al.*, *Nature* **403**, 203 (2000).
9. S. Kubis *et al.*, *Plant Cell* **15**, 1859 (2003).
10. Y. Ivanova, M. D. Smith, K. Chen, D. J. Schnell, *Mol. Biol. Cell* **15**, 3379 (2004).
11. J. P. Stanga, K. Boonsirichai, J. C. Sedbrook, M. S. Otegui, P. H. Masson, *Plant Physiol.* **149**, 1896 (2009).
12. W. Huang, Q. Ling, J. Bédard, K. Lilley, P. Jarvis, *Plant Physiol.* **157**, 147 (2011).
13. S. L. Stone *et al.*, *Plant Physiol.* **137**, 13 (2005).
14. R. J. Deshaies, C. A. Joazeiro, *Annu. Rev. Biochem.* **78**, 399 (2009).
15. R. D. Vierstra, *Nat. Rev. Mol. Cell Biol.* **10**, 385 (2009).
16. G. Shen, Z. Adam, H. Zhang, *Plant J.* **52**, 309 (2007).
17. S. Lee *et al.*, *Plant Cell* **21**, 3984 (2009).
18. B. M. Basnayake *et al.*, *Plant Cell Rep.* **30**, 37 (2011).
19. W. Li *et al.*, *PLoS ONE* **3**, e1487 (2008).
20. B. Zhang *et al.*, *Cell Res.* **18**, 900 (2008).
21. E. Braschi, R. Zunino, H. M. McBride, *EMBO Rep.* **10**, 748 (2009).
22. N. Livnat-Levanon, M. H. Glickman, *Biochim. Biophys. Acta* **1809**, 80 (2011).
23. J. Myung, K. B. Kim, C. M. Crews, *Med. Res. Rev.* **21**, 245 (2001).
24. W. Huang *et al.*, *Plant Cell* **18**, 2479 (2006).
25. Materials and methods and further information are available as supplementary materials on *Science* Online.
26. D. Lu *et al.*, *Science* **332**, 1439 (2011).
27. S. Xu, G. Peng, Y. Wang, S. Fang, M. Karbowski, *Mol. Biol. Cell* **22**, 291 (2011).
28. S. Prakash, T. Inobe, A. J. Hatch, A. Matouschek, *Nat. Chem. Biol.* **5**, 29 (2009).
29. N. Mochizuki, R. Susek, J. Chory, *Plant Physiol.* **112**, 1465 (1996).
30. S. Schelbert *et al.*, *Plant Cell* **21**, 767 (2009).

Acknowledgments: We thank M. Rashbrooke for assistance with initial phenotype analyses and rough mapping of *sp1*; U. Ranganathan for her contribution to the analysis of *SPL1*; R. Patel and R. Berkeley for excellent technical assistance; N. Allcock and S. Hyman for electron microscopy (EM) carried out within the EM Laboratory, University of Leicester; C. Dean and R. Trösch for helpful comments on the manuscript; U. Flores-Perez for antigen preparation (atToc132 and atToc34); M. Boutry (PMA2), N.E. Hoffman (LHCP), K. Inoue (OEP80), F. Kessler (atToc159), and G. Thorlby (SFR2) for antibodies; C.E. Stebbins for the AtUBC8 clone; and the Salk Institute Genomic Analysis Laboratory (SIGnAL) and the Nottingham *Arabidopsis* Stock Centre (NASC) for the *sp1-2* and *sp1-3* alleles. This study was supported by grants from the Biotechnology and Biological Sciences Research Council (BBSRC; BB/D016541/1 and BB/H008039/1) to P.J., by the Royal Society Rosenheim Research Fellowship to P.J., and by a Royal Society International Incoming Fellowship to W.H. This work is the subject of patent application number GB 1216090.9, which covers the role of the ubiquitin-proteasome system in the control of plastid development. The data are presented in the manuscript and in the supplementary materials.

Supplementary Materials

www.sciencemag.org/cgi/content/full/338/6107/655/DC1
Materials and Methods
Figs. S1 to S12
Table S1
References (*31*–*63*)

22 May 2012; accepted 14 September 2012
10.1126/science.1225053

Tricking the Guard: Exploiting Plant Defense for Disease Susceptibility

J. Lorang,[1] T. Kidarsa,[1]* C. S. Bradford,[1]† B. Gilbert,[1] M. Curtis,[1] S.-C. Tzeng,[2] C. S. Maier,[2] T. J. Wolpert[1]‡

Typically, pathogens deploy virulence effectors to disable defense. Plants defeat effectors with resistance proteins that guard effector targets. We found that a pathogen exploits a resistance protein by activating it to confer susceptibility in *Arabidopsis*. The guard mechanism of plant defense is recapitulated by interactions among victorin (an effector produced by the necrotrophic fungus *Cochliobolus victoriae*), TRX-h5 (a defense-associated thioredoxin), and LOV1 (an *Arabidopsis* susceptibility protein). In LOV1's absence, victorin inhibits TRX-h5, resulting in compromised defense but not disease by *C. victoriae*. In LOV1's presence, victorin binding to TRX-h5 activates LOV1 and elicits a resistance-like response that confers disease susceptibility. We propose that victorin is, or mimics, a conventional pathogen virulence effector that was defeated by LOV1 and confers virulence to *C. victoriae* solely because it incites defense.

Disease susceptibility and resistance are normally considered opposite plant responses to pathogen challenge. However, for disease caused by the fungus *Cochliobolus victoriae*, susceptibility and the host resistance response appear to be one and the same (*1*). Most pathogens gain virulence by expressing effectors that target proteins integral to host defense. The guard model posits that plants defeat pathogen virulence by guarding effector targets with resistance (R) proteins in a process called effector-triggered immunity or R-gene resistance (*2*, *3*). The largest class of R proteins consists of nucleotide-binding leucine-rich repeat (NB-LRR) proteins related to innate immune response proteins in animals (*2*, *3*). The *Arabidopsis thaliana* gene *LOV1* encodes a typical NB-LRR but is unique because it confers sensitivity to the fungal toxin victorin, and thus susceptibility (S) rather than resistance to *C. victoriae* (*1*). Although *LOV1* conditions disease susceptibility, it initiates a defense-like response and requires structural features identical to those of resistance-associated NB-LRRs (*1*, *4*). Additionally, *LOV1* is widespread and conserved in *Arabidopsis*, implying that it is maintained for resistance to an unidentified pathogen (*4*). In support of this presumption is the original description of *C. victoriae*

[1]Department of Botany and Plant Pathology and Center for Genome Research and Biocomputing, Oregon State University, Corvallis, OR 97331, USA. [2]Department of Chemistry, Oregon State University, Corvallis, OR 97331, USA.

*Present address: Horticultural Crops Research Lab, USDA-ARS, Corvallis, OR 97331, USA.
†Present address: Department of Environmental and Molecular Toxicology, Oregon State University, Corvallis, OR 97331, USA.
‡To whom correspondence should be addressed. E-mail: wolpertt@science.oregonstate.edu

as causal to Victoria blight of oats. Victoria blight affects oats bred for single-gene (*Pc2*) resistance to the crown rust pathogen, *Puccinia coronata* (*5*). The locus conferring *C. victoriae* susceptibility, *Vb*, and *Pc2* were never genetically resolved and are surmised to be one and the same (*5*). Hence, multiple lines of evidence associate susceptibility to *C. victoriae* with disease resistance, but mechanistic proof of this association is lacking.

We propose that susceptibility to *C. victoriae* conforms to the guard model of plant defense. We find that victorin, an effector required by *C. victoriae* for pathogenesis, binds to thioredoxins (TRXs). TRXs regulate the redox homeostasis of cells by functioning as protein disulfide oxidoreductases. Victorin exhibits characteristics of a canonical virulence effector by targeting TRX-h5, a thioredoxin required for redox control of the transcriptional regulator, NPR1 (*6*). As a key regulator of local and systemic acquired resistance (*7*), NPR1 presents a conspicuous effector target. We also find that LOV1 is activated (causes cell death) when TRX-h5 binds victorin. However, activation of this NB-LRR guard (LOV1) leads to disease susceptibility instead of resistance, presumably by facilitating *C. victoriae*'s necrotrophic exploitation of the associated host cell death (*1*). Thus, victorin is an atypical virulence effector because it confers virulence by evoking rather than suppressing defense.

Thioredoxins (TRXs) regulate the redox homeostasis of cells by functioning as protein disulfide oxidoreductases. TRXs contain two active-site cysteines that form an oxidized disulfide or exist as free sulfhydryls that reduce and regulate the activity of target proteins. Of the eight *Arabidopsis* h-type TRXs, only TRX-h5 is genetically required for victorin sensitivity (*8*) and induced by biotic stress (*9*). Although TRX-h5 mutants are completely victorin-insensitive, overexpression of TRX-h3, the constitutive leaf TRX-h, can partially rescue TRX-h5 mutants (*8*).

Victorin sensitivity in *Arabidopsis* requires the TRX-h5 protein but not its enzymatic activity, because mutation of the TRX-h5 essential active-site Cys^{42} or both thioredoxin reductases does not compromise victorin-induced cell death. Mutation of TRX-h5 at active-site Cys^{39} (TRX-h5C39S) does abolish victorin-induced cell death (*8*). Because TRX-h5 but not its enzymatic activity is required for LOV1 function, and because NB-LRR proteins are known to survey host proteins for modification, we evaluated TRX-h5 for victorin-induced modifications (*10*). We found that TRX-h5 exhibits a ~1-kD shift in electrophoretic mobility when treated with victorin in vivo (Fig. 1). The victorin molecule (~1 kD) induced a similar shift to all thioredoxins tested (fig. S1), which suggests that victorin is generally reactive to thioredoxins. Furthermore, biotin-labeled victorin coimmunoprecipitated with shifted TRX-h5, indicating that victorin binds TRX-h5 (Fig. 1B). A covalent association of victorin with TRX-h5 was confirmed by mass spectrometry (fig. S2). The ability of TRX-h5C42S but not TRX-h5C39S to bind victorin correlated with the respective abilities of these proteins to support victorin-induced cell death (Fig. 1A and fig. S3), which suggests that victorin binding is essential for cell death and occurs at Cys^{39}. We provide several lines of evidence that this is the case. First, victorin's aldehyde moiety is essential for both toxicity (*11*) and binding to TRX-h5 (Fig. 1C). Second, victorin binds TRX-h5 under

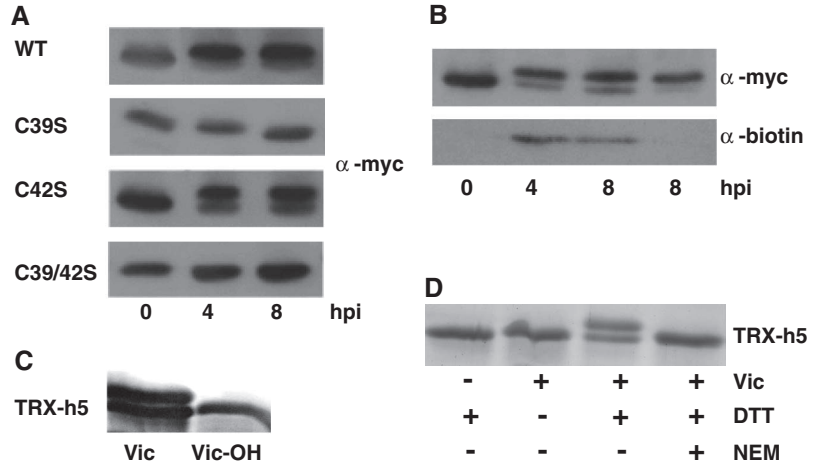

Fig. 1. Victorin binds to TRX-h5. (**A** and **B**) Immunoblot of wild-type and mutant, myc-tagged TRX-h5 proteins from *Arabidopsis* leaves hours after treatment (hpi) with victorin (A) or biotinylated victorin (B). Proteins were detected with antibody to myc (A) or immunoprecipitated with antibody to myc and detected with antibodies to biotin and myc (B). Victorin binding is seen as a ~1-kD increase in the apparent mass of TRX-h5. (**C**) Purified, His-tagged TRX-h5 incubated in vitro with 1 mM dithiothreitol (DTT) and 10 μM native victorin or victorin in which the aldehyde moiety has been reduced to a primary alcohol (Vic-OH). Protein detected by silver staining. (**D**) Purified, His-tagged TRX-h5 incubated in vitro with or without 10 μM victorin, 1 mM DTT, and 1 mM *N*-ethylmaleimide and detected by Coomassie staining.

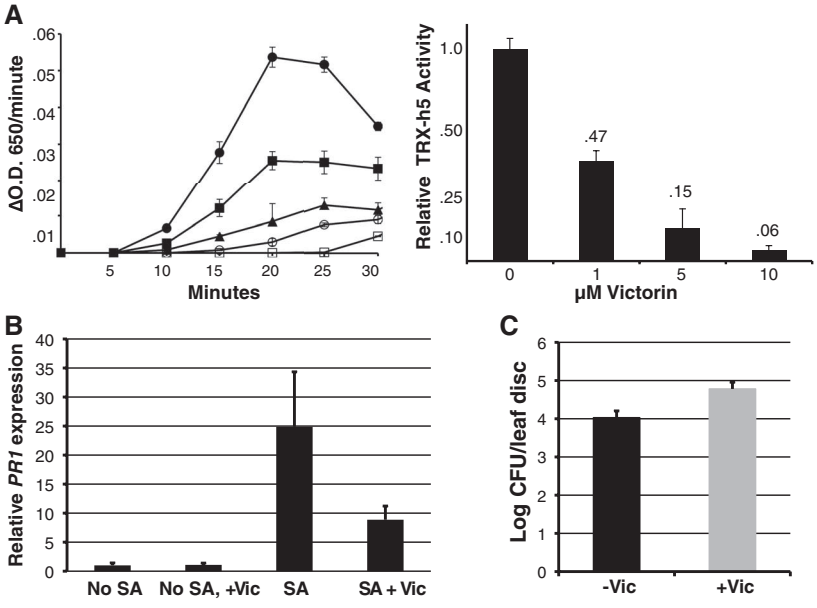

Fig. 2. Victorin inhibits thioredoxin activity. (**A**) Left: TRX-h5–catalyzed reduction of insulin measured by change in optical density at 650 nm (ΔOD_{650}) of insulin (0.1% w/v) in the presence of 1 mM DTT (solid circles) or 1 mM DTT and 1 μM (solid squares), 5 μM (triangles), or 10 μM (open circles) victorin. Open squares denote insulin reduction in the presence of 1 mM DTT without TRX-h5. Right: Relative specific activity of TRX-h5 in the presence of 0, 1, 5, or 10 μM victorin. Error bars represent SE from triplicate assays. (**B**) Quantitative reverse transcription polymerase chain reaction analysis of *PR1* from leaves of 3-week-old *Arabidopsis* (*lov1, lov1*) grown in hydroponic solution and transferred to water or victorin (20 μg/ml) 48 hours before spraying with water or 1 mM salicylic acid (SA). RNA was isolated 24 hours after SA treatment. SE bars represent $N = 8$ (4 biological × 2 technical replicates). Data were reproducible in separate experiments. (**C**) Colony-forming units of *Pseudomonas syringae* pv. *maculicola* (*Psm*) from 3-week-old *Arabidopsis* (*lov1, lov1*) leaves 2 days after treatment with *Psm*, 0.1 OD_{600}. Leaves were infiltrated with water or victorin (100 μg/ml) 2 hours before treatment with *Psm*. SE bars represent $N = 6$ biological replicates containing three leaf discs each.

reducing conditions (free sulfhydryls), but not under nonreducing conditions or in the presence of the sulfhydryl blocker *N*-ethylmaleimide (Fig. 1D). Finally, mutation of the only cysteine in TRX-h5 (Cys^{10}) other than the active-site cysteines does not affect victorin binding or induced cell death (fig. S3). Collectively, these data suggest that victorin binds TRX-h5 at the active-site Cys^{39}, which is required for LOV1 activation.

Activation of LOV1 upon victorin binding to TRX-h5 implies that TRX-h5 is guarded because it plays a role in defense. One defense function of TRX-h5 is to regulate the redox state of NPR1 (*6*). NPR1 normally exists in the cytosol as a thiol-bound oligomer. Upon pathogen challenge or treatment with salicylic acid, *TRX-h5* is upregulated (*6*, *9*). TRX-h5 then reduces NPR1 oligomers, resulting in monomer release, translocation to the nucleus, and regulation of defense gene expression associated with both local and systemic resistance (*6*). Because victorin binds to the TRX-h5 active site, it should inhibit its activity. We measured TRX-h5 activity in vitro using a reduction-of-insulin assay (*10*) and found that victorin markedly inhibited TRX-h5 activity (Fig. 2A). Accordingly, victorin inhibition of TRX-h5 activity in planta (in the absence of *LOV1*) should compromise defense-gene expression conferred by NPR1. We found that seedlings (*lov1*/*lov1*) treated with victorin exhibited salicylic acid–induced *PR1* expression (a reporter for NPR1 activation) that was lower than in controls by a factor of 3 (Fig. 2B). This extent of *PR1* repression is equivalent to that reported for TRX and thioredoxin reductase mutants (*6*). We also found that victorin increased susceptibility to *Pseudomonas syringae* pv. *maculicola* (*Psm*) (Fig. 2C). This increase in disease susceptibility is equivalent to that displayed by an *NPR1* mutant (*6*, *7*) (fig. S4), statistically significant by *t* test ($P < 0.001$) and highly reproducible. In this capacity, and as implicated by the guard model, victorin acts as a canonical virulence effector through its inhibition of thioredoxin and subsequent repression of local resistance to *Psm*. Systemic application of victorin also inhibited salicylic acid–induced resistance (fig. S5). Salicylic acid is associated with both local and systemic acquired resistance. However, because pathogens secrete effectors locally, the potential to inhibit systemic acquired resistance is difficult to place in a biological context. Interestingly, systemic acquired resistance discourages sequential infection of an individual plant and thus could provide formidable defense against pathogens that undergo polycyclic infection, such as rusts (*12*).

Heterologous expression of NB-LRR proteins in *Nicotiana benthamiana* often results in NB-LRR autoactivation or activation in the presence of the cognate pathogen effector (*3*). Expression of only *LOV1* in *N. benthamiana* did not result in cell death, even after treatment with victorin. However, coexpression of *TRX-h5* and *LOV1* conferred victorin sensitivity (Fig. 3A). Thus, LOV1 activation relies on TRX-h5, and their coexpression is both necessary and sufficient to confer victorin sensitivity. Furthermore, as in *Arabidopsis* (Fig. 1) (*8*), the ability of TRX-h5 to bind victorin is required for LOV1 activation (fig. S3).

Because LOV1 requires *TRX-h5* coexpression and is activated when TRX-h5 (or enzymatically inactive TRX-h5) binds victorin, we explored the possibility that LOV1 and TRX-h5 interact. Yeast two-hybrid analyses demonstrated that TRX-h5 interacts strongly with the LOV1 CC domain but not the LRR domain, and weakly with full-length LOV1 (Fig. 3B). In contrast, TRX-h3 interacted only weakly with the LOV1 CC domain (Fig. 3B). A fluorescent fusion of LOV1 exclusively labeled the cell periphery (Fig. 3C), and subcellular fractionation revealed that LOV1 and TRX-h5 copurify with the plasma membrane (Fig. 3D) even though TRX-h5 predominantly occupies the cytoplasm. TRX-h5 localization to the plasma membrane was also independently corroborated by proteome analyses (*13*). Finally, bimolecular fluorescence complementation (BiFC) supported an interaction of LOV1 and TRX-h5 at the plasma membrane

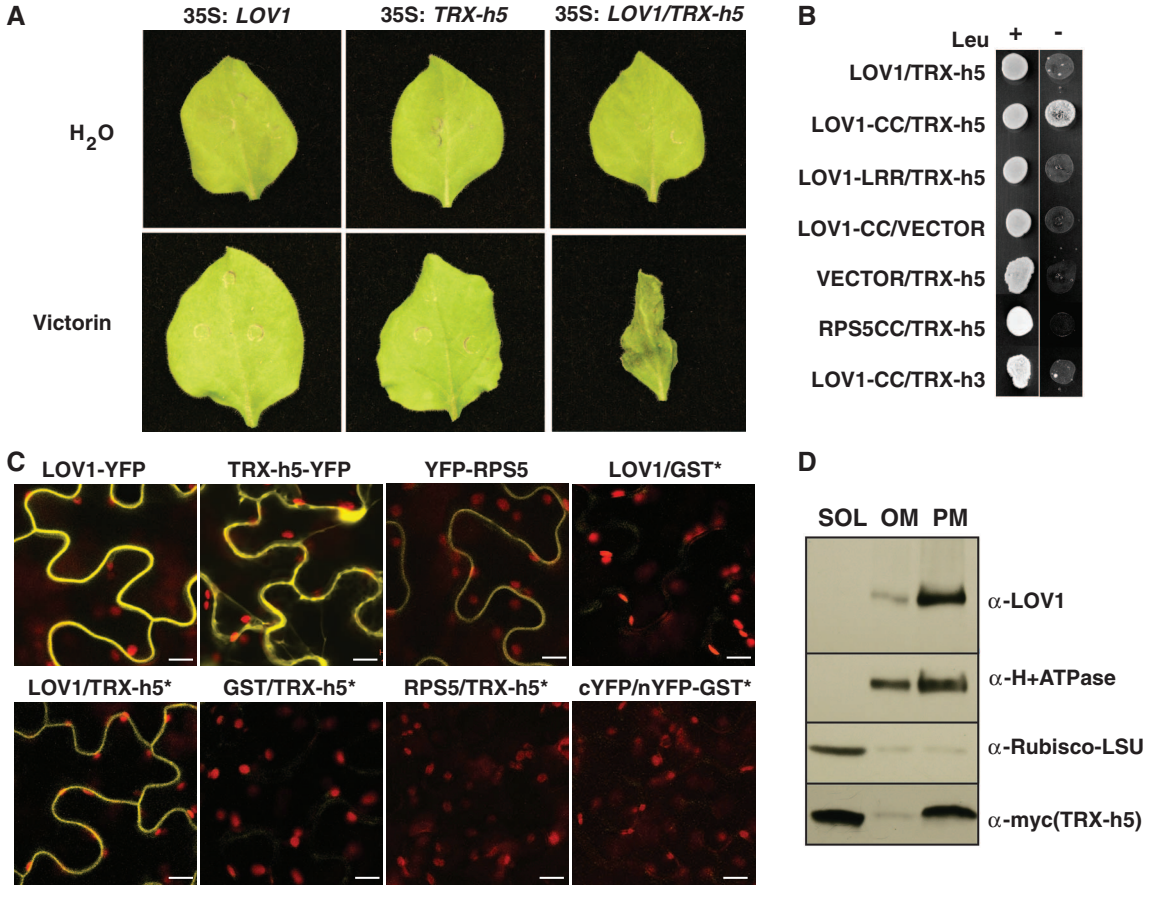

Fig. 3. LOV1 guards TRX-h5. (**A**) Transient expression of LOV1 (left), TRX-h5 (center), or LOV1 and TRX-h5 (right) in *N. benthamiana* infiltrated with water or victorin (1 μg/ml). (**B**) Yeast two-hybrid assay of LOV1, TRX-h5, and control proteins on SD/-Trp/-His medium (left) and SD/-Leu/-Trp/-His medium (right). (**C**) Confocal fluorescence microscopy of *N. benthamiana* leaves transiently expressing proteins tagged with yellow fluorescent protein (YFP) or split-YFP* (BiFC). From left to right: top row, 35S:*LOV1-YFP*; 35S:*TRX-h5-YFP*; 35S:*YFP-RPS5*; 35S:*cYFP-LOV1*+35S:*nYFP-GST*; bottom row, 35S:*cYFP-LOV1*+35S:*nYFP-TRX-h5*; 35S:*cYFP-GST*+35S:*nYFP-TRX-h5*; 35S:*cYFP-RPS5*+35S:*nYFP-TRX-h5*; 35S:*cYFP*+35S:*nYFP-GST*. Red, chlorophyll autofluorescence; yellow, YFP fluorescence. Scale bars, 10 μm. (**D**) Immunoblot of 10 μg of soluble (SOL), other membrane (OM), or plasma membrane (PM) protein fractions from two-phase extraction of *N. benthamiana* transiently expressing LOV1 and myc-TRX-h5. H+ATPase is used as a plasma membrane marker; Rubisco (ribulose-1,5-bisphosphate carboxylase-oxygenase) is used as a marker for soluble proteins.

(Fig. 3C). Coimmunoprecipitation of LOV1 and TRX-h5 was not successful, possibly because of conditions required for solubilizing LOV1. Nonetheless, the cumulative data indicate that LOV1 and TRX-h5 interact in some manner at the plasma membrane, consistent with the idea that TRX-h5 is guarded by LOV1.

The guard model accounts for plants having immunity to a myriad of pathogens while possessing a limited number of *R* genes (*2*, *3*). *R* gene limitation is possible because effector targets are limited, and pathogens (however numerous) secrete functionally redundant virulence effectors. This implies that *R* genes across plant species evolve to guard common targets (*14*). We have observed victorin sensitivity in oats, *Arabidopsis*, barley, rice, *Brachypodium* (*15*), and bean (fig. S6). Because victorin binds diverse thioredoxins (fig. S1) and sensitivity is conditioned by a NB-LRR gene (*LOV1*) in *Arabidopsis*, inseparable from the *Pc2* resistance gene in oats, and mapped to a genomic region rich in NB-LRR genes in barley (*15*), the data suggest that victorin sensitivity is evoked by a common mechanism across these species: by victorin binding to a thioredoxin that is guarded by a NB-LRR protein. Given this and the important defense functions of TRXs (*6*), it is possible that multiple pathogens target thioredoxins to enhance virulence (i.e., redundant virulence effectors). Notably, *C. victoriae* does not cause disease in *Arabidopsis* in the absence of *LOV1* or in oats in the absence of *Vb* (*5*). This is important because it implies that victorin production did not evolve in *C. victoriae* to inhibit TRX-h5–conferred defense. Rather, *C. victoriae* uses victorin solely in its capacity as a defeated effector to exploit *R* gene–mediated defense for disease susceptibility. This suggests that other defeated effectors could confer virulence if expressed by the appropriate pathogen.

Susceptibility to three other necrotrophic pathogens has been associated with *R*-like genes (*16*, *17*). Given the numbers of *R* genes in plant genomes and defeated virulence effectors collectively deployed by biotrophic pathogens, this study underpins the importance of understanding the limits to necrotroph exploitation of effector-triggered immunity (resistance-mediated susceptibility), so that future deployment of resistance does not lead to the emergence of new disease.

References and Notes

1. J. M. Lorang, T. A. Sweat, T. J. Wolpert, *Proc. Natl. Acad. Sci. U.S.A.* **104**, 14861 (2007).
2. J. D. G. Jones, J. L. Dangl, *Nature* **444**, 323 (2006).
3. B. J. DeYoung, R. W. Innes, *Nat. Immunol.* **7**, 1243 (2006).
4. T. A. Sweat, J. M. Lorang, E. G. Bakker, T. J. Wolpert, *Mol. Plant Microbe Interact.* **21**, 7 (2008).
5. T. J. Wolpert, L. D. Dunkle, L. M. Ciuffetti, *Annu. Rev. Phytopathol.* **40**, 251 (2002).
6. Y. Tada *et al.*, *Science* **321**, 952 (2008).
7. H. Cao, S. A. Bowling, A. S. Gordon, X. Dong, *Plant Cell* **6**, 1583 (1994).
8. T. A. Sweat, T. J. Wolpert, *Plant Cell* **19**, 673 (2007).
9. C. Laloi, D. Mestres-Ortega, Y. Marco, Y. Meyer, J. P. Reichheld, *Plant Physiol.* **134**, 1006 (2004).
10. See supplementary materials on *Science* Online.
11. T. J. Wolpert, V. Macko, W. Acklin, D. Arigoni, *Plant Physiol.* **88**, 37 (1988).
12. C. C. Mundt, *Phytopathology* **99**, 1116 (2009).
13. A. Marmagne *et al.*, *Mol. Cell. Proteomics* **6**, 1980 (2007).
14. T. Wroblewski *et al.*, *Plant Physiol.* **150**, 1733 (2009).
15. J. Lorang, A. Cuesta-Marcos, P. M. Hayes, T. J. Wolpert, *Mol. Breed.* **26**, 545 (2010).
16. E. D. Nagy, J. L. Bennetzen, *Genome Res.* **18**, 1918 (2008).
17. J. D. Faris *et al.*, *Proc. Natl. Acad. Sci. U.S.A.* **107**, 13544 (2010).

Acknowledgments: We thank J. Chang and M. Behrenfeld for valuable discussion. This work was supported in part by the Agriculture and Food Research Initiative Competitive Grants Program from the USDA National Institute of Food and Agriculture (grants 2005-35319-15361 and 2008-35319-18651) and by NSF grant IOS-0724954. OSU's mass spectrometry facility and core is in part supported by National Institute of Environmental Health Sciences grant P30ES200210.

Supplementary Materials

www.sciencemag.org/cgi/content/full/science.1226743/DC1
Materials and Methods
Figs. S1 to S6
References (*18*–*27*)

29 June 2012; accepted 5 September 2012
Published online 18 October 2012;
10.1126/science.1226743

Tug-of-War in Motor Protein Ensembles Revealed with a Programmable DNA Origami Scaffold

N. D. Derr,[1,2,3]* B. S. Goodman,[1]* R. Jungmann,[4,5] A. E. Leschziner,[6] W. M. Shih,[2,3,5] S. L. Reck-Peterson[1]†

Cytoplasmic dynein and kinesin-1 are microtubule-based motors with opposite polarity that transport a wide variety of cargo in eukaryotic cells. Many cellular cargos demonstrate bidirectional movement due to the presence of ensembles of dynein and kinesin, but are ultimately sorted with spatial and temporal precision. To investigate the mechanisms that coordinate motor ensemble behavior, we built a programmable synthetic cargo using three-dimensional DNA origami to which varying numbers of DNA oligonucleotide-linked motors could be attached, allowing for control of motor type, number, spacing, and orientation in vitro. In ensembles of one to seven identical-polarity motors, motor number had minimal affect on directional velocity, whereas ensembles of opposite-polarity motors engaged in a tug-of-war resolvable by disengaging one motor species.

Cytoplasmic dynein and kinesin-1 (referred to as "dynein" and "kinesin" here) are opposite-polarity, microtubule-based motors that are responsible for producing and maintaining subcellular organization via the transport of many cargos in eukaryotic cells (*1*, *2*). Defects in these transport processes have been linked to neurological diseases (*1*, *3*, *4*). Microtubules contain inherent structural polarity, polymerizing rapidly at their "plus" ends and more slowly at their "minus" ends (*5*), with dynein and kinesin driving most minus- and plus-end–directed microtubule transport, respectively (*2*). Although some transport tasks require a single motor type, many cargos use both dynein and kinesin and move bidirectionally on microtubules (*1*, *6*, *7*). The mechanisms that allow ensembles of identical-polarity motors to coordinate their activity and ensembles of opposite-polarity motors to achieve both processive movement and rapid switches in direction are unknown.

To dissect the biophysical mechanisms of motor-driven cargo transport, we designed a programmable, synthetic cargo using three-dimensional DNA origami (*8*, *9*) (also see supplementary materials and methods). The cargo consisted of a 12-helix bundle with 6 inner and 6 outer helices (Fig. 1A and fig. S1) (*10*). We refer to this structure as a "chassis," akin to an automobile chassis that serves as a skeletal frame for the attachment of additional components. The origami chassis was made by rapidly heating and slowly cooling an 8064-nucleotide, single-strand DNA (ssDNA) "scaffold" in the presence of 273 short, ssDNA "staples" (fig. S1A and tables S1 to S3), which hybridize with discontinuous regions of the scaffold to fold it into a desired shape. Selective inclusion of staples with extra "handle" sequences that project out from the chassis provide site- and sequence-specific attachment points for motors, fluorophores, or other chemical moieties (Fig. 1B).

[1]Department of Cell Biology, Harvard Medical School, Boston, MA 02115, USA. [2]Dana-Farber Cancer Institute, Boston, MA 02115, USA. [3]Department of Biological Chemistry and Molecular Pharmacology, Harvard Medical School, Boston, MA 02115, USA. [4]Department of Systems Biology, Harvard Medical School, Boston, MA 02115, USA. [5]Wyss Institute for Biologically Inspired Engineering, Harvard University, Boston, MA 02115, USA. [6]Department of Molecular and Cellular Biology, Harvard University, Cambridge, MA 02138, USA.

*These authors contributed equally to this work.
†To whom correspondence should be addressed. E-mail: reck-peterson@hms.harvard.edu

Next, we purified well-characterized model dynein and kinesin motors and covalently linked them to DNA oligonucleotide "antihandles" complementary to the handle sequences on the chassis. We used a minimal dimeric *Saccharomyces cerevisiae* dynein (*11*, *12*) and a minimal dimeric human kinesin-1 (*13*), both of which contained a $SNAP_f$-tag at their cargo-binding domain for oligonucleotide antihandle attachment.

We next assessed motor-chassis complex assembly. Gel-shift assays of the dynein chassis indicated an ~80% probability for individual dynein occupancy at each motor site on the chassis (Fig. 1C and fig. S2A). Due to kinesin's small size relative to dynein, similar assays with the kinesin chassis did not allow individual occupancy numbers to be resolved (fig. S2B). When the kinesin antihandle was used with dynein, however, we again observed ~80% occupancy, indicating no handle-sequence–specific effects on motor-chassis linking (fig. S2, C and D). Super-resolution fluorescence imaging with the use of DNA-PAINT (*14*) revealed that submaximal handle incorporation into the folded chassis was probably responsible for incomplete motor occupancy (fig. S3), in agreement with previous reports (*15*, *16*). Negative-stain transmission electron microscopy (TEM) of fully assembled chassis structures showed dynein motors occupying sites on the chassis at the programmed locations (Fig. 1D).

We quantified the motile properties of dynein alone or dynein ensembles on the chassis with one, two, four, or seven motor-attachment sites (1D, 2D, 4D, and 7D, respectively) on microtubules at the single-molecule level using total internal reflection fluorescence microscopy (Fig. 2A). The average velocity of a single dynein was similar to that of the 1D and 2D ensembles, whereas 4D and 7D ensembles moved slightly slower (Fig. 2B and fig. S4A). The characteristic run length (total distance moved) and time (total duration of the run) of the dynein ensembles increased with the number of motor sites for the 1D, 2D, and 4D ensembles (Fig. 2, C and D, and fig. S4, B and C). The 4D and 7D ensembles were

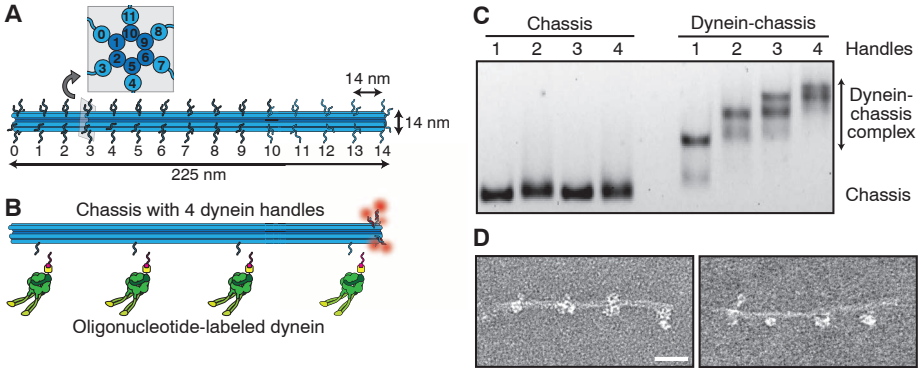

Fig. 1. Design and validation of a three-dimensional DNA origami synthetic cargo. (**A**) Schematic of the 12-helix-bundle chassis structure with 6 inner and 6 outer helices. Each outer helix contains up to 15 optional handles, yielding 90 uniquely addressable sites. Each handle consists of an unpaired 21-bp (~7 nm) oligonucleotide sequence for hybridization to complementary antihandle sequences covalently attached to motors or fluorophores. The inset shows an orthogonal cross section. (**B**) Schematic of a chassis labeled with five fluorophores (red) at handle position 14 on each of five outer helices and dynein handles at positions 1, 5, 9, and 13 on a single outer helix. Oligonucleotide-labeled dynein is also shown. (**C**) Agarose gel-shift assay of a carboxytetramethylrhodamine (TAMRA)–labeled chassis containing one to four handles in the absence (left lanes) or presence (right lanes) of dynein labeled with an antihandle oligonucleotide. Chassis are visualized by TAMRA fluorescence. See fig. S2B for occupancy quantification. (**D**) Negative-stain TEM images of the four-dynein–chassis complex. Scale bar, 40 nm.

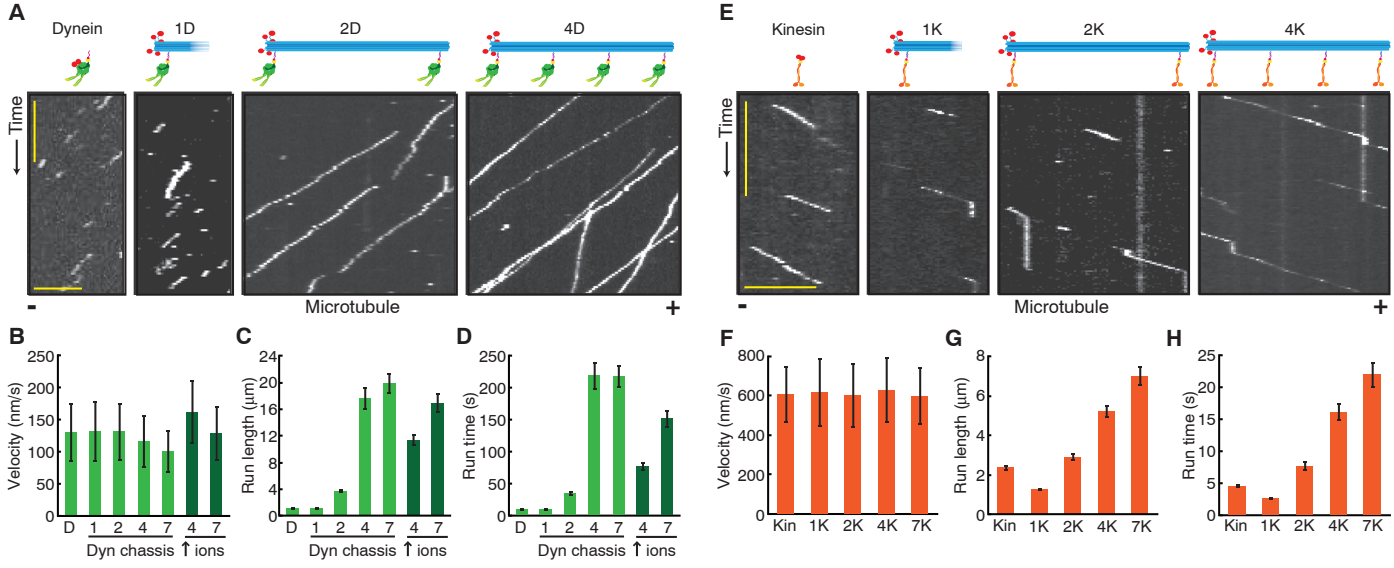

Fig. 2. Single-molecule motile properties of chassis-motor complexes. (**A**) Kymographs of a tetramethylrhodamine (TMR)–labeled dynein alone and a TAMRA-labeled chassis with 1, 2, or 4 dyneins. Plus (+) and minus (-) denote microtubule polarity. Scale bars: 1 min (*x* axis), 5 μm (*y* axis). (**B**) Quantification of average segment velocities ± SD (error bars) of dynein and dynein-chassis complexes. The 4D and 7D ensembles moved significantly slower than dynein alone or the 1D or 2D ensembles (one-tailed *t* test, $P < 0.001$; $N \geq 211$ runs). In higher ionic concentration (↑ ions), the 4D and 7D ensemble velocities were significantly different (one-tailed *t* test, $P < 0.001$; $N \geq 208$). (**C**) Quantification of run lengths ± SE (error bars) of dynein and dynein-chassis ensembles ($N \geq 208$). (**D**) Quantification of total run times ± SE (error bars) of dynein and dynein-chassis ensembles ($N \geq 208$). (**E**) Kymographs of TMR-labeled kinesin alone and a TAMRA-labeled chassis with 1, 2, or 4 kinesins. Scale bars: 1 min (*x* axis), 5 μm (*y* axis). (**F**) Quantification of average segment velocities ± SD (error bars) of kinesin and kinesin-chassis ensembles. Comparison of velocities yielded no statistical differences (analysis of variance test, $P > 0.05$; $N \geq 301$). (**G**) Quantification of run lengths ± SE (error bars) of kinesin and kinesin-chassis ensembles ($N \geq 301$). (**H**) Quantification of total run times ± SE (error bars) of kinesin and kinesin-chassis ensembles ($N \geq 301$). For additional statistical analysis, see figs. S4 to S6.

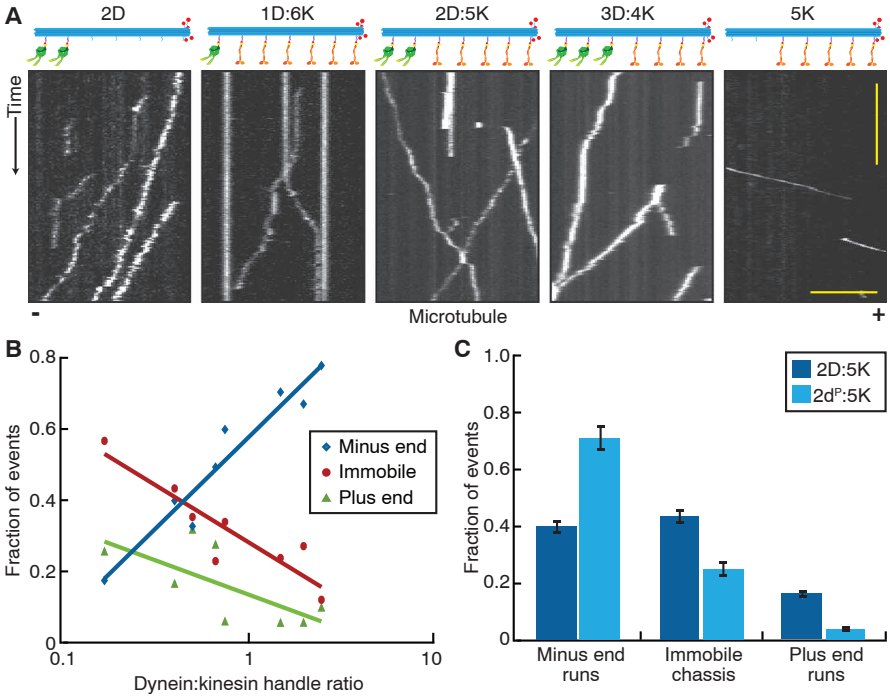

Fig. 3. Chassis attached to dynein and kinesin frequently engage in a stalled tug-of-war. (**A**) Kymographs of a TAMRA-labeled chassis attached to dynein only (leftmost panel), kinesin only (rightmost panel), or varying ratios of dynein and kinesin motors (middle panels). Plus (+) and minus (-) denote microtubule polarity. Scale bars: 1 min (*x* axis), 5 μm (*y* axis). (**B**) Quantification of the fraction of events for each chassis observed as defined by their dynein–to–kinesin-handle ratio. Chassis were immobile, moving toward the minus end, or moving toward the plus end ($N \geq 221$) (table S6). The *x* axis of dynein-to-kinesin ratios is a logarithmic scale, and linear-log fits highlight the trends observed. (**C**) Quantification of the fraction of events ± SE (error bars) observed to be immobile, moving toward the minus end, or moving toward the plus end for mixed ensembles containing two dyneins and five kinesins ($N \geq 352$). The dyneins were either wild type (D) or a highly processive mutant (d^P).

so processive that their run lengths and times were similar to each other in standard assay buffer, where microtubule length and imaging duration become limiting (Fig. 2, C and D). However, when assayed in high–ionic strength buffer, which decreases dynein's processivity (*17*), the 7D ensemble was more processive than the 4D ensemble (Fig. 2, C and D, and figs. S4 and S5).

We performed a similar analysis of kinesin alone and kinesin ensembles on the chassis with one, two, four, or seven motor-attachment sites (1K, 2K, 4K, and 7K, respectively; Fig. 2, E to H). The average velocities of the kinesin ensembles remained constant (Fig. 2F and fig. S6A), whereas run lengths and times increased with increasing motor number (Fig. 2, G and H, and fig. S6, B and C).

Recent models of motor ensemble behavior using a transition-state framework predict run lengths that are several orders of magnitude higher than what we observed (*18*). In contrast, our data suggest that motor microtubule binding dynamics may be influenced by the presence and number of other motors on a shared cargo, similar to previous work (*19*–*22*). For one to seven kinesins or one or two dyneins, velocity was unaffected by motor number. However, for 4D and 7D ensembles, velocity was decreased, suggesting that intermotor interference can affect motor stepping rate. To test this hypothesis, we engineered the chassis with locations for inactive mutant dyneins (denoted d^I) incapable of binding adenosine triphosphate (ATP) at dynein's main site of ATP hydrolysis; this mutant binds microtubules tightly, but does not move (*23*). Dynein ensembles programmed

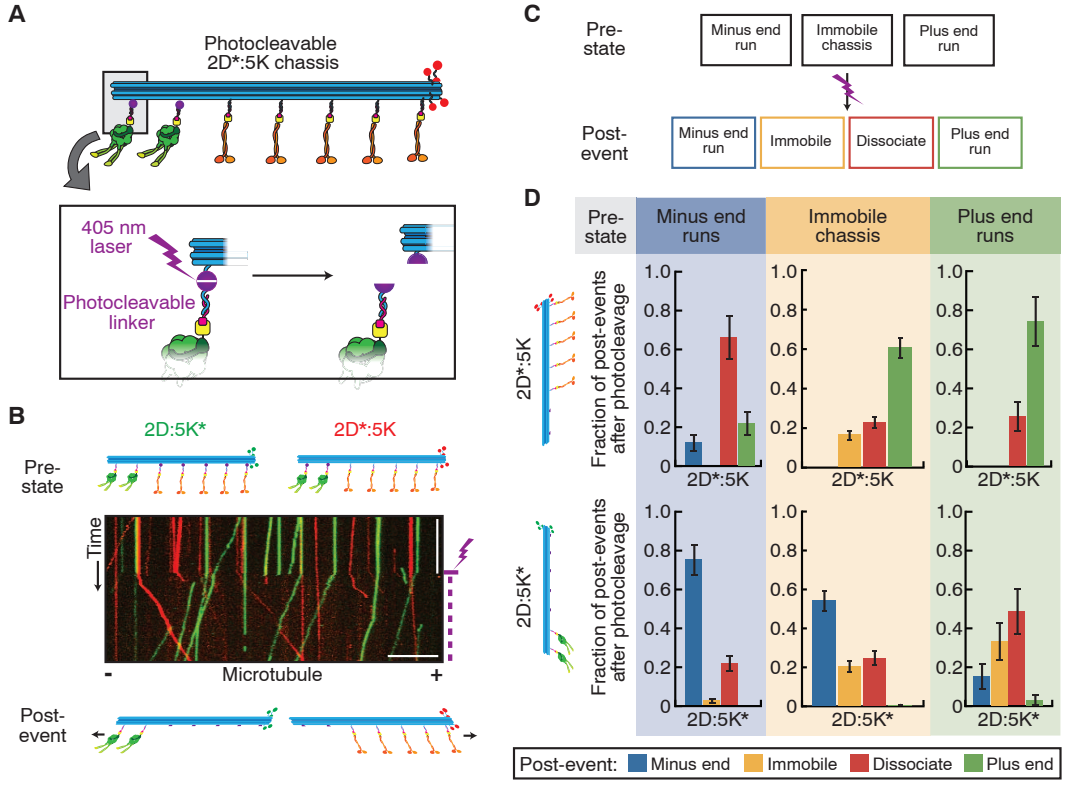

Fig. 4. Disengagement of one motor species resolves the stalled tug-of-war. (**A**) Schematic of a mixed-motor chassis with dynein attached via photocleavable handles (purple circles). Photocleavage is induced by 405-nm laser pulses (inset). (**B**) Kymograph of the 2D:5K*(green) and the 2D*:5K (red) chassis. The purple lightning bolt indicates the start of laser pulses. Plus (+) and minus (-) denote microtubule polarity. Scale bars: 1 min (*x* axis), 10 μm (*y* axis). (**C**) Chassis classification scheme for data presented in (D). Before (prestate) and after (postevent) laser photocleavage, the chassis were characterized as immobile, minus-end–directed, or plus-end–directed. Possible postevents also included dissociation from the microtubule. (**D**) Quantification of the postphotocleavage event motility of the 2D*:5K (top) and the 2D:5K* (bottom) chassis as a function of their prestates ($N \geq 286$). Each individual postevent fraction was calculated relative to the number of events within that given prestate. Error bars indicate SD.

to bind differing ratios of active and inactive motors (table S6) moved with reduced velocity (fig. S7), demonstrating that intermotor negative interference decreases cargo velocity.

We next investigated the motility of the chassis linked to mixed ensembles of opposite-polarity motors. We quantified the motility of the chassis as a function of the dynein-to-kinesin (D:K) ratio (table S6). All mixed-motor ensembles moved unidirectionally (Fig. 3A) with no reversals detected at a precision of ~10 nm. With the exception of the 1D:6K chassis, all ensembles were more likely to move toward the minus end of the microtubules (Fig. 3B). Mixed-motor ensembles were relatively insensitive to increasing the number of kinesin motors compared with increasing the number of dynein motors, which could be due to kinesin ensembles operating predominantly through the actions of fewer motors at any given time (*24*). Based on the stall forces of dynein [~5 pN (*25*)] and kinesin [~7 pN (*26*)], we expected that kinesin plus-end runs would have been more dominant. In contrast, our results suggest that stall force was not the only parameter governing the behavior of opposite-polarity motor ensembles (*27*). Other parameters, such as microtubule affinity, detachment force, and velocity-dependent on-rates, could also be relevant (*20*–*22*, *28*–*31*). Mixed-motor ensembles moved more slowly and for longer periods of time than did equivalent single-motor–type ensembles (fig. S8, A and B), with the magnitude of this effect being more pronounced in the plus-end direction. Notably, mixed ensembles of dynein and kinesin were more likely to be immobile than identical-motor ensembles, suggesting that opposite-polarity motors engage in a tug-of-war that prevents cargo movement (Fig. 3B).

Based on the longer run lengths and times of yeast dynein compared with human kinesin, we hypothesized that dynein runs dominated in mixed-motor ensembles due to dynein's higher microtubule affinity. To test this, we purified a mutant dynein with a higher processivity and affinity for microtubules (denoted d^P) (*17*) and paired it with kinesins. The $2d^P$:5K ensemble was even more likely to move in the dynein direction and had fewer immobile chassis structures compared with the 2D:5K ensemble containing wild-type (WT) dynein (Fig. 3C). These results suggest that track affinity is a key motor property in governing opposite-polarity motor ensemble motility. Mixed ensembles containing the high-affinity dynein mutant also produced slower plus-end runs and longer run times in both directions compared with the equivalent WT system (fig. S8, C and D).

We wanted to determine if mixed-motor ensembles were nonmotile due to a stalled tug-of-war. To regulate motor attachment to the chassis, we introduced photocleavable linkers in selected handles such that illumination with a 405-nm laser released one motor type from the chassis (Fig. 4A). We designed two modified chassis: (i) 2D:5K*, with photocleavable (*) kinesins, and (ii) 2D*:5K, with photocleavable dyneins. We monitored the motile properties of these chassis structures before and after laser-induced photocleavage (Fig. 4B). Cleavage was rapid (fig. S9); within seconds of photocleaving motors of one type, immobile chassis moved in the direction of the remaining motors (Fig. 4B). We classified the state of each chassis before and after photocleavage (Fig. 4C) and found that the majority of stalled tug-of-war events were resolved into active motility (Fig. 4D), indicating that disengagement of one motor type can resolve tug-of-war events between dynein and kinesin. Though we also observed rare events in which ensembles switched directions after photocleavage, we more commonly observed that chassis would dissociate when moving in the direction of the cleaved motor (fig. S10).

Using DNA origami, we built a versatile, synthetic cargo system that allowed us to determine the motile behavior of microtubule-based motor ensembles. In ensembles of identical-polarity motors, the motor number had a minimal affect on directional velocity, whereas ensembles of opposite-polarity motors engaged in a tug-of-war resolvable by disengaging one motor species. Yeast dynein's high microtubule affinity allowed it to dominate in mixed ensembles, whereas the ratio of dynein to kinesin dictated cargo directionality, supporting experiments performed in vivo or in cell-free lysates (*32*–*34*). The reduction in velocity reported here for opposite polarity motor ensembles also agrees with in vivo reports of dynein and kinesin tug-of-war (*32*, *35*). The high probability with which mixed ensembles of active dynein and kinesin motors were immobile suggested that, for this motor pair, efficient bidirectional transport requires extrinsic regulation (*36*). Motors with comparable microtubule affinities and binding kinetics, such as those that coevolved in the same biological system, may produce bidirectional transport characteristics similar to those observed in vivo (*6*, *37*, *38*). The system we built provides a powerful platform to investigate the motile properties of any combination of identical- or opposite-polarity motors and could also be used to investigate the role of motor regulation.

References and Notes

1. N. Hirokawa, S. Niwa, Y. Tanaka, *Neuron* **68**, 610 (2010).
2. R. D. Vale, *Cell* **112**, 467 (2003).
3. R. B. Vallee, J.-W. Tsai, *Genes Dev.* **20**, 1384 (2006).
4. G. T. Banks, E. M. C. Fisher, *Genome Biol.* **9**, 214 (2008).
5. A. Desai, T. J. Mitchison, *Annu. Rev. Cell Dev. Biol.* **13**, 83 (1997).
6. M. A. Welte, *Curr. Biol.* **14**, R525 (2004).
7. S. A. Bryantseva, O. N. Zhapparova, *Cell Biol. Int.* **36**, 1 (2012).
8. P. W. K. Rothemund, *Nature* **440**, 297 (2006).
9. S. M. Douglas *et al.*, *Nature* **459**, 414 (2009).
10. S. M. Douglas *et al.*, *Nucleic Acids Res.* **37**, 5001 (2009).
11. S. L. Reck-Peterson *et al.*, *Cell* **126**, 335 (2006).
12. W. Qiu *et al.*, *Nat. Struct. Mol. Biol.* **19**, 193 (2012).
13. R. B. Case, D. W. Pierce, N. Hom-Booher, C. L. Hart, R. D. Vale, *Cell* **90**, 959 (1997).
14. R. Jungmann *et al.*, *Nano Lett.* **10**, 4756 (2010).
15. Y. Ke, N. V. Voigt, K. V. Gothelf, W. M. Shih, *J. Am. Chem. Soc.* **134**, 1770 (2012).
16. S. H. Ko, G. M. Gallatin, J. A. Liddle, *Adv. Funct. Mater.* **22**, 1015 (2012).
17. W. B. Redwine *et al.*, *Science* **337**, 1532 (2012).
18. S. Klumpp, R. Lipowsky, *Proc. Natl. Acad. Sci. U.S.A.* **102**, 17284 (2005).
19. C. Leduc, N. Pavin, F. Jülicher, S. Diez, *Phys. Rev. Lett.* **105**, 128103 (2010).
20. A. R. Rogers, J. W. Driver, P. E. Constantinou, D. Kenneth Jamison, M. R. Diehl, *Phys. Chem. Chem. Phys.* **11**, 4882 (2009).
21. H. Lu *et al.*, *J. Biol. Chem.* **287**, 27753 (2012).
22. J. Xu, Z. Shu, S. J. King, S. P. Gross, *Traffic* **13**, 1198 (2012).
23. T. Kon, M. Nishiura, R. Ohkura, Y. Y. Toyoshima, K. Sutoh, *Biochemistry* **43**, 11266 (2004).
24. D. K. Jamison, J. W. Driver, A. R. Rogers, P. E. Constantinou, M. R. Diehl, *Biophys. J.* **99**, 2967 (2010).
25. A. Gennerich, A. P. Carter, S. L. Reck-Peterson, R. D. Vale, *Cell* **131**, 952 (2007).
26. A. Yildiz, M. Tomishige, A. Gennerich, R. D. Vale, *Cell* **134**, 1030 (2008).
27. P. E. Constantinou, M. R. Diehl, *J. Biomech.* **43**, 31 (2010).
28. M. Y. Ali *et al.*, *Proc. Natl. Acad. Sci. U.S.A.* **108**, E535 (2011).
29. R. D. Vale, F. Malik, D. Brown, *J. Cell Biol.* **119**, 1589 (1992).
30. A. Kunwar, M. Vershinin, J. Xu, S. P. Gross, *Curr. Biol.* **18**, 1173 (2008).
31. D. K. Jamison, J. W. Driver, M. R. Diehl, *J. Biol. Chem.* **287**, 3357 (2012).
32. V. Levi, A. S. Serpinskaya, E. Gratton, V. Gelfand, *Biophys. J.* **90**, 318 (2006).
33. M. Schuster, R. Lipowsky, M.-A. Assmann, P. Lenz, G. Steinberg, *Proc. Natl. Acad. Sci. U.S.A.* **108**, 3618 (2011).
34. M. Amrute-Nayak, S. L. Bullock, *Nat. Cell Biol.* **14**, 416 (2012).
35. V. Soppina, A. K. Rai, A. J. Ramaiya, P. Barak, R. Mallik, *Proc. Natl. Acad. Sci. U.S.A.* **106**, 19381 (2009).
36. A. Kunwar *et al.*, *Proc. Natl. Acad. Sci. U.S.A.* **108**, 18960 (2011).
37. S. E. Encalada, L. Szpankowski, C.-H. Xia, L. S. B. Goldstein, *Cell* **144**, 551 (2011).
38. M. J. Egan, K. Tan, S. L. Reck-Peterson, *J. Cell Biol.* **197**, 971 (2012).

Acknowledgments: We thank C. Lin for assistance with electron microscopy; F. Aguet for assistance with data analysis; J. Huang, W. Qiu, W.B. Redwine, and A. Roberts for helpful advice and critical reading of the manuscript; members of the Reck-Peterson and Shih labs for advice and helpful discussions; and J. Iwasa for illustrations. EM data were collected at the Center for Nanoscale Systems, Harvard University. DNA-PAINT data were collected at the Nikon Imaging Center, Harvard Medical School. R.J. is supported from the Alexander von Humboldt Foundation through a Feodor Lynen fellowship. S.L.R.-P. is funded by the Rita Allen Foundation, the Harvard Armenise Foundation, and a NIH New Innovator award (1 DP2 OD004268-1). W.M.S. is funded by NIH awards (1U54GM094608 and 1DP2OD004641) and ONR awards (N000014091118 and N000141010241).

Supplementary Materials

www.sciencemag.org/cgi/content/full/science.1226734/DC1
Materials and Methods
Figs. S1 to S10
Tables S1 to S6
Scaffold Sequence
References (*39*, *40*)
caDNAno File of Chassis Structure

29 June 2012; accepted 21 September 2012
Published online 11 October 2012;
10.1126/science.1226734

Synchronizing Nuclear Import of Ribosomal Proteins with Ribosome Assembly

Dieter Kressler,[1,2*†] Gert Bange,[1*] Yutaka Ogawa,[3] Goran Stjepanovic,[1] Bettina Bradatsch,[1] Dagmar Pratte,[2] Stefan Amlacher,[1] Daniela Strauß,[1] Yoshihiro Yoneda,[3] Jun Katahira,[3] Irmgard Sinning,[1†] Ed Hurt[1†]

Ribosomal proteins are synthesized in the cytoplasm, before nuclear import and assembly with ribosomal RNA (rRNA). Little is known about coordination of nucleocytoplasmic transport with ribosome assembly. Here, we identify a transport adaptor, symportin 1 (Syo1), that facilitates synchronized coimport of the two 5*S*-rRNA binding proteins Rpl5 and Rpl11. In vitro studies revealed that Syo1 concomitantly binds Rpl5-Rpl11 and furthermore recruits the import receptor Kap104. The Syo1-Rpl5-Rpl11 import complex is released from Kap104 by RanGTP and can be directly transferred onto the 5*S* rRNA. Syo1 can shuttle back to the cytoplasm by interaction with phenylalanine-glycine nucleoporins. X-ray crystallography uncovered how the α-solenoid symportin accommodates the Rpl5 amino terminus, normally bound to 5*S* rRNA, in an extended groove. Symportin-mediated coimport of Rpl5-Rpl11 could ensure coordinated and stoichiometric incorporation of these proteins into pre-60*S* ribosomes.

Ribosomes perform their role in translation in the cytoplasm, but ribosome assembly occurs predominantly in a specialized nuclear compartment, the nucleolus (*1*–*4*). The construction of ribosomes follows an ordered assembly of ~80 ribosomal proteins (r-proteins) and four ribosomal RNAs (rRNAs) into a small (40*S*) and large (60*S*) ribosomal subunit. This process is spatially and temporally coordinated, starting with cotranscriptional assembly of a first preribosomal particle (90*S*) in the nucleolus that is subsequently separated into pre-40*S* and pre-60*S* ribosomes, which follow independent processing and maturation steps before export into the cytoplasm (*5*–*8*). R-proteins are synthesized in the cytoplasm and are imported into the nucleus by nuclear import receptors of the importin-β/karyopherin family (*9*, *10*). These transport receptors recognize different types of nuclear localization sequences (NLSs), and hence a number of import receptors have been implicated in decoding NLSs of r-proteins in a redundant way (*9*, *11*). After nuclear import and before incorporation into nascent ribosomes, r-proteins are released from the transport receptor by its interaction with RanGTP (*12*). At present, it is thought that each r-protein is individually transported into the nucleus by its import receptor. However, a number of r-proteins form functional clusters on the ribosomal surface or assemble at distinct temporal or spatial entry points during ribosome formation (*13*–*15*), thus raising the possibility of coordinated nuclear import and assembly of r-proteins.

One such pair of functionally related r-proteins is Rpl5 and Rpl11, which are close to each other on the mature 60*S* subunit and bind to opposite sites on the 5*S* rRNA (Fig. 1A) (*13*). 5*S* rRNA transport has been extensively studied in the *Xenopus* oocyte system. However, this is a special case because 5*S* rRNA is exported into the cytoplasm for storage, either with ribosomal protein L5 [5*S* ribonucleoprotein (RNP)] or transcription factor IIIA (7*S* RNP) (*16*, *17*). In contrast, 5*S* rRNA export may not occur in somatic cells, and only a few studies have addressed 5*S* RNP biogenesis in this case. One of these investigations reported that yeast Rpl5 and Rpl11 form a ribonucleoprotein particle with the 5*S* rRNA that could be incorporated with the aid of two biogenesis factors, Rpf2 and Rrs1, into pre-60*S* ribosomes (*18*). However, it is not known how Rpl5 and Rpl11 enter the nucleus and whether this is coordinated with their assembly onto the 5*S* rRNA. We performed tandem affinity purification (TAP) of TAP-tagged *Saccharomyces cerevisiae* Rpl5 and observed coenrichment of Rpl11 and the uncharacterized yeast protein Ydl063c (Fig. 1B, lane 1). Ydl063c, which we named Syo1 (for synchronized import or briefly symportin), is present in all eukaryotes, including the eukaryotic thermophile *Chaetomium thermophilum* and *Homo sapiens*. Reciprocal tagging of Syo1 with Flag–tobacco etch virus–protein A and subsequent affinity purification revealed copurification of Rpl5 and Rpl11, but not other r-proteins (Fig. 1B, lane 2).

Yeast two-hybrid (Y2H) assays indicated that Syo1 binds both Rpl5 and Rpl11 (Fig. 1C). To further dissect these interactions and gain high-resolution structural data, we performed in vitro reconstitution studies with Syo1, Rpl5, and Rpl11 from the thermophilic fungus *C. thermophilum* (*ct*) (*19*), owing to their improved biochemical properties compared to the orthologous *S. cerevisiae* proteins. These investigations demonstrated that *ct*Syo1 can bind to either *ct*Rpl5 or *ct*Rpl11 (Fig. 1D). Moreover, it was possible to reconstitute the heterotrimeric *ct*Syo1-*ct*Rpl5-*ct*Rpl11 complex, and size exclusion chromatography in line with static light scattering and refractive index measurements revealed a 1:1:1 stoichiometry of the three components (Fig. 1E and table S1). Likewise, we assembled a stoichiometric complex between yeast Syo1 and Rpl5 expressed in *Escherichia coli* (fig. S1B), but expression of yeast Rpl11 yielded largely insoluble protein, which hindered binding studies with Syo1. Taken together, in vivo and in vitro analyses demonstrated that Syo1 can simultaneously bind Rpl5 and Rpl11 to form a heterotrimeric Syo1-Rpl5-Rpl11 complex.

To gain further insight into the in vivo role of Syo1 with respect to the Rpl5-Rpl11 interaction, we returned to the yeast system. Dot spot growth analysis showed that cells with chromosomally disrupted *SYO1* (*syo1*Δ) were viable, but exhibited reduced cell growth, especially at lower temperatures (Fig. 1F). Analysis of ribosome and polysome profiles of *syo1*Δ cells showed a significant reduction of free 60*S* subunits relative to 40*S* subunits, and consequently, the appearance of half-mer polysomes was observed (Fig. 1G). Subsequent genetic analyses revealed a functional link between Syo1 and Rpl5, as evidenced by (i) synthetic lethality between *syo1*Δ and *rpl5* alleles, (ii) high-copy suppression of the cold-sensitive *syo1*Δ phenotype by *RPL5*, and (iii) a complete rescue of the slow-growth or lethal phenotypes of distinct *rpl5* mutant alleles (e.g., *rpl5L104S*) by Syo1 overexpression (Fig. 1H and fig. S2). Together, these data point to a role for Syo1 in ribosome synthesis, possibly by facilitating assembly of Rpl5-Rpl11 onto the pre-60*S* subunit.

To obtain insight into the function of Syo1 at the atomic level, we determined the crystal structure of *ct*Syo1 at 2.1 Å resolution by single-anomalous dispersion (SAD) (table S2). Syo1 forms an all α-helical elongated superhelix or α-solenoid (Fig. 2A), which is typical for nuclear transport receptors (*20*, *21*). Whereas importin-α, the import adaptor for classical NLSs, exclusively contains ARM repeats, importin-β transport receptors are exclusively composed of HEAT repeats. Syo1 is an unusual chimera of four complete ARM repeats (residues 65 to 260) followed by six HEAT repeats (residues 274 to 675), whose inner surfaces form an extensive groove (Fig. 2, A and B). Karyopherins contain binding sites for NLSs and phenylalanine-glycine (FG) repeats of nucleoporins on their inner and outer α-solenoid surfaces, respectively (*22*). By analogy, Syo1 may act as a nuclear import receptor or adaptor by binding to a linear motif of Rpl5 or Rpl11 and/or interacting with FG repeats.

Rpl5 is composed of a globular domain flanked by N- and C-terminal extensions that clamp the

[1]Biochemie-Zentrum der Universität Heidelberg, Im Neuenheimer Feld 328, Heidelberg D-69120, Germany. [2]Unit of Biochemistry, Department of Biology, University of Fribourg, Chemin du Musée 10, CH-1700 Fribourg, Switzerland. [3]Biomolecular Networks Laboratories, Graduate School of Frontier Biosciences, Osaka University, 1-3 Yamadaoka, Suita, Osaka 565-0871, Japan.

*These authors contributed equally to this work.
†To whom correspondence should be addressed. E-mail: dieter.kressler@unifr.ch (D.K.); irmi.sinning@bzh.uni-heidelberg.de (I.S.); ed.hurt@bzh.uni-heidelberg.de (E.H.)

5*S* rRNA within the 60*S* subunit (*13*) (see also Fig. 1A). Y2H analyses and in vitro binding assays revealed that the N-terminal 41 amino acids of Rpl5 (L5-N) are required and sufficient for a robust interaction with Syo1 (fig. S1). To gain structural insight into the Syo1-Rpl5 interaction, we determined the crystal structure of *ct*Syo1 in complex with *ct*L5-N at 2.95 Å resolution by molecular replacement using the *ct*Syo1 structure as the search model (Fig. 2, B and D, and table S2). The side chains and main-chain carbonyls were well defined in the electron density map, and residues 2 to 20 of *ct*Rpl5 could be unambiguously traced (Fig. 2, C and D). L5-N forms an elongated peptide chain with a short helical segment (Tyr^{12} to Phe^{16}), which binds into the extended groove formed by *ct*Syo1 and primarily interacts with residues of HEAT repeats 1 to 4 of *ct*Syo1 (binding interface: 980 Å^2; for a more detailed description, see fig. S3). Therefore, Rpl5 binding to Syo1 results in extensive shielding of an Rpl5 region involved in 5*S* rRNA binding. Moreover, L5-N binding induces a slight conformational rearrangement of the ARM and HEAT domains of Syo1 (fig. S4). L5-N binding to Syo1 seems to slightly "open" the α-solenoid structure of Syo1, which could be of functional relevance but may also reflect a crystal-packing artifact. Taken together, the mode of Rpl5 recognition by Syo1 is reminiscent of the interaction between linear motifs (e.g., from Nup2) and the α-solenoid surface of importin-α (*23*, *24*) (fig. S5).

In the case of Rpl11, we could not restrict the primary sequence into a linear motif that efficiently binds to Syo1. This implies that the interaction between Rpll1 and Syo1 could be more complex, possibly involving part of the Rpl11 fold (see Fig. 1A for Rpl11 structure). To determine the Rpl11 binding surface on Syo1, we performed ^{1}H/^{2}H exchange mass spectrometry (HX-MS) labeling experiments. Specifically, free *ct*Syo1 and the *ct*Syo1-*ct*Rpl11 heterodimer were, after completion of the HX labeling, digested with pepsin, and the resulting peptide fragments were analyzed by electrospray ionization–mass spectrometry. Only

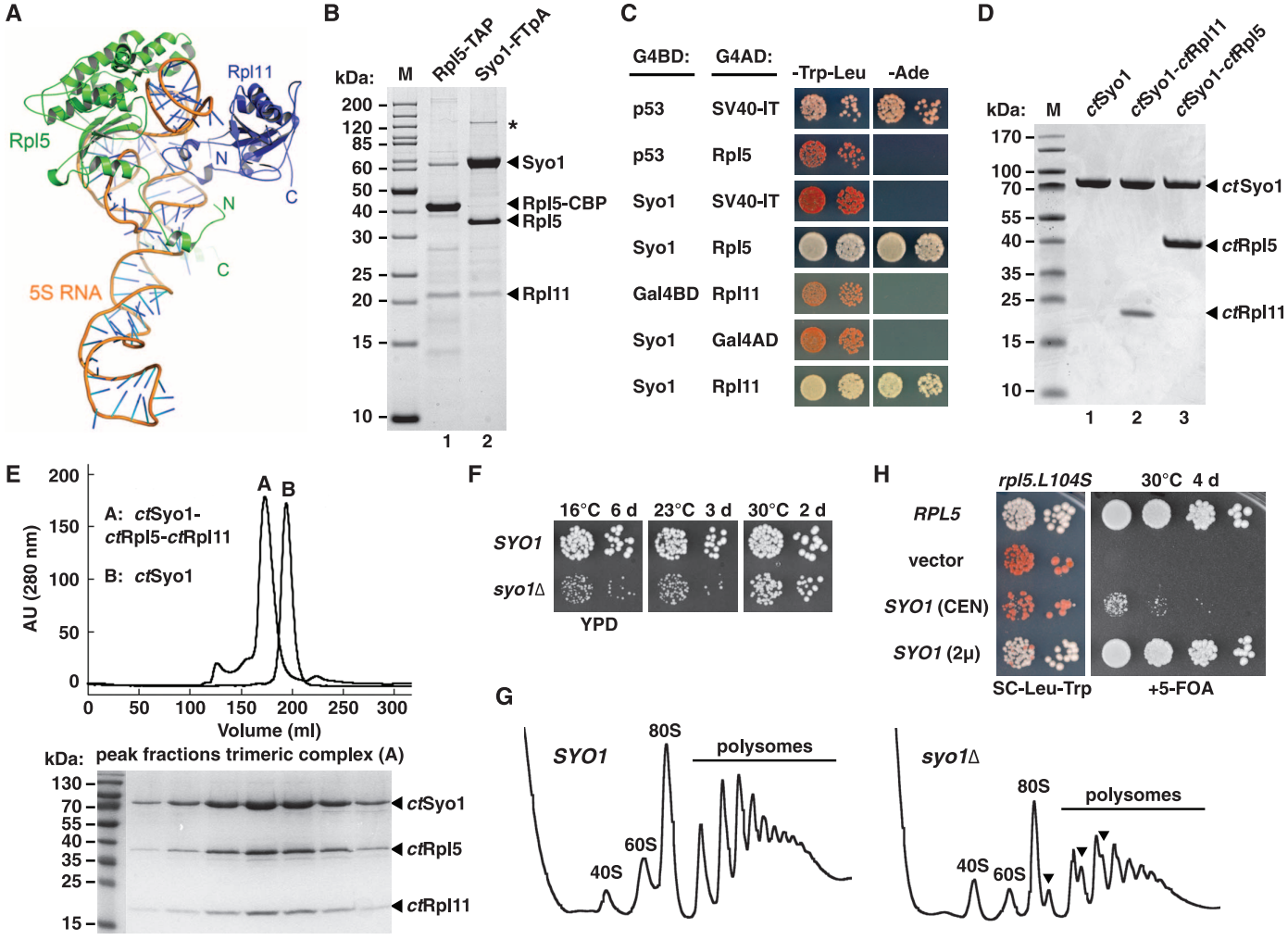

Fig. 1. Syo1 forms a trimeric complex with Rpl5 and Rpl11. (**A**) Structure of the 5*S* RNP (5*S* rRNA-Rpl5-Rpl11) as observed in the *S. cerevisiae* 80*S* ribosome (PDB 3U5D and 3U5E) (*13*). The 5*S* rRNA is shown in orange, Rpl5 in green (residues 2 to 297), and Rpl11 in blue (residues 6 to 174). N and C termini are labeled in the respective colors. (**B**) Identification of Syo1 as an Rpl5 binding protein. Tandem-affinity purification of TAP-tagged Rpl5 (lane 1) and FTpA-tagged Syo1 (lane 2) from yeast cell lysates. Final eluates were analyzed by SDS-PAGE (polyacrylamide gel electrophoresis) and Coomassie staining. The indicated proteins were identified by mass spectrometry. Asterisk indicates the common contaminant Tif4631. M, molecular weight standard. (**C**) Y2H interaction between Syo1 and Rpl5 or Rpl11. (**D**) In vitro binding assay between *ct*Syo1 and *ct*Rpl5 or *ct*Rpl11. Proteins were (co-)expressed in *E. coli*, purified via Ni-affinity purification and revealed by SDS-PAGE and Coomassie staining. Lanes: 1, *ct*Syo1-(His)$_6$; 2, *ct*Syo1-(His)$_6$/*ct*Rpl11; 3, *ct*Syo1/*ct*Rpl5-(His)$_6$; M, molecular weight standard. (**E**) Size exclusion chromatography of reconstituted *ct*Syo1/*ct*Rpl5-(His)$_6$/*ct*Rpl11 heterotrimer (chromatogram A) and *ct*Syo1 (chromatogram B). The peak fractions of chromatogram A were analyzed by SDS-PAGE and Coomassie staining. (**F**) The *syo1*Δ null mutant displays a slow-growth phenotype at low temperatures. Growth analysis of wild-type (*SYO1*) and isogenic *syo1*Δ (*syo1*Δ) deletion mutant. (**G**) Syo1 is required for efficient synthesis of 60*S* ribosomal subunits. Polysome profiles of wild-type (*SYO1*) and *syo1*Δ (*syo1*Δ) cells grown at 23°C. Free 40*S* and 60*S* subunits, 80*S* ribosomes, and polysomes are indicated; arrowheads indicate half-mer polysomes. (**H**) Overexpression of Syo1 rescues the lethal phenotype of the *rpl5L104S* allele.

the very C-terminal part of the *ct*Syo1 disordered loop (residues 395 to 408) showed a decrease in deuterium incorporation upon *ct*Rpl11 binding, indicating shielding of this *ct*Syo1 region (fig. S6A). Consistent with these data, deletion of residues 393 to 397 in the disordered loop abolished binding to *ct*Rpl11 (fig. S6, B and C). Moreover, Y2H assays indicated that the ARM domain of Syo1 contributes to Rpl11 binding (fig. S7). From these results, we conclude that the disordered loop of Syo1 in conjunction with the ARM domain provides the interaction site for Rpl11 (for a model, see fig. S8).

To act as import receptor, Syo1 must pass through the hydrophobic FG-meshwork of the nuclear pore complex (NPC) transport channel. Shuttling karyopherin transport receptors do so by binding with low (micromolar) affinity to FG repeats of nucleoporins (*12*, *25*). We found that Syo1 and *ct*Syo1 bind to FG-rich repeats of distinct nucleoporins with a binding constant in the low micromolar range (Fig. 3, A and B, and fig. S9, A and B). Moreover, Syo1 can translocate into the nucleus on its own in the absence of cytosol, which provides karyopherin transport receptors and RanGTP, when tested in an in vitro nuclear import assay with permeabilized HeLa cells (*26*, *27*) (Fig. 3C and fig. S9, C and D). In agreement with translocation across the NPC channel, Syo1 did not show nuclear accumulation when permeabilized HeLa cells were incubated with wheat germ agglutinin (WGA), a specific inhibitor of nucleocytoplasmic transport that sterically blocks the FG-repeat meshwork of the NPC transport channel (Fig. 3E and fig. S9, C and D). Thus, Syo1 can directly pass through the NPC by low-affinity interaction with FG repeats of NPC-channel nucleoporins.

However, and in contrast to *ct*Syo1 alone, the reconstituted *ct*Syo1-*ct*Rpl11, *ct*Syo1-*ct*Rpl5, and *ct*Syo1-*ct*Rpl5-*ct*Rpl11 complexes were inefficiently imported into the nucleus in the absence of cytosol and energy (Fig. 3C and fig. S10B). Consistent with this observation, the *ct*Syo1-*ct*Rpl11 and *ct*Syo1-*ct*Rpl5-*ct*Rpl11 complexes, and to a lesser extent the *ct*Syo1-*ct*Rpl5 complex, exhibited reduced binding to FG repeats (Fig. 3B and fig. S10C), suggesting that recruitment of Rpl5/Rpl11 masks or alters the FG-binding site(s) on Syo1. Notably, nuclear import of the *ct*Syo1-*ct*Rpl5-*ct*Rpl11 complex was markedly stimulated by addition of cytosol and energy (Fig. 3C), but did not occur at 4°C or in the presence of WGA or the guanosine triphosphatase (GTPase)–deficient Ran(Q69L) mutant (*28*) (Fig. 3, D and E). Thus, we conclude that a RanGTP-dependent importin-β transport receptor mediates nuclear import of the Syo1-Rpl5-Rpl11 complex. Moreover, Syo1, released from Rpl5 and Rpl11 after nuclear import, could shuttle back to the cytoplasm on its own. In support of this possibility, Syo1 alone traverses the NPC in both directions in permeabilized HeLa cells (Fig. 3 and fig. S9), and Syo1-GFP (green fluorescent protein) is located both in the nucleus and cytoplasm in yeast cells (fig. S12, C and D).

To identify the import receptor of the Syo1-Rpl5-Rpl11 complex, we took advantage of the observation that low amounts of Kap104 were sometimes coenriched when Syo1 was affinity-purified from yeast (fig. S11A). Kap104 is a member of the conserved karyopherin-β2/transportin receptor subfamily (*9*), which recognizes a non-classical NLS of the hydrophobic or basic proline-tyrosine (PY)–NLS type with the C-terminal consensus signature R/K/H-X_{2-5}-P-Y/L (*29*, *30*) (fig. S11B). Notably, Syo1 contains a conserved putative basic PY-NLS at its N terminus. In vitro binding assays revealed that this PY-NLS is necessary and sufficient for the interaction of Syo1 with Kap104 (fig. S11C and fig. S12A). Moreover, the PY-NLS can target an attached GFP reporter into the nucleus in vivo and is required for the in vivo function of Syo1 and nuclear

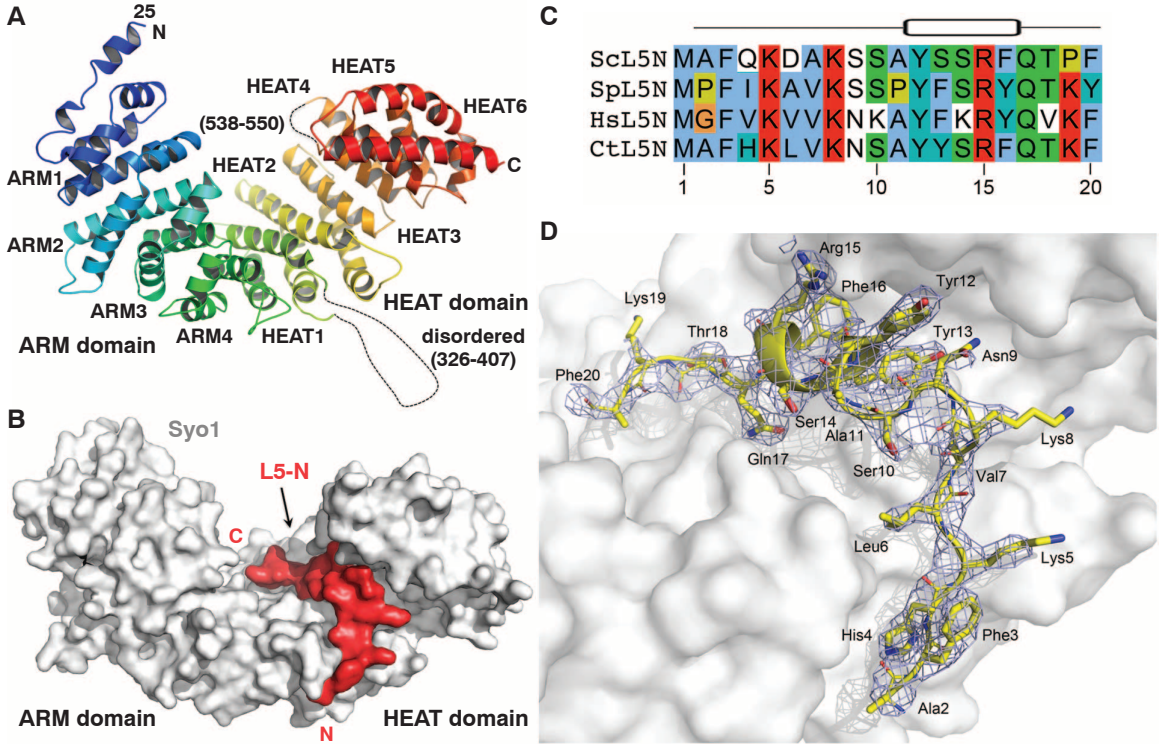

Fig. 2. Syo1 is structurally related to importins and binds the N-terminal residues of Rpl5 in an extended groove. (**A**) Crystal structure of *ct*Syo1 (residues 25 to 675). Cartoon representation showing that *ct*Syo1 is an extended α-solenoid, which consists of four complete ARM repeats (residues 65 to 260) followed by six HEAT repeats (residues 274 to 675). The ARM and HEAT repeats are indicated and "rainbow" colored from the N to the C terminus. Dashed lines indicate disordered regions. (**B**) Surface representation of the *ct*Syo1/*ct*L5-N complex. Residues 2 to 20 of *ct*Rpl5 (L5-N, red) are accommodated in an extensive groove of *ct*Syo1 (gray). (**C**) Multiple sequence alignment of residues 2 to 20 of L5-N from *S. cerevisiae* (Sc), *Schizosaccharomyces pombe* (Sp), *Homo sapiens* (Hs), and *C. thermophilum* (Ct). Single-letter abbreviations for the amino acid residues are as follows: A, Ala; D, Asp; F, Phe; G, Gly; H, His; I, Ile; K, Lys; L, Leu; M, Met; N, Asn; P, Pro; Q, Gln; R, Arg; S, Ser; T, Thr; V, Val; and Y, Tyr. (**D**) Enlargement of the *ct*L5-N/*ct*Syo1 interaction. The $2F_{obs} - F_{calc}$ electron density of *ct*L5-N at 1.3σ after final refinement is shown.

localization of Syo1-GFP (fig. S11D and fig. S12, B and C). Consistent with the proposal that Kap104 is the predominant import receptor of Syo1, we could not observe nuclear accumulation of Syo1-GFP in temperature-sensitive *kap104-16* mutant cells (*31*) (fig. S12D).

To test the model of Kap104 as the principal transport receptor for a trimeric import complex comprising Syo1-Rpl5-Rpl11, we reconstituted the

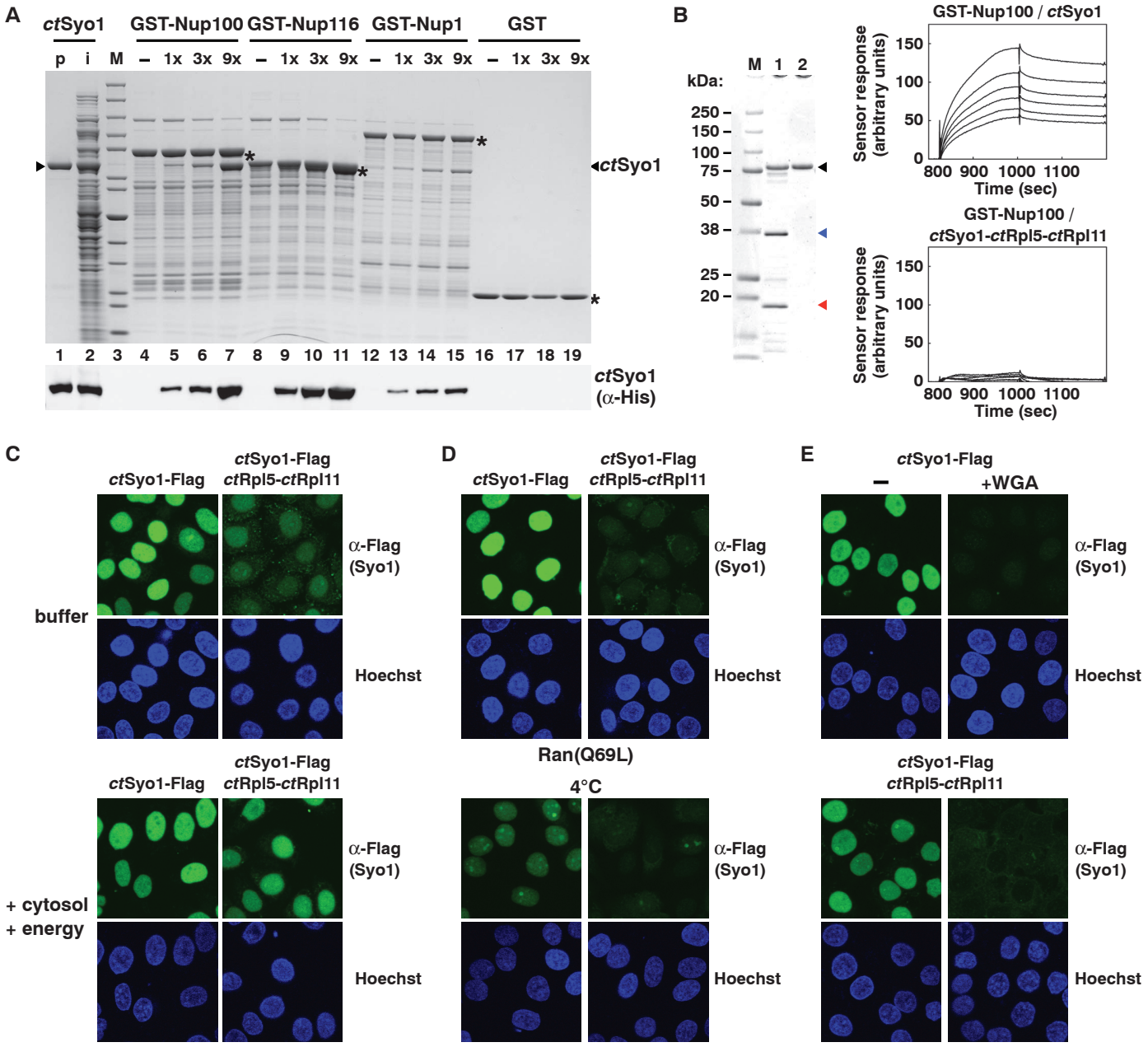

Fig. 3. The Syo1-Rpl5-Rpl11 complex is actively imported into the nucleus. (**A** and **B**) *ct*Syo1 interacts with FG repeats of nucleoporins. (A) Binding of recombinant *ct*Syo1 to immobilized FG-repeat domains of nucleoporins (GST-Nup) in the presence of competitor *E. coli* lysate. Lane 1, purified *ct*Syo1 (p); lane 2, *ct*Syo1 mixed with *E. coli* lysate (input, i); lane 3, molecular weight standard (M), same as in Fig. 1B; lanes 4 to 19, proteins bound to the indicated glutathione *S*-transferase (GST)–Nups or the GST control in the absence (–) or presence of increasing amounts of *ct*Syo1 (1×, 3×, 9×). Bound proteins were analyzed by SDS-PAGE and Coomassie staining (upper panel) or Western analysis (lower panel) with anti-penta-His antibody (*ct*Syo1). (B) BIAcore analysis of the interaction between the FG-repeat domain of Nup100 and *ct*Syo1 or the trimeric *ct*Syo1-*ct*Rpl5-*ct*Rpl11 complex. Protein input for BIAcore measurement (left panel); *ct*Syo1-Flag-$(His)_6$ (lane 2) and *ct*Syo1-Flag/*ct*Rpl5/*ct*Rpl11-$(His)_6$ (lane 1) were purified by nickel–ion affinity chromatography and analyzed by SDS-PAGE and Coomassie staining. Black, blue, and red arrowheads indicate *ct*Syo1-Flag/*ct*Syo1-Flag-$(His)_6$, *ct*Rpl5, and *ct*Rpl11-$(His)_6$, respectively. M, molecular weight standard. GST-Nup100 was immobilized and different concentrations (0.09 to 0.48 μM) of purified *ct*Syo1-Flag-$(His)_6$ (upper right panel) or *ct*Syo1-Flag/*ct*Rpl5/*ct*Rpl11-$(His)_6$ (lower right panel) were injected over the sensor chip, and sensor responses (arbitrary units) were recorded. (**C** to **E**) In vitro nuclear import assays. HeLa cells were permeabilized by digitonin and incubated with purified *ct*Syo1 or *ct*Syo1-*ct*Rpl5-*ct*Rpl11 complex in transport buffer [(C), upper panel], transport buffer containing either cytosol/energy (guanosine triphosphate/adenosine triphosphate) at 30°C [(C), lower panel] or 4°C [(D), lower panel], or cytosol/energy/Ran(Q69L) [(D), upper panel]. Permeabilized HeLa cells were first treated with transport buffer containing cytosol/energy in the absence or presence of WGA before performing the import reactions (E). Nuclear translocation of *ct*Syo1 or the trimeric complex was revealed by indirect immunofluorescence against Flag-tagged *ct*Syo1. Nuclei were revealed by staining DNA with Hoechst.

interaction of Kap104 with this complex using recombinant proteins derived from either *C. thermophilum* or yeast (Fig. 4A and fig. S12E). Size-exclusion chromatography revealed formation of a stable *ct*Kap104-*ct*Syo1-*ct*Rpl5-*ct*Rpl11 import complex (Fig. 4A) with a 1:1:1:1 stoichiometry of the four components, as determined by static light scattering and refractive index measurements (table S1). Addition of RanGTP was sufficient to release the trimeric *ct*Syo1-*ct*Rpl5-*ct*Rpl11 cargo complex from *ct*Kap104 (Fig. 4B). These findings indicate that Syo1 can serve as the import adaptor for Rpl5-Rpl11 with Kap104 as the cognate import receptor for the heterotrimer. Given that Syo1 is not an essential protein, it is apparent that alternative import routes for Rpl5 and Rpl11 must exist, which could involve other transport receptors or diffusion across the NPC.

After nuclear transport and RanGTP-mediated release of Syo1-Rpl5-Rpl11 from Kap104, the complex could be transferred onto the newly synthesized 5*S* rRNA in the nucleus. To test the possibility of a direct transfer in vitro, we produced *C. thermophilum* 5*S* rRNA by in vitro transcription and added it to the preformed *ct*Syo1-*ct*Rpl5-*ct*Rpl11 complex (Fig. 4, C and D). This binding assay revealed that 5*S* rRNA was efficiently bound to *ct*Syo1-*ct*Rpl5-*ct*Rpl11, as evidenced by a strict coelution of heterotrimer and rRNA on the gel filtration column (Fig. 4D). In contrast, 5*S* rRNA alone eluted in later fractions from this column. Thus, 5*S* rRNA can directly bind to the Syo1-Rpl5-Rpl11 complex. Removal of Syo1 from the 5*S* rRNP likely occurs at a subsequent maturation step, possibly during incorporation of the 5*S* RNP into preribosomal particles, which may require also other factors, such as Rpf2 and Rrs1 (*18*).

Our study has uncovered a mechanism that allows simultaneous nuclear import of more than one cargo, coupling nucleocytoplasmic transport

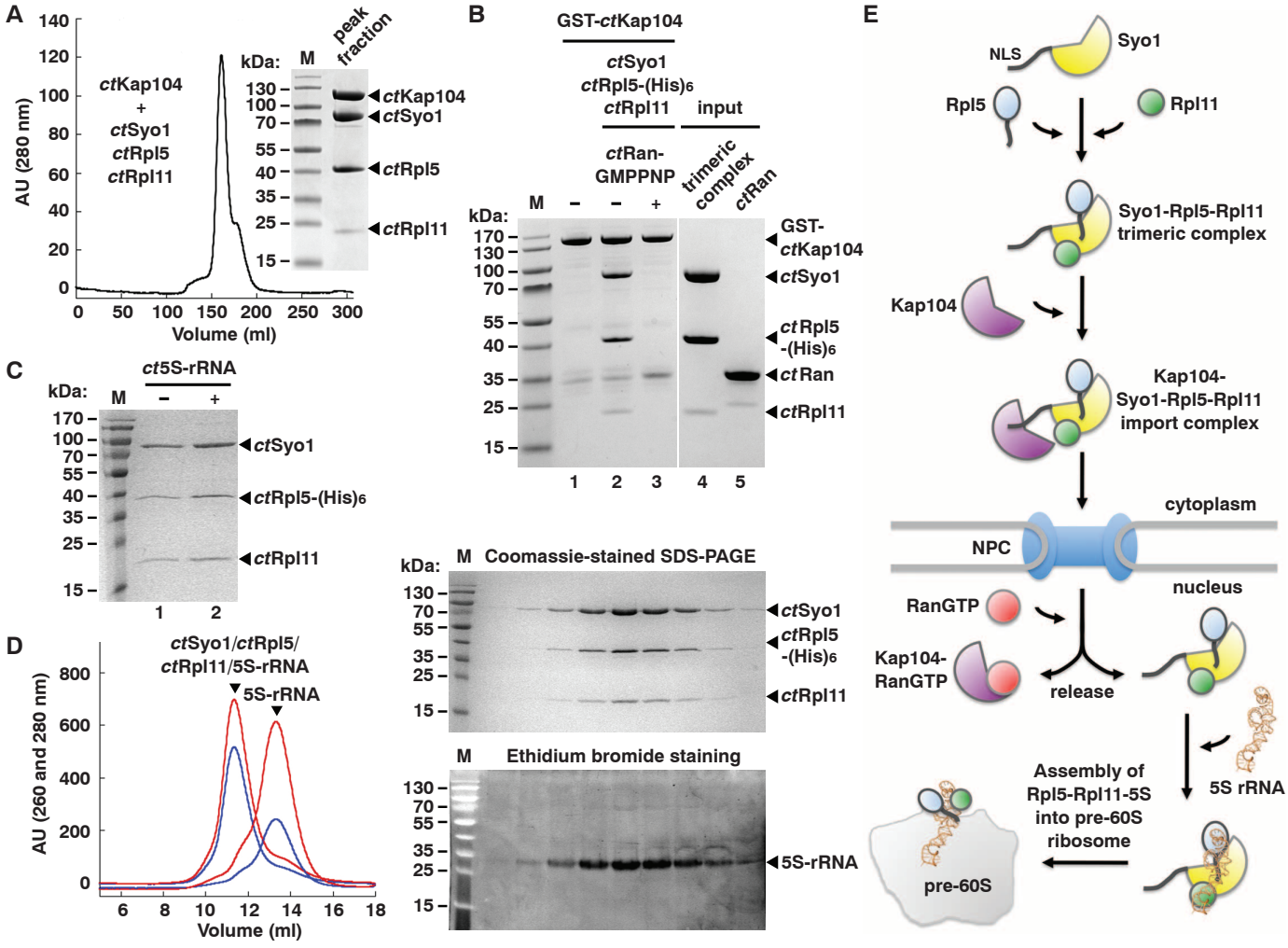

Fig. 4. The Syo1-Rpl5-Rpl11 complex is imported into the nucleus via Kap104 and binds to the 5*S* rRNA. (**A**) Size exclusion chromatography of the reconstituted *ct*Kap104-*ct*Syo1-*ct*Rpl5-*ct*Rpl11 heterotetrameric import complex. The peak fraction was analyzed by SDS-PAGE and Coomassie staining. (**B**) RanGMPPNP promotes release of the *ct*Syo1-*ct*Rpl5-*ct*Rpl11 complex from *ct*Kap104. The trimeric *ct*Syo1-*ct*Rpl5-*ct*Rpl11 complex (lane 4) was bound to immobilized GST-ctKap104 (lane 1) and incubated in the absence (lane 2) or presence (lane 3) of RanGMPPNP (lane 5). Input and bound proteins were revealed by SDS-PAGE and Coomassie staining. M, molecular weight standard. (**C**) Coomassie-stained SDS-PAGE of an in vitro binding assay of *ct*Syo1-*ct*Rpl5-*ct*Rpl11 in the absence or presence of *ct*5S rRNA. The presence of 5*S* rRNA did not lead to disassembly of the *ct*Syo1-*ct*Rpl5-*ct*Rpl11 complex. (**D**) The *ct*5S rRNA and *ct*Syo1-*ct*Rpl5-*ct*Rpl11 form a stable complex on size exclusion chromatography. Size exclusion chromatogram for free *ct*5S rRNA and the *ct*5S rRNA-*ct*Syo1-*ct*Rpl5-*ct*Rpl11 complex at two different wavelengths [i.e., 260 nm (red) and 280 nm (blue), upper panel]. SDS-PAGE of the peak fractions stained with Coomassie (middle panel) and ethidium bromide (lower panel) to detect the proteins and the 5*S* rRNA, respectively, present in the *ct*5S rRNA-*ct*Syo1-*ct*Rpl5-*ct*Rpl11 complex. (**E**) The transport adaptor Syo1 synchronizes nuclear import of Rpl5 and Rpl11. Syo1 simultaneously interacts with Rpl5 and Rpl11 in the cytoplasm, thus enabling formation of a tetrameric Kap104-Syo1-Rpl5-Rpl11 import complex. RanGTP binding to Kap104 in the nucleus promotes release of the trimeric Syo1-Rpl5-Rpl11 complex, which recruits the 5*S* rRNA. Rpl5, Rpl11, and the 5*S* rRNA are then incorporated with the aid of assembly factors (not shown) into pre-60*S* ribosomes. See text for details.

to stoichiometric assembly of proteins into macromolecular machines. Key to this mechanism is a nuclear import adaptor, Syo1, that specifically recruits the two functionally and topologically linked r-proteins Rpl5 and Rpl11. It guarantees that this cargo pair remains bound together from the time of synthesis in the cytoplasm until delivery to the nascent 5*S* rRNA in the nucleus (see Fig. 4E). In the broader sense, synchronous nuclear transport of topologically linked and/or functionally related cargo may represent a general strategy to streamline downstream nuclear processes that depend on temporally or spatially controlled assembly steps.

References and Notes

1. F. M. Boisvert, S. van Koningsbruggen, J. Navascués, A. I. Lamond, *Nat. Rev. Mol. Cell Biol.* **8**, 574 (2007).
2. D. L. Lafontaine, D. Tollervey, *Nat. Rev. Mol. Cell Biol.* **2**, 514 (2001).
3. T. Pederson, R. Y. Tsai, *J. Cell Biol.* **184**, 771 (2009).
4. J. R. Warner, *Trends Biochem. Sci.* **24**, 437 (1999).
5. A. K. Henras *et al*., *Cell. Mol. Life Sci.* **65**, 2334 (2008).
6. D. Kressler, E. Hurt, J. Bassler, *Biochim. Biophys. Acta* **1803**, 673 (2010).
7. J. P. Staley, J. L. Woolford Jr., *Curr. Opin. Cell Biol.* **21**, 109 (2009).
8. H. Tschochner, E. Hurt, *Trends Cell Biol.* **13**, 255 (2003).
9. Y. M. Chook, K. E. Süel, *Biochim. Biophys. Acta* **1813**, 1593 (2011).
10. M. P. Rout, G. Blobel, J. D. Aitchison, *Cell* **89**, 715 (1997).
11. D. Görlich, U. Kutay, *Annu. Rev. Cell Dev. Biol.* **15**, 607 (1999).
12. M. Stewart, *Nat. Rev. Mol. Cell Biol.* **8**, 195 (2007).
13. A. Ben-Shem *et al*., *Science* **334**, 1524 (2011).
14. S. Ferreira-Cerca *et al*., *Mol. Cell* **28**, 446 (2007).
15. G. Pöll *et al*., *PLoS ONE* **4**, e8249 (2009).
16. M. Ciganda, N. Williams, *Wiley Interdiscip. Rev. RNA* **2**, 523 (2011).
17. M. Claussen, F. Rudt, T. Pieler, *J. Biol. Chem.* **274**, 33951 (1999).
18. J. Zhang *et al*., *Genes Dev.* **21**, 2580 (2007).
19. S. Amlacher *et al*., *Cell* **146**, 277 (2011).
20. M. A. Andrade, C. Petosa, S. I. O'Donoghue, C. W. Müller, P. Bork, *J. Mol. Biol.* **309**, 1 (2001).
21. D. Xu, A. Farmer, Y. M. Chook, *Curr. Opin. Struct. Biol.* **20**, 782 (2010).
22. K. E. Süel, A. E. Cansizoglu, Y. M. Chook, *Methods* **39**, 342 (2006).
23. M. Marfori *et al*., *Biochim. Biophys. Acta* **1813**, 1562 (2011).
24. Y. Matsuura, M. Stewart, *EMBO J.* **24**, 3681 (2005).
25. R. Bayliss, T. Littlewood, L. A. Strawn, S. R. Wente, M. Stewart, *J. Biol. Chem.* **277**, 50597 (2002).
26. S. A. Adam, R. S. Marr, L. Gerace, *J. Cell Biol.* **111**, 807 (1990).
27. B. Bradatsch *et al*., *Mol. Cell* **27**, 767 (2007).
28. F. R. Bischoff, C. Klebe, J. Kretschmer, A. Wittinghofer, H. Ponstingl, *Proc. Natl. Acad. Sci. U.S.A.* **91**, 2587 (1994).
29. B. J. Lee *et al*., *Cell* **126**, 543 (2006).
30. K. E. Süel, H. Gu, Y. M. Chook, *PLoS Biol.* **6**, e137 (2008).
31. J. D. Aitchison, G. Blobel, M. P. Rout, *Science* **274**, 624 (1996).

Acknowledgments: We thank A. Hendricks and C. Déforel for technical assistance, J. Kopp and C. Siegmann from the BZH Cluster of Excellence:CellNetworks crystallization platform, J. Lechner and his team for mass spectrometry, T. Ruppert and M. Mayer (Zentrum für Molekulare Biologie Heidelberg) for access to the core facility for mass spectrometry for the HX-MS experiments, J. Woolford for sharing published *rpl5* mutant plasmids, and L. Dimitrova (Hurt laboratory) for providing the full-length *ct*KAP104 clone. Data collection was performed at the European Synchrotron Radiation Facility, Grenoble. This work was funded by the German Research Council (Hu363/9-4 to E.H. and SFB 638 to I.S.), the Swiss National Science Foundation (PP00P3_123341 to D.K.), and the Japan Society for the Promotion of Science (no. 21570195 and no. 21247032 to J.K. and Y.Y., respectively). I.S. and E.H. are investigators of the Cluster of Excellence:CellNetworks, and G.B. is a fellow of the Peter and Traudl Engelhorn Foundation. D.K., G.B., I.S., and E.H. conceived the experiments. D.K., G.B., J.K., I.S., and E.H. analyzed the data. D.K., G.B., I.S., and E.H. wrote the paper. D.K. and D.S. constructed yeast strains and carried out all yeast genetic experiments. D.K., G.B., and S.A. constructed plasmids. D.K. carried out tandem-affinity purifications of yeast proteins. G.B. and D.K. performed binding assays. G.B. determined crystal structures. G.S. carried out the HX-MS experiments. D.P. and D.S. performed fluorescence microscopy of live yeast cells. B.B. performed in vitro FG-repeat binding assays. Y.O. performed in vitro import assays with permeabilized HeLa cells under the supervision of J.K. in the laboratory of Y.Y. J.K. measured binding constants by BIAcore. D.K. and G.B. contributed equally to this study. All authors commented on the manuscript. Atomic coordinates and structure factors for the reported crystal structures have been deposited with the Protein Data Bank (PDB) under accession codes 4GMNO (*ct*Syo1) and 4GMN (*ct*Syo1/*ct*L5-N). The authors declare no competing financial interests. Correspondence and requests for materials should be addressed to D.K. (dieter.kressler@unifr.ch), I.S. (irmi.sinning@bzh.uni-heidelberg.de), or E.H. (ed.hurt@bzh.uni-heidelberg.de).

Supplementary Materials

www.sciencemag.org/cgi/content/full/338/6107/666/DC1
Materials and Methods
Figs. S1 to S12
Tables S1 to S5
References (*32*–*50*)

4 July 2012; accepted 6 September 2012
10.1126/science.1226960

Gene Loops Enhance Transcriptional Directionality

Sue Mei Tan-Wong,[1]* Judith B. Zaugg,[2]* Jurgi Camblong,[1]* Zhenyu Xu,[3] David W. Zhang,[4] Hannah E. Mischo,[1] Aseem Z. Ansari,[4] Nicholas M. Luscombe,[2,5,6] Lars M. Steinmetz,[3]† Nick J. Proudfoot[1]†

Eukaryotic genomes are extensively transcribed, forming both messenger RNAs (mRNAs) and noncoding RNAs (ncRNAs). ncRNAs made by RNA polymerase II often initiate from bidirectional promoters (nucleosome-depleted chromatin) that synthesize mRNA and ncRNA in opposite directions. We demonstrate that, by adopting a gene-loop conformation, actively transcribed mRNA encoding genes restrict divergent transcription of ncRNAs. Because gene-loop formation depends on a protein factor (Ssu72) that coassociates with both the promoter and the terminator, the inactivation of Ssu72 leads to increased synthesis of promoter-associated divergent ncRNAs, referred to as Ssu72-restricted transcripts (SRTs). Similarly, inactivation of individual gene loops by gene mutation enhances SRT synthesis. We demonstrate that gene-loop conformation enforces transcriptional directionality on otherwise bidirectional promoters.

Eukaryotic genomes are ubiquitously transcribed, generating an extensive network of noncoding RNAs (ncRNAs) (*1*, *2*). Most ncRNAs are made by RNA polymerase II (Pol II), which can initiate transcription nonspecifically and bidirectionally on nucleosome-depleted chromatin (*3*–*5*). Although this promiscuous transcription is partly restricted by rapid transcript degradation (*6*, *7*), we demonstrate that actively transcribed genes adopt a gene-loop conformation that reduces aberrant transcription by focusing Pol II into productive mRNA synthesis (see the supplementary materials and methods). Gene-loop formation depends on both promoter-associated transcription factors and polyadenylation complex (pAC) factors (*8*–*11*) such as Ssu72, localized at the 5′ and 3′ ends of genes (*12*, *13*). On the basis of quantitative 3C analysis, we initially confirmed that mutation of Ssu72 (*ssu72-2*) prevents gene-loop formation across *FMP27* (Fig. 1A). We also detected an increase in promoter-associated antisense ncRNA and increased Pol II density over the *FMP27* promoter region in *ssu72-2* (Fig. 1, B and C). Furthermore, we observed unanticipated genetic interactions between either Ssu72- or pAC-associated Pta1 and the nuclear exosome component Rrp6, which is responsible for the degradation of many ncRNAs, especially cryptic unstable transcripts (CUTs) (fig. S1) (*6*, *7*). Taken together, our initial results indicate that the loss of gene-loop formation by inactivation of Ssu72 results in the production of

[1]Sir William Dunn School of Pathology, University of Oxford, South Parks Road, Oxford OX1 3RE, UK. [2]European Molecular Biology Laboratory, European Bioinformatics Institute, Cambridge CB10 1SD, UK. [3]Genome Biology Unit, European Molecular Biology Laboratory, Meyerhofstrasse 1, 69117 Heidelberg, Germany. [4]Department of Biochemistry, University of Wisconsin–Madison, 433 Babcock Drive, Madison, WI 53706, USA. [5]University College London Genetics Institute, Gower Street, London WC1E 6BT, UK. [6]Cancer Research UK London Research Institute, 44 Lincoln's Inn Fields, London WC2A 3LY, UK.

*These authors contributed equally to this work.
†To whom correspondence should be addressed. E-mail: larsms@embl.de (L.M.S.); nicholas.proudfoot@path.ox.ac.uk (N.J.P.)

aberrant ncRNAs that are stabilized in *Δrrp6* mutant cells.

We next compared the effect of mutating *RRP6* and *SSU72* alone or together on the genomic profile of coding and ncRNAs. Total RNA from wild-type (WT), *ssu72-2*, *Δrrp6*, and double *ssu72-2Δrrp6* strains grown at 32°C (semipermissive conditions) was hybridized to strand-specific *Saccharomyces cerevisiae* tiling arrays. The profiles obtained confirmed that loss of Rrp6 causes accumulation of CUTs, especially from bidirectional promoters (*7*). However, *ssu72-2* mutation alone or in combination with *Δrrp6* gave rise to many additional ncRNAs (Fig. 2A).

Ssu72 is involved in the transcription termination of small nucleolar RNAs, as is clearly revealed by the widespread appearances of extended transcripts for these genes in *ssu72-2* (fig. S2A, I) (*14*). The profiles also unveil a role of Ssu72 in transcriptional termination of CUTs, as many show 3′ extensions in the *ssu72-2Δrrp6* double mutant compared with *Δrrp6* (fig. S2A, II). Ssu72 inactivation also leads to increased initiation of new cryptic transcripts. Like CUTs, Ssu72-restricted transcripts (SRTs) often run in a divergent orientation from bidirectional promoters. We detected some SRTs in the single *ssu72-2* mutant strain and others only in combination with *RRP6* deletion (Fig. 2A). The array data demonstrated the presence of 605 SRTs in addition to the expected 1982 CUTs (Fig. 2B), as validated in specific cases (fig. S2B).

CUT and SRT initiation is associated with mRNA transcription start sites (TSSs) (Fig. 2B) (*6*, *7*). To focus on promoter-associated ncRNAs (pncRNAs), we selected CUTs and SRTs that are positioned between tandem open reading frames (ORFs) (hereafter referred to as pCUTs and pSRTs). 678 pCUTs and 135 pSRTs initiate antisense transcription between tandem ORFs. Promoters that generate a divergent pncRNA tend to express more mRNA (down ORF) (Fig. 2C). In contrast, we found no correlation in mRNA expression level (up ORF) with downstream-positioned ncRNAs. We further showed that SRT expression is not due to loss of nuclear pre-mRNA down-regulation–dependent CUT termination or differential RNA stability effects (fig. S3, A and B). Finally, a genome-wide Pol II occupancy profile of the *ssu72-2* mutant (*12*) revealed a distinct peak upstream of the TSS, which is absent in the wild type (Fig. 2D), as well as a higher Pol II occupancy over SRT transcript regions in the mutant compared with the wild type (fig. S3C). Overall these results established that the loss of Ssu72 promotes de novo initiation of pSRTs.

Publicly available genome-wide data revealed that pSRT-associated promoters are especially depleted of histone H4 acetylation (*15*), implying a more repressed transcriptional state also shown in four selected pSRT-producing promoters (Fig. 3A). Loss of Ssu72 seems to relax this repressed chromatin structure by promoting histone acetylation and consequent pSRT expression. A genome-wide analysis of *S. cerevisiae* nascent transcripts reported a potentially similar connection between ncRNA levels and histone deacetylation (*16*). Loss of histone deacetylase Rco1 (in Rpd3S complex) known to contribute to H4 deacetylation in gene 3′ regions also increased antisense transcription, suggesting its potential role in promoter directionality. However, antisense transcripts may derive from antisense initiation at gene 3′ ends (*17*). We compared pSRTs to antisense ncRNA induced in *Δrco1* [*Rco1*-restricted transcripts (RRTs)] by generating transcriptome profiles for *Δrco1 and Δrco1Δrrp6* matching our *ssu72-2* profiles. To distinguish between transcripts arising from gene 5′ or 3′ ends, we selected tandem genes separated by either more or less than 400 base pairs (bp) (fig. S4A). We showed that RRT expression (in regions where pSRTs are also detected) in *Δrco1Δrrp6* versus *Δrrp6* is clearly greater in close tandem gene configurations than in distant ones, which indicates that RRTs are produced from gene terminator regions. We therefore performed a metagene analysis on tandem gene pairs more than 400 bp apart that have a pncRNA arising between them. SRTs peak near the TSS, whereas RRTs align with the transcription termination site (TTS) (Fig. 3B) also validated for specific tandem and divergent gene pairs (fig. S4B). The terminator association of RRTs fits with the known gene 3′ end association of Rpd3S (*18*, *19*). Collectively we show that, contrary to previous interpretation (*16*), antisense RRTs are terminator-derived, whereas SRTs are promoter-derived. Ssu72 thus enforces promoter directionality. We also detected a small but significant trend of decreased expression in *ssu72-2* for tandem genes that generate pSRTs (fig. S5), which suggests that the loss of promoter directionality results in decreased genic transcription. Because Ssu72 is required for gene-loop formation, we tested whether other gene-loop–associated factors similarly act to restrict pncRNA synthesis. Inactivation of TFIIB (Sua7) or other pAC components (Pta1, Rna14, and Rna15) has been shown to restrict gene-loop formation (*10*, *11*). Similarly we show that their inactivation caused an increase in pncRNA in a range of *S. cerevisiae* genes (fig. S6).

Because gene loops require both an active promoter and functional polyA signals (PASs) (*20*), we tested the effect of terminating transcription on pSRT formation by directly replacing the PAS with an Rnt1 cleavage signal (RCS) that promotes efficient termination but not mRNA polyadenylation (*21*). Plasmid constructs containing *CYC1* with transcription initiated on a *GAL1* promoter and terminated by either a PAS or a RCS were transformed into *Δrrp6* strain. After galactose induction, chromatin was subjected to 3C analysis (Fig. 4A, I). A clear peak of interaction between the promoter and a PAS (but not a RCS) was evident, confirming that RCS-mediated Pol II termination prevents gene looping. Next, we measured transcript levels of *CYC1* mRNA and pncRNA in transformed *Δrrp6* strains (Fig. 4A, II and III). The *GAL1* promoter–associated pncRNA was enhanced in level when the *CYC1* PAS was converted into a RCS due to loss of the PAS-dependent gene loop. In a genomic context, conversion of the *MSN5* (which generates a pSRT) (Fig. 2A and fig. S2B) PAS into a RCS showed loss of gene looping and a threefold increase in pSRT production, mimicking the effect

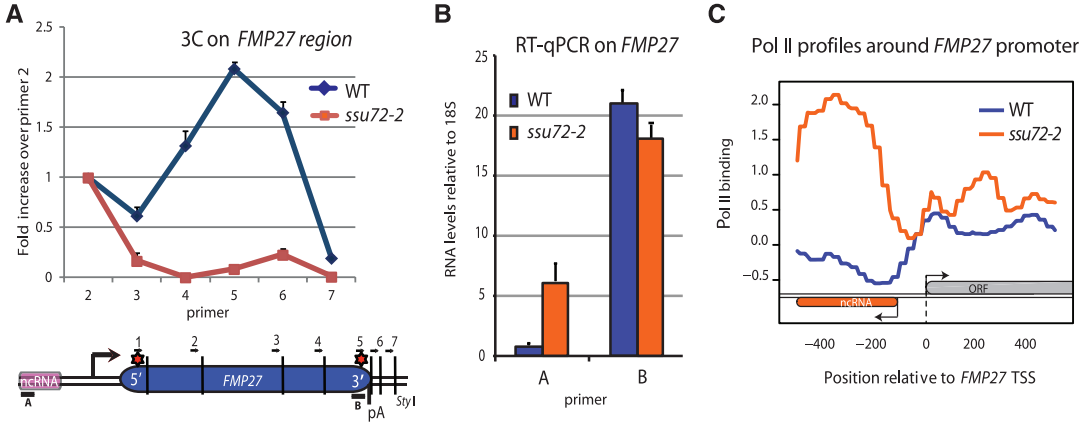

Fig. 1. Ssu72 inactivation abrogates FMP27 gene loop and enhances antisense transcription. (**A**) Graphical representation of 3C interaction levels in *ssu72-2* versus the wild type across *FMP27*. Red stars show significant 3C interaction. The positions of 3C primers are indicated, as are reverse transcription quantitative polymerase chain reaction (RT-qPCR) amplicons. For 3C analysis, primer 1 (anchor) was combined sequentially with downstream primers 2 to 7. Error bars represent SEM. (**B**) RT-qPCR analysis of *FMP27* mRNA and ncRNA in *ssu72-2* versus the wild type. Error bar represent SEM. (**C**) Pol II profile (ChIP-seq) across the *FMP27* promoter region (*12*) in *ssu72-2* versus the wild type.

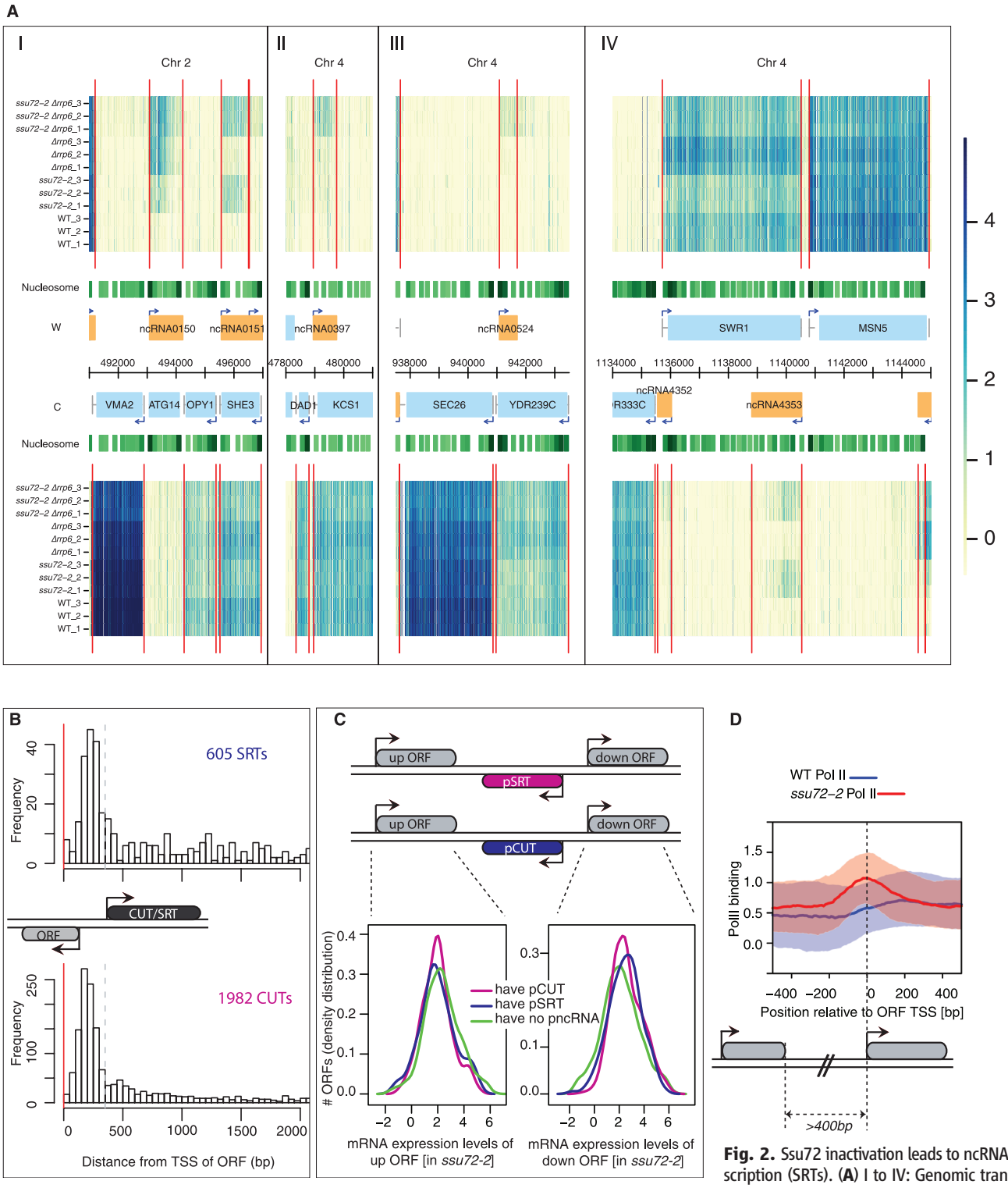

Fig. 2. Ssu72 inactivation leads to ncRNA transcription (SRTs). (**A**) I to IV: Genomic transcription across 28 kilobases of chromosomes 2 and 4 (*x* axis) for the Watson (W, top) and the Crick (C, bottom) strands. For the whole genome, see http://steinmetzlab.embl.de/proudfoot_lab/index.html. Normalized signal intensities are shown for profiled samples (*y* axis). Triplicate data are shown for the wild type (1 to 3), *ssu72-2* (1 to 3), *Δrrp6* (1 to 3), and *ssu72-2Δrrp6* (1 to 3) strains. Red vertical lines represent inferred transcript boundaries. Nucleosome positions [green tracks (darker for higher occupancy) (*25*) and genome annotations are shown in the center: annotated ORFs (blue boxes), ncRNAs (orange boxes), and TSSs (arrows)]. (I) ncRNA0151, (II) ncRNA0397, (III) ncRNA0524, and (IV) ncRNA4353 represent promoter-associated SRTs. (**B**) Distribution of relative distances of 605 SRTs (upper panel) versus 1982 CUTs (lower panel) to their nearest ORF TSS (red line). Dashed lines (350 bp) indicate the cut-off position used to define intergenic cryptic transcription—sharing ORF promoters. (**C**) Distributions of gene expression levels are shown for downstream (down) and upstream (up) ORFs of tandem genes [three categories: downstream promoter pSRT (blue), pCUT (purple), or no pncRNA (green)]. Downstream ORFs with pncRNAs are significantly higher expressed than those without ($P = 0.001$ [pSRT] and $P < 2.2 \times 10^{-16}$ [pCUTs]). No significant association was found for upstream ORFs. (**D**) Pol II profiles for *ssu72-2* (red) and the wild type (blue) around the ORF promoter in tandem genes that are more than 400 bp apart. Solid lines indicate median Pol II occupancy; shaded areas denote 25 to 75 percentiles. Pol II occupancy increases upstream of TSSs in *ssu72-2*.

of Ssu72 inactivation (Fig. 4B). Finally, an integrated β-globin gene construct with a SV40 late PAS or mutated version (*22*) in human embryonic kidney 293 cells displays a gene-loop conformation with the wild type, but not the mutant PAS construct. Similarly we observed a threefold increase in the levels of divergent pncRNA with the mutated PAS (Fig. 4C), indicating a similar effect in a mammalian system.

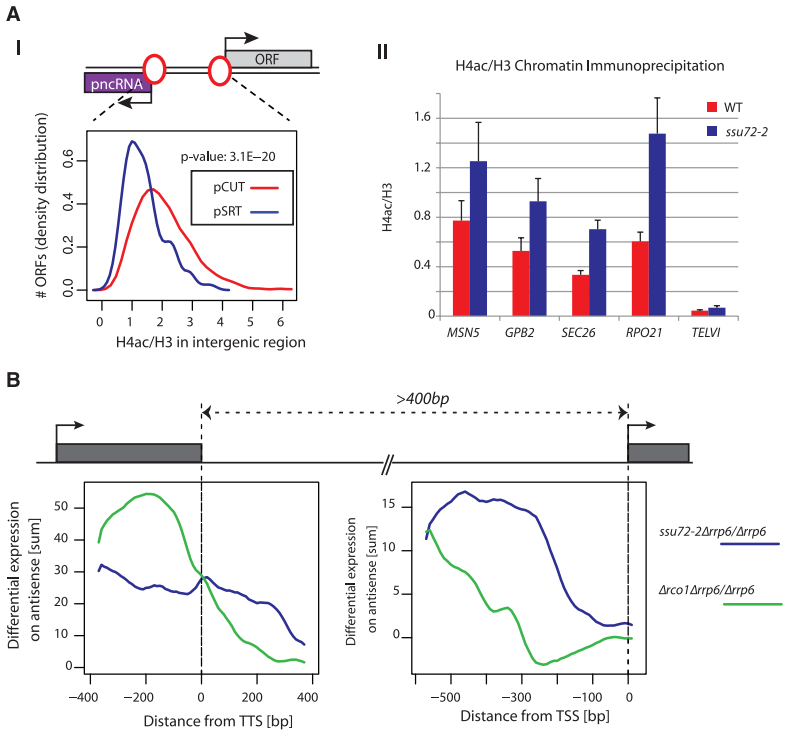

Fig. 3. pSRTs initiate from bidirectional promoters. (**A**) I: Histone H4 acetylation (as a ratio with H3) compared over the intergenic region between ORF TSSs and divergent pSRT (blue) or pCUT (red) TSSs in WT strains. Intergenic regions of pCUTs show higher H4 acetylation levels than those of pSRTs. II: Chromatin immunoprecipitation analysis across the promoter regions of the indicated loci with WT- and *ssu72-2*-derived chromatin using anti-H4ac. Ssu72 inactivation caused H4 acetylation increase at all four loci. Telomeric region (*TELV1*) was used as a negative control. Error bars represent SEM. (**B**) Metagene analysis of Δ*rco1*Δ*rrp6* versus Δ*rrp6* (green) and *ssu72-2*Δ*rrp6* versus Δ*rrp6* (blue) differential expression levels for all antisense ncRNAs that initiate between tandem genes in relative position to the upstream gene TTSs and downstream gene TSSs.

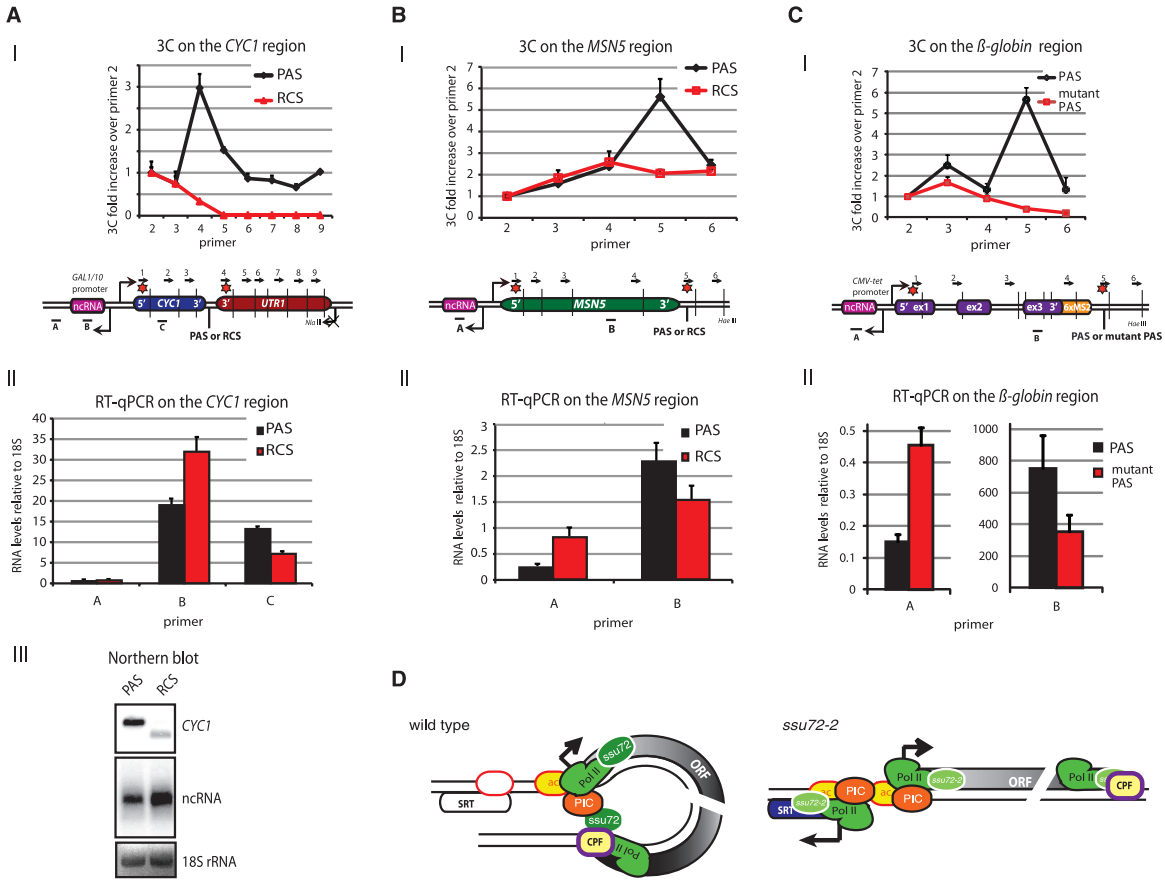

Fig. 4. Gene-loop disruption by PAS mutation enhances divergent transcription. (**A** to **C**) I: Graphical representation of 3C interaction analyses for the *CYC1* plasmid (A), *MSN5* (B), and a mammalian β-globin gene construct (C), as in Fig. 1A. II: RT-qPCR analyses of mRNA versus pncRNAs. (A) III: Northern blot for *CYC1* transcripts. Note that the *CYC1* mRNA is smaller with RCS replacement, due to lack of a pA tail. Also, *UTR1* downstream of CYC1 is inactive due to promoter deletion, denoted by the crossed arrow in (A, I). Error bars represent SEM. (**D**) The gene loop defines the transcription unit and promotes transcription directionality. Loss of the gene loop in *ssu72-2* or with PAS mutation increases antisense pncRNA transcription. Gene loops involving Ssu72 (green ovals) may act to maintain nucleosome (yellow bubbles; ac denotes H4Ac) positions, preventing association of a second preinitiation complex (PIC) (red), leading to divergent transcription initiation.

Our results indicate that gene loops act to maintain the directionality of transcription. The loss of a mammalian gene's PAS can directly influence the recruitment of transcription factors, with a consequent reduction in gene expression (*22*). PAS mutation has also been shown to increase levels of divergent transcripts (*23*). On the basis of our results, such effects are directly explicable by the loss of gene-loop formation and the potential to recycle factors from the terminator back to the promoter (see model, Fig. 4D). The role of Rpd3S in restricting antisense terminator transcripts (Fig. 3) clearly illustrates the importance of histone deacetylation in preventing inappropriate ncRNA synthesis. We predict that gene loops may similarly act to influence the recruitment of 5′ localized histone deacetylases such as Set3 (*24*). This would maintain promoters in a deacetylated, inactive state until gene activation selectively promotes transcription of genes rather than divergent pSRTs. We postulate that gene looping contributes to determining which transcription units are fully productive.

References and Notes

1. J. S. Mattick, R. J. Taft, G. J. Faulkner, *Trends Genet.* **26**, 21 (2010).
2. P. Carninci, *Nature* **457**, 974 (2009).
3. L. J. Core, J. T. Lis, *Science* **319**, 1791 (2008).
4. P. Preker *et al.*, *Science* **322**, 1851 (2008).
5. A. C. Seila *et al.*, *Science* **322**, 1849 (2008).
6. H. Neil *et al.*, *Nature* **457**, 1038 (2009).
7. Z. Xu *et al.*, *Nature* **457**, 1033 (2009).
8. J. M. O'Sullivan *et al.*, *Nat. Genet.* **36**, 1014 (2004).
9. A. Ansari, M. Hampsey, *Genes Dev.* **19**, 2969 (2005).
10. B. N. Singh, M. Hampsey, *Mol. Cell* **27**, 806 (2007).
11. S. Medler *et al.*, *J. Biol. Chem.* **286**, 33709 (2011).
12. D. W. Zhang *et al.*, *J. Biol. Chem.* **287**, 8541 (2012).
13. D. L. Pappas Jr., M. Hampsey, *Mol. Cell. Biol.* **20**, 8343 (2000).
14. E. J. Steinmetz, D. A. Brow, *Mol. Cell. Biol.* **23**, 6339 (2003).
15. D. K. Pokholok *et al.*, *Cell* **122**, 517 (2005).
16. L. S. Churchman, J. S. Weissman, *Nature* **469**, 368 (2011).
17. S. C. Murray *et al.*, *Nucleic Acids Res.* **40**, 2432 (2012).
18. M. J. Carrozza *et al.*, *Cell* **123**, 581 (2005).
19. M. C. Keogh *et al.*, *Cell* **123**, 593 (2005).
20. K. J. Perkins, M. Lusic, I. Mitar, M. Giacca, N. J. Proudfoot, *Mol. Cell* **29**, 56 (2008).
21. A. G. Rondón, H. E. Mischo, J. Kawauchi, N. J. Proudfoot, *Mol. Cell* **36**, 88 (2009).
22. C. K. Mapendano, S. Lykke-Andersen, J. Kjems, E. Bertrand, T. H. Jensen, *Mol. Cell* **40**, 410 (2010).
23. P. Preker *et al.*, *Nucleic Acids Res.* **39**, 7179 (2011).
24. T. Kim, S. Buratowski, *Cell* **137**, 259 (2009).
25. T. N. Mavrich *et al.*, *Genome Res.* **18**, 1073 (2008).

Acknowledgments: We thank B. Dichtl and J. Kufel for strains and H. Wijayatilake for *FMP27* and β-*globin* 3C reagents. This work was supported by the Wellcome Trust (N.J.P.), the NIH and Deutsche Forschungsgemeinschaft (L.M.S.), European Molecular Biology Laboratory (J.B.Z., N.M.L., L.M.S.), and the Swiss National Fonds and European Molecular Biology Organization (J.C.). Genomic data are deposited at http://steinmetzlab.embl.de/proudfoot_lab/index.html (E-TABM-936).

Supplementary Materials

www.sciencemag.org/cgi/content/full/science.1224350/DC1
Materials and Methods
Figs. S1 to S6
Tables S1 to S8
References (*26*–*35*)

7 May 2012; accepted 14 September 2012
Published online 27 September 2012;
10.1126/science.1224350

Trade-Offs of Chemotactic Foraging in Turbulent Water

John R. Taylor[1] and Roman Stocker[2]*

Bacteria play an indispensable role in marine biogeochemistry by recycling dissolved organic matter. Motile species can exploit small, ephemeral solute patches through chemotaxis and thereby gain a fitness advantage over nonmotile competitors. This competition occurs in a turbulent environment, yet turbulence is generally considered inconsequential for bacterial uptake. In contrast, we show that turbulence affects uptake by stirring nutrient patches into networks of thin filaments that motile bacteria can readily exploit. We find that chemotactic motility is subject to a trade-off between the uptake benefit due to chemotaxis and the cost of locomotion, resulting in an optimal swimming speed. A second trade-off results from the competing effects of stirring and mixing and leads to the prediction that chemotaxis is optimally favored at intermediate turbulence intensities.

The average milliliter of seawater contains a million heterotrophic bacteria that play an essential role in remineralizing dissolved organic matter (DOM) by decomposing 35 to 80% of net primary production (*1*) and converting it into particulate form, available for consumption by larger organisms. Most marine environments are turbulent, ranging from the energetic mixed-layer and surf zone to calmer thermoclines, yet the effect of turbulence on bacterial uptake of DOM has remained elusive. This is due in part to the difficulty of quantifying the microscale biogeochemical variability generated by turbulence. At the same time, the physics of transport at micrometer scales dictates that DOM uptake occurs primarily by diffusion of nutrient molecules to cells (*2*). In a homogeneous nutrient environment, marine turbulence is insufficient to increase bacterial uptake (*2*, *3*), at least for low–molecular weight substrates. For example, relatively strong turbulence ($\epsilon = 10^{-6}$ W kg^{-1}, where ϵ is the turbulent dissipation rate) increases the uptake of amino acids by <1%, and as a result turbulence has been considered inconsequential for bacterial uptake (*2*).

Many DOM sources occur as small, discrete patches, including cell lysis, phytoplankton exudation, marine snow particles, oil droplets, and excretions by larger organisms (*4*, *5*). Numerous bacterial taxa have evolved the ability to sense chemical gradients associated with patches and swim toward more favorable conditions (*5*–*8*), a process called chemotaxis. Chemotaxis can affect marine biogeochemical cycles by increasing remineralization rates (*5*, *9*), and community composition by affording motile bacteria a benefit over nonmotile competitors (*7*). Yet, most knowledge of chemotactic foraging is based on studies in still fluid, simple flows, or synthetic advection (*7*, *10*, *11*).

Here, we show that turbulence can affect the relative uptake of DOM by motile and nonmotile bacteria by reshaping the nutrient landscape to which chemotactic bacteria respond. To study the trade-offs of chemotaxis in the turbulent ocean, we used direct numerical simulations (DNS) (*12*). This method has been applied extensively to model passive scalars in turbulence (*13*). We use it to resolve the smallest turbulent scales and quantify their impact on the nutrient competition between motile and nonmotile bacteria.

A range of spatial scales affect bacterial foraging in the ocean (Fig. 1). Bacteria experience turbulence as smooth, slowly varying velocity gradients, because their size (≈1 μm) is considerably smaller than the Kolmogorov scale, l_K (≈1 to 10 mm in the ocean) (*3*), the smallest scale at which turbulent velocity fluctuations occur. Gradients in nutrient concentration persist down to a smaller scale, the Batchelor scale l_B (≈10 to 300 μm in the ocean) (*14*). Motile bacteria can exploit nutrient gradients if their "motility range"—the distance they can cover over the lifetime of the patch—is larger than the Batchelor scale (Fig. 1). This is generally the case, because bacteria swim up gradients at 5 to 40 μm s^{-1} (*8*, *15*) and can thus travel a distance of l_B in a few seconds.

To determine the impact of turbulence on chemotactic foraging, we used DNS to simulate the competition between motile and nonmotile bacteria for a DOM patch occurring in a turbulent flow (*16*). The two bacterial species were

[1]Department of Applied Mathematics and Theoretical Physics, University of Cambridge, Wilberforce Road, Cambridge CB3 0WA, UK. [2]Ralph M. Parsons Laboratory, Department of Civil and Environmental Engineering, Massachusetts Institute of Technology, 77 Massachusetts Avenue, Cambridge, MA 02139, USA.

*To whom correspondence should be addressed. E-mail: romans@mit.edu

initially distributed uniformly, each with concentration $B_0 = 2.5 \times 10^{11}$ cells m^{-3}. Bacteria consume nutrients at a rate $1/\tau_U$, where $\tau_U \approx 200$ s is a typical uptake time scale (*16*). Nonmotile bacteria remain uniformly distributed and rely on diffusion to obtain nutrients. Motile bacteria swim up nutrient gradients with a chemotactic velocity that increases with the gradient's magnitude, up to a maximum velocity V_C (*16*). Using dissolved organic carbon as a representative nutrient, we assumed an initial peak concentration of $C_0 = 10\ \mu M_C$ to reflect the approximately three orders of magnitude concentration enhancement within patches compared to background levels (typically, 0.1 to 50 nM_C) (*17*). In this large difference lies the potential benefit of chemotaxis.

Turbulence affects uptake by reshaping the patch into a complex nutrient landscape (movie S1), dramatically changing the gradients experienced by chemotactic bacteria. Consider motile bacteria ($V_C = 20\ \mu m\ s^{-1}$) in relatively strong turbulence ($\epsilon = 10^{-6}$ W kg^{-1}) (Fig. 2 and movie S1). Within seconds, turbulence stirs the patch into filaments and sheets as thin as l_B (Fig. 2, top row), which the chemotactic bacteria quickly locate (Fig. 2, bottom row). Fifteen seconds after release of the patch, nutrient filaments are pervasive and harbor concentrations of motile bacteria 50% above background. At 30 s, the patch has morphed into a web of tangled filaments, whose topology is mirrored in the distribution of motile bacteria. After 60 s, the remaining nutrients are well-mixed (the standard deviation of the nutrient concentration is 3.5% of its initial value) and the clustering of motile bacteria begins to fade.

Accumulation of motile bacteria within nutrient-rich filaments increases their uptake rate compared with nonmotile bacteria (Fig. 3A). The difference in the population-averaged, per-cell uptake rate between motile and nonmotile bacteria (*16*) is a measure of the motility benefit. After rescaling

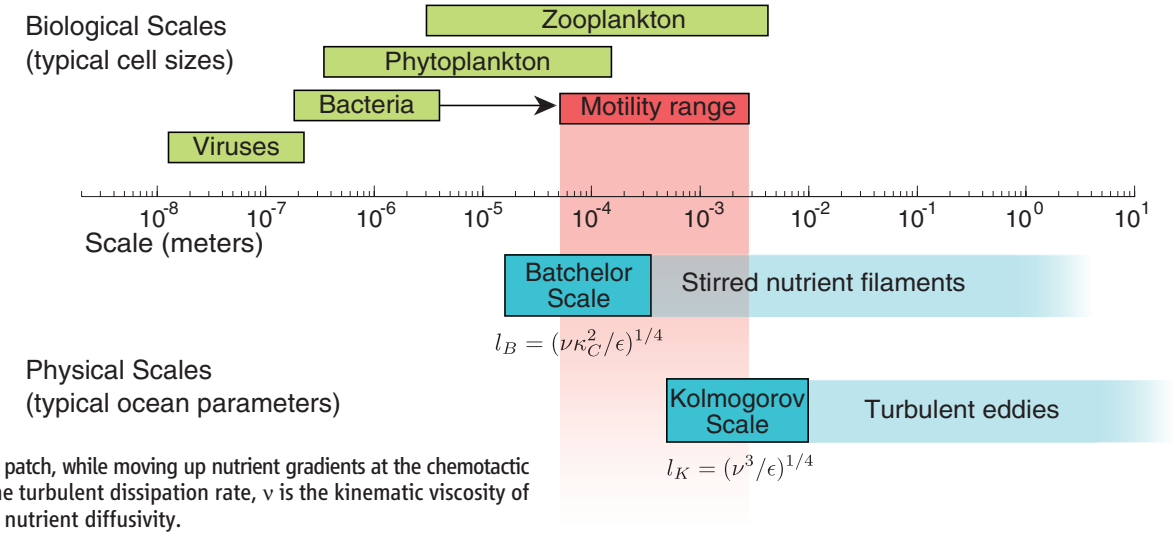

Fig. 1. Physical and biological length scales in the ocean. Turbulent stirring generates variance in the distribution of dissolved nutrients on scales as small as the Batchelor scale, l_B, but does not directly affect the diffusive flux of nutrients on the scales of bacterial cells. However, motile bacteria sample spatial scales considerably larger than their size: Their "motility range" is the distance that they can travel during the lifetime of a typical nutrient patch, while moving up nutrient gradients at the chemotactic velocity V_C. Here, ϵ is the turbulent dissipation rate, ν is the kinematic viscosity of seawater, and κ_C is the nutrient diffusivity.

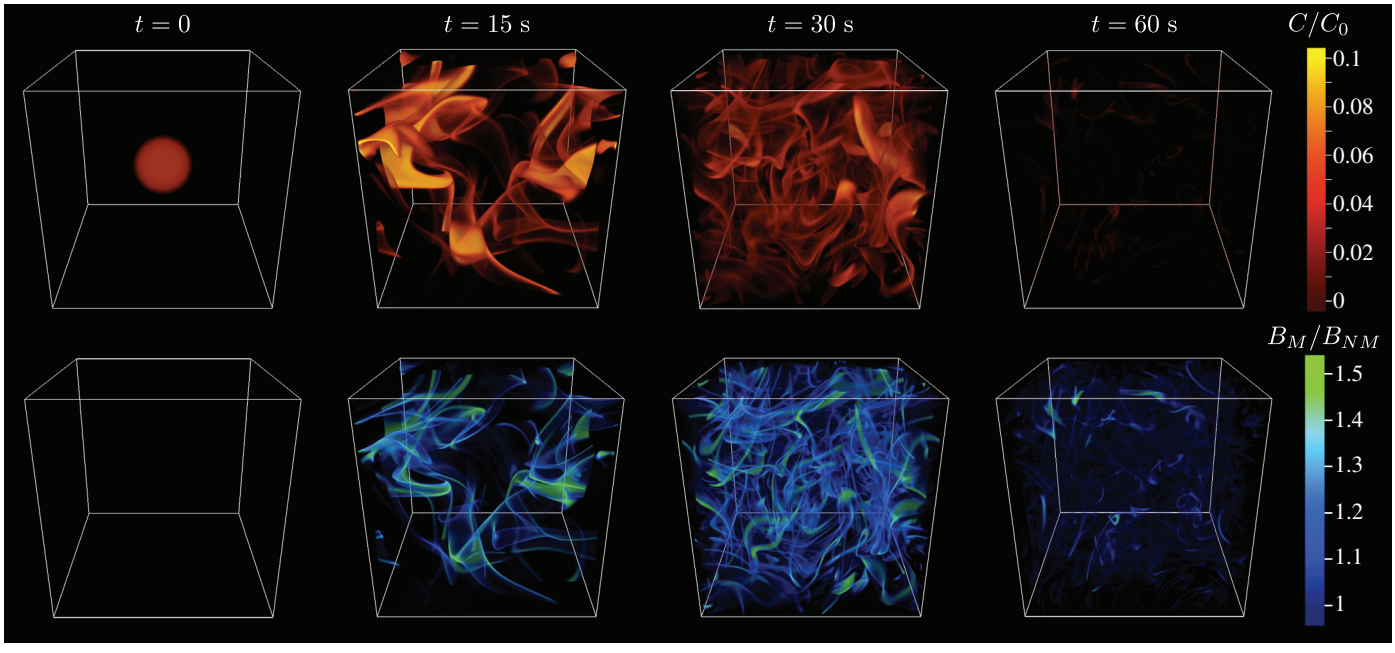

Fig. 2. Stirring of a nutrient patch and response of chemotactic bacteria. As a nutrient patch is stirred by a turbulent flow (top row, showing nutrient concentration C), chemotactic bacteria respond by accumulating within nutrient filaments (bottom row, showing concentration of motile bacteria B_M), thereby enhancing their uptake. For this simulation, the chemotactic velocity was $V_C = 20\ \mu m\ s^{-1}$, the turbulent dissipation rate $\epsilon = 10^{-6}$ W kg^{-1}, and the domain size $L = 5.65$ cm. Values of C and B_M are normalized by the initial maximum nutrient concentration, C_0, and the concentration of nonmotile bacteria, B_{NM}, respectively. The lowest value on each color scale is made transparent, and opacity increases linearly with concentration. Images generated using Vapor (www.vapor.ucar.edu).

by the number of patches occurring in the computational volume in a day, based on a carbon injection rate of $\dot{C}_{inj} = 0.12\ g_C\ m^{-3} day^{-1}$ (*16*), and by the carbon content in one cell (*16*), the motility benefit can be expressed in units of new cell equivalents produced by each bacterium per day. For the scenario shown in Fig. 2, the motility benefit peaks 13.2 s after injection of the patch. At this time, motile cells consume 23% more than nonmotile cells, an equivalent benefit of more than one new cell per day (per individual) if the uptake difference was sustained at this level (relative to 4.5 new cells per day produced by each cell of either species in the absence of chemotaxis). Instead, the motility benefit nearly vanishes after 50 s, even though 59% of the nutrient is still available, because what remains has been mixed, erasing any advantage of motility. The instantaneous motility benefit, like the nutrient filaments, is therefore highly transient.

To determine the chemotactic velocity that optimizes foraging, we performed competition simulations where we varied the maximum chemotactic velocity, V_C, while keeping the turbulence intensity constant at an intermediate level ($\epsilon = 1.2 \times 10^{-8}$ W kg^{-1}). The advantage afforded by chemotaxis depends strongly on V_C (Fig. 3, A and B). The motility benefit is weak throughout the patch lifetime for slow chemotaxers. For example, motility enhances the instantaneous uptake by at most 15%, affording a time-averaged benefit of 0.3 new cells per day, for $V_C = 5\ \mu m\ s^{-1}$. A chemotactic velocity of this order is typical of the enteric bacterium *Escherichia coli* ($V_C = 0.6$ to 13.8 μm s^{-1}) (*15*), the traditional model organism for the study of chemotaxis. In contrast, marine bacteria are capable of much higher swimming speeds (up to a few hundred μm s^{-1}) and high-performance chemotaxis (*6*, *7*, *18*). For chemotactic velocities of $V_C = 20$ to 60 μm s^{-1}, associated with swimming speeds of $V_S = 60$ to 170 μm s^{-1} (*16*), the motility benefit can be much larger, with motile cells instantaneously consuming up to 58 to 133% more than nonmotile cells and experiencing a time-averaged benefit of 1.1 to 2.3 additional new cells per day (Fig. 3, A and B).

Motility can be costly for marine bacteria. The motility benefit grows approximately linearly with chemotactic velocity (Fig. 3B), whereas propulsive power increases quadratically with the swimming speed (*16*). This suggests a trade-off between enhanced uptake and swimming cost, and the existence of an optimal chemotactic velocity. To test this prediction, we computed the

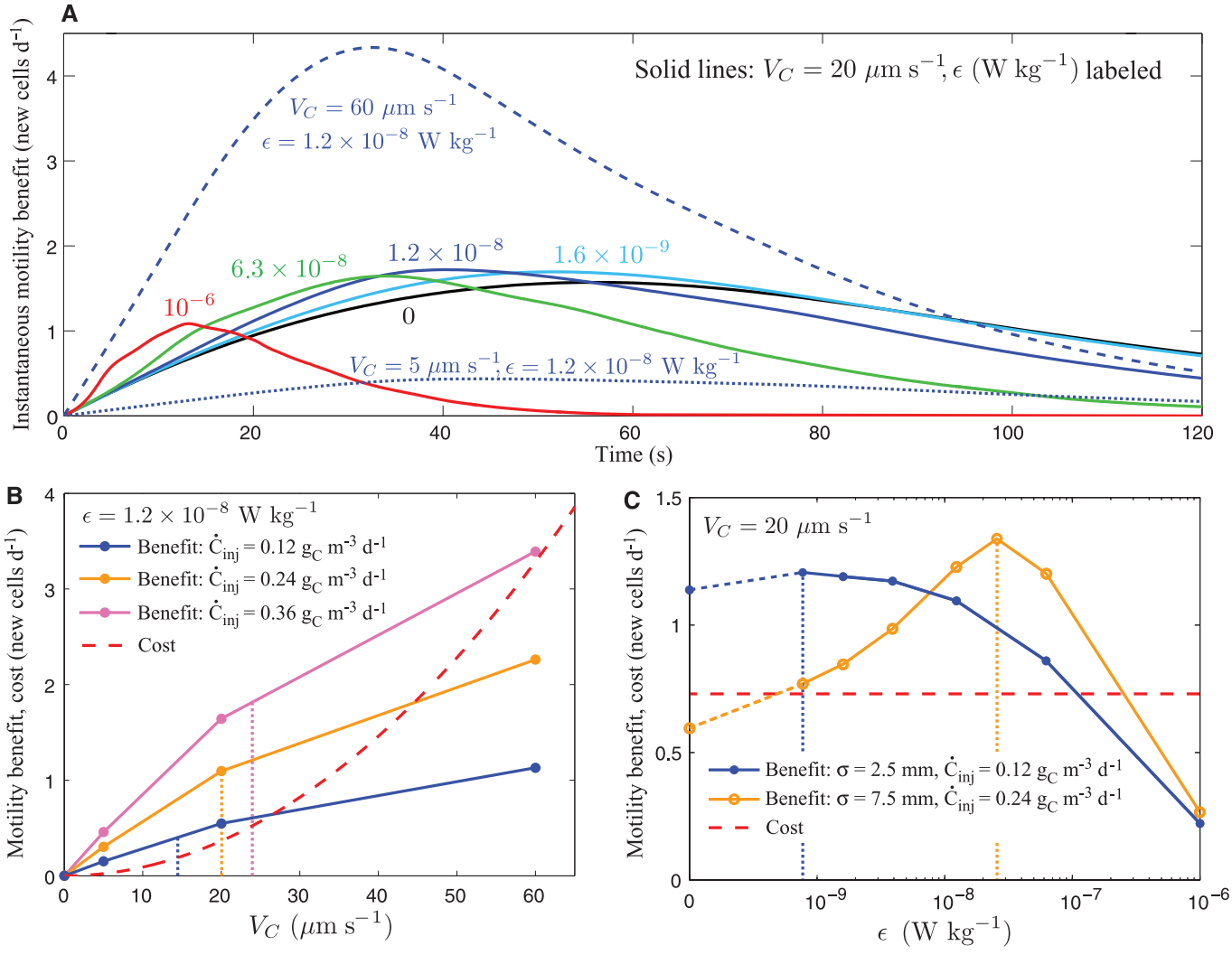

Fig. 3. Trade-offs of chemotactic foraging. (**A**) The instantaneous motility benefit as a function of time since release of the nutrient patch, for different turbulence intensities ϵ and chemotactic velocities V_C. (**B**) The motility benefit, shown for three carbon injection rates $\dot{C}_{inj}$ (solid lines), increases with the chemotactic velocity V_C, but the cost of swimming (dashed red line) increases more rapidly (quadratically) with V_C. The trade-off between motility benefit and swimming cost results in an optimal chemotactic velocity (dotted lines) of $V_C \approx 15$ to 25 μm s^{-1}. (**C**) The trade-off between stirring and mixing results in an optimal value of turbulence (dotted lines) that depends on the initial patch size, σ. For large patches, the motility benefit is optimal in moderate turbulence (orange line), whereas smaller patches lead to an optimum in weak turbulence (blue line). Values of the motility benefit in the absence of flow ($\epsilon = 0$) are connected with dashed lines (values of $\epsilon < 7.7 \times 10^{-10}$ W kg^{-1} were not considered owing to computational restrictions).

net motility benefit as the difference between the motility benefit and the power required for swimming (*16*). In intermediate turbulence ($\epsilon = 1.2 \times 10^{-8}$ W kg^{-1}), the net motility benefit is maximal for $V_C \approx 15$ to 25 μm s^{-1} (Fig. 3B), corresponding to swimming speeds V_S of 45 to 70 μm s^{-1} (*16*). These values are in good agreement with speeds recorded for several species of marine bacteria (*6*–*8*, *18*, *19*), suggesting that motility in marine bacteria might be under selection for chemotactic fitness.

The effectiveness of chemotaxis as a foraging strategy further depends on the intensity of turbulence through the stirring and mixing of nutrient patches. We quantified this dependence by varying the turbulence intensity, while keeping the chemotactic velocity constant ($V_C = 20$ μm s^{-1}). For an initial patch size of $\sigma = 2.5$ mm, chemotaxis is optimally favored at weak turbulence intensities ($\epsilon \approx 10^{-9}$ W kg^{-1}), characteristic of the ocean thermocline (*20*), where the motility benefit is slightly larger than in the absence of turbulence (Fig. 3C). In contrast, the motility benefit is fivefold smaller at $\epsilon = 10^{-6}$ W kg^{-1} (Fig. 3C), indicating that chemotaxis is less effective in highly turbulent regions, such as the upper ocean. For larger patches the optimum turbulence intensity shifts to intermediate values ($\epsilon \approx 10^{-8}$ to 10^{-7} W kg^{-1} for $\sigma = 7.5$ mm; Fig. 3C), characteristic of the upper thermocline (*20*). Although observations of motility in the ocean are insufficient to test these predictions, it will be interesting to determine whether changes in the prevalence of motility and chemotaxis with depth revealed by metagenomic studies (*21*) are in part determined by turbulence levels.

The existence of an optimal turbulence intensity points to a second, more subtle trade-off: that between stirring and mixing. Stirring increases the surface area between the nutrient patch and the surrounding water (Fig. 2). Mixing refers to homogenization of the nutrients, which is aided by stirring but ultimately occurs by molecular diffusion. Stronger turbulence produces thinner filaments and steeper nutrient gradients that elicit faster chemotaxis, but also accelerates mixing, which erases the motility benefit. This trade-off results in an optimal turbulence intensity, whereby the maximum motility benefit depends jointly on the size and lifetime of DOM filaments.

Constraints on chemotaxis can be understood in terms of three fundamental time scales (*16*). The chemotaxis time scale, $\tau_C = l_B/V_C$, is the time it takes a bacterium to swim to the core of a nutrient filament, whose characteristic width is the Batchelor scale, l_B. Stronger turbulence creates finer filaments (smaller l_B and τ_C), but also decreases the filaments' lifetime, which is characterized by the mixing time scale, $\tau_M = l_B^2/\kappa_C$, where κ_C is the nutrient diffusivity. One thus expects that the motility benefit depends on the relative magnitude of τ_C and τ_M. A further condition for motility to be beneficial is that the consumption of the patch through uptake is slower than chemotactic migration, i.e., $\tau_C < \tau_U$. We quantify the relative magnitude of the three time scales by means of two Frost numbers, $Fr_M = \tau_C/\tau_M$ and $Fr_U = \tau_C/\tau_U$ (*16*, *22*). When $Fr_M >> 1$ or $Fr_U >> 1$, chemotaxis is too slow relative to mixing (the "mixing-limited regime") or consumption (the "uptake-limited regime"), respectively, for motile bacteria to gain appreciable benefit. This argument is verified by a formal scaling analysis (*16*), whose prediction (Eq. S40) is in good agreement with the DNS results.

In addition to swimming speed and turbulence intensity, the net benefit of chemotaxis depends on multiple features of the nutrient landscape, as additional simulations reveal (*16*). The total nutrient injection rate must be sufficient to justify the investment in motility. We used a baseline value of 0.12 g_C m^{-3} day^{-1}, representative of relatively nutrient-rich conditions (*1*, *16*). Fast chemotaxis is optimal at higher injection rates (Fig. 3B), whereas lower input rates shift the competition in favor of nonmotile bacteria, in line with evidence that abundant species in the oligotrophic open ocean are nonmotile (*23*). The benefit of chemotaxis further depends on patch size. In the absence of flow, the motility benefit is optimal for a patch size of $\sigma \approx 650$ μm; larger patches are too vast for bacteria to reach their nutrient-rich core, whereas smaller patches quickly diffuse away. The motility benefit is less dependent on the initial patch size in a turbulent flow, because the patch is stirred into Batchelor-scale filaments. Therefore, turbulence can significantly favor the utilization of larger patches by motile bacteria (Fig. 3C). Finally, an important role is played by the nutrient diffusivity, because higher–molecular weight solutes, abundant in the ocean, diffuse more slowly, prolonging the filaments' lifetime and favoring chemotaxis (*16*). Taken together, these findings indicate that, although our fundamental conclusions apply to a broad range of nutrient conditions, the net motility benefit is environment-dependent: It will be lower than predicted here, or vanish entirely, for oligotrophic conditions or very small patches, and it might be higher for intermediate patch sizes or high–molecular weight solutes.

Our results indicate that, in contrast to *E. coli* (*24*), motile marine bacteria spend a sizable fraction of their metabolic budget on locomotion. Whereas many coastal ocean bacteria are motile (*9*, *25*), dominant clades in the open ocean, like SAR11 (*23*), are nonmotile, providing evidence that motility is not without cost. We propose that a fundamental determinant of the prevalence of motility in a given environment is the trade-off between motility benefit and swimming cost. Chemotaxis in the heterogeneous, time-varying nutrient landscape prevalent in the ocean should be seen as an optimal foraging problem, where the most successful strategy depends on the nutrient distribution and turbulence intensity. In addition to the trade-offs presented here, other factors can affect the optimal foraging behavior. Additional costs, associated with biosynthesis of flagella, operation of chemotaxis pathways, increased encounter rates with predators, and less effective uptake kinetics, might reduce the optimal chemotactic velocity and the net motility benefit. In contrast, the benefits of motility could be augmented by the ability of fast cells to escape capture (*26*) or to modulate swimming so as to combine intermediate exploration speeds with fast exploitation speeds (*27*). Indeed, most bacteria remain outside of nutrient filaments (e.g., less than 1.7% of the cells experience $C > 0.01 C_0$ at any given time) and can be considered in "exploration mode," using undirected motility to search for a chemical signal that they can exploit through chemotaxis.

DNS provides a quantitative framework to investigate this optimal foraging problem, and we have applied it to show that turbulence can affect the competition between motile and nonmotile bacteria. The outcome of this competition will be an important determinant of species succession when environmental conditions change—for example, during algal blooms or oil spills, when the abundance of DOM sources varies greatly. More broadly, DNS promises to be a valuable tool to address the elusive effects of turbulence on microscale biophysical processes, such as gamete encounter rates (*28*), phytoplankton patchiness (*29*), microbial productivity in bioreactors (*30*), and the fate of microbial nutrient sources, including particle plumes and oil droplets.

The results presented here upend the prevailing view on the effect of turbulence on aquatic microorganisms. Contrary to current understanding, based on homogeneous nutrient environments where turbulence is inconsequential for bacterial uptake (*2*), motile bacteria are directly affected by fluid motion in a heterogeneous environment, where they can exploit thin nutrient filaments generated by turbulence. This process generalizes to a broad spectrum of nutrient sources, because turbulence will stir even large DOM patches into a tangled web of filaments. Accordingly, the nutrient landscape experienced by aquatic microorganisms might be even more heterogeneous and intermittent than previously thought (*4*), renewing the challenge of capturing the effect of this variability on microbial adaptations and marine biochemistry.

References and Notes

1. C. Duarte, J. Cebrian, *Limnol. Oceanogr.* **41**, 1758 (1996).
2. L. Karp-Boss, E. Boss, P. Jumars, *Oceanogr. Mar. Biol. Annu. Rev.* **34**, 71 (1996).
3. J. Lazier, K. Mann, *Deep Sea Res. A* **36**, 1721 (1989).
4. F. Azam, F. Malfatti, *Nat. Rev. Microbiol.* **5**, 782 (2007).
5. N. Blackburn, T. Fenchel, J. Mitchell, *Science* **282**, 2254 (1998).
6. J. G. Mitchell, L. Pearson, S. Dillon, *Appl. Environ. Microbiol.* **62**, 3716 (1996).
7. R. Stocker, J. R. Seymour, A. Samadani, D. E. Hunt, M. F. Polz, *Proc. Natl. Acad. Sci. U.S.A.* **105**, 4209 (2008).
8. J. R. Seymour, R. Simó, T. Ahmed, R. Stocker, *Science* **329**, 342 (2010).
9. T. Fenchel, *Science* **296**, 1068 (2002).

10. T. Kiørboe, G. Jackson, *Limnol. Oceanogr.* **46**, 1309 (2001).
11. J. Muñoz-García, Z. Neufeld, C. Torney, *New J. Phys.* **12**, 103043 (2010).
12. P. Moin, K. Mahesh, *Annu. Rev. Fluid Mech.* **30**, 539 (1998).
13. D. Donzis, K. Sreenivasan, P. Yeung, *Flow Turbul. Combus.* **85**, 549 (2010).
14. G. Batchelor, *J. Fluid Mech.* **5**, 113 (1959).
15. T. Ahmed, R. Stocker, *Biophys. J.* **95**, 4481 (2008).
16. Supplementary materials are available on *Science* Online.
17. P. Williams, in *Microbial Ecology of the Oceans*, D. L. Kirchman, Ed. (Wiley, New York, 2000), pp. 153–200.
18. L. Xie, T. Altindal, S. Chattopadhyay, X. L. Wu, *Proc. Natl. Acad. Sci. U.S.A.* **108**, 2246 (2011).
19. A. Hütz, K. Schubert, J. Overmann, *Appl. Environ. Microbiol.* **77**, 4412 (2011).
20. M. Gregg, D. Winkel, T. Sanford, H. Peters, *Dyn. Atmos. Oceans* **24**, 1 (1996).
21. E. F. DeLong *et al.*, *Science* **311**, 496 (2006).
22. D. Grünbaum, *Hydrobiologia* **480**, 175 (2002).
23. R. M. Morris *et al.*, *Nature* **420**, 806 (2002).
24. E. Purcell, *Am. J. Phys.* **45**, 3 (1977).
25. H. Grossart, L. Riemann, F. Azam, *Aquat. Microb. Ecol.* **25**, 247 (2001).
26. C. Matz, K. Jürgens, *Appl. Environ. Microbiol.* **71**, 921 (2005).
27. J. Seymour, Marcos, R. Stocker, *Am. Nat.* **173**, E15 (2009).
28. J. Crimaldi, H. Browning, *J. Mar. Syst.* **49**, 3 (2004).
29. W. M. Durham, E. Climent, R. Stocker, *Phys. Rev. Lett.* **106**, 238102 (2011).
30. J. Marshall, Y. Huang, *Chem. Eng. Sci.* **65**, 3865 (2010).

Acknowledgments: We thank W. M. Durham, R. Ferrari, M. Follows, M. Garren, F. Menolascina, S. Merrifield, T. Pedley, S. Smriga, and R. Watteaux for helpful comments and suggestions. The calculation of the resistive force coefficient for a bacterium was performed by Marcos. J.R.T. was supported by an NSF Mathematical Sciences Postdoctoral Research Fellowship. R.S. acknowledges NSF grants OCE-0744641-CAREER and CBET-1066566.

Supplementary Materials
www.sciencemag.org/cgi/content/full/338/6107/675/DC1
Materials and Methods
Supplementary Text
Figs. S1 to S9
Table S1
References
Movie S1

20 January 2012; accepted 2 August 2012
10.1126/science.1219417

Asymmetric Division of *Drosophila* Male Germline Stem Cell Shows Asymmetric Histone Distribution

Vuong Tran,* Cindy Lim,* Jing Xie, Xin Chen†

Stem cells can self-renew and generate differentiating daughter cells. It is not known whether these cells maintain their epigenetic information during asymmetric division. Using a dual-color method to differentially label "old" versus "new" histones in *Drosophila* male germline stem cells (GSCs), we show that preexisting canonical H3, but not variant H3.3, histones are selectively segregated to the GSC, whereas newly synthesized histones incorporated during DNA replication are enriched in the differentiating daughter cell. The asymmetric histone distribution occurs in GSCs but not in symmetrically dividing progenitor cells. Furthermore, if GSCs are genetically manipulated to divide symmetrically, this asymmetric mode is lost. This work suggests that stem cells retain preexisting canonical histones during asymmetric cell divisions, probably as a mechanism to maintain their unique molecular properties.

Although all cells in an organism contain the same genetic material, different genes are expressed in specific cell types, allowing them to differentiate along distinct pathways. Epigenetic mechanisms regulate gene expression and maintain a specific cell fate through many cell divisions (*1*–*3*). Stem cells have the remarkable ability to both self-renew and generate daughter cells that enter differentiation (*4*). Epigenetic mechanisms have been reported to regulate stem cell activity in multiple lineages (*5*–*7*). However, there has been little direct in vivo evidence demonstrating whether stem cells retain their epigenetic information.

The *Drosophila* male GSCs are well characterized in terms of their physiological location, microenvironment (i.e., niche), and cellular structures (*8*, *9*) (Fig. 1, A and B). Male GSCs can be identified precisely by their distinct anatomical positions and morphological features. A GSC usually divides asymmetrically to produce a self-renewed GSC and a daughter cell gonialblast (GB) that undergoes differentiation. Therefore, GSCs can be examined at single-cell resolution for a direct comparison.

In eukaryotes, the basic unit of chromatin called nucleosome contains histone octamer [2×(H3, H4, H2A, H2B)] and DNA wrapping around them. Indeed, histones are one of the major carriers of epigenetic information (*10*). To address how histones are distributed during the GSC asymmetric division, we developed a switchable dual-color method to differentially label "old" versus "new" histones (Fig. 1C) that uses both spatial (by Gal4; UAS system) and temporal (by heat shock induction) controls to switch labeled histones from green [green fluorescent protein (GFP)] to red [monomeric Kusabira-Orange (mKO)]. Heat shock treatment induces an irreversible DNA recombination to shut down expression of GFP-labeled old histones and initiate expression of mKO-labeled new histones. If the old histones are partitioned nonselectively, the GFP will initially exhibit equal distribution in the GSC and GB, and will be gradually replaced by the mKO (Fig. 1D). However, if the old histones are preferentially retained in the GSCs to constitute potentially GSC-specific chromatin structure, the GFP will be detected specifically in the GSCs (Fig. 1E). During DNA replication–dependent canonical histone deposition, histones H3 and H4 are incorporated as a tetramer, and histones H2A and H2B are incorporated as dimers (*11*–*15*). Therefore, we generated independent transgenic strains for H3 and H2B, respectively. On the other hand, histone variants are incorporated into chromatin in a transcription-coupled but DNA replication–independent manner (*16*, *17*). Therefore, the histone variant H3.3 was used as a control for canonical histones.

To avoid potential complications caused by heat shock–induced DNA recombination on either one or both chromosomes in GSCs, each of the three transgenes (H3, H2B, and H3.3) was integrated as a single copy and analyzed in heterozygous flies. Examination of testes with the transgenes revealed nuclear GFP but little mKO signal before heat shock. After heat shock, mKO signals were detectable (fig. S1). Different GSCs undergo mitosis asynchronously, and an average cell cycle length of GSCs is approximately 12 to 16 hours. Among all GSCs, 75 to 77% are in G_2 phase, 21% are in S phase, fewer than 2% are in mitosis, and G_1-phase GSCs are almost negligible (*18*–*22*). Moreover, the GSC and GB arising from an asymmetric division remain connected after mitosis by a cellular structure known as the spectrosome, when they undergo the next G_1 and S phases synchronously (*19*, *21*).

To examine the distribution of old versus new histones in GSC and GB after a round of DNA replication–dependent histone deposition, we studied testes 16 to 20 hours after heat shock (Fig. 2A). In particular, GSC-GB pairs connected by spectrosomes were examined (Fig. 2, B and H, arrows). On the basis of cell cycle length of GSCs, these GSC-GB pairs were from GSCs that switched from *histone-GFP* to *histone-mKO* genetic code during their G_2 phase and then underwent the first mitosis followed by G_1, S, and G_2 phase and the second mitosis (Fig. 2A). Within this time frame, both old histones

Department of Biology, Johns Hopkins University, Baltimore, MD 21218, USA.

*These authors contributed equally to this work.
†To whom correspondence should be addressed. E-mail: xchen32@jhu.edu

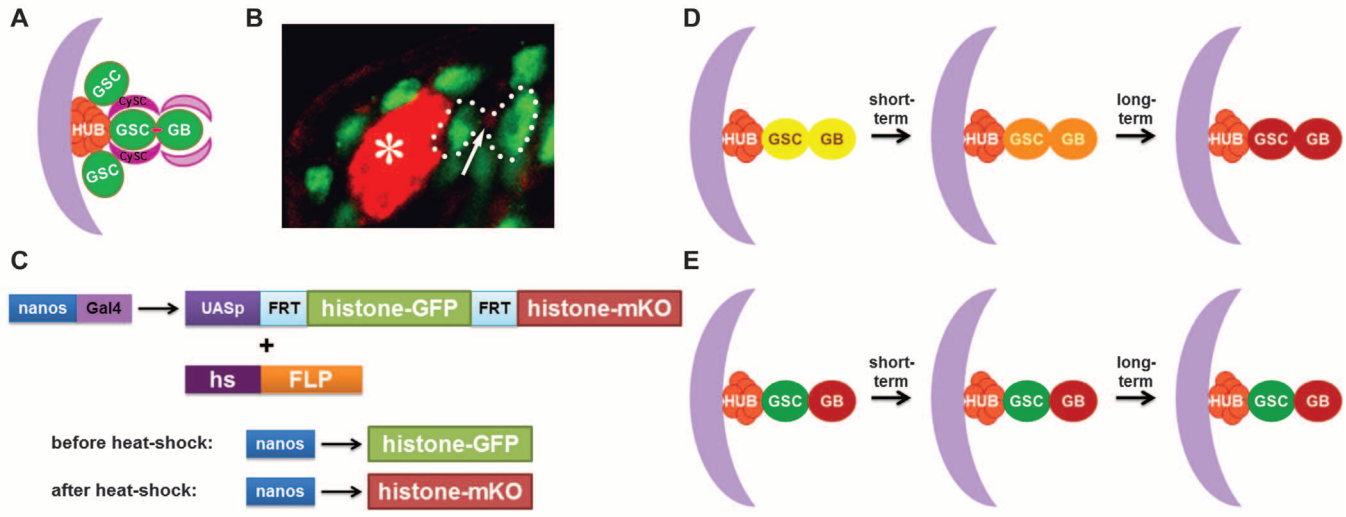

Fig. 1. Experimental design and potential results. (**A**) Diagram of the GSC niche. HUB, hub cells; CySC, cyst progenitor/somatic stem cell. (**B**) Immunofluorescent image of the niche: HUB (anti–Fas III, red, asterisk), GSC-GB pair expressing H3-GFP (green, dotted outline) connected by a spectrosome (anti-α-spectrin, red, arrow). (**C**) The *UASp-FRT-histone-GFP-PolyA-FRT-histone-mKO-PolyA* transgene. UAS, upstream activating sequence; FRT, FLP (flippase) recombination target; histone, H3, H2B, or histone variant H3.3; *nanos-Gal4*, a germline-specific driver; *hs-FLP*, the yeast FLP recombinase controlled by the heat shock (*hs*) promoter. (**D** and **E**) Two potential results. For simplicity, only one GSC-GB pair is shown, and each entire cell is colored according to histone fluorescence.

Fig. 2. H3 is asymmetrically segregated during the second GSC division after heat shock. (**A**) Heat shock regime. (**B** to **G**) H3 is distributed asymmetrically in GSC versus GB (B to D) but symmetrically in two-cell spermatogonia (E to G). (**H** to **J**) H3.3 is distributed symmetrically in GSC versus GB. (**K** to **S**) H3 distribution pattern in GSCs: (K to M) G_2 phase, (N to P) anaphase, (Q to S) telophase. Scale bars, 5 μm. Asterisk, HUB (anti–Fas III); arrow, spectrosome (anti-α-spectrin). (**T**) Quantification of GFP and mKO fluorescence intensity ratio (table S2). H3 GSC/GB GFP ratio > 1 (*$P < 10^{-4}$), GSC/GB mKO ratio < 1 (*$P < 10^{-4}$), $N = 15$. H3 two-cell spermatogonial (SG) SG1/SG2 GFP ratio (#$P = 0.103$) and mKO ratio (#$P = 0.684$) are insignificantly different from 1, $N = 16$. H3.3 GSC/GB GFP ratio (#$P = 0.513$) and mKO ratio (#$P = 0.532$) are insignificantly different from 1, $N = 12$. Error bars: SE; P value: one-sample t test.

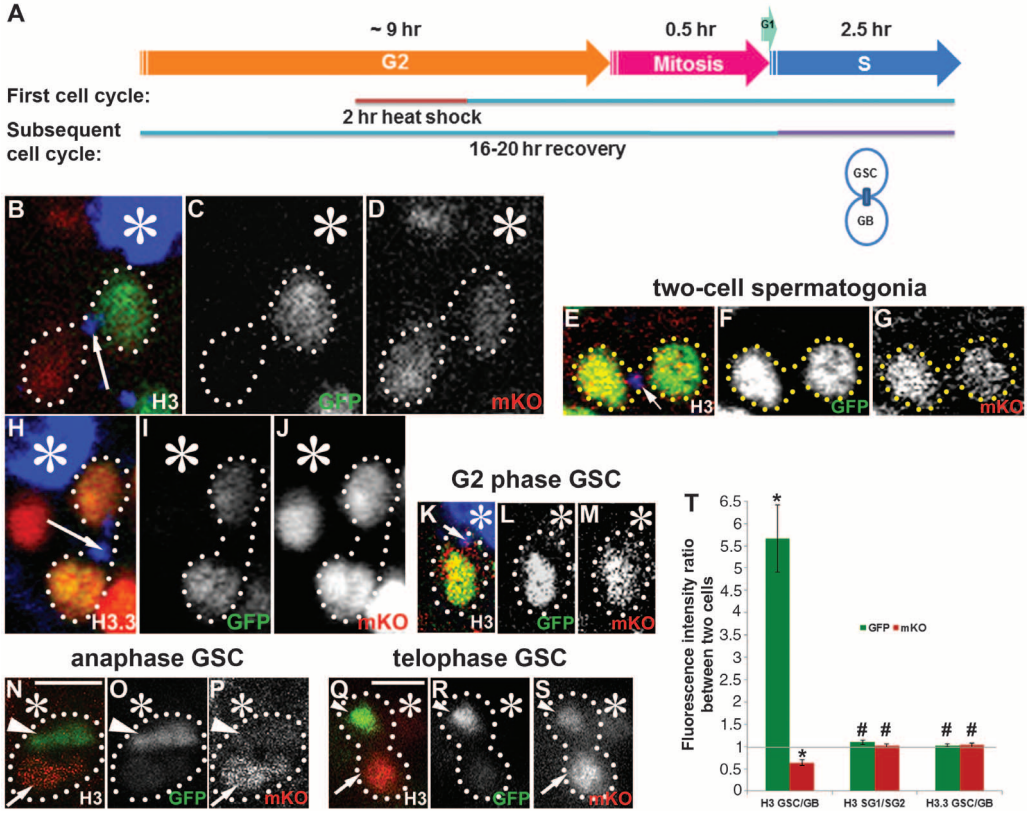

and new histones were detectable in GSCs at the second G_2 phase (Fig. 2, K to M, and table S1) because new histones had been synthesized and incorporated during the first S phase. For histone H3, the GFP signal was detected primarily in the GSC but not in the GB (Fig. 2C). By contrast, the mKO signals were present in both the GSC and the GB, with a relatively higher level in the GB (Fig. 2, B and D). The asymmetric distribution of histone H3 was specific for GSC divisions, because both the GFP and mKO signals were equally distributed in spermatogonial cells derived from a symmetric division of the GB in the same testis samples (Fig. 2, E to G). Quantification of fluorescence intensity revealed that the old H3 (GFP-labeled) signal was more enriched in the GSC than in the GB by a factor of ~5.7, whereas new H3 (mKO-labeled) signal was more enriched in the GB than in the GSC by a factor of ~1.6 (H3 GSC/GB data in Fig. 2T and tables S1 and S2). By contrast, this differential distribution of old versus new histone was not detected for symmetrically dividing spermatogonial cells (H3 SG1/SG2 data in Fig. 2T,

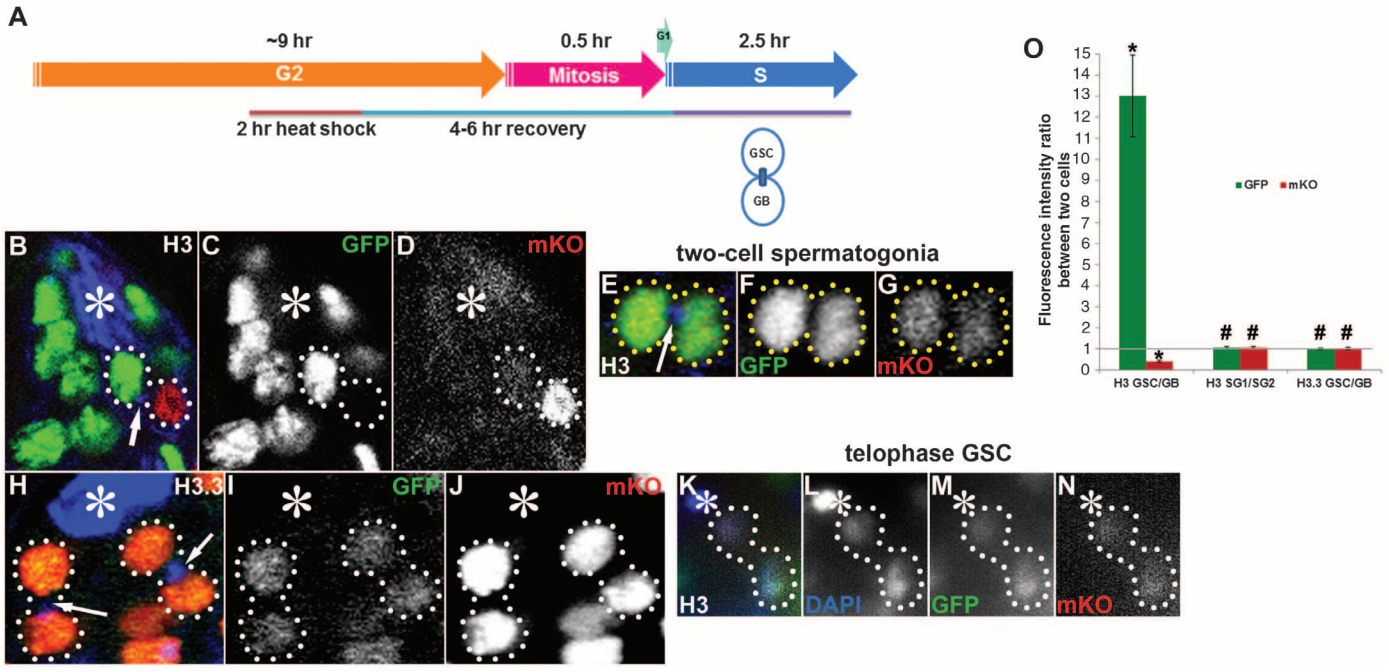

Fig. 3. H3 is asymmetrically distributed after the first GSC division after heat shock. (**A**) Heat shock regime. (**B** to **G**) H3 is distributed asymmetrically in GSC versus GB (B to D) but symmetrically in two-cell spermatogonia (E to G). (**H** to **J**) H3.3 is distributed symmetrically in GSC versus GB. (**K** to **N**) A telophase GSC. Asterisk, HUB (anti–Fas III); arrow, spectrosome (anti–α-spectrin). (**O**) Quantification of GFP and mKO fluorescence intensity ratio (table S4). H3 GSC/GB GFP ratio > 1 ($*P < 10^{-4}$), GSC/GB mKO ratio < 1 ($*P < 10^{-4}$), $N = 12$. H3 two-cell spermatogonial (SG) SG1/SG2 GFP ratio ($\#P = 0.225$) and mKO ratio ($\#P = 0.365$) are insignificantly different from 1, $N = 11$. H3.3 GSC/GB GFP ratio ($\#P = 0.970$) and mKO ratio ($\#P = 0.594$) are insignificantly different from 1, $N = 13$. Error bars: SE; P value: one-sample t test.

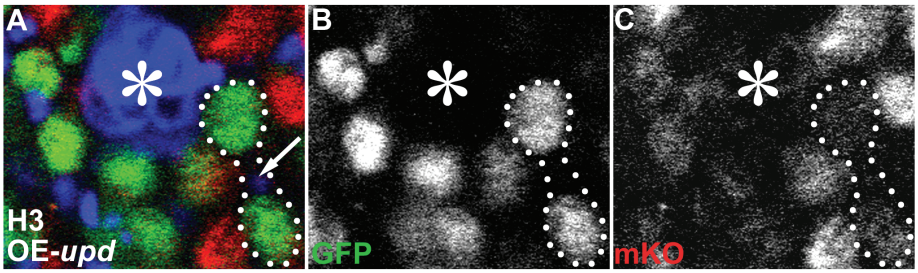

Fig. 4. Loss of asymmetric H3 distribution pattern upon overexpression of *upd*. (**A** to **C**) In *nanos-Gal4*; *UAS-upd* testis. (A), both H3-GFP (B) and H3-mKO (C) are symmetrically distributed in overproliferative GSC-like cells. Asterisk, HUB (anti–Fas III).

tables S1 and S2: H3-GFP ratio in SG1/SG2 = 1.09; H3-mKO ratio in SG1/SG2 = 1.02).

In contrast to the asymmetric distribution pattern for the canonical histone H3, the histone variant H3.3 did not show this asymmetry during GSC divisions, by fluorescence images (Fig. 2, H to J) and by quantification (H3.3 GSC/GB data in Fig. 2T, tables S1 and S2: H3.3-GFP ratio in GSC/GB = 1.03; H3.3-mKO ratio in GSC/GB = 1.03). The symmetry of the histone variant H3.3 suggests that the asymmetric mode is specific for canonical histone H3.

Fewer than 2% of all GSCs are undergoing mitosis; thus, all analyses above were based on postmitotic GSC-GB pairs. To further examine the histone segregation pattern during mitosis, we screened for mitotic GSCs. Indeed, old histones were mainly associated with the chromatids segregated to the GSC side at metaphase (fig. S2), anaphase (Fig. 2, N to P, fig. S2, arrowheads), and telophase (Fig. 2, Q to S, arrowheads). By contrast, new histones were more enriched at the chromatids segregated to GB side (Fig. 2, N, P, Q, and S, and fig. S2, arrows). These results suggest that the sister chromatids preloaded with old histones are preferentially retained in GSCs and that the ones enriched with new histones are partitioned to GBs during GSC mitosis.

Next, we examined the histone distribution pattern during the first GSC division by recovering GSCs for 4 to 6 hours after heat shock (Fig. 3A). An asymmetric distribution pattern was also found in the GSC-GB pairs with the H3 transgene (Fig. 3, B to D). By contrast, a symmetric distribution pattern was observed for both dividing spermatogonial cells with the H3 transgene (Fig. 3, E to G) and H3.3 during GSC division (Fig. 3, H to J). Quantification of fluorescence intensity revealed that the old H3-GFP signal was enriched in the GSC by a factor of ~13 relative to the GB, whereas the new H3-mKO signal was enriched in the GB by a factor of ~2.4 relative to the GSC (H3 GSC/GB data in Fig. 3O, tables S3 and S4). By contrast, there was no differential distribution of the old versus new histone for the symmetrically dividing spermatogonial cells (H3 SG1/SG2 data in Fig. 3O, tables S3 and S4: H3-GFP ratio in SG1/SG2 = 1.07; H3-mKO ratio in SG1/SG2 = 1.06), or H3.3 during GSC division (H3.3 GSC/GB data in Fig. 3O, tables S3 and S4: H3.3-GFP ratio in GSC/GB = 1.00; H3.3-mKO ratio in GSC/GB = 1.02). Although an asymmetric histone distribution pattern was detected in postmitotic GSC-GB pairs, examination of the mitotic GSC at this stage did not show any asymmetry (Fig. 3, K to N). These data suggest that the asymmetric segregation mode (Fig. 2, N to S) relies on replication-dependent histone incorporation prior to mitosis. However, the factor of >10 difference of GFP signal between GSC and GB could be contributed by faster turnover of old histones in GBs, probably as a mechanism to reset the chromatin for differentiation. By contrast, the difference of mKO in GSC and GB was less substantial, probably as a result of new histone synthesis in both cells. Furthermore, the H2B transgene

showed a similar pattern to H3 after the first GSC division (fig. S3).

The consistent asymmetric cell divisions of GSCs could be lost under certain conditions, such as ectopic activation of the key JAK-STAT signaling pathway in the niche (*23*–*25*). It has been shown that overexpression of the JAK-STAT ligand *unpaired* (OE-*upd*) induces overpopulation of GSCs (*23*, *24*). Consistent with the loss of asymmetry in expanded GSCs, the asymmetric distribution pattern of the histone H3 was not observed in OE-*upd* testes 16 to 20 hours after heat shock (Fig. 4). These results demonstrate that the asymmetric histone distribution pattern is dependent on GSC asymmetric divisions. We propose a two-step process as our favored explanation (fig. S4A; an alternative explanation is discussed in fig. S4B): Old and newly synthesized histones are incorporated to different sister chromatids during S phase; then, during mitosis, the sister chromatid preloaded with old histones is preferentially segregated to GSC.

These data reveal that stem cells preserve preexisting histones through asymmetric cell divisions. The JAK-STAT signaling pathway required for the asymmetric GSC divisions contributes to the asymmetric histone distribution pattern. This work provides a critical first step toward identifying the detailed molecular mechanisms underlying old histone retention during GSC asymmetric division. These findings in the well-characterized GSC model system will facilitate understanding of how epigenetic information could be maintained by stem cells or reset in their sibling cells that undergo cellular differentiation.

References and Notes

1. L. Ringrose, R. Paro, *Annu. Rev. Genet.* **38**, 413 (2004).
2. J. J. Jacobs, M. van Lohuizen, *Biochim. Biophys. Acta* **1602**, 151 (2002).
3. B. M. Turner, *Cell* **111**, 285 (2002).
4. J. A. Knoblich, *Cell* **132**, 583 (2008).
5. S. H. Eun, Q. Gan, X. Chen, *Curr. Opin. Cell Biol.* **22**, 737 (2010).
6. R. Jaenisch, R. Young, *Cell* **132**, 567 (2008).
7. M. Buszczak, A. C. Spradling, *Cell* **125**, 233 (2006).
8. M. T. Fuller, A. C. Spradling, *Science* **316**, 402 (2007).
9. V. P. Losick, L. X. Morris, D. T. Fox, A. Spradling, *Dev. Cell* **21**, 159 (2011).
10. T. Kouzarides, *Cell* **128**, 693 (2007).
11. M. Xu *et al.*, *Science* **328**, 94 (2010).
12. V. Jackson, R. Chalkley, *J. Biol. Chem.* **256**, 5095 (1981).
13. V. Jackson, R. Chalkley, *Cell* **23**, 121 (1981).
14. G. Russev, R. Hancock, *Nucleic Acids Res.* **9**, 4129 (1981).
15. A. T. Annunziato, R. K. Schindler, M. G. Riggs, R. L. Seale, *J. Biol. Chem.* **257**, 8507 (1982).
16. H. Tagami, D. Ray-Gallet, G. Almouzni, Y. Nakatani, *Cell* **116**, 51 (2004).
17. K. Ahmad, S. Henikoff, *Mol. Cell* **9**, 1191 (2002).
18. J. Cheng *et al.*, *Nature* **456**, 599 (2008).
19. X. R. Sheng, E. Matunis, *Development* **138**, 3367 (2011).
20. Y. M. Yamashita, D. L. Jones, M. T. Fuller, *Science* **301**, 1547 (2003).
21. S. Yadlapalli, J. Cheng, Y. M. Yamashita, *J. Cell Sci.* **124**, 933 (2011).
22. Y. M. Yamashita, A. P. Mahowald, J. R. Perlin, M. T. Fuller, *Science* **315**, 518 (2007).
23. A. A. Kiger, D. L. Jones, C. Schulz, M. B. Rogers, M. T. Fuller, *Science* **294**, 2542 (2001).
24. N. Tulina, E. Matunis, *Science* **294**, 2546 (2001).
25. J. L. Leatherman, S. Dinardo, *Cell Stem Cell* **3**, 44 (2008).

Acknowledgments: We thank J. Prado for discussions to develop a controlled gene expression system and the *FRT-MCS-SV40 Poly A-FRT* plasmid; A. Talaga, A. Chin, A. Kim, and B. Weber for experimental assistance; K. Ahmad for plasmids containing *H3*, *H2B*, and *H3.3* sequences; A. Nakamura for the *UAS-mKO-vasa* strain; S. DiNardo for the *UAS-upd* strain; Y. Yamashita for GSC cell cycle information and insightful suggestions; and R. Kuruvilla, K. Zhao, Y. Zheng, H. Zhao, M. Van Doren, D. Drummond-Barbosa, A. Hoyt, and Chen lab members for critical reading. Supported by NICHD/NIH grants R21HD065089 and R01HD065816, the David & Lucile Packard Foundation, American Federation of Aging Research, and JHU start-up (X.C.).

Supplementary Materials

www.sciencemag.org/cgi/content/full/338/6107/679/DC1
Materials and Methods
Figs. S1 to S4
Tables S1 to S4
References (*26*–*31*)

13 June 2012; accepted 4 September 2012
10.1126/science.1226028

Some Consequences of Having Too Little

Anuj K. Shah,[1]* Sendhil Mullainathan,[2] Eldar Shafir[3]

Poor individuals often engage in behaviors, such as excessive borrowing, that reinforce the conditions of poverty. Some explanations for these behaviors focus on personality traits of the poor. Others emphasize environmental factors such as housing or financial access. We instead consider how certain behaviors stem simply from having less. We suggest that scarcity changes how people allocate attention: It leads them to engage more deeply in some problems while neglecting others. Across several experiments, we show that scarcity leads to attentional shifts that can help to explain behaviors such as overborrowing. We discuss how this mechanism might also explain other puzzles of poverty.

The poor often behave in ways that reinforce poverty. For instance, low-income individuals often play lotteries (*1*, *2*), fail to enroll in assistance programs (*3*), save too little (*4*), and borrow too much (*5*). Currently there are two ways to explain this behavior. The first focuses on the circumstances of poverty, such as education (*6*), health (*7*), living conditions (*8*), political representation (*9*), and numerous demographic and geographic variables (*10*, *11*). Put simply, the poor live in environments (for sociological, political, economic, or other reasons) that promote these behaviors. The second view focuses on personality traits of the poor (*12*–*14*). But we suggest a more general view: Resource scarcity creates its own mindset, changing how people look at problems and make decisions.

To understand this hypothesis, consider how people manage expenses. When money is abundant, basic expenses (e.g., groceries, rent) are handled easily as they arise. These expenses come and go, rarely requiring attention and hardly lingering on the mind. But when money is scarce, expenses are not easily met. Instead of appearing mundane, they feel urgent. The very lack of available resources makes each expense more insistent and more pressing. A trip to the grocery store looms larger, and this month's rent constantly seizes our attention. Because these problems feel bigger and capture our attention, we engage more deeply in solving them. This is our theory's core mechanism: Having less elicits greater focus.

This view is not bound to the specific circumstances of poverty, nor does it make assumptions about the dispositions of the poor. This mindset stems from the most fundamental feature of poverty: having less. And this hypothesis is about scarcity more generally, not just poverty. Indeed, just as expenses capture the attention of the poor, researchers have found that people who are hungry and thirsty focus more on food- and drink-related cues (*15*, *16*). Likewise, the busy (facing time scarcity) respond to deadlines with greater focus on the task at hand (*17*). Across many contexts, we see a similar psychology. People focus on problems where scarcity is most salient.

The second part of our theory follows readily from the first. Because scarcity elicits greater engagement in some problems, it leads to neglect of others. While focusing on the groceries from week to week, we might neglect next month's rent. While consumed with meeting tomorrow's

[1]Booth School of Business, University of Chicago, Chicago, IL 60637, USA. [2]Department of Economics, Harvard University, Cambridge, MA 02138, USA. [3]Department of Psychology and Woodrow Wilson School of Public and International Affairs, Princeton University, Princeton, NJ 08544, USA.

*To whom correspondence should be addressed. E-mail: anuj.shah@chicagobooth.edu

manuscript deadline, we might fail to prepare next week's lecture. Attentional neglect appears in many domains. Low-income homeowners often do not attend to regular home maintenance while they focus on more pressing expenses (*18*). Neglected, these small repairs become major projects. Similarly, in areas where water-borne illness is common, families might focus on pressing daily expenses while failing to procure periodic water treatments (*19*).

Attentional neglect can explain another particularly striking behavior: why low-income individuals take short-term, high-interest loans, with interest rates that can approach 800% (*20*–*22*). These loans make it easier to meet today's needs, but the loans' deferred costs make it difficult to meet future expenses. If scarcity creates a focus on pressing expenses today, then attention will go to a loan's benefits but not its costs. This suggests a clear prediction: Scarcity, of any kind, will create a tendency to borrow, with insufficient attention to whether the benefits outweigh the costs.

Consistent with this prediction, the busy also borrow. Facing tight budgets (i.e., deadlines), they borrow time by taking extensions. Like the poor, the busy often take extensions because they focus on urgent tasks, but neglect important tasks that seem less pressing (*23*). We suggest that both forms of borrowing stem from how scarcity shifts attention.

We test this theory with the use of an approach that psychologists have employed to study other social problems, such as obedience to authority (*24*), helping behavior (*25*), and conformity (*26*). Simple experiments can distill a problem's primary features in the lab, abstracting from the complexities of the world and highlighting how selected features guide behavior. Here, we distill scarcity and test its influence on how people borrow. Experiments 1 and 2 show that scarcity creates increased focus. Experiments 2 to 5 demonstrate how (and why) scarcity leads people to borrow.

In all experiments, participants were randomly assigned budgets; "poor" participants had smaller budgets than "rich" participants [see (*27*) for a full description]. These budgets were distributed in "paychecks" across multiple rounds of a game. Poor participants had proportionally smaller paychecks than rich participants. On each round, participants used the resources to earn rewards. If participants moved on from a round without exhausting their paycheck, unspent units were saved for future use. Participants were also assigned to different borrowing conditions. Some could not borrow—when a paycheck was exhausted, they moved to the next round. Other participants could borrow at a cost *R*: Borrowing an additional resource unit for the current round subtracted *R* units from their overall budget.

In experiment 1, 60 participants played a version of *Wheel of Fortune* (*WoF*). Scarcity was manipulated by budgeting participants' chances to guess letters in word puzzles. Poor participants had 84 total guesses (6 per round); rich participants had 280 guesses (20 per round). Previous work suggests that greater engagement in *WoF* will cause cognitive fatigue and worse performance on subsequent cognitive tasks (*28*). As a measure of cognitive fatigue, after *WoF*, participants completed a version of the Dots-Mixed task, which assesses executive functions such as attention and cognitive control (*29*). Participants responded to visual stimuli presented to the left or right of a fixation cross. On congruent trials, participants had to press a key on the same side as the stimulus; on incongruent trials, they had to press a key on the opposite side. Congruent and incongruent trials (40 each) were randomly presented. Although *WoF* included a scarcity manipulation, the Dots-Mixed task was identical for all participants.

A simple model of effort might suggest that the rich should be more fatigued because they spent more time and made more guesses playing *WoF*. In our model, however, the poor would engage more deeply and could be more fatigued despite spending less time.

We measured the total number of correct responses in the attention task. Four participants were removed from the analyses for having zero correct responses. Poor participants performed worse (mean ± SD, 45.12 ± 15.87) than did rich participants (52.93 ± 12.79) [$F(1, 54) = 4.16$, $P < 0.05$, effect size $\eta_p^2 = 0.07$; see table S1 for performance based on trial type]. Scarcity seems to have created greater engagement: Even with less time played (and fewer guesses made), the poor were more depleted.

Experiment 2 offers a more precise look at how scarcity changes engagement. Sixty-eight participants played a video game similar to Angry Birds. They fired shots from a slingshot, earning points for clearing targets. The poor had budgets of 30 shots (3 per level); the rich had 150 shots (15 per level). Some participants could not borrow shots, whereas others could borrow with $R = 2$ (essentially, 100% interest). Participants played until exhausting their budget.

To analyze how scarcity affected focus, we measured how long participants spent aiming each shot (i.e., how careful they were with their resources). Poor participants spent more time aiming the first shot of each level (log-transformed milliseconds, 8.08 ± 0.42) than did rich participants (7.73 ± 0.39) [$F(1, 64) = 12.96$, $P < 0.001$, $\eta_p^2 = 0.17$]. These results held for subsequent shots as well. Because the rich could always earn more points (and each additional point increased the chances of winning a prize), they had an incentive to remain engaged and use their resources well. Yet they were less engaged than the poor. Still, one might argue that these differences are driven by rich participants losing interest later in the game. However, these differences emerged on the very first shot of the game (poor: 8.19 ± 0.52; rich: 7.86 ± 0.52) [$F(1, 64) = 6.58$, $P < 0.05$].

This engagement had some benefits for the poor. Among participants who could not borrow, the poor earned more points per shot (2.31 ± 0.60) than did the rich (1.67 ± 0.37) [$F(1, 31) = 11.92$, $P < 0.005$]. Rich participants had 5 times as many shots as the poor, but earned far fewer than 5 times as many points. If the rich had played as if they were poor, they would have performed better. It seems that to understand the psychology of scarcity, we must also appreciate the psychology of abundance. If scarcity can engage us too much, abundance might engage us too little.

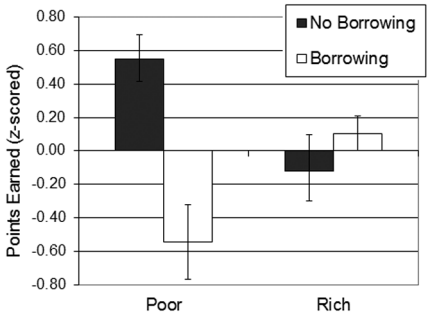

Fig. 1. Performance in experiment 1: Standardized points earned by the rich and poor. Error bars represent SE of the mean.

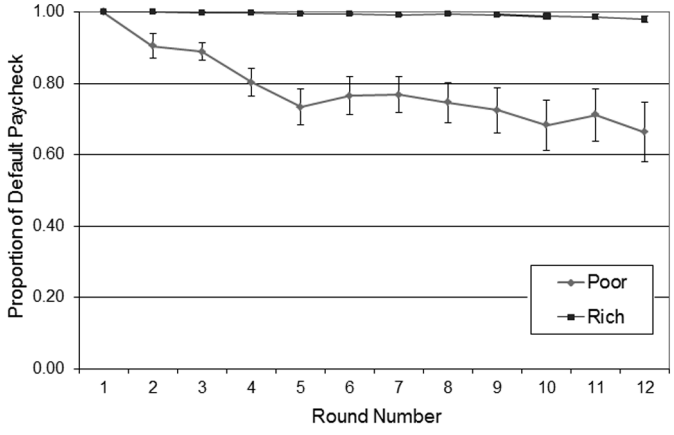

Fig. 2. The accumulation of debt in experiment 4. The paycheck for each round is shown as a proportion of the default paycheck allocated. Errors bars represent SE of the mean. Data are shown for the median number of rounds completed by all participants.

These results illustrate scarcity's focusing effect. Field data also show scarcity-induced focus. For instance, instead of offering bulk discounts, some retailers raise the per-unit cost of an item as purchase quantity increases. Most people overlook these occasional "quantity surcharges," but low-income consumers are more likely to notice these surcharges (*30*). Low-income consumers are also more sensitive to "hidden" taxes—those not included in the posted price (*31*).

Our experiments also suggest that scarcity leads people to neglect future rounds and borrow away from them. In experiment 2, each shot used beyond a round's paycheck counted as a shot borrowed. Borrowed shots were summed across a participant's game. As a fraction of their budget, poor participants borrowed more shots (0.24 ± 0.15) than the rich (0.02 ± 0.05) [$F(1, 33) = 27.53$, $P < 0.001$].

Performance data suggest that this borrowing was counterproductive. We measured performance in *z*-scores, standardizing points earned separately for the poor and the rich (Fig. 1; see table S2 for unstandardized data). Rich participants performed similarly whether they could not borrow (–0.12 ± 0.77) or could (0.10 ± 1.18), whereas poor participants fared better when they could not borrow (0.55 ± 0.65) than when they could (–0.55 ± 1.00) [scarcity × borrowing interaction, $F(1, 64) = 8.47$, $P < 0.005$, $\eta_p^2 = 0.12$]. This suggests that the poor overborrowed.

The amount of borrowing by the poor was significantly correlated with measures of engagement. On rounds where poor participants borrowed, the average amount of time spent aiming each shot in their paycheck correlated positively with how many shots they subsequently borrowed [$r(38) = 0.34$, $P < 0.05$]. The more focused the poor were on the current round, the more they neglected (and borrowed away from) future rounds.

To ensure that this was not an artifact of a particular context, we considered a different form of scarcity: having too little time. In experiment 3, 143 participants were given budgets of time with which to play *Family Feud*, a trivia game where each question allows multiple answers. Each round consisted of a new question and participants earned points for each correct answer. Poor participants had budgets of 300 s (15 per round); rich participants had 1000 s (50 per round). Participants played until exhausting their budget. There were three borrowing conditions: no borrowing, borrowing with $R = 1$ (i.e., "without interest"), and borrowing with $R = 2$ ("with interest").

Regardless of interest rate, poor participants borrowed a greater proportion of their budget (0.22 ± 0.15) than did rich participants (0.08 ± 0.15) [$F(1, 102) = 22.39$, $P < 0.001$]. Once again, the poor overborrowed [interaction $F(1, 137) = 6.54$, $P = 0.002$, $\eta_p^2 = 0.09$; see table S3 for unstandardized data]. Rich participants performed similarly whether they had no option to borrow (0.06 ± 1.10), borrowed without interest (–0.31 ± 0.88), or borrowed with interest (0.25 ± 0.98) [$F(1, 137) = 2.14$, $P = 0.15$]. The poor performed best when they could not borrow (0.60 ± 1.14), less well when they borrowed without interest (0.08 ± 0.67), and worst when they borrowed with interest (–0.48 ± 0.94) [$F(1, 137) = 7.49$, $P < 0.001$].

The effects of scarcity appear to be quite general. But one concern with these studies might be that the consequences of borrowing, which were not felt until the end, were not sufficiently salient. In experiment 4, we therefore modified the game so that borrowing would create "debt" in subsequent rounds. That is, the size of each paycheck varied depending on how people borrowed or saved. Initial paychecks were the same as in experiment 3, but on subsequent rounds, paychecks equaled the total time remaining divided by the number of remaining rounds. Participants played until they exhausted their budget or completed 20 rounds, whichever came first. Excessive borrowing on one round would therefore lead to a smaller paycheck on the next round. Some participants could not borrow, whereas others could borrow with $R = 2$.

Poor participants borrowed a greater proportion of their budget (0.27 ± 0.14) than did rich participants (0.03 ± 0.04) [$F(1, 56) = 70.50$, $P < 0.001$] and consequently saw their paychecks shrink during the game (Fig. 2). For this analysis, each round's paycheck was converted to a proportion of the default paycheck (i.e., dividing by 15 for the poor and by 50 for the rich). We regressed these proportions on the round numbers and analyzed the slopes for each participant. The poor accumulated debt at a higher rate (mean of slope ± SD, –0.13 ± 0.18) than did the rich (–0.01 ± 0.01) [Mann-Whitney test, $z = 5.46$, $P < 0.001$]. Furthermore, the poor did not adjust their borrowing as they accumulated debt. Instead, as their budgets shrunk, they gradually increased their borrowing relative to their remaining budget (*27*). As a result, rich participants performed similarly when they could not borrow (–0.09 ± 0.81) and when they could (0.11 ± 1.20). The poor performed better when they could not borrow (0.54 ± 0.77) than when they could (–0.49 ± 0.94) [interaction $F(1, 114) = 12.81$, $P < 0.001$, $\eta_p^2 = 0.10$; see table S4 for unstandardized data].

As in these experiments, neglect also creates many forms of borrowing (beyond conventional loans) among the poor in the world. For example, the poor often focus on certain expenses while neglecting utility payments, thereby incurring reconnection fees that are like interest payments—"borrowing" by paying the bill late (*32*).

Experiment 5 offers more direct support for the notion that scarcity creates attentional neglect. One hundred thirty-seven participants played *Family Feud.* Some participants could see previews of the subsequent round's question at the bottom of the screen; others could not. We expected that poor participants would be too focused on the demands of the current round to consider what comes next, whereas rich participants would be able to consider future rounds and whether moving on was beneficial. All participants could borrow with $R = 3$. As predicted, poor participants performed similarly with previews (–0.02 ± 0.87) and without (0.02 ± 1.11), while rich participants performed better with previews (0.32 ± 0.98) than without (–0.35 ± 0.92) [scarcity × borrowing interaction, $F(1, 133) = 4.29$, $P < 0.05$, $\eta_p^2 = 0.03$; for unstandardized scores, see table S5]. One concern might be that the poor did not have enough time to consider the previews. But the experiments above found that the poor were using too much; they were overborrowing. Their performance in the no-preview condition left substantial room for improvement. Even if poor participants had used some of the borrowed time to consider the previews and move on sooner, they could have improved. That is, the previews benefited the rich by helping them save more; they could have benefited the poor by helping them borrow less. But it appears they were too focused on the current round to benefit.

Taken together, these studies provide compelling support for the notion that scarcity elicits greater engagement and that a focus on some problems leads to neglect of others (manifesting in behaviors such as overborrowing). An alternative account might be that the poor and rich approached these tasks with the same mindset—playing each round until they were satisfied with their progress before moving on. By this account, the poor borrowed only because they were facing more severe constraints. But evidence from experiments 1 and 2 suggests that the poor and rich did not approach the tasks in the same way. The poor were more engaged.

Another explanation might be that scarcity creates cognitive load, thereby diminishing performance. Cognitive load might prevent people from figuring out the optimal borrowing rates, or it might lead people to use their resources less efficiently or make riskier financial decisions. Although we agree that scarcity creates load, our theory is more specific about the origins of that load and its effects. We suggest that cognitive load arises because people are more engaged with problems where scarcity is salient. This consumes attentional resources and leaves less for elsewhere.

Once we appreciate where attention is drawn under scarcity, we see how this mechanism can explain behaviors other than overborrowing. Scarcity-induced focus is not myopia, nor does it necessarily imply steeper discount rates. The poor often save for the future. However, their savings are not set aside in a generic account, but rather are geared toward specific expenses. That is, the poor often save for the same reason they borrow. This has clear policy implications. Interventions that draw people's attention to specific future needs should be particularly effective at increasing savings (*33*). This mechanism also

explains why the poor in many countries have a patchwork of financial instruments, with high turnover across accounts. A scarcity mindset leads people to choose the most locally convenient response to pressing demands, leading to constant financial juggling (*34*).

Questions surrounding poverty are large. Poverty has long occupied philosophers, social scientists, and policy-makers. No experiment can fully explain how poverty, and scarcity more generally, guides behavior. But the hypotheses, methods, and results above offer an approach to unpacking this problem. This paradigm can shed light on the cognitive consequences of poverty. Future research might also suggest ways to alleviate the taxing cognitive consequences of having too little. Finally, this approach can help us to understand circumstances even broader than poverty, because scarcity underlies problems as dire as hunger and as mundane as busyness. These problems have traditionally been studied within their own limited domains. A more general study of scarcity can inform our understanding of many specific contexts at once. This may be the key to a deeper appreciation of the vast psychology that stems from having too little.

References and Notes

1. C. Clotfelter, P. Cook, *Selling Hope: State Lotteries in America* (Harvard Univ. Press, Cambridge, MA, 1991).
2. E. Haisley, R. Mostafa, G. Loewenstein, *J. Risk Uncertain.* **37**, 57 (2008).
3. M. Bertrand, S. Mullainathan, E. Shafir, *Am. Econ. Rev.* **94**, 419 (2004).
4. D. S. Shurtleff, Improving savings incentives for the poor (National Center for Policy Analysis Brief Analysis No. 672, 2009); www.ncpa.org/pub/ba672.
5. D. Mendel, *Advocasey* **7**, 4 (2005); www.aecf.org/upload/publicationfiles/advocasey-%20winter%202005.pdf.
6. B. D. Bernheim, D. M. Garrett, D. Maki, *J. Public Econ.* **80**, 435 (2001).
7. R. W. Johnson, G. B. T. Mermin, D. Murphy, The impact of late-career health and employment shocks on Social Security and other wealth (Urban Institute Discussion Paper 07-07, 2007); www.urban.org/UploadedPDF/411591_impact_social_security.pdf.
8. J. Ludwig, G. J. Duncan, P. Hirschfield, *Q. J. Econ.* **116**, 655 (2001).
9. F. Cleaver, *World Dev.* **33**, 893 (2005).
10. S. W. Allard, *Access to Social Services: The Changing Urban Geography of Poverty and Service Provision* (Brookings Foundation, Washington, DC, 2004).
11. S. Spilerman, D. Elesh, *Soc. Probl.* **18**, 358 (1971).
12. O. Lewis, in *On Understanding Poverty: Perspectives from the Social Sciences*, D. P. Moynihan, Ed. (Basic Books, New York, 1969), pp. 187–200.
13. M. Salling, M. E. Harvey, *Environ. Behav.* **13**, 131 (1981).
14. T. J. Kane, *Soc. Serv. Rev.* **61**, 405 (1987).
15. R. Radel, C. Clément-Guillotin, *Psychol. Sci.* **23**, 232 (2012).
16. H. Aarts, A. Dijksterhuis, P. De Vries, *Br. J. Psychol.* **92**, 631 (2001).
17. S. J. Karau, J. R. Kelly, *J. Exp. Soc. Psychol.* **28**, 542 (1992).
18. L. Acquaye, *Comm. Dev.* **42**, 16 (2011).
19. A. Banerjee, E. Duflo, *Poor Economics* (Public Affairs, New York, 2011).
20. S. Bair, *Low-Cost Payday Loans: Opportunities and Obstacles* (Annie E. Casey Foundation, Baltimore, 2005); www.aecf.org/upload/publicationfiles/fes3622h334.pdf.
21. *The High Cost of Being Poor: What It Takes for Low-Income Families to Get By and Get Ahead in Rural America* (Annie E. Casey Foundation, Baltimore, 2004); www.aecf.org/upload/publicationfiles/rf2022k560.pdf.
22. P. Chen, *Univ. Ill. Law Rev.* **2004**, 723 (2004).
23. L. A. Perlow, *Admin. Sci. Q.* **44**, 57 (1999).
24. S. Milgram, *J. Abnorm. Soc. Psychol.* **67**, 371 (1963).
25. J. M. Darley, C. D. Batson, *J. Pers. Soc. Psychol.* **27**, 100 (1973).
26. S. E. Asch, *Psychol. Monogr.* **70**, 1 (1956).
27. See supplementary materials on *Science* Online.
28. B. J. Schmeichel, K. D. Vohs, R. F. Baumeister, *J. Pers. Soc. Psychol.* **85**, 33 (2003).
29. M. C. Davidson, D. Amso, L. C. Anderson, A. Diamond, *Neuropsychologia* **44**, 2037 (2006).
30. J. K. Binkley, J. Bejnarowicz, *J. Retailing* **79**, 27 (2003).
31. J. Goldin, T. Homonoff, "Smoke Gets in Your Eyes: Cigarette Tax Salience and Regressivity," http://scholar.princeton.edu/jgoldin/files/goldin_homonoff.pdf.
32. M. S. Barr, *No Slack* (Brookings, Washington, DC, 2012).
33. D. Karlan, M. McConnell, S. Mullainathan, J. Zinman, Getting to the top of mind: How reminders increase saving (NBER Working Paper No. 16205, 2010); www.nber.org/papers/w16205.
34. D. Collins, J. Morduch, in *Insufficient Funds*, R. M. Blank, M. S. Barr, Eds. (Russell Sage Foundation, New York, 2009), chap. 4.

Acknowledgments: Supported by NSF award 0933497 and by the Canadian Institute for Advanced Research. Data are available at http://theslab.uchicago.edu/browse/scidata.

Supplementary Materials

www.sciencemag.org/cgi/content/full/338/6107/682/DC1
Materials and Methods
Tables S1 to S5

26 March 2012; accepted 13 September 2012
10.1126/science.1222426

AAAS 2013 ANNUAL MEETING
14-18 FEBRUARY • BOSTON

THE BEAUTY AND BENEFITS OF SCIENCE

HYNES CONVENTION CENTER

Join Us in Boston

Participate in seminars on the biology and evolution of human language, global fisheries and food supply, the brain's plasticity, and communicating science as well as 150 symposia across 14 tracks that cover the breadth of science, engineering, education, and policy.

- Share ideas with leaders in science and technology.
- Learn about recent developments in education and policy.
- Network with colleagues and make new connections.

View full program and take advantage of early registration and hotel discounts
www.aaas.org/meetings

Follow us on Twitter
www.twitter.com/AAASMeetings
#AAASmtg

Reporters: The EurekAlert! website hosts the AAAS Meeting Newsroom. Reporters can obtain details and register
www.eurekalert.org/newsroom

AAAS
ADVANCING SCIENCE, SERVING SOCIETY

AAAS presents the

2013 AAAS ANNUAL MEETING

THE BEAUTY AND BENEFITS OF SCIENCE

William H. Press
AAAS President and 2013 Program Chair

Dear Colleagues,

On behalf of the AAAS Board of Directors, it is my honor to invite you to join us in Boston for the 2013 AAAS Annual Meeting, 14-18 February. As you may know, this annual event is one of the most widely recognized global science gatherings, with hundreds of networking opportunities and broad U.S. and international media coverage.

The meeting's theme — *The Beauty and Benefits of Science* — points to the "unreasonable effectiveness" of the scientific enterprise in creating economic growth, solving societal problems, and satisfying the essential human drive to understand the world in which we live.

The phrase "unreasonable effectiveness" was coined in 1960 by physicist Eugene Wigner, who explored the duality of mathematics — both beautiful unto itself, and also eminently practical, often in unexpected ways. The scientific program will highlight the rich and complicated connections between basic and applied research, and how they bring about both practical benefits and the beauty of pure understanding.

Everyone is welcome at the AAAS Annual Meeting. Those who join us will have the opportunity to choose among a broad range of activities, including plenary and topical lectures by some of the world's leading scientists and engineers, multidisciplinary symposia, cutting-edge seminars, career development workshops, and an international exhibition. You and your family can also enjoy Family Science Days, a free event open to the general public.

The Annual Meeting reflects tremendous efforts from the AAAS sections, divisions, and committees, which I gratefully acknowledge. I also extend a personal thanks to the members of the Scientific Program Committee who selected and assembled the many excellent ideas and proposals into this outstanding meeting.

Please join us in Boston.

William H. Press
AAAS President and Program Chair;
Warren J. and Viola M. Raymer Professor in Computer Science and Integrative Biology
University of Texas at Austin

President's Address

Thursday, 14 February

William H. Press
Warren J. and Viola M. Raymer Professor in Computer Science and Integrative Biology, University of Texas at Austin

Dr. Press is a noted researcher in computer science, genomics, statistical methods, astrophysics, and international security. He is a member of the President's Council of Advisors on Science and Technology. His current research focus is bioinformatics and whole-genome genetics. He previously served as deputy laboratory director for science and technology at the Los Alamos National Laboratory and as a professor of astronomy and physics at Harvard University. He is a member of the U.S. National Academy of Sciences, a fellow of the American Academy of Arts and Sciences, and a member of the Council on Foreign Relations.

Plenary Speakers

Friday, 15 February

Sherry Turkle
Abby Rockefeller Mauzé Professor of the Social Studies of Science and Technology in the Program in Science, Technology, and Society, MIT

The Robotic Moment: What Do We Forget When We Talk to Machines?

Dr. Turkle is founder and director of the MIT Initiative on Technology and Self. She received a joint doctorate in sociology and personality psychology from Harvard University and is a licensed clinical psychologist. Her research focuses on the psychology of human relationships with technology, especially in the realm of how people relate to computational objects. She is an expert on mobile technology, social networking, and sociable robotics and a regular media commentator on the social and psychological effects of technology. Her most recent book is *Alone Together: Why We Expect More from Technology and Less from Each Other.*

Saturday, 16 February

Nathan Myhrvold
Founder and Chief Executive Officer, Intellectual Ventures

Modernist Cuisine: The Art and Science of Cooking

Dr. Myhrvold founded Intellectual Ventures after retiring as chief strategist and chief technology officer of Microsoft Corporation. At Intellectual Ventures, he is focused on a variety of business interests relating to the funding, creation, and commercialization of inventions. During his tenure at Microsoft, he was responsible for founding Microsoft Research and technology groups that resulted in many successful products. He has extensive experience linking research to product development and commercialization and holds hundreds of patents. As a postdoctoral fellow in applied mathematics and theoretical physics at Cambridge University, he worked with Stephen Hawking on research in cosmology, quantum field theory in curved space time, and quantum theories of gravitation. He earned a doctorate in theoretical and mathematical physics and a master's degree in mathematical economics from Princeton University. He also has a master's degree in geophysics and space physics and a bachelor's degree in mathematics from University of California, Los Angeles.

Sunday, 17 February

Robert Kirshner
Clowes Professor of Science, Harvard University

The Beauty of the Accelerating Universe

Dr. Kirshner is an astrophysicist studying the physics of supernovae and observational cosmology. He is a member of the High-z Supernova Search Team that used observations of extragalactic supernovae to discover the accelerating universe, which implied the existence of dark energy. Dr. Kirshner's graduate students Brian Schmidt and Adam Riess shared the 2011 Nobel Prize in Physics with Saul Perlmutter for the discovery of cosmic acceleration. He teaches a popular course for Harvard undergraduates called "The Energetic Universe" and is author of the book *The Extravagant Universe: Exploding Stars, Dark Energy, and the Accelerating Cosmos.* He is a past president of the American Astronomical Society, a member of the National Academy of Sciences, and a 2012 Guggenheim Fellow.

Monday, 18 February

Cynthia Kenyon
American Cancer Society Professor and Director of the Hillblom Center for the Biology of Aging, University of California, San Francisco

Mechanisms for Life Extension in *C. elegans*

Dr. Kenyon is a molecular biologist whose discovery with colleagues that a single-gene mutation could double the lifespan of the worm *C. elegans* sparked an intensive study of the molecular biology of aging. Her findings have since led to the discovery that an evolutionarily conserved hormone signaling system controls aging in other organisms as well, including mammals. As a doctoral student at Massachusetts Institute of Technology, she was the first to look for genes on the basis of their expression profiles, discovering that DNA damaging agents activate a battery of DNA repair genes in *E. coli.* She is a member of the U.S. National Academy of Sciences and the Institute of Medicine, a fellow of the American Academy of Arts and Sciences, and a past president of the Genetics Society of America.

Topical Lectures

Richard Alley
Evan Pugh Professor, Department of Geosciences, and Earth and Environmental Systems Institute, Pennsylvania State University
Ice Sheets, Sea Level, and Other Surprises: Benefits of Understanding Some Beautiful Places

Karl Deisseroth
Associate Professor of Bioengineering and Psychiatry, Stanford University
Optogenetics: Development and Application

Felice Frankel
Research Scientist, Center for Materials Science and Engineering, Massachusetts Institute of Technology
More Than Pretty Pictures: How the Process of Making Science Images and Graphics Clarifies Understanding

Nina Jablonski
Distinguished Professor of Anthropology, Pennsylvania State University
The Evolution and Meanings of Human Skin Color

Chad Mirkin
Director of International Institute for Nanotechnology and George B. Rathmann Professor of Chemistry, Northwestern University
"Artificial Atoms" Formed from Nucleic Acid Nanoparticle Conjugates: The Dawn of a New Periodic Table

Peter Norvig
Director of Research, Google Inc.
Technology for Educating Everyone

GEORGE SARTON MEMORIAL LECTURE IN THE HISTORY AND PHILOSOPHY OF SCIENCE

Silvan Schweber
Emeritus Professor of Physics and Richard Koret Professor in the History of Ideas, Brandeis University
Hans Bethe and Physics in the 20th Century

Topical Panel: European Science Policy on the Move

European science policy is as dynamic as ever. The new chief scientific advisor position to the European Commission President has been filled. National research councils are becoming more organized with the new Science Europe organization. Bottom-up research is increasingly supported at the European level. A bigger and larger EU research funding program, "Horizon 2020," will be launched next year from the European Commission. Four high-level experts will be asked to address questions about where European science policy is headed.

Moderated by: William H. Press, AAAS President and Program Chair; Warren J. and Viola M. Raymer Professor in Computer Science and Biology, University of Texas at Austin

Paul Boyle
President, Science Europe; Chief Executive, U.K. Economic and Social Research Council

Anne Glover
Chief Scientific Advisor to European Commission President, European Union

Helga Nowotny
President, European Research Council

Robert-Jan Smits
Director-General, Directorate-General for Research and Innovation, European Commission

To browse the updated program, register, and reserve hotel rooms, visit **www.aaas.org/meetings.**

Special Sessions

International Teacher-Scientist Partnership Conference
Wednesday, 13 February - Thursday, 14 February
Pre-registration required

Responsible Professional Practices in a Changing Research Environment
Thursday, 14 February
Pre-registration required

***Curiosity*'s Mission at Gale Crater, Mars**
Friday, 15 February
John Grotzinger, Fletcher Jones Professor of Geology, and Project Scientist, Mars Science Laboratory, California Institute of Technology
Open to all attendees

Seminars

Thursday, 14 February

Communicating Science

Scientific and technological issues increasingly trigger societal conflicts whenever they intersect with personal or political views. Particularly amid pressures on research and development budgets, and related concerns about transparency and accountability, today's scientists and engineers are challenged to communicate and engage with the public, reporters, and policy-makers. This seminar will share science communication expertise in working with different types of content, across a range of presentation formats, for various audiences.

Organized by: Cornelia Dean, *The New York Times;* Dennis Meredith, Science Communication Consultant

Working with Print, Broadcast, and Online Media

SPEAKERS
Juliet Eilperin, *The Washington Post*
Science Reporting at Newspapers in an Age of Tight Budgets, Constant Deadlines, Political Polarization, and Industry Upheaval

Chris Joyce, National Public Radio
Science Journalism: Alive and Kicking

Alan Boyle, NBCNews.com
Science Journalism: On Internet Time

Communicating Science to Policy-Makers

SPEAKERS
David Goldston, Natural Resources Defense Council
Why Can't They Just Do What's Right?: Misperceptions and Barriers to Science Communication

* Bill Foster, United States House of Representatives

Arthur Lupia, University of Michigan
Communicating Science in Politicized Environments

Visualizing Science

SPEAKERS
Felice Frankel, Massachusetts Institute of Technology
Tell Me What You See: Understanding Science Images

Erik Olsen, *The New York Times*
Explaining Science in Video

Yael Fitzpatrick, AAAS/*Science*
Starting with the Basics, Ending with a Bang

Engaging with Social Media

SPEAKERS
Scicurious, Neurotic Physiology
Science Blogging for Fun and Profit

Christie Wilcox, University of Hawaii
Science in a Digital Age

Dominique Brossard, University of Wisconsin, Madison
Science and the Public in New Information Environments

Friday, 15 February

The Biology and Evolution of Human Language

The human ability to learn and use language is deeply rooted in the biology of our species and processes of cultural evolution. We are biologically equipped for language in general, but inherit the specific cultural form of the languages in which we are socialized. The creation of new languages provides unique perspectives on language acquisition.

The Language Organ: The Bases of Human Language in Human Biology

Organized by: Stephen Anderson, Yale University

SPEAKERS
Stephen Anderson, Yale University
Human Language in the Broader Biological Context

Steven Pinker, Harvard University
Language as an Adaptation to the Cognitive Niche

Janet F. Werker, University of British Columbia
Infant Speech Perception: Biological Beginnings and Experiential Influences

Erich Jarvis, Duke University Medical Center
Learned Birdsong and the Neurobiology of Human Language

David Poeppel, New York University
What We Know About the Brain Bases of Language

Karen Emmorey, San Diego State University
The Generality of the Language Faculty: Biological Bases of Signed Language

Historical Syntax

Organized by: David Lightfoot, Georgetown University; Joseph Salmons, University of Wisconsin, Madison

SPEAKERS
David Lightfoot, Georgetown University
Phase Transitions in Language History

Tony Kroch, University of Pennsylvania
Studying the Diffusion of Syntactic Changes in Historical Corpora

Michel DeGraff, Massachusetts Institute of Technology
A Null Theory of Creole Formation

DISCUSSANT
Mark Liberman, University of Pennsylvania

Language Evolving: Genes and Culture in Ongoing Language Evolution

Organized by: Stephen C. Levinson, Max Planck Institute for Psycholinguistics; Karen Emmorey, San Diego State University

SPEAKERS
Simon E. Fisher, Max Planck Institute for Psycholinguistics
Language, Evolution, and the Genomics Revolution

Russell Gray, University of Auckland
Evolutionary Principles and the Diversification of Linguistic Form

Carol Padden, University of California, La Jolla
Culture Before Genes: The Case of a Village Sign Language

DISCUSSANTS
Dan Dediu, Max Planck Institute for Psycholinguistics; Fiona Jordan, Max Planck Institute for Psycholinguistics

**Invited*

Saturday, 16 February

Brain Function and Plasticity

Early experience has a lasting impact on our ability to perceive the world. It is widely understood that the brain is initially plastic and that its connections are tuned by early experience to match the environment. Recent evidence indicates that there is also considerable residual plasticity in the adult brain, which has implications for treatment of brain injury and recovery of lost function.

The Connectome: From the Synapse to Brain Networks in Health and Disease

Organized by: David Holtzman, Washington University, St. Louis

SPEAKERS

Mark F. Bear, Massachusetts Institute of Technology
Molecules and Mechanisms Involved in Synaptic Plasticity in Health and Disease

Jeff Lichtman, Harvard University
Connectomics: Developing a Wiring Diagram for the Mammalian Brain

Steve Petersen, Washington University, St. Louis
The Human Connectome Project

Marcus E. Raichle, Washington University, St. Louis
The Brain's Dark Energy and the Default Mode Network

Nicole Calakos, Duke University
Synaptic Plasticity in the Basal Ganglia in Health and Disease

William W. Seeley, University of California, San Francisco
Brain Networks: Linking Structure and Function in Neurodegenerative Diseases

Old Dogs, New Tricks: How Plastic Is the Adult Human Brain?

Organized by: Daphne Maurer, McMaster University; Susan M. Fitzpatrick, James S. McDonnell Foundation

SPEAKERS

Daphne Maurer, McMaster University
Improving Vision After the Critical Period

Alex R. Carter, Washington University School of Medicine, St. Louis
A "New Trick" for Neuro-Rehabilitation: Treating Networks Not Spots

Arthur Kramer, University of Illinois, Urbana-Champaign
Physical Fitness Effects on Brain and Cognition

DISCUSSANT

Susan M. Fitzpatrick, James S. McDonnell Foundation

Teaching the Brain to Speak Again: New Frontiers in Trauma and Stroke Recovery

Organized by: Nan Ratner, University of Maryland; Margaret Rogers, American Speech-Language-Hearing Association

SPEAKERS

Julius Fridriksson, University of South Carolina
Real-Time Audiovisual Feedback Enables Stroke Patients to Reacquire Speech

Cynthia Thompson, Northwestern University
Neurocognitive Mechanisms of Syntactic Recovery in Agrammatism

Sheila Blumstein, Brown University
Auditory Modeling Improves Aphasic Speech Production Recovery

Sunday, 17 February

Global Fisheries and Food Supply

Ecosystem sustainability may be endangered by exploitation. As the rising world population increases demand for food production, the sustainable development of goods and services and the protection of ocean and fisheries environments will be a formidable challenge. Cooperation across scientific disciplines and international borders is crucial to securing the future ocean.

Realizing Jacques Cousteau's Vision of Aqua-Farming Replacing Hunting of the Sea

Organized by: KeShun Liu and Jeffrey Silverstein, U.S. Department of Agriculture (USDA) Agricultural Research Service

SPEAKERS

Margareth Overland, Norwegian University of Life Sciences
Sustainable Ingredient Development for Aquaculture Feed

Steven Summerfelt, The Conservation Fund Freshwater Institute
Responsible Aquaculture by Minimizing Environmental Impacts on Land and Water

Jeffrey Silverstein, USDA Agricultural Research Service
Responsible Aquaculture Development: A Holistic Approach

Moving Toward Sustainable Development of Large Marine Ecosystems
Organized by: Kenneth Sherman, National Oceanic and Atmospheric Administration (NOAA)

SPEAKERS

Hashali Hamukuaya, Benguela Current Commission
The Resilience and Robustness of the Benguela Current Large Marine Ecosystem

Yihang Jiang, United Nations Development Program/Global Environment Facility Yellow Sea Project
The Resilience and Robustness of the Yellow Sea Large Marine Ecosystem

Michael Akester, United Nations Office for Project Services
The Resilience and Robustness of the Humboldt Current Large Marine Ecosystem

Weaving the Future Ocean Web Through Collaboration: the Nereus Program

Organized by: Yoshitaka Ota and Villy Christensen, University of British Columbia

SPEAKERS

Henrik Osterblom, Stockholm University
Weaving the Future Ocean Food Web: The Nereus Diagram

Ryan Rykaczewski, Princeton University
Linkages Between the Carbon Cycle and Biota in the Global Ocean

Andre Boustany, Duke University
Habitat and Fisheries Interactions: Spatial Patterns Under Climate Change

Marc Metian, Stockholm Resilience Center
Bridging Demand and Supply of Seafood: Sustainable Aquaculture in a Changing World

Chris McOwen, United Nations Environment Program, World Conservation Monitoring Center
Linking Terrestrial Processes, Coastal Landscapes, and Marine Ecosystems

DISCUSSANTS

Claire Nouvian, BLOOM Association; Philippe Cury, Center for Mediterranean and Tropical Fisheries Research, France

Symposium Tracks

Animal, Plant, and Food Sciences

Advancing Food Safety in a Global Marketplace

Organized by Nicola J. Stagg, Dow AgroSciences; P. Michael Bolger, Retired

Alternate Paths to Food Security: Making the Right Choices While Feeding the World

Organized by Albert G. Medvitz, McCormack Sheep and Grain

Employing Cutting-Edge Plant Science To Address Global Issues that Threaten Mankind

Organized by Melvin J. Oliver, U.S. Department of Agriculture

Fixing the Broken Tomato: What We Like and Why We Like It

Organized by Linda M. Bartoshuk and Harry J. Klee, University of Florida

How Microbes Can Help Feed the World

Organized by Ann Reid, American Academy of Microbiology

Plant Viruses: Mutualists, Modulators, and Manipulators
Organized by Ulrich Melcher, Oklahoma State University; Nilsa A. Bosque-Pérez, University of Idaho

Power of New Generation Biotechnology To Transform Global Food Security
Organized by Jenny Gu and Larry Beach, U.S. Agency for International Development

Transforming Productivity and Incomes of Poor Farm Households in the Developing World
Organized by Jerry Glover and Elizabeth Skewgar, U.S. Agency for International Development

Why a Calorie Is Not a Calorie and Why It Matters for Human Diets
Organized by Rachel N. Carmody and Richard Wrangham, Harvard University

Anthropology, Culture, and Language

Beyond Color: How Human Skin Interacts with Our World
Organized by Nina Jablonski, Pennsylvania State University; Ellen E. Quillen, Texas Biomedical Research Institute

Democratizing Science: Virtualization and Global Natural History Repositories
Organized by Herbert D.G. Maschner, Idaho Museum of Natural History; Corey D. Schou, Idaho State University

The Scars of Human Evolution
Organized by Karen Rosenberg, University of Delaware; Rachel Caspari, Central Michigan University

The Whole of Culture: Anthropology Back on Track
Organized by Dwight Read, University of California, Los Angeles; Fadwa El Guindi, Qatar University

Atmospheric, Hydrospheric, and Oceanic Sciences

Advancing the Frontiers of Understanding the Ocean and Its Role in the Earth System
Organized by Robert A. Weller, Woods Hole Oceanographic Institution

Can Oceans Help Meet the Century's Looming Food Security Challenges?
Organized by Steven Gaines, University of California, Santa Barbara

Contributions of Citizen Scientists to Climate Science
Organized by Imke Durre

Electric Oceans: Finding the Space for Marine Renewable Energy in Crowded Waters
Organized by Jodie Toft and Mary Ruckelshaus, Natural Capital Project

Green Dreams, Blue Waves, and Shades of Gray: The Reality of Water
Organized by E. John Sadler, U.S. Department of Agriculture; Fred Vocasek, Servi-Tech Laboratories

The National Climate Assessment: Draft Findings for 2013 and Sustaining the Process
Organized by Emily Therese Cloyd, U.S. Global Change Research Program; Kathy Jacobs, Office of Science and Technology Policy, Executive Office of the U.S. President

U.S. Climate and Weather Extremes: Past, Present, and Future
Organized by Connie Woodhouse, University of Arizona; Gregory Wiles, The College of Wooster; Ester Sztein, U.S. National Academies

Biological Science and Genomics

A Decade After "Forensic Science: Oxymoron?": Will There Be Real Change?
Organized by Clifford H. Spiegelman, Texas A&M University

Confluence of Streams of Knowledge: Biotechnology and Nanotechnology
Organized by Elicia M.A. Maine, Simon Fraser University; James M. Utterback, Massachusetts Institute of Technology

Dragons of the East: China's Paleontological Riches
Organized by Richard A. Stone, AAAS/*Science*

Evolution of Giants: The Great Whales
Organized by Jere H. Lipps, Cooper Archaeological and Paleontological Center; Nicholas D. Pyenson, Smithsonian National Museum of Natural History

How Macro-Evolutionary Studies Call for an Extended Synthesis
Organized by Nathalie L. Gontier, University of Lisbon; Emanuele Serrelli, University of Milan-Bicocca

How Symbiosis, Horizontal Gene Transfer, and Virolution Call for an Extended Synthesis
Organized by Nathalie L. Gontier, University of Lisbon

Innovations in Imaging
Organized by Amy S. Gladfelter, Dartmouth College

Interfacing with the Body Using Implants and Prostheses
Organized by Erin Heath, AAAS Office of Government Relations

New Frontiers in Single Molecule Detection and Single Cell Analysis
Organized by X. Nancy Xu, Old Dominion University

Personal Genetics: An Intersection Between Science, Society, and Policy
Organized by Peter Yang, Brenna Krieger, and Kevin Bonham, Harvard University

Resurrected Ancestral Proteins: Fundamentals and Applications
Organized by Antony Dean and Romas Kazlauskas, University of Minnesota

The Architecture of the Cell Nucleus
Organized by Gary Felsenfeld, National Institute of Diabetes and Digestive and Kidney Diseases

The Invisible Revealing the Dangerously Beautiful
Organized by Isabelle Boscaro-Clarke, Diamond Light Source

The Science of Uncertainty in Genomic Medicine
Organized by Shili Lin, Ohio State University; Reed E. Pyeritz, University of Pennsylvania

Visualizing Chemistry: Seeing Another Dimension of Plants and Animals
Organized by Barbara Illman, U.S. Forest Service; Janos Kirz, Lawrence Berkeley National Laboratory

Cognitive, Neural, and Social Sciences

Advances in Brain-Machine Interfaces: Applications and Implications
Organized by Peyton West and Jennifer Wiseman, AAAS Dialogue on Science, Ethics, and Religion

Breakthroughs in Our Understanding of Primate Cognition and Psychopathology
Organized by Neal D. Barnard, George Washington University

Computation, Computational Efficiency, and Cognitive Science
Organized by Robert C. Berwick, Massachusetts Institute of Technology; Anna Maria Di Sciullo, University of Quebec, Montreal

Evidence from Music, Fiction, and Visual Arts: Transfer of Learning from the Arts?
Organized by Ellen Winner, Boston College

The Economic Costs of Crime and Justice in the United States
Organized by William Alex Pridemore, Indiana University

The Elusive Common Good: What Moral Psychology and Neuroscience Now Tell Us
Organized by Robert E. Fay, Westat

Understanding Memory: The Legacy of Case H.M.
Organized by Howard Eichenbaum, Boston University

Why Is Living Healthily So Difficult?
Organized by Benedikt Herrmann and Geraldine Barry, Joint Research Center, European Commission

Communication and Public Programs

A New Social (Media) Contract for Science
Organized by Elizabeth Neeley, COMPASS

Artful Science
Organized by John R. Jungck, Beloit College

Creative and Participatory Methods in Climate Communication
Organized by Eli Kintisch, AAAS/*Science*; Juliette N. Rooney-Varga, University of Massachusetts, Lowell

Engaging Lay Publics in Museums on Provocative Societal Questions Related to Science
Organized by Larry Bell, Museum of Science, Boston

In the Eye of the Beholder: Engaging the Public in Societal Implications of Science
Organized by Larry Bell and David Sittenfeld, Museum of Science, Boston

New Tools to Engage Publics and Assess the Impact of Science Communication
Organized by David Herring, NOAA

Science Festivals: Grand Experiments in Public Outreach
Organized by Ben Wiehe, MIT Museum

Scientists' Understanding of the Public
Organized by John C. Besley, Michigan State University

Synthetic Biology and Public Perceptions: Communication and Engagement
Organized by Peyton West, AAAS Dialogue on Science, Ethics, and Religion; Tiffany Lohwater, AAAS Office of Public Programs

The Beauty and Benefits of Escaping the Ivory Tower
Organized by Dawn J. Wright, Environmental Systems Research Institute; Elizabeth Hadly, Stanford University

Wild Weather, Climate Change, and Media: Communicating Science, Uncertainty, and Impact
Organized by James McCarthy and Cristine Russell, Harvard University

Writing About Science for the Public
Organized by Daniel Levitin, McGill University

Education and Human Resources

Accelerating School Readiness and Cumulative Academic Performance: Birth to Age 10
Organized by David L. Featherman, University of Michigan

Animals on Exhibit
Organized by Joe Zammit-Lucia, Artist and Independent Scholar; Linda Kalof, Michigan State University

Benefits Beyond Beauty: Integration of Art into STEM Education and Research
Organized by Rieko Yajima, AAAS Center of Science, Policy, and Society Programs; Gunalan Nadarajan, Maryland Institute College of Art

Creating Interdisciplinary Competency-Based Curricula for Undergraduate Students
Organized by Dee U. Silverthorn, University of Texas, Austin; William R. Galey, Howard Hughes Medical Institute

Engaging Students in Complex Science Learning via Games and Simulations
Organized by Susannah Gordon-Messer, Massachusetts Institute of Technology; Jody Clarke Midura, Harvard Graduate School of Education

For Scientists and Society: A New Vision of Chemistry Graduate Education
Organized by Bassam Shakhashiri, University of Wisconsin, Madison

How K-12 Curriculum Reform Can and Will Affect University Studies
Organized by Arthur Eisenkraft, University of Massachusetts, Boston

Increasing Diversity in Science: Learning from Successful Program Models
Organized by Rebecca L. Smith, University of California, San Francisco

Overcoming Dualisms and Promoting Minority Inclusion in Science Networks and Pipelines
Organized by Roberta Spalter-Roth, American Sociological Association

Preparing Our Future Scientific Work Force to Ensure the Success of Science
Organized by Cynthia N. Fuhrmann, University of Massachusetts Medical School; Bill Lindstaedt, University of California, San Francisco; Bruce M. Alberts, AAAS/*Science*

Science After School: Scientists Inspire the Next Generation Outside of the Classroom
Organized by Carol M. Tang, Coalition for Science After School; Elizabeth Stage, University of California, Berkeley

The 25th Anniversary of the First Collection in the History of Women in Science
Organized by Pnina G. Abir-Am, Brandeis University; Joy Harvey, Independent Scholar

Undergraduate Science Education at a Crossroad: Responding to Research Findings
Organized by Jay B. Labov, U.S. National Academy of Sciences; Susan Singer, Carleton College; Martin Storksdieck, U.S. National Research Council

Where and How Are Research and Innovation Fostering Job Creation?
Organized by Florent Bernard, European Commission

Environment and Ecology

A 50 Year Legacy: Why does Rachel Carson Matter?
Organized by Gregg Zachary and Jane Maienschein, Arizona State University

A Science and Art Interface: Geographic Information Systems and Remotely Sensed Images
Organized by Daniel Griffith, University of Texas, Richardson; Ren Vasiliev, State University of New York, Geneseo

Building Resilience of Coastal Communities to Environmental and Institutional Shocks
Organized by Richard Pollnac, University of Rhode Island; Joshua E. Cinner, James Cook University

Converging on Climate Change: From Middens to Models, the Savannah to Snæfellsjökull
Organized by Samantha Christey, European Research Council

Environmental Challenges and Adaptation in Cities
Organized by Matthias Ruth, University of Maryland

Finding the Fault: Sampling the Source of the M9.0 Tohoku Earthquake
Organized by Charna Meth, Consortium for Ocean Leadership

Indigenous and Western Science: Collaborating for Better Research and Education
Organized by Patricia B. Campbell, Campbell-Kibler Associates

New Dimensions of Biodiversity Science and Application
Organized by Julia K. Parrish, University of Washington; Sandy J. Andelman, Conservation International

Partners for the Earth: Scientists and Religious Groups Working for the Environment
Organized by Jennifer Wiseman and Peyton West, AAAS Dialogue on Science, Ethics, and Religion

Spatially Distributed Environmental Factors and Health Effects
Organized by Katherine B. Ensor, Rice University

The Toxicological Impact of the Gulf of Mexico Oil Spill on Human and Wildlife Health
Organized by John Pierce Wise, University of Southern Maine; R. Joseph Griffitt, University of Southern Mississippi

Global Perspectives and Issues

A Tale of Two Networks: Connecting the African Drylands, Rio de Janeiro, and Women
Organized by Marcelo Vinces, AAAS Science and Technology Policy Fellow, National Science Foundation; Riju Srimal, AAAS Science and Technology Policy Fellow, National Institutes of Health; Gillian Bowser, Colorado State University

Bridging the Gap Between Global Environmental Change Research and Development
Organized by Timothy L. Killeen, National Science Foundation; Erika von Schneidemesser, AAAS Science and Technology Policy Fellow, National Science Foundation

Future Earth: International Coordination of Research for Global Sustainability
Organized by Roberta Quadrelli, Julie DeMeester, and Anne-Sophie Stevance, International Council for Science

Global Food Security in Relation to Climate, Population, Technology, and Earth Changes
Organized by Alfred M. Powell and Felix Kogan, NOAA

Lead: The Global Poison — Humans, Animals, and the Environment
Organized by Mark A. Pokras, Tufts University; Ronnie Levin, U.S. Environmental Protection Agency

Measurement of Economic and Social Impacts of Science and Technology Investments
Organized by Yuko Ito and Aska Takeshiro, National Institute of Science and Technology Policy, Japan

Networks of Discovery: Delivering Unsurpassed Insight into Changing Global Ecosystems
Organized by Kristen Milligan and Joe A. Tyburczy, Oregon State University

Science from the International Space Station
Organized by Julie A. Robinson, NASA Johnson Space Center; Christopher L. Martin, Oberlin College

Smart Phones, Smart Devices, Social Networks, and Smart Health Care
Organized by Vinton Cerf, Google Inc.; Ram Sriram, National Institute of Standards and Technology

The Invisible Beauty: How Security Research Helped in Real Life, but Nobody Noticed
Organized by Stephan Lechner, Joint Research Center, European Commission

The Role of Higher Education in Science Diplomacy: Possibilities and Potential Pitfalls
Organized by Elizabeth E. Lyons, U.S. Department of State

Unreasonable Usefulness of Test-Ban Verification for Disaster Warning and Science
Organized by Annika Thunborg, Preparatory Commission for the Comprehensive Nuclear-Test-Ban Treaty Organization

Health and Pharmaceutical Science

Clinical Trial and Error: Beauty and the Beast
Organized by Aidan Gilligan, SciCom–Making Sense of Science; Thomas Hartung, Johns Hopkins University

Control Engineering of Brain in Health and Disease
Organized by Steven J. Schiff, Mauricio Terrones, and Alok Sinha, Pennsylvania State University

Cultivating the Science and Scientists for 21st Century Drug Discovery and Development
Organized by Alice Clark, University of Mississippi

Engineering the Nervous System: Solutions to Restore Sight, Hearing, and Mobility
Organized by Sanna Fowler, Ecole Polytechnique Fédérale, Lausanne

Monitoring and Assuring the Quality of Essential Medicines
Organized by Gaurvika Nayyar and Joel Breman, National Institutes of Health

Multi-Scale Study of Cancer
Organized by Mark Alber, University of Notre Dame; Jill P. Mesirov, Broad Institute of Massachusetts Institute of Technology and Harvard University

Pathways to Health Equity for Aboriginal Peoples
Organized by Danièle St-Jean, Canadian Institutes of Health Research

Scientific Advances and New Strategies for Reconstruction of Oral and Facial Tissues
Organized by Paul Krebsbach, University of Michigan; Barbara D. Boyan, Georgia Institute of Technology

Stem Cell-Based Bioartificial Tissues and Organs
Organized by Sabina Bossi, Karolinska Institute

Stroke Research: New Concepts and Innovative Solutions
Organized by Ruxandra Draghia-Akli and Virginija Dambrauskaite, European Commission

The Benefits of Randomized Experiments for Science and Society
Organized by Daniel McCaffrey, RAND Corp.

Materials Science and Chemistry

Attosecond Science in Chemical, Molecular Imaging, Spintronics, and Energy Science
Organized by Andre D. Bandrauk, University of Sherbrooke; Margaret M. Murnane, University of Colorado, Boulder

Nucleic Acid Nanotechnology
Organized by Andrew D. Ellington, University of Texas, Austin

Quantum Sensors: Toward the Ultimate Limits
Organized by Martin Laforest, University of Waterloo

Remembering Galileo: Lithium Ion Batteries, Atomic Clocks, and Other Stories
Organized by Carlos Saraiva Martins, European Commission

Surprises at the Frontier of the Periodic Table: Novel Paradigms in Actinide Science
Organized by Geraldine Barry and Roberto Caciuffo, Joint Research Center, European Commission

Translation of Mussel Adhesion to Beneficial New Concepts and Materials
Organized by Herbert Waite and Alison Butler, University of California, Santa Barbara

Watching Atoms Move: From Structures to Dynamics to Mesoscale Processes
Organized by Eric Stach, Brookhaven National Laboratory; Donald Baer, Pacific Northwest National Laboratory

Physical Sciences

Beauty and the Beast: Supersymmetry and the Dark Matter in the Universe
Organized by Maria Spiropulu, California Institute of Technology

Compressive Sensing: Sensing Sparse Phenomena in Theory and Practice
Organized by Mark Davenport, Georgia Institute of Technology; Emmanuel Candès, Stanford University

Exploring Other Worlds and Seeing Our Own Anew
Organized by Samuel P. Kounaves, Tufts University

How Fundamental Computing Research Touches Everyday Lives
Organized by Andrew Bernat and Erwin P. Gianchandani, Computing Research Association

Is Beauty Truth? Mathematics in Physics from Dirac to the Higgs Boson and Beyond
Organized by Thomas J. Kelleher, Basic Books

Mathematics of Tipping Points: Framework, Applications, and Prediction
Organized by Mary Silber, Northwestern University; Mary Lou Zeeman, Bowdoin College

Neutrinos: Nature's Smallest Surprises
Organized by Janet Conrad, Massachusetts Institute of Technology

Predictability: From Physical to Data Sciences
Organized by Albert-Laszlo Barabasi, Northeastern University

Predictive Model of the Internal Combustion Engine
Organized by Nils Hansen and Ahren Jasper, Sandia National Laboratories

The Beauty and Utility of Scientific Images
Organized by Kartik Sheth, National Radio Astronomy Observatory; Margaret Meixner, Space Telescope Science Institute

The Higgs Boson: Past, Present, and Future
Organized by James Gillies, European Organization for Nuclear Research (CERN)

The Mirror World of Antiatoms and Antimolecules
Organized by Charles W. Clark, Joint Quantum Institute; Michael J. Brunger, Flinders University

Tiny But Mighty: Neutrinos and the New Frontiers of Science
Organized by Katie Yurkewicz, Fermi National Accelerator Laboratory

Understanding the Universe Through Images of the Cosmic Microwave Background
Organized by Asantha Cooray, University of California, Irvine

What's Hot in Cold
Organized by Charles W. Clark, Joint Quantum Institute

Worldwide Progress Toward Fusion Energy
Organized by Ned R. Sauthoff, Oak Ridge National Laboratory

Public Policy

Advanced Manufacturing: Today, Tomorrow, and Beyond
Organized by Stephanie Shipp, Science and Technology Policy Institute

Can Exposure Science Quell the Furor over Environmental Endocrine Disruption?
Organized by Justin G. Teeguarden, Pacific Northwest National Laboratory

Capturing "Complicated Duality": Evaluating the Outcomes and Impacts of Science
Organized by Julia E. Melkers, Georgia Institute of Technology

Coal, Communities, Commerce, and China: A Nexus for the Sciences and Public Policy
Organized by Donna Gerardi Riordan, DGR Strategies

Convergence of Physical, Engineering, and Life Sciences: Next Innovation Economy
Organized by Larry A. Nagahara, National Cancer Institute

Effective Science for Community Adaptation to Climate Change
Organized by Thomas Webler, Social and Environmental Research Institute

Getting What We Pay For: Incentives, Peer Review, and Conservatism in Science
Organized by P. Kyle Stanford, University of California, Irvine

Predicting Major Events and Planning for Hazards: An Art or Science?
Organized by Julia Wilson, Sense About Science; Albert Yuan, *San Lian Life Weekly*

Promoting Collaborative, Policy-Relevant Science: Learning from Fulbright
Organized by Patrick Feng, University of Calgary; Walter E. Baethgen, Columbia University

Role of Science in the American Democracy: Roots, Tensions, and Paths Forward
Organized by Peter Frumhoff and Pallavi Phartiyal, Union of Concerned Scientists; James McCarthy, Harvard University

Tales of the Unexpected: How Science Advisers Manage Uncertainty
Organized by Geraldine Barry, Joint Research Center, European Commission

The Beauty, Benefits, and Challenges of Transformative Research
Organized by Bhavya Lal, Science and Technology Policy Institute; Edward J. Hackett, Arizona State University

The Science of Politics
Organized by Barbara Jasny, AAAS/*Science*; David Lazer, Northeastern University

Toward Bridging the Duality of Science: Seed-Push, Issue-Driven, or "Encounter"?
Organized by Tateo Arimoto, National Graduate School for Policy Studies, Japan; Chikako Maeda, Japan Science and Technology Agency; Yuko Harayama, Organization for Economic Cooperation and Development

Understanding and Communicating Uncertainty in Climate Change Science
Organized by Richard L. Smith, University of North Carolina, Chapel Hill

Sustainability and Resource Management

From Promise to Proof: How Ecosystem Service Science Is Transforming Real Decisions
Organized by Karen L. McLeod and Erica Goldman, COMPASS; Heather Tallis, Natural Capital Project

Getting to Global Ecological Sustainability: Climate and Small-Planet Ethics
Organized by Kai Ming A. Chan and Paige Olmsted, University of British Columbia

Global Health and Environmental Impacts of E-Waste Recycling
Organized by Erica L. Dahl, SafeBridge Consultants Inc.; Bruce A. Fowler, ICF International

Is the Future of Conservation at a Crossroads?
Organized by Jennifer Howard, AAAS Science and Technology Policy Fellow, NOAA; Colin F. Quinn, NOAA

Socio-Hydrology: Co-Evolution and Future of Human-Water Resource Systems
Organized by Veena Srinivasan, Pacific Institute

Sustainable Chemical Manufacturing in a Resource-Limited World
Organized by Susannah Scott, University of California, Santa Barbara

Water Purification and Monitoring Under Minimal Resource Setting
Organized by Sushanta Mitra and Thomas Thundat, University of Alberta; Ni-Bin Chang, University of Central Florida

What Are the Roles of Knowledge Institutions in Sustainability?
Organized by David D. Hart, University of Maine; Lewis Gilbert, University of Minnesota, Saint Paul; Margaret A. Palmer, National Socio-Environmental Synthesis Center

What Is Science's Role in Developing Aquaculture as a Sustainable Use of the Ocean?
Organized by Paul A. Sandifer, NOAA; Barry Costa-Pierce, University of New England; Michael Rust, NOAA

AAAS, publisher of *Science*, thanks the sponsors and supporters of the 2013 Annual Meeting

EUROPEAN COMMISSION
European Research Area

AAAS thanks

THE KAVLI FOUNDATION

for its generous support of the Science Journalism Awards

Register Today at Discounted Rates

Registration

Discounted advance registration rates are available until Monday, 21 January 2013.

Take advantage of unlimited access to all symposia, seminars, topical lectures, plenary events, career workshops, the Exhibit Hall, and a variety of networking opportunities.

Professional
$295 Member/ $375 New Member/ $399 Non-Member

Postdoc
$235 Member/ $315 New Member/ $335 Non-Member

K-12 Teacher
$235 Member/ $315 New Member/ $355 Non-Member

Emeritus
$235 Member/ $315 New Member/ $355 Non-Member

Student
$60 Member/ $70 New Member/ $90 Non-Member

After 21 January 2013, on-site rates apply.

For more information, visit **www.aaas.org/meetings**

Housing

Special room rates and travel benefits are available to Annual Meeting registrants.

Sheraton Boston Hotel
Rate: $205 single/double

Hilton Back Bay
Rate: $197 single/ $207 double

Boston Marriott Copley Place
Rate: $192 single/ $208 double

Rooms are available on a first-come, first-served basis until 21 January 2013.

AAAS 2013 ANNUAL MEETING
14-18 FEBRUARY • BOSTON

Science Careers Advertising

For full advertising details, go to ScienceCareers.org and click For Employers, or call one of our representatives.

Tracy Holmes
Worldwide Associate Director
Science Careers
Phone: +44 (0) 1223 326525

THE AMERICAS

E-mail: advertise@sciencecareers.org
Fax: 202-289-6742

Tina Burks
East Coast/West Coast/South America
Phone: 202-326-6577

Allyson Rosen
Midwest/Canada/Corporate
Phone: 202-326-6578

Marci Gallun
Sales Administrator
Phone: 202-326-6582

Online Job Posting Questions
Phone: 202-312-6375

EUROPE & REST OF WORLD

E-mail: ads@science-int.co.uk
Fax: +44 (0) 1223 326532

Lucy Nelson
Phone: +44 (0)1223 326527

Kelly Grace
Phone: +44 (0) 1223 326528

JAPAN

Yuri Kobayashi
Phone: +81-50-3696-5100
E-mail: ykobayas@aaas.org

CHINA & TAIWAN

Ruolei Wu
Phone: +86-1367-1015-294
E-mail: rwu@aaas.org

NAVAL RESEARCH LABORATORY
Superintendent, Materials Science and Technology Division
www.nrl.navy.mil
Senior Executive Service Career Opportunity
ES-806, 1301, or 1310: $119,554 to $179,700 per annum*

*Actual salary may vary depending on the scope and complexity of the position and the qualifications and current compensation of the selectee.

Become a member of an elite research and development community involved in basic and applied scientific research and advanced technological development for tomorrow's Navy and for the Nation

The Superintendent of the Materials Science and Technology Division located at the Naval Research Laboratory, Washington, DC, is responsible for the oversight of approximately 172 employees (including government, contract and post doctorate fellows), most of whom are professional scientists and engineers. The Division consists of: the Multifunctional Materials Branch, the Materials and Sensors Branch, The Center for Computational Materials Science, and the Special Projects Group. Division research is at the frontiers of materials science and technology and encompasses the intrinsic behavior of metals, alloys, ceramics, glasses, and composites and their performance and reliability in Naval structures and devices. The ultimate goal is to provide materials knowledge that enables new and/or improved military performance that lead to transformational capabilities. The Division has an annual budget of over $38 million.

The Superintendent is responsible for:

- Technical and administrative management of a broad program of highly sophisticated basic and applied research and exploratory and advanced development of materials; and technical management of industrial contract programs which provide new and improved materials for new weapons systems;
- Overall planning and direction of a coordinated research and development program related to materials science designed to meet the present and future needs of the Navy;
- Obtaining support for work of the various Division programs, stimulating interest and activity on the part of the Division personnel, and providing creative thinking, suggestions and judgments with respect to major research encountered;
- Acting as principal consultant to the Navy, other agencies and nations on the science and developing applications for the research programs under his/her cognizance.

Applicants should be recognized as national/international authorities and should have planned and executed difficult programs of national significance that show outstanding attainment in the field of materials science. For information regarding this vacancy and specific instructions on how to apply, go to **www.usajobs.gov** and enter the following announcement number: **NW2XXXX-00-752920K9464770-S**. The announcement closes on **30 November 2012**. Contact Ginger Kisamore at **ginger.kisamore@nrl.navy.mil** if you need additional information. E-mailed resumes **cannot** be accepted.

NRL is an Equal Opportunity Employer

NRL• 4555 Overlook Ave SW, Washington DC 20375

Research Scientist (Molecular Catalysis)
Division: Chemical Sciences

The Joint Center for Artificial Photosynthesis (JCAP) will focus on the development of molecularly designed, inorganic catalysts for electrocatalytic water splitting. JCAP is a Solar Fuels Innovation Hub recently funded by the Department of Energy (122 M, 5 years) with physical location at the sites of its major partners, Caltech (South) and Lawrence Berkeley National Laboratory (North). The researcher will take major responsibility for the synthetic and catalyst evaluation efforts in the Molecular Catalysis Project located at JCAP North Site.

For a Molecular Catalysis Chemist, this position offers a unique opportunity for an early career researcher to assume a key role at the inception of the JCAP research effort in development of efficient electrocatalysts for artificial photosynthesis. Anticipated activities involve novel synthetic approaches, including those based on molecular design and precursor chemistry, for targeting novel catalytic structures such as inorganic clusters, nanostructures, and stabilized, surface-bound catalytic centers. Significant effort will also involve electrochemical studies for the evaluation of new catalysts, and for characterizations of active catalytic centers and catalytic mechanisms.

For more information about this position and to apply online, visit **http://go.lbl.gov/75229** and follow the instructions to complete the application process.

Berkeley Lab is an affirmative action/equal opportunity employer committed to the development of a diverse workforce.

BERKELEY LAB

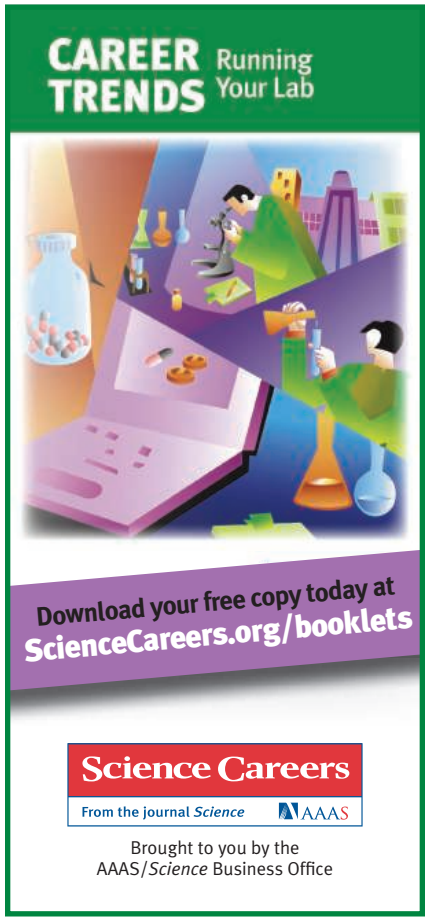

TEXAS TECH UNIVERSITY HEALTH SCIENCES CENTER™
Senior Vice President for Research

GENERAL SUMMARY: Texas Tech University Health Sciences Center (TTUHSC) invites nominations and applications for the position of Senior Vice President for Research. TTUHSC is a member of the Texas Tech University System which also includes Texas Tech University in Lubbock and Angelo State University in San Angelo. The Senior Vice President will serve as the chief administrative officer responsible for all research enterprises at the TTUHSC campuses located in Lubbock, Amarillo, Abilene, El Paso, Dallas, Midland and Odessa. Reporting directly to the President of TTUHSC, the Senior Vice President will actively promote the research enterprises of TTUHSC within the Texas Tech University System as well as champion its research mission at both the state and national level. This individual will be the principal architect for strengthening and growing the research enterprise of TTUHSC.

KEY RESONSIBILITIES

1. Oversees the overall research program and infrastructure of TTUHSC.
2. Develops, together with university faculty engaged in research, a strategic plan for growing and enhancing the quality, visibility, and impact of basic, translational, and clinical research conducted within the university.
3. Oversees the budget for the Office of Research and component functions as well as funds/resources for the development of research efforts on all campuses.
4. Expands and strengthens the basic and clinical research enterprise at TTUHSC, particularly focusing on faculty hiring, strategic investments in facilities and space, and increasing external research funding from national, state and local sources.
5. In close coordination with the Texas Tech University (TTU) Senior Vice President for Research, grows and explores strategic research collaborations between the two institutions.
6. Works closely with the TTU Vice Chancellor for Research, Commercialization and Federal Relations and the TTUHSC Assistant Vice Chancellor for Institutional Development in identifying, establishing, and maintaining collaborations with external stakeholders such as corporations, government officials, and foundations that will provide support for basic, translational, and clinical research and commercialization at the university.
7. Provides supervision for the Research Integrity Office (RIO), responsible for ensuring compliance with agency guidelines; Office of Sponsored Programs (OSP) review and approval of proposals for extramural funding and the acceptance of extramural grants for research, training and services; responsible for the Laboratory Animal Research Center (LARC) including maintenance and health of animals used in research.
8. Responsible for reporting compliance issues to federal agencies for activities related to the Institutional Review Board (IRB), Institutional Animal Care and Use Committee (IACUC), and financial conflicts of interest in research.
9. Actively enhances the visibility of university research and provides external agencies, corporations and foundations with information on the research, training and service capabilities of the university.
10. Provides administrative oversight in implementing the university's agreements with state and federal agencies, corporations, and foundations in the conduct of research and development activities.
11. Provides recommendations, leadership and management of proposals for large-scale research activities such as university-wide research and pilot centers, centralized research facilities, interdisciplinary research programs and inter-institutional research agreements.
12. Leads efforts to develop and stimulate participation in activities that encourage interaction between the university and the private sector.
13. Encourages and assists faculty and other university personnel in developing opportunities for patents, licensing and commercialization.
14. Promotes research integrity and responsibility and ensures that all university personnel adhere to regulations, policies, procedures, and strict standards of ethical conduct in planning, conducting and reporting research and scholarly activity.
15. Serves on the President's Executive Council.
16. Undertakes additional assignments in research affairs at the direction of the president.
17. Advises the president on strategic plans for development and renovation of research space.

MINIMUM QUALIFICATIONS: The successful candidate for Senior Vice President for Research must have a PhD and/or MD degree with academic credentials for appointment to the rank of full professor; work experience that demonstrates a successful and continuous record of scholarship and success in obtaining federal peer-reviewed funding for research; outstanding achievement in developing and managing a diverse staff; a commitment to quality and integrity; engaging interpersonal and public communication skills; and a demonstrated record of significant, successful administrative experience in higher education, including actual experience in research administration. Experience as a chair, vice-chair, division director, etc., preferred. Demonstrated knowledge of indirect costs, effort reporting, responsible conduct of research, federal and state regulations relating to grants, human and animal use in research required.

Nominations and applications will be received until the position is filled. Applications should include: curriculum vitae; statement summarizing the relevant credentials of the candidate; and complete contact information for at least three professional references. All materials should be submitted electronically. TTUHSC is committed to diversity and encourages nominations and applications from all qualified individuals. Application should be made through TTUHSC's website (**http://jobs.texastech.edu/postings/48499**). Confidential requests for information and nominations should be directed to:

Matthew B. Grisham, PhD.
Chair, Search Committee for the Senior Vice President for Research
c/o Ms. Alicia Gauna
Department of Immunology and Molecular Microbiology
Texas Tech University Health Sciences Center
3601 4th Street STOP 6591
Lubbock, TX 79430-6591
806-743-2414
alicia.gauna@ttuhsc.edu

TTUHSC is an Equal Opportunity/Affirmative Action Employer.

BIOCHEMISTRY ASSISTANT PROFESSOR
CALIFORNIA STATE UNIVERSITY FULLERTON

The **Department of Chemistry and Biochemistry, California State University Fullerton**, **http://chemsrvr2.fullerton.edu/employment.asp** invites applications for a **full-time tenure-track Assistant Professor** position to begin in August 2013. Applicants shall have a Ph.D. in biochemistry or a related field as well as relevant postdoctoral experience. We are particularly interested in candidates whose research complements the department's existing research programs or further expands opportunities at the interface of chemistry and biology. The candidates will be expected to maintain an active, externally funded research program involving undergraduate and M.S. students, and be committed to excellence in teaching and mentoring a diverse student population.

Please submit the following required application materials as pdf documents to **biochem-search@fullerton.edu**: (a) cover letter, (b) *curriculum vitae*, (c) a statement of teaching philosophy and experience that addresses teaching diverse populations (3 page limit), (d) a statement of research plans that addresses projects to engage undergraduate and M.S. students and strategies to obtain funding (3 page limit), (e) reprints of relevant peer-reviewed publications, (limit of 3), and (f) names and contact information for 3 individuals who will send letters of recommendation. The recommenders are required to directly send a signed letter on official letterhead either via email to **biochem-search@fullerton.edu** or by mail to **Chair, Biochemistry Search Committee, Department of Chemistry and Biochemistry, California State University, Fullerton, CA 92834-6850**. Review of applications will begin **December 15, 2012**, and continue until suitable candidate(s) are appointed. **Position #23603G-13-032**.

See full job announcement **http://diversity.fullerton.edu/jobs/ft/ChemBioChemTT.asp**

Cal State Fullerton is an Equal Opportunity/title IX/503/504/VEVRAA/ADA Employer.

NATIONWIDE CHILDREN'S
When your child needs a hospital, everything matters.℠

THE OHIO STATE UNIVERSITY

FACULTY POSITION
CENTER FOR VACCINES AND IMMUNITY

The CENTER FOR VACCINES AND IMMUNITY at The Research Institute at Nationwide Children's Hospital and The Ohio State University Department of Pediatrics is seeking PhD, MD or MD/PhD candidates for a tenure-track position at the Associate or Professor level. The successful candidate will have an established, independent research program on virus infections of the human respiratory tract. Research on innate or humoral immunity is preferred to complement existing NIH-funded programs on the immunology and virology of viral and polymicrobial respiratory tract infections. Research on respiratory tract infections in the Center for Vaccines and Immunity is supported by a close working relationship with the Infectious Diseases Division of Nationwide Children's Hospital including access to large patient populations for translational studies and a special infectious diseases unit dedicated to facilitating patient identification and recruitment. The Center has a facility that produces well differentiated human airway epithelial cultures. The Institute has an AAALAC-accredited vivarium with expertise in animal infection, particularly rodent and non-human primates and provides state-of-the-art core services for flow cytometry, bioinformatics, morphology, viral vector production, genomics, ES cell, transgenic and small animal imaging. The OSU campus provides many other cores.

Start-up support and joint appointments within OSU graduate departments and with clinical divisions at Nationwide Children's Hospital are available. For more information, please visit our website at **http://www.nationwidechildrens.org/center-for-vaccines-and-immunity**

Send curriculum vitae with contact information for three references to: **Mark.Peeples@nationwidechildrens.org**

The Ohio State University is an Equal Opportunity, Affirmative Action Employer. Women, minorities, veterans, and individuals with disabilities are encouraged to apply.

中国科学院生物和化学交叉研究中心（中国 上海）
Interdisciplinary Research Center of Biology and Chemistry (IRCBC) - Exciting Biomedical Research Career Opportunity in Shanghai, China

The Interdisciplinary Research Center on Biology and Chemistry (IRCBC), the Chinese Academy of Sciences, Shanghai, is an exciting new collaborative research center in China in collaboration with the Shanghai Institute of Materia Medica and the Shanghai Institute of Organic Chemistry. The vision of IRCBC is to bring outstanding biologists and outstanding chemists to work side-by-side at the interface of biology and chemistry using tools of chemistry, cell biology, molecular biology, proteomics, bioinformatics and genomics to address the most interesting and important biological questions that are relevant to neurological and neurodegenerative diseases. The IRCBC offers long-term stable support for research (¥2-3 million per year), highly competitive salary (upto ¥600,000 per year), benefits and generous housing allowance, new laboratory space and state-of-art core facilities. The IRCBC invites applications from outstanding candidates from all stages of career, especially junior investigators who are looking for their first independent research opportunities, to apply for one of the two career tracks: Principle Investigators (PI), who will run independent research laboratories; or Technology Specialists (TS), who will run the platform technology facilities.

The IRCBC is seeking applicants with expertise in following areas:
Cellular and molecular biology; Proteomic and mass spectrometry; Chemical biology; Medicinal chemistry; Bioinformatics; Cellular neurobiology; Electrophysiology; Vertebrate and invertebrate animal models of neurological and neurodegenerative diseases; Behavioral neurobiology; Structural biology; Genomics.

Please submit a curriculum vitae with links to representative publication in the PubMed, one-page description of current research program and accomplishments, two-page description of future plans with relevance to neurological and neurodegenerative diseases and the names of three references by email to"**IRCBC@mail.shcnc.ac.cn**".

Applications will be accepted until the positions are filled. Reviews of applications will begin in **September 2012**.

AAAS is here –
bringing educational infrastructure to the developing world.

AAAS is helping the Rwandan government rebuild its educational infrastructure as a way to help drive economic growth and development. By providing materials such as the Project 2061 *Atlas of Science Literacy*, lesson plans from Science NetLinks, and access to *Science* digital libraries, AAAS is helping the people of Rwanda work toward a future built around science and technology. As a AAAS member your dues support these efforts. If you're not yet a AAAS member, join us. Together we can make a difference.

To learn more, visit
aaas.org/plusyou/rwanda

AAAS + U = Δ

WASHINGTON STATE UNIVERSITY
HEALTH SCIENCES

FACULTY POSITIONS
MEDICAL SCIENCES

Washington State University Division of Health Sciences, located on the Riverpoint campus in Spokane, invites applications for two tenure-track faculty positions at the rank of Assistant or Associate Professor and one at the rank of Professor in its new Medical Sciences section. Applicants must have an advanced degree (Ph.D. or M.D. or equivalent) in the basic, clinical, or translational medical sciences and a track record of scholarly accomplishments. Successful candidates will be expected to maintain an active, extramurally funded research program, to mentor graduate students and fellows, and to teach in the professional and/or graduate curricula. The successful candidate for the Professor position will additionally be expected to take a leadership role in rapidly expanding medical research in Spokane, including recruitment of faculty and programmatic development.

Areas of research interest are open, but key areas of planned growth in the program include molecular, cellular, physiological and systems biology approaches to: neurosciences/behavioral neurosciences (sleep, addictions, pain, anesthesia), senescence and immortality (stem cells, cancer, aging, regenerative medicine), microbiology (antimicrobial resistance, virology), and metabolic diseases (obesity, diabetes, renal and cardiovascular disease). Washington State University is substantially building its research and graduate education capacity in the medical sciences. The Medical Sciences section also participates in preclinical medical education in the WWAMI program, which is a collaborative medical education program with the University of Washington School of Medicine.

Screening of applications will begin immediately and will continue until a suitable candidate is identified. To apply visit: **www.wsujobs.com**. Applications must include a current curriculum vitae and letter of application describing professional goals, research, and teaching experience. Before interviews commence four letters of reference will be required. **Contact Kim Noe, Administrative Manager**, at **knoe@wsu.edu** or **509-358-7515** for questions, assistance with the application process or confidential expressions of interest.

Women and minorities are particularly encouraged to apply. Washington State University Is An Equal Opportunity/affirmative Action Educator And Employer.

Western University of HEALTH SCIENCES
The discipline of learning. The art of caring.

www.westernu.edu

Faculty Positions in Biochemistry and other disciplines available for 2013

The College of Osteopathic Medicine of the Pacific – Northwest (COMP-Northwest) inaugurated its first class of physicians-in-training in Lebanon, Oregon in Fall, 2011. As the newest expansion of Western University of Health Sciences in Pomona, California (COMP-Pomona), we have established a thriving center for medical education and human health care in Oregon.

A major responsibility of the Department of Basic Medical Sciences is to provide preclinical education for first and second-year students in COMP. Our current initiative is to add instructional and research strength within the discipline of Biochemistry. This is a 12-month, tenure-track appointment at the Assistant/ Associate/ or Full Professor rank depending upon qualifications. Successful candidates will join a large intercampus faculty in Basic Medical Sciences and be located at the new campus in Lebanon, Oregon. Applicants must have a Ph.D. in Biochemistry and at least two years of postdoctoral experience. Similar positions in microbiology and pharmacology are also available at both the Lebanon, OR and Pomona, CA campuses. Preference is given to effective educators with a record of excellence in teaching, significant scholarly activity and strong potential for independent grant-supported research. Submit a current curriculum vitae and a cover letter describing your teaching experience, research activity and goals. Please include contact information for at least three references. These positions will remain open until filled.

Nissar A. Darmani, PhD
Associate Dean for Basic Sciences and Research
Department of Basic Medical Sciences
College of Osteopathic Medicine of the Pacific
Western University of Health Sciences
309 E. Second Street, Pomona, CA 91766-1854
Email Address: ndarmani@westernu.edu

Western University of Health Sciences is an equal opportunity employer.

MRC | Laboratory of Molecular Biology

Cambridge, UK

Programme Leaders in Neurobiology

Coinciding with the move of the MRC Laboratory of Molecular Biology (LMB) into a new state-of-the-art research building from January 2013 (**http://www2.mrc-lmb.cam.ac.uk/about-lmb/new-building**), the Division of Neurobiology wishes to recruit talented scientists interested in developing an independent programme of research. We are particularly interested in individuals working in the area of molecular/cellular neurobiology or neurodegeneration. Current interests in the Division include mechanisms of synaptic transmission, protein misfolding in relation to neurodegenerative diseases, visual and olfactory processing and circadian rhythms (**www2.mrc-lmb.cam.ac.uk/NB/**). Scientific excellence and potential for major impact are paramount. Synergy with existing research programmes would be an advantage.

The LMB provides an excellent environment for hands-on research. Core-funding by the Medical Research Council provides long-term support for ambitious projects, while administrative duties are minimal and no teaching is required. Interactions across the four Divisions of the Laboratory are encouraged. There is extensive central support, including electronic and instrumentation workshops, imaging and transgenic mouse facilities. The University of Cambridge and affiliated institutions form a vibrant Neuroscience community (**http://www.neuroscience.cam.ac.uk/**).

Candidates should have a PhD and/or MD and will have completed a period of postdoctoral training or equivalent, with an excellent track record, and show outstanding potential for independent research. The successful candidate will lead a small team and substantial funding will be available.

These appointments will be made at either Programme Leader-track or Programme Leader level, depending on achievements and experience. Programme Leader-track appointments will be made for those who demonstrate the potential to develop into Programme Leaders within six years. Candidates for Programme Leader positions should have a strong international track record of relevant independent research and a proven ability to lead a research team, pursuing original approaches to long-term research goals. Salaries are competitive (Programme Leader-track £35,935-£48,000 per annum; Programme Leader £45,213-£70,000 per annum).

These positions will remain open until they are filled; applications received by **30th November 2012** will be given priority.

Informal enquiries can be addressed to Michel Goedert (**mg@mrc-lmb.cam.ac.uk**).

Applications should include a covering letter and full CV, an outline of current research interests (1 page) and a proposal for future research (up to 2 pages), along with the names and addresses of three professional referees who have agreed to be contacted prior to interview. Applications are handled by the RCUK Shared Services Centre; to apply please visit our job board at http://www.topcareer.jobs/Vacancy/irc69837_2430.aspx. If you are unable to apply online please contact us on 01793 867003 quoting reference IRC69837.

This position is subject to pre-employment screening.
For further information about the MRC visit **www.mrc.ac.uk**
The Medical Research Council is an Equal Opportunities Employer

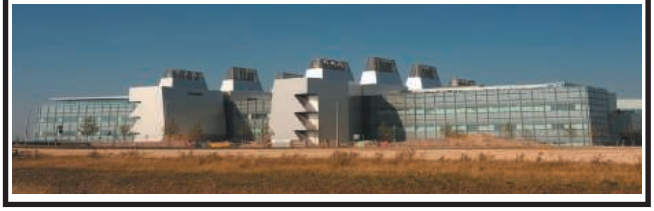

ETH

Eidgenössische Technische Hochschule Zürich
Swiss Federal Institute of Technology Zurich

Assistant Professor (Tenure Track) of Ecology of Infectious Disease

The Department of Environmental Systems Science at ETH Zurich (www.usys.ethz.ch) invites applications for the above-mentioned position. Candidates with outstanding scientific track records in any related field will be considered, but preference may be given to ecologists working on interactions between the environment and disease dynamics. The new professor should establish a world-class research group and integrate into research activities in related fields at ETH Zurich.

The successful candidate is expected to contribute to the teaching of undergraduate (German or English) and graduate level courses (English) for students of the Departments of Environmental Systems Science and Biology. The professorship will be equipped with a generous personnel and operational budget, but the candidate will be expected to obtain further funds for research through competitive grants.

This assistant professorship has been established to promote the careers of younger scientists. The initial appointment is for four years with the possibility of renewal for an additional two-year period and promotion to a permanent position.

Your application should include your curriculum vitae, a list of publications, and a statement of your research and teaching interests. The letter of application should be addressed **to the President of ETH Zurich, Prof. Dr. Ralph Eichler. The closing date for applications is 31 December 2012.** ETH Zurich is an equal opportunity and affirmative action employer. In order to increase the number of women in leading academic positions, we specifically encourage women to apply. ETH Zurich is further responsive to the needs of dual career couples and qualifies as a family friendly employer. **Please apply online at www.facultyaffairs.ethz.ch.**

ETH

Eidgenössische Technische Hochschule Zürich
Swiss Federal Institute of Technology Zurich

Assistant Professor of Structural Biology / Biophysics

The Department of Biology (www.biol.ethz.ch) at ETH Zurich invites applications for above-mentioned assistant professorship.

The successful candidate is expected to study the molecular mechanisms of biological reactions and to build an innovative and internationally competitive research program within the Institute of Molecular Biology and Biophysics (www.mol.biol.ethz.ch), which provides an excellent scientific environment and access to state-of-the-art equipment. The search is not limited to a specific research field or technology, but we are specifically encouraging candidates with expertise in methods complementary to those already used at the Institute, e.g. single particle cryo-electron microscopy or single molecule spectroscopy. For electron microscopy, transmission electron microscopes (including a FEI Tecnai G2 F20 cryo and a Titan Krios) are available within the Electron Microscopy Center of ETH Zurich. The new professor will be expected to teach undergraduate level courses (German or English) and graduate level courses (English) for students of the Department of Biology, and to actively contribute to an interactive, scientific environment at ETH Zurich.

This assistant professorship has been established to promote the careers of younger scientists. The initial appointment is for four years with the possibility of renewal for an additional two-year period.

Your application should include your curriculum vitae, a list of publications, the names of at least three referees, and a short overview of your research interests. The letter of application should be addressed **to the President of ETH Zurich, Prof. Dr. Ralph Eichler. The closing date for applications is 31 December 2012.** ETH Zurich is an equal opportunity and affirmative action employer. In order to increase the number of women in leading academic positions, we specifically encourage women to apply. ETH Zurich is further responsive to the needs of dual career couples and qualifies as a family friendly employer.
Please apply online at **www.facultyaffairs.ethz.ch**.

AAAS is here – helping scientists achieve career success.

Every month, over 400,000 students and scientists visit ScienceCareers.org in search of the information, advice, and opportunities they need to take the next step in their careers.

A complete career resource, free to the public, *Science* Careers offers a suite of tools and services developed specifically for scientists. With hundreds of career development articles, webinars and downloadable booklets filled with practical advice, a community forum providing answers to career questions, and thousands of job listings in academia, government, and industry, *Science* Careers has helped countless individuals prepare themselves for successful careers.

As a AAAS member, your dues help AAAS make this service freely available to the scientific community. If you're not a member, join us. Together we can make a difference.

To learn more, visit **aaas.org/plusyou/sciencecareers**

AAAS + U = Δ

NEW
Women in Science Booklet

Science and the L'Oréal Foundation present

Read inspiring profiles of women making a difference in biology.

Free download at ScienceCareers.org/LOrealWIS

POSITIONS OPEN

UCIRVINE

SENIOR PROFESSOR in Materials Engineering, Physics, or Chemistry
University of California, Irvine-

The Henry Samueli School of Engineering and the School of Physical Sciences at the University of California, Irvine (UCI) announces an endowed chair faculty search at the senior level in the field of experimental materials science. We are seeking a distinguished scientist and educator who directs a field-leading research program in materials engineering, physics, or chemistry in which transmission electron microscopy plays an integral roll. In addition, this individual will lead the build-out of our campus-wide materials characterization infrastructure, including the establishment of a state-of-the-art facility for transmission electron microscopy. A record of teaching excellence at the undergraduate and graduate levels is required. The successful candidate will occupy either the Henry Samueli Endowed Chair in the Henry Samueli School of Engineering or the Donald Bren Chair in the School Physical Sciences.

Founded in 1965, the University of California, Irvine is at the forefront of education and research in the science and engineering disciplines that will shape the future of the nation and the world. In 2012, U.S. News & World Report ranked UCI 45th among national universities and 13th among public universities in the U.S. Graduate programs that were ranked in that report included: organic chemistry (11), information systems (11), physical chemistry (12), theoretical chemistry (18), experimental psychology (19), chemistry (26), aerospace engineering (29), computer science (29), physics (29), mechanical engineering (30), civil engineering (31), biological sciences (32), environmental engineering (34), biomedical engineering (40), engineering (41), medicine (41), materials science engineering (45), mathematics (47), and electrical engineering (49). NRC rankings, based upon 2006 data, place Chemistry, Earth System Science, Mathematics, and Physics & Astronomy in the top quartile nationally. An analysis by *Times Higher Education*, released in May 2012, ranked UCI first in the U.S. and fourth in the world among the 100 best universities less than 50 years old. The "100 Under 50" list aims to show institutions poised to become future world leaders.

Applications should contain a cover letter and a complete curriculum vita including publication list, a list of references, and summary of research funding. Completed applications should be sent electronically, via **website: https://recruit.ap.uci.edu.** To ensure full consideration, applications and supporting materials should be received by January 1, 2013. *The University of California, Irvine is an Equal Opportunity/Affirmative Action Employer committed to excellence through diversity. UC Irvine has an active ADVANCE Gender Equity Program.*

MULTIPLE FACULTY POSITIONS

The University of Washington (UW) School of Public Health is recruiting multiple full-time faculty positions at the **ASSISTANT, ASSOCIATE**, and **PROFESSOR** level as identified in our Strategic Plan. Applicants must have a doctoral degree in a relevant field. Application review begins November 19, 2012 and will continue until filled. For complete advertisement, visit **website: http://sph.washington.edu/fachires/**. University of Washington faculty engage in teaching, research, and service.

The UW is an Affirmative Action/Equal Opportunity Employer. Women and minority candidates are strongly encouraged to apply.

ASSISTANT PROFESSOR of Biology (with expertise in anatomy)

The Biology Department at Coe College seeks applications for a full-time tenure-track position beginning fall 2013. A Ph.D. in the biological sciences, with research and/or teaching expertise in anatomy is required. For position details and application process, visit **website: http://www.coe.edu/aboutcoe/employment**.

POSITIONS OPEN

UMBC
AN HONORS UNIVERSITY IN MARYLAND

CHAIR
Department of Chemistry and Biochemistry
University of Maryland, Baltimore County

Applications from outstanding scientists are invited for the position of Chair of the Department of Chemistry and Biochemistry at University of Maryland, Baltimore County (UMBC). The Department offers graduate and undergraduate degrees in both chemistry and biochemistry with a highly cross-disciplinary and interactive group of faculty and lecturers. Cutting-edge research is carried out by postdoctoral fellows, Ph.D., M.S., and undergraduate students working in excellent laboratory facilities in a recently renovated building. The University is strategically situated on a suburban campus in the intellectually and culturally vibrant Baltimore-Washington corridor, which enhances the dynamic educational and research opportunities afforded by its diversity, intermediate size, and world-class infrastructure. The Chair will be expected to provide vigorous leadership toward expanding the department's current research profile and directing the next stage of departmental growth. Applications are invited from internationally recognized scholars in any area who have a commitment to superior research and innovative teaching at both the graduate and undergraduate levels. Applicants should submit a letter of application, curriculum vitae, and the names of three persons who can be contacted for supporting letters to: **Chair, Faculty Search Committee, Department of Chemistry and Biochemistry, University of Maryland, Baltimore County, 1000 Hilltop Circle, Baltimore, MD 21250**. Electronic submissions can be made to **e-mail: chemsearch@umbc.edu**. Applications will enter the review process as soon as they are received and consideration of applications will continue until the position is filled. *UMBC is an Equal Opportunity/Affirmative Action Employer; and applications from women, minorities, and individuals with disabilities are especially encouraged.*

LECTURER IN BIOLOGY

The Department of Biology at University of North Carolina at Charlotte invites applications for a non-tenure track, nine-month, full-time position, as Lecturer in Biology, beginning August 15, 2013. Required qualifications include: Master's degree in an area of the Biological Sciences; expertise in the field and laboratory techniques needed for development and revision of laboratory exercises; knowledge of laboratory safety procedures; and the ability to supervise graduate teaching assistants. Desired qualifications include a Ph.D. in an area of the Biological Sciences and previous experience working with graduate teaching assistants. The position includes responsibilities for teaching lecture and laboratory introductory coursesfor Biology majors and contributing to Ecology instruction. *The Department and College strongly support and value diversity among their students and faculty.*

Candidates must apply online at **website: http://jobs.uncc.edu, position number: 6280**. Please provide a complete curriculum vitae, statement of teaching philosophy including teaching in an ethnically diverse environment, and contact information for three references. Screening of applicants will begin on December 1, 2012 and continue until the position is filled.

For more information, please contact **Dr. Inna Sokolova** (**e-mail: isokolov@uncc.edu**), Lecturer Search Committee Chair, and/or the Biology Department **website: http://biology.uncc.edu**.

The University of North Carolina at Charlotte is an Equal Opportunity Employer/Affirmative Action Employer and an ADVANCE Institution that strives to create an academic climate in which the dignity of all individuals is respected and maintained. Therefore, we celebrate diversity that includes, but is not limited to ability/disability, age, culture, ethnicity, gender, language, race, religion, sexual orientation, and socio-economic status.

POSITIONS OPEN

INTERDISCIPLINARY POSTDOCTORAL TRAINING in Physiological, Pathological, and Cellular/Biochemical Aspects of Hemorrhagic Shock

A postdoctoral position is available immediately in the Departments of Emergency Medicine and Biochemistry and Molecular Biology in conjunction with the Virginia Commonwealth University Reanimation Engineering Science Center (VCURES; **website: http://www.vcu.edu/vcures/index.html**) at the Virginia Commonwealth University (VCU) School of Medicine. VCURES is an internationally recognized center of excellence devoted to the study of critical illness and injury. The current position is funded for three years by a grant from the Department of the Army to study the role of AMP-dependent protein kinase in cellular metabolic homeostasis during hemorrhagic shock and resuscitation. Outstanding candidates with an M.D., D.V.M., or a Ph.D. in physiology, biochemistry, cell and molecular biology, pharmacology, or a related discipline will be considered. Special consideration will be given to individuals who have some background either in cell and molecular biology or in whole animal physiology. This training offers the unique opportunity for individuals who have been trained in molecular biology to broaden their base to learn whole animal physiology/pathophysiology and preclinical translational research, and for individuals trained in whole animal biology to learn biochemical and molecular techniques. Salary is determined by NIH postdoctoral fellowship stipend levels, and health insurance is included.

Please send curriculum vitae, a statement of research interests and the names/contact information of three references to **R. Wayne Barbee,** Ph.D., Professor of Emergency Medicine, at **e-mail: rwbarbee@vcu.edu**, or **Paul H. Ratz**, Ph.D., Professor of Biochemistry and Molecular Biology, at **e-mail: phratz@vcu.edu.**

VCU is an Equal Opportunity/Affirmative Action Institution and does not discriminate on the basis of race, color, national origin, age, gender, religion, sexual orientation, political affiliation, veterans' status, or disability.

TENURE-TRACK POSITION
Department of Biological Sciences
Texas Tech University

The Department of Biological Sciences at Texas Tech University (TTU) invites applications for a tenure-track **ASSISTANT PROFESSOR** position, beginning September 1 for the 2013–2014 academic year. We seek an outstanding individual within the broad area of Microbiology/Immunology with an emphasis on host-pathogen interactions. The successful candidate will complement existing strengths in Cell and Molecular Bioogy within the Department. Candidates must have a Ph.D. and or M.D., a proven track record of postdoctoral accomplishment in appropriate fields, and demonstrate their ability or strong potential to secure competitive extramural funding. Successful candidates are expected to develop/maintain and expand an innovative extramurally funded research program, contribute to both graduate and undergraduate education and provide services to the department and the University as necessary. The Department and TTU have resources including flow cytometry/cell sorting, imaging, proteomics/structural, and biology/genomics facilities available on campus. The position includes a competitive salary and startup package. All candidates must submit their application through **website: http://jobs.texastech.edu/postings/49501, position T93553**. The online application should include a cover letter and curriculum vitae, in addition please combine into a single PDF a summary of past research and teaching experience, statements of research interests and teaching philosophy, and copies of two recent publications as well as the names and contact information for three professional references. Review of applications will begin November 15 and continue until filled.

Texas Tech University is committed to enhancing the diversity of its faculty and staff and encourages applications from women, minorities, people with disabilities and veterans. TTU is an Equal Employment Opportunity/Affirmative Action Employer.

COLUMBIA UNIVERSITY
IN THE CITY OF NEW YORK

The 2013 Louisa Gross Horwitz Prize for Biology or Biochemistry

The Louisa Gross Horwitz Prize was established under the will of the late S. Gross Horwitz through a bequest to Columbia University and is named to honor the donor's mother. Louisa Gross Horwitz was the daughter of Dr. Samuel David Gross (1805-1889), a prominent surgeon of Philadelphia and author of the outstanding *Systems of Surgery* who served as President of the American Medical Association.

Each year since its inception in 1967, the Louisa Gross Horwitz Prize has been awarded by Columbia University for outstanding basic research in the fields of biology or biochemistry. The purpose of this award is to honor a scientific investigator or group of investigators whose contributions to knowledge in either of these fields are deemed worthy of special recognition.

The Prize consists of an honorarium and a citation which are awarded at a special presentation event. Unless otherwise recommended by the Prize Committee, the Prize is awarded annually. Dr. Richard Losick, Harvard University, Cambridge, MA, Dr. Joe Lutkenhaus, University of Kansas Medical Center, Lawrence, KA and Dr. Lucy Shapiro, Stanford University School of Medicine, Stanford, CT were the 2012 awardees.

QUALIFICATIONS FOR THE AWARD

The Prize Committee recognizes no geographical limitations. The Prize may be awarded to an individual or a group. When the Prize is awarded to a group, the honorarium will be divided among the recipients, but each member will receive a citation. Preference will be given to work done in the recent past.

Nominations must be submitted electronically at: **http://www.cumc.columbia.edu/research/horwitz-prize**
All communications and materials must be written in the English language.

Re-nomination(s) are by invitation only.

Nominations should include:

1) A summary, preferably less than 500 words, of the research on which this nomination is based.
2) A summary, preferably less than 500 words, of the significance of this research in the fields of biology or biochemistry.
3) A brief biographical sketch of the nominee, including positions held and awards received by the nominee.
4) A listing of up to ten of the nominee's most significant publications relating to the research noted under item 1.
5) A copy of the nominee's curriculum vitae.

Deadline date: January 31, 2013

POSITIONS OPEN

ASSISTANT/ASSOCIATE/ FULL PROFESSOR (Computational Biology-Microbiology/Metagenomics/Tenure-track) Department of Biological Sciences Louisiana State University

The Department of Biological Sciences at Louisiana State University (LSU) invites applications for a tenure-track Microbiologist position at the level of Assistant Professor or above. Required Qualifications: Ph.D. in Biological Sciences, Microbiology, or related discipline; record of productive research. Additional Qualifications Desired: Postdoctoral experience. The successful candidate will be expected to develop a strong, competitively funded research program and will complement the department's existing strengths in systematics, ecology, and evolution. We are especially interested in applicants that specialize in computational biology, and whose research employs "omics" approaches for understanding microbes in complex systems. Applicants will be expected to teach an undergraduate course in microbiology and a graduate course in their area of expertise. An offer of employment is contingent on a satisfactory pre-employment background check. Application deadline is December 21, 2012 or until a candidate is selected. The anticipated start date is August 2013. While we anticipate hiring at the Assistant Professor level, candidates at higher rank are also encouraged to apply. Apply online and view a more detailed ad at **website: http://www.lsusystemcareers.lsu.edu. Position #020243**.

LSU is an Equal Opportunity/Equal Access Employer and strongly encourage applications from women and minorities.

ASSISTANT PROFESSOR (Marine/Coastal/Wetland/ Aquatic Ecologist/Tenure-track) Department of Biological Sciences Louisiana State University

The Department of Biological Sciences at Louisiana State University (LSU) invites applications for a tenure-rack Ecologist position at the level of Assistant Professor. Required Qualifications: Ph.D. in Biological Sciences or related field; successful track record of productive research. Additional Qualifications Desired: Postdoctoral experience. The successful candidate is expected to develop a strong, competitively funded research program, and develop courses in their area of interest. We seek an outstanding ecologist working in either freshwater, marine, coastal or wetland systems. Research interests may be at any level. Candidates should complement existing research strengths in the Systematics, Ecology, and Evolution division of the Department of Biological Sciences at LSU. An offer of employment is contingent on a satisfactory pre-employment background check. Application deadline is December 7, 2012 or until a candidate is selected. The anticipated start date is August 2013. Apply online and view a more detailed ad at **website: http://www.lsusystemcareers.lsu.edu. Position #021646**.

LSU is an Equal Opportunity/Equal Access Employer and strongly encourage applications from women and minorities.

FACULTY POSITIONS - MEDICAL SCHOOL

The Saint James School of Medicine, an international medical school (**website: http://www.sjsm.org**), invites applications from candidates with teaching and/or research experience in any of the basic medical sciences for its Caribbean campuses. Faculty positions are currently available in Anatomy, Physiology, Pathology, Microbiology, and Pharmacology. Applicants must be M.D., D.O., and/or Ph.D..

Teaching experience in the U.S. system is desirable but not required. Retired persons are encouraged to apply. Attractive salary and benefits. Submit curriculum vitae electronically to **e-mail: mjansen@mail.sjsm.org** or mail to: **HRDS Inc., 1480 Renaissance Drive. Suite 300, Park Ridge, IL 60068.**

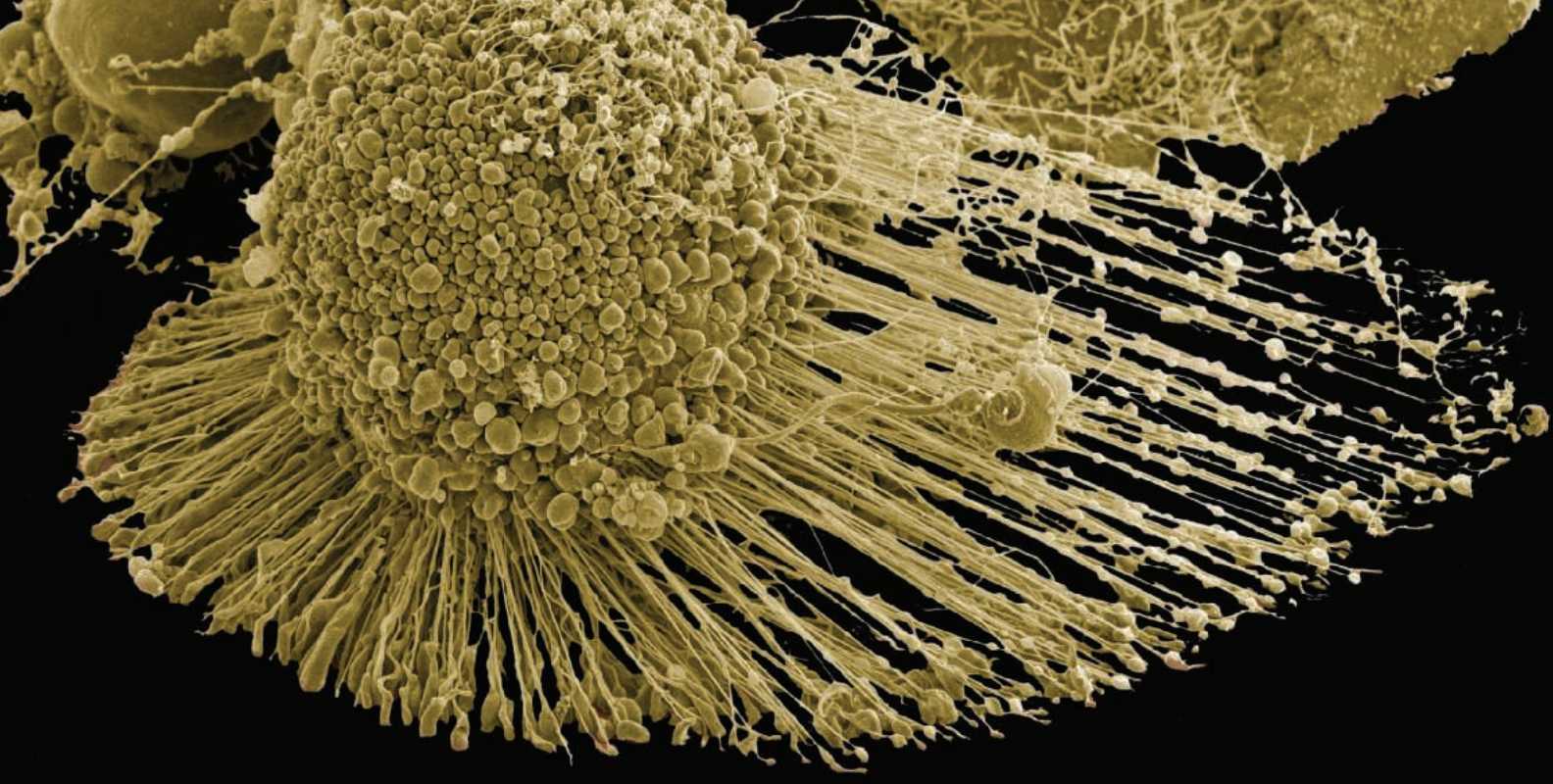

Hi

my name is HeLa
but you may also know me as Hep-2, or even as KB

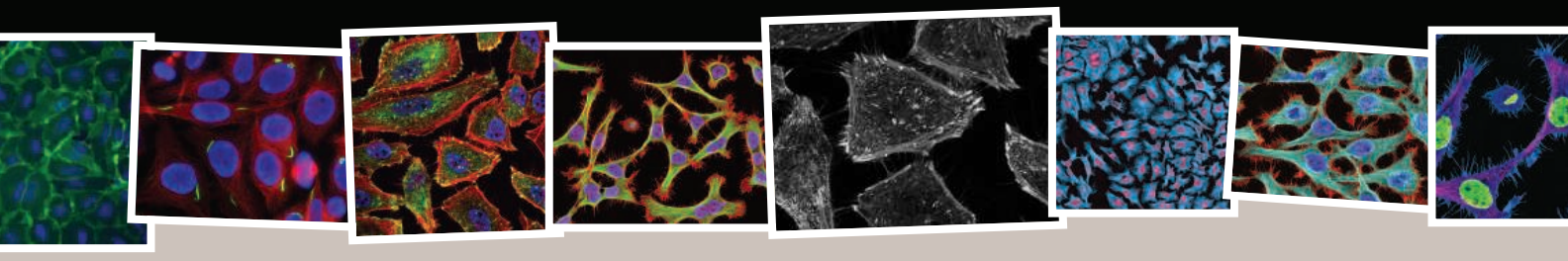

ATCC™

Learn how to avoid cell misidentification, visit **www.atcc.org/trustedsource**

ATCC performs a combination of test methods, including Human STR analysis, COI testing, Mycoplasma testing, Human viral testing, and Sterility testing, on all cell lines to ensure the highest quality and authenticity.

Your trusted source since 1925

EMD MILLIPORE

Rethink Western blotting.
Take protein detection to new dimensions.

Biology isn't flat—neither are your Westerns.
Meet the fast, versatile SNAP i.d.® 2.0 system, to fully exploit three-dimensional reagent distribution. Unlike conventional Western blotting, where diffusion is the primary means of reagent transport, the SNAP i.d.® 2.0 system applies a vacuum to actively drive antibodies and buffers right through the membrane. This advanced technology promotes antigen binding and thorough washing, enabling you to better optimize your Western blotting conditions.

www.emdmillipore.com/SNAP

EMD Millipore is a division of Merck KGaA, Darmstadt, Germany

NEW ENGLAND BioLabs® Inc.
enabling technologies in the life sciences

Stick together.

New DNA Ligases and Ligase Master Mixes

New England Biolabs offers the most extensive selection of high-quality and performance-optimized DNA ligases and ligase master mixes to streamline your cloning experiments.

Our expanded portfolio now includes:

- Blunt/TA Ligase Master Mix, optimized for blunt-end and single-base overhang substrates
- Instant Sticky-end Ligase Master Mix, uniquely formulated for the rapid ligation of sticky-end substrates
- T7 DNA Ligase, specific for sticky ends
- ElectroLigase,™ directly compatible with electroporation

Stick together with DNA Ligases and Ligase Master Mixes from NEB.

To request a FREE SAMPLE of our new DNA Ligase Master Mixes, visit **NEBStickTogether.com**

Blunt/TA Ligase Master Mix outperforms the competition

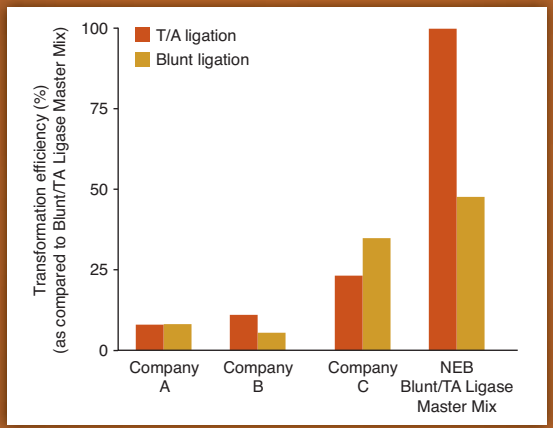

Duplicate ligation reactions of blunt or T/A vector/insert pairs were set up according to the master mix vendors' suggestions. Equal amounts of ligated DNA were used to transform NEB 10-beta Competent E. coli (NEB #C3019) and triplicate plating was performed. Transformation results were averaged and graphed as a percentage of the highest performing reaction, T/A ligation using the Blunt/TA Ligase Master Mix.

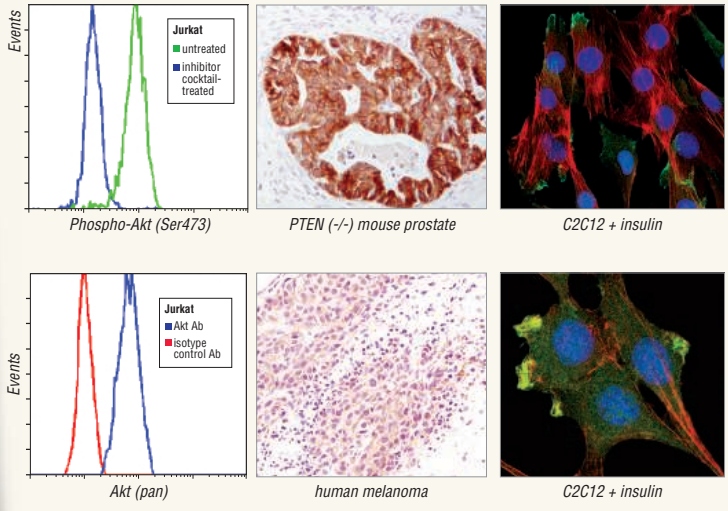

Phospho-Akt (Ser473) (D9E) XP® Rabbit mAb #4060 *(upper)*
and ***Akt (pan) (C67E7) Rabbit mAb #4691*** *(lower).*
For full validation details see www.cellsignal.com

The Highest Quality
Akt Antibodies
are from Cell Signaling Technology

Over 45 thoroughly validated Akt Antibodies available

Cell Signaling Technology offers the widest range of phospho and total protein Akt antibodies. These reagents are the most thoroughly validated, widely used, and highly cited Akt antibodies available.

:: CST™ phospho and total protein Akt antibodies offer **unsurpassed specificity, sensitivity, and performance**.

:: **Extensive in-house validation** in a wide range of applications means that optimization is not left up to you, the user.

:: **Technical support is provided by scientists** who produce the products and know them best.

Unparalleled product quality, validation, and technical support

for quality products you can trust...

www.cellsignal.com

Cell Signaling TECHNOLOGY®

The moment your data change scientific minds.

This is the moment we work for.

Visit Carl Zeiss Microscopy at the Annual Meeting of the American Society for Cell Biology 2012 in San Francisco. You will get a glimpse of Lightsheet Z.1, the unique light sheet microscope, capable of obtaining brilliant time lapse images of whole developing embryos.

www.zeiss.com/lightsheet

ZEISS

We make it visible.

Lead the way on epigenetics

abcam®
discover more

Let our EpiSeeker kits guide you through

The **EpiSeeker** range of kits for epigenetics is all you need to get the best results in no time. From histone modification quantification to methylated DNA ChIP kits, you have the right tool at your hands.

- **Simple and reliable assays**
- **Ready to go - All essential components present in the kit**

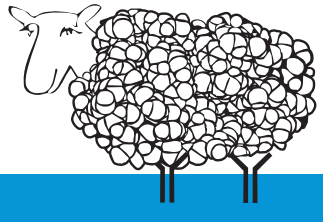

473_12_MF

Discover more at abcam.com/episeeker

Thermo SCIENTIFIC

Quantify, verify,

In science there are always essential steps in any workflow. Accurate measurements of DNA, RNA and protein samples are critical for confidence in qPCR, sequencing, microarrays or bioproduction, but there's a better alternative to the time and complexity of conventional methods. Using minimal sample (0.5 – 2.0 µL), **Thermo Scientific NanoDrop** instruments make concentration and purity analysis so incredibly easy, and so much faster, you won't notice this step on the way to your ultimate discovery.

simplify

- Realize the difference.
Try any NanoDrop instrument for FREE.
www.thermoscientific.com/nanodrop

NanoDrop™ Lite
Basic microvolume measurements

NanoDrop™ 2000C
Full-spectrum microvolume and cuvette measurements in a single instrument

NanoDrop™ 2000
Full-spectrum microvolume measurements

NanoDrop 8000
Higher throughput, full-spectrum microvolume measurements

NanoDrop 3300
Full-spectrum microvolume fluorescence measurements

WEBINAR

Microfluidic Electrophoresis Assays for Rapid Characterization of Protein in Research and Development

Wednesday, November 14, 2012

12 noon ET, 9 a.m. PT, 4 p.m. UK, 5 p.m. CET

Therapeutic proteins are large complex molecules that are often heterogeneous in molecular structures. The control and characterization of biotherapeutic protein quality throughout the development process has been a major focus of the biotechnology industry. Studies to test the effect of cell culture conditions on posttranslational modifications or to monitor the purification process of the proteins produces a large number of samples that can easily exceed the capacity of modern analytical laboratories. High throughput analytical platforms with high precision, automation, and ease-of-use are therefore in great demand. Microfluidic-based assays for screening protein product quality are finding wide use because they address the limitations of SDS-PAGE as well as other separation assays that depend on conventional capillary electrophoresis. These assays leverage microfluidic technology to reduce analysis times dramatically compared with conventional techniques, to a minute or less per sample. In this presentation we will discuss the use of microfluidic-CE platforms for characterization assays such as purity assessment of monoclonal antibodies under reducing and nonreducing conditions, N-glycan profiling, and determination of protein charge heterogeneity.

During the webinar, the viewers will:

- Learn about the pros and cons of using microfluidics for high throughput protein analysis
- Obtain expert advice on setting up and validating microfluidics-based assays
- Compare results obtained using microfluidics assays to conventional methods
- Have their questions answered live during the broadcast!

PARTICIPANTS:

Joey Studts, Ph.D.
Boehringer Ingelheim Pharma GmbH & Co. KG
Biberach, Germany

Tim Blanc, Ph.D.
ImClone Systems
Branchburg, NJ

Bahram Fathollahi, Ph.D.
PerkinElmer
San Francisco, CA

REGISTER NOW!
webinar.sciencemag.org

Webinar sponsored by

PerkinElmer®
For the Better

Brought to you by the *Science*/AAAS Custom Publishing Office

Science
AAAS

Personal Flow Cytometry from BD Biosciences

BD Pharmingen™ reagents and BD Accuri™ C6

BD

Helping all people live healthy lives

Best-in-class meets best time to buy.

10% OFF

40% OFF

Now you can speed discovery with the power of multiparameter cell analysis using the best-in-class BD Accuri™ C6 personal flow cytometer. Never before have the power and insight of personal flow cytometry been more within reach. Today, you can take advantage of an unprecedented value package including 10% savings on the BD Accuri C6 and 40% savings on the high quality BD reagents you'll use with it for a full two years.

With this package, you get 4-color cell analysis in an affordable, transportable, and easy-to-use format that serves both novice and experienced researchers well, right from the benchtop.

The software's intuitive interface guides you through workflows, making it easy to begin collecting and analyzing data—even if you have little flow cytometry know-how. Setup and maintenance are also simplified to increase availability and up-time.

Take advantage of this value package today at bdbiosciences.com/go/accuri.

Flow cytometry within reach.™

Some limitations apply. Vist bdbiosciences.com/go/accuri for more information.

23-14402-00

BD Biosciences
2350 Qume Drive
San Jose, CA 95131
bdbiosciences.com

Reagent Proteins

Discover the Source

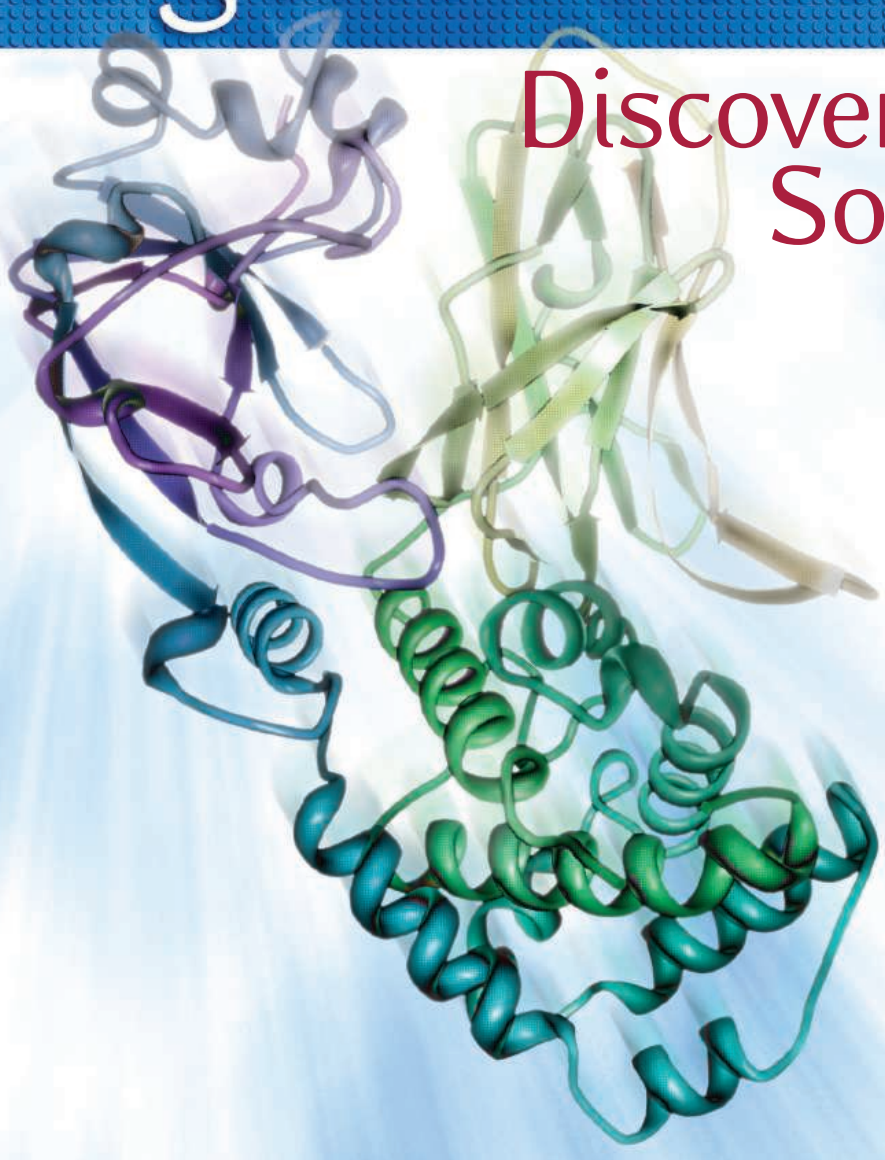

Reagent Proteins is the source

With over 5,000 recombinant proteins available, *Reagent* Proteins provides seamless access to the highest quality reagent, pre-clinical and cGMP grade proteins for research purposes.

Reagent Proteins
A DIVISION OF Pfēnex Inc.

phone 858 · 352 · 4400 **reagentproteins.com** fax 858 · 352 · 4602

Announcing our new partnership with NASA Federal Credit Union

Dear Member:

AAAS is committed to offering you member benefits that fit your needs and make your membership more valuable.

With that in mind AAAS is embarking on a new partnership with NASA Federal Credit Union that will provide you with access to a wide range of financial tools and products. Like AAAS, NASA Federal Credit Union is dedicated to serving the scientific community. This shared perspective is just one of the many reasons that we are embarking on this partnership.

As you may know, we have recently ended our banking relationship with Bank of America, but we're confident that our new partnership with NASA FCU will provide you with a superior banking experience. NASA FCU offers members better ways to save and smarter ways to borrow with friendly, professional service – along with anytime, anywhere account access.

Moreover, unlike other financial institutions that have public stockholders, NASA FCU is a not-for-profit financial cooperative where being a member means being an owner, too. And as a member/owner, you will enjoy unique benefits like: better loan rates, higher dividends and state-of-the-art products and services.

We'll be sending you more information about this great new benefit over the coming months. In the meantime, be sure to visit **nasafcu.com/AAASpackage** to apply for the new AAAS Platinum Advantage Rewards or Platinum Cash Rewards credit cards. You can also take a sneak peek at the AAAS Check Card and Checks coming soon.

Sincerely,

Ian King
Director of Marketing and Membership, AAAS

New Products: General Lab Equipment

INVERTED MICROSCOPE SYSTEMS

The new IX3 series of inverted research microscope systems are designed for effortless, intuitive live cell imaging, and clinical analysis. This includes the fully automated IX83 for high-end research applications; the flexible IX73, which can be configured in manual, semi-motorized; or motorized modes; and the easy-to-use IX53 with fluorescent capabilities, which is optimized for the routine examination of tissue samples. Built using worldwide customer feedback and designed to meet the needs of a wide range of users, the new systems offer exceptional ease-of-use and unprecedented optical flexibility via a new, customizable light path. New components can be easily slid into the light path using a series of swappable decks. This opens up many new avenues for exploration, allowing researchers to follow their imaginations. The new systems also utilize the latest Olympus innovations in frame design, optics, and software—providing exceptional stability, optical quality, accuracy, and reliability.

Olympus

For info: +49-40-23773-0 | www.microscopy.olympus.eu

ELISA READER

The Apollo 11 is a dedicated absorbance reader characterized by long-time proven and continuously optimized optics as well as a modern LED light source which has a principally endless lifetime. Up to six filters can be used with the instrument enabling the performance of all important applications including DNA quantification, protein quantification, enzyme activities, β-Galactosidase (reporter gene), alkaline phosphatase (ELISA), and horseradish peroxidase (ELISA). Besides a large dynamic range of 3.7 OD—which covers customary assays—the sophisticated optics and the robust mechanical design, together with the integrated auto-check function, guarantee extraordinary accuracy and precision. A very small footprint and the PhotoRead software showing all necessary settings and displays needed during operation on a single screen are additional attractive features of the Apollo 11.

BertholdTechnologies

For info: +49-70-81177-0 | www.berthold.com

COMPACT RECIRCULATING CHILLER

The new compact, economical recirculating chiller is designed to provide reliable heat removal for lasers and other precision laboratory equipment. Capable of maintaining process temperatures from 41°F to 95°F (5°C to 35°C), the Durachill 1.5 HP Chiller provides up to 6,328 watts of cooling at 68°F (20°C) ambient and is available with a built-in heater for use with equipment that must be brought up to elevated temperatures before operation can begin. For optimum operational versatility and flexibility, it comes with a wide variety of standard and optional features. The DuraChill 1.5 HP Chiller offers exceptional performance, reliability, and operational simplicity. All models feature a microprocessor-based controller, digital temperature display, one-touch set point display, and digital pressure/flow-rate display. Plus for optimal operational and process safety, these rugged chillers also feature user-adjustable fluid temperature, pressure, and flow rate alarms as well as a high ambient temperature alarm.

Polyscience

For info: 800-229-7569 | www.polyscience.com

ULTRAPURE WATER SYSTEMS

Three new product lines extend the successful arium lab water family: the arium pro ultrapure water system, the arium advance pure water system, and the arium comfort combination system. These new product lines generate Type 1 to Type 3 ultrapure and pure water, delivering the right water quality for any laboratory application. The highlight of these new lines is the arium comfort series. In addition to providing ASTM Type 1 ultrapure water, this space-saving combination unit also produces Type 2 and Type 3 pure water. Low quantities of organic contaminants in water are all it takes to have a negative impact on laboratory tests. The new arium ultrapure water systems deliver water quality that meets, and even exceeds, the ASTM Type 1 Standard. Its integrated ultraviolet lamp prevents microbiological growth, thus reducing the total organic carbon content to a minimum. If a Sartopore 2 sterilizing grade filter is used on arium, ultrapure water is practically free of microorganisms when dispensed.

Sartorius

For info: +49-55-1308-0 | www.sartorius.com

CO_2 INCUBATORS

The new In-VitroCell ES (Energy Saver) line of microbiological CO_2 incubators feature seven direct heat models. In-VitroCell CO_2 incubators are designed with the NuTouch Intelligent Interface. NuTouch is a user-friendly color touchscreen offered in English, Spanish, German, and French. Chamber parameters are easily controlled by the touch of a finger. All In-VitroCell models utilize a single source dual wave infrared sensor to maintain accurate CO_2 gas levels in the growth chamber. The wavelengths used are absorbed by only CO_2, making the measurement insensitive to other components such as water vapor. A large seven cubic foot (200 L) interior chamber is surrounded by heating elements on all six sides of the chamber encased by high-density R5 insulation to produce a smaller incubator footprint. Dual temperature sensor probes maintain precise temperature uniformity while an individual door heater minimizes condensation build up on the inner glass door.

NuAire

For info: 800-328-3352 | www.nuaire.com

Electronically submit your new product description or product literature information! Go to **www.sciencemag.org/products/newproducts.dtl** for more information.

Newly offered instrumentation, apparatus, and laboratory materials of interest to researchers in all disciplines in academic, industrial, and governmental organizations are featured in this space. Emphasis is given to purpose, chief characteristics, and availability of products and materials. Endorsement by *Science* or AAAS of any products or materials mentioned is not implied. Additional information may be obtained from the manufacturer or supplier.

AAAS, publisher of *Science*, thanks the sponsors and supporters of the 2013 Annual Meeting

SUBARU

NSF

EUROPEAN COMMISSION
European Research Area

ACS Chemistry for Life®
American Chemical Society

HELMHOLTZ ASSOCIATION

Canada

AAAS thanks

THE KAVLI FOUNDATION

for its generous support of the Science Journalism Awards

Register Today at Discounted Rates

Registration

Discounted advance registration rates are available until Monday, 21 January 2013.

Take advantage of unlimited access to all symposia, seminars, topical lectures, plenary events, career workshops, the Exhibit Hall, and a variety of networking opportunities.

Professional
$295 Member/ $375 New Member/ $399 Non-Member

Postdoc
$235 Member/ $315 New Member/ $335 Non-Member

K-12 Teacher
$235 Member/ $315 New Member/ $355 Non-Member

Emeritus
$235 Member/ $315 New Member/ $355 Non-Member

Student
$60 Member/ $70 New Member/ $90 Non-Member

After 21 January 2013, on-site rates apply.

For more information, visit **www.aaas.org/meetings**

Housing

Special room rates and travel benefits are available to Annual Meeting registrants.

Sheraton Boston Hotel
Rate: $205 single/double

Hilton Back Bay
Rate: $197 single/ $207 double

Boston Marriott Copley Place
Rate: $192 single/ $208 double

Rooms are available on a first-come, first-served basis until 21 January 2013.

AAAS 2013 ANNUAL MEETING
14-18 FEBRUARY • BOSTON

PICTURE YOURSELF AS A AAAS SCIENCE & TECHNOLOGY POLICY FELLOW

Make a Difference.
Help give science a greater voice in Washington, DC! Since 1973, AAAS Fellows have applied their skills to federal decision-making processes that affect people in the U.S. and around the world, while learning first-hand about the government and policymaking.

Join the Network.
Year-long fellowships are available in the U.S. Congress and federal agencies. Applicants must hold a PhD or equivalent doctoral-level degree in any behavioral/social, biological, computational/mathematical, earth, medical/health, or physical science, or any engineering discipline. Individuals with a master's degree in engineering and three years of professional experience also may apply. Federal employees are not eligible and U.S. citizenship is required.

Apply.
The application deadline for the 2013-2014 AAAS Science & Technology Policy Fellowships is 5 December. Fellowships are awarded in the spring and begin in September. Stipends range from $74,000 to $97,000.

Note: Additional fellowships are available through approximately 30 scientific society partners. Individuals are encouraged to apply with AAAS as well as with any scientific societies for which they qualify.

Full details at: **fellowships.aaas.org**

Enhancing Public Policy, Advancing Science Careers

Sabrina McCormick, PhD

Sociology and Environmental Sciences, Brown University

2009-11 S&T Policy Fellow, Environmental Protection Agency, Office of Research and Development

Now president, Evidence Based Media

SCIENCE & TECHNOLOGY
POLICY FELLOWSHIPS
AAAS

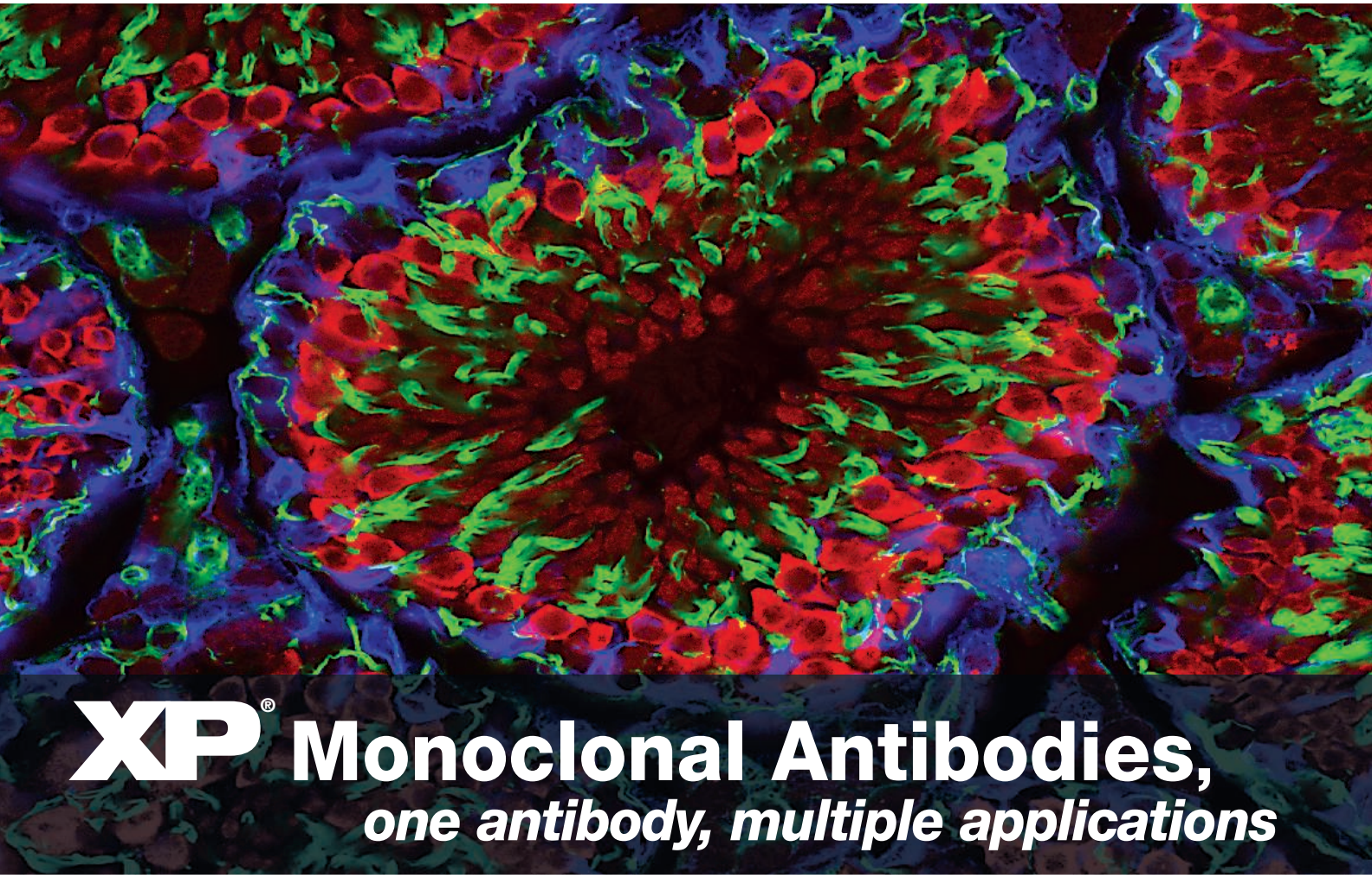

XP® Monoclonal Antibodies,
one antibody, multiple applications

Unparalleled product quality, validation, and technical support.

XP® monoclonal antibodies are a line of high quality rabbit monoclonal antibodies exclusively available from Cell Signaling Technology. Any product labeled with XP has been carefully selected based on superior performance in the most relevant applications.

XP monoclonal antibodies are generated using XMT® technology, a proprietary monoclonal method developed at Cell Signaling Technology. This technology provides access to a broad range of antibody-producing B cells unattainable with traditional monoclonal technologies, allowing more comprehensive screening and the identification of XP monoclonal antibodies.

eXceptional specificity
As with all of our antibodies, the antibody is specific to your target of interest, saving you valuable time and resources.

+ eXceptional sensitivity
The antibody will provide a stronger signal for your target protein in cells and tissues, allowing you to monitor expression of low levels of endogenous proteins, saving you valuable materials.

+ eXceptional stability and reproducibility
XMT technology combined with our stringent quality control ensures maximum lot-to-lot consistency and the most reproducible results.

= eXceptional Performance™
XMT technology coupled with our extensive antibody validation and stringent quality control delivers XP monoclonal antibodies with eXceptional Performance in the widest range of applications.

Above: Confocal IF analysis of rat testis using Miwi (D92B7) XP® Rabbit mAb #6915 (red pseudocolor) and Vimentin (D21H3) XP® Rabbit mAb (Alexa Fluor® 647 Conjugate) #9856 (blue pseudocolor). Actin filaments were labeled with DY-554 phalloidin (green pseudocolor).

For experimental details, additional information, and a complete list of available XP® monoclonal antibodies visit…

www.cellsignal.com

Cell Signaling TECHNOLOGY®

Orders (toll-free) 1-877-616-2355 | **Technical support** (toll-free) 1-877-678-8324 support@cellsignal.com | **Inquiries** info@cellsignal.com | **Environmental Commitment** eco.cellsignal.com